frontiers | Research Topics

Recent advances in renewable energy automation and energy forecasting, 2nd Edition

Edited by
Sarat Kumar Sahoo, Franco Fernando Yanine, Vikram Kulkarni and Akhtar Kalam

Published in
Frontiers in Energy Research
Frontiers in Energy Efficiency

ISSN 1664-8714
ISBN 978-2-8325-4167-8
DOI 10.3389/978-2-8325-4167-8

About Frontiers

Frontiers is more than just an open access publisher of scholarly articles: it is a pioneering approach to the world of academia, radically improving the way scholarly research is managed. The grand vision of Frontiers is a world where all people have an equal opportunity to seek, share and generate knowledge. Frontiers provides immediate and permanent online open access to all its publications, but this alone is not enough to realize our grand goals.

Frontiers journal series

The Frontiers journal series is a multi-tier and interdisciplinary set of open-access, online journals, promising a paradigm shift from the current review, selection and dissemination processes in academic publishing. All Frontiers journals are driven by researchers for researchers; therefore, they constitute a service to the scholarly community. At the same time, the *Frontiers journal series* operates on a revolutionary invention, the tiered publishing system, initially addressing specific communities of scholars, and gradually climbing up to broader public understanding, thus serving the interests of the lay society, too.

Dedication to quality

Each Frontiers article is a landmark of the highest quality, thanks to genuinely collaborative interactions between authors and review editors, who include some of the world's best academicians. Research must be certified by peers before entering a stream of knowledge that may eventually reach the public - and shape society; therefore, Frontiers only applies the most rigorous and unbiased reviews. Frontiers revolutionizes research publishing by freely delivering the most outstanding research, evaluated with no bias from both the academic and social point of view. By applying the most advanced information technologies, Frontiers is catapulting scholarly publishing into a new generation.

What are Frontiers Research Topics?

Frontiers Research Topics are very popular trademarks of the *Frontiers journals series*: they are collections of at least ten articles, all centered on a particular subject. With their unique mix of varied contributions from Original Research to Review Articles, Frontiers Research Topics unify the most influential researchers, the latest key findings and historical advances in a hot research area.

Find out more on how to host your own Frontiers Research Topic or contribute to one as an author by contacting the Frontiers editorial office: frontiersin.org/about/contact

Recent advances in renewable energy automation and energy forecasting, 2nd Edition

Topic editors

Sarat Kumar Sahoo — Parala Maharaja Engineering College (P.M.E.C), India
Franco Fernando Yanine — Universidad Finis Terrae, Chile
Vikram Kulkarni — SVKM's NMIMS University, India
Akhtar Kalam — Victoria University, Australia

Citation

Sahoo, S. K., Yanine, F. F., Kulkarni, V., Kalam, A., eds. (2023). *Recent advances in renewable energy automation and energy forecasting, 2nd Edition*. Lausanne: Frontiers Media SA. doi: 10.3389/978-2-8325-4167-8

Publisher's note: In this 2nd edition, the following article has been added:

Yanine F, Sahoo SK, Sanchez-Squella A, Barrueto A and Krishna Rao C (2023) Energy homeostasis model for electrical and thermal systems integration in residential buildings: a means to sustain distributed generation systems integration. *Front. Energy Effic*. 1:1258384. doi: 10.3389/fenef.2023.1258384

Table of contents

frontiers | Frontiers in Energy Research

TYPE Editorial
PUBLISHED 10 May 2023
DOI 10.3389/fenrg.2023.1195418

OPEN ACCESS

EDITED AND REVIEWED BY
ZhaoYang Dong,
Nanyang Technological University,
Singapore

*CORRESPONDENCE
Sarat Kumar Sahoo,
sksahoo.ee@pmec.ac.in

RECEIVED 28 March 2023
ACCEPTED 04 May 2023
PUBLISHED 10 May 2023

CITATION
Sahoo SK, Yanine FF, Kulkarni V and Kalam A (2023), Editorial: Recent advances in renewable energy automation and energy forecasting. *Front. Energy Res.* 11:1195418. doi: 10.3389/fenrg.2023.1195418

Editorial: Recent advances in renewable energy automation and energy forecasting

Sarat Kumar Sahoo[1]*, Franco Fernando Yanine[2], Vikram Kulkarni[3] and Akhtar Kalam[4]

[1]Parala Maharaja Engineering College (BPUT), Brahmapur, India, [2]Faculty of Engineering, Universidad Finis Terrae, Santiago, Chile, [3]Mukesh Patel School of Technology Management and Engineering, SVKM's NMIMS University, Mumbai, India, [4]School of Engineering and Science, Victoria University, Melbourne, VIC, Australia

KEYWORDS

renewable energy, machine learning, energy forecasting, control and optimization, real-time monitoring

Editorial on the Research Topic
Recent advances in renewable energy automation and energy forecasting

Renewable energy sources like solar, wind, and hydroelectric power are gaining popularity as we work towards a more sustainable future. However, their intermittent and often unpredictable nature, creates challenges for the energy industry in terms of being able to ensure continuous electric power generation over regular periods of time. Thus, accurate forecasting of renewable energy output is crucial for their reliable integration into the power grid. In this regard, automation and machine learning have made significant improvements in energy forecasting by enabling more precise predictions of energy output. Advanced algorithms and high-performance computing systems allow for better grid management and increased power generation systems' efficiency. Automation is also being used for the operation and maintenance of renewable energy systems. Real-time monitoring and control systems enable a rapid response to changes in weather conditions, optimizing energy production. This editorial summarizes recent advancements in renewable energy automation and energy forecasting, which are critical areas for achieving a sustainable energy future. The Research Topic covers areas like machine learning-based energy forecasting, control and optimization of renewable energy systems, and the integration of renewable energy into microgrids as shown in Figure 1. Continued research and development in renewable energy automation and energy forecasting are essential for the transition towards a sustainable energy future.

The global energy crisis on one hand and the advancement of climate change threat on the other have prompted countries worldwide to seek alternative energy solutions, such as solar, wind, hydrogen, etc., accelerating the pace towards decarbonization of their energy matrix. Thus, renewable power generation, and the advancement of sustainable energy are becoming an important concern for many countries. With these important priorities, so grows the need for advanced technologies that can support such transformation in the countries' power grid to transition towards renewable and sustainable energy future. These technologies must be able to monitor systems continuously and safeguard their continuous operation over regular periods of time so as to ensure the technical and economic feasibility of such large-scale projects. However, the electrical power being produced at the generation

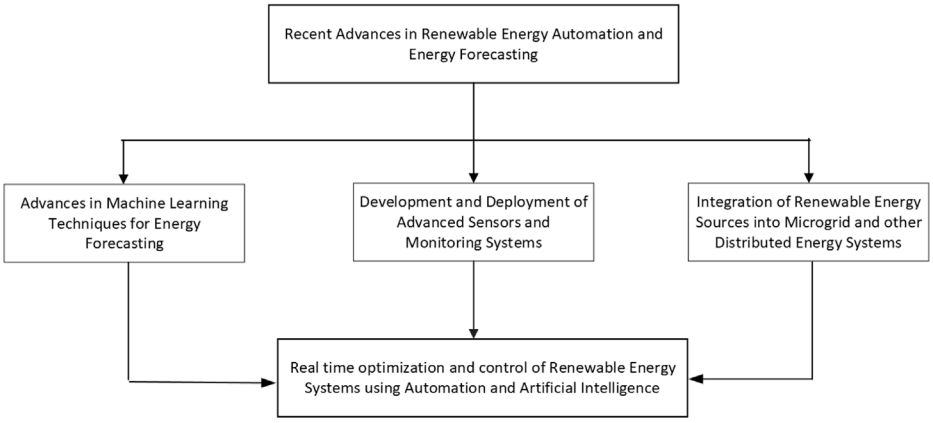

FIGURE 1
Recent advances in Renewable Energy Automation and Energy Forecasting.

plants is transmitted to the points of utilization, which is achieved by means of the power grids (an interconnected network for electricity transmission and distribution from producers to the consumers). Hence, traditional power grids support a one-way flow of power from centralized sources, such as gas, nuclear and hydroelectric to points of consumption. Therefore, based on the devices used and their functionality, the electric power grids are classified into two categories:

- Conventional grid
- Smart grid

A smart grid is much different from the conventional power grid in the sense that it provides more reliable and consistent electric power supply, thanks to advanced power electronics, control and communications systems. The smart grid is the electrical system which is capable for monitoring the activities of the grid connected system and provides the real-time information of all the events occurring in the power system. Part of the technology that goes into a smart grid are advanced sensors and real-time advanced data processing systems, with machine learning capabilities incorporated in such systems, which can ensure the continuous monitoring of all of the systems that comprise the smart grid, thus safeguarding its continuous operation. The emergence of improved sensors, actuators, and automation technologies has consequently improved the control, monitoring and communication techniques within the energy sector, helping to advance the smart grid system. Thus, with the support of aforementioned modern technologies, the information flows in two-ways between the consumer and supplier. This data communication helps the supplier in overcoming challenges like integration of renewable technologies, management of energy demand, load automation and control. Renewable energy (RE) is intermittent in nature and therefore difficult to predict. The accurate RE forecasting is very essential to improve the power system operations. The forecasting models are based on complex functions' combination that include seasonality, fluctuation, and dynamic nonlinearity. The advanced intelligent computing algorithms for forecasting should consider the proper parameter determinations for achieving optimization process. For this we need, new generation research areas like Machine learning (ML), and Artificial Intelligence (AI) to enable the efficient integration of distributed and renewable generation at large scale and at all voltage levels. The modern research in the above areas will improve the efficiency, reliability and sustainability of the Smart grid.

The energy grid is one of the most complex infrastructures and requires quick decision-making in real-time, which big data and AI algorithms enable for utilities. Beyond grid analytics and management, AI's applications in the renewable sector include power consumption forecasting and predictive maintenance of renewable energy sources. It further enables the internet of energy applications that predict grid capacity levels and carry out time-based autonomous trading and pricing. Future smart power systems need the intelligent field devices to help in the implementation of effective control mechanisms and protection schemes. The researchers should focus on development of human and machine interaction (HMI) system based on advanced AI and ML techniques in plant control and monitoring systems. An increase in the application of advanced automation by RE based research may lead to an eventual total shift from conventional energy sources to RE.

This Research Topic is entitled "*Recent advances in renewable energy automation and energy forecasting*." It aims to bring out new methods and models that can help improve the operations on RE, improves grid security and can sustainable energy future. This Research Topic calls for novel and innovative research submissions that focus on application-oriented studies improving RE automation and Energy forecasting models.

Specific Research Topic of interest include (but are not limited to):

- Intelligent systems, solving methods, optimization, and advanced heuristics for improving operation of renewable integrated energy systems;
- Advanced control and operation methods to improve power system flexibility;

- Artificial intelligence and its application in RE automation;
- Modelling of Intelligent Field Devices;
- Smart energy, IoT and modern power systems modelling of RE operations;
- Energy-forecasting technologies;
- Deep learning and machine learning applications in smart grids;
- Modelling of data analytics for smart grid operations;
- Business models for different electricity market players;

The Smart Grid concept has been defined as the integration of the electrical generation, transmission and distribution networks and the data communications networks. As such, Smart Grid systems use digital and other advanced technologies to monitor and manage the transport of electricity from all generation sources to meet the varying electricity demands of end users. Reviewing the literature, we find, for example, that Praveena et al. proposed a new optimization method that combines Crow Search Algorithm and Harris Hawks Optimization to improve power quality and reduce harmonic distortion in microgrid systems with photovoltaic systems and multi-level inverters. By optimizing the performance of a recurrent neural network controller, the proposed approach outperforms other methods in enhancing power quality and reducing THD. The authors suggest its potential for application in other microgrid systems with different configurations to enhance renewable energy system performance.

Likewise, Kondaiah et al. projected a modified deep residual network (MDRN) for short-term load forecasting (STLF) that enhances accuracy and efficiency. Combining the residual network and convolutional neural network, the MDRN comprises four main components and outperforms other deep learning models, including (Long-Short Term Memory) LSTM model and (Contextual LSTM) CLSTM, an extension of the recurrent neural network LSTM, in forecasting accuracy and computational efficiency. The proposed MDRN can potentially enhance energy management systems' accuracy and efficiency and may be useful in other time-series forecasting applications.

A major Research Topic within energy management systems, especially in the context of renewables being incorporated to the energy matrix and the enhancement of Smart Grid technologies, are the strong non-linear and non-stationary characteristics of power loads, wherein there is the need to develop short-term power load forecasting methods based on bald eagle search (BES) optimization variational mode decomposition (VMD), convolutional bi-directional long short-term memory (CNN-Bi-LSTM) network and considering error correction are developed to improve the accuracy of such load forecasting. In this context Wang and Li recommended a BES-VMD and CNN-Bi-LSTM method with an error correction mechanism for short-term power load forecasting. The method outperforms traditional methods, including ARIMA and CNN-Bi-LSTM without error correction, in accuracy and efficiency. The authors suggest its potential for other time-series forecasting problems.

With regard to the Smart Grid and demand response management —a major Research Topic within the subject's key areas of research—most consumers of energy are familiar with the grid and its hourly periods of high and low electricity rate of consumption. Thus, demand response programs seek to give consumers the opportunity to voluntarily reduce or shift their electricity consumption during peak hours by incentivizing them with lower rates or other forms of compensation. This way, demand response programs are being used by utilities and operators to balance supply and demand of electricity in an evolving market. In this context, Puppala et al. proposed a demand response program for a smart grid that incentivizes customers to reduce peak electricity demand through rebates. The framework outperforms other programs in reducing peak demand and improving customer satisfaction. It can scale up to support energy sustainability and grid stability. Along the same line, Vishnuvardhan et al. proposed a review of technical advancements and stability analysis in wind-penetrated power generation systems. The authors emphasize the significance of integrating renewable energy into the power grid and the challenges associated with high wind penetration. The review discusses recent advancements in power electronic devices, grid-forming inverters, and control strategies, as well as stability challenges like frequency and voltage stability. The review highlights the current state-of-the-art in wind-penetrated power generation systems and identifies the need for further research. The findings can inform policy and strategy for grid stability and wind energy integration.

The growing need to diversify the energy matrix and the electric power distribution sector has drawn electric utilities to pursue renewable energy projects that can advance the green energy agenda towards 2030 and beyond. In this context, Din et al. examine the public perception and willingness to pay (WTP) for renewable energy in Pakistan using the theory of planned behaviour (TPB). The study employs a survey questionnaire to investigate public attitudes, subjective norms, perceived behavioural control, and WTP for renewable energy. The results reveal that public attitudes and subjective norms have a significant influence on WTP for renewable energy, while perceived behavioural control has a weaker effect. The authors suggest that these findings can inform policy and strategy development to encourage renewable energy adoption in Pakistan and other developing countries.

An important Research Topic that is also at centre stage in the Smart Grid discussion is the potential impact of electric vehicles (EVs) on global energy systems. There is no doubt that the growing trend in the electrification of private and public transport vehicles accelerating at a somewhat rapid pace towards 2035, energy producers and distributors need to take into account and plan ahead for the potential impact of EVs on electricity demand. Thus, Dharavat et al. emphasized a review on the impact of plug-in electric vehicles (PEVs) on grid integration with distributed energy resources (DERs). They discuss the challenges and opportunities of PEV integration, such as the need for grid infrastructure upgrades and the potential for PEVs to provide grid services. The authors also explore strategies and technologies, including vehicle-to-grid systems and smart charging, to manage the impact of PEVs on the grid. The review provides an overview of the current state-of-the-art in PEV grid integration and highlights the need for further research.

High impedance faults (HIF) are abnormal conditions in power distribution networks, that occur when an energized primary conductor establishes an improper contact with a highly resistive surface. Therefore, the need to prevent such occurrences are also a major Research Topic of research. To accomplish this, HIF detection

methods are employed considering the presence of non-linear loads in the distribution network. Along this line, Gogula and Edward recommended a new method for detecting high-impedance faults in a distribution network, where they propose to use a combination of discrete wavelet transform (DWT) and radial basis function (RBF) neural network. The authors highlight the difficulties in detecting such faults using traditional methods due to their low fault currents, hence they may go generally undetected for extensive periods of time, decreasing the distribution network's reliability and effectiveness. Moreover, energized conductor on the ground present great risk of electric shock to anyone nearby. The proposed method of the authors is evaluated using simulations and outperforms traditional methods in accuracy. This study's findings can inform the development of more effective fault detection methods for distribution networks, improving grid reliability and reducing downtime.

Bishwal et al. have proposed a differential evolution (DE) algorithm to optimize an IPIDF controller for frequency management in a networked power system with superconducting magnetic energy storage (SMES) and high-voltage direct current (HVDC) links. The DE algorithm finds the optimal values of the IPIDF controller's parameters for stable frequency response in the system. The study shows that the optimized IPIDF controller provides better frequency response than traditional PI controllers, particularly in scenarios with power system disturbances. The study suggests that the DE-optimized IPIDF controller is a promising approach for managing frequency in networked power systems with SMES and HVDC links.

Research on methods and techniques to optimize the energy efficiency in industrial processes, are also an important area of development, seeking to optimize the use of energy and enhance process optimization in various industrial sectors. In this vein, Parekh et al. review different techno-managerial methods for optimizing energy use in chemical process industries, such as energy audits, pinch analysis, process integration, advanced process control, and machine learning. The authors discuss the benefits and limitations of each approach, and emphasize that combining them can lead to substantial energy and cost savings, stressing the importance of considering both technical and managerial factors when implementing energy optimization strategies.

Power systems expansion parallels the increase in load demand both from residential and industrial users, especially now that large influx of renewable energy is being incorporated into the power systems almost everywhere, to satisfy the increasing load demand. Regarding this, Chetan H. R. et al. explain that with its potential to generate power and compensate for a large portion of the load demand, wind generators make a major renewable power contribution. Chetan H. R. et al. used an optimized PI controller with a static synchronous series compensator (SSSC) to improve the transient stability of a wind power conversion system. The optimized PI controller enhanced damping and stability, making it a promising approach for power system disturbances.

Finally, Ravinder and Kulkarni highlight the importance of safeguarding smart meters' integrity when they state that the intrusion detection in network traffic for crucial smart metering applications based on radio sensor networks is becoming very important in the Smart Grid area. The network's structure for smart meters under investigation should consider important security factors. Thus, they report on research using machine learning to detect intrusions in smart meter data. Their results show that three algorithms, including random forest, can effectively detect intrusions. The study concludes that machine learning can enhance smart grid security and privacy.

Author contributions

SS and FY: Contribute the aims and objectives of the Research Topic, writing—review and editing, VK and AK: present the contributing articles of the Research Topic, original draft preparation. All authors listed have made a substantial, direct, and intellectual contribution to the work and approved it for publication. All authors contributed to the article and approved the submitted version.

Conflict of interest

The authors declare that the research was conducted in the absence of any commercial or financial relationships that could be construed as a potential conflict of interest.

Publisher's note

frontiers | Frontiers in Energy Research

TYPE Original Research
PUBLISHED 12 October 2022
DOI 10.3389/fenrg.2022.1038819

OPEN ACCESS

EDITED BY
Sarat Kumar Sahoo,
Parala Maharaja Engineering College, India

REVIEWED BY
Rakhee Panigrahi,
Parala Maharaja Engineering College, India
Sudhakaran M,
Pondicherry Engineering College, India
Rabindra Kumar Sahu,
Veer Surendra Sai University of Technology, India
Ashwin Sahoo,
C. V. Raman College of Engineering, India

*CORRESPONDENCE
B. Saravanan,
bsaravanan@vit.ac.in

SPECIALTY SECTION
This article was submitted to Smart Grids, a section of the journal Frontiers in Energy Research

RECEIVED 07 September 2022
ACCEPTED 22 September 2022
PUBLISHED 12 October 2022

CITATION
Kondaiah VY and Saravanan B (2022), A modified deep residual network for short-term load forecasting.
Front. Energy Res. 10:1038819.
doi: 10.3389/fenrg.2022.1038819

A modified deep residual network for short-term load forecasting

V. Y. Kondaiah and B. Saravanan*

School of Electrical Engineering, Vellore Institute of Technology, Vellore, India

The electrical load has a prominent position and a very important role in the day-to-day operations of the entire power system. Due to this, many researchers proposed various models for forecasting load. However, these models are having issues with over-fitting and the capability of generalization. In this paper, by adopting state-of-the-art of deep learning, a modified deep residual network (deep-ResNet) is proposed to improve the precision of short-term load forecasting and overcome the above issues. In addition, the concept of statistical correlational analysis is used to identify the appropriate input features extraction ability and generalization capability in order to progress the accuracy of the model. Two utility (*ISO-NE and IESO-Canada*) datasets are considered for evaluating the proposed model performance. Finally, the prediction results obtained from the proposed model are promising as well as accurate when compared with the other existing models in the literature.

KEYWORDS

load forecasting, smart/ micro-grid, feature selection, ANN, artificial neural networks, short term load forecasting, deep learning

1 Introduction

Estimating the electricity demand is vital to the growth and development of current existing power systems. Making accurate projections of future loads over various time horizons is essential to the steady and effective operation of decision makers, scheduling, and allocating sources in power systems. Specifically, STLF is concerned with estimating the subsequent future loads for a time-period ranging from a few minutes to a week Kondaiah et al. (2022). In addition, a reliable and efficient STLF also assists utilities and energy suppliers in meeting the difficulties posed by the increased penetration of renewable energy sources and the progression of the electricity sector with more complicated pricing techniques in future smart grids.

Researchers over the years have proposed various STLF methods. Some of the models used for STLF include linear or nonparametric regression Ferraty et al. (2014), support vector regression (SVR) Zhang and Guo (2020), autoregressive models Taylor (2010), fuzzy logic approach Ali et al. (2021), etc. In addition, the references Kondaiah et al. (2022); Kuster et al. (2017); Hippert et al. (2001) provide reviews and assessments of the various available approaches. However, most of the suggested models were over-parameterised, and the findings they offered were neither

persuasive nor sufficient Hernández et al. (2014). Furthermore, the construction of STLF systems via artificial neural networks (ANN) has been one of the more conventional approaches to tackling the forecasting challenge. In addition, increasing the several input parameters, hidden nodes, or layers may increase the size of ANN, but another critique is that networks are prone to the issue of "overfitting" Velasco et al. (2018). Despite this, other kinds and subcategories of ANN, such as radial basis function (RBF) neural networks Cecati et al. (2015), wavelet-based neural networks Liu et al. (2013), and extreme learning machines (ELM) Li et al., 2016b, to mention a few, have been suggested and used to STLF.

Moreover, Computer vision, natural language processing (NLP), and speech recognition have been greatly influenced by recent advances in neural networks (especially deep-ResNets) Li et al. (2022). Mostly, Scientists are now incorporating their knowledge of various applications into neural network architectures instead of relying on pre-designed superficial neural network configurations. The addition of other building modules, such as convolutional neural networks (CNN) Amarasinghe et al. (2017) and long short-term memory (LSTM) Wang et al. (2019), has made it possible for deep neural networks to be very versatile and efficient. In addition, numerous training methods have been suggested to train neural networks properly with multiple layers without the gradients disappearing or severe overfitting. Furthermore, the use of deep learning models for STLF is a subject that has just recently gained attention. For forecasting various loads, researchers have utilized Restricted Boltzmann Machines (RBM) and feed-forward neural networks with many layers Li C. et al. (2021); Rafi et al. (2021). Nonetheless, as the number of layers rises, it becomes more difficult to train these models; hence, the number of hidden layers is often somewhat limited, thereby limiting the performance of the models. And also, numerous studies have indicated that feature selection from input data impacting hourly load profile might enhance prediction performance Zhang and Guo (2020); Bento et al. (2019).

Furthermore, using a multi-sequence-LSTM-based network architecture, Jiao et al. (2018), developed a framework for commercial load forecasting. This approach accurately captures the complex relationships among sequences. The contribution of DNN in the actual load dataset was explored in reference Chitalia et al. (2020), and it was shown that a wide variety of activation functions could be employed to create reliable load predictions. A model that is mainly focused on LSTM-RNN was suggested in reference Kong et al. (2019) to forecast the short-term residential load. This model is able to estimate the overall load of a single home quite precisely. The residual network was suggested in reference Kaiming et al. (2015). Applying DNNs has become feasible according to this technique. A modified residual network was presented by Chen et al. (2019). Here, the network's input would be the average value of the multi-layer output rather than the output of the layer that came before it. To avoid such complexity, a model for STLF is developed in this paper with the assistance of the DNN. Also, we used a deep-ResNet model to make our prediction and over-fitting methods more reliable. The critical difference between the proposed and other existing models is that in this approach, we don't stack several hidden layers over each other since this would lead to severe over-fitting.

Consequently, in this proposed work, we have used the state-of-the-art deep neural network (DNN) architectures and implementation approaches to enhance the existing ANN structures for STLF. A unique DNN model for estimating the day-ahead (24-Hours) load has been suggested based on the residual network (ResNet) topology introduced in Chen et al. (2019); Kondaiah and Saravanan (2021) instead of stacking numerous hidden layers. The most important vital contributions of the work proposed in this paper are as follows. First, an effective end-to-end model for STLF based on deep-ResNets is proposed. The suggested model used an appropriate feature extraction or selection method with adequate statistical correlation analysis. The findings suggest that enhancing the neural network topology may significantly improve predicting performance. Second, the integration of the building blocks with pre-existing methodologies for feature extraction and selection is an essential process that has the potential to result in significant improvements in accuracy. Furthermore, the fundamental components of the model that has been described are easily adaptable to other neural-network-based STLF models already in existence. In addition, when compared to various models, the suggested STLF model outperforms in terms of precision and reliability. Concurrently, we utilised DNN to make the prediction model more robust and to reduce over-fitting. Typically, the output of an aggregated model of neural networks is the combination of many individual models. One drawback is that it takes a substantial amount of processing capacity to execute. But, just a single training session is required for the proposed approach in this paper.

According to the following outline, the rest of the paper is organised as follows. First, the process of selecting appropriate inputs from the dataset is described in **Section 2**. The details of the proposed methodology are presented in **Section 3**. The results of the proposed STLF model are described in **Section 4**. Additionally, we compare the model performance with other approaches. Finally, **Section 5** concludes the paper with a summary of the findings and suggestions.

2 Features selection for the model

Meteorological conditions or variables[1] and the price of electricity, as we all know, considerably influence

1 such as temperature, relative humidity, wind speed, and precipitation.

TABLE 1 Pearson's correlational coefficient variables.

Correlational coefficients

Range	Relation
0.8 to 1.0	*Extremely strong*
0.6 to 0.8	*Strong*
0.4 to 0.6	*Medium*
0.2 to 0.4	*Weak*
0.0 to 0.2	*Extremely weak*
0.0	*No relation*
-0.0 to -1.0	*Negative relation*

electricity consumption Liu et al. (2018); Kwon et al. (2020); Kim et al. (2020). However, because of the intricate relation between those variables, it is difficult to characterise the interactions between them. Therefore, there are additional benefits to selecting several input parameters in general. On the other hand, numerous variables might have certain drawbacks Memarzadeh and Keynia (2021).

Consequently, Pearson's correlation approach was used for correlation analysis to find the association between input parameters and the actual load. The relationship between the various variables can be understood in detail based on the correlation coefficients generated by this method Zhang and Guo (2020). The following is the formula that is used while calculating Pearson's correlation:

$$Corr\left(x_i, y_j\right) = \frac{n\sum x_i y_j - \sum x_i \sum y_j}{\sqrt{n\left[x_i^2 - (x_i)^2\right]\left[n\sum y_j^2 - \left(y_j\right)^2\right]}} \quad (1)$$

Where $Corr(x_i, y_j)$ denotes the relational degree between input variables x_i and actual load demand y_j, and n represents the total number of data points. The values of the reference coefficients of the correlation (-1.0 to 1.0) are given in **Table 1**.

Correlation analysis was performed on the data from 1 January 2010, to 31 December 2014. This dataset consists of different variables, such as, "the hourly temperature (Tem), wind speed (WS), relative humidity (RH), precipitation (Pr) and solar radiation (SR), air pressure (AP), and the actual load demand (LD)". There are several extremely interesting observations to be made, as explained in **Section 4.1**.

3 Proposed methodology

Deep residual networks (deep-ResNet) are the foundation of our model for day-ahead load forecasting, which we presented in this study. We begin by formulating the low-level fundamental structure of the model, which consists of numerous layers that are all completely related to one another, and process the inputs of the model to create tentative predictions for the next 24 hours. After then, the preliminary projections are processed by a comprehensive residual network. Following the presentation of the topology of the ResNet, many adjustments are done in order to further improve its capacity for learning.

3.1 Deep neural networks

Deep Neural Networks (DNNs) are ANNs with numerous hidden layers between the input layer and the output layer Ma (2021). The linear and non-linear associations between data characteristics are modelled by using DNN. In modeled, the propensity to overfit may be mitigated by using dropout, a technique in which neurons are removed from the network in either a random or a systematic manner Salinas et al. (2020). Since their inception, DNNs have made significant achievements in a wide range of areas of study. According to Subbiah and Chinnappan (2020), the field of deep learning exploded after their original publication was released in 2006. Through the use of the summation and product procedures, the non-linear function that effectively represents the data is determined in the neural networks. **Figure 1** depicts an ANN-based DNN structure. There are three layers in the DNN: an input layer, a hidden layer, and an output layer. Each layer is made up of neurons that do not communicate with each other. There are, nevertheless, complete weighted connections between neurons between layers. The fundamental formulae of DNN in classic networks are as follows;

$$y_{output} = F\left(x_{input}\right) \quad (2)$$

Where the input of the neuron is denoted by x_{input} and the output of the neuron is denoted by y_{output}.

DNNs are able to extract highly abstracted characteristics from training data because of their multiple hidden layers, which provide this power. Since load profiles include nonlinear features among the different components that determine the morphologies of load patterns, it is possible to use DNN as a prediction model under these circumstances. However, the DNNs have two problems when they are being trained to do a task: gradient explosion/vanish and network degeneration.

3.2 Deep residual networks

The aforementioned model is used in order to discover the nonlinear connection that exists between the input data and the output value. In general, the neural network's learning capacity improves as the model depth is increased. However, there is a possibility that the performance of the deep learning model would suffer in reality. The inherent quality of the data or the challenging nature of the deep learning model might both be to responsible for the deteriorating performance. For greater

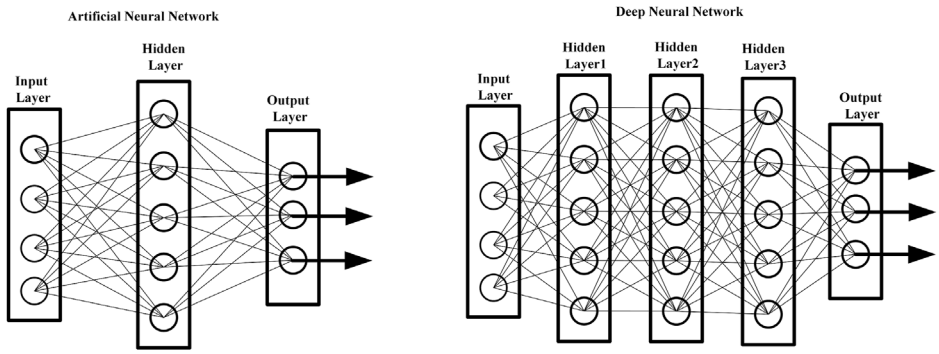

FIGURE 1
The structure of ANN-based DNN.

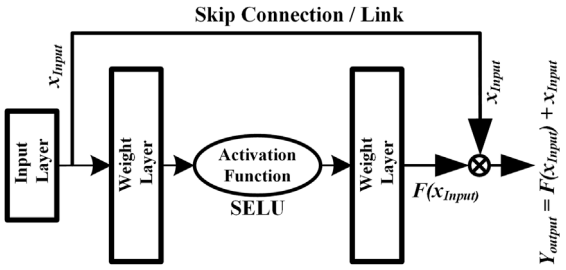

FIGURE 2
The basic structure of Residual Network (ResNet).

performance, Zhang et al. (2018) presented an approach that used ResNet instead of stacking concealed layers. ResNet has a unique structure in comparison to nested layers. It is essentially the same as the framework suggested in Zhang et al. (2021), which is often employed for the picture/image classification issue but with a few key differences. In the ResNet building block, the skip link/connection typically has input and output dimensions that are the same, but in a residual block, the input (x_{input}) and output (y_{output}) dimensions are different. A ResNet, as seen in **Figure 2**, has two stacked levels and one skip link/connection.

Typically, a skip connection is an identical mapping when its input and output are of the same dimension. For this case, the output of the appropriate ResNet is as follows:

$$y_{output} = F\left(x_{input}\right) + x_{input} \tag{3}$$

If the dimensions of the input and output are not the same, then the skip connection act as a linear projection. In this case, the associated ResNet produces an output with linear projection (L_p) as follows:

$$y_{output} = F\left(x_{input}\right) + L_p * x_{input} \tag{4}$$

The skip connection signifies that the ResBlock/ResNet learning ability is no weaker than that of the stacked layers when both have the same number of hidden layers. The formula for forward-propagation if n residual blocks are formed one after the other is given as follows:

$$y(x) = x_{initial} + \sum_{j=1}^{n} F\left(x_j - 1\right) \tag{5}$$

Where $x_{initial}$ represents the very first input that the network receives. In point of fact, the residual block builds an artificial identity map by performing an addition that combines the input and output of the neural unit in a straightforward manner. Experiments have shown that the residual block is an effective solution to the issue of deterioration that occurs in DNNs. Sheng et al. (2021), explained the residual block, both from the point of view of advancing propagation and backward propagation [30].

3.3 A modified structure of deep residual network

The proposed model is presented in this subsection; it is based on the model structure shown in **Figure 2**. As a result of its design, the proposed model can learn both deep and superficial characteristics or features from the input data that is fed into it. Furthermore, the ResBlocks structure enables that the modified deep-ResNet learning capacity is equivalent to that of a shallow ResNet. According to Zhang et al. (2018), there is a way to expand the deep-ResNet by adding more shortcuts. Although the formulations of the forward and backward propagation of responses and gradients are somewhat different, the network features are the same after adding the additional shortcut links. In order to enhance ResNet learning capacity, we make structural changes to the network. The convolutional network designs suggested in Chen et al. (2019) and Kondaiah and Saravanan (2021) served as inspiration for our proposal of

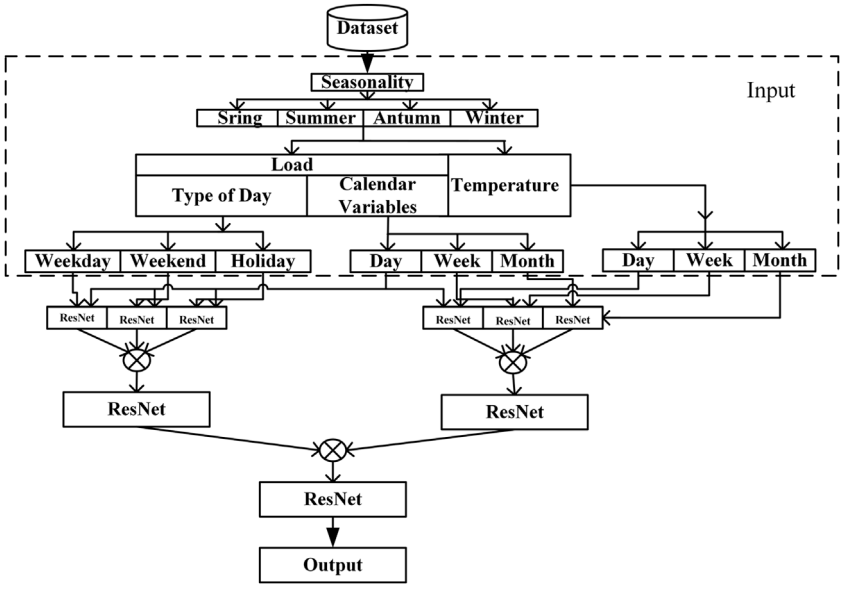

FIGURE 3
The Proposed Structure of a modified deep-ResNet.

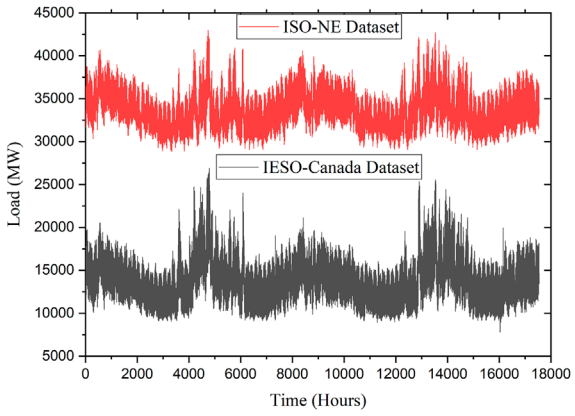

FIGURE 4
Time-Series load data from the two-utility dataset.

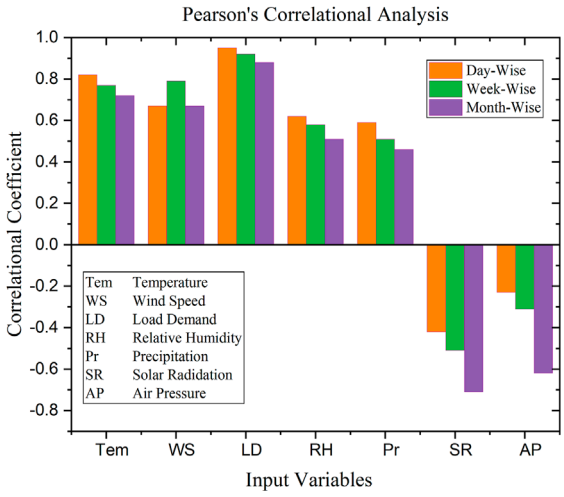

FIGURE 5
Correlational Analysis between the input variables.

the modified deep-ResNet, the structure of which is seen in Figure 3.

A sequence of ResNets is added to the model first (the residual blocks on the right). The input of both side residual blocks is the combination of load values regarding the calendar variables with day type, and the temperature information, respectively, unlike the implementation in Xu et al. (2020) (except for the first side residual block, whose input is the input of the network). This layer output is averaged across the outputs of each of the primary residual blocks. Then the outputs are linked to all of the major remaining blocks in the following layers, much like the tightly connected network in Li Z. et al. (2021). After averaging all connections from the blocks on the right and the network output, the following major residual block is provided as an input. As a result of the extra side residual blocks and dense shortcut connections, it is anticipated that the network representation capabilities and error back-propagation efficiency would increase. In the next section of this study, we will evaluate and contrast the performance of the proposed model.

TABLE 2 Input Features for the model.

Name of the input features	Index of the variable(s)		
	Day_wise	Week-Wise	Month-Wise
Temperature (Tem)	Tem_h^{Day}	Tem_h^{Week}	Tem_h^{Month}
Load Demand (LD)	LD_h^{Day}	LD_h^{Week}	LD_h^{Month}
Wind Speed (WS)	WS_h^{Day}	WS_h^{Week}	WS_h^{Month}
Relative Humidity (RH)	RH_h^{Day}	RH_h^{Week}	RH_h^{Month}
Precipitation (Pr)	Pr_h^{Day}	Pr_h^{Week}	Pr_h^{Month}

TABLE 3 Additional input variables for the model.

Dummy Variables	Code	Indication Meaning
Seasonality (S)	1	*spring*
	2	*Summer*
	3	*Antumn*
	4	*Winter*
Week-Index (WI)	0	*Weekday*
	1	*Weekend*
Holiday-Index (HI)	0	*Holiday*
	1	*Non-Holiday*

4 Results and discussion

The proposed model in this experiment is trained by the *Adam optimizer* with default parameters, as mentioned in Kondaiah and Saravanan (2021). The models are accomplished by adopting *Keras 2.2.4* with *Tensorflow 1.11.0* as the backend in the *Python* 3.6 environment. Note that adaptive adjustment of the learning rate during the training process is used. The models are trained on an *Intel(R) Core(TM)- i5-3230M*-powered *Acer* laptop. Moreover, the generalizability of the developed model was investigated in two case studies with *IESO-Canada* and *ISO-NE datasets*, respectively. Finally, the proposed model performance was verified using real-time data. To train the model, 3 years of data were used, which was taken around 1.5 h for 700 epochs. When training all models, the total training duration is under 8 hours. "Mean absolute percentage error (MAPE), Root mean square error (RMSE), and Mean absolute error (MAE)" are the most significant indices when comparing the results of various STLF models Li et al., 2016b. They are described as follows:

$$MAPE = \frac{1}{N}\sum_{n=1}^{N}\left(\left|\frac{Load_{Actual_n} - Load_{Predicted_n}}{Load_{Actual_n}}\right| * 100\right) \quad (6)$$

$$RMSE = \sqrt{\frac{1}{N}\sum_{n=1}^{N}\left(Load_{Actual_n} - Load_{Predicted_n}\right)^2} \quad (7)$$

$$MAE = \frac{1}{N}\sum_{n=1}^{N}\left|Load_{Actual_n} - Load_{Predicted_n}\right| \quad (8)$$

Where N is the total number of input values,$Load_{Actual_n}$ and $Load_{Predicted_n}$ are the average values of the actual and predicted load, respectively.

4.1 Analysis of input data

4.1.1 Data pre-processing

The gathered dataset(s) may have multiple anomalies, including missing values, incomplete data, noises, and raw format Shi et al. (2018). The unprocessed data contains flaws and contradictions that might lead to misunderstanding and indicate a lack of proper data analysis. Therefore, the pre-processing stage that is part of the data refining process is particularly crucial for real-world datasets since it ensures the performance and reliability of the system to find information from real-world data. In most cases, the pre-processing data stage consists of many fundamental sub-steps or phases that are applied to raw data before they are refined. These phases and sub-steps are as follows: 1) Data-Cleaning, 2) Data-Transformation, 3) Data-Reduction, 4) Data- Discretization, respectively. These stages are primarily employed in the pre-processing step to improve and evaluate data in order to efficiently and accurately anticipate. As a result, a variety of sub-phases may be effectively used based on the data format, strategy, and input requirements for the suggested methodology.

4.1.2 Description of the data

Two different public data sets are utilized in this work, both of which contain hourly load and weather related data. The first dataset is New England's independent system operator (ISO-NE)[2] dataset Chen et al. (2019). The time range of this dataset is from March 2003 to December 2014. The second dataset is Canada's Independent Electricity System Operator (IESO)[3] dataset El-Hendawi and Wang (2020). The time scope

2 https://class.ee.washington.edu/555/el-sharkawi.

3 http://reports.ieso.ca.

TABLE 4 The month-wise estimation results (% MAPE) of the proposed model with other model(s) on the ISO-NE dataset.

Name of the Month	Forecasted Results (%MAPE)				
	Name of the Model(s)				Proposed Model
	SIWNN [Chen et al. (2010)]	WT_ELM_PLSR [Li et al. (2016c)]	WT_ELM_MABC Li et al. (2016b)	ResNetPlus [Chen et al. (2019)]	
January	1.60	–	1.52	1.619	1.423
February	1.43	-	1.28	1.308	1.252
March	1.47	–	1.37	1.172	1.032
April	1.26	–	1.05	1.340	1.212
May	1.61	–	1.23	1.322	1.245
June	1.79	–	1.54	1.411	1.331
July	2.70	–	2.07	1.962	1.523
August	2.62	–	2.06	1.549	1.329
September	1.48	–	1.41	1.401	1.321
October	1.38	–	1.23	1.293	1.133
November	1.39	–	1.33	1.507	1.361
December	1.75	–	1.65	1.465	1.373
Average	1.75	1.489	1.48	1.447	**1.294**

TABLE 5 Year-Wise forecasted results (%MAPE) of the proposed model with other model(s) on the ISO-NE dataset.

Year	Name of the model(s)	Forecasted results (%MAPE)
2010	*RBFN-ErrCorr* [Yu et al. (2014)]	1.80
	RBFN-ErrCorr [Cecati et al. (2015)]	1.75
	WT-ELM-PLSR [Li et al. (2016c)]	1.50
	ResNetPluse [Chen et al. (2019)]	1.50
	Proposed	**1.308**
2011	*RBFN-ErrCorr* [Yu et al. (2014)]	2.02
	RBFN-ErrCorr [Cecati et al. (2015)]	1.98
	WT-ELM-PLSR [Li et al. (2016c)]	1.80
	ResNetPluse [Chen et al. (2019)]	1.64
	Proposed	**1.423**

TABLE 6 Day-wise forecasted results (%MAPE) of the model on the ISO-NE dataset.

Day Index	Year-wise forecasted MAPE (%)		
	2006	2010	2011
Weekdays	1.289	1.273	1.296
Weekends	1.296	1.387	1.279
Average	1.2925	1.3300	1.2875

TABLE 7 Holiday(s)-wise forecasted results (%MAPE) of the model on the ISO-NE dataset.

Name of the Holiday	MAPEs (%)		
	2006	2010	2011
New Year	1.343	1.322	1.287
Martin Luther King Jr.Day	1.284	1.395	1.303
	1.333	1.364	1.329
Memorial Day	1.148	1.102	1.245
Independence Day	1.276	1.355	1.395
Labor Day	1.397	1.298	1.269
Veterans Day	1.265	1.226	1.313
Thanks Giving Day	1.309	1.361	1.268
Christmas Day	1.237	1.328	1.256
Pre-New year's Day	1.348	1.332	1.301
Average	1.294	1.3083	1.2966

of this dataset is from 1st January 2002 to 12th November 2021. These datasets are time series, which are taken into account in minutes, hours, or even days. Trend, cycle, seasonal variation, and erratic fluctuations are the most common features of time series data. In a time series context, a trend is an upward and downward movement that depicts the long-term advancement or deterioration. "Cycle" refers to the periodic oscillations that take place around a trend level. In time series, seasonal variation refers to the recurrence of time interval patterns that complete themselves inside a year's calendar and reoccur annually. Any movement in a time series that does not follow the regular pattern, known as an irregular variation, is unforeseen and unexpected. For example, the data that we collected for the load in the case study is presented as a time series that is denoted by the hour, as depicted in Figure 4.

The 2-year load demand of both utilities is shown graphically in Figure 4. As seen in Figure, the ISO-NE grid data shows a repeating and cyclic load pattern. In addition to that, the seasonal fluctuation may be noted as well. Nevertheless, the shape of the curve remains the same throughout each year. Furthermore, the IESO data also has the same repeating and cyclic load pattern. This indicates that the load data are subject to annual and seasonal changes. Additionally, the characteristics of load data are as follows. From the hourly load demand as shown in

TABLE 8 The month_wise estimation results (% MAPE) of the proposed model with other model(s) on the IESO-Canada dataset.

Name of the Month	Forecasted Results (%MAPE)		Proposed Model
	Name of the Model(s)		
	WT-NN [El-Hendawi and Wang (2020)]	*A novel WT_Ensemble* [Kondaiah and Saravanan (2022)]	
January	1.504	1.354	1.254
February	1.618	1.266	1.218
March	1.888	1.339	1.252
april	1.763	1.634	1.229
May	1.406	1.354	1.255
June	1.961	1.799	1.233
July	1.638	1.323	1.232
August	1.627	1.512	1.232
September	1.508	1.236	1.216
October	1.434	1.273	1.223
November	1.757	1.554	1.238
December	2.024	1.692	1.227
Average	1.677333	1.444667	**1.234083**

Figure 4; observation reveals that the daily, weekly, and annual patterns represent the most significant seasonal components of load demand. Furthermore, daily load characteristics exhibit a distinct seasonality pattern due to the same fluctuations in load demand as the delayed load variables for seasonal components. In terms of weekday consumption patterns, there is a lot of overlap with weekend consumption patterns. In addition, the workday has a more prominent peak demand than the weekend. And also, the public holidays are characterised by a high demand for electricity on weekends and special days. On the other hand, the everyday power consumption is equivalent to that of a special day. Due to various anthropogenic activities, such as public sector celebrations and festivities, the demand for power increases. There is a significant seasonal variation in the amount of power used. Therefore, the observation results reveal that the lagged load parameters exhibited a substantial correlation and seasonal dependence on the actual load.

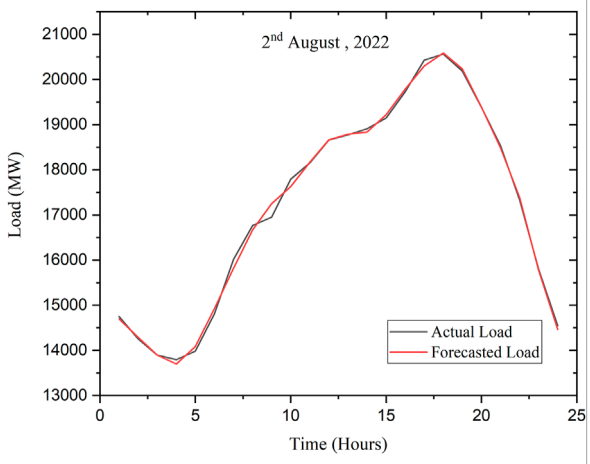

FIGURE 6
The forecasted and actual load for *2nd* August 2022.

4.1.3 Inputs selection for the model

As mentioned earlier the datasets consist of different variables. The correlation analysis was performed on the input data by using Eq. 1. As a result, there are several extremely interesting observations to be made, as seen in Figure 5.

Among the several climatic factors that affect electrical load, the temperature is the one that has the most extraordinary sensitivity. The warmer it is throughout the summer months (*June, July, and August*), the greater the electrical grid demand is expected. So, a positive relationship exists respectively between the actual load and temperature. There is a negative correlation between actual load and the relative humidity in the winter months (December, January, February) and a positive correlation in other months (*June to September*). This may be due to the fact that the heating load is reduced in winter. At the same time, the warming in summer increases load consumption for air conditioners and other electrical-related machinery for cooling purposes. There will be large increases in the power consumption utilised for heating during the chilly winter with high relative humidity; summer precipitation has a considerable negative association with the actual load; because precipitation cools the weather and reduces the need for refrigeration, this may be the reason. In the winter and summer, wind speed has an opposing influence on load; the temperature may have dropped because of the strong wind. As heating loads rise in the winter, air conditioners and fans must work harder, whereas cooling

loads fall in the summer. In all seasonal months, solar radiation and air pressure have negligible influence on load; several research studies are confident that forecasting performance may be enhanced by eliminating factors with marginal correlation with load demand Zhang and Guo (2020). Because of the low correlation between SR and AR, only the hourly-based (h)-Tem, WS, RH, and Pr were selected as inputs for load forecasting in this study. These are all listed in **Table 2**.

From the perspective of several research works, special days[4], seasonality, and normal working days have somewhat distinct load series characteristics. For example, enhancing predicting accuracy may be achieved by using separate systems for special days and normal workdays Song et al., 2005; Fidalgo and Peças Lopes, 2005[35,36]. For this consequence, dummy variables were implemented (see **Table 3**) in order to partition the data set into three distinct subgroups.

4.1.4 Performance analysis of the proposed model

4.1.4.1 Case study 1: With ISO-NE dataset

The first case study uses the ISO-NE utility dataset. This dataset from the New England utility contains previous load and weather variables at a 1-h resolution. Also, it covers data between 1st March 2003 and 31st December 2014. Furthermore, this case study is concerned with estimating the load for the year 2006. Therefore, the complete details of the input, training, and test data required for the proposed model are as follows to achieve this objective.

The 2 years earlier to 31st December 2014, are utilised as the test set and the training set. To be more explicit, there are two beginning dates that are utilised for the training sets. These starting dates are the first of March 2004 and the first of January 2010. We adjust the hyper-parameters by utilising the last ten percent of the training set that contains this beginning date since it is revealed in studies that are published in the literature. The hyper-parameters are the same for the model that was trained with 2 years of extra data.

ResNet is adopted for the proposed model, and then each residual block is constructed with a hidden layer that has 20 nodes and typically uses an activation function as SELU[5]. The block outputs have the same 24 elements size as their respective inputs. Such a way that, the proposed network consisting of sixty layers is created by stacking a total of thirty residual blocks. Five different models are trained for each implementation with 600, 650, and 700 epochs respectively.

If we look at the contrast of the proposed model with others, the day-based wavelet neural network (SIWNN) model shown in reference Chen et al. (2010) is trained using data from 2003 to 2005, whereas the models presented in references Li et al., 2016b, Li et al. (2016a), and Chen et al. (2019) utilise data from March 2003 to December 2005 for their training. The month-wise proposed model MAPE findings are shown in **Table 4**. There is no specific reporting of the MAPEs for the whole year 2006 in reference number Li et al., 2016b. As is evident from the information shown in the Table, the suggested model has the lowest MAPE throughout the year 2006. Despite this, we are able to draw the conclusion that the proposed model is capable of high generalisation across a variety of datasets since the majority of the hyper-parameters are not adjusted using the ISO-NE dataset.

Using data from 2010 to 2011, we further evaluate the proposed model generalisation capabilities. In this scenario, we used the same model developed for the year 2006 and train it using data collected between 2004 and 2009. The results of the proposed model are summarized in **Table 5** and compared with the results of the other models discussed in Yu et al., 2014, Cecati et al (2015), and Li et al (2016c), Chen et al (2019). According to the obtained results, the suggested deep-ResNet model performs better than the already available models in terms of the total MAPE for both years It is significant to note that the proposed model is implemented without even additional tuning, while all previous models were tuned using the ISO-NE dataset during the period of 2004–2009.

Furthermore, the proposed model generalization capabilities were investigated on the load estimation in weekday/end(s) and holiday(s) wise during the years 2006,2010, and 2011 respectively. For this case, we used the same model developed for estimating the load of the year 2006. The suggested model results are summarised in **Table 6** and **Tables 7**. However, the suggested model has slightly different MAPE values in the results of the year 2010. The reason may be the model was confused while at the training period due to the variance in the data. From these results, the suggested model performs better in estimation and has minimal MAPE. It is significant to note that the proposed model is implemented without even additional tuning.

4.1.4.2 Case study 2: With IESO-Canada dataset

The secondary intention of this research is to investigate the generalizability of the developed model. For this purpose, we train the prediction model with the IESO-Canada dataset by adopting the significant number of the hyper-parameters of deep-ResNet optimized for the New England utility dataset. Take into consideration that the methodology utilized here is quite similar to case Study 1. This case study's primary goal is to forecast 2006s load like the prior scenario. As a result, the training set consists of data collected before 12 November 2021, while the test set consists of data collected 2 years before that date.

In **Table 8**, we validated the performance of the proposed model with that of the models presented in El-Hendawi and

4 Saturday, Sunday, holidays.

5 Scaled exponential linear unit.

Wang (2020) and Kondaiah and Saravanan (2022). From the information shown in the table, it can conclude that the suggested model is more effective than the other prediction models. In addition to being more efficient than competing models, the presented model has less MAPE. If additional data is supplied to the training set, the model test loss may be decreased even more.

4.1.4.3 Case study 3: Testing of the proposed model using real-time data

In this context, to verify the proposed model using real-time data, we have forecasted the load for the next day from the IESO-Canada utility dataset. For this purpose, the model was trained and tested with the data taken from the same dataset as per the procedure followed in the second case study. Furthermore, a significant number of hyper-parameters were adopted by the optimized model in that same case study. As result, the forecasted and actual load for 2nd August 2022 was shown in **Figure 6**, and the (%) MAPE is only 1.19045.

5 Conclusion

A model for STLF based on a modified version of a DNN was suggested in this paper. By utilizing a statistical correlation approach, the appropriate inputs to the model were chosen. The efficacy of the proposed model was evaluated with different test scenarios on the ISO-NE and IESO-Canada utility datasets. The suggested model has been proved to be better regarding the accuracy of its forecasts based on comparisons with other models already in existence.

The MAPE (%) using the modified deep-ResNet method for ISO-NE data is 1.294, which is comparatively less to other models available in the literature. Simillarly, the MAPE (%) for IESO-Canada data is 1.234083, which is also less and the same is represented in **Table 8**. These results shows the effectiveness of the proposed model (deep-ResNet). Also, in case 3, the model was tested with real-time data, and the error MAPE is 1.19045%

There is still a considerable amount of work to be done as future work. We have considered the basis of the possibility of DNNs here, but there are probably many different architectures of these networks that could be combined with the model to improve its performance. However, it is also possible to explore further research on the technique of probabilistic load forecasting with DNN. Additionally, the model accuracy can be improved by considering a more significant number of meteorological factors.

Data availability statement

The raw data supporting the conclusions of this article will be made available by the authors, without undue reservation.

Author contributions

VK has analyzed and implemented the STLF application methodology in the smart grid environment. And also prepared the original manuscript. BS has supervised the work and reviewed/edited the manuscript. VK and BS have conceptualized, validated, and investigated.

Conflict of interest

The authors declare that the research was conducted in the absence of any commercial or financial relationships that could be construed as a potential conflict of interest.

Publisher's note

References

Ali, M., Adnan, M., Tariq, M., and Poor, H. V. (2021). Load forecasting through estimated parametrized based fuzzy inference system in smart grids. *IEEE Trans. Fuzzy Syst.* 29, 156–165. doi:10.1109/TFUZZ.2020.2986982

Amarasinghe, K., Marino, D. L., and Manic, M. (2017). Deep neural networks for energy load forecasting. *IEEE Int. Symposium Industrial Electron.* doi:10.1109/ISIE.2017.8001465

Bento, P. M., Pombo, J. A., Calado, M. R., and Mariano, S. J. (2019). Optimization of neural network with wavelet transform and improved data selection using bat algorithm for short-term load forecasting. *Neurocomputing* 358, 53–71. doi:10.1016/j.neucom.2019.05.030

Cecati, C., Kolbusz, J., Rózycki, P., Siano, P., and Wilamowski, B. M. (2015). A novel RBF training algorithm for short-term electric load forecasting and comparative studies. *IEEE Trans. Ind. Electron.* 62, 6519–6529. doi:10.1109/TIE.2015.2424399

Chen, K., Chen, K., Wang, Q., He, Z., Hu, J., and He, J. (2019). Short-term load forecasting with deep residual networks. *IEEE Trans. Smart Grid* 10, 3943–3952. doi:10.1109/TSG.2018.2844307

Chen, Y., Luh, P. B., Guan, C., Zhao, Y., Michel, L. D., Coolbeth, M. A., et al. (2010). Short-term load forecasting: Similar day-based wavelet neural networks. *IEEE Trans. Power Syst.* 25, 322–330. doi:10.1109/TPWRS.2009.2030426

Chitalia, G., Pipattanasomporn, M., Garg, V., and Rahman, S. (2020). Robust short-term electrical load forecasting framework for commercial buildings using deep recurrent neural networks. *Appl. Energy* 278, 115410. doi:10.1016/j.apenergy.2020.115410

El-Hendawi, M., and Wang, Z. (2020). An ensemble method of full wavelet packet transform and neural network for short term electrical load forecasting. *Electr. Power Syst. Res.* 182, 106265. doi:10.1016/j.epsr.2020.106265

Ferraty, F., Goia, A., Salinelli, E., and Vieu, P. (2014). "Peak-load forecasting using a functional semi-parametric approach," in *Springer proceedings in mathematics and statistics*. doi:10.1007/978-1-4939-0569-0_11

Fidalgo, J. N., and Peças Lopes, J. A. (2005). Load forecasting performance enhancement when facing anomalous events. *IEEE Trans. Power Syst.* 20, 408–415. doi:10.1109/TPWRS.2004.840439

Hernández, L., Baladrón, C., Aguiar, J. M., Carro, B., Sánchez-Esguevillas, A., and Lloret, J. (2014). Artificial neural networks for short-term load forecasting in microgrids environment. *Energy* 75, 252–264. doi:10.1016/j.energy.2014.07.065

Hippert, H. S., Pedreira, C. E., and Souza, R. C. (2001). Neural networks for short-term load forecasting: A review and evaluation. *IEEE Trans. Power Syst.* 16, 44–55. doi:10.1109/59.910780

Jiao, R., Zhang, T., Jiang, Y., and He, H. (2018). Short-term non-residential load forecasting based on multiple sequences LSTM recurrent neural network. *IEEE Access* 6, 59438–59448. doi:10.1109/ACCESS.2018.2873712

Kaiming, H., Xiangyu, Z., Shaoqing, R., and Jian, S. (2015). Deep residual learning for image recognition. *Proc. IEEE Comput. Soc. Conf. Comput. Vis. Pattern Recognit.*

Kim, W., Han, Y., Kim, K. J., and Song, K. W. (2020). Electricity load forecasting using advanced feature selection and optimal deep learning model for the variable refrigerant flow systems. *Energy Rep.* 6, 2604–2618. doi:10.1016/j.egyr.2020.09.019

Kondaiah, V. Y., Saravanan, B., Sanjeevikumar, P., and Khan, B. (2022). A review on short-term load forecasting models for micro-grid application. *J. Eng.* 202, 665–689. doi:10.1049/tje2.12151

Kondaiah, V. Y., and Saravanan, B. (2022). Short-term load forecasting with a novel wavelet-based ensemble method. *Energies* 15, 5299. doi:10.3390/en15145299

Kondaiah, V. Y., and Saravanan, B. (2021). "Short-term load forecasting with deep learning," in *3rd IEEE international virtual conference on innovations in power and advanced computing technologies*. i-PACT 2021. doi:10.1109/i-PACT52855.2021.9696634

Kong, W., Dong, Z. Y., Jia, Y., Hill, D. J., Xu, Y., and Zhang, Y. (2019). Short-term residential load forecasting based on LSTM recurrent neural network. *IEEE Trans. Smart Grid* 10, 841–851. doi:10.1109/TSG.2017.2753802

Kuster, C., Rezgui, Y., and Mourshed, M. (2017). Electrical load forecasting models: A critical systematic review. *Sustainable Cities and Society*. 35. 257-270. doi:10.1016/j.scs.2017.08.009

Kwon, B. S., Park, R. J., and Song, K. B. (2020). Analysis of the effect of weather factors for short-term load forecasting. *Transactions of the Korean Institute of Electrical Engineers*. 69. Seoul, Korea. 985-992. doi:10.5370/KIEE.2020.69.7.985

Li, C., Liang, G., Zhao, H., and Chen, G. (2021a). A demand-side load event detection algorithm based on wide-deep neural networks and randomized sparse backpropagation. *Front. Energy Res.* 9. doi:10.3389/fenrg.2021.720831

Li, J., Sun, A., Han, J., and Li, C. (2022). A survey on deep learning for named entity recognition. *IEEE Trans. Knowl. Data Eng.* 34, 50–70. doi:10.1109/TKDE.2020.2981314

Li, S., Goel, L., and Wang, P. (2016a). An ensemble approach for short-term load forecasting by extreme learning machine. *Appl. Energy* 170, 22–29. doi:10.1016/j.apenergy.2016.02.114

Li, S., Wang, P., and Goel, L. (2016b). A novel wavelet-based ensemble method for short-term load forecasting with hybrid neural networks and feature selection. *IEEE Trans. Power Syst.* 31, 1788–1798. doi:10.1109/TPWRS.2015.2438322

Li, Z., Li, Y., Liu, Y., Wang, P., Lu, R., and Gooi, H. B. (2021b). Deep learning based densely connected network for load forecasting. *IEEE Trans. Power Syst.* 36, 2829–2840. doi:10.1109/TPWRS.2020.3048359

Liu, D., Zeng, L., Li, C., Ma, K., Chen, Y., and Cao, Y. (2018). A distributed short-term load forecasting method based on local weather information. *IEEE Syst. J.* 12, 208–215. doi:10.1109/JSYST.2016.2594208

Liu, Z., Li, W., and Sun, W. (2013). A novel method of short-term load forecasting based on multiwavelet transform and multiple neural networks. *Neural computing and applications*. 22. 271–277. doi:10.1007/s00521-011-0715-2

Ma, S. (2021). A hybrid deep meta-ensemble networks with application in electric utility industry load forecasting. *Inf. Sci.* 544, 183–196. doi:10.1016/j.ins.2020.07.054

Memarzadeh, G., and Keynia, F. (2021). Short-term electricity load and price forecasting by a new optimal LSTM-NN based prediction algorithm. *Electr. Power Syst. Res.* 192, 106995. doi:10.1016/j.epsr.2020.106995

Rafi, S. H., Al-Masood, N., Deeba, S. R., and Hossain, E. (2021). A short-term load forecasting method using integrated CNN and LSTM network. *IEEE Access* 9, 32436–32448. doi:10.1109/ACCESS.2021.3060654

Salinas, D., Flunkert, V., Gasthaus, J., and Januschowski, T. (2020). DeepAR: Probabilistic forecasting with autoregressive recurrent networks. *Int. J. Forecast.* 36, 1181–1191. doi:10.1016/j.ijforecast.2019.07.001

Sheng, Z., Wang, H., Chen, G., Zhou, B., and Sun, J. (2021). Convolutional residual network to short-term load forecasting. *Appl. Intell. (Dordr).* 51, 2485–2499. doi:10.1007/s10489-020-01932-9

Shi, H., Xu, M., and Li, R. (2018). Deep learning for household load forecasting-A novel pooling deep RNN. *IEEE Trans. Smart Grid* 9, 5271–5280. doi:10.1109/TSG.2017.2686012

Song, K.-b., Baek, Y.-s., Hong, D. H., and Jang, G. (2005). Short-term load forecasting for the holidays using. *IEEE Trans. Power Syst.*

Subbiah, S. S., and Chinnappan, J. (2020). An improved short term load forecasting with ranker based feature selection technique. *J. Intelligent Fuzzy Syst.* 39, 6783–6800. doi:10.3233/JIFS-191568

Taylor, J. W. (2010). Triple seasonal methods for short-term electricity demand forecasting. *Eur. J. Operational Res.* 204, 139–152. doi:10.1016/j.ejor.2009.10.003

Velasco, L. C. P., Polestico, D. L. L., Abella, D. M. M., Alegata, G. T., and Luna, G. C. (2018). Day-ahead load forecasting using support vector regression machines. *Int. J. Adv. Comput. Sci. Appl.* 9. doi:10.14569/IJACSA.2018.090305

Wang, Y., Gan, D., Sun, M., Zhang, N., Lu, Z., and Kang, C. (2019). Probabilistic individual load forecasting using pinball loss guided LSTM. *Appl. Energy* 235, 10–20. doi:10.1016/j.apenergy.2018.10.078

Xu, Q., Yang, X., and Huang, X. (2020). Ensemble residual networks for short-term load forecasting. *IEEE Access* 8, 64750–64759. doi:10.1109/ACCESS.2020.2984722

Yu, H., Reiner, P. D., Xie, T., Bartczak, T., and Wilamowski, B. M. (2014). An incremental design of radial basis function networks. *IEEE Trans. Neural Netw. Learn. Syst.* 25, 1793–1803. doi:10.1109/TNNLS.2013.2295813

Zhang, G., and Guo, J. (2020). A novel method for hourly electricity demand forecasting. *IEEE Trans. Power Syst.* 35, 1351–1363. doi:10.1109/TPWRS.2019.2941277

Zhang, K., Sun, M., Han, T. X., Yuan, X., Guo, L., and Liu, T. (2018). Residual networks of residual networks: Multilevel residual networks. *IEEE Trans. Circuits Syst. Video Technol.* 28, 1303–1314. doi:10.1109/TCSVT.2017.2654543

Zhang, Y., Tian, Y., Kong, Y., Zhong, B., and Fu, Y. (2021). Residual dense network for image restoration. *IEEE transactions on pattern analysis and machine intelligence*. 43. 2480-2495. doi:10.1109/TPAMI.2020.2968521

Nomenclature

ANN Artificial Neural Network

CNN Convolutional Neural Network

deep – ResNet Deep Residual Network

DNN Deep Neural Network

ELM Extreme Learning Machine

IESO – Canada Independent Electricity System Operator-Canada

ISO – NE Independent System Operator-New England

LSTM Long Short-Term Memory

MAE Mean Absolute Error

MAPE Mean Absolute Percentage Error

NLP Natural Language Processing

RBF Radial Basis Function

RBM Restricted Boltzmann Machine

ResNet Residual Network

RMSE Root Mean Square Error

STLF Root Mean Square Error

SVR Support Vector Regression

frontiers | Frontiers in Energy Research

TYPE Original Research
PUBLISHED 10 November 2022
DOI 10.3389/fenrg.2022.1038533

OPEN ACCESS

EDITED BY
Sarat Kumar Sahoo,
Parala Maharaja Engineering College (P. M. E. C), India

REVIEWED BY
Indragandhi Vairavasundaram,
VIT University, India
Deep Kiran,
Indian Institute of Technology Roorkee, India
Balamurugan M.,
Dayananda Sagar College of Engineering, India
Ashish Paramane,
National Institute of Technology, Silchar, India

*CORRESPONDENCE
Sathishkumar K.,
kansathh21@yahoo.co.in

†These authors have contributed equally to this work

SPECIALTY SECTION
This article was submitted to Smart Grids, a section of the journal Frontiers in Energy Research

RECEIVED 07 September 2022
ACCEPTED 26 September 2022
PUBLISHED 10 November 2022

CITATION
A. P and K. S (2022), Optimized RNN-oriented power quality enhancement and THD reduction for micro grid integration of PV system with MLI: Crow Search-based Harris Hawks Optimization concept.
Front. Energy Res. 10:1038533.
doi: 10.3389/fenrg.2022.1038533

Optimized RNN-oriented power quality enhancement and THD reduction for micro grid integration of PV system with MLI: Crow Search-based Harris Hawks Optimization concept

Praveena A.† and Sathishkumar K.*†

School of Electrical Engineering, Vellore Institute of Technology, Vellore, Tamil Nadu, India

Grid-connected Photo Voltaic (PV) power systems are becoming increasingly popular in several nations. The goal of achieving maximum power and acceptable power quality in a grid-connected PV power system is considered a major difficulty. Hence, this paper develops an artificial intelligence-based optimization concept for PV system and novel cascaded Multi Level Inverter (MLI) for the grid integration of PV system. The cascaded MLI was designed with fewer power electronic switches and can function at asynchronous voltage sources, making it the most suitable for PV systems. This novel inverter minimizes the THD at the output with the help of enhancing the output voltage level. It also improves the power quality of the system. The micro grid integration of the introduced inverter is controlled by Optimized Recurrent Neural Network (ORNN), where the hidden neurons are tuned by novel hybrid meta heuristic algorithm by merging Crow Search Algorithm (CSA) and Harris Hawks Optimization (HHO) leading to Crow Search-based Harris Hawks Optimization (CS-HHO). The proposed model is designed at several loading conditions and weather conditions. The simulation findings proved the efficiency of the developed system.

KEYWORDS

multi level inverter, power quality enhancement, total harmonic distortion reduction, micro grid integration, Optimized Recurrent Neural Network and Crow Search-based Harris Hawks Optimization, photo voltaic system

1 Introduction

PV systems have evolved as a viable substitute for traditional power production systems owing to their ease of upkeep, eco-friendliness, low noise, and widespread availability (Liu et al., 2008). The arduous work involved with solar power generation is collecting maximum power and reversing the PV system's output electricity into useable ac to feed the grid. MPP of the PV system must be tracked continually using a MPPT

controller for extracting maximum solar power (Pai and Chao, 2010). In recent years, small solar power producing units installed on building rooftops have become popular, and they may also serve as an alternate major source of energy for home needs during a power outage. To supply the electric grid, the PV array's DC power must be reversed into AC power (Killi and Samanta, 2015). A dc-dc power converter as well as a MLI is usually included in the CC. To eliminate voltage mismatch among the DC voltage bus and PV source, a dc-dc converter is used, which boosts the low-level PV voltage to the DC bus voltage level (Abdelsalam et al., 2011). Inverters are then used to transform the increased DC solar power into AC electricity. PV array as well as power CC efficiency should be high to minimize power waste. Several researchers have built MLI having higher voltage levels, greater conversion ratio, lower harmonic content, and a minimal interface to electromagnetic interface over the last few years (Bhukya and Kota, 2018). Conventional MLI architectures, like flying capacitor and diode-clamped topologies, use CCs to create multiple voltage levels. The main disadvantage of these two arrangements is that the voltage between the capacitors cannot be regulated (Graditi et al., 2014). Furthermore, as the voltage level is enhanced, conversion effectiveness falls. CHB converters are well suited to producing many voltage levels using asymmetric voltage technology, although they need additional switching devices (Adinolfi et al., 2015).

Another development in the solitary MLI family is the development of asymmetrical sources on the basis of MLI, which is gaining popularity (Motahhir et al., 2018). This is because, when asymmetrical inputs are used in MLI topologies, they yield a much greater count as symmetrical-oriented MLI (Eltawil and Zhao, 2013). THD is reduced in waveforms having a larger count of levels. It is not necessary after a specific count of levels because the THD is low enough to meet the IEEE 5l9 standard. The binary as well as trinary configurations (Macaulay and Zhou, 2018) are two typical asymmetrical source selection approaches. Non-universal sources selection schemes are also implemented in some topologies. Because many contemporary MLI are modular, making them easily expandable, implementing asymmetrical sources is significantly more beneficial (Yang and Wen, 2018).

The modulation method is another important feature of an inverter, and it is directly connected to THD and effectiveness (Dileep and Singh, 2017). Implementing conventional PWM at a greater level might be difficult because a larger count of carriers is required. This raises the PWM's intricacy and necessitates more computing power. Low switching frequency approaches, in which the needed switching angles are predicted previously, can be, employed rather (Wang et al., 2017). They want to produce a waveform that nearly mimics a pure sinusoid by obtaining the most precise switching angles. Low switching frequency modulation also aids in lowering total switching loss (Haddadi et al., 2019). Nevertheless, because of the large low order harmonic content, it may enhance THD. As a result, functioning will mitigate the aforementioned issue (Moradi-Shahrbabak et al., 2014). The aforesaid constraints of the present method suggest that a new PV inverter architecture may be developed. The paper contributions are.

- To develop an artificial intelligence-based optimization concept for PV system and novel cascaded MLI for the grid integration of PV system.
- To minimize the THD at the output with the help of enhancing the output voltage level and also improving the power quality of the system.
- To control the micro grid integration of the introduced inverter by ORNN, where the hidden neurons are tuned with the consideration of THD minimization.
- To develop a novel form of optimization algorithm referred as CS-HHO for fulfilling the THD minimization objective and to prove the efficiency of the developed system by comparing it with various existing methods in terms of several analysis.

The paper organization is. **Section 1** is the introduction of PV system with MLI. **Section 2** is literature survey. **Section 3** is PV system. **Section 4** is MLI. **Section 5** is ORNN and proposed CS-HHO. **Section 6** is results. **Section 7** is conclusion. The description of symbols and abbreviations are listed in Nomenclature.

2 Literature survey

2.1 Related works

Sonti et al. (2020) have introduced a novel three-phase three-level CMLI on the basis of NPC DC decoupling approach. As a result, a common zero state is detected in the entire three phases, and the level of the common mode or terminal voltage is held constant at its prior active state level utilizing clamping circuitry. The simulation as well as experimental data reported in this short also corroborates the provided analysis. This brief provides comprehensive information on the planned CMLI's functioning, modeling, and experimental findings.

Bhukya et al. (2019) have proposed a new PV inverter topology that includes a novel MPPT strategy on the basis of shading pattern identification with an ANN, a SIMO converter, and a MLI. Under partially shadowed conditions, the suggested MPPT system's performance is benchmarked. The PV voltage is supplied into the SIMO converter, which generates four separate voltages having varying magnitudes. The MLI reduces harmonic distortion by converting the SIMO converter's dc output voltage to ac to feed the utility. This MLI has eight switching devices and

delivers 31. The suggested MPPT method harvests maximum power, which is a key component of the introduced topology. To validate the effectiveness of the suggested PV inverter architecture, an operational prototype is modeled and produced. The FPGA Spartan training kit was employed to programmed the pulses necessary for the suggested topology's converter and MLI.

Hamidi et al. (2021) for use in a 31-level asymmetrical switch-diode-oriented MLDCL inverter, a POVR and a CC circuit have been developed. This method is used to manage the voltage as well as supply the maximum power at load condition. The solo system provides 97.21 percent of the theoretical maximum power under full load. In particular, when delivering power to inductive loads, CC is used to reduce voltage spikes at the output. It effectively removes spikes while also lowering THD of output voltage and current as specified by IEEE 519.

Nazer et al. (2021) have presented the TFL scale to assess alternative inverter topologies in terms of energy losses and reliability. The TFL index takes into account the repair costs, initial cost, financial losses owing to element and downtime losses, as well as environmental factors. When the TFL is reduced, the best inverter structure and switching frequency are found utilizing this universal index. The actual failure rates of susceptible parts like switches, capacitors, diodes, and the cooling system are determined, given that the dependability of power electronic equipment is greatly influenced by power losses and ambient circumstances. The Markov approach is used to assess the system reliability and the frequency of experiencing failure situations. Therefore, among the regularly employed two-level as well as three-level topologies, the best solar inverter for the 150 kW power range is chosen.

Hamidi et al. (2020) for PV renewable energy systems, a novel theoretical foundation of asymmetrical MLI having optimal amount of parts has been developed. In comparison to prior configurations, the goal is to minimize the amount of components necessary to generate a large count of output levels. This approach is utilized rather than the traditional PWM methodology. With respect to the amount of elements, the suggested inverter is a better alternative than traditional MLI topologies. It also maintains a reasonable balance among the overall blocking voltage and the count of components. As a result, its installation will take up less room and cost less money. The suggested topology also has the advantage of producing AC output having reduced THD and great effectiveness. The suggested process was confirmed by experimental investigation.

Mahendiran (2020) has developed hybrid control architecture for grid-connected hybrid systems using CMLI. CHA and XGBOOST are combined in the suggested control topology. The goal of the CMLI simulation was to obtain the best control signal. The suggested CMLI was made up of a smaller count of switches, diodes, and sources. The suggested control approach aims to fulfill load power demand while also maintaining power regulation or maximization of energy conversion in solar and wind subsystems. The suggested approach strongly precludes the presence of a difference at the CMLI output voltage. In this case, CHA was used to determine the ideal gain parameters in light of a wide range of source currents compared to the normal value, and it may also be used to generate an optimal control signal dataset offline. The XGBOOST analyzes and forecasts the most optimum control signals of the CMLI in an online manner based on the completed dataset. The IGBT of CMLI were controlled using the resulting control signals. Here, the developed model was adopted in the MATLAB/Simulink working phase, with prior methodologies taken into account. The effectiveness of different sources was also examined utilizing suggested and current methods. The suggested technology's PV and wind effectiveness is 99.3975 percent and 91.2138 percent, respectively. Generally, the results of the comparison suggest that the developed strategy was superior and that it has the ability to address the problem.

Katir et al. (2020) have looked at the modeling framework made up of boost converters, solar arrays, N-CHBMI, DC bus capacitors, and an L-filter. This research aimed to achieve three control goals. The attainment of these goals was made possible by a multi-loop architecture regulator. Furthermore, every panel was separately managed to extract maximum power, while two cascaded loops strive to ensure DC-link voltage management and adequate power factor correction. The suggested regulator was created by combining a nonlinear back stepping technique with certain Lyapunov stability tools. The simulated results achieves its goals and has intriguing tracking and control performance.

Fernão Pires et al. (2018) a multilevel three-phase VSI has been suggested. Conventional multilevel PWM techniques could be used to control the T3VSI. A control scheme was also described, as well as a PDPWM suited for the multilevel T3VSI, to assure the transmission of energy produced by PV generators to the grid. Simulation as well as experimental findings would be used to demonstrate the grid-connected PV multilevel T3VSI's performance. Numerous experimental findings corroborate the multilayer T3VSI PV system's predicted properties.

Janardhan et al. (2020) a revolutionary micro MLI-based hold solar PV system has been proposed. A micro MLI was a miniature inverter with a multilayer construction. On the MATLAB platform, a solar PV system having a micro MLI is formed and recreated; the impact has been probed, as well as the main impact on the load. A five-level MLI was installed underneath each of the two solar panels and a level shifting sinusoidal PWM technology was used to regulate micro MLI switching. The findings were achieved at different modulation indexes, and an over modulation was selected to decrease the switching losses and lower order harmonic content. The overall harmonic distortion attained was extremely low, and a laboratory model was being created to verify the simulated results. The experimental and simulation findings were nearly identical.

Chandrasekaran et al. (2021) the speed of response as well as harmonics have been studied, and the general efficiency of the model has been improved. A FLC regulates the speed of the motor. The PI controller's output was compared to the FLC's. The present system was tested using an experimental setup, and the new system was tested using MATLAB and Simulink, with the findings being documented.

3 Photovoltaic system for the power quality enhancement and THD reduction

3.1 Mathematical description of PV system

It is impossible to get consistent irradiance throughout the system owing to barriers like as building shadows, passing clouds, dust deposits on panels, and bird faeces. As a result, the effective irradiance (H_F) of every PV module differs, and it may be expressed as,

$$H_F = (1 - T)\,H \tag{1}$$

H shows the irradiance on un-shaded portions, and T shows the panel's shading ratio. The shading ratio defines the proportion of darkened area of a module to its entire area. The PV module's output current is specified as,

$$J = J_{Pi} - J_E\left[\exp\frac{\left(r\left(W_{PV} + J_{PV}S_T\right)\right)}{\left(O_T B C_L U\right)} - 1\right] - \frac{\left(W_{PV} + J_{PV}S_T O_T\right)}{\left(O_T\right)S_{Ti}} \tag{2}$$

Here, J_{Pi} shows the photogenerated current (A), J_E shows the diode saturation current (A), W_{PV} shows the panel voltage (V), J_{PV}shows the panel current (A), S_T shows the series resistance (Ω), O_T shows the count of PV cells joined in series, B shows the diode ideality factor, C_L shows the Boltzmann constant, U shows the temperature on the panel (°C), and S_{Ti} shows the parallel resistance (Ω).

Specifically, photo-generated current having shaded as well as un-shaded cells may be represented as,

$$J_{Pi(H_1)} = \left(J_{SD,Reg} + L_{ISD}\left(U - U_{Reg}\right)\right)\frac{H_1}{H_{Reg}} \tag{3}$$

$$J_{Pi(H_2)} = \left(J_{SD,Reg} + L_{ISD}\left(U - U_{Reg}\right)\right)\frac{H_2}{H_{Reg}} \tag{4}$$

$$J_{Pi(H_3)} = \left(J_{SD,Reg} + L_{ISD}\left(U - U_{Reg}\right)\right)\frac{H_3}{H_{Reg}} \tag{5}$$

$$J_{Pi(H_4)} = \left(J_{SD,Reg} + L_{ISD}\left(U - U_{Reg}\right)\right)\frac{H_4}{H_{Reg}} \tag{6}$$

$J_{Pi(H1)}$, $J_{Pi(H2)}$, $J_{Pi(H3)}$, and $J_{Pi(H4)}$ are photo produced currents in relation to the irradiance on the panel surface (A), L_{ISD} stands for current coefficient, $J_{(SD,Reg)}$ stands for short circuit current at STC (A), U_{Reg} stands for temperature at STC (°C), H_{Reg} stands for irradiance at STC (W/m2), H_1, H_2, H_3, and H_4 stands for individual panel irradiance (W/m2).

PV system output current as well as voltage for a 2S2P setup beneath PSC are represented as,

$$J_{PV} = Min\left(J_1, J_2, J_3, J_4\right) \tag{7}$$

$$W_{PV} = W_1, W_2, W_3, W_4 \tag{8}$$

J_1, J_2, J_3, and J_4 represents panel currents computed by inserting $J_{Pi(H1)}$, $J_{Pi(H2)}$, $J_{Pi(H3)}$, and $J_{Pi(H4)}$ in **Eqs 3–6**. The output current as well as voltage beneath PSC may be represented as if the PV system contains "o" count of modules linked in series. If $J_{PV} > J_{Pi(o-1)}$, then

$$J_{PV} = J_{Pi}\left(H_0\right) - J_E\left[\exp\left(\frac{rW_{PV} + J_{PV}ST}{O_T B C_L U}\right) - 1\right] - \frac{W_o + J_{PV}S_T O_T}{O_T S_{Si}} \tag{9}$$

$$W_{PV} = W_o \tag{10}$$

If $J_{Pi(o-2)} < J_{PV} < J_{Pi(o-1)}$, then

$$J_{PV} = J_{Pi}\left(H_{(0-1)}\right) - J_E\left[\exp\left(\frac{rW_{(0-1)} + J_{PV}ST}{O_T B C_L U}\right) - 1\right] - \frac{W_{(o-1)} + J_{PV}S_T O_T}{O_T S_{Si}} \tag{11}$$

$$W_{PV} = W_o - W_{(o-1)} \tag{12}$$

Consequently, if $J_{PV} < J_{Pi1}$

$$J_{PV} = J_{Pi}\left(H_{(1)}\right) - J_E\left[\exp\left(\frac{rW_1 + J_{PV}ST}{O_T B C_L U}\right) - 1\right] - \frac{W_1 + J_{PV}S_T O_T}{O_T S_{Si}} \tag{13}$$

$$W_{PV} = W_1 + W_2 + \cdots + W_o \tag{14}$$

The total power (Q_U) of a PV system is reduced when it is partially shaded.

$$Q_U = Q_1 H_{F_1} + Q_2 H_{F_2} + \cdots + Q_o H_{F_o} \tag{15}$$

The efficient irradiances of the PV modules are $F_1, F_2, \ldots, F_o$. The PV system with MLI is shown in **Figure 1**.

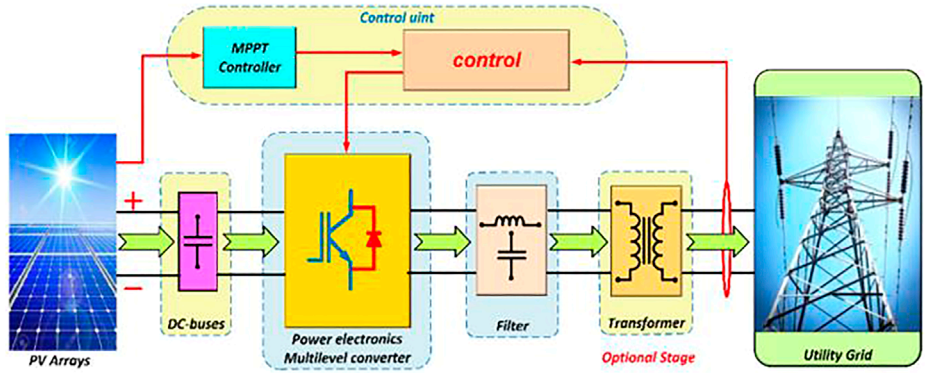

FIGURE 1
Pv system with MLI.

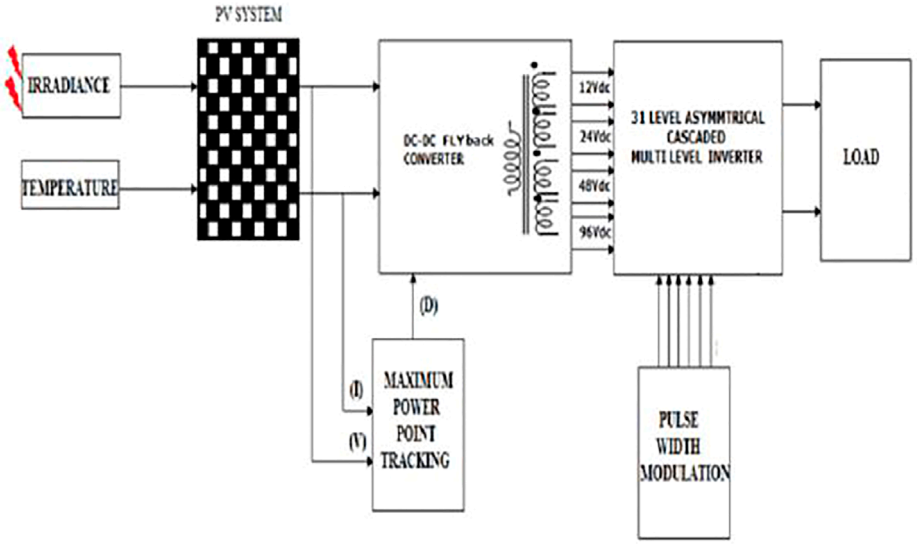

FIGURE 2
31-level proposed CMLI for the PV system.

3.2 MPPT objective (PV voltage regulator design)

The characteristics of PV modules are affected by variations in temperature, insolation, and load. As a result, using the MPPT is required to keep the operating voltage in around MPP and to achieve the necessary output voltage having the smallest amount of solar panels feasible (Bhandari et al., 2014). The familiar PO "Perturb and Observe algorithm" approach is utilized to attain the following aims because it is easier and requires minimal measurable parameters. The PV voltage as well as current represents the PO block's input signals, which result to a PV reference voltage in the output. The boost regulator uses the latter as a references Aourir et al. (2020) and Abouloifa et al. (2018).

The PV arrays are being used to supply DC voltages to the technology being examined. The current control method's goal is to achieve a DC voltage across every solar array's output that is near to its MPPs, so that the settings of every DC/DC boost converter may be controlled to enhance the PV level voltage that will be utilized subsequently by the CHBMI. The back stepping method describes a regulation approach that allows this goal to be achieved. The back stepping technique is accomplished in two phases to attain the control laws because the subsystems beneath examination contain a comparative degree of two. The recommended topology's averaged paradigm may be represented as below:

$$D_d y_{1,l} = J_{p,vl} - y_{2,l} \tag{16}$$

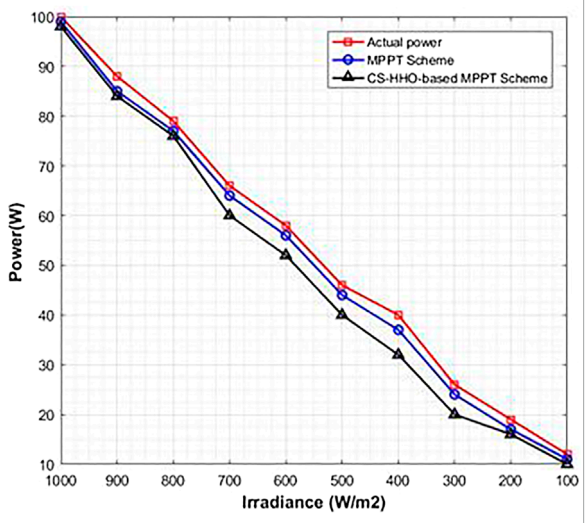

FIGURE 3
PV power analysis.

$$M_d y_{2,l} = s_{d,l} y_{2,l} + y_{1,l} - (1 - v_{1,l}) y_{3,l} \tag{17}$$

Here, $y_{(1,l)}$ and $y_{(2,l)}$ signify the voltage throughout the PV arrays as well as the boost converters' input current, correspondingly; and $y_{(3,l)}$ signifies the DC-link voltages. The current of the PV arrays is shown by $j_{(pv,l)}$ respectively.

3.2.1 Step 1

Sub-system stabilization **Eq. 17**

$$f_{1,l} = D_d \left(y_{1,l} - \overset{*}{\hat{y}}_{1,l} \right) \tag{18}$$

Time-derivation provides the below tracking error dynamics utilizing **Eq. 16** and **Eq. 18**:

$$f_{1,l} = J_{pv,l} - y_{1,l} D_d \overset{\prime}{\hat{y}}_{1,l} \tag{19}$$

We choose the below candidate Lyapunov function, keeping in mind that the Lyapunov function must be positive and its counterpart must be negative:

$$W_{1,l} = 0.5 f_{1,l}^2 \tag{20}$$

Its temporal derivative, in fact, corresponds to:

$$W_{1,l} = f_{1,l} f_{1,l} = -d f_{1,l}^2 < 0 \tag{21}$$

Here, d_1 shows a design parameter that is positive.

The lth stabilising function linked with the subsystems (9a) is produced as below: Given y_2,l as the lth virtual control input signal and the Lyapunov function **Eq. 20** and its dynamic **Eq. 21**:

$$y_{2,l}^{*} = d_1 f_{1,l} + j_{pv,l} - D_d \overset{*}{\hat{y}}_{1,l} \tag{22}$$

Because $y\_(2,l)$ is not the real control rule, the second tracking error is proceeded as follows:

$$f_{2,l}^{*} = M_d \left(y_{2,l} - \overset{*}{\hat{y}}_{2,l} \right) \tag{23}$$

Utilizing **Eqs 22**, **23** and **Eq. 21fd21** is changed to:

$$f_{1,l} = -d_1 f_{1,l}^2 - \frac{f_{2,l}}{M_d} \tag{24}$$

As a result, the Lyapunov function's time-derivation updates to:

$$W_{1,l} = -d f_{1,l}^2 - \frac{f_{1,l} f_{2,l}}{M_d} \tag{25}$$

3.2.2 Step 2

Sub-system stabilization **Eq. (18)**: The error variables f_1 and $f_2$must fade away in order to attain the control laws, which attempt to regulate the voltages across the PV modules and increase the input voltages. Time-derivation of the second tracking error using equations **Eqs 18**, **19** yields:

$$f_{2,l}' = -s_{d,l} y_{d,l} + y_{1,l} - (1 - v_{d,l}) y_{3,l} - M_d \overset{*}{\hat{y}}_{2,l} \tag{26}$$

Assume the enhanced Lyapunov function with the below parameters:

$$W_{2,l} = 0.5 f_{d,l}^2 + W_{1,l} \tag{27}$$

Eqs 26, **25** yield the following:

$$W_{1,l} = -d_1 f_{1,l}^2 + f_{2,l} f_{2,l}' - \frac{f_{1,l} f_{2,l}}{M_d} \tag{28}$$

The goal is to make $W_{2,l}$ negative by selecting the following option:

$$f_{2,l}' - \frac{f_{1,l}}{M_d} = -d_2 f_{2,l} < 0 \tag{29}$$

It is worth noting that d_2 shows a positive regulator. The control rules provided by the equation are obtained by combining equations **Eqs 26**, **29**.

$$v_{d,l} = 1 + \frac{1}{y_{3,l}} \left[s_{d,l} y_{2,l} - d_2 f_{2,l} - y_{1,l} + M_d \overset{\prime}{\hat{y}}_{1,l} + \frac{f_{1,l}}{M_d} \right] \tag{30}$$

The creation of O appropriate gate signals for the control of the O boost DC-DC converters is accomplished by utilizing the control principles given in **Eq. 24** to PWM generators.

3.2.3 Proposition

The dynamic behaviour linked with the lth closed loop system in the $f_{1,l}$, $f_{2,l}$ coordinates may be stated as follows, using the control rules **Eq. 31** and the averaged computational formalism provided by equations **Eqs 16**, **17**.

$$\begin{pmatrix} f_{1,l}' \\ f_{2,l}' \end{pmatrix} = \begin{pmatrix} -d_1 & -1/M_d \\ 1/M_d & -d_2 \end{pmatrix} \begin{pmatrix} f_{1,l} \\ f_{2,l} \end{pmatrix} \tag{31}$$

Consequently, the error variables $f_{1,l}$ and $f_{2,l}$ monotonically dissipate.

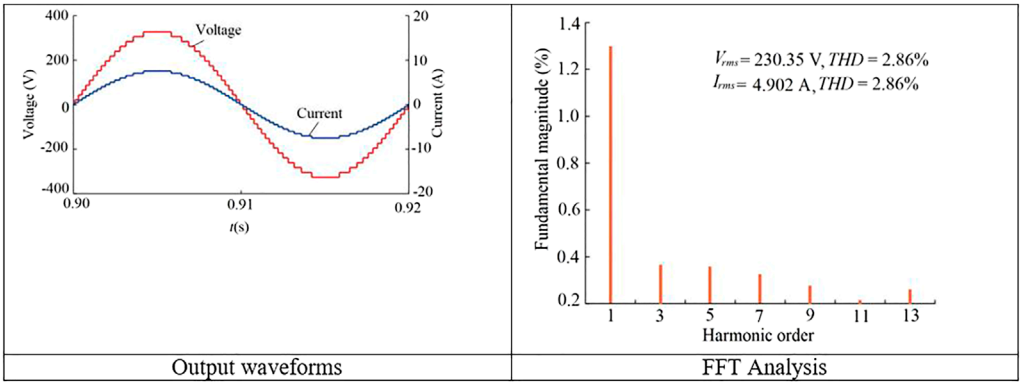

FIGURE 4
Operation beneath full load operation.

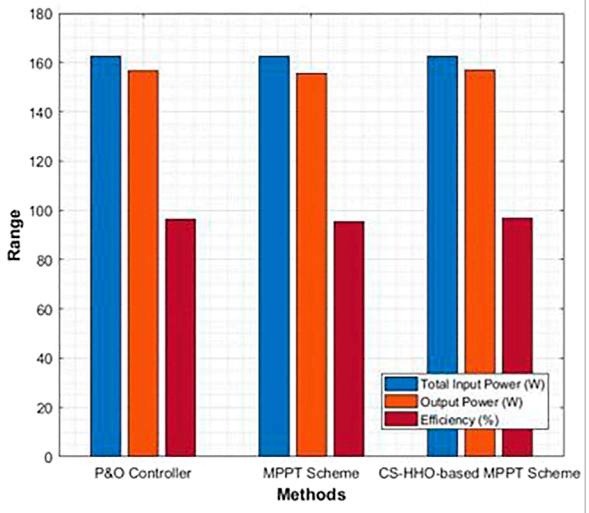

FIGURE 5
Efficiency analysis.

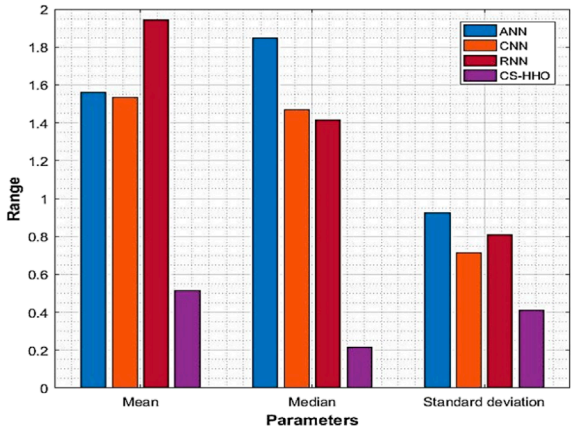

FIGURE 6
Statistical analysis.

4 Multi-level inverter for the power quality enhancement and THD reduction

4.1 Inverter topology with configuration

There are four steps to the recommended PV system's total setup. PV arrays are the initial stage, accompanied by boost DC-DC converters, DC-AC inverters, and finally load. *Via* voltage feedback control, the boost converters must deliver the necessary voltage level to the inverter. In this study, the suggested MLI was employed as a DC-AC inverter. The inverter's output could then be utilized to power isolated AC loads. The suggested 31-Level inverter architecture with asymmetrical sources was explained. The boost converter outputs were used as DC sources in this study. Two unidirectional switches $T_{M/S,1}$ and $T_{M/S,3}$ one bidirectional switch $T_{M/S,2}$, and two voltage sources $W_{M/S,2}$ and $W_{M/S,2}$ make up every basic unit. Six unidirectional switches were included in the H-Bridge component ($T_{D,1}, T_{D,2}, T_{D,3}, T_{D,4}, T_{D,5}$, and $T_{D,6}$).

The topology is able to construct 31 output levels by employing asymmetrical DC sources whose values are picked on the basis of geometric progression having a factor of two. Based on the switching states, the levels were obtained by adding the DC sources in sequence. The topology may operate in either a binary or a trinary series of DC sources, however the former could create the most output levels. Symmetrical sources can also be configured at the expense of a smaller count of output levels. The DC sources must be chosen in the ratio $W_{M,1}:W_{M,2}:W_{S,1}:W_{S,2} = W_{DC}:2W_{DC}:4W_{DC}:8W_{DC}$ to

10.3389/fenrg.2022.1038533

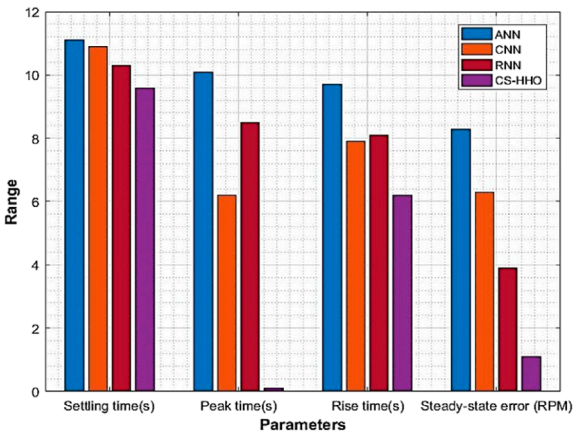

FIGURE 7
Time domain parameter analysis.

perform the binary sequence. The suggested topology is not limited to merely producing 31 levels. The setup can be cascaded into as various stages as needed to create a greater degree of output. The following formulas can be used to calculate the count of switching devices (O_{SX}), gate drivers (O_H), DC sources (O_{DC}), output levels (O_{OM}), and maximum magnitude of output voltage (w_{max}):

$$O_{SX} = 7k \tag{32}$$

$$O_H = 6k \tag{33}$$

$$O_{DC} = 2k \tag{34}$$

$$O_M = 0.5\left(4^{k+1} - 2\right) \tag{35}$$

$$W_{max} = \sum_{o=1}^{\infty} \left[W_{LO,1} + W_{LO,2} + W_{RO,1} + W_{RO,2}\right] \tag{36}$$

Here, o shows the count of cascaded stages and k shows the count of basic units. Only even numbers of fundamental units are taken into account. Nevertheless, by deleting any one among the units as well as $T_{D,5}$ and $T_{D,6}$, it is still feasible to provide an odd count of fundamental units. The 31-level introduced CMLI for the PV system is shown in **Figure 2**.

4.2 THD

The signal is warped and displays in many shapes, like square, triangular, and saw-tooth waves, underneath this circumstance (Alhafadhi, 2016). Due to the obvious existence of odd as well as even harmonics, the waveform is non sinusoidal, with the former being more harmful than the latter. THD is represented as:

$$THD\% = 100^{*}\sqrt{\frac{Q_2 + Q_2 + Q_3 + \cdots + Q_o}{Q_1}} \tag{37}$$

$Q_o$is the number of watts. THD is computed as below if the measurement data is in volts:

$$THD\% = 100^{*}\sqrt{\frac{W_2^2 + W_2^2 + W_3^2 + \cdots + W_o^2}{W_1^2}} \tag{38}$$

W_o stands for root mean square voltage. The harmonic count o is represented in both equations. Apart from the numerous benefits of PV solar energy, grid integration of PV systems creates a number of operational issues. Changes in weather temperature and solar irradiance generate oscillations in the PV system's output power, which are two of the major causes of harmonics. Power electronic components utilized in power converters, in contrast to solar irradiance, causes quality issues like harmonic distortion. The performance of a PV system with respect to power quality is solely dependent on the usage of inverters, solar irradiation, and temperature, all of which can alter the generated voltage, power, and current profiles. Harmonic distortion in PV systems can be caused by both inherent and external factors. Intrinsic harmonic distortions are caused by inverter flaws like control loops and nonlinear component, measurement errors, and low PWM precision (Du et al., 2018 and Sunny and Anto, 2013).

Reactive power and current THD are both connected to output active power levels, which change depending on solar irradiation. The current THD value is risen dramatically all through low irradiance levels (e.g., sunset, sunrise, and cloudy days), but it is noticeably lowered and attains its nominal value. The current distortion behaviour is described by the inherent features of the nonlinear components and control circuit of the PV inverter.

Voltage as well as frequency variations or sag/well patterns in the grid are caused by different power resulting in substantial harmonic distortion (Makbul et al., 2008). Various MPPT algorithms and power electronic topologies have been utilised to overcome these limitations and improve the maturity of innovation in this sector. As a result, a new methodology must be devised to address the aforementioned shortcomings of present methods. Harmonics are problematic not just for the PV module, but also for the overall power supply. THD inside the power signal must be eliminated as much as possible to eradicate this problem.

10.3389/fenrg.2022.1038533

5 Optimized Recurrent Neural Network and proposed Crow Search-Based Harris Hawks Optimization for the power quality enhancement and THD reduction

5.1 Optimized RNN

Here, the hidden neurons of RNN are tuned by CS-HHO with the consideration of THD minimization thus referred as ORNN. The RNN may be characterised by the below state-space equations when non-linear activation functions are employed for the hidden units and linear activation functions are utilized for the input units:

$$y(l) = g\left[(X_1 y(l-1) + \tau(l-1)) + X_{J\phi}(l-1)\right] \tag{39}$$

$$\tau(l) = X_p y(l) \tag{40}$$

$$d(l) = T_1 \tau(l) + T_2 \tau(l) \tag{41}$$

X_J, X_I, X_P, T_1, and T_2 represents weight matrices, while $\phi(l)$, y(l), d(l), and $\tau(l)$ represents the network's input vectors, hidden units' outputs, context layer's outputs, and network's outputs, accordingly. The following equations are obtained:

Assume q represent the count of input layer units, r represent the count of hidden and context layer units, and s represent the count of output layer units. After that, T_1 and T_2 are provided by:

$$T_1 = \alpha K \tag{42}$$

$$T_2 = \gamma J \tag{43}$$

I shows the q identity matrix, and K shows a s×rmatrix with complete members equal to 1. **Eqs 32–43** when combined produces:

$$d(l) = [\alpha K X_1 X_P + \gamma J X_1]\, d(l-1) + [\alpha K X_1 X_P + \gamma J X_1]\, \phi(l-1) \tag{44}$$

This is in the following format:

$$d(l) = L_1 d(l-1) + L_2 \phi(l-1) \tag{45}$$

$L_1 = [\alpha K X_I X_P + \gamma J X_I]$ represents a r×rmatrix, while $L_2 = [\alpha K X_P X_J + \gamma J X_J]$ represents a r×q matrix. **Eq. 10** clearly shows the governing equations of a generic 0^{th}-order system with d as the state vector. During training, the components of L_1 and L_2 may be changed to fit any arbitrary 0^{th}-order system.

5.2 Proposed CS-HHO

The proposed CS-HHO is used for the THD reduction through the optimization of the hidden neurons of RNN.

Step 1: Start
Step 2: Population initialization
Step 3: Parameter initialization
Step 4: Fitness calculation
while iter<iter+1
if AP< 0.5,
$y^{(j,itr+1)} = y^{(j,itr)} + s_j - fm^{(j,itr)}[(n^{(k,itr)} - y^{(j,itr)}]$
else
iter=iter+1
Step 5: Stop

Algorithm 1. Proposed CS-HHO.

The cooperative behaviour and pursuit manner of Harris' hawks in essence, known as surprise pounce, seems to be the fundamental source for HHO (Heidari et al., 2019). The HHO has various advantages such as finding excellent solutions, superior outcomes, *etc.* It, however limits from binary as well as the multi objective versions, cannot compete distinct constraint solving strategies, *etc.* Thus, to overcome its limitations, CSA is combined into it and the so formed algorithm is named as CS-HHO. This HHO can handle various strategies as well as solves the multi objective versions of optimization problems, *etc.* CSA (Askarzadeh, 2016) is a demographically strategy that relies on the premise that crows store their extra food in hiding places and recover it when it is necessary. In CSA, the component of AP is primarily responsible for intensification and diversification. By lowering the AP number, CSA is more likely to focus its search on a small area where a suitable answer is currently available. As a consequence, employing low AP levels boosts intensification. On the other extreme, when the AP value rises, the likelihood of CSA searching in the region of already good solutions drops, and the search space is explored on a global scale (pseudo random). As a reason, using big AP values boosts diversity. The proposed CS-HHO is developed on the basis of AP concept. If AP ≤ 0.5, then the update takes place by CSA as below.

$$y^{j,itr+1} = y^{j,itr} s_j \times fm^{(j,itr)} \times n^{(k,itr)} - y^{(j,itr)} \tag{46}$$

$fm^{j,itr}$ signifies the flight length of crow j at iteration itrand s_j defines a random number with uniform distribution between 0 and 1. Otherwise, if $AP > 0.5$, then the update takes place by exploration phase of HHO as in **Eq. 47**.

$$Y(itr+1) = \begin{cases} Y_{rd}(itr) - s_1 |Y_{rd}(itr) - 2s_2 Y(itr)|; r \geq 0.5 \\ Y_{rabbit}(itr) - Y_n(itr) - s_3 (LB + s_4 (UB - LB)); r < 0.5 \end{cases} \tag{47}$$

Here, $Y(itr+1)$ represents the hawks' position vector, Y_{rabbit} (itr) represents the position of rabbit, Y (itr) represents the current hawks' position vector, s_1, s_2, s_3, s_4, and r represents random numbers, LB and UB represents the upper and lower

10.3389/fenrg.2022.1038533

TABLE 1 Simulation parameters.

Parameters	Values
Network	210V/50 Hz
PWM Frequency	8 kHz
Cascaded Count	31
PC Voltage regulator	7,000, 14,000

bounds, Y_{rd} (itr) represents a randomly selected hawk and the average position of the current hawks population is shown by Y_n. The pseudocode of CS-HHO is in **Algorithm 1**.

6 Results

6.1 Experimental results

The researched system is built in MATLAB/SIMULINK/SimPowerSystems environment to assess the performance and show proof of the developed regulator. The simulation is run to keep the study focused on cascaded H-bridge cells. The system as well as the simulation parameter of the controller is displayed in **Table 1**.

6.2 PV power analysis

In comparison to real available power and traditional MPPT controller, **Table 2** shows total power gathered by the introduced CS-HHO-based MPPT scheme under variable irradiance. **Figure 3** shows PV analysis based on proposed method.

6.3 Voltage and THD analysis

The harmonic spectrums of the output voltage and current waveforms under testing conditions are shown in **Figure 4**. THD is 2.86 percent for both voltage and current. This is significantly below the IEEE 519 standard's 5-percentage-point restriction. The circuit is not activated while employing a totally resistive load since there exists no reactive power component and the power factor is at unity. Excluding the amplitude, the waveforms of voltage as well as current are quite identical. On both waveforms, the 31-level output is readily visible.

6.4 Efficiency analysis

Table 3 shows the efficiency study of the suggested asymmetrical 31-level inverter architecture utilizing the load. Simply multiply the rms current, rms voltage, and power factor yields the output power. The efficiency continues to be amazing. 96.81 percent is the value. The power distributed by the resistive load is identical to the power distributed by the resistive load. When compared to various DC sources, single DC source is determined to be roughly 23 percent higher than the prior source as shown in **Figure 5**. The power distribution is comparable to what was found in the simulation research. Efficiency is defined as the amount of energy produced divided by the amount of energy input and expressed as a percentage. Ultimately, diminishing harmonics and statistical measurements are used to show that the established procedure is capable throughout entire instances. Similarly, a well-proven approach optimally manages DC connection voltages and collects grid currents.

6.5 Statistical analysis

Since the statistical measures are stochastic in nature, it is required to perform the optimization a minimum of five times in order to attain the best optimal solution. In **Figure 6**, different measures such as mean, median, and standard deviation are considered. The considered measures clearly reveal the betterment of the proposed method in terms of the considered measures than the existing methods as listed in **Table 4**.

6.6 Time domain parameter analysis

The time domain parameter analysis in terms of various measures such as settling time, peak time, rise time, and steady state error with respect to methods like ANN, CNN, RNN and introduced CS-HHO is shown in **Figure 7**. **Table 5** clearly reveals that the time utilized is less with the proposed

TABLE 2 PV power analysis.

Irradiance	Actual power	MPPT Shimi et al. (2013)	Proposed method
1000 W/m2	100	99	98
800 W/m2	78	77	78
600 W/m2	58	56	57
400 W/m2	40	37	38
200 W/m2	19	17	18

TABLE 3 Efficiency comparison.

Analysis	P&O Kumari et al. (2012)	MPPT Shimi et al. (2013)	Proposed scheme
Total Input Power	162.56 (W)	162.51 (W)	162.59 (W)
Output Power	156.73 (W)	155.71 (W)	157.12 (W)
Efficiency (%)	96.40%	95.21%	96.81%

TABLE 4 Statistical comparison.

Methods	ANN Nambiar et al. (2015)	CNN Ramasamy and Perumal (2021)	CRNN Yildirim (2005)	Proposed CS-HHO
Mean	1.5625	1.5342	1.9428	0.5136
Median	1.8500	1.4702	1.4138	0.2175
SD	0.9254	0.7152	0.8110	0.4102

TABLE 5 Time domain parameter analysis Comparison.

Methods	Settling time (s)	Peak time (s)	Rise time (s)	Steady-state error (RPM)
ANN Nambiar et al. (2015)	11.1	10.1	9.7	8.3
CNN Ramasamy and Perumal (2021)	10.9	6.2	7.9	6.3
RNN Yildirim (2005)	10.3	8.5	8.1	3.9
CS-HHO	9.6	0.1	6.2	1.1

CS-HHO than the other methods. Hence, it can be clearly stated that the time domain parameter analysis is better with CS-HHO than the other methods for the developed PV system with MLI.

7 Conclusion

This paper proposed an artificial intelligence-based PV system optimization concept as well as an unique cascaded MLI for PV system grid integration. The cascaded MLI was the best ideal for PV systems since it has fewer power electronic switches and could operate at asynchronous voltage sources. By increasing the output voltage level, this unique inverter reduced THD at the output. It also enhanced the system's power quality. ORNN controlled the micro grid integration of the introduced inverter, with hidden neurons tuned by a novel hybrid meta heuristic algorithm that combined CSA and HHO, resulting in CS-HHO. The suggested model was tested under a variety of loads and weather situations. The simulation results validated the created system's efficiency.

Data availability statement

The original contributions presented in the study are included in the article/supplementary material, further inquiries can be directed to the corresponding author.

Author contributions

All authors listed have made a substantial, direct, and intellectual contribution to the work and approved it for publication.

Conflict of interest

The authors declare that the research was conducted in the absence of any commercial or financial relationships that could be construed as a potential conflict of interest.

The reviewer [IV] declared a shared affiliation with the authors at the time of the review.

Publisher's note

All claims expressed in this article are solely those of the authors and do not necessarily represent those of their affiliated organizations, or those of the publisher, the editors and the reviewers. Any product that may be evaluated in this article, or claim that may be made by its manufacturer, is not guaranteed or endorsed by the publisher.

References

Abdelsalam, A. K., Massoud, A. M., Ahmed, S., and Enjeti, P. N. (2011). High-performance adaptive perturb and observe mppt technique for photovoltaic-based microgrids. *IEEE Trans. Power Electron.* 26, 1010–1021. doi:10.1109/TPEL.2011.2106221

Abouloifa, A., Aouadi, C., Lachkar, I., Boussairi, Y., Aourir, M., and Hamdoun, A. (2018). Output-feedback nonlinear adaptive control strategy of the single-phase grid-connected photovoltaic system. *J. Sol. Energy* 2018, 1–14. doi:10.1155/2018/6791056

Adinolfi, G., Graditi, G., Siano, P., and Piccolo, A. (2015). Multiobjective optimal design of photovoltaic synchronous boost converters assessing efficiency, reliability, and cost savings. *IEEE Trans. Ind. Inf.* 11, 1038–1048. doi:10.1109/TII.2015.2462805

Alhafadhi, L. A. (2016). "Total harmonics distortion reduction using adaptive, weiner, and kalman filters,". Ph.D. thesis. Michigan: Scholarworks@WMU.

Aourir, M., Abouloifa, A., Lachkar, I., Aouadi, C., Giri, F., and Guerrero, J. M. (2020). Nonlinear control and stability analysis of single stage grid-connected photovoltaic systems. *Int. J. Electr. Power & Energy Syst.* 115, 105439. doi:10.1016/j.ijepes.2019.105439

Askarzadeh, A. (2016). A novel metaheuristic method for solving constrained engineering optimization problems: Crow search algorithm. *Comput. Struct.* 169, 1–12. doi:10.1016/j.compstruc.2016.03.001

Bhandari, B., Poudel, S. R., Lee, K.-T., and Ahn, S.-H. (2014). Mathematical modeling of hybrid renewable energy system: A review on small hydro-solar-wind power generation. *Int. J. Precis. Eng. Manuf. -Green. Tech.* 1, 157–173. doi:10.1007/s40684-014-0021-4

Bhukya, M., and Kota, V. (2018). DCA-TR-based MPP tracking scheme for photovoltaic power enhancement under dynamic weather conditions. *Electr. Eng.* 100, 2383–2396. doi:10.1007/s00202-018-0710-z

Bhukya, M. N., Kota, V. R., and Depuru, S. R. (2019). A simple, efficient, and novel standalone photovoltaic inverter configuration with reduced harmonic distortion. *IEEE Access* 7, 43831–43845. doi:10.1109/ACCESS.2019.2902979

Chandrasekaran, S., Durairaj, S., and Padmavathi, S. (2021). A performance evaluation of a fuzzy logic controller-based photovoltaic-fed multi-level inverter for a three-phase induction motor. *J. Frankl. Inst.* 358, 7394–7412. doi:10.1016/j.jfranklin.2021.07.032

Dileep, G., and Singh, S. N. (2017). Selection of non-isolated dc-dc converters for solar photovoltaic system. *Renew. Sustain. Energy Rev.* 76, 1230–1247. doi:10.1016/j.rser.2017.03.130

Du, Y., Lu, D., Zobaa, A., Aleem, S., and Balci, M. (2018). "Harmonic distortion caused by single-phase grid-connected pv inverter," in *Power system harmonics: Analysis, effects and mitigation solutions for power quality improvement*. Editors A. F. Zobaa, S. Aleem, and M. E. Balci (Norderstedt, Germany: BoD – Books on Demand), 51.

Eltawil, M. A., and Zhao, Z. (2013). Mppt techniques for photovoltaic applications. *Renew. Sustain. Energy Rev.* 25, 793–813. doi:10.1016/j.rser.2013.05.022

Fernão Pires, V., Cordeiro, A., Foito, D., and Silva, J. F. (2018). Three-phase multilevel inverter for grid-connected distributed photovoltaic systems based in three three-phase two-level inverters. *Sol. Energy* 174, 1026–1034. doi:10.1016/j.solener.2018.09.083

Graditi, G., Adinolfi, G., and Tina, G. M. (2014). Photovoltaic optimizer boost converters: Temperature influence and electro thermal design. *Appl. Energy* 115, 140–150. doi:10.1016/j.apenergy.2013.10.031

Haddadi, A. M., Farhangi, S., and Blaabjerg, F. (2019). A reliable three-phase single-stage multiport inverter for grid-connected photovoltaic applications. *IEEE J. Emerg. Sel. Top. Power Electron.* 7, 2384–2393. doi:10.1109/JESTPE.2018.2872618

Hamidi, M., Ishak, D., Zainuri, M., and Ooi, C. (2020). An asymmetrical multilevel inverter with optimum number of components based on new basic structure for photovoltaic renewable energy system. *Sol. Energy* 204, 13–25. doi:10.1016/j.solener.2020.04.056

Hamidi, M. N., Ishak, D., Zainuri, M. A. A. M., Ooi, C. A., and Tarmizi, T. (2021). Asymmetrical multi-level dc-link inverter for pv energy system with perturb and observe based voltage regulator and capacitor compensator. *J. Mod. Power Syst. Clean Energy* 9, 199–209. doi:10.35833/MPCE.2019.000147

Heidari, A. A., Mirjalili, S., Faris, H., Aljarah, I., Mafarja, M., and Chen, H. (2019). Harris hawks optimization: Algorithm and applications. *Future gener. Comput. Syst.* 97, 849–872. doi:10.1016/j.future.2019.02.028

Janardhan, K., Mittal, A., and Ojha, A. (2020). Performance investigation of stand-alone solar photovoltaic system with single phase micro multilevel inverter. *Energy Rep.* 6, 2044–2055. doi:10.1016/j.egyr.2020.07.006

Katir, H., Abouloifa, A., Lachkar, I., Noussi, K., Giri, F., and Guerrero, J. (2020). Advanced nonlinear control of a grid-connected photovoltaic power system using n-cascaded h-bridge multilevel inverters. *IFAC-PapersOnLine* 53, 12859–12864. doi:10.1016/j.ifacol.2020.12.2095

Killi, M., and Samanta, S. (2015). Modified perturb and observe mppt algorithm for drift avoidance in photovoltaic systems. *IEEE Trans. Ind. Electron.* 62, 5549–5559. doi:10.1109/TIE.2015.2407854

Kumari, J. S., Babu, D. C. S., and Babu, A. K. (2012). Design and analysis of p&o and ip&o mppt techniques for photovoltaic system. *Int. J. Mod. Eng. Res.* 2, 2174–2180.

Liu, F., Duan, S., Liu, F., Liu, B., and Kang, Y. (2008). A variable step size inc mppt method for pv systems. *IEEE Trans. Ind. Electron.* 55, 2622–2628. doi:10.1109/TIE.2008.920550

Macaulay, J., and Zhou, Z. (2018). A fuzzy logical-based variable step size P&O MPPT algorithm for photovoltaic system. *Energies* 11, 1340. doi:10.3390/en11061340

Mahendiran, T. V. (2020). A color harmony algorithm and extreme gradient boosting control topology to cascaded multilevel inverter for grid connected wind and photovoltaic generation subsystems. *Sol. Energy* 211, 633–653. doi:10.1016/j.solener.2020.09.079

Makbul, A., Hamid, M. I., and Taufik, T. (2008). "Power quality behavior of single phase fed adjustable speed drive supplied from grid of pv generation," in 2008 IEEE 2nd International Power and Energy Conference (IEEE), 1098–1102.

Moradi-Shahrbabak, Z., Tabesh, A., and Yousefi, G. R. (2014). Economical design of utility-scale photovoltaic power plants with optimum availability. *IEEE Trans. Ind. Electron.* 61, 3399–3406. doi:10.1109/TIE.2013.2278525

Motahhir, S., El Hammoumi, A., and El Ghzizal, A. (2018). Photovoltaic system with quantitative comparative between an improved mppt and existing inc and p&o methods under fast varying of solar irradiation. *Energy Rep.* 4, 341–350. doi:10.1016/j.egyr.2018.04.003

Nambiar, N., Palackal, R. S., Greeshma, K. V., and Chithra, A. (2015). "Pv fed mli with ann based mppt," in 2015 International Conference on Computation of Power, Energy, Information and Communication (ICCPEIC), India, April 22,23, 2015. 0293–0300 doi:10.1109/ICCPEIC.2015.7259478

Nazer, A., Driss, S., Haddadi, A. M., and Farhangi, S. (2021). Optimal photovoltaic multi-string inverter topology selection based on reliability and cost analysis. *IEEE Trans. Sustain. Energy* 12, 1186–1195. doi:10.1109/TSTE.2020.3038744

Pai, F.-S., and Chao, R.-M. (2010). A new algorithm to photovoltaic power point tracking problems with quadratic maximization. *IEEE Trans. Energy Convers.* 25, 262–264. doi:10.1109/TEC.2009.2032575

Ramasamy, S., and Perumal, M. (2021). Cnn-based deep learning technique for improved h7 tli with grid-connected photovoltaic systems. *Int. J. Energy Res.* 45, 19851–19868. doi:10.1002/er.7030

Shimi, S. L., Thakur, T., Kumar, J., Chatterji, S., and Karanjkar, D. (2013). "Mppt based solar powered cascade multilevel inverter," in 2013 Annual International Conference on Emerging Research Areas and 2013 International Conference on Microelectronics, Communications and Renewable Energy. 1–5. doi:10.1109/AICERA-ICMiCR.2013.6576041

Sonti, V., Jain, S., and Pothu, B. S. K. R. (2020). Leakage current minimization using npc dc decoupling method for three-phase cascaded multilevel pv inverter. *IEEE Trans. Circuits Syst. Ii.* 67, 3247–3251. doi:10.1109/TCSII.2020.2984014

Sunny, R., and Anto, R. (2013). Control of harmonics and performance analysis of a grid connected photovoltaic system. *Int. J. Adv. Res. Electr. Electron. Instrum. Eng.* 2, 37–45.

Wang, L., Wu, Q., and Tang, W. (2017). Energy balance control of a cascaded multilevel inverter for standalone solar photovoltaic applications. *Energies* 10, 1805. doi:10.3390/en10111805

Yang, Y., and Wen, H. (2018). Adaptive perturb and observe maximum power point tracking with current predictive and decoupled power control for grid-connected photovoltaic inverters. *J. Mod. Power Syst. Clean. Energy* 7, 422–432. doi:10.1007/s40565-018-0437-x

Yildirim, S. (2005). Design of adaptive robot control system using recurrent neural network. *J. Intell. Robot. Syst.* 44, 247–261. doi:10.1007/s10846-005-9012-6

Nomenclature

PV photo voltaic
MPPT maximum power point tracking
MLI multi level inverter
THD total harmonic distortion
ORNN Optimized Recurrent Neural Network
CSA crow search algorithm
CC conversion circuit
ANN artificial neural network
CHB cascade h-bridge
HHO harris hawks optimization
PWM pulse width modulation
NPC neutral point clamped
P&O perturb and observe
CS-HHO Crow Search-based Harris Hawks Optimization
SIMO single-input and multi-output
CMLI cascaded multi-level inverter
MLDCL multi-level DC-link
TFL total financial losses
CHA color harmony algorithm
POVR P&O based voltage regulator
XGBOOST eXtreme Gradient BOOSTing
IGBT Insulated Gate Bi-polar swiTches
VSI voltage source inverter
PDPWM phase disposition pulse width modulation
FLC fuzzy logic controller
STC standard test conditions
PI proportional-integral
AP Awareness Probability

frontiers | Frontiers in Energy Research

TYPE Review
PUBLISHED 19 December 2022
DOI 10.3389/fenrg.2022.1091512

OPEN ACCESS

EDITED BY
Sarat Kumar Sahoo,
Parala Maharaja Engineering College (P.M.E.C), India

REVIEWED BY
Saroj Padhan,
Parala Maharaja Engineering College (P.M.E.C), India
Rabindra Kumar Sahu,
Veer Surendra Sai University of Technology, India

*CORRESPONDENCE
B. Saravanan,
bsaravanan@vit.ac.in

SPECIALTY SECTION
This article was submitted to Smart Grids, a section of the journal Frontiers in Energy Research

RECEIVED 07 November 2022
ACCEPTED 02 December 2022
PUBLISHED 19 December 2022

CITATION
Yadav VV and Saravanan B (2022), Technical advances and stability analysis in wind-penetrated power generation systems—A review.
Front. Energy Res. 10:1091512.
doi: 10.3389/fenrg.2022.1091512

Technical advances and stability analysis in wind-penetrated power generation systems—A review

V. Vishnuvardhan Yadav and B. Saravanan*

School of Electrical Engineering, Vellore Institute of Technology, Vellore, India

Recently, wind power from renewable energy power generation has been extended quickly to another level. To the grid, most renewable generators synchronize through the power electronic converters controlled flexibly. The high-level wind power penetration into the power generation system affects the dynamic performance of the power system and presents substantial uncertainties in system operation. This study mainly focuses on reviewing the various types of stability analyses in high-level wind penetration of power generation systems. It describes several challenges and simulation analyses related to stability issues. A comparative analysis has also been carried out for the various types of stability related to different research studies. The data show that transient stability has been significantly focused on in most of the studies.

KEYWORDS

stability analysis, wind turbine, power generation system, microgrid, transient stability

1 Introduction

Renewable energy resources increasingly penetrate modern power systems because of energy shortage crisis and environmental pressure. Recently, wind power integration projects have been launched in various countries. Wind power integration on a large scale presents substantial economic and environmental benefits to the society. The system exhibits several challenges in maintaining stability due to its stochastic nature and highly intermittent state. The power system stability can be affected after the integration of wind power into the utility grid due to several aspects, such as the replacement of the synchronous generator can reduce the effective inertia of the system. Due to the power electronics converter, the system alters its characteristics dynamically. The synchronous generator dispatch changes fast through the transmission network, power flow direction, and magnitude fluctuation (Xu et al., 2018). This proposed study reviews several types of stability issues of wind power integration in power systems and uncertainties present in the generation of wind power and satisfies the requirement of transient stability with several practices aimed at optimizing the system's operating state.

The doubly fed induction generator (DFIG) model analyzed the stability in wind power systems. The DFIG consists of an induction generator with a mechanically driven rotor through a gearbox by a wind turbine and a rotor side convertor (RSC). It is electrically excited through the grid and exhibits a power electronic-based interface. The complex control system is responsible for efficient wind energy conversion to power electricity for proper electrical and mechanical dynamics regulation. The small-signal stability region (SSSR) concept extends to the robust small-signal stability region (RSSSR), wherein the system maintains the stability even during perturbations that occur due to renewable energy power generation's volatile nodal injections and uncertainties (Pan et al., 2018).

Wind generators must provide ancillary services for systems with high-level wind penetration. As wind generation facilities increase worldwide, transmission system operators (TSOs) have changed grid code criteria. Under particular grid regulations, wind farms must provide inertial support, frequency regulation, and damping control. Synchronous generators typically deliver these services. However, due to the time-varying nature of such resources and the inherent modeling uncertainties that come along with their large-scale integration, this presents a formidable challenge. As a result, a sufficiently deterministic model of wind-dominated power systems is difficult to ensure. In the study by Husham et al. (2022), a Koopman-based model predictive controller (KMPC) was proposed to suppress the oscillations due to wind speed variations with climatic conditions and improve the control methodology for active and reactive power injections to the respective converters. Rahman et al. (2022) discussed clustering algorithms for large-scale wind power farms to access power system stability. Clustering algorithms are used to determine a probabilistic group of clusters representing equivalent wind farms and would hold true for most wind conditions throughout the year. The four aggregated wind farm models are subjected to small disturbances, frequency, and voltage stability analyses, also these wind farm models are analyzed considering a single unit for a better understanding.

A crucial sub-synchronous resonance (SSR) event in October 2009, persuaded by fixed series compensation, occurred in a wind farm with DFIG in Texas, United States. The SSR effect could not reflect critical factors like wind speed distribution, wind farms' spatial distribution, wind turbine generators' diversity, and network topology (Liu et al., 2018a). The developing VSC-MTDC grid shows some technological benefits concerning economics, modularity, and controllability focused on managing the frequency stability of traditional onshore AC grids (Wen et al., 2018). This study analyzes the robustness in the stability analysis of the wind power penetrated power system through stochastic optimization, which is risk-based, and estimates wind uncertainty. Furthermore, using devices such as ESS will reduce the required energy storage services (ESS) size by reactive power capabilities and wind farms. If the preferred voltage stability margin (VSM) increases, then the required ESS also increases as was shown by Jalali and Aldeen (2019).

The main contribution of this study involves

- reviewing the various research studies related to wind-penetrated power generation systems in terms of various types of stability,
- observing and studying the different techniques involved in improving the various types of stability issues and comparing them, and
- pictorially representing the analysis here in this review.

1.1 Article organization

This article is organized as follows: Section 2 describes the review of the stability analysis and the issues in wind-penetrated power generation systems. Various types of stability, namely, transient stability, dynamic stability, voltage stability, parametric stability, frequency stability, and other types of stability in power systems, are explained briefly, followed by a comparative analysis discussed in Section 3. The evaluation of the stability analysis is elaborated further. Finally, this article concludes in Section 4.

2 Types of stability in wind-penetrated power systems

Various types of stabilities, namely, transient stability, dynamic stability, voltage stability, parametric stability, frequency stability, and other such types of stability in power systems, are explained briefly in Figure 1.

2.1 Transient stability

Transient stability is "the ability of the system to remain in synchronism when subjected to large disturbances." Large disturbances can cause a variety of issues, such as faults, switching loads, and tripping. In most cases, the effects of these disturbances can lead to a large deviation of the generator rotor angles. It affects system synchronism to maintain stability.

Xu et al. (2018) developed a robust dispatch approach for the power system's operation state optimization while sustaining transient stability with stochastic wind power generation and high variability. As an increased optimal power flow framework, the system is designed with differential-algebraic equations and uncertain variables. Based on the trajectory sensitivity analysis and one-machine infinite-equivalence of bus, the approximately equivalent algebraic equations are obtained by conversion using

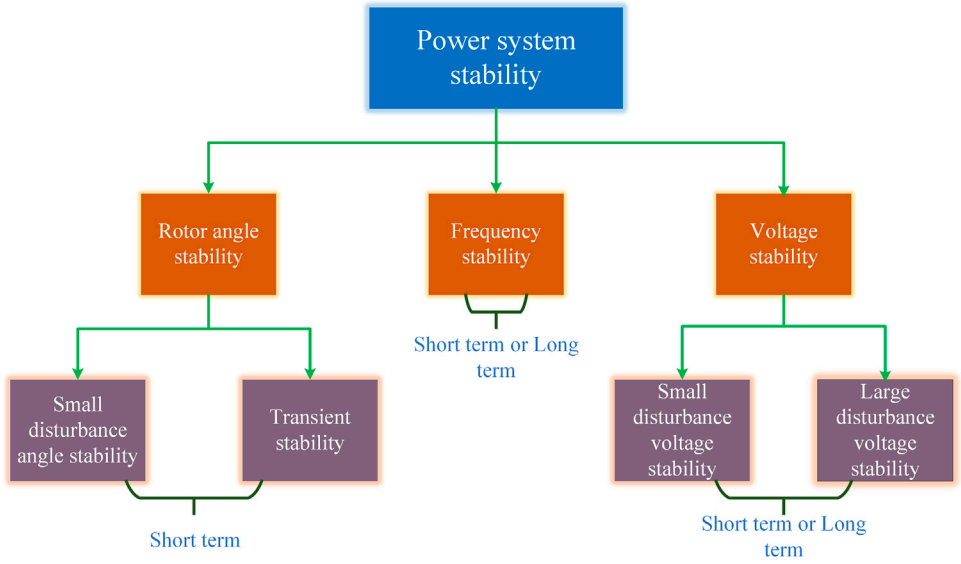

FIGURE 1
Different types of stabilities in power systems.

stability constraints. A small number of strategically represented chosen testing states are due to the uncertainty in wind power generation. This problem was solved iteratively by dividing the actual model into master problems and a sequence of slave issues based on the developed decomposition-based computation approach. This proposed method of dispatch focuses on a single period, i.e., 1 h. If we are to consider the dispatch of a multi-period, then the wind farm power output's temporal dependency should be well designed.

Wang et al. (2018a) focused on the multi-machine power system's stability improvement, combined with a hybrid wind-photovoltaic (PV) farm on a large scale using a supercapacitor (SC)-based energy storage unit. A wind turbine generator (WTG) of 300 MW simulated the hybrid and wind PV farm characteristics. The proposed SC connected with a proportional integral derivative supplementary damping controller (PID-SDC) and rendered efficient the damping characteristics that enhanced the transient performance of the proposed system subjected to a fault in three phases and short-circuited.

Ma et al. (2018a) explored the doubly fed induction generator (DFIG) current source–based model to analyze stability in wind power systems. Wind generator manufacturers developed this model, and generic models have simplified it. Moreover, it uses the current source–based model. Based on limited accurate measurements and chosen simulation scenarios, the proposed model was validated. The drawback was that the validity had not undergone any theoretical and systematic analysis of the current source model, and it may be considered unsuitable for application in real engineering. Hence, this study presents the current source model conditions for the analysis of stability in power systems. Furthermore, it investigates the model under asymmetrical and symmetrical fault conditions. This present source-based DFIG model has been practiced for validation in North China's real wind farms.

Hui et al. (2019) proposed a robust feedback control method on the basis of linear parameter varying (LPV) for interconnected systems' transient stability. This proposed method used mechanical power and DC channel power control in an interconnected system for the transient stability enhancement of the wind farm interconnected system. As a variable parameter linear model, the transient process has been designed mainly focusing on the interconnected system's robust nonlinear characteristics and the transient process's wind power uncertainty output. Four equal-value grids evaluated the proposed method in an interconnected system on a digital simulation platform through AC and DC lines. The proposed method exhibits better transient ability control impacts and response characteristics for wind power interconnected systems. Due to severe grid faults by loss of synchronization, wind farm tripping occurs.

During severe faults in a grid, the system requires dynamic properties with special requirements for maintaining the wind farm synchronization with the power grid. The grid synchronization by Ma et al. (2018b) is explained as autonomous nonlinear differential equation motion with particular initial states. However, synchronization stability occurs due to deprived system dynamic properties and unsuitable initial states. The proposed method satisfies the requirements by adjusting the wind farm's active and reactive

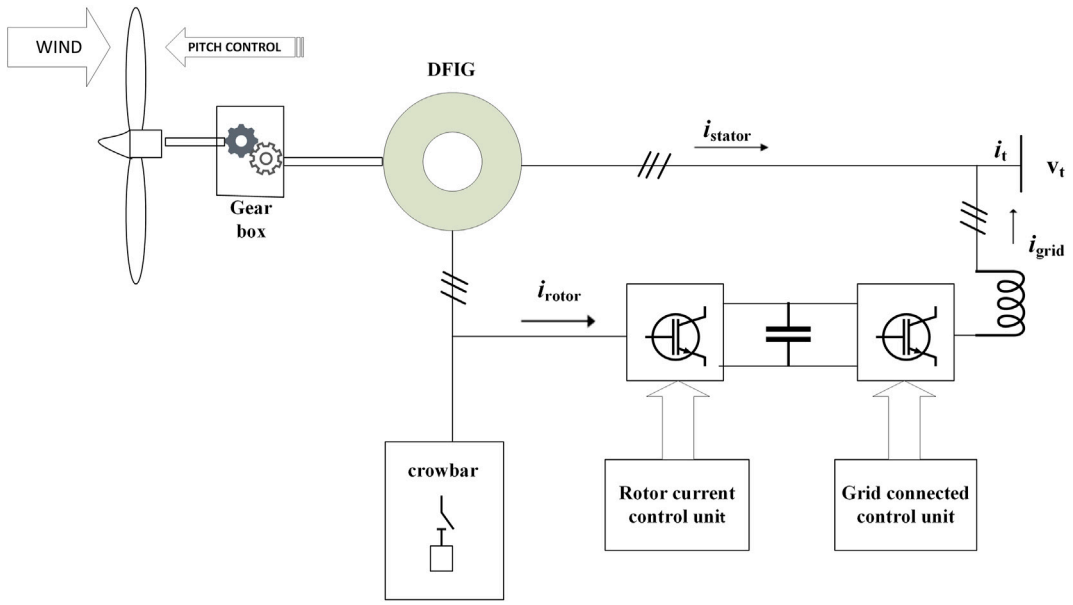

FIGURE 2
Transient stability control of the DFIG wind farm.

output current during severe faults in a grid. The proposed method was executed and analyzed on DFIG- and PMSG-based wind farms. Figure 2 shows the schematic diagram of transient stability control of the DFIG.

In the study by Yu et al. (2018), power system control considers the post-contingency–based online identification of transient stability as significant since it enables the grid operator to decide and synchronize correction control actions during system failure. Machine learning methods used with synchrophasor measurements were used for evaluating transient stability and received more attention in protection and control systems. Based on a long short-term memory (LSTM) network, this proposed study developed the transient ability assessment system. This self-adaptive scenario balanced the accuracy and response time after the assessment and subsidized better accuracy. This proposed system exhibited a fast-training process and lesser difficulty. The proposed assessment system's transient stability efficacy has been validated further in this study. The study by Ortega and Milano (2018) offers an in-depth stochastic analysis of the ESS impact on the transmission grid's transient stability. This stated impact was verified by considering the mixed effects of network topologies, fault-clearing times, and various ESS technologies. In addition, the synchronous machines, storage devices, and the fault's relative position were also considered. The stochastic time-domain simulations have also been considered for the all-island, Irish transmission system, 1479-bus model, resulting in nonintuitive endings.

Tang et al. (2018) developed a phase/magnitude dynamical model with unnatural consideration of timescale controller on rotor speed control for the theoretical evaluation of transient stability of DFIG-based wind turbines. This current model describes the unfair active power and active or reactive power output relationships. The synchronous generator and DFIG-based internal voltage vector show similarity but differ in the transient phase. The DFIG-based wind turbine system's transient stability is analyzed in case of new instability, recognizing the variation from the synchronization generator system.

Datta et al. (2019) examined the battery energy storage system (BESS) performance and static compensator (STATCOM) in improvising the tremendous power system frequency stability and transient voltage, the additional capacity of power export enhancing among two interconnected power systems. A multi-machine power system proposes a BESS controlled by PI lead and lead-lag to give concurrent frequency regulation and voltage among the defined battery charge range and the system performance evaluated by the Finnish transmission grid. The proposed method compares with conventional methods based on several permanent and temporary fault conditions rendered by the Australian electricity market grid requirements. BESS results from improvements like power export show a 44% increase, while failure cases are seen in STATCOM. Moreover, the BESS lead-lag establishes better performance than PI lead–controlled BESS under the permanent and temporary faults in divergent events.

In DFIG, the low-voltage ride through the LVRT requirements changes the DFIG running state and brings about the system's transient stability secondary impact. The DFIG output power mixes with the system's mechanical power. This study minimizes the mathematical relationship and analyzes the superconducting magnetic energy storage (SMES) relationship, improving transient stability and access location (Jiang and Zhang, 2019). Dynamic characteristics of wind farms connected with the grid improved and obtained more extraordinary transient stability performance.

In the study by Pico and Johnson (2019), the transmission defects due to recent the California wildfires stimulated utility-scale disconnection conversion in PV plants. The investigations described that the PLL and DC side dynamics caused tripping commands that are typically un-modeled in a classical stability analysis. Because of these authors introduce a positive-sequence model for photovoltaic power plants that is derived on the fundamental principles of physics and controls to predict during the faults. For addressing the disadvantage, a sequence of PV plant models was derived from physical principles. The three-phase converter scale shows that the framework comprises closed-loop controllers, DC side dynamics, and PLL.

The principal purpose of the study by Eshkaftaki et al. (2020) was to improve the SG's dynamic and transient performance using wind turbines with local DFIGs. The DFIG block is controlled by a designed transient controller (TC) and uses a modified generator in a motor regime operation mode. Furthermore, the electromagnetic torque band damping controller (ETBDC) consisting of two damping controllers is recommended to enhance the SG's dynamic stability. There are three types of feedback: DFIG electromagnetic torque, SG speed modified torque, and SG electromagnetic torque in every damping controller. The genetic algorithm adjusts these controlled parameters. By comparing the transient indexes system, namely, SG accelerating energy, with and without using TC of DFIG inertia energy in two area network and critical clearing time (CCT), the TC performance is evaluated. Moreover, the dynamic performance indexes of the system like settling time, SG's damping torque, eigenvalue, and overshoot have been related with and without using the two dynamic controllers. Moreover, these observe the proposed controller's effectiveness in the study.

Liu et al. (2016) proposed a new strategy that was a coordinated "switching power system stabilizer" (SPSS) to enhance the multi-machine power system stability. Simulations consist of 4 generators, 11-bus power systems, and IEEE 68-bus with 16 generator power systems in which SPSS assesses the damping ability in aspects of enhancements in transient stability. Renedo et al. (2016) analyzed an active power control strategy for a multi-terminal VSC-HVDC system that enhances the transient stability of AC/DC hybrid grids—the weighted-average frequency observed by the MTDC system's VSCs (WA-F). When compared to a strategy based on local frequency (LF), the study by Yousefian et al. (2017) mainly focused on an energy-based wide-area control on integrated power grids with wind. They proposed an algorithm of a nonlinear optimal control with "reinforcement learning (RL) and neural networks (NNs)," which, in using "approximate dynamic programming (ADP)," improves the wind-integrated power grid closed-loop performance. We observed that the suggested RL-based WAC enhanced system responses in simulations using the modified IEEE 68-bus system.

2.2 Small-signal stability

The small-signal stability in a power system is "the ability of the system to remain in synchronism when subjected to small disturbances." If power system oscillations are suppressed during the disturbances, the system's stability can be maintained over a long period.

Pan et al. (2018) addressed the small-signal stability region (SSSR) concept extension to the robust small-signal stability region" (RSSSR). The structured perturbation theory was first employed for the nodal injection perturbations in state-space formulations. This study considers the locations and intensity of the perturbations; RSSR in parameter subspace definition influences the structured singular value theory and stability radius theory. The "small-signal stability" of the power system's systematic analysis enables region-wise perturbations. Furthermore, the system maintains stability even during renewable generation's volatile nodal injections and uncertainty during perturbations. For the RSSSR boundaries, it constructs a linear closed-form approximation by the hyperplane approximation technique. Moreover, to make and learn from the RSSR boundary predictions, machine learning (ML) approaches have been employed.

The ML approaches' learning ability speeds up the computation on boundary significantly and simplifies the robust stability analysis of vast and complex power systems. Sadamoto et al. (2018) addressed the wind power integration concerned with the various growth of stability and power system dynamics retrofit control terms a new control design. Using retrofit controller, the rotor voltages of the induction generators that were doubly fed controlled for tie line power flow oscillations suppressing initiated by the wind farm's inside disturbance. The major drawback considered was that closed-loop system stability has not been assured theoretically. The requirement of an exact wind farm model is necessary, and in future, the problem can be resolved by designing the controller using robust control theory. Huang et al. (2020) carried out a novel investigation where online detection of wind farm generalized short-circuit ratio (gSCR) was studied using current and voltage data from PMUs, which enables convenient online stability monitoring of wind farms. Ma et al. (2017a) found that on virtual inertia control, DFIG impacts the "power system small-signal stability" by considering

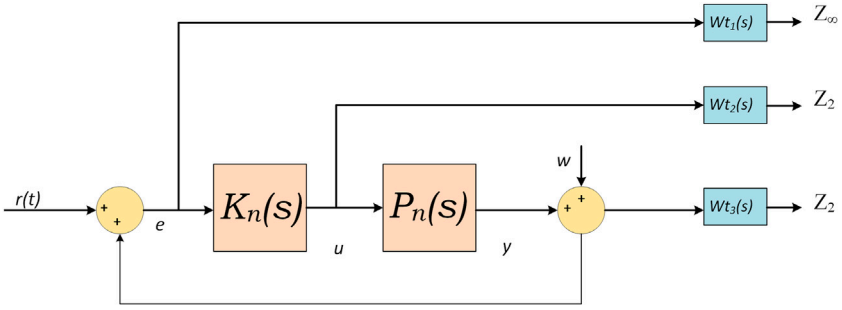

FIGURE 3
Robust mixed damping controller *H2/H∞* block diagram.

the "phase-locked loop" (PLL). For a DFIG interconnected with conventional synchronous generators, it considers PLL and virtual inertia. The system's dynamic characteristics vary due to the DFIG participating in electromechanical oscillations controlled by varying the PI values in PLL and virtual inertia.

In the study by Ma et al. (2017b), the robust stochastic "small-signal stability" of the DFIG was integrated into a power system with virtual inertia, as mentioned earlier, and the methodology used was the sensitivity analysis method, which determined the connection between the state matrix variables and stochastic parameters using analytic function relationships. The stochastic power system stability issue turns into a solution for the problem of feasibility. Wen et al. (2017) proposed power electronics–based distributed power system stability analysis using "active front end (AFE) converters," "voltage source inverters (VSIs)," and "grid-tied inverters (GTIs)" to process power flow as an analysis of AC stability and DQ frame impedance parameters. Liu et al. (2020a) investigated grid-integrated DFIG wind farms' PLL parameters and power grid strength that impacts small-signal stability issues. They focused on finding the PLL oscillation mechanism and its influencing factors and developed a damping solution to that oscillation mode. To abate the PLL oscillations, they designed a different robust damping controller H_2/H_∞ for DFIG, which reduces the oscillations and improves small-signal stability. The structure of the robust damping controller is shown in Figure 3, where "r(t)" is the input signal of the controller and "e" is the error signal. "$K_n(s)$" and "$P_n(s)$" are controller gains; "$Wt_1(s)$, $Wt_2(s)$, and $Wt_3(s)$" are weighting functions, and "Z_∞" is the output channel associated with H∞ performance. "Z_2" is the output channel associated with H_2 performance.

2.3 Stability of sub-synchronous resonance

"Subsynchronous resonance is a phenomenon in which one or more of the resonant frequencies of the turbine generator shaft in thermal power units coincides through the generator with a natural resonant frequency of the electrical system with a long radial transmission network with series capacitors."

In series, the compensated systems with several wind farms have detected the sub-synchronous resonance (SSR) issue elaborated by Liu et al. (2018a). The single-machine infinite bus system design has been simplified and used for further evaluation. It does not reflect the SSR effect, which is not from critical factors like wind speed distribution. This article, based on SSS, proposes a wind farm's spatial distribution, wind turbine generators diversity, network topology, and an INM-impedance network model.

Moreover, with lumped independence, the INM was combined. The SSR stability was quantified by new stability criteria, which analyzed the features of impedance frequency. Even for wind power systems on a large scale, this proposed system has analyzed the SSR issue. For DFIG-based wind turbines interconnected with compensated transmission systems series, Karunanayake et al. (2020) specified the nonlinear sliding mode control SMC based on the mitigation method as a sub-synchronous resonance (SSR). This proposed method controls the rotor side converter by assuring the reactive power, and the decoupled torque of DFIG control ability sustains to mitigate SSR. For validations, on the model of DFIG wind turbines, the proposed method is executed on the Real Time Digital Simulator (RTDS) platform. At damping SSR, the controller shows positivity obtained from the results tested on different wind speeds and compensation levels.

Ma et al. (2020) concentrated on sub-synchronous oscillations of DFIG stability estimations based on energy dissipation intensity analysis. According to the Lyapunov stability theory, the model of DFIG consists of an internal control and external network. Here, the proposed assessment method is represented in a logical diagram as shown in Figure 4. In this first step, collecting all the data of electrical variables at DFIG terminals with the help of phasor measurement units compares with steady-state values. Next, at the DFIG, variations of transient energy are estimated and the oscillation

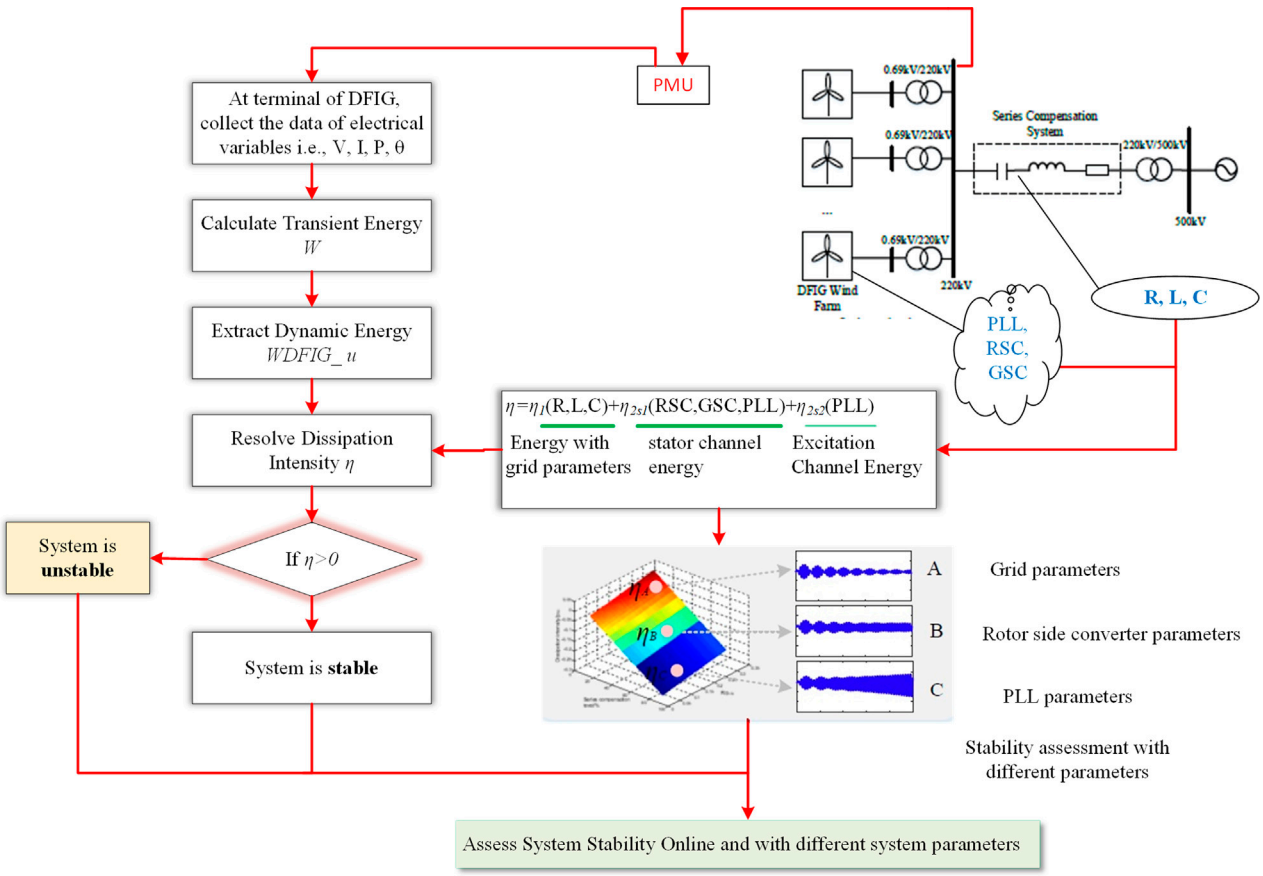

FIGURE 4
Logical representation of the assessment method.

frequency and DFIG transient energy variation are obtained. Then, the dissipation intensity η can be calculated. The system's stability can be judged by the value of η; when $\eta > 0$, the system is stable, and a larger value of η indicates higher stability. Also, when $\eta = 0$, the system is marginally stable, while $\eta < 0$ is negative stability and SSR oscillations diverge.

2.4 Probabilistic stability of sub-synchronous resonance

"In power system stability analysis, the system performance is based on a predefined scenario and ignores uncertainties in the system states and parameters. In modern power systems, consider all the uncertainties in the probabilistic approach to get accurate results." The probabilistic approaches are highly appropriate for random and uncertain system analysis, which are the essential features of future power systems.

Chen et al. (2018) focused on assessing the probabilistic stability of SSR by using the piecewise probabilistic collocation method (PPCM), which concerns random wind speed. Because of the switching among various operational modes of the DFIG, the PPCM tackles the inherent nonlinearity. The lesser computational difficulty and damping accuracy in the probability density function (PDF) is achieved using the proposed PPCM. Various existing methods are available to describe the probabilistic distribution of wind speed: Rayleigh, Weibull, and Lognormal distribution methods. Among these methods, Weibull distribution ideally suits wind speed as a frequency histogram. The Weibull probabilistic model has also been designed in this study with two-year statistical wind speed data. Compared with the Monte Carlo method, consistency is obtained from using this proposed method. The SSR events field data in real-world wind farms offer effectiveness validation of the current model.

In their research work, Bian et al. (2016) carried out "power system stabilizers" (PSS) and "static VAR compensator" (SVC) damping controller coordination and optimizing these parameters to improve the "probabilistic small-signal stability" of the wind farm integrated power system. This novel algorithm

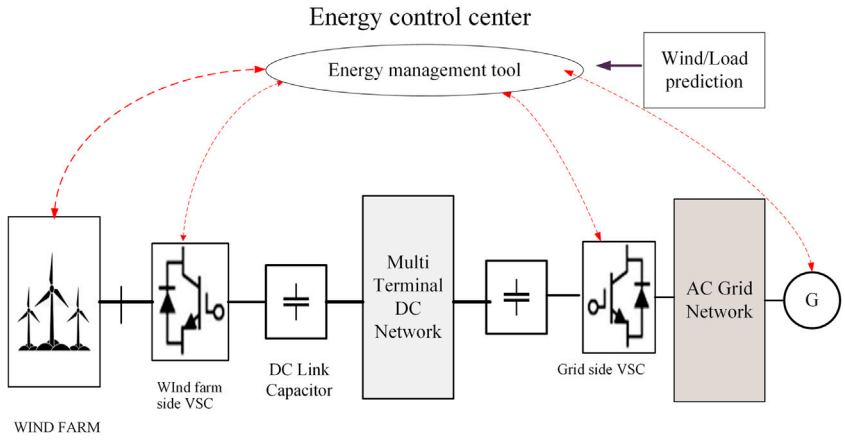

FIGURE 5
AC-VSC-based MTDC system's integrated configuration.

is known as the "modified fruit fly optimization algorithm" (MFOA). With this, to coordinate and optimize the parameters, the probabilistic eigenvalue method was used. The proposed method improved the "parabolic small-signal stability" of DFIG-based wind firms integrated with synchronous generators.

2.5 Frequency stability

Frequency stability means "the ability of a power system to maintain steady frequency following a severe disturbance between generation and load." Frequency stability depends on the ability to restore equilibrium between load and system generation. It can also lead to sustained frequency swings that can cause the generating system or load tripping.

In the study by Wen et al. (2018), the onshore AC grid and offshore multiterminal DC grid–based voltage source convertor VSC-MTDC operation were examined to improve the system's frequency stability by the unit commitment (UC) framework. Furthermore, it recognized three standard types of outages like wind farm side VSC loss, synchronous unit loss, and grid side VSC loss, which correspond to frequency dynamic constraints. Based on these, it integrated the AC/VSC MTDC system from the proposed frequency dynamics. Moreover, it effectively stabilized two grids among the GVSCs and WVSCs and examined the coordinated control approach. In Figure 5, the configuration of the AC/VSC-based MTDC system is shown. Here, the MTDC network is connected to offshore wind farms through the wind farm side voltage source converters (WVSC) and DC link capacitor. Similarly, the onshore AC grid is connected to the offshore VSC-MTDC grid through grid side voltage source converters (GVSC) and submarine HVDC cables. All the converters communicate with the energy management tool and track the voltages and power with local frequency control to detect any disturbance.

Renewable energy penetration has increased into the latest power systems, getting new oscillatory stability focused on this. Zhan et al. (2019) developed the analysis of the frequency-domain modal technique. It evaluated the dominant component's participation, and several oscillatory modes were concerned. The oscillatory modes by loop impedance matrix or matrix of nodal admittance determinant's zeroes located were worked out by the target system represented with impedance model network. The oscillation mode's origin, respective components, and oscillation path were understood by the loop or nodal participation factors, component sensitivity, and branch observability derivation. The above-stated experiment was performed on a practical wind power system and a primary passive circuit that practices real sub-synchronous resonance. In addition, its effectiveness was evaluated by using electromagnetic transient simulations and theoretical results. This study evaluated the massive power systems with high penetration renewables.

Han et al. (2022) discussed the frequency oscillation problem, and a novel discrete-time domain modal analysis, proposing to reduce the sub-synchronous oscillations of RES connected to the power system. In this method, first, in the discrete-time domain, the frequency and damping ratio were calculated, and the system stability was evaluated from the calculated eigenvalues in discrete-time. Furthermore, the origin location, contributive components, and propagation paths of the oscillatory mode were determined by calculating the participation factors, component participation, branch current/node voltage observability matrix, and distribution coefficient for all modes based on matrix decomposition and node equations of the system-level model.

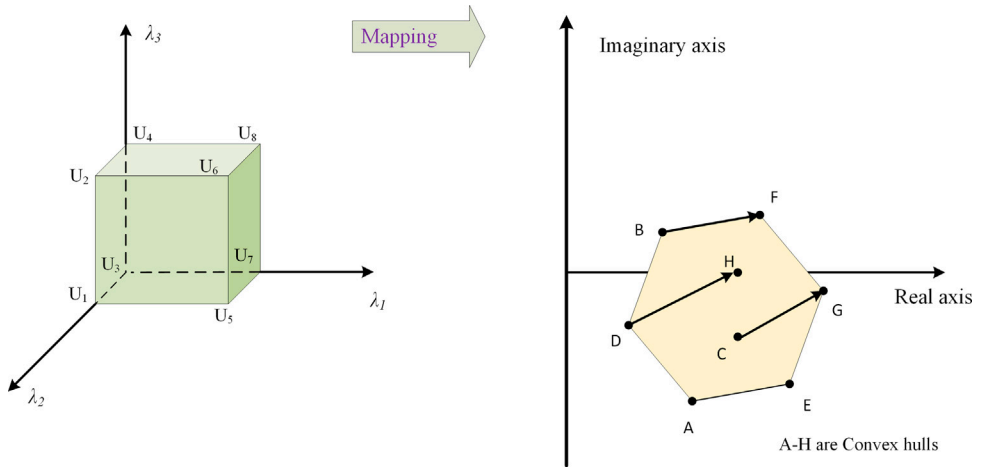

FIGURE 6
Structure of the mapping theorem.

A supplementary optimal frequency controller was designed for variable speed wind turbines to be integrated into the power system to improve system stability in a study by Toulabi et al. (2018). The proposed controller regulates the frequency variations in wind farms, and the controller design parameters are designed using genetic algorithms.

Yang et al. (2022) described the power compensation control for a weak grid-connected DFIG wind farm. The synchronization of the wind farm to the weak grid during severe grid faults was studied to improve the frequency stability. The analysis was performed in a simulation and verified with experimental results.

In the study by Li et al. (2021), a SMES-based damping controller was designed to reduce low-frequency oscillations for enhancing the power system's frequency stability. A finite Markov decision process that utilizes a deep reinforcement learning (DRL)–based agent was used to achieve the best possible results in terms of parameter optimization.

2.6 Dynamic stability

"Dynamic stability is the ability of a power system to return to a steady state of operation after significant disturbances (short circuit, the shutdown of any element of the power system, etc.)."

Shi et al. (2019) investigated the wind power penetrated power system's robust stability analysis. The power system analysis can be imposed on the (D-stability) issue by focusing on the constraint of the damping ratio. The most familiar mapping theorem $\det(I - M(s)\Delta)$ was applied for robust stability evaluation, and sufficient condition and multivariable stability margin K_m were provided. Uncertainty effects turn transparent while analyzing these values. It was tested on North China system's machine and 11-bus test 4 generator power system, and the structure of mapping theorems as shown in Figure 6. "$P(s, Q) = \{p(s, \lambda) = \det(I - M(s)\Delta) \mid \lambda \in Q\}$" are multi-linear parameters. Here, U_1–U_8 are the "k vertices" of the hypercube Q.

Li et al. (2019) concentrated on real-world wind farms where the weak grid's interconnection observed 4 and 30 Hz oscillations. The delivery of wind power is limited by these stability problems. This study proposes that the overall system stability improvises the mechanism-based feedback control approaches appropriate for voltage source converters that were vector based and engaged in type-3 and type-4 wind testbeds. The weak grid stability problem has to be demonstrated by the simplified linear model, and the reason was the power delivery coupling and voltage of the point of common coupling (PCC). The PCC voltage reduces when the power delivery increases, and hence the weak grid leads to instability. The feedback control approaches modulate DC-link voltage and power order through PCC voltage as input or the d-axis current. Finally, we see the efficient capability of stability improvement and wind power delivery further enhanced.

When a harmonic grid with parallel compensation joins the DFIG system, the harmonics and high-frequency resonance (HFR) exhibiting the frequency range may show intersections. Nian and Pang (2019) revealed that the coupling between the harmonics suppression control and HFR damping control provided by the harmonics suppressor and HFR damping led to an unstable situation of the DFIG system. Extra detection time of frequency of HFR results in HFR damping performance deterioration. Moreover, it achieves the harmonic current suppression and HFR damping control to further enhance DFIG system power quality associated with parallel compensation of the harmonic grid.

The IEEE 118-bus system uses a 12-bus system to evaluate the performance and effectiveness of the current study. Xiong et al. (2019) presented an optimal virtual inertia planning approach for power system stability improvement with renewable resources of large volumes penetrated by the DFIGs. The critical frequency drops are also exhibited in this study, and the DFIG stability are analyzed first. It calculates the local virtual inertia function form by the stability margin defined by the DFIG's two predefined operation curves. Then, the planning strategy of virtual inertia is proposed, and the non-convex optimization issue is followed from the homogeneity of the stability margin. It uses the Lyapunov function to resolve these issues. The general stability was promoted, and the coherency level of the system stability margin improved, resulting in the proposed method. In the study by Liu et al. (2020b), with increased wind power penetration, the stability problems of the poor AC grid connection and DFIG-based wind turbines during low voltage could not be neglected. The exploration of the instability process of the DFIG system during the process of weak grid fault and a model based on the small-signal state are specified in this article. The article's outcome depicted that the work was impacted by the rotor current control loop, phase-locked loop (PLL), and terminal voltage during dominant factor processing.

The system impact factor evaluated comprehensively indicated that the controller bandwidth in the expected condition does not apply to the fault because of the interaction between the grid and controller. It follows the optimized proportion that could be improved significantly. Experiments and simulations have evaluated the efficiency of the suggested system. The permanent magnet synchronous generator depends on wind turbines, and the virtual synchronous machine (VSM) was proposed by Muftau et al. (2020), and all operating modes allow continuous operation and guarantee maximum power point tracking in grid connected operations. In islanded operations, the power generation follows a load. During faults, the lower voltage ride-through capability exists. The optimal performance obtained by VSM stability in all operating models examines large and small perturbations. The linearized state-space model and participator factor analysis perform the VSM's small-signal stability analysis using participator factor analysis and derived dominant mode controller effects. The VSM's nonlinear model, dynamic performance, and transient stability analyzed. The VSM's design guidelines and operational limits were recognized. Li et al. (2016) focused on multiple time delays of delay-dependent stability control for the power system. They designed a multiple time-delayed power system model consisting of PSS with time delays. Two H_{∞} controls develop schemes for time-varying multiple delayed systems by considering the "Lyapunov stability theory" and "linear matrix inequality" (LMI) method. The New England 10-machine, 39-bus system and a 2-area 4-machine power system were employed to demonstrate the effectiveness of the proposed methods.

Wang et al. (2017) proposed a novel framework consisting of "stochastic differential equations" (SDE) to ease the "long-term stability" analysis with spasmodic wind power generations. This framework considers discrete dynamics, playing a significant role in the "long-term stability" analysis. They developed a "deterministic hybrid model (DHM)" for the "stochastic hybrid model (SHM)." The computing burden of the uncertainty of wind power was reduced, which improves the dynamic stability under mild conditions.

2.7 Parametric stability

The parametric analysis was used to enhance the system stability in wind-penetrated power systems. In parametric analysis, more uncertain parameters were considered to enhance the power system stability.

In wind power assimilated power systems, Shi et al. (2018) focused on the analysis of parametric stability, and for that, they developed the rational fractional representation technique. It improves accuracy when using rational fractional parameters in a fitted parametric state matrix instead of conventional polynomials. For robust stability analysis, the generalized linear fractional transformation was used for standard linear $M(s) - \Delta$ system of feedback, to formulate determinant of return difference matrix of value set plots, to apply the mapping theorem, i.e., instead of $M(s) - \Delta$, $1 - M(s) - \Delta$ is applied, and finally, to exhibit rational fractional uncertainty from the power system's robust stability. At the same time, analyzing these values is tested on the North China system's 8647-bus model 547 machine and 11-bus test 4 generator power system, only considering a single DFIG for analysis.

2.8 Voltage stability

Voltage stability means "the ability of a system to maintain steady-state voltages at all the system buses when subjected to a disturbance. If the disturbance is large, then it is called large-disturbance voltage stability."

Jalali and Aldeen (2019) considered the energy storage devices (ESS), optimal placement, and sizing in wind-intensive power distributed generation. The expected voltage stability margin (VSM) should attain and require ESS size minimization. This study also focuses on reducing the reactive power import and reactive power loss from a network upstream through stochastic optimization, which is risk based and estimates the wind uncertainty. Furthermore, the ESS size required is reduced by additional means such as ESS devices' reactive power capabilities and wind farms. If the preferred VSM increased, then the required ESS also increased asshown in the results. Yet, this kind of increase shortens using active network

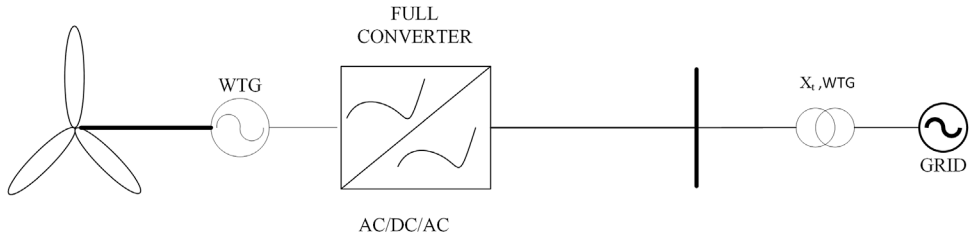

FIGURE 7
Wind turbine with full converter.

management (ANM) tools and voltage stability constraints, which are risk based. The traditional VAR compensation devices have become old and show minor changes for short-term voltage stability of high requirement satisfaction in power systems penetrated with high-level wind power. Hence, Liu et al. (2018b) proposed the STATCOMs technique for optimal dynamic VAR devices and also the power system upgraded with penetration of higher wind power and more excellent retirement of equipment. Three objectives have to be minimized, namely, proximity to steady-state index voltage collapse, retirement costs and upgrades, and unaccepted performance of the transient voltage index by the multi-objective optimization technique. Indefinite dynamic load models and several contingencies are considered in the real-world operating situation simulation. Through wind farm abilities, it designs low- and high-voltage rides. The New England 39-bus system of testing evaluates the proposed method.

Kawabe et al. (2017) specified the photovoltaic (PV) system's novel dynamic voltage support capability to improve the short-term voltage stability of the power system. The proposed DVS capability injects both active and reactive power in an organized manner. Souxes et al. (2020) focused on enhancing the power system stability issues under unfavorable network conditions with necessary support from wind farm power electronic converters. Protection schemes proposed for a weak transmission and network are integrated into wind farms to enhance long-term voltage stability during reactive emergency support. The schematic diagram of the full converter-based wind turbine is shown in Figure 7.

Milano (2016) proposed power and current injections for voltage and angle stability analysis, the comparison made with two formulations of both current and voltage injections on a dynamic 1479-bus model.

2.9 Small-signal angular stability

Small-signal angular stability means "the ability of synchronous machines of an interconnected power system to remain in synchronism after being subjected to a disturbance."

Du et al. (2019) evaluated the power system's small-signal angular stability affected by the virtual synchronous generator (VSG). Based on these two subsystems of the interconnected model the small signal angular stability evaluated. The other subsystem was the rest of the power system (ROPS). Based on these two subsystems of the interconnected model, and evaluated. When the VSG subsystem oscillation mode was in nearness to ROPS subsystem's electromechanical oscillation mode, the damping torque analysis applied indicated to VSG's strong dynamic interactions for the small-signal angular stability decrease in the power system. Both subsystems' modal proximity evaluates after setting the VSG parameters and avoids VSG due to the harmful effect of small-signal angular stability's decrease in the power system. However, the modal proximity is avoided by this proposed article which assists in VSG design parameters. For wind power generation, finally, it offers two example power systems with several VSGs and transmission. Ma et al. (2017c) elaborated the angle stability analysis with multiple operating conditions by considering cascading failures of the power system. Based on the flow transfer theory, the power system divides into various operating conditions. The discrete Markov model establishes to analyze the angle stability.

2.10 Rotor angle stability

Rotor angle stability means "the ability of the system to remain in synchronism when subjected to a disturbance." The rotor angle depends on the balance between a generator's electromagnetic and mechanical torque to maintain stability.

To ensure grid security, Zhang et al. (2020) demonstrated that the frequency stability of the current dynamic analysis showed insufficiency because the virtual inertia control had impacted the first swing's rotor angle stability. The novel virtual inertia control approach investigated in this study for wind turbines enhances the rotor angle stability of the first swing in the interconnected power grid. Here, the virtual inertia's virtual energy in wind turbines was investigated and evaluated. The conversion of the transient energy system is

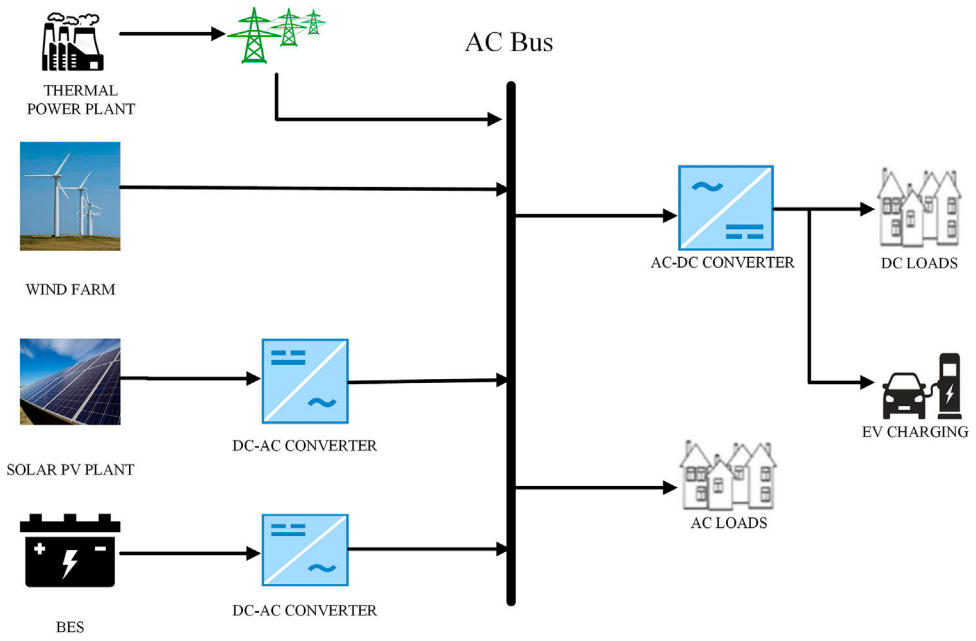

FIGURE 8
Microgrid structure.

grouped on the forward and backward directions of the swings of the rotor angle, and their virtual energies effect the two coherent generator groups. High wind penetration with 35% in a two-area interconnected power system has been provided in this study. Furthermore, it is comprised of two DFIG-based wind farms and simulated four traditional power plants. By regulating variable inertias and minimizing the rotor angle difference among coherent generator groups, wind turbines of virtual inertia support with more reliability resulted.

2.11 Stability issues in microgrids

Majumder (2013) described different stability aspects in microgrids and discussed various methods in improving power system stability in DC microgrids. As illustrated in Figure 8, a microgrid can be represented by various micro sources and loads.

The research study by Bhosale and Agarwal (2019) used a fuzzy logic-based novel scheme for power flow control from a ultracapacitor in a battery. To regulate the DC bus voltage firmly, a fuzzy logic controller determines the UC convertor current reference. Low bandwidth controllers were developed to enhance current drawing quality from the battery. The fuzzy controller is simple to develop and does not require the understanding of the mathematical model of the system. Low complexity is assured during execution since it is a controller of single input and single output. Wind-up problems are not visible and faster controller is seen. Compared with the traditional frequency-based control approach, the proposed method shows better performance.

Wang et al. (2018b) described the stability analysis of a microgrid system consisting of a "seashore wave farm" (SWF), an "offshore wind farm" (OWF), and an "offshore tidal farm" (OTF) fed to the onshore power grid through a high-voltage DC (HVDC) link. They proposed VSC-based HVDC link with a PID damping controller, which evaluates a systematic approach by frequency domain analysis based on nonlinear simulations during severe three-phase faults at the power grid side. Puchalapalli et al. (2020) proposed a hybrid energy generation-based microgrid. It designs a bidirectional buck-boost DC-DC converter to improve the microgrid's stability in various wind and solar weather conditions.

Xia et al. (2022) discussed the large signal stability of the AC microgrid, which is a single energy storage–based AC microgrid, with the nonlinear reduced order model designed to determine system stability during large disturbances.

Krismanto et al. (2021) studied the stability issues in grid-connected microgrids during uncertain conditions in RES. In order to confirm and characterize the modal interaction, three analytical methods were proposed: eigen-trajectories, the cross-participation factor, and the modal interaction index (MII). Monte Carlo (MC) simulation was proposed to determine the eigenvalues of the system and determine the small-signal stability of the system.

TABLE 1 Comparison of types of stability with the various existing research studies.

S. no	References	Techniques	Key findings	Type of stability
1	Xu et al. (2018)	A robust dispatch approach was developed to optimize the operation of a power system while sustaining its transient stability	• A quantitative stability assessment for the original DAE model is proposed	Transient stability
			• Translation of the stability constraints to equivalent algebraic terms	
			• The model is also used to solve a large-scale system problem	
2	Wang et al. (2018a)	Hybrid wind–photovoltaic PV farm in large scale employing supercapacitor (SC) combined with the designed PID-SDC	• The proposed SC is connected with a "proportional integral derivative–supplementary damping controller" (PID-SDC) designed to enhance a system's transient response subjected to a short circuit fault	Transient stability
3	Ma et al. (2018a)	The doubly fed induction generation (DFIG) model for analysis of stability in wind power system	• The authors focused on the development and validation of the DFIG model. The current source model conditions for the analysis of stability in the power system was presented	Transient stability
4	Hui et al. (2019)	A robust feedback control method was proposed based on linear parameter varying LPV for the interconnected system's transient stability improvement	• A novel transient stability control method was proposed for solving the Hco robust optimal control algorithm based on point-linearization and transient multiparameter	Transient stability
5	Ma et al. (2018b)	The proposed method satisfies the requirements, which adjust the wind farm's active and reactive output current during the faults in the severe grid	• The proposed method shows better transient ability control impacts and response characteristics for wind power interconnected systems	Transient stability
6	Yu et al. (2018)	The transient ability assessment system was developed based on the "long short-term memory" (LSTM) network	• Machine learning methods with synchrophasor measurements were used for evaluating transient stability and got more attention in protection and control systems	Transient stability
7	Ortega and Milano (2018)	In-depth stochastic analysis of ESS impact on transmission grid's transient stability	• The stochastic time-domain simulations have also been considered for the all-island, Irish transmission system, 1479-bus model, resulting in nonintuitive endings	Transient stability
8	Tang et al. (2018)	Phase/magnitude dynamical model unnatural consideration of timescale controller on rotor speed control for the theoretical evaluation of transient stability of DFIG wind turbines	• The DFIG wind turbine system's transient stability analyzed in case of new instability problem. It shows variation from unstable equilibrium point of traditional synchronous generation system	Transient stability
9	Datta et al. (2019)	Battery energy storage system (BESS) performance and also static compensator (STATCOM) in improvising the power system frequency stability and transient voltage	• BESS results in improvements such as the power export shows 44% increase while failure cases are seen in STATCOM. Moreover, the BESS lead-lag establishes better performance than PI-lead BESS under the permanent and temporary faults in divergent events	Transient stability
10	Jiang and Zhang (2019)	The DFIG output power mixes with system mechanical power and minimizes the mathematical relationship and analyzes the superconducting magnetic energy storage (SMES) relationship, which improves transient stability and access location	• Dynamic characteristics of wind farms connected with the grid are improved and obtain a greater transient stability performance	Transient stability
11	Pico and Johnson (2019)	The proposed power plant model considers several factors: PV side dynamics, a closed-loop controller, and a PLL. It is compatible with bulk power system models	• The three-phase converter scale shows that the framework comprises closed-loop controllers, DC side dynamics, and PLL	Transient stability
12	Eshkaftaki et al. (2020)	A designed transient controller (TC) controls the DFIG block, which modifies the generator to the motor regime operation mode	• Furthermore, to enhance SG's dynamic stability, it recommends the ETBDC-electromagnetic torque band damping controller, which is also known as two damping controllers	Transient stability
13	Liu et al. (2016)	It employs a locally installed SPSS, switching power system stabilizers for coordination	• Installed SPPS can communicate with the different generators to improve stability	Transient stability
14	Renedo et al. (2016)		• In maximum cases, results were very similar. There are no relevant differences	Transient stability

(Continued on following page)

TABLE 1 (*Continued*) Comparison of types of stability with the various existing research studies.

S. no	References	Techniques	Key findings	Type of stability
		It develops a novel active power control strategy for the VSC-HVDC MTDC system by utilizing weighted-average frequency		
15	Yousefian et al. (2017)	Proposed WAC algorithm with "reinforcement learning" (RL) and "neural networks" (NNS)	• By observing the results, WAC increases CCT and stability margins fast	Transient stability
16	Husham et al. (2022)	Decentralized stability enhancement in DFIG	• A data-centric model predictive control (MPC) is proposed to supplementary controlling • Koopman-based model predictive controller (KMPC) design used to design converter controlling technique	Small-signal stability
17	Pan et al. (2018)	The small-signal stability (SSSR) region concept extension to the robust small stability region (RSSSR) wherein the system maintains the stability even during perturbations	• Machine learning employs ML approaches to learn and implement RSSR boundary predictions • The ML approaches learning ability speeds up the computation on boundary significantly and simplifies the robust stability analysis of vast and difficult power systems	Small-signal stability
18	Sadamoto et al. (2018)	Retrofit control	• It designs the decentralized controllers for the DFIGs, which improves the oscillation dampings in the wind-penetrated power systems • The major drawback considered is closed-loop system stability that has not been assured theoretically	Small-signal stability
19	Huang et al. (2020)	Online identification of generalized short circuit ratio	• Using PMU's online stability monitoring is very convenient	Small-signal stability
20	Ma et al. (2017a)	Virtual inertia control of DFIG by considering PLL	• To extend this work for all large-scale interconnected systems during different operating conditions with mechanical inertia on system stability with all aspects	Small-signal stability
21	Ma et al. (2017b)	Robust stochastic stability	• It presents stability improvement methods by considering stochastic parameters with virtual inertia and PLL of DFIG	Small-signal stability
22	Wen et al. (2017)	Decoupled DQ frame dynamics with generalized Nyquist stability criterion (GNC)	• It demonstrates stability studies of various power-electronics devices with characteristics of distributed power systems with the new DQ framework	Small-signal stability
23	Liu et al. (2020a)	Damping solutions for PLL oscillations and their influence factor	• A new mixed damping controller H_2/H∞ was designed for DFIG to minimize PLL oscillations	Small-signal stability
24	Liu et al. (2018a)	It uses the single machine infinite-bus system design	• By new stability criteria, it quantifies SSR stability, which analyzes the features of impedance frequency • Even for wind power systems on a large scale, this proposed system has analyzed the SSR issue	Stability of SSR
25	Karunanayake et al. (2020)	Nonlinear sliding mode control SMC proposed based on mitigation method as sub-synchronous resonance (SSR)	• This proposed method controls the rotor side converter, assuring the sustainability of reactive power and decoupled torque of DFIG control ability to mitigate SSR	Stability of SSR
26	Ma et al. (2020)	Lyapunov stability criteria	• The DFIG dynamic energy was determined with negative gradient intensity, comparing PLL parameters, line resistance, and series compensations to enhance stability	Stability of SSR
27	Rahman et al. (2022)	A probabilistic clustering approach is proposed	• A probabilistic clustering framework that uses four different clustering algorithms to represent the aggregated wind farm model that occurs most frequently over the course of an entire year	Probabilistic stability
28	Chen et al. (2018)	Assessing the probabilistic stability of SSR using piecewise probabilistic collocation method (PPCM) with respect to random wind speed	• Because of the switching among DFIG's various operational modes, the PPCM tackles the inherent nonlinearity	Probabilistic stability of SSR

(Continued on following page)

TABLE 1 (*Continued*) Comparison of types of stability with the various existing research studies.

S. no	References	Techniques	Key findings	Type of stability
29	Bian et al. (2016)	"Modified fruit fly optimization algorithm (MFOA) with a probabilistic approach"	• "Modified fruit fly optimization algorithm" (MFOA) employed • The best coordination between PSS and SVC damping controllers, which improves the entire "probabilistic small-signal stability" of grid integrated wind farms	Probabilistic stability of SSR
30	Wen et al. (2018)	AC/VSC-based MTDC system	• It examines the onshore AC grid and offshore multiterminal DC grid-based voltage source convertor VSC-MTDC operation to improve its frequency stability • Among the GVSCs and WVSCs, the coordinate control approach is expected to be examined	Frequency stability
31	Zhan et al. (2019)	Analysis of frequency-domain modal technique	• For finding electromagnetic oscillations, the frequency-domain method is developed • It is verified on two case studies and verified with EMT simulations	Frequency stability
32	Han et al. (2022)	Discrete-time domain modal analysis	• SSO issues are investigated using discrete-time domain modal analysis • The frequency and damping ratio in the discrete-time domain calculated • Eigenvalues calculated in depth by using participation factors	Frequency stability
33	Toulabi et al. (2018)	Supplementary frequency optimal controller designed	• A proportional-derivative frequency controller is proposed and tested in a wind farm with several VSWTs	Frequency stability
34	Yang et al. (2022)	Power compensation control schemes proposed for power converters	• In order to compensate for the power loss on the network, the active power of WT is subject to control	Frequency stability
35	Li et al. (2021)	SMES-based damping controller is designed	• In the article, a finite Markov decision process is utilized and an agent that is based on deep reinforcement learning (DRL) is selected in order to obtain the optimal parameters	Frequency stability
36	Shi et al. (2019)	Wind power penetrated power system's robust stability analysis is investigated	• Dynamic stability (D-stability) issue analyzed by focusing on the constraint of damping ratio for power system analysis	Dynamic stability
37	Li et al. (2019)	Feedback control approaches were appropriate for vector-based voltage source converters and engaged in type-3 and type-4 wind testbeds	• The feedback control approaches modulate the order of DC-link voltage and power order • Finally, the efficient capability of stability improvement is seen with further enhancement in wind power delivery	Dynamic stability
38	Nian and Pang (2019)	When a harmonic grid with parallel compensation joins the DFIG system, the harmonics and high-frequency resonance (HFR) exhibiting the frequency range may show intersections	• Coupling among harmonics suppression control and HFR damping control leads to an unstable situation of the DFIG system	Dynamic stability
39	Xiong et al. (2019)	An optimal virtual inertia planning approach for power system stability improvement	• The non-convex optimization issue followed from the homogeneity of stability margin is solved by using the Lyapunov function • To evaluate the performance and effectiveness of the current study, it uses IEEE 118-bus system and a 12-bus system	Dynamic stability
40	Liu et al. (2020b)	DFIG-based wind turbines during low voltage	• The instability process of the DFIG system during the process of weak grid fault, a model based on the small-signal state has been specified	Dynamic stability
41	Muftau et al. (2020)	For permanent magnet synchronous generator that depends on wind turbines, the virtual synchronous	• It uses linear and nonlinear models	Dynamic stability

(Continued on following page)

TABLE 1 (*Continued*) Comparison of types of stability with the various existing research studies.

S. no	References	Techniques	Key findings	Type of stability
		machine (VSM) is proposed in this article that allows continuous operation in all operating modes	• It recognizes the VSM's design guidelines and operational limits	
42	Li et al. (2016)	"Lyapunov stability theory" and "linear matrix inequality" (LMI) method	• By utilizing Lyapunov stability theory, it designs a new Hꝏ controller	Dynamic stability
43	Wang et al. (2017)	Developed "deterministic hybrid model" (DHM) for the "stochastic hybrid model" (SHM)	• By considering various uncertainties to extend this work with this framework further to studying the stability analysis of power systems	Dynamic stability
44	Shi et al. (2018)	Developed a rational fractional representation technique	• Focused on the analysis of parametric stability	Parametric stability
			• The power system's robust stability	
			• Exhibits a rational fractional uncertainty	
			• It considers only a single DFIG for analysis	
45	Jalali and Aldeen (2019)	Energy storage services (ESS) in wind intensive power distributed generation and voltage stability	• For ESS size minimization, the expected voltage stability margin (VSM) should be attained	Voltage stability
			• Active network management (ANM) tools and constraints of voltage stability for minimization, which it considers as risk-based	
46	Liu et al. (2018b)	Proposed STATCOMs techniques for the optimal dynamic VAR devices with multi-objective optimization techniques	• The power system upgraded with penetration of higher wind power and greater retirement of equipment	Voltage stability
47	Kawabe et al. (2017)	A novel dynamic voltage support (DVS) capability	• It improves short-term voltage stability of PV farm with novel DVS capability	Voltage stability
48	Souxes et al. (2020)	Emergency maximum reactive	• Long-term voltage stability of wind farms tested	Voltage stability
		Support control scheme		
49	Milano (2016)	Computational current and power injection models	• The proposed formulation for current and power injection methods for angle and voltage stability	Voltage stability
50	Du et al. (2019)	The modal proximity avoided by this proposed article which assisted VSG design parameters	• After setting the VSG parameters, it evaluates the two-subsystem modal proximity and avoids VSG due to the harmful effect of small-signal angular stability's decrease in the power system	Small-signal angular stability
51	Ma et al. (2017c)	Cascading failure	• It proposes the discrete Markov power system model considering cascading failure during different operating conditions for determining angle stability of power system	Small-signal angular stability
52	Zhang et al. (2020)	The novel virtual inertia control approach is investigated in this study for wind turbines that enhances the rotor angle stability of the first swing in the interconnected power grid	• It simulates two DFIG-based wind farms and four traditional power plants	Rotor angle stability
53	Majumder (2013)	Improvement of various types of stability issues in microgrids	• It describes different types of microgrid stability studies with enhanced methods	Microgrid stability
54	Bhosale and Agarwal, (2019)	For ultracapacitor, it proposes the fuzzy logic-based novel scheme for power flow control	• It can enhance with AI and machine learning	Microgrid stability
55	Wang et al. (2018b)	Designed a damper controller placed at the converter station of the HVDC link	• A grid-connected microgrid structure consisting of a large DFIG "offshore wind farm," PMSG-based "offshore tidal farm," and DFIG-based "seashore wave farm," stability improvement, and power flow control methods proposed	Microgrid stability
56	Puchalapalli et al. (2020)	"Rotor side VSC and bidirectional buck-boost converter" proposed	• A microgrid is developed consisting of DFIG, DG, and solar PV array with BES, and steady-state and dynamic performance of the microgrid studied	Microgrid stability

(Continued on following page)

TABLE 1 (*Continued*) Comparison of types of stability with the various existing research studies.

S. no	References	Techniques	Key findings	Type of stability
57	Xia et al. (2022)	"Large-signal stability analysis and control in AC microgrid"	• The nonlinear reduced-order model of small-scale alternating current microgrids with a single storage is established as valid	Microgrid stability
58	Krismanto et al. (2021)	Grid-connected microgrid stability in uncertain RES	• Monte Carlo (MC) simulation is proposed to determine the eigenvalues of the system	Microgrid stability
59	Mohamed et al. (2022)	"Enhancement the frequency stability and protection of interconnected microgrid"	• A fractional order load frequency controller with superconducting magnetic energy storage (SMES) virtual inertia system is used to assess and improve digital frequency relay coordination	Microgrid stability
60	Zhang et al. (2021)	"Voltage-based segmented control of superconducting magnetic energy storage in DC microgrid"	• Voltage-based segment control is used to improve the transient stability of DC microgrid when the DC voltage deviation is within the tolerant range • VBS control allows SMES to function in the energy storage mode	Microgrid stability

Hence, the table elaborates the comparative analysis of various references in terms of types of stability, and the data analysis is depicted in a diagrammatic form in Figure 9.

TABLE 2 Different controllers used to improve the various types of stability.

S. no	Type of stability	Type of controller
1	Transient stability	P, PI, and PID-SDC fuzzy controllers
2	Small-signal stability	P, PI, robust controller, H2 and H∞ controller
3	Stability of SSR	PI and H∞ controller
4	Frequency stability	PI, PID, and optimal frequency damping controller
5	Dynamic stability	PI, high-frequency resonance damping control, and H∞ controller
6	Parametric stability	PI, robust controller, fuzzy controller, and H2 and H∞ controller
7	Small-signal angular stability	Fuzzy controller, PI, robust controller, and H2 and H∞ controller
8	Voltage stability	PI, PID, and fuzzy controller
9	Probabilistic stability of SSR	Optimal PI, PID, fuzzy controllers
10	Rotor angle stability	Robust controller, fuzzy controller, and H2 and H∞ controller

Mohamed et al. (2022) explored frequency stability enhancement in an interconnected microgrid. This article uses a fractional order load frequency controller with superconducting magnetic energy storage (SMES) virtual inertia system to assess and improve digital frequency relay coordination. Optimized fractional order controller based on slime mould optimization algorithm improves the coordination method (SMA). In the study by Zhang et al. (2021), voltage-based segment control was used to enhance the transient stability of the DC microgrid. When the DC voltage deviation is within the tolerant range, the VBS control allows SMES to function in the energy storage mode. When the voltage is outside the normal range because of transient power fluctuations, the SMES will carry out transient power regulation.

Hence, the above stated references have been reviewed based on types of stability, and the results of all the analyses are validated using the simulation method, namely, MATLAB/SIMULINK.

3 Comparison analysis

The following section describes the type of stability related to wind power in the power system, comparatively analyzed further and briefly tabulated below in Table 1.

Figure 9 depicts the type of stability used in every referenced article and states that transient stability is analyzed primarily in most research studies for other types of stability.

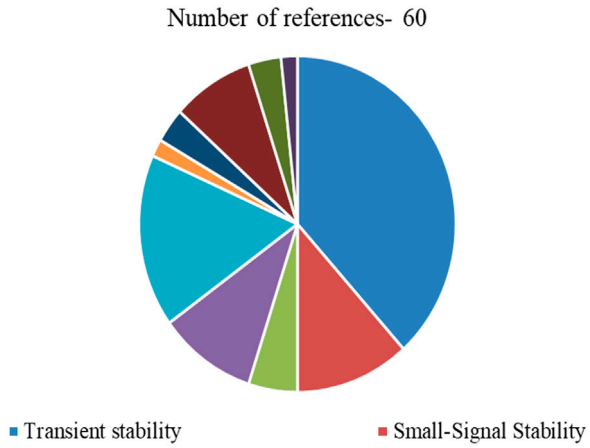

FIGURE 9
Types of stability reviewed.

Table 2 represents the different controllers used to improve the various types of stability.

4 Conclusion

This article gives a concise summary of power system stability issues in large-scale wind-integrated power systems. The increasing wind power penetration has shown several challenges toward the stability types in power system generation due to uncertainty of wind speed. The system dynamic depicts variations in the performance of wind turbines that was also seen in this proposed study. This proposed review focused mainly on the types of stability toward the penetration in wind power generation systems. In most research works, a comparative analysis of sustainability has shown that transient stability has been substantially analyzed and compared with other types of stability like parametric stability, dynamic stability, frequency stability, and others. In recent years, many researchers have focused their studies on stability issues of renewable energy sources–based microgrids. It is the new trend in investigating the stability problems of microgrids. In the future, several other types of stability and analyses of the respective simulations and of their results should be studied in depth.

Author contributions

VY: conceptualization, methodology, software, formal analysis, writing—original draft, and data curation. BS: conceptualization, methodology, validation, investigation, resources, writing—review and editing, visualization, supervision, and project administration.

Conflict of interest

The authors declare that the research was conducted in the absence of any commercial or financial relationships that could be construed as a potential conflict of interest.

Publisher's note

All claims expressed in this article are solely those of the authors and do not necessarily represent those of their affiliated organizations, or those of the publisher, editors, and reviewers. Any product that may be evaluated in this article, or claim that may be made by its manufacturer, is not guaranteed or endorsed by the publisher.

References

Bhosale, R., and Agarwal, V. (2019). Fuzzy logic control of the ultracapacitor interface for enhanced transient response and voltage stability of a dc microgrid. *IEEE Trans. Ind. Appl.* 55 (1), 712–720. doi:10.1109/TIA.2018.2870349

Bian, X. Y., Geng, Y., Lo, K. L., Fu, Y., and Zhou, Q. B. (2016). Coordination of PSSs and SVC damping controller to improve probabilistic small-signal stability of power system with wind farm integration. *IEEE Trans. Power Syst.* 31 (3), 2371–2382. doi:10.1109/TPWRS.2015.2458980

Chen, W., Xie, X., Wang, D., Liu, H., and Liu, H. (2018). Probabilistic stability analysis of subsynchronous resonance for series-compensated DFIG-based wind farms. *IEEE Trans. Sustain. Energy* 9 (1), 400–409. doi:10.1109/TSTE.2017.2737599

Datta, U., Kalam, A., and Shi, J. (2019). Battery energy storage system to stabilize transient voltage and frequency and enhance power export capability. *IEEE Trans. Power Syst.* 34 (3), 1845–1857. doi:10.1109/TPWRS.2018.2879608

Du, W., Fu, Q., and Wang, H. F. (2019). Power system small-signal angular stability affected by virtual synchronous generators. *IEEE Trans. Power Syst.* 34 (4), 3209–3219. doi:10.1109/TPWRS.2019.2896149

Eshkaftaki, A. A., Rabiee, A., Kargar, A., and Boroujeni, S. T. (2020). An applicable method to improve transient and dynamic performance of power system equipped with DFIG-based wind turbines. *IEEE Trans. Power Syst.* 35 (3), 2351–2361. doi:10.1109/TPWRS.2019.2954497

Han, Y., Sun, H., Huang, B., and Qin, S. (2022). Discrete-time domain modal analysis of oscillatory stability of renewables integrated power systems. *IEEE Trans. Power Deliv.* 37 (5), 4248–4260. doi:10.1109/TPWRD.2022.3148187

Huang, L., Xin, H., Li, Z., Ju, P., Yuan, H., and Wang, G. (2020). Identification of generalized short-circuit ratio for on-line stability monitoring of wind farms. *IEEE Trans. Power Syst.* 35 (4), 3282–3285. doi:10.1109/TPWRS.2020.2975413

Hui, Q., Yang, J., Yang, X., Chen, Z., Li, Y., and Teng, Y. (2019). A robust control strategy to improve transient stability for AC-DC interconnected power system

with wind farms. *CSEE J. Power Energy Syst.* 5, 259. doi:10.17775/CSEEJPES.2019.00250

Husham, A., Kamwa, I., Abido, M. A., and Supreme, H. (2022). Decentralized stability enhancement of DFIG-based wind farms in large power systems: Koopman theoretic approach. *IEEE Access* 10, 27684–27697. doi:10.1109/ACCESS.2022.3157747

Jalali, A., and Aldeen, M. (2019). Risk-based stochastic allocation of ESS to ensure voltage stability margin for distribution systems. *IEEE Trans. Power Syst.* 34 (2), 1264–1277. doi:10.1109/TPWRS.2018.2873774

Jiang, H., and Zhang, C. (2019). A method of boosting transient stability of wind farm connected power system using S magnetic energy storage unit. *IEEE Trans. Appl. Supercond.* 29 (2), 1–5. doi:10.1109/TASC.2019.2892291

Karunanayake, C., Ravishankar, J., and Dong, Z. Y. (2020). Nonlinear SSR damping controller for DFIG based wind generators interfaced to series compensated transmission systems. *IEEE Trans. Power Syst.* 35 (2), 1156–1165. doi:10.1109/TPWRS.2019.2938230

Kawabe, K., Ota, Y., Yokoyama, A., and Tanaka, K. (2017). Novel dynamic voltage support capability of photovoltaic systems for improvement of short-term voltage stability in power systems. *IEEE Trans. Power Syst.* 32 (3), 1796–1804. doi:10.1109/TPWRS.2016.2592970

Krismanto, A. U., Mithulananthan, N., Setiadi, H., Setyawan, E. Y., and Abdillah, M. (2021). Impacts of grid-tied microgrid on stability and interaction of power systems considering RE uncertainties. *Sustain. Energy, Grids Netw.* 28, 100537. doi:10.1016/j.segan.2021.100537

Li, J., Chen, Z., Cai, D., Zhen, W., and Huang, Q. (2016). Delay-dependent stability control for power system with multiple time-delays. *IEEE Trans. Power Syst.* 31 (3), 2316–2326. doi:10.1109/TPWRS.2015.2456037

Li, T., Hu, W., Zhang, B., Zhang, G., Zhang, Z., and Chen, Z. (2021). SMES damping controller design and real-time parameters tuning for low-frequency oscillation. *IEEE Trans. Appl. Supercond.* 31 (8), 1–4. doi:10.1109/TASC.2021.3099759

Li, Y., Fan, L., and Miao, Z. (2019). Stability control for wind in weak grids. *IEEE Trans. Sustain. Energy* 10 (4), 2094–2103. doi:10.1109/TSTE.2018.2878745

Liu, H., Xie, X., Gao, X., Liu, H., and Li, Y. (2018). Stability analysis of SSR in multiple wind farms connected to series-compensated systems using impedance network model. *IEEE Trans. Power Syst.* 33 (3), 3118–3128. doi:10.1109/TPWRS.2017.2764159

Liu, J., Xu, Y., Dong, Z. Y., and Wong, K. P. (2018). Retirement-driven dynamic VAR planning for voltage stability enhancement of power systems with high-level wind power. *IEEE Trans. Power Syst.* 33 (2), 2282–2291. doi:10.1109/TPWRS.2017.2732441

Liu, J., Yao, W., Wen, J., Fang, J., Jiang, L., He, H., et al. (2020). Impact of power grid strength and PLL parameters on stability of grid-connected DFIG wind farm. *IEEE Trans. Sustain. Energy* 11 (1), 545–557. doi:10.1109/TSTE.2019.2897596

Liu, R., Yao, J., Wang, X., Sun, P., Pei, J., and Hu, J. (2020). Dynamic stability analysis and improved LVRT Schemes of DFIG-Based wind turbines during a symmetrical fault in a weak grid. *IEEE Trans. Power Electron.* 35 (1), 303–318. doi:10.1109/TPEL.2019.2911346

Liu, Y., Wu, Q. H., Kang, H., and Zhou, X. (2016). Switching power system stabilizer and its coordination for enhancement of multi-machine power system stability. *CSEE Power Energy Syst.* 2 (2), 98–106. doi:10.17775/CSEEJPES.2016.00027

Ma, J., Qiu, Y., Li, Y., Zhang, W., Song, Z., and Thorp, J. S. (2017). Research on the impact of DFIG virtual inertia control on power system small-signal stability considering the phase-locked loop. *IEEE Trans. Power Syst.* 32 (3), 2094–2105. doi:10.1109/TPWRS.2016.2594781

Ma, J., Shen, Y., and Phadke, A. G. (2020). Stability assessment of DFIG subsynchronous oscillation based on energy dissipation intensity analysis. *IEEE Trans. Power Electron.* 35 (8), 8074–8087. doi:10.1109/TPEL.2019.2962217

Ma, J., Song, Z., Zhang, Y., Zhao, Y., and Thorp, J. S. (2017). Robust stochastic stability analysis method of DFIG integration on power system considering virtual inertia control. *IEEE Trans. Power Syst.* 32 (5), 4069–4079. doi:10.1109/TPWRS.2017.2657650

Ma, J., Wang, S., Qiu, Y., Li, Y., Wang, Z., and Thorp, J. S. (2017). Angle stability analysis of power system with multiple operating conditions considering cascading failure. *IEEE Trans. Power Syst.* 32 (2), 1–882. doi:10.1109/TPWRS.2016.2566672

Ma, J., Zhao, D., Yao, L., Qian, M., Yamashita, K., and Zhu, L. (2018). Analysis on application of a current-source based DFIG wind generator model. *CSEE J. Power Energy Syst.* 4 (3), 352–361. doi:10.17775/CSEEJPES.2018.00060

Ma, S. K., Geng, H., Liu, L., Yang, G., and Pal, B. C. (2018). Grid-synchronization stability improvement of large scale wind farm during severe grid fault. *IEEE Trans. Power Syst.* 33 (1), 216–226. doi:10.1109/TPWRS.2017.2700050

Majumder, R. (2013). Some aspects of stability in microgrids. *IEEE Trans. Power Syst.* 28 (3), 3243–3252. doi:10.1109/TPWRS.2012.2234146

Milano, F. (2016). On current and power injection models for angle and voltage stability analysis of power systems. *IEEE Trans. Power Syst.* 31 (3), 2503–2504. doi:10.1109/TPWRS.2015.2449765

Mohamed, E. A., Aly, M., Elmelegi, A., Ahmed, E. M., Watanabe, M., and Said, S. M. (2022). Enhancement the frequency stability and protection of interconnected microgrid systems using advanced hybrid fractional order controller. *IEEE Access* 10, 111936–111961. doi:10.1109/ACCESS.2022.3216212

Muftau, B., Fazeli, M., and Egwebe, A. (2020). Stability analysis of a PMSG based virtual synchronous machine. *Electr. Power Syst. Res.* 180, 106170. doi:10.1016/J.EPSR.2019.106170

Nian, H., and Pang, B. (2019). Stability and power quality enhancement strategy for DFIG system connected to harmonic grid with parallel compensation. *IEEE Trans. Energy Convers.* 34 (2), 1010–1022. doi:10.1109/TEC.2018.2866619

Ortega, Á., and Milano, F. (2018). Stochastic transient stability analysis of transmission systems with inclusion of energy storage devices. *IEEE Trans. Power Syst.* 33 (1), 1077–1079. doi:10.1109/TPWRS.2017.2742400

Pan, Y., Liu, F., Chen, L., Wang, J., Qiu, F., Shen, C., et al. (2018). Towards the robust small-signal stability region of power systems under perturbations such as uncertain and volatile wind generation. *IEEE Trans. Power Syst.* 33 (2), 1790–1799. doi:10.1109/TPWRS.2017.2714759

Pico, H. N. V., and Johnson, B. B. (2019). Transient stability assessment of multi-machine multi-converter power systems. *IEEE Trans. Power Syst.* 34 (5), 3504–3514. doi:10.1109/TPWRS.2019.2898182

Puchalapalli, S., Tiwari, S. K., Singh, B., and Goel, P. K. (2020). A microgrid based on wind-driven DFIG, DG, and solar PV array for optimal fuel consumption. *IEEE Trans. Ind. Appl.* 56 (5), 4689–4699. doi:10.1109/TIA.2020.2999563

Rahman, M. T., Hasan, K. N., and Sokolowski, P. (2022). Evaluation of wind farm aggregation using probabilistic clustering algorithms for power system stability assessment. *Sustain. Energy, Grids Netw.* 30, 100678. doi:10.1016/j.segan.2022.100678

Renedo, J., Garcia-Cerrada, A., and Rouco, L. (2016). Active power control strategies for transient stability enhancement of AC/DC grids with VSC-HVDC multi-terminal systems. *IEEE Trans. Power Syst.* 31 (6), 4595–4604. doi:10.1109/TPWRS.2016.2517215

Sadamoto, T., Chakrabortty, A., Ishizaki, T., and Imura, J. I. (2018). Retrofit control of wind-integrated power systems. *IEEE Trans. Power Syst.* 33 (3), 2804–2815. doi:10.1109/TPWRS.2017.2750411

Shi, P., Jiang, C., Gan, D., Xin, H., Jia, L., Gao, X., et al. (2019). New value set approach for robust stability of power systems with wind power penetration. *IEEE Trans. Sustain. Energy* 10 (2), 811–821. doi:10.1109/TSTE.2018.2848703

Shi, P., Zhou, J., Gan, D., and Wang, Z. (2018). A rational fractional representation method for wind power integrated power system parametric stability analysis. *IEEE Trans. Power Syst.* 33 (6), 7122–7131. doi:10.1109/TPWRS.2018.2849400

Souxes, T., Parasidis, A., and Vournas, C. D. (2020). Stabilizing controls for wind generators participating in transmission V/Q support. *IEEE Trans. Power Syst.* 35 (5), 3627–3635. doi:10.1109/TPWRS.2020.2974956

Tang, W., Hu, J., Chang, Y., and Liu, F. (2018). Modeling of DFIG-based wind turbine for power system transient response analysis in rotor speed control timescale. *IEEE Trans. Power Syst.* 33 (6), 6795–6805. doi:10.1109/TPWRS.2018.2827402

Toulabi, M., Bahrami, S., and Ranjbar, A. M. (2018). Optimal supplementary frequency controller design using the wind farm frequency model and controller parameters stability region. *ISA Trans.* 74, 175–184. doi:10.1016/j.isatra.2018.01.011

Wang, L., Lin, C. Y., Wu, H. Y., and Prokhorov, A. V. (2018). Stability analysis of a microgrid system with a hybrid offshore wind and ocean energy farm fed to a power grid through an HVDC link. *IEEE Trans. Ind. Appl.* 54 (3), 2012–2022. doi:10.1109/TIA.2017.2787126

Wang, L., Vo, Q. S., and Prokhorov, A. V. (2018). Stability improvement of a multimachine power system connected with a large-scale hybrid wind-photovoltaic farm using a supercapacitor. *IEEE Trans. Ind. Appl.* 54 (1), 50–60. doi:10.1109/TIA.2017.2751004

Wang, X., Wang, T., Chiang, H. D., Wang, J., and Liu, H. (2017). A framework for dynamic stability analysis of power systems with volatile wind power. *IEEE J. Emerg. Sel. Top. Circuits Syst.* 7 (3), 422–431. doi:10.1109/JETCAS.2017.2657627

Wen, B., Burgos, R., Boroyevich, D., Mattavelli, P., and Shen, Z. (2017). AC stability analysis and <italic>dq</italic> frame impedance specifications in power-electronics-based distributed power systems. *IEEE J. Emerg. Sel. Top. Power Electron.* 5 (4), 1455–1465. doi:10.1109/JESTPE.2017.2728640

Wen, Y., Zhan, J., Chung, C. Y., and Li, W. (2018). Frequency stability enhancement of integrated AC/VSC-MTDC systems with massive infeed of offshore wind generation. *IEEE Trans. Power Syst.* 33 (5), 5135–5146. doi:10.1109/TPWRS.2018.2792906

Xia, Y., Lv, Z., Wei, W., and He, H. (2022). Large-signal stability analysis and control for small-scale AC microgrids with single storage. *IEEE J. Emerg. Sel. Top. Power Electron.* 10 (4), 4809–4820. doi:10.1109/JESTPE.2021.3135892

Xiong, L., Li, P., Wu, F. W., and Wang, J. (2019). Stability enhancement of power systems with high DFIG-wind turbine penetration via virtual inertia planning. *IEEE Trans. Power Syst.* 34 (2), 1352–1361. doi:10.1109/TPWRS.2018.2869925

Xu, Y., Yin, M., Dong, Z. Y., Zhang, R., Hill, D. J., and Zhang, Y. (2018). Robust dispatch of high wind power-penetrated power systems against transient instability. *IEEE Trans. Power Syst.* 33 (1), 174–186. doi:10.1109/TPWRS.2017.2699678

Yang, Y., Zhu, D., Zou, X., Chi, Y., and Kang, Y. (2022). Power compensation control for DFIG-based wind turbines to enhance synchronization stability during severe grid faults. *IEEE Trans. Power Electron.* 37 (9), 10139–10143. doi:10.1109/TPEL.2022.3168883

Yousefian, R., Bhattarai, R., and Kamalasadan, S. (2017). Transient stability enhancement of power grid with integrated wide area control of wind farms and synchronous generators. *IEEE Trans. Power Syst.* 32 (6), 4818–4831. doi:10.1109/TPWRS.2017.2676138

Yu, J. J. Q., Hill, D. J., Lam, A. Y. S., Gu, J., and Li, V. O. K. (2018). Intelligent time-adaptive transient stability assessment system. *IEEE Trans. Power Syst.* 33 (1), 1049–1058. doi:10.1109/TPWRS.2017.2707501

Zhan, Y., Xie, X., Liu, H., Liu, H., and Li, Y. (2019). Frequency-domain modal analysis of the oscillatory stability of power systems with high-penetration renewables. *IEEE Trans. Sustain. Energy* 10 (3), 1534–1543. doi:10.1109/TSTE.2019.2900348

Zhang, T. L., Zhou, Q., Mu, S., Li, H., Li, Y. J., and Wang, J. (2021). Voltage-based segmented control of superconducting magnetic energy storage for transient power fluctuation suppression in Island DC microgrid. *IEEE Trans. Appl. Supercond.* 31 (8), 1–5. doi:10.1109/TASC.2021.3101760

Zhang, X., Zhu, Z., Fu, Y., and Li, L. (2020). Optimized virtual inertia of wind turbine for rotor angle stability in interconnected power systems. *Electr. Power Syst. Res.* 180, 106157. doi:10.1016/J.EPSR.2019.106157

frontiers | Frontiers in Energy Research

TYPE Original Research
PUBLISHED 23 December 2022
DOI 10.3389/fenrg.2022.1102898

OPEN ACCESS

EDITED BY
Sarat Kumar Sahoo,
Parala Maharaja Engineering College (P.M.E.C), India

REVIEWED BY
Balamurugan M,
Dayananda Sagar College of Engineering, India
Saroj Padhan,
Parala Maharaja Engineering College (P.M.E.C), India
Saravanan B,
VIT University, India

*CORRESPONDENCE
Ashutosh Biswal,
linku.ashutosh@gmail.com

SPECIALTY SECTION
This article was submitted to Smart Grids, a section of the journal Frontiers in Energy Research

RECEIVED 19 November 2022
ACCEPTED 12 December 2022
PUBLISHED 23 December 2022

CITATION
Biswal A, Dwivedi P and Bose S (2022), DE optimized IPIDF controller for management frequency in a networked power system with SMES and HVDC link. *Front. Energy Res.* 10:1102898. doi: 10.3389/fenrg.2022.1102898

DE optimized IPIDF controller for management frequency in a networked power system with SMES and HVDC link

Ashutosh Biswal*, Prakash Dwivedi and Sourav Bose

Department of Electrical Engineering, National Institute of Technology (NIT), Uttarakhand, India

A major concern is frequency change with load. So, Load Frequency Control (LFC) of an interconnected power system is proposed in this research using a unique integral plus proportional integral derivative controller with filter (IPIDF). The Differential Evolution (DE) algorithm is used to optimize the integral plus proportional integral derivative controller with filter controller parameters for a two-area power system. By contrasting the results of the proposed method with those of recently published optimization techniques for the same power system, such as the Particle Swarm Optimization (PSO), Genetic Algorithm (GA), Firefly Algorithm (FA), and Differential Evolution (DE) based Proportional integral derivative (PID) and PIDF controllers, the superiority of the integral plus proportional integral derivative controller with filter approach is made clear. It is possible to determine the system performance index like integral time multiplied the absolute error (ITAE) and the settling time (Ts). The power system with superconducting magnetic energy storage and an HVDC link is also included in the proposed work, and the values of the suggested integral plus proportional integral derivative controller with filter controllers are evaluated using the Differential Evolution method. By comparing the outcomes with the Differential Evolution tuned PIDF controller for the identical power systems, the suggested controller's superiority is demonstrated. To show the stability of the recommended Differential Evolution algorithm tuned integral plus proportional integral derivative controller with filter controller, the speed governor, turbine, synchronizing coefficient, and frequency bias parameters' time constants and operating load conditions are varied in the range of +25 to −25% from their nominal values, along with the magnitude and location of step load perturbation and pulse load perturbation, to perform sensitivity analysis. According to research, proposed integral plus proportional integral derivative controller with filter controllers offer greater dynamic response by minimizing time required to settle and undershoots than Proportional integral derivative controllers and PIDF controllers. MATLAB/Simulink is used to run the simulations.

KEYWORDS

load frequency control (LFC), differential evolution (DE) algorithm, proportional integral derivative (PID), integral plus proportional integral derivative controller with filter (IPIDF), superconducting magnetic energy storage system (SMES)

1 Introduction

Frequency drift with load is a major concern. Total generation equals the sum of load power and losses under steady state conditions. However, a user who is uninformed of the creation alters the load at random. Any imbalance between supply and demand has a direct impact on rotor speed, and consequently, system frequency. A shift in frequency and power flow in tie line results from the majority of systems being interconnected. Since maintaining the balance between supply and load is particularly challenging, a good controlling mechanism is needed to maintain the system frequency within the desired range. One such control is load frequency control (LFC), which attempts to reduce frequency deviation by reducing steady state error to zero while regulating the producing units' active power (Elgerd, 2000; Ram Babu and Saikia, 2021; Soni et al., 2021; Peng, 2022). For the purpose of lowering the frequency and power of tie line fluctuation in the load frequency control problem, the area control error is sent to the controller (Karn et al., 2022; Yang et al., 2022).

The power system will be out of equilibrium as a result of the continuous rise in load demand; as a result, the frequency of the system continues to drop until it reaches its lowest allowable value (Sun and Duan, 2022). Subsequently, a further rise in load will cause more frequent drops, necessitating the use of load shedding. If we employ an energy storage system or another source of power supply in addition to the electricity generated by the system, load shedding can be avoided. In a superconducting magnetic energy storage system (SMES), energy is retained in a superconducting coil by use of a magnetic field (Padhan et al., 2014a). The direct current (DC) passing through the coil is what generates the magnetic field. In order to transport the current, the conductor needs to be sufficiently cooled. At cryogenic temperatures, where it is a superconductor and has almost no resistive losses, the conductor generates the magnetic field. Superconducting Magnetic Energy Storage (SMES), an active power source with a quick response that can absorb frequency fluctuations, is extremely successful at enhancing the power system's dynamic performance. The governor system's slow response prevents it from doing so (Luo et al., 2021). The frequency regulation of a networked system with SMES has been documented in the literature (Banerjee et al., 1990; Sudha and Vijaya, 2012; Luo et al., 2021) for enhancing system performance. There have been reports in the literature (Dekaraja, Chandra Saikia; Wang et al., 2021) about the effects of various FACTS controllers for AGC when used in conjunction with SMES (Luo et al., 2021).

Researchers throughout the world suggest a number of LFC solutions to keep the power flow in tie line and frequency at their specified levels throughout normal operation and even in the presence of minor fluctuations (Sahu et al., 2016). Compares the performance of a number of classical controller structures used in the AGC for multi-area interconnected thermal systems, including the integral (I), proportional integral (PI), integral derivative (ID), PID, and integral double derivative (IDD) (Luo et al., 2021). Over the past few decades, numerous scholars have suggested various control strategies for LFC of power systems (Sahu et al., 2016; Ahmed et al., 2022; El-Ela et al., 2022). Recently Rabindra et al. (Sahu et al., 2016), proposed a TIDF controller in a three unequal area interconnected power system and then TCSC is installed in tie line and performance of the TIDF controller is investigated with GA (Ali and Abd-Elazim, 2011), BFOA (Ali and Abd-Elazim, 2011), PSO (Panda et al., 2013), FA-PID (Padhan et al., 2014b) and DE-PID (Sahu et al., 2016).

Storm and Price first presented the population-based stochastic search technique called Differential Evolution (DE) in 1995 (Stron and Prince, 1995). With only a few, easily selectable control parameters, this global optimization technique can handle objective functions that are non-differentiable, non-linear, and multimodal. The Greedy selection process was employed in DE algorithm with inherent elitist features. The literature review makes it abundantly evident that the controller structure as well as the artificial intelligence approaches used have an impact on the system's performance. In light of the aforementioned, an attempt has been made to create the best DE-based IPIDF controller for the LFC of a power system in this work.

In light of the foregoing survey:

(a) To study Load frequency control
(b) To successfully implement the DE algorithms in the Simulink models.
(c) To develop a simple two area power system with a thermal unit in each area utilizing a new IPIDF controller.
(d) To illustrate the benefits of the proposed IPIDF controller over the PID controller.
(e) To perform a sensitivity study by altering the system's attributes from their actual range in order to examine the suggested controller's resilience.
(f) To conduct robustness analysis to examine the effectiveness of the system by varying load pattern.

2 Materials and methods

2.1 Power system under investigation

In this paper, a commonly used non-reheat thermal power plant connected by tie-line is considered for system under study (Ali and Abd-Elazim, 2011; Panda et al., 2013; Padhan et al., 2014b; Sahu et al., 2016). A speed-governing system, a turbine, and a generator are present in each section

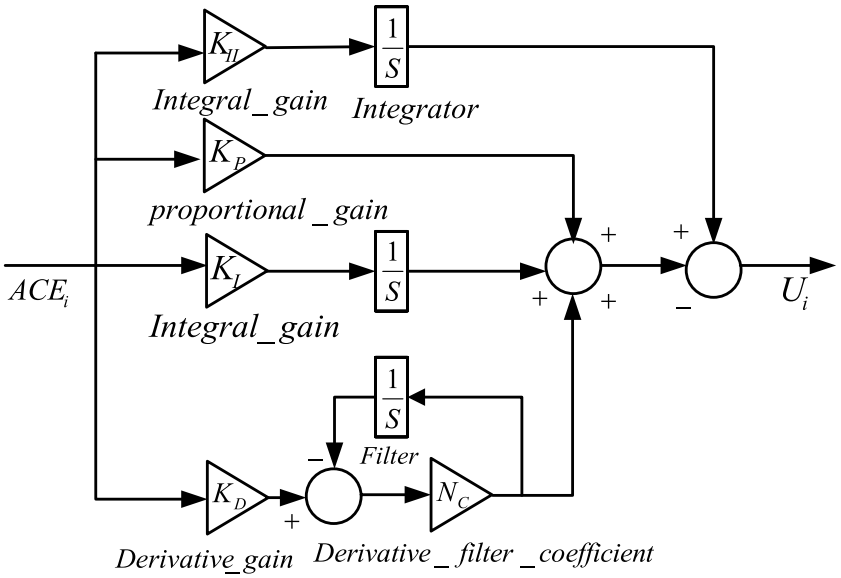

FIGURE 1
Controller structure for IPIDF.

of a power plant having two outputs and three inputs. The inputs are the tie-line power error (ΔP_{Tie}), load disturbance (ΔP_D), and controller input (written as u). Area Control Error and Generator Frequency (ΔF) are the outputs (ACE). Each area has a rating of 2000 MW and a nominal load of 1,000 MW. ACE_1 and ACE_2 are area control errors; B_1 and B_2 are the frequency bias parameters; u_1 and u_2 are the control outputs from the controller; R_1 and R_2 are the governor speed regulation parameters in p.u. Hz; T_{G1} and T_{G2} are the speed governor time constants in sec; T_{T1} and T_{T2} are the turbine time constant in sec; ΔP_{D1} and ΔP_{D2} are the load demand changes; ΔP_{Tie} is the incremental change in tie line power in p.u; K_{P1} and K_{P2} are the power system gains; T_{P1} and T_{P2} are the power system time constant in sec; T_{12} is the synchronizing coefficient and ΔF_1 and ΔF_2 are the system frequency deviations in Hz. The nominal parameters of the system are given in Appendix.

2 2 The controller architecture and purpose

The two-area power system has IPIDF controllers available in each region to regulate the frequency. Standard PID controllers with static values do not offer satisfactory accuracy across a wide variety of operating situations (Sahu et al., 2016). IPIDF controller design therefore enters the picture for the purpose of enhancing system performance. The IPIDF controller combines the PIDF controller and the traditional I controller. Where KII is the I controller's integral gain.

In contrast to PID controller, IPIDF controller is displayed in Figure 1. It has a transient response to instruction intake ratio that is good over a larger range of plant component fluctuation, is simple to calibrate, and has more reliable regulation. In addition to being simpler than PID, IPIDF designing and tuning is also quicker. The transfer function of the IPIDF controller is shown in Eq. 1.

$$TF_{I-PIDF} = \frac{K_{II}}{s} + K_P + \frac{K_I}{s} + K_D\left(\frac{N_C s}{s + N_C}\right) \tag{1}$$

In order to build controllers that use optimization techniques and to fine-tune controller parameters in accordance with performance indices, objective functions are used. Control designs often employ one of four basic types of objective functions (Shabani et al., 2013). The target function ITAE is used in this paper because it shortens peak overshoot and settling rate. It cannot be done using IAE or ISE-based correction, though. The mathematical formulas for the ITAE are shown in Eq. 2 (Sahu et al., 2016).

$$J = ITAE = \int_0^{t_{sim}} \left(|\Delta f_1| + |\Delta f_2| + |\Delta P_{Tie}|\right) \cdot t \cdot dt \tag{2}$$

3 Differential evolution

The Differential Evolution (DE) algorithm, a straightforward, effective, and dependable heuristic search technique with minimal coding, was first introduced by Storn

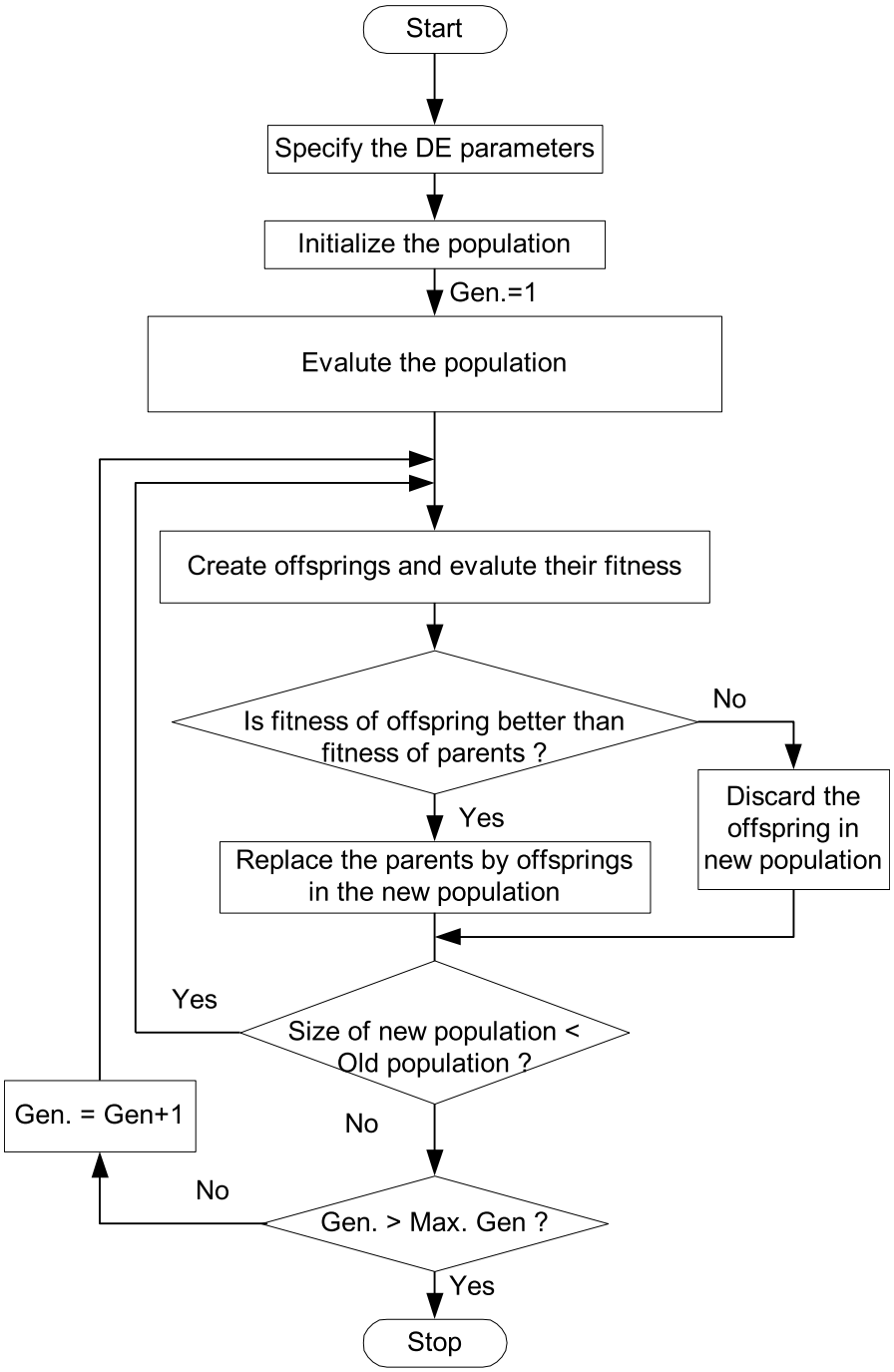

FIGURE 2
Flow chart of DE optimization approach.

and Price (Stron and Prince, 1995). The Genetic Algorithm (GA) employs crossover operator for evolution based on the difference of randomly picked pairs of solutions in the population, whereas DE uses mutation operation, making it more favorable than GA. The DE algorithm employs two Generation, one of which is the old generation and the other is the new generation, both of which have the same population size and are controlled by the parameter Np, which is initialized at random (Pang et al., 2022) within the parameter constraints. A D-dimensional vector can serve as a representation for the D variables in an

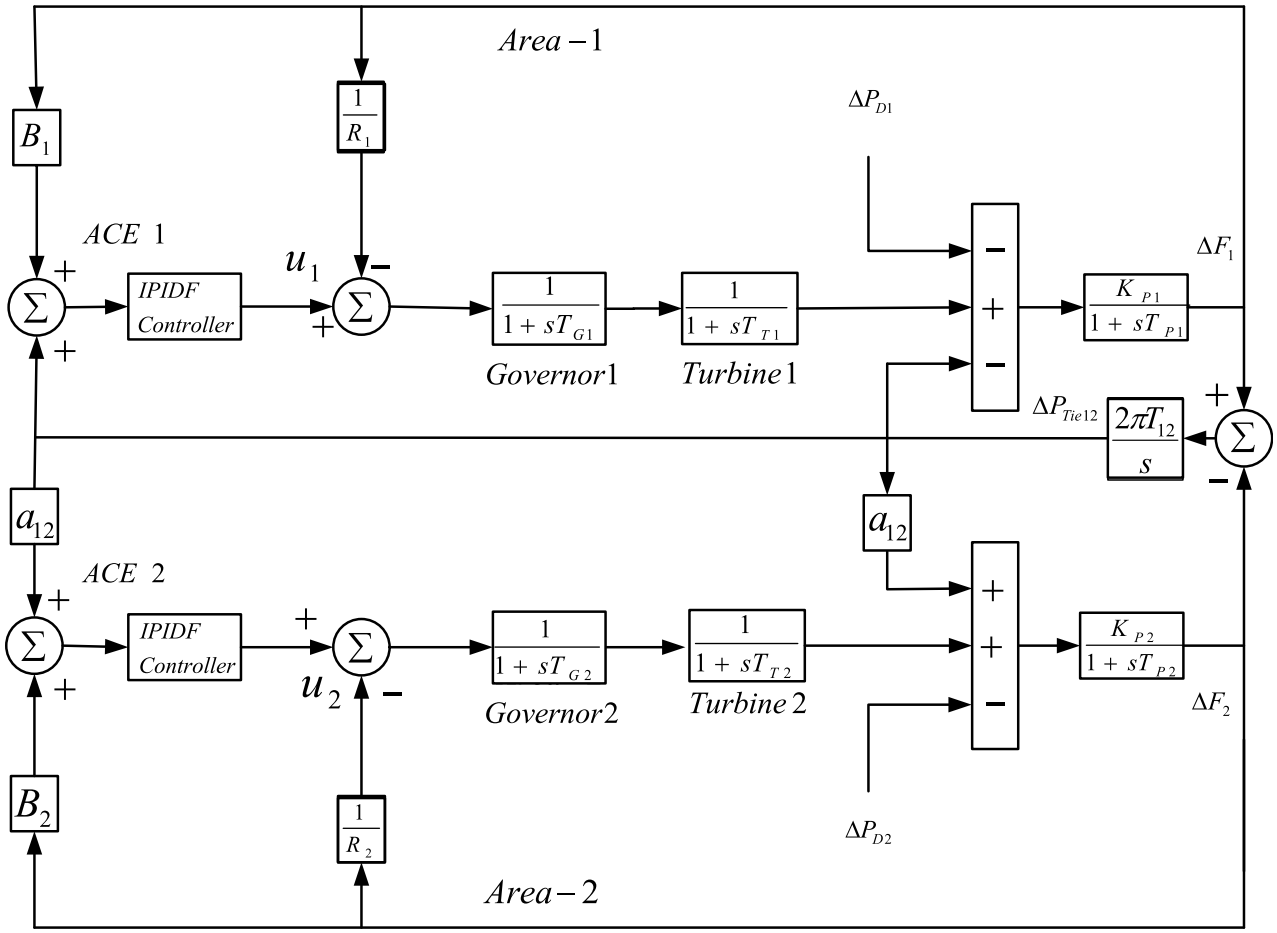

FIGURE 3
MATLAB/SIMULINK model interconnected power system.

TABLE 1 Optimized IPIDF gain parameters for two-area thermal power system.

Variables	GA: PID Sahu et al., (2016)	PSO: PID Sahu et al., 2016	FA: PID Sahu et al., (2016)	DE: PID Sahu et al., (2016)	DE: PIDF	DE: IPIDF
K_{II}	------	------	------	------	------	1.6965
K_P	.4005	1.5378	1.0556	1.2885	1.8044	1.9917
K_I	1.6870	1.1341	1.0373	1.2861	1.9861	.8657
K_D	.8475	.7705	.9626	.9618	1.0300	1.0384
N_C	------	------	------	------	165.3426	213.1675

optimization job. Three key procedures are used to carry out the optimization process: mutation, crossover, and selection (Pant et al., 2020).

The target vectors for the following generation are people in the existing population (Sahu et al., 2016). Old and fresh generations of the same population size are used in the DE method. The present population's individuals become the target vectors for the following generation. By adding the weighted difference between two randomly selected vectors to a third vector, the mutation process

TABLE 2 Values of the Comparative Performance Index while region 1 is under 10% load.

Controller	ITAE	Peak undershoot x10^{-3}			Settling time (sec)		
		ΔF_1	ΔF_2	ΔP_{tie}	ΔF_1	ΔF_2	ΔP_{tie}
GA: PID Sahu et al., (2016)	**.4967**	−8.74	−5.22	−2.01	6.93	6.74	4.87
PSO: PID Sahu et al., (2016)	**.4854**	−8.58	−4.36	−1.57	5.30	6.41	5.03
FA: PID Sahu et al., (2016)	**.4714**	−7.88	−4.28	−1.71	4.25	5.49	4.78
DE: PID Sahu et al., (2016)	**.3391**	−7.80	−3.92	−1.53	3.58	4.85	4.20
DE: PIDF	**.1764**	−7.48	−3.41	−1.24	2.47	3.70	3.21
DE: IPIDF	**.1238**	−7.36	−3.30	−1.18	1.89	3.00	2.67

TABLE 3 Sensitive investigation using IPIDF controllers under various conditions of T_G, T_T, T_{12}, and B.

Parameter variation	%Change	Peak undershoot (x 10^{-3})			Settling time T_S (sec)			ITAE
		ΔF_1	ΔF_2	ΔP_{tie}	ΔF_1	ΔF_2	ΔP_{tie}	
Nominal	0	−.0977	−.1535	−.0001	3.02	3.93	2.66	**.2892**
T_G	+25	−.1019	−.1641	−.0002	2.99	3.90	2.65	**.2826**
	−25	−.0949	−.1420	−.0001	3.04	3.97	2.68	**.2958**
T_T	+25	−.1108	−.1714	−.0002	2.84	3.89	2.60	**.2702**
	−25	−.0871	−.1333	−.0001	3.16	3.94	2.73	**.3105**
T_{12}	+25	−.1028	−.1518	−.0002	2.95	3.78	2.57	**.2861**
	−25	−.0917	−.1552	−.0001	3.13	4.13	2.82	**.2957**
B	+25	−.0774	−.1351	−.0001	2.81	4.10	2.75	**.2411**
	−25	−.1301	−.1798	−.0002	3.46	3.06	2.57	**.3795**

TABLE 4 Tuned IPIDF controller parameters with SMES and HVDC Link.

Parameters	DE: PIDF	DE: IPIDF
K_{II}	------	1.4192
K_P	1.1636	1.9510
K_I	1.9495	1.9927
K_D	1.0593	1.1991
N_C	93.6275	262.3740

creates a mutant vector for each target vector. By combining the properties of the mutant vector and those of the target vector, the crossover procedure creates a trial vector. If the trial vector achieves a higher fitness value than the target vector, it replaces the target vector in the following generation. The flow chart of the DE algorithm is shown in Figure 2.

4 Findings and discussion

4.1 Execution of DE

The MATLAB/SIMULINK environment was used to create the model of the system under study depicted in Figure 3 and a DE program was constructed (. mfile). The present work chooses −2.0 and 2.0 as the lowest and maximum values for controller parameters. The objective function, which is computed in the. m file, is used by the optimization process. In the current study, the population size NP = 100, generation number G = 100, step size F = .8, and crossover probability CR = .8 have all been used. With a situation of a 10% shift in the burden in Area-1 only at t = 0 s, the output/gain of the controller are optimized here by the DE method, and their control parameters are displayed in Table 1. The final value that is determined by repeating the optimization procedure 50 times will be determined by the optimal value for each parameter.

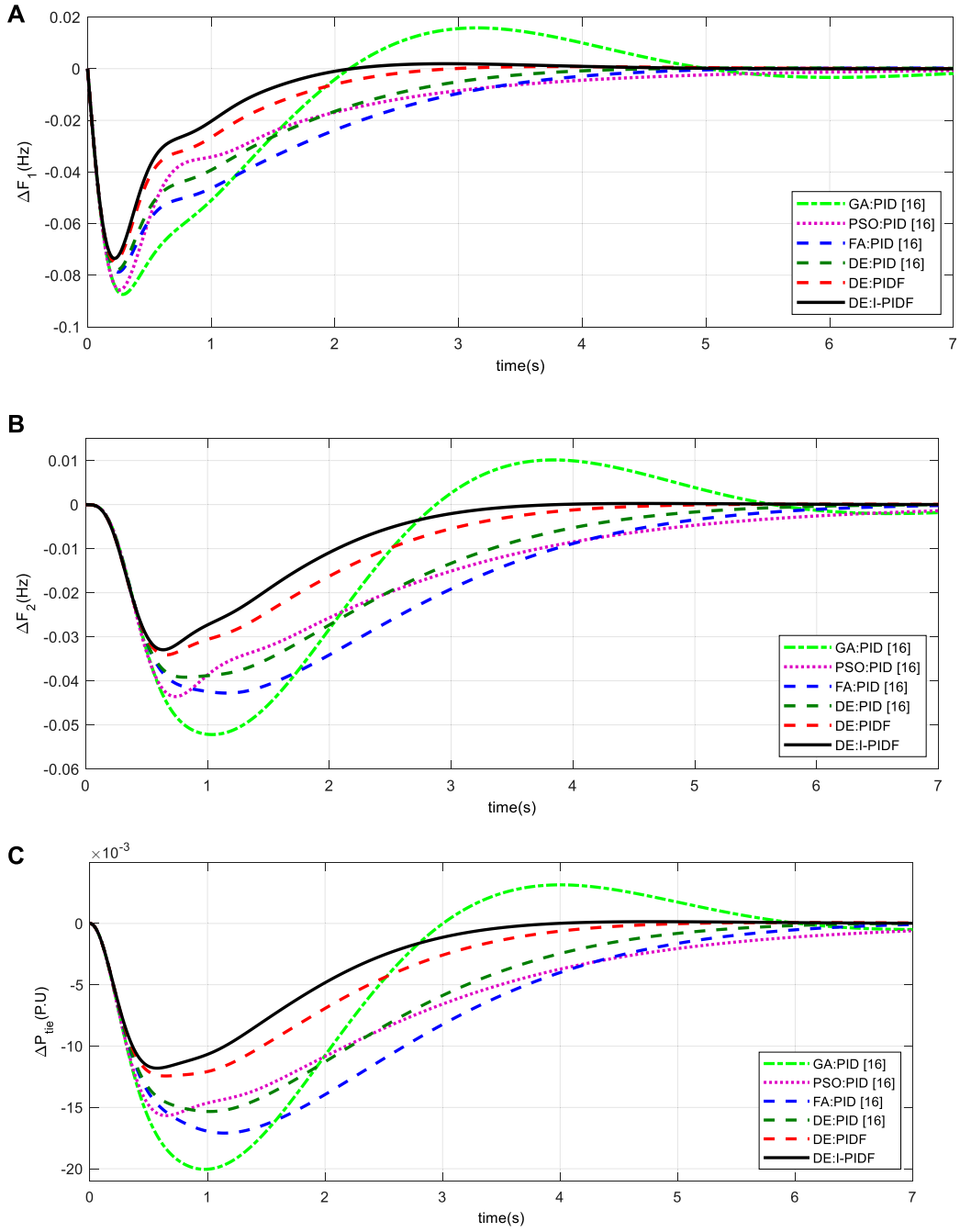

FIGURE 4
System dynamic responses for 10% shift in the burden in Area -1 only **(A)** frequency shift in Area 1 **(B)** frequency shift in Area 2 **(C)** power change in tie-line.

4.2 Analysis of results

Three examples can be taken into account in order to examine the dynamic performance of the system under examination. In the first scenario, Area-1 is the only one to receive the 10% step load; in the second, Area -2 is the only one to receive the 10% load disturbance; and, in the third scenario, Area -1 and Area -2, respectively, are the recipients of 10% and 20% step load. The effectiveness indicator values are given in Table 2 for the first case, where a 10% shift in the burden is applied to Area -1 at time t = 0 s. Figure 4 displays the associated frequency change in the area and Power

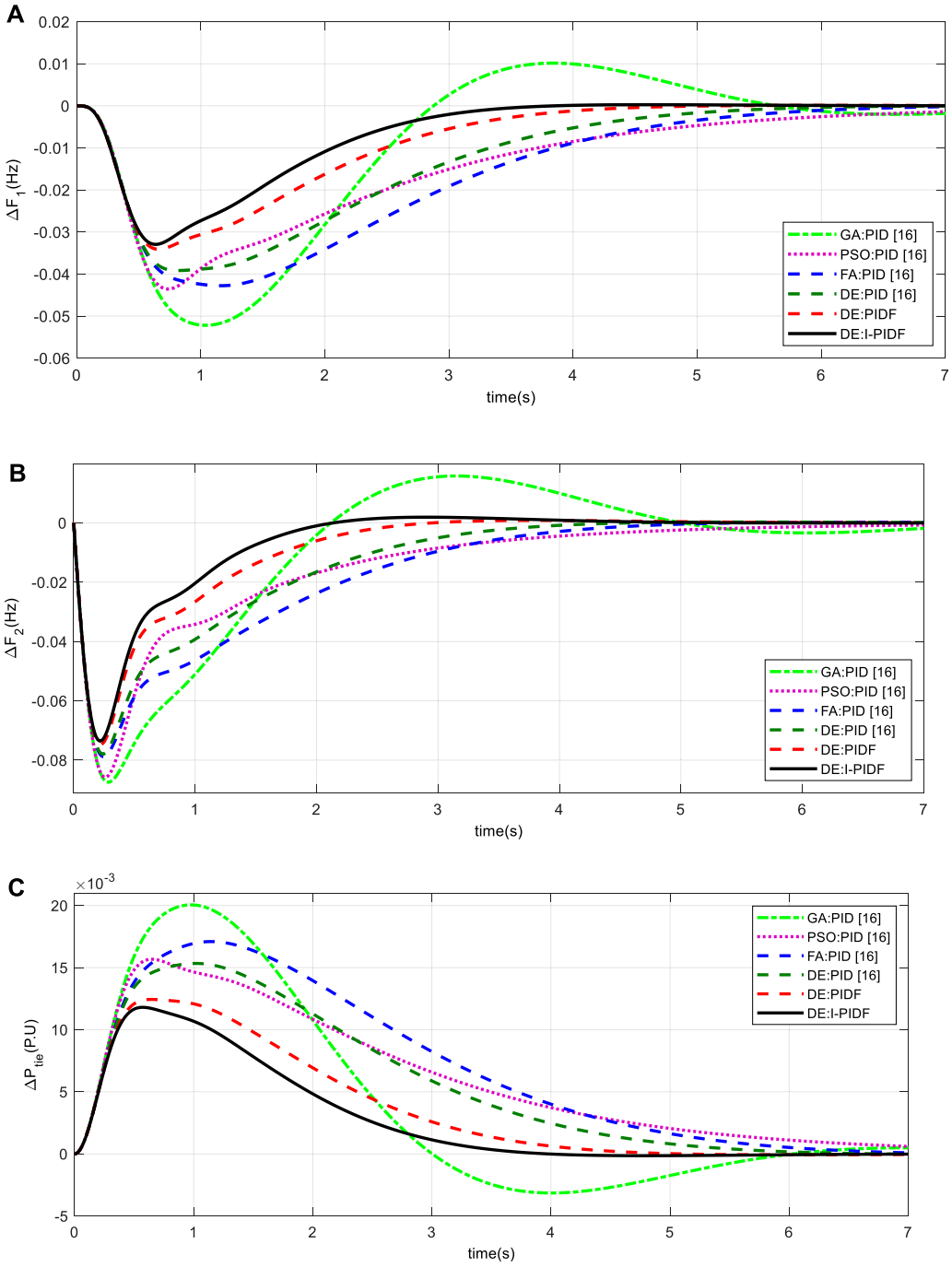

FIGURE 5
System dynamic responses for 10% shift in the burden in Area-2 only **(A)** frequency shift in Area 1 **(B)** frequency shift in Area 2 **(C)** power change in tie-line.

variations along the tie line. In contrast to GA PID (Sahu et al., 2016), PSO PID (Sahu et al., 2016), FA PID (Sahu et al., 2016), DE: PID (.3391) (Sahu et al., 2016), and DE: PIDF (.1764), the IPIDF controller yields a reduced ITAE (.1238). When compared to other controllers, the proposed IPIDF controller reduces the ITAE value by 12.38%. The change in error is then displayed in Figure 5 when a similar operation is carried out with a 10% shift in the burden in Area -2 only at t = 0 s. Finally, Area -1 and Area -2, respectively, receive 10% and 20% step disruption. In

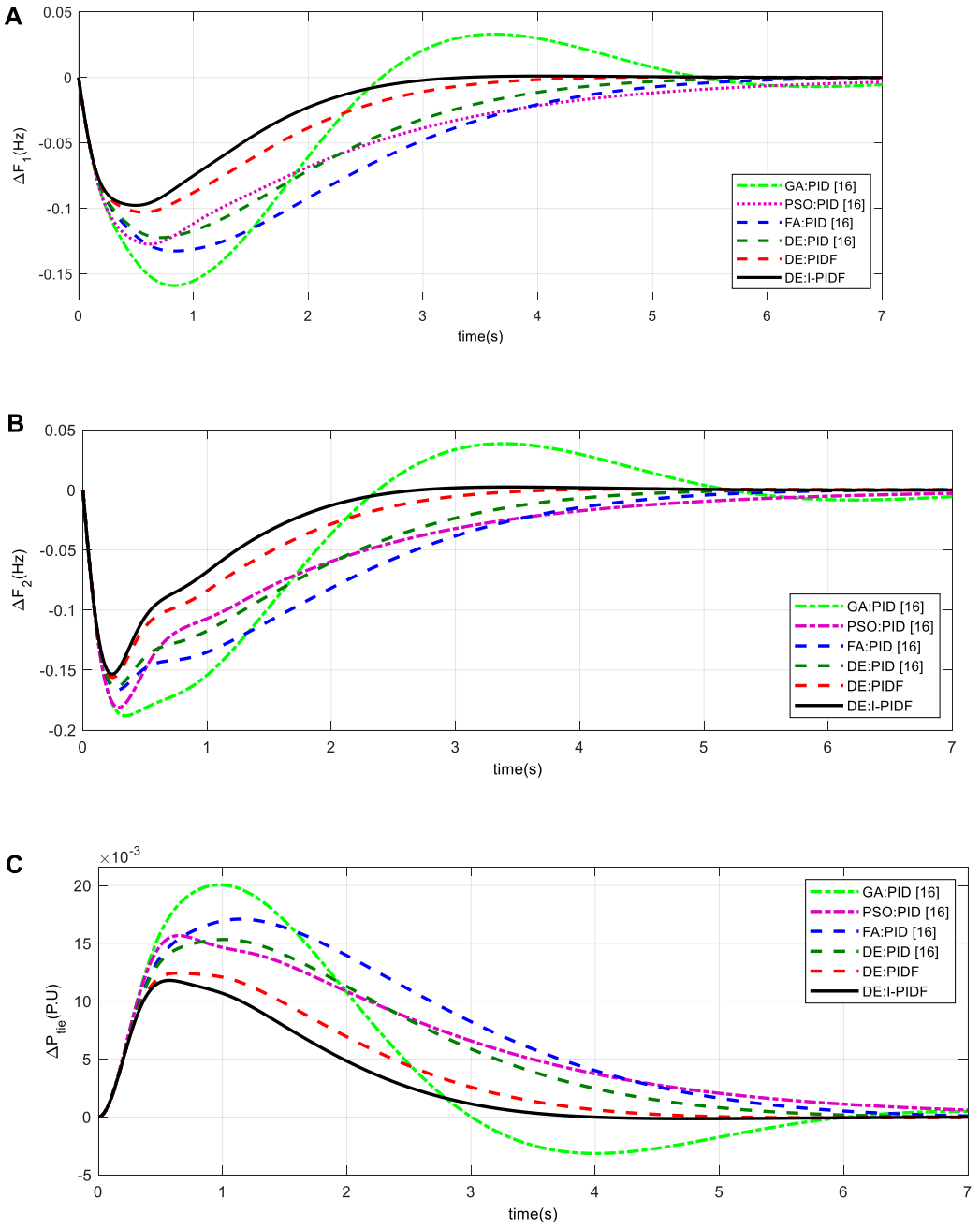

FIGURE 6
System dynamic responses for 10% shift in the burden in Area-1 and 20% in Area 2 **(A)** frequency shift in Area 1 **(B)** frequency shift in Area 2 **(C)** power change in tie-line.

Figure 6, the dynamic reaction is displayed. The figure clearly shows that the IPIDF controller functions more effectively analyzing peak overshoot and undershoot, as well as settling time. The yielded results of the IPIDF controller are therefore evidently better than that of the PIDF controller.

4.3 Sensitivity analysis

Changes to the system's operating circumstances and system parameters are made as part of the sensitivity study, which examines the proposed system's resilience (Ali and Abd-Elazim, 2011; Panda et al., 2013; Padhan et al., 2014b; Sahu et al., 2016).

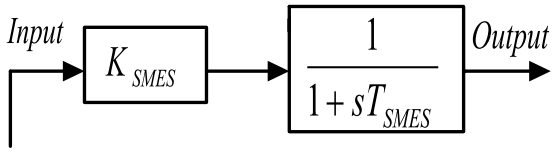

FIGURE 7
Structure of SMES.

Here, the reliability of the system is evaluated by altering the value of T_G, T_T, T_{12}, and B in the range of ±25% for the same controller value. Here, under changing load conditions, a sensitivity study is conducted for 10% and 20% shift in burden in Area 1 and Area 2 respectively. Table 3's listing of the system characteristics demonstrates how the IPIDF controller is resistant to various parameter variations.

5 Investigation with SMES and HVDC link

5.1 Modelling of SMES

The SMES's capacity to store electrical energy in the form of magnetic energy and its ability to deliver enormous amounts of power instantly are two of its key capabilities. Because all of a SMES unit's components are static, it is more stable than other power storage devices. Pradhan et al. (2016); model the SMES and connect in the power system to investigate the system. The model for SMES is shown in Figure 7. Two SMES units are set up in areas 1 and 2 in the current study to stabilize frequency oscillations, as depicted in Figure 9. The input signal of the SMES controller is p.u. frequency deviation (ΔF) and the output is change in control vector (ΔP_{SMES}). The values of the time constant T_{SMES} and the controller gains K_{SMES} are .03 s and .12, respectively.

5.2 Modelling of HVDC

A HVDC link is taken into consideration in parallel with the HVAC system in order to enhance the dynamic performance of the power system. Figure 8 depicts the single line diagram of a two-area power system with parallel HVAC/HVDC linkages. The HVDC link's control system responds promptly to a step load disruption by suppressing the peak value of the transient frequency deviation. The governors then eliminate the steady state inaccuracies of the frequency deviation. The dynamics of the governors in both areas can be ignored for the purpose of simplicity in the control design of the HVDC link. The change in output in area-1 of an HVDC link can be expressed as follows for a sudden step load perturbation:

$$\Delta P_{DC} = \frac{K_{DC}}{1 + ST_{DC}} \Delta F_1$$

Where K_{DC} is gain of a HVDC link and T_{DC} is time constant of HVDC link in seconds.

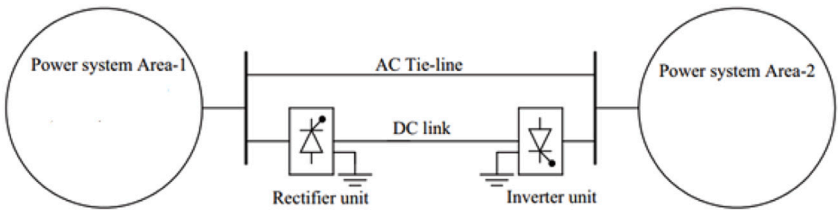

FIGURE 8
Two-area interconnected power system with HVDC.

TABLE 5 Performance index values with SMES and HVDC Link.

Controller	ITAE	Peak undershoot			Settling time (S)		
		ΔF_1	ΔF_2	ΔP_{tie}	ΔF_1	ΔF_2	ΔP_{tie}
DE: PIDF	**.3279**	−.0603	−.0168	−.0121	3.13	5.52	3.58
DE: IPIDF	**.1330**	−.0555	−.0141	−.0089	1.88	3.84	2.64

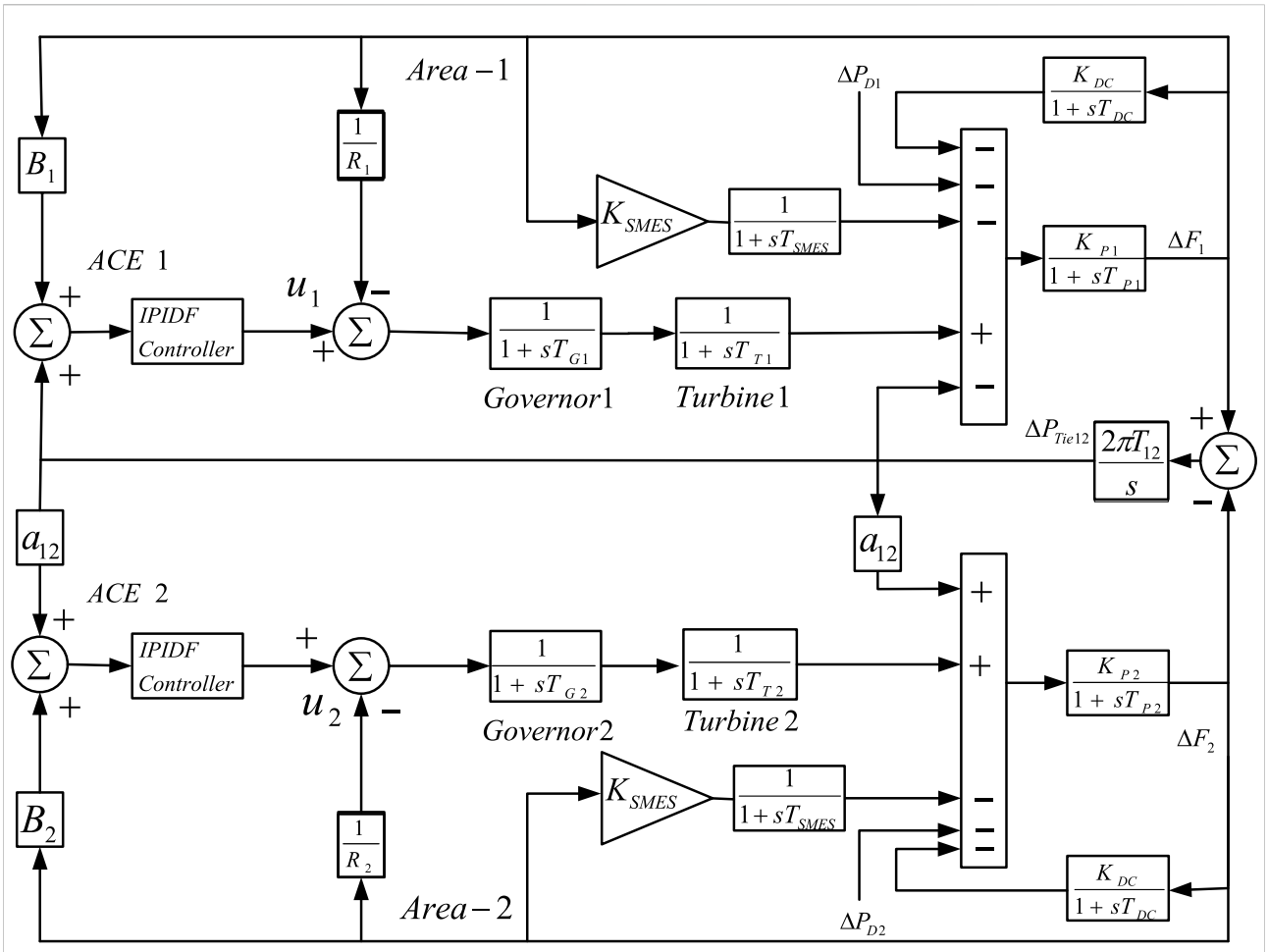

FIGURE 9
Thermal power system with SMES and HVDC Link MATLAB/SIMULINK model.

TABLE 6 Sensitive analysis with IPIDF controllers when T_G, T_T, T_{12} and B are varied.

Parameter variation	% Change	Peak undershoot (x 10^{-3})			Settling time Ts (sec)			ITAE
		ΔF_1	ΔF_2	ΔP_{tie}	ΔF1	ΔF2	ΔPtie	
Nominal	0	−.0555	−.0141	−.0089	1.88	3.84	2.64	**.1330**
T_G	+25	−.0587	−.0150	−.0090	1.87	3.81	2.63	**.1329**
	−25	−.0520	−.0138	−.0088	1.90	3.86	2.66	**.1332**
T_T	+25	−.0599	−.0156	−.0092	1.84	3.75	2.59	**.1351**
	−25	−.0501	−.0135	−.0086	1.94	3.92	2.70	**.1327**
T_{12}	+25	−.0550	−.0164	−.0096	1.96	3.66	2.48	**.1243**
	−25	−.0562	−.0126	−.0080	1.87	4.13	2.87	**.1527**
B	+25	−.0510	−.0118	−.0085	1.71	3.61	2.70	**.1138**
	−25	−.0614	−.0186	−.0093	2.36	4.22	2.58	**.1857**

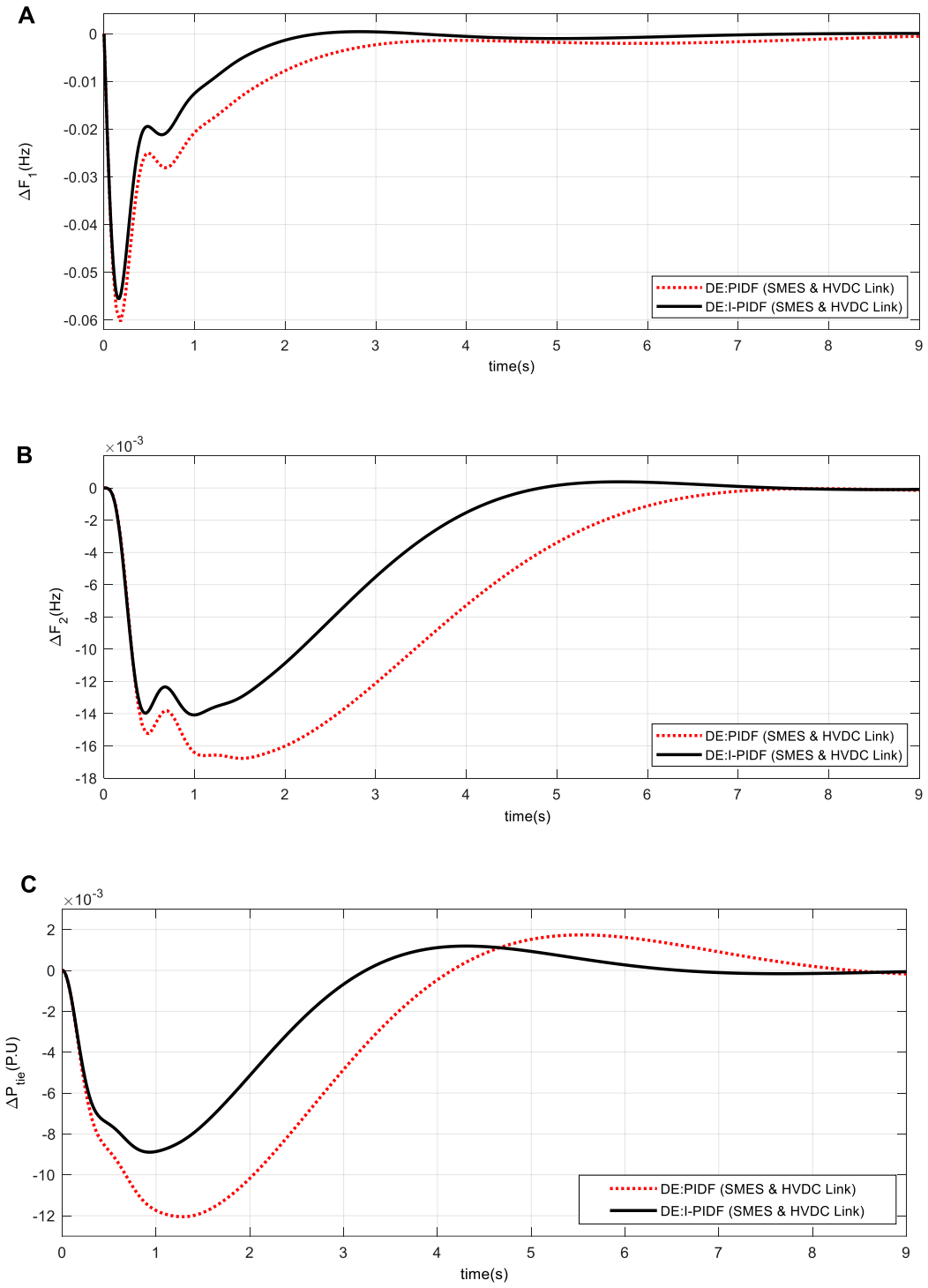

FIGURE 10
System dynamic responses for 10% shift in the burden in Area -1 only **(A)** frequency shift in Area 1 **(B)** frequency shift in Area 2 **(C)** power change in tie-line.

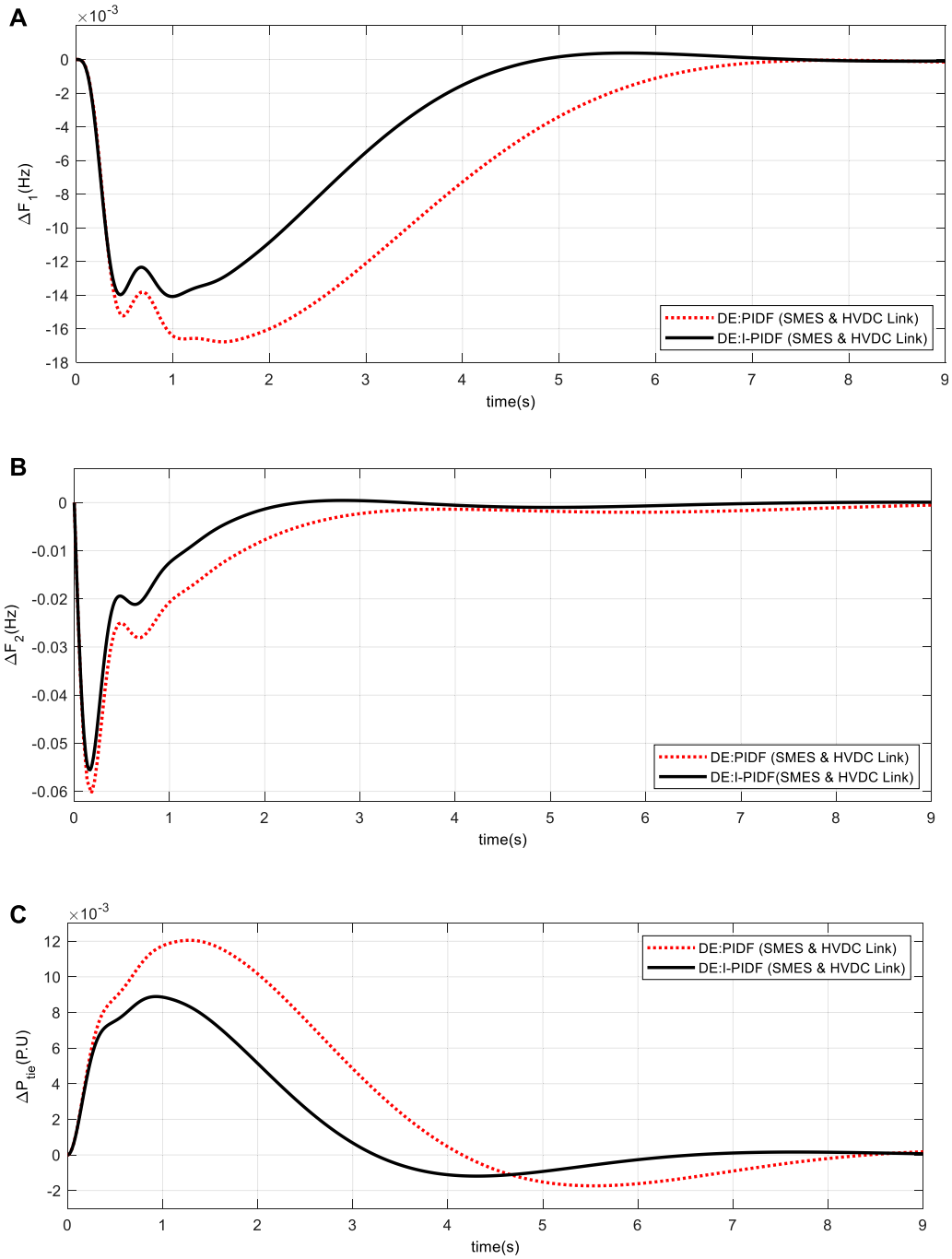

FIGURE 11
System dynamic responses for 10% shift in the burden in Area -2 only **(A)** frequency shift in Area 1 **(B)** frequency shift in Area 2 **(C)** power change in tie-line.

5.3 Two area units non-reheat thermal power system with SMES and HVDC link

To demonstrate the efficacy of the suggested IPIDF controller, the study is further extended with SMES and HVDC link (Pradhan et al., 2016; Dekaraja et al., 2022; Ramoji, 2022; Sivadanam et al., 2022) as shown in Figure 9. The MATLAB/SIMULINK environment was used to create the model of the system under study depicted in Figure 9, and a DE program was constructed (. mfile). The present

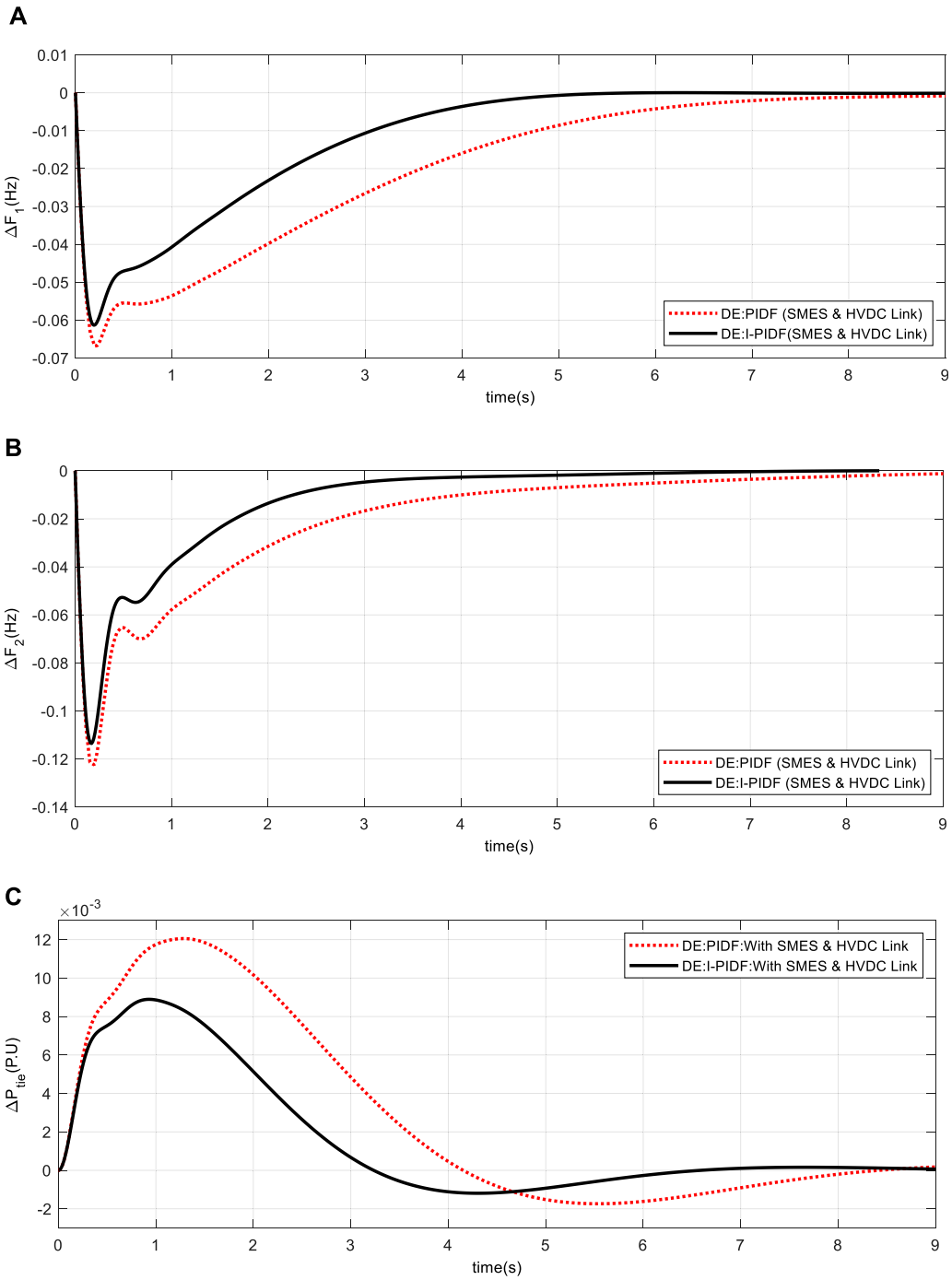

FIGURE 12
System dynamic responses for 10% shift in the burden in Area -1 and 20% in Area 2 **(A)** frequency shift in Area 1 **(B)** frequency shift in Area 2 **(C)** power change in tie-line.

work chooses −2.0 and 2.0 as the lowest and maximum values for controller parameter for K_{II}, K_P, K_I, and K_D. The lowest and maximum value for the filer (N_C) is taken 1 and 300 respectively. With a situation of a 10% shift in the burden in Area -1 only at t = 0 s, the output/gain of the controller are optimized here by the DE method. The same DE method, where the 50 best final solutions from the 50 optimization runs were utilized to establish the controller's settings. The top 50 concluding responses from the 50 runs are shown in Table 4.

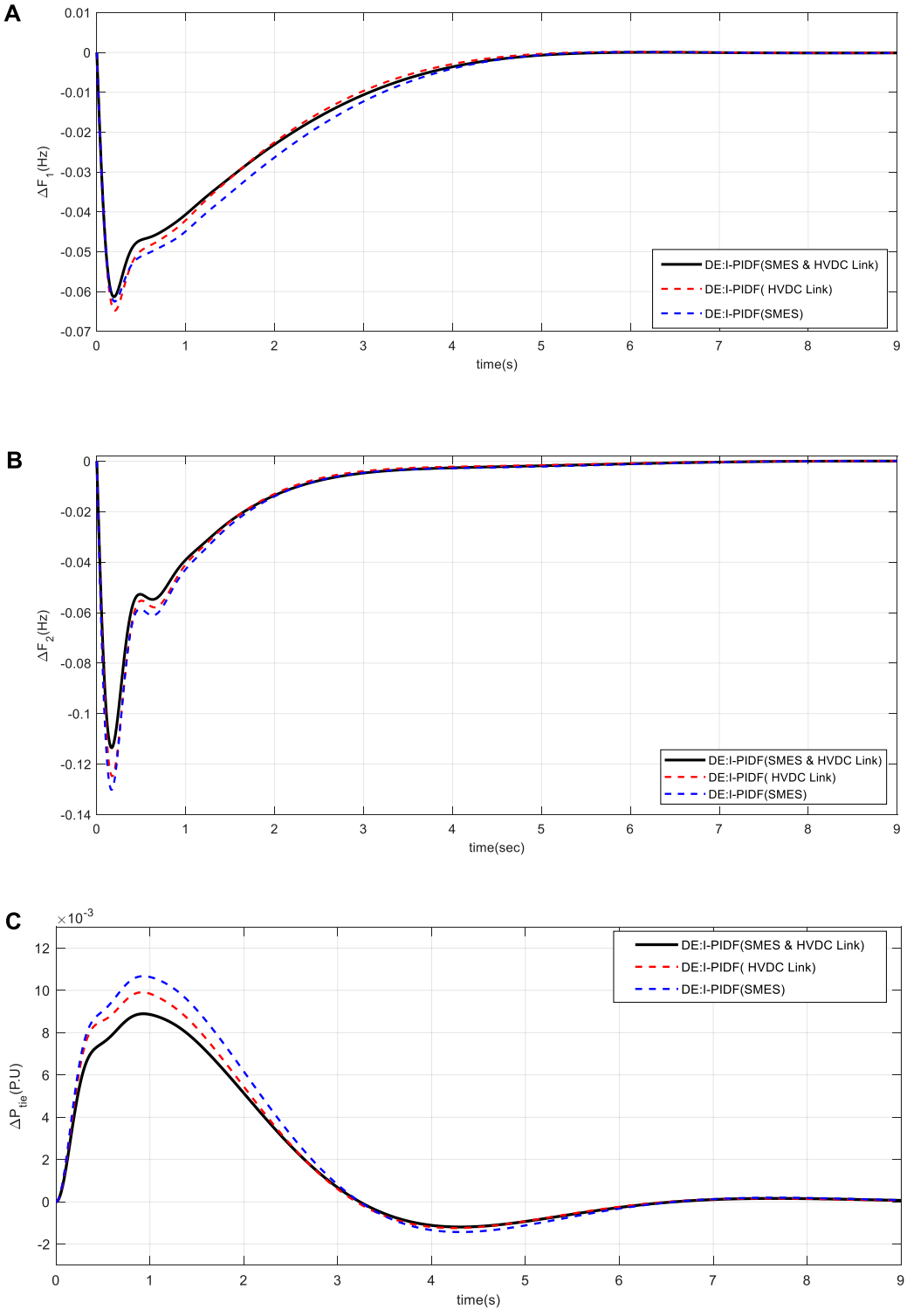

FIGURE 13
System dynamic responses for 10% shift in the burden in Area -1 and 20% in Area 2 **(A)** frequency shift in Area 1 **(B)** frequency shift in Area 2 **(C)** power change in tie-line.

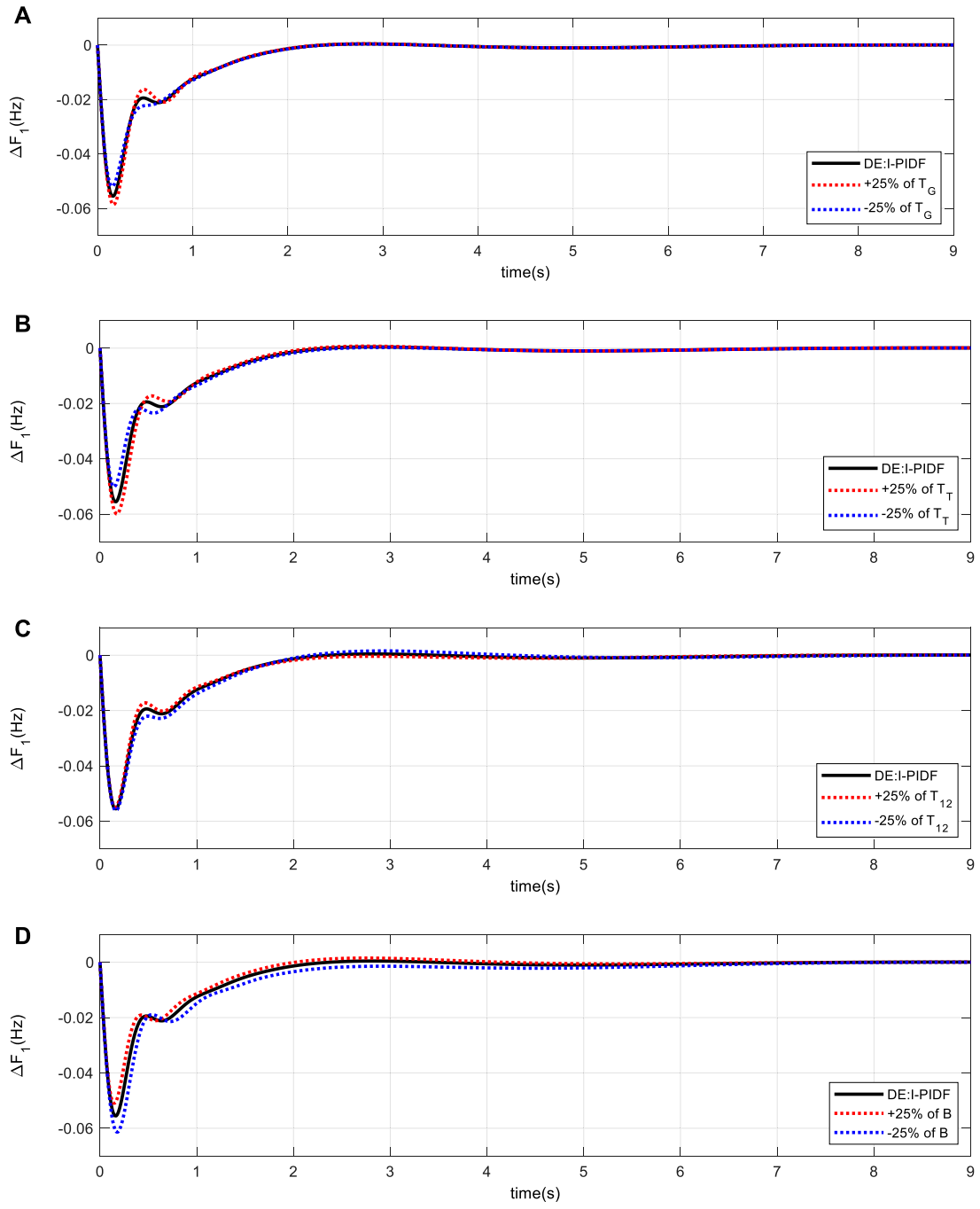

FIGURE 14
Area-1 frequency variation with .1 p.u. of load with variation of **(A)** T_G **(B)** T_T **(C)** T_{12} **(D)** B.

5.4 Analysis of the findings

Table 5 shows the outcome of the system DE-optimized IPIDF controller for the fast scenario, where Area -1 is subjected to a burden of 10% load at time t = 0 s. Performance of the proposed IPIDF controller is compared to that of PIDF. Table 5 makes it very evident that the IPIDF controller produces a lower ITAE value than the PIDF (ITAE = .3279 vs. .1330). Area -2 is the only location in the second scenario to have a burden of 10%. Finally, to investigate the dynamic performance of system 10% and 20% shift in burden is given to Area -1 and Area

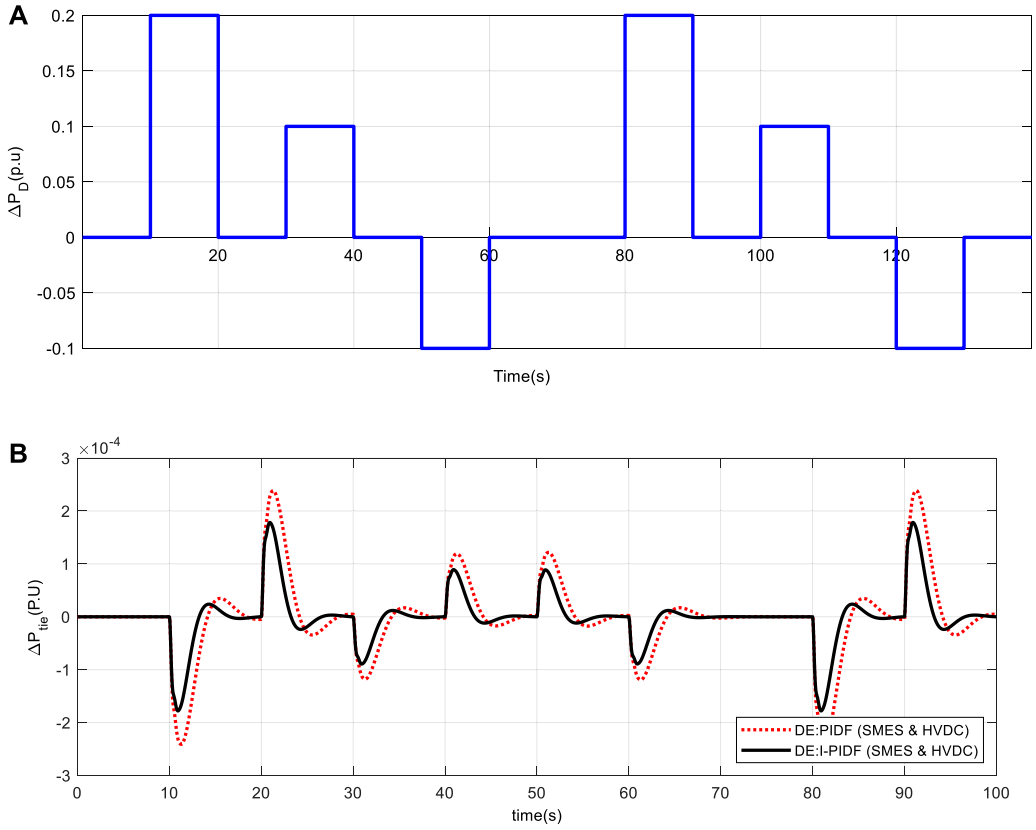

FIGURE 15
(A) Random step load **(B)** tie-line power deviation between area 1 and area 2.

-2 accordingly. The dynamic reaction is seen in Figure 10–12. It is obvious that, in terms of output performance, the IPIDF controller surpasses the PIDF controller (minimal Peak undershoot, frequency settling durations, and power variations in tie-line).

Individual system performance of the system with just SMES and only HVDC connection is compared to the system with both SMES and HVDC link in order to demonstrate the effectiveness of adding both SMES and HVDC link to the systems. The change in errors for the 10% and 20% loads to Areas 1 and 2 is presented in Figure 13. From Figure 13, it is evident that the system clearly performs better when SMES and HVDC links are included in the system.

5.5 Sensitivity analysis

The reliability of the system (Figure 9) is evaluated by altering the value of T_G, T_T, T_{12}, and B in the range of ±25% for the same controller value. Here, under changing load conditions, a sensitivity study is conducted for 10% shift in burden in Area 1 only. Table 6's listing of the system characteristics demonstrates how the IPIDF controller is resistant to various parameter variations. Table 6 makes it evident that the performance index values fluctuate within allowable limits and are typically identical to the standard value. Dynamic nature of the system for different parameter variation is shown in Figure 14.

5.6 Assessment of the effectiveness under various load disturbance scenarios

A performance analysis of the suggested system is also done for several load perturbations, such as step load and pulse load to Area 1 (Sahu et al., 2016). Figure 15A depicts the application of a step load to region 1 that has a period of 140 s and a breadth of 10 s (Sahu et al., 2016). Figure 15B depicts the corresponding tie-line power exchange. Area 1 is then put under a pulse (Sahu et al., 2016) change with an initial magnitude of 10% P.U and a frequency of .025 Hz shown in Figure 16A. Figure 16B depicts the change in tie-line power. We can infer from all of the findings that the IPIDF controller reduces oscillation.

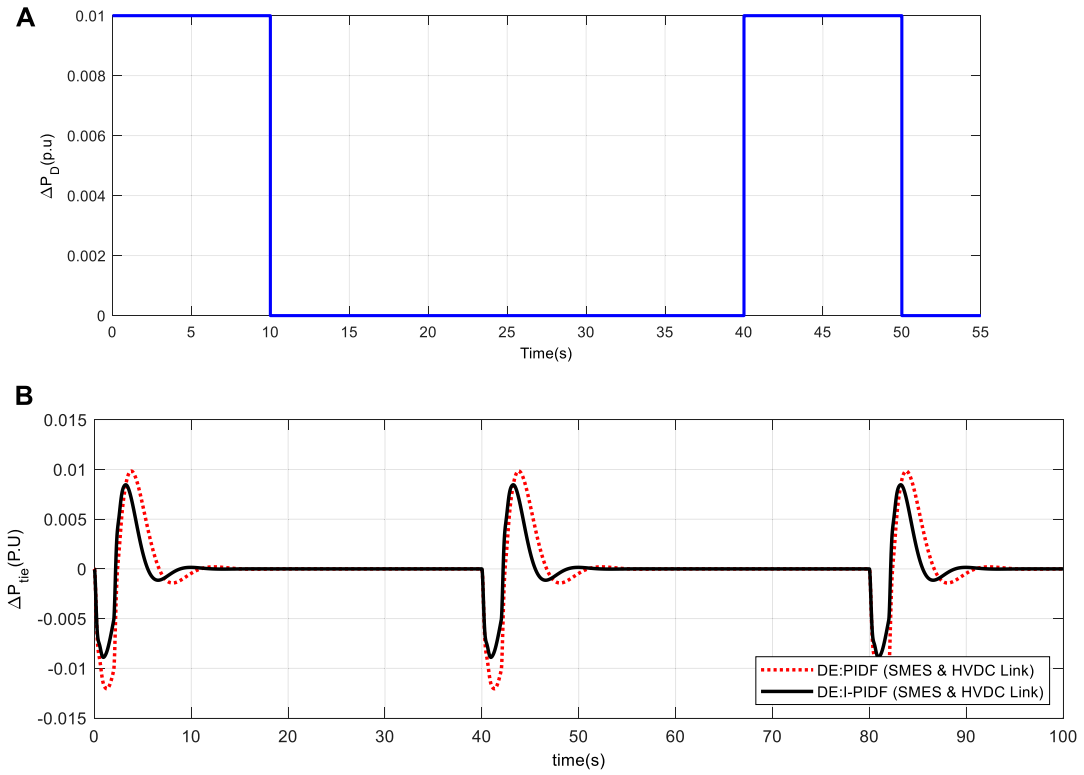

FIGURE 16
(A) Pulse load **(B)** tie-line power deviation between area 1 and area 2.

6 Conclusion

This work has addressed the Load Frequency Control (LFC) of a two-area linked system using a special IPIDF controller. The Differential Evolution approach was employed to improve the IPIDF controller's settings with an ITAE-based fitness function. By comparing the outcomes with those of other recently published optimization approaches, such as Particle Swarm Optimization (PSO), Firefly Algorithm (FA), and Differential Evolution (DE) algorithm based PID and PIDF controllers, the supremacy of the IPIDF controller is shown. A two-area system that takes into consideration both a HVDC connection and a superconducting magnetic energy storage device is added to the recommended method. There have been reports of considerable improvements in dynamic responsiveness when the IPIDF controller is used in conjunction with superconducting magnetic energy storage and an HVDC link. Additionally, a sensitivity study of the operational state and system parameters in the range of +25 to -25% from their nominal values is conducted to evaluate the system's resilience. Next, the efficacy of the presented method is reviewed under several load perturbations, such as step load and pulse load. The results demonstrate that the created controller is trustworthy and perform admirably under a variety of operating circumstances, system characteristics, and load patterns.

Data availability statement

The original contributions presented in the study are included in the article/supplementary material, further inquiries can be directed to the corresponding author.

Author contributions

All authors listed have made a substantial, direct, and intellectual contribution to the work and approved it for publication.

Conflict of interest

The authors declare that the research was conducted in the absence of any commercial or financial relationships that could be construed as a potential conflict of interest.

The handling editor declared a shared affiliation with the reviewer SP at the time of the review.

Publisher's note

References

Ahmed, M., Magdy, G., Khamies, M., and Kamel, S. (2022). Modified TID controller for load frequency control of a two-area interconnected diverse-unit power system. *Int. J. Electr. Power & Energy Syst.* 135, 107528. doi:10.1016/j.ijepes.2021.107528

Ali, E. S., and Abd-Elazim, S. M. (2011). Bacteria foraging optimization algorithm-based load frequency controller for interconnected power system. *Int. J. Electr. Power Energy Syst.* 33, 633–638. doi:10.1016/j.ijepes.2010.12.022

Banerjee, S., Chatterjee, J. K., and Tripathy, S. C. (1990). Application of magnetic energy storage unit as load-frequency stabilizer. *Trans. Energy Conv.* 5, 46–51. doi:10.1109/60.50811

Dekaraja, B., and Chandra Saikia, L. (2022). Impact of energy storage and flexible alternating current transmission devices in combined voltage and frequency regulation of multiarea Multisource Interconnected Power System. *Energy Storage* 4, e317. doi:10.1002/est2.317

Dekaraja, B., Saikia, L. C., Ramoji, S. K., Behera, M. K., and Bhagat, S. K. (2022). Performance analysis of diverse energy storage on combined ALFC and AVR control of multiarea multiunit system with AC/HVDC interconnection. *IFAC-Papers Line* 551, 479–485. doi:10.1016/j.ifacol.2022.04.079

El-Ela, A. A. A., El-Sehiemy, R. A., Shaheen, A. M., and Diab, A. E. G. (2022). Design of cascaded controller based on coyote optimizer for load frequency control in multi-area power systems with renewable sources. *Control Eng. Pract.* 121, 105058. doi:10.1016/j.conengprac.2021.105058

Elgerd, O. I. (2000). *Electric energy systems theory (2000) – an introduction*. New Delhi: Tata McGraw Hill.

Karn, A. K., Hameed, S., Sarfraz, M., Ro, J. S., and Khalid, M. R. (2022). Load shedding for frequency and voltage control in the multimachine system using a heuristic knowledge discovery method. *Front. ENERGY Res.* 10. doi:10.3389/fenrg.2022.1002064

Luo, K., Jiao, Y., and Zhu, J. (2021). Perturbation observer based fractional-order control for SMES systems based on jellyfish search algorithm. *Front. Energy Res.* 695. doi:10.3389/fenrg.2021.781774

Padhan, S., Sahu, R. K., and Panda, S. (2014). Application of Firefly algorithm for load frequency control of multi-area interconnected power system. *Electr. Power Compon. Syst.* 42, 1419–1430. doi:10.1080/15325008.2014.933372

Padhan, S., Sahu, R. K., and Panda, S. (2014). Automatic generation control with thyristor-controlled series compensator including superconducting magnetic energy storage units. *Ain Shams Eng. J.* 5 (3), 759–774. doi:10.1016/j.asej.2014.03.011

Panda, S., Mohanty, B., and Hota, P. K. (2013). Hybrid BFOA–PSO algorithm for automatic generation control of linear and nonlinear interconnected power systems. *Soft Comput.* 13 (12), 4718–4730. doi:10.1016/j.asoc.2013.07.021

Pang, S., Liu, J., Zhang, Z., Fan, X., Zhang, Y., Zhang, D., et al. (2022). A photovoltaic power predicting model using the differential evolution algorithm and multi-task learning. *Front. Mater.* 9, 938167. doi:10.3389/fmats.2022.93816

Pant, M., Zaheer, H., Garcia-Hernandez, L., and Abraham, A. (2020). Differential evolution: A review of more than two decades of research. *Eng. Appl. Artif. Intell.* 90, 103479. doi:10.1016/j.engappai.2020.103479

Peng, Bo (2022). Coordinated AGC control strategy for an interconnected multi-source power system based on distributed model predictive control algorithm. *Front. Energy Res.* 1678.

Pradhan, P. C., Sahu, R. K., and Panda, S. (2016). Firefly algorithm optimized fuzzy PID controller for AGC of multi-area multi-source power systems with UPFC and SMES. *Int. J.* 19, 338–354. doi:10.1016/j.jestch.2015.08.007

Ram Babu, N., and Saikia, L. C. (2021). Load frequency control of a multi-area system incorporating realistic high-voltage direct current and dish-Stirling solar thermal system models under deregulated scenario. *IET RPG* 15 (5), 1116–1132. doi:10.1049/rpg2.12093

Ramoji, S. K. (2022). "Repercussions of SMES and HVDC link in amalgamated voltage and frequency regulation of multi-area multi-unit interconnected power system," in 2022 4th International Conference on Energy, Power and Environment (ICEPE), Shillong, India, 29 April 2022-01 May 2022.

Sahu, R. K., Panda, S., Biswal, A., and Chandra Sekhar, G. T. (2016). Design and analysis of tilt integral derivative controller with filter for load frequency control of multi-area interconnected power systems. *ISA Trans.* 61, 251–264. doi:10.1016/j.isatra.2015.12.001

Shabani, H., Vahidi, B., and Ebrahimpour, M. (2013). A robust PID controller based on imperialist competitive algorithm for load-frequency control of power systems. *Trans* 52, 88–95. doi:10.1016/j.isatra.2012.09.008

Sivadanam, N., Bhookya, N., and Maheswarapu, S. (2022). Stochastic and iterative based optimization for enhancing dynamic performance of interconnected power system with hybrid energy storage. *Front. Energy Res.* 10, 175. doi:10.3389/fenrg.2022.845686

Soni, V., Parmar, G., and Kumar, M. (2021). A hybrid grey wolf optimisation and pattern search algorithm for automatic generation control of multi-area interconnected power systems. *Int. J. Adv. Intell. Paradig.* 18 (3), 265. doi:10.1504/IJAIP.2021.10035674

Stron, R., and Prince, K. (1995). Differential evolution- a simple and efficient adaptive scheme for global optimization over continuous spaces. *J. Glob. Optim.* 11, 341–359. doi:10.1023/A:1008202821328

Sudha, K. R., and Vijaya, S. R. (2012). Load frequency control of an interconnected reheat thermal system using type-2 fuzzy system including SMES units" Int. *J. Elec. Power Energy Syst.* 43, 1383–1392.

Sun, Y., and Duan, W. (2022). Stability analysis of load frequency control for power systems with interval time-varying delays. *Front. Energy Res.* 1507.

Wang, X., Gu, L., and Liang, D. (2021). Decentralized and multi-objective coordinated optimization of hybrid AC/DC flexible distribution networks. *Front. Energy Res.* 9, 646. doi:10.3389/fenrg.2021.762423

Yang, C., Sun, W., Dong, H., and Yin, X. (2022). Research on power system flexibility considering uncertainties. *Front. Energy Res.* 1343. doi:10.3389/fenrg.2022.967220

Nomenclature

f nominal system frequency (Hz)

ΔP_{Tie} tie-line power error

u controller Output

ACE Area Control Error

B frequency bias parameter

T_T turbine time constant in sec

T_P power system time constant in sec

t_{sim} time range of simulation

$\mathbf{K_{SMES}}$ gain of the SMES

$\mathbf{K_{DC}}$ gain of a HVDC link

i subscript referred to area i (1–2)

ΔP_D load disturbance in p.u

ΔF frequency deviations in Hz

R governor speed regulation parameters in p.u. Hz

T_G speed governor time constants in sec

K_P power system gain

T_{12} synchronizing coefficient

$\mathbf{\Delta P_{SMES}}$ output signal of SMES

$\mathbf{T_{SMES}}$ time constant of the SMES

$\mathbf{T_{DC}}$ time constant of HVDC link in sec

Appendix

The system being studied has the following nominal parameters: (Padhan et al., 2014a; Sahu et al., 2016; Luo et al., 2021).

$P_{R1} = P_{R2} =$ 2000 MW (rating), $P_{L1} = P_{L2} =$ 1,000 MW (nominal loading), f = 60 Hz, $B_1 = B_2 =$ .045 p.u. MW/Hz, $R_1 = R_2 =$ 2.4 Hz/p.u., $T_{G1} = T_{G2} =$ .08 s, $T_{T1} = T_{T2} =$ .03 s, $K_{PS1} = K_{PS2} =$ 120 Hz/p.u. MW, $T_{PS1} = T_{PS2} =$ 20 s, $T_{12} =$ .545 p.u., a_{12} =-1, $K_{SMES} =$ .12, $T_{SMES} =$ .03 s, $K_{DC} =$ 1.0, $T_{DC} =$ 0.2 s.

frontiers | Frontiers in Energy Research

TYPE Original Research
PUBLISHED 04 January 2023
DOI 10.3389/fenrg.2022.1079695

OPEN ACCESS

EDITED BY
Sarat Kumar Sahoo,
Parala Maharaja Engineering College (P.M.E.C), India

REVIEWED BY
Sakda Somkun,
Naresuan University, Thailand
Suresh Kumar Velu,
Thiagarajar College of Engineering, India
Saroj Padhan,
Parala Maharaja Engineering College (P.M.E.C), India

*CORRESPONDENCE
Belwin Edward Jeyaraj,
jbelwinedward@vit.ac.in

SPECIALTY SECTION
This article was submitted to Smart Grids, a section of the journal Frontiers in Energy Research

RECEIVED 25 October 2022
ACCEPTED 15 November 2022
PUBLISHED 04 January 2023

CITATION
Puppala R, Jeyaraj BE, Isaac JR and CH HB (2023), Framework for smart grid to implement a price elasticity-based peak time rebate demand response program.
Front. Energy Res. 10:1079695.
doi: 10.3389/fenrg.2022.1079695

Framework for smart grid to implement a price elasticity-based peak time rebate demand response program

Rajendhar Puppala[1], Belwin Edward Jeyaraj[2]*, Jacob Raglend Isaac[2] and Hussaian Basha CH[3]

[1]Electrical Engineering Department, Smt.Indira Gandhi College of Engineering, Navi Mumbai, India, [2]School of Electrical Engineering, Vellore Institute of Technology, Vellore, Tamilnadu, India, [3]Department of Electrical and Electronics Engineering, Nitte Meenakshi Institute of Technology, Bangalore, India

The smart grid model is developed with some changes to help in implementing a demand response program which was initially developed for a Pecan Street project. Correspondingly, the real-time solar and load data are collected from the data port for the city of Austin. A single day is selected for our analysis of all four seasons of the year. The flat rate, and real-time and day-ahead pricing information are collected from ComEd. The key challenge for addressing business problems is the flexibility of consumption. However, without considering the properties of loss aversion, the system would not be a practical solution. So, in this article, a dynamic demand response program based on price elasticity that integrates loss aversion characteristics is proposed. The proposed system is compared for all pricing schemes and all seasons. Four scenarios are created for peak time rebate with different combinations of loss aversion factor values and all the possible combinations of rebates. This article directs how these combinations could change the demand curve and how the utility can make a decision about the specific importance of the criteria, such as the total demand carrying capacity, peak demand reduction, and in obtaining optimum profit for utility and the consumer.

KEYWORDS

demand response (DR), electricity market, loss aversion, price elasticity of demand, peak time rebate (PTR), smart grid

Introduction

Motivation

In most countries, on one hand, the growing population of the world and on the other hand, the rise in electricity consumption *per capita* have contributed to the management of the demand side being more significant. DR is regarded as one of the most impressive methods of demand-side management, where the peak of consumers will be shifted from

high-price hours to low-price hours (Abapour et al., 2020). For implementing innovative DR programs, tariffs for electricity purchases must be designed to maximize the economic interest and to alter the pattern of consumption. This can be achieved by introducing incentive mechanisms. The first one is to decrease the customer demand by attempting to offer rewards to the customer during peak hours. The second means is to avoid the occurrence of supply–demand imbalance as far as possible (Ajoulabadi et al., 2020).

The DR programs are classified based on the control mechanism, offered motivations, and decision variable which was clearly described by Rajendhar and Belwin Edward (2019). The programs discussed here like the flat rate(FR), real-time pricing (RTP), day-ahead pricing (DAP), and peak time rebate (PTR) programs fall under time-based DR programs. The earlier studies explored the elasticity of residential loads, that is, the potential elasticity of demand and reduction of demand with regard to various prices (H. A. Aalami et al., 2019). Furthermore, there are some major variables that have not been completely discussed. To be addressed: most of the previous market elasticity studies are focused on price-based DR, such as the possible reduction in demand with a dynamic pricing scheme (Hosseini et al., 2019; Monfared, Ghasemi et al., 2019). There is, however, little work performed to target incentive-based DR′s (IBDR) elasticity, namely, the relationship between the reduction of overall peak demand and financial incentives.

Literature survey

Based on the DR, Jiang et al. (2019) proposed an efficient real-time pricing model. In order to express the relationship between price and energy consumption dynamics, price elasticity is used. RTP can offer many advantages as a measure of demand-side management, such as peak shaving, generation deferral, and network investment, promoting the introduction of renewable energy. The authors introduced a new model in Sharifi et al. (2018) for DR programs for economic models, based on the methodology of time-of-use. The essential advantages of the model were demonstrated based on price-elasticity. In a smart grid system, the real-time electricity pricing mechanism is applied compared to the flat rate pricing mechanism. It results in monetary savings due to the reduction of electricity bills and to involve the consumer directly in the reduction of peak loads by reducing the grid burden and encouraging the interaction of renewable sources with the grid (Dhundia, 2016).

Lu and Hong (2019) proposed a new real-time incentive-based demand response algorithm for reinforcement learning and deep neural network smart grid systems. It intended to help the service provider to buy energy resources from its subscribing customers to manage energy volatility and strengthen the grid. In particular, deep neural networks are used to forecast unpredictable prices and demands for energy in order to solve the potential uncertainties. Reinforcement learning is then implemented to achieve the optimum reward rates for various clients, taking into account the income of both service providers and clients. Chai et al. (2019) suggested an incentive-based demand response model to optimize the benefits of electricity retailers. The breakthrough is that, given their diverse activities during both peak and valley times, the models provide utility and elasticity of different customers. The optimum reduction of clients with a certain reward price can be achieved by solving the customer benefit optimization model at peak times. The variance of customers can be measured with a certain reward price, according to the elasticity during the valley times. Then, the optimum incentive price can be found based on the suggested DR model by evaluating the sensitivity of incentive prices to retailer benefits.

From utility‘s viewpoint, IBDR has significant prospects for power system peak demand control. Shi et al. (2020) incorporated a systematic approach by integrating the technological model and the social–behavioral survey to determine IBDR ability. The outcome validates the strategy suggested and acts as guidance for IBDR initiatives for utilities.

The Pecan Street research network, which was established in 2009, is the world’s only real power, gas, and water test bed. More than 1,000 houses, 250 solar homes, and 65 electric vehicle users have contributed data to it. Every home’s energy production and consumption are tracked continuously, 24/7/365, and can be dissected down to the circuit level. These high-resolution data shed light on the production, usage, and storage of energy (Residential data page of Pecan street data port, 2022).

Exelon Corporation (NASDAQ: EXC), a Fortune 100 energy corporation with around 10 million customers for electricity and natural gas, is based in Chicago and owns ComEd. More than 4 million customers, or 70% of the state’s population, in northern Illinois rely on ComEd for power. The service area of ComEd is essentially bordered to the south by Iroquois County (about Interstate 80), to the north by Wisconsin, to the west by Iowa, and to the east by Indiana (ComEd’s Hourly Pricing, 2011).

Objectives and novelty

The objectives of the article are as follows:

1. To develop a smart grid simulation setup to implement a dynamic DR program with real-time data on load, generation, pricing signals, and seasons;
2. To test the system for different pricing signals and different scenarios of loss aversion, rebates, and elasticity constants.

The novelties of the article are as follows:

1. To propose a dynamic DR program based on price elasticity that integrates with the loss aversion characteristics;

2. To see how a demand price characteristic would be effected and to suggest the best ways based on the priorities of the parameters such as the peak demand, load demand, and overall cost for the given conditions, combinations, and seasons.

Modeling and data fetching for a smart grid system to incorporate a DR program

The flow diagram of the article is depicted in Figure 1. The simulation model of the proposed system is depicted in Figure 2. The model for the smart grid is based on the model developed by the Centre of Electromechanics, University of Texas (Austin), for the Pecan Street Project including some modifications (University of Texas, 2011; Dhundia, 2016). A substation is represented by a three-phase source with a Ph–Ph voltage of 13.8 kV, which is connected to a static load that is represented by a three-phase series RLC load through a cable. A three-winding residential transformer is tapped from the output of the cable.

It is of 50 KVA power rating with a voltage ratio of 13.8 kV/120V–120 V. The secondary voltages of the transformer are as follows: Line 1 to Neutral= 120 V ∠ 0°, Line 2 to Neutral= 120 V ∠ 180°, Line1 to Line 2 = 240 V ∠ 0°, and neighborhoods 1 and 2 are connected to the output of the transformer. Each neighborhood is connected with five homes. Homes with data ids 7951, 8386, 661, 3039, and 3538 of the Pecan Street Project are connected to Neighborhood 1. Homes with data ids 8565, 9922, 4031, 6139, and 9278 are connected to Neighborhood 2. Out of those previously mentioned, homes with data ids 661, 3039, 3538, 4031, 6139, and 9278 are having PV connections. The loading scenario and PV generation data on all houses are obtained from the Pecan Street project dataport that is used to get the grid power ("Residential data page of Pecan street data port," n. d.).

$$P_{Grid} = P_{used} - P_{PV}, \tag{1}$$

where P_{PV} is the power generated by PV arrays for a given temperature and irradiance. This P_{Grid} is the power used to calculate the electricity charges incurred by the user. The PV profile, grid profile, and load profile of all the seasons are shown in Figure 3.

The Pecan Street dataport continuously monitors each home's energy use and production at intervals of 1 s to 1 min and beyond. The time slots are on the horizontal axes. Here, 15 min is referred to as a single time slot. The analysis is conducted throughout each of the four seasons for an entire day. Even though we can collect data for 24 h by using a 60-min time slot, a 15-min time slot provides higher resolution data for outcome analysis. This high-resolution data shed light on the production, usage, and storage of energy.

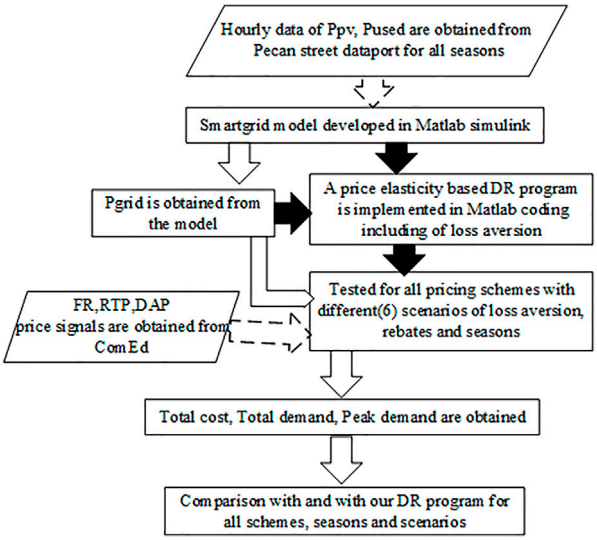

FIGURE 1
Flow diagram of the article.

The total power distributed among the legs is as follows: $P_{Total} = P_{Grid}$;

The total power consumed by the split phase load is as follows:

$$P_{Total} = P_1 + P_2 + P_3, \tag{2}$$

where P_1 = Power to Leg 1 at 120V; P_2 = Power to Leg 2 at 120V; and P_3 = Power to Leg 3 at 240V. Since only P_{Total} is known, we randomly distribute the total power to each leg as follows.

Choosing

$$P_3 = P_{Total} * (a\ random\ distribution\ number\ between\ 0\ and\ 1), \tag{3}$$

$$P_{remaining} = P_{Total} - P_3 \tag{4}$$

Then,

$$P_1 = 0.75 * P_{remaining};\ P_2 = 0.25 * P_{remaining} \tag{5}$$

Each leg current phasor is calculated from the basic power equation

$$P = \frac{1}{2}\left(V_{pk} I_{pk}^{*}\right) \tag{6}$$

Then,

$$I_{pk} = \left(2 * \frac{P}{V_{pk}}\right)^{*} \tag{7}$$

where [*] = complex conjugate, V_{pk} = voltage phasor (peak), and I_{pk} = current phasor (peak). Once the current for each phase is computed, it is used to drive to consumer power from the grid. I=P/V.

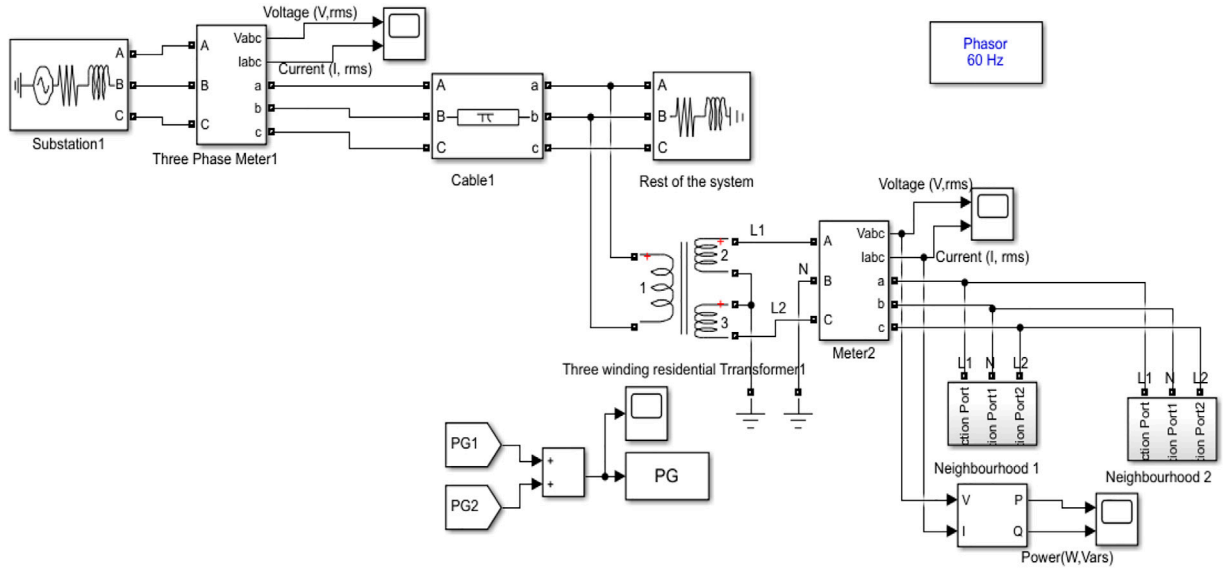

FIGURE 2
Schematic representation of a data-driven smart grid system for incorporating a DR program.

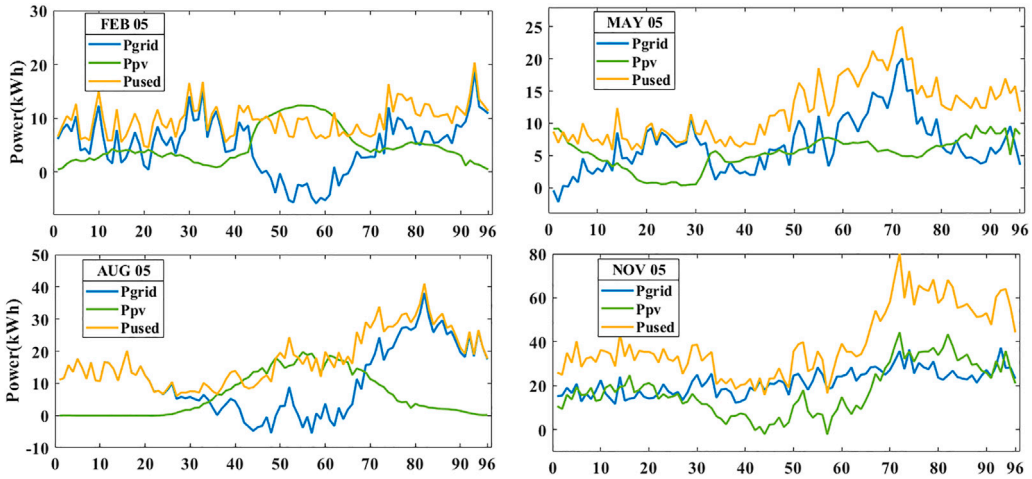

FIGURE 3
Power profile of all seasons.

The energy supply charges (ESCs) can be calculated for different pricing schemes as follows:

For the flat-rate mechanism,

$$ESC = \sum Total\,kWh\,drawn\,from\,the\,grid * Flat\,rate\,(\$/kWh) \quad (8)$$

where the flat rate value is calculated as an average of the RTP pricing of the day.

For the RTP mechanism,

$$ESC = \sum Hourly\,kWh\,drawn\,from\,the\,grid * Hourly\,RTP\,(\$/kWh) \quad (9)$$

For the DAP mechanism,

$$ESC = \sum Hourly\,kWh\,drawn\,from\,the\,grid * Hourly\,prices\,that\,are\,informed\,a\,day\,before \quad (10)$$

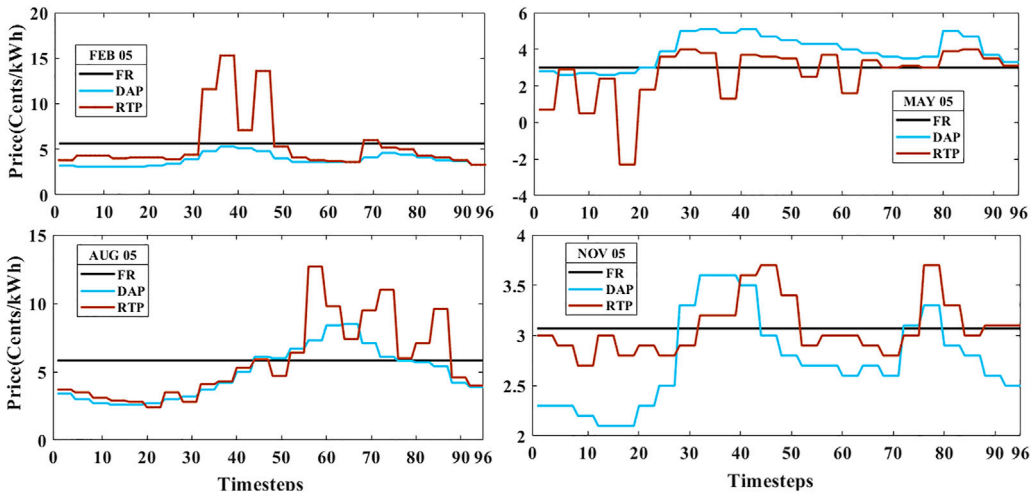

FIGURE 4
Price profile of all the seasons and schemes.

For PTR pricing,

$$ESC = \left(Total\,kWh\,drawn\,from\,the\,grid * Flat\,rate\left(\frac{\$}{kWh}\right)\right) - (Total\,kWh\,drawn\,from\,the\,grid\,during\,peak\,hours * Reward) \quad (11)$$

The standard seasonal information on Austin is categorized as summer, fall, winter, and spring. During the year of case study conduction, 20 June to 22 September is summer, 22 September to 21 December is fall, 21 December to 20 March is winter, and 20 March to 20 June is spring. A single day from each season has been considered for our analysis, that is, February 5, May 5, August 5, and November 5. The days of February and November are on the weekend. The days of May and August are on a weekday. So, the seasonal behavioral analysis can also be performed with these data. As mentioned previously, P_{PV}, P_{Used}, and P_{Grid} information on all those days are obtained from the Pecan Street Project dataport. The price information is obtained from the Common Wealth Edison company dataport ("ComEd's Hourly Pricing," 2011). The price information on all the seasons for the flat rate, RTP, and DAP is shown in Figure 4.

Proposed price elasticity-based demand response program

Loss aversion

Risk aversion is the behavior of human beings (in particular, investors and consumers) in finance and economics, who strive to minimize uncertainty, if they are subjected to uncertainty. It is the reluctance of a person to participate in an unpredictable payoff scenario rather than a more predictable payoff but maybe a lower expected payoff scenario. (For example, a risk-averse investor may prefer to invest their money in a lower but guaranteed bank rate instead of a stock that may have a high return rate, which also involves an opportunity to lose value) (Mohajeryami, Schwarz, & Baboli, 2015).

The fact that losses and disadvantages have a greater effect on perceptions than benefits and advantages is a well-established behavioral fact. This results in a feature of utility that is steeper for losses than for gains. A traditional presumption that assumes a symmetry between the gain and loss value simplifies the study of an individual decision. However, it is not practical. It can, therefore, lead to over- or under-estimated assumptions. In Figure 5, a clear illustration of a value function, that can describe a broad range of outcomes, is shown. In riskless and risky situations, loss aversion is distinct. In risky situations, the value function of loss aversion is clearly steeper. The riskless scenarios include both real-time pricing and peak time discounts.

During peak hours, the utilities charge more in real-time pricing (RTP), so any load that can be shifted to peak hours appears to the consumer as a loss relative to the price of off-peak times. On the other hand, based on their load reduction, the peak time rebate (PTR) relies on rewarding the clients at the peak time. Any load that can be shifted to off-peak times is also equivalent to a gain. Their perceived value, therefore, belongs to the two opposite sides of the value function, although they are the same method, namely, shifting the flexible loads from peak to off-peak times.

Price elasticity-based demand response program:

The price-elasticity curve is shown in Figure 6. When the price decreases, the demand for almost all goods and services increases. This demand shift is not linear. The non-linear

demand curve can be linearized around the particular time to quantify this effect. It is regarded as the demand elasticity of the price. In other words, market elasticity is a standardized indicator of the shift in demand because price increases.

$$E = \frac{P_0}{d_0} \cdot \frac{\partial d}{\partial p} \tag{12}$$

Here, E = demand elasticity; d = the value of demand; P = the price of electricity; and P_0 and d_0 are the initial price of electricity and the demand value, respectively. If electricity prices differ over different periods, the following reactions to demand are

(i) Some of the loads (e.g., illuminating loads) are not capable of moving from one time to the next and can only be on/off. Thus, these loads have just a single period of sensitivity and it is called "self-elasticity," and it often has a negative value:

$$E_{xx} = \frac{\Delta d_x}{\Delta p_x} \leq 0. \tag{13}$$

(ii) Such periods of consumption can be changed from high to off-peak or low periods. Such behavior is referred to as sensitivity for several periods, and "cross-elasticity" is measured. This value is positive at all times.

$$E_{xy} = \frac{\Delta d_x}{\Delta p_y} \geq 0, \tag{14}$$

where Δd_x is the change in demand in period 'x'; Δp_x is the change in price in period 'x'; and Δp_y is the variation in price in period 'y'.

In this article, we will model the DR program depending on price elasticity and articulate how RTP, DAP, and PTR programs affect the prices and demands of electricity and how these programs can achieve the maximum customer benefit.

Modeling for a single period

Assume that

d(i) is the consumer's demand; p(i) is the electricity spot price; I(i) is the incentive ($/kWh); and R (d(i)) is the revenue of the consumer. Also suppose that, depending on the price chosen for the incentive I(i)), the consumer changes his/her own demand from d_0(i) (original value) to d(i). Thus, due to running PTR, P ($) would be as P (Δd(i)) = I(i).Δd(i) (H. Aalami et al., 2008).

Assume that the consumer's benefit for the *i*th period is as shown in

$$B(d(i)) = R(d(i)) - d(i).p(i) + P(\Delta d(i))(\$), \tag{15}$$

$$P(\Delta d(i)) = \lambda.IB(i).\Delta d(i), \tag{16}$$

where IB(i) is an incentive bonus, and in this scenario, this is a reward paid on every peak decrease in kWh. λ, It is a coefficient that represents the actual value of the incentive or reward's nominal payment. It is believed that each person is trying to maximize their benefit. So,

$$\frac{\partial B(d(i))}{\partial d(i)} = \frac{\partial R(d(i))}{\partial d(i)} - p(i) + \frac{\partial P(\Delta d(i))}{\partial d(i)} = 0. \tag{17}$$

Consequently,

$$\frac{\partial R(d(i))}{\partial d(i)} = p(i) + \lambda.IB(i). \tag{18}$$

Marginal utility is equivalent to the energy price at the optimum value. According to H. Aalami et al. (2008), for quadratic customer revenue function, the Taylor series expansion is used. So,

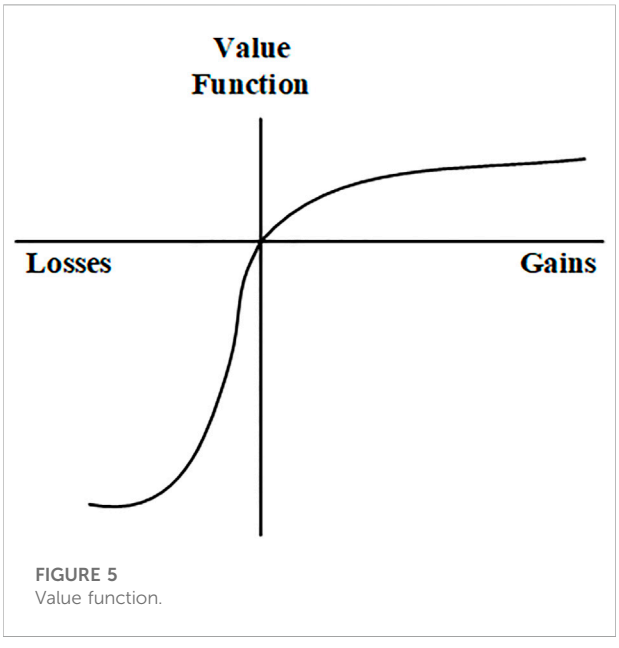

FIGURE 5
Value function.

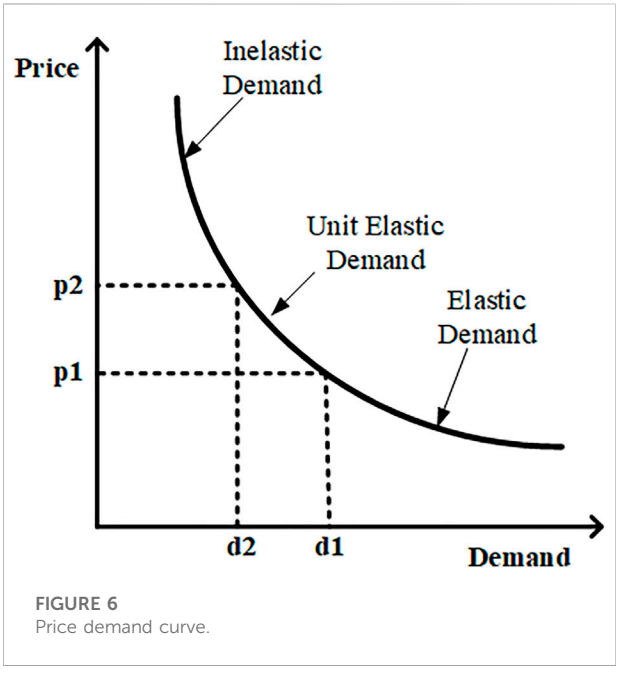

FIGURE 6
Price demand curve.

$$R(d(i)) = R(d_0(i)) + \frac{\partial R(d_0(i))}{\partial d(i)} \times \Delta d(i) + \frac{1}{2} \times \frac{\partial^2 R(d_0(i))}{\partial d^2(i)} \times (\Delta d(i))^2, \quad (19)$$

where d(i) represents a change from d_0(i) (optimal point) in client demand. The following relation must be maintained if the initial demand is optimum prior to the introduction of the DR program.

$$\frac{\partial B_0}{\partial d(i)} = \frac{\partial R(d_0(i))}{\partial d(i)} - p_0 = 0, \quad (20)$$

$$\frac{\partial R(d_0(i))}{\partial d(i)} = p_0. \quad (21)$$

Using (18) and the concept of demand price elasticity (12),

$$\frac{\partial^2 R(d(i))}{\partial d^2(i)} = \frac{\partial p}{\partial d} = \frac{1}{E} \times \frac{p_0}{d_0}. \quad (22)$$

Plugging (21) and (22) into the extension to the Taylor series gives

$$R(d(i)) = R(d_0(i)) + p_0.\Delta d(i) + \frac{1}{2}.\frac{1}{E(i)}.\frac{p_0}{d_0}.(\Delta d(i))^2. \quad (23)$$

It is easy to rewrite Eq. 23 as follows:

$$R(d(i)) = R(d_0(i)) + p_0.\Delta d(i)\left[1 + \frac{\Delta d(i)}{2 \times E(i) \times d_0}\right] \quad (24)$$

Expanding d(i) = d(i)-d_0(i) and afterward relating (24) to (18) offer

$$p(i) + \lambda.\mathrm{IB(i)} = p_0(i) \times \left[1 + \frac{d(i) - d_0(i)}{E(i) \times d_0(i)}\right], \quad (25)$$

$$p(i) + \lambda.\mathrm{IB(i)} = p_0(i) + p_0(i) \times \frac{d(i) - d_0(i)}{E(i) \times d_0(i)}. \quad (26)$$

So, the consumption of the consumer can also be evaluated as follows:

$$d(i) = d_0(i) \times \left[1 + \frac{Ei \times p(i) - p_0(i) + \lambda.\mathrm{IBi})}{p_0(i)}\right]. \quad (27)$$

When I(i) is zero (i.e., no incentive award) in the aforementioned equation, d(i) would be equal to d_0(i). Consequently, the price of energy would not change and the elasticity of the price will be equal to 0.

Modeling for the multi-period

The cross-elasticity between the periods i and j is described as follows:

$$E(i,j) = \frac{P_0(j)}{d_0(i)} \times \frac{\partial d(i)}{\partial p(j)}, \; i \neq j, \quad (28)$$

$$\begin{cases} E(i,j) \leq 0, if\ i = j, \\ E(i,j) \geq 0, if\ i \neq j. \end{cases}$$

In (28), we conclude that $\frac{\partial d(i)}{\partial p(j)}$ is constant. The demand response to price variance could, therefore, be characterized as a linear function. Here, 15 min is known as a one-time slot. The demand response model for 24 (96-time slots) hours a day can be obtained by incorporating self- and cross-elasticity of demand as follows:

$$d(i) = d_0(i) + Ei \times \frac{d_0(i)}{p_0(i)} \times p(i) - p_0(i) + \lambda.\mathrm{IB(i)} + \sum_{\substack{j=1 \\ j \neq i}}^{96} E(i,j) \times \frac{d_0(i)}{p_0(j)} \times (p(j) - p_0(j) + \lambda.\mathrm{IB(j)}), \quad i = 1, 2 \ldots 96. \quad (29)$$

The aforementioned equation shows how high the customer's consumption should be in order to reach maximum profits in 24 h. The change in demand in Eq. 29 comes from two sources. The source is self-elasticity, expressed in the first term, and cross-elasticity, expressed in the second term, is the other source. Both price- and reward-sensitive demands are expressed in the model. In order to achieve the maximum profit in 24 h, the aforementioned equation indicates how high the consumption of the consumer should be. In the following section, we will illustrate how incentives could change the demand curve through executing FR, RTP, DAP, and PTR programs in the numerical results segment. Load profiles of the consumers are now pre-classified as low consumption, off peak and peak

TABLE 1 Categorization of the load profile.

	February 5		May 5		August 5		November 5	
	Load profile	Interval	Load profile	Interval	Load profile	Interval	Load profile	Interval
Low consumption	0–4 kW	14–28	0–5 kW	1–24	(-50) to 5 kW	26–66	(-5) to 8 kW	39–63
		48–64		32–43				
Off-peak	4–8 kW	1–13, 35–47, and 65–88	5–10 kW	25–31	5–20 kW	1–25	9–20 kW	1–38 and 64–67
				44–66		67–72		
Peak	8–16 kW	29–34	>10 kW	67–96	20–36 kW	73–96	20–30 kW	68–96
		89–96						

TABLE 2 Self and cross elasticities.

	Peak	Off-peak	Low
Peak	-0.10	0.005	0.005
Off-peak	0.005	-0.10	0.003
Low	0.003	0.005	-0.10

categories based on the different bands of power consumption and the time duration where it was obtained. The categorization of load profile is shown in Table 1. The self and cross elasticity values are fixed based on the literature and by examining with various set of values to obtain the desired outcomes. The pre-fixed self and cross elasticity values are shown in Table 2.

Analysis and discussion of results

The flat rate is assumed as the average electricity price of dynamic RTP. Real-time pricing (RTP) is a service that specifically provides consumers with real-time hourly rates. In day-ahead pricing (DAP), a consumer will be told a day in advance of the price of electricity. A peak time rebate (PTR) is a program in which clients earn discounts during peak hours. Loss aversion is not considered ($\lambda = 1$) in the PTR_1 program. Loss aversion is considered in the PTR_2 program ($\lambda = 0.5$). Any dollar lost is considered to be twice the worth of any dollar gained. The PTR_3 program is the same as PTR2, except for the doubling of the cross-elasticity constants. In $PTR_{1,2,3}$ programs, the reward awarded to a client is assumed to be 2.6 times the flat rate value during peak hours. PTR_4 is the same as PTR_1, except that the reward being awarded is doubled, that is, 5.2 times the flat rate value.

A peak price only applies during the designated summer days, that is, June–September. Also, a very low night-time rate that applies during the five windiest months, that is, March–May and November–December (e.g., 5 August, 0.0583$, 5 May, 0.03$, and 5 November, 0.0307$). The experimental rate will be the same as the normal Austin energy rate (e.g., 5 February 0.0564$) for the remaining 3 months of January, February, and October ("ComEd's Hourly Pricing," 2011; McCracken and George, 2014).

Scenario 1: Impact of pricing systems on all season parameters and to illustrate the numerical results of how incentives could alter the demand curve

The impact of the pricing scheme on the total cost, total demand, and peak demand for all seasons has been clearly analyzed here. Initially, the analysis has been done for 5th of February. Corresponding results are tabulated in Table 3. In contrast to flat-rate pricing, the RTP scheme does not show any effect on parameters such as overall cost, total demand, and peak demand here. However, with a loss of utility income of −30% without any impact on the total demand and peak demand, the DAP scheme will have a negative impact. Compared to other pricing schemes, peak demand was reduced in the case of $PTR_{1,2,3}$ (−13.06 percent to −26.13 percent). A fair amount of peak demand is reduced in PTR_1, that is., -26 percent with a loss of -15 percent in utility profits. The potential to minimize the peak demand to half (-26.13 percent to -13.06 percent) and half of the utility income (15.26 percent to -7.63 percent) can be saved relative to PTR_1 by considering the loss aversion ($\lambda = 0.5$) in PTR_2. In conclusion, PTR_2 has a moderate impact as opposed to PTR_1, both in terms of peak reduction and total cost. The doubling of the cross-elasticity values in PTR_3 as opposed to PTR_2 indicates no effect in terms of peak reduction. However, it shows a good impact in maintaining utility in profits (-7.63% to -1.2%) and also by improving the overall carrying capacity of the demand (2.53 percent to 8.96 percent).

In the case of PTR_4, the peak demand was drastically reduced, that is, -50 percent with a huge compromise of -64.6 percent in the total utility income, which is an adverse effect and not advisable. Of all PTR conditions, PTR_3 is the best solution for peak reduction (-13 percent) without compromising on utility revenue (-1.2 percent) with load

TABLE 3 Results of February 05.

Pricing scheme	Price in $/kWh	Reward in $/kWh	Total cost in $	Total demand in kWh	Peak demand in kWh
Flat rate	0.0564		24.83	440.08	130.99
RTP	Dynamic		23.57 (-5.08%)	433.82 (-1.42%)	132.72 (+1.31%)
DAP	0.0392, Dyn		17.23 (-30.6%)	436.82 (-0.74%)	130.83 (-0.12%)
PTR_1	0.0564	0.1475	21.04 (-15.26%)	462.4 (+5.07%)	96.75 (-26.13%)
PTR_2	0.0564	0.1475	22.93 (-7.63%)	451.24 (+2.53%)	113.87 (-13.06%)
PTR_3	0.0564	0.1475	24.53 (-1.2%)	479.52 (+8.96%)	113.87 (-13.06%)
PTR_4	0.0564	0.282	8.77 (-64.64%)	482.75 (+9.69%)	65.53 (-49.97%)

capacity improvement (9 percent) as a result of the shifting load to non-peak hours and low-price hours. Figure 7 shows the demand curve of all pricing schemes for the month of February. Figures 8, 9 shows the bar chart of all parameters and all pricing schemes for the month of February and May respectively. Figure 8 shows the bar chart of all parameters and all pricing schemes for the month of February.

Then, the analysis has been done for 5th of May, August and November. Corresponding results are tabulated in Tables 4–6 respectively. If utility income is only the criterion, DAP is considered the best in May. According to the Pecan Street report (Rate Structure Information for Time-of-Use Pricing, 2011; McCracken and George, 2014), the explanation for low income in May is due to the very low night-time rate that applies during the five windiest months (March–May and November–December). When the key concern is peak demand reduction, then PTR_1 is the best option. However, because of the compromise in utility revenue (36.2 percent), it is not advisable. As far as all parameters are concerned, then PTR_3 is the best choice for May with all the parameters in a moderate range. In PTR_3, with a compromise of 9.5% utility revenue, 13.09% peak demand can be reduced with increased loading capability by 9.7%. In August and November, the trend of all the parameters remains the same. PTR_3 is the optimal solution by keeping all parameters in concern.

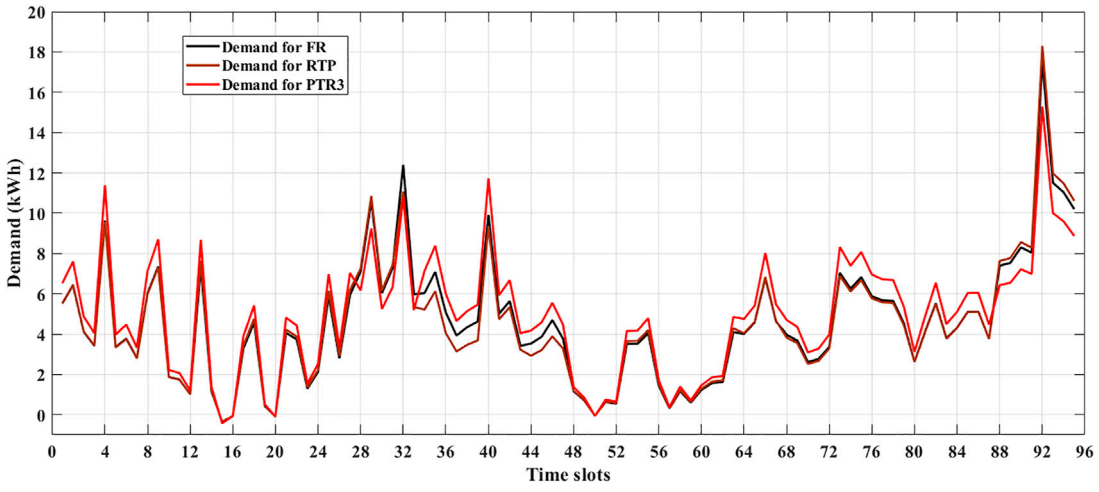

FIGURE 7
Demand curve of all pricing schemes for February 05.

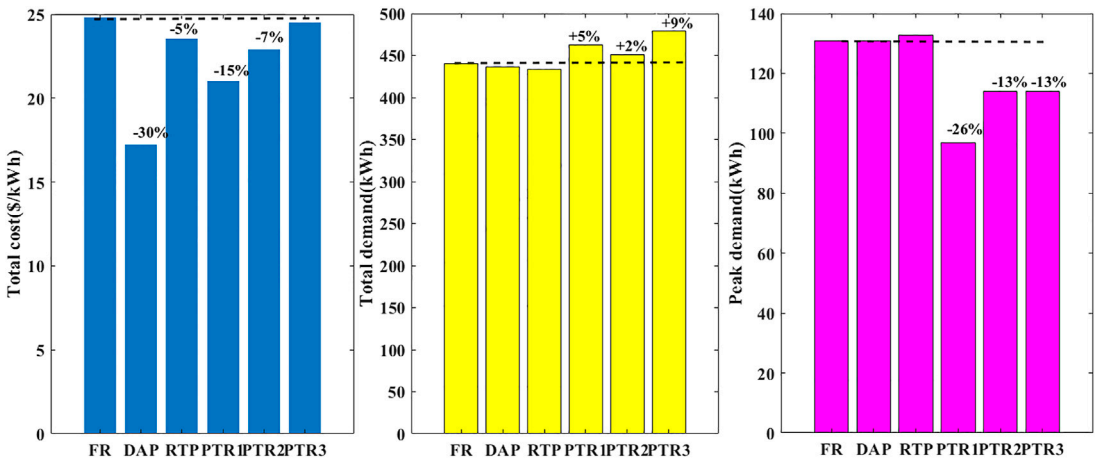

FIGURE 8
Bar chart of all parameters and all pricing schemes for February 05.

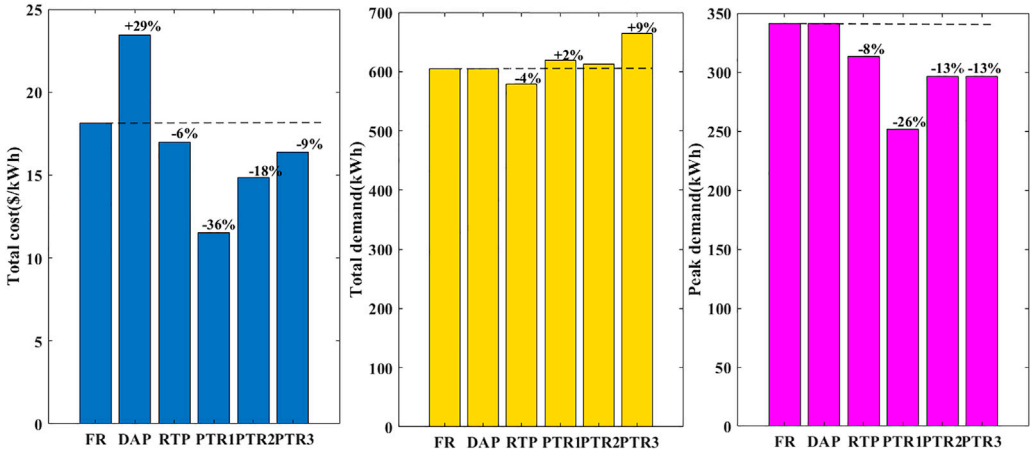

FIGURE 9
Bar chart of all parameters and all pricing schemes for the month of May.

TABLE 4 Results of May 05.

Pricing scheme	Price in $/kWh	Reward in $/kWh	Total cost in $	Total demand in kWh	Peak demand in kWh
Flat rate	0.03		18.13	605.25	341.11
RTP	Dynamic		16.98 (-6.34%)	579.45 (-4.2%)	313.49 (-8.1%)
DAP	0.0389, Dyn		23.43 (+29.2%)	604.6 (-0.1%)	341.19 (0.02%)
PTR_1	0.03	0.07845	11.55 (-36.2%)	619.68 (+2.3%)	251.79 (-26.18%)
PTR_2	0.03	0.07845	14.84 (-18.1%)	612.47 (+1.19%)	296.45 (-13.09%)
PTR_3	0.03	0.07845	16.4 (-9.5%)	664.34 (+9.7%)	296.45 (-13.09%)

TABLE 5 Results of August 05.

Pricing scheme	Price in $/kWh	Reward in $/kWh	Total cost in $	Total demand in kWh	Peak demand in kWh
Flat rate	0.0583		62.78	1,076.6	596.43
RTP	Dynamic		60.47 (-3.6%)	1,068.37 (-0.7%)	562.59 (-5.6%)
DAP	0.0460,Dyn		50.1 (-20.1%)	1,102.34 (+2.39%)	596.75 (+0.05%)
PTR_1	0.058315	0.1524	38.71 (-38.3%)	1,071.31 (-0.49%)	440.56 (-26.1%)
PTR_2	0.058315	0.1524	50.75 (-19.1%)	1,073.95 (-0.24%)	518.5 (-13%)
PTR_3	0.058315	0.1524	55.14 (-12.1%)	1,149.24 (+6.74%)	518.5 (-13%)

TABLE 6 Results of November 05.

Pricing scheme	Price in $/kWh	Reward in $/kWh	Total cost in $	Total demand in kWh	Peak demand in kWh
Flat rate	0.03067		33.64	1,097	648.7
RTP	Dynamic		33.68 (0.09%)	1,099 (0.18%)	646.6 (-0.325%)
DAP	0.0275, Dyn		30.14 (-10.41%)	1,098.1 (0.09%)	644.6 (-0.638%)
PTR_1	0.307	0.0803	20.01 (-40.5%)	1,097.4 (0.03%)	478.9 (-26.18%)
PTR_2	0.307	0.0803	26.83 (-20.25%)	1,097.2 (0.015%)	563.8 (-13.09%)
PTR_3	0.307	0.0803	29.44 (-12.49%)	1,182.3 (+7.77%)	563.8 (-13.09%)

Scenario 2: Impact of pricing schemes for all seasons on all parameters and contrast between seasons

The percentage change in total cost, total demand, and peak demand is shown in bar charts for all pricing schemes in Figures 10–12, respectively. Percentage change in total cost: utility revenue has dropped in the range of 3% to 6 percent for RTP pricing in all seasons, and PTR_1 for utility revenue or total cost of all seasons has dropped in the range of 15% to 40 percent. Due to λ 's variation from 1 to 0, the total cost of PTR_2 is half of PTR_1. A range of 1 percent decreased to 12 percent for PTR_3. Percentage change in total demand: the total demand reduction is in the range of 1 to 4 percent for RTP pricing in all seasons. The percent increase in the total demand range is 0 to +5 percent in PTR_1. In PTR_2, the percentage increase in the total demand range is 0 to +2%, that is, the exact half of PTR_1. Percentage change in peak demand: the percentage peak decrease range for RTP is 0 to −8 percent. The percentage peak reduction range for PTR_1 is 26 percent. The percentage peak reduction range for PTR_2 is exactly half of PTR_1 at −13 percent. The percentage peak reduction range for PTR_3 is exactly the same as PTR_2 at 13 percent.

PTR_1 has a positive effect on the reduction of peak demand (-26%) and the rise in total demand (0–5%). However, the reduction in utility income also had a major effect (15 to 40 percent). The credit for $PTR_{2,3}$ is half the credit for PTR_1 in all seasons. The cause is that $\lambda = 0.5$ is taken into account in $PTR_{2,3}$, and in the demand response equation, reward 0 is replaced by 0.5*reward0. The value of λ is also expressed in the value of the credit. At the $\lambda = 1$ condition, peak demand is drastically reduced in all the seasons. Peak demand

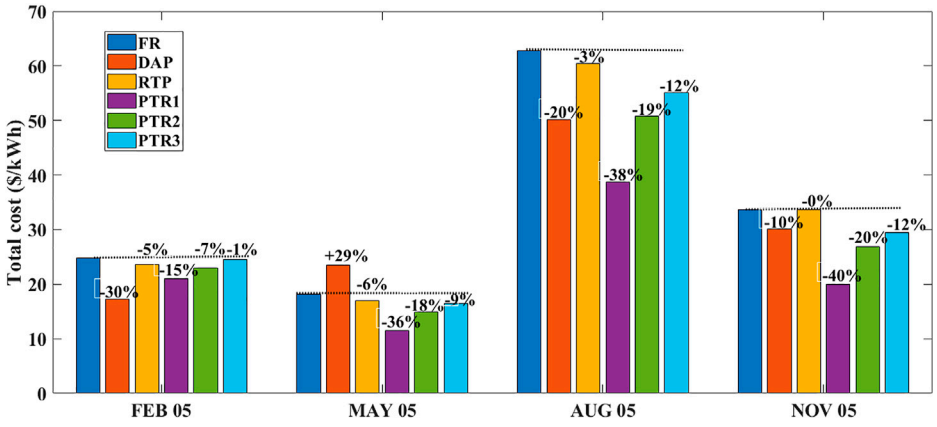

FIGURE 10
Percentage change in the total cost for all seasons and all pricing schemes.

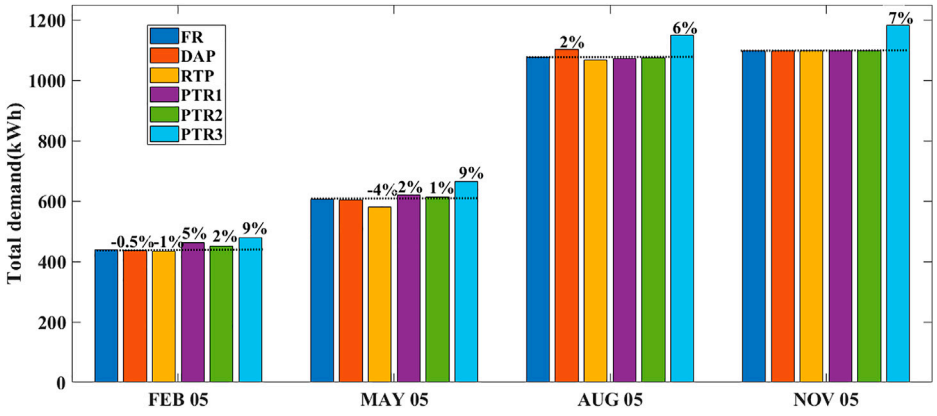

FIGURE 11
Percentage change in total demand for all seasons and all pricing schemes.

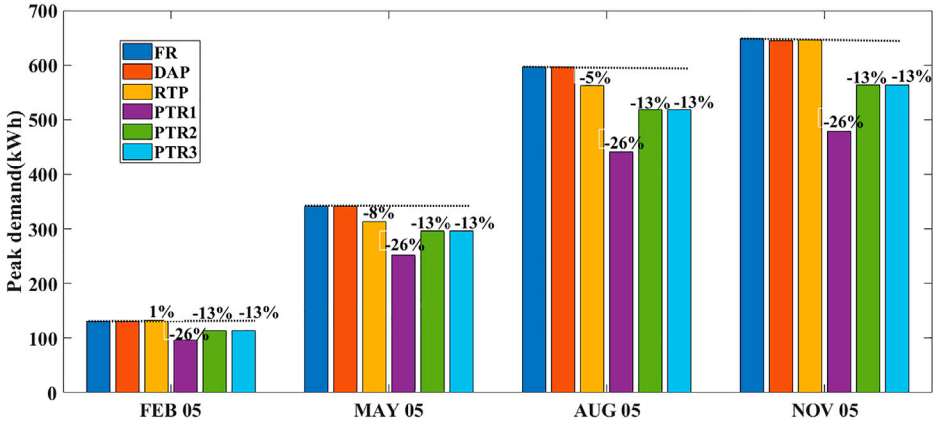

FIGURE 12
Percentage change in peak demand for all seasons and all pricing schemes.

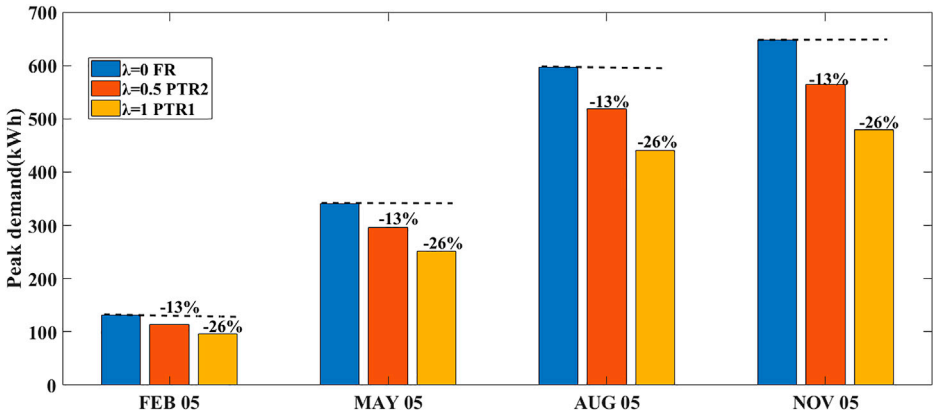

FIGURE 13
Percentage change in peak demand for all seasons and all values of loss aversion.

is decreased and halved at $\lambda = 0.5$ compared to $\lambda = 1$; peak demand comparison at different conditions of $\lambda = 0$(FR), 0.5(PTR_2), and 1(PTR_1) is shown in Figure 13.

The total demand for February and May is between 440 and 660 units. Also, the total cost is between $11 and $24 with average flat rate values of 0.0564 and 0.03. The total demand surged by almost 80% in August and November, that is, in the range of 1,050 to 1180 kwh, and cost ranges from 33 $to 50$.With the same range of the total demand, the total cost of November is almost half of that of August because the RTP price signal variation is based on the season and nature of the day. For the total demand range of ≈440units in February and ≈1,097 units in November, it charges almost in the same range of ≈24 to 30 $.

Scenario 3: Rebate or reward that has given during peak hours is 2.6 times of the flat rate (PTR_4). If it is doubled, that is, the reward is equal to 5.2 times the flat rate, what will be the response?

The FEB is reviewing this situation. The corresponding changes in parameters due to doubling of rebate are tabulated in Table 7. The flat rate is 0.0564 for the FEB. The incentive is now boosted to 0.2820 (i.e., 5.2 times the flat rate) during peak hours. Peak demand is decreased by 49 percent relative to the flat rate. Also, the total demand is raised by 9%, and the utility's total revenue is decreased by 64%. Compared to PTR_1, just by changing the rebate value, much change has

TABLE 7 Doubling of the rebate scenario.

Pricing scheme	Reward in $/kWh	Total cost in $	Total demand in kWh	Peak demand in kWh
FR		24.83	440.08	130.9
PTR_1	2.6*0.0564	21.04	462.4	96.75
PTR_4	5.2*0.0564	8.77	482.7	65.53

been observed in the percentage change in peak demand and total cost. However, it is not at all suggested as it is happening at the loss of utility revenue.

Scenario 4: Equal loss scenario and peak reduction scenario (for any season)

The equal loss scenario criterion is the one that evaluates how much peak reduction can be accomplished with the same amount of economic loss. In the peak reduction scenario, utilities are interested in peak reduction, regardless of the cost. The month of May is considered for analyzing these scenarios. For equal loss scenario, total demand and peak demand responses are shown in Figure 14. The implications of equal loss scenario and peak reduction scenario on the parameters are listed out in Tables 8, 9 respectively.

To retain equivalent financial loss, i.e., −6.34 percent, the PTR_1 rebate is reduced to 0.0343 from $0.07845 per kWh. PTR_1 can achieve a −11.4 percent peak reduction in PTR_1 without taking into account the loss aversion scenario (i.e., $\lambda = 1$), compared to a −8.1 percent peak reduction in RTP. In the same way, a −7.91 percent reduction compared to RTP is accomplished by considering loss aversion in PTR_2. In terms of peak reduction, PTR_3 shows the same effect as PTR_1, i.e., −11.51 percent. The added advantage with PTR_3 is the improvement in total demand serving capability of 8.5% and peak reduction of −11.4% is attained by considering loss aversion and doubling the cross elasticity constants.

Compared to RTP, the corresponding peak reduction of 8.11 percent in PTR is achieved at $\lambda = 0.31$. RTP is responsible for utility loss of 6.34 percent for the same peak load reduction, while 11.24 percent in PTR_1. Compared to RTP (4.26 percent), the total demand serving capacity is better in PTR_1 (+0.7 percent). The selection of either RTP or PTR_1 is solely

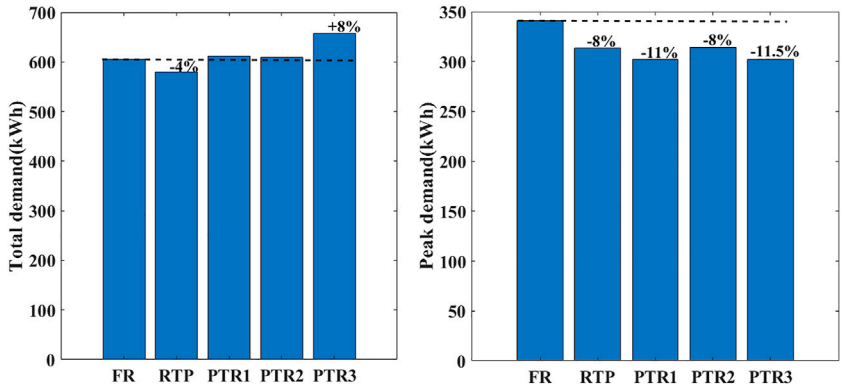

FIGURE 14
Total demand and peak demand for the equal loss scenario.

TABLE 8 Equal loss scenario.

Pricing scheme	Price in $/kWh	Reward in $/kWh	Total cost in $	Total demand in kWh	Peak demand in kWh
FR	0.03		18.13	605.25	341.1
RTP	Dynamic		16.98 (-6.34%)	579.45 (-4.26%)	313.4 (-8.09%)
PTR_1	0.03	0.0343	16.98 (-6.34%)	611.56 (+1.04%)	302.0 (-11.44%)
PTR_2	0.03	0.0474	16.98 (-6.33%)	609.61 (+0.72%)	314.12 (-7.91%)
PTR_3	0.03	0.069	16.98 (-6.36%)	657.23 (+8.58%)	301.83 (-11.51%)

TABLE 9 Peak reduction scenario.

Pricing scheme	Price in $/kWh	Reward in $/kWh	Total cost in $	Total demand in kWh	Peak demand in kWh
FR	0.03		18.13	605.25	341.11
RTP	Dynamic		16.98 (-6.34%)	579.45 (-4.26%)	313.49 (-8.09%)
PTR_1	0.03	0.07845	16.09 (-11.24%)	609.73 (+0.73%)	313.42 (-8.11%)

TABLE 10 For different values of loss aversion.

Season	May				August			
Pricing scheme	λ	Reward	Total demand	Peak demand	λ	Reward	Total demand	Peak demand
FR								
RTP	0		579.4	313.4	0		1,068.3	562.5
PTR_2	0.5	0.07845	612.4	296.4	0.5	0.1524	1,073.9	518.5
PTR_1	1	0.07845	619.6	251.8	1	0.1524	1,071.3	440.5

TABLE 11 Doubling of the elasticity constant case.

	May					August				
	λ	Reward	Elasticity constant	Total demand	Peak demand	λ	Reward	Elasticity constant	Total demand	Peak demand
PTR2	0.5	0.07845	0.005 and 0.003	612.4	296.4	0.5	0.0583	0.005 and 0.003	1,073.9	518.5
PTR3	0.5	0.07845	0.01 and 0.006	664.3 (+7%)	296.4	0.5	0.0583	0.01 and 0.006	1,149.2 (+8.4%)	518.5

dependent on the priority of the cost, else load demand serving capacity for the same peak reduction.

Scenario 5: For the same value of rebate, if λ is changed from 0 (FR), 0.5 (PTR_2), and 1 (PTR_1), then what will happen?

For the same value of rebate, change in loss aversion value effects the parameters that are shown in Table 10. For the same reward value, a decrease in peak demand is caused by λ approaching from 0 to 1. The value range is from 313.4 to 251.4 for May and 562.5 to 440.5 for August. At the same time, this allows the total demand to rise. For May, its value ranges from 579.4 to 619.6 and for August, it ranges from 1,068.3 to 1,071.3. In conclusion, the pattern of a significant reduction in peak demand and a rise in total demand is observed as λ approaches 0 to 1.

Scenario 6: For the same value of reward and λ values, are elasticity constants doubled?

For the same value of reward and λ values, but elasticity constants are doubled. Then the corresponding implications on the parameters are shown in Table 11. The total demand is significantly increased through the doubling of cross elasticity values. Their values change from 612 to 664 for May. The range is 1,073–1,149 for August. The peak demand remains unchanged for May (296–296) and August (518–518). Therefore, the peak demand has been shown to remain unaltered, and overall demand has risen by 7–8.4 percent.

Conclusion

The potential of demand response initiatives has offered new perspectives for the electricity market to participate in the process of making decisions by the clients. Time-based DR programs help enhance the indices of service and reliability. Choosing the right one among them depends on financial and technical aspects. These aspects should be integrated into the utility function of the customer. The influence of loss aversion is studied on the PTR program with different scenarios in this paper. Of all PTR conditions, without sacrificing on utility revenue with load capacity increase, PTR_3 is the best option for peak reduction. There are also season-based conclusions, such as a drastic change in some parameters for a specific season or between different

seasons in relation to other parameters. It also discusses the situations that make the system financially and technically unviable. The best outcomes of the peak load reduction scenario and equal loss scenario are well-explored. In conclusion, as λ approaches 0 to 1, the trend of a sharp reduction in the peak demand and an increase in the total demand is observed. The peak demand has been shown to remain constant, and the total demand has increased by doubling the cross-elasticity values.

Data availability statement

Publicly available datasets were analyzed in this study. These data can be found at: ComEd's Hourly Pricing. (2011). Retrieved from https://dataport.pecanstreet.org/academic and from https://dataport.pecanstreet.org/academic.

Author contributions

RP has conceptualised, implemented, investigated and validated the proposed methodology for the smart grid environment. And also prepared the original manuscript. BJ has supervised the whole work and reviewed the manuscript. JI has given valuable inputs in implementing of the the work. HC has edited the manuscript for better visualization.

Acknowledgments

PR received his Bachelor of Technology degree from Kakatiya University College of Engineering, Telangana, India, in 2007. He obtained master's degree from JNTU, Hyderabad, India. He has completed his doctoral degree from the School of Electrical Engineering, Vellore Institute of Technology, Tamil Nadu, India. He has more than 11 years of teaching and research experience in electrical engineering in reputed organizations including VIT and Ministry of Manpower, Sultanate of Oman. His research interest includes energy management, demand-side management/demand response, optimization, energy efficiency in buildings, and grid-connected PV Systems, IoT. JB (corresponding author) received his B.E. in Electrical Engineering from Manonmaniam Sundaranar University, Tamilnadu, India, in 1999, an ME in Power Systems from Annamalai University, Tamil Nadu, India, in 2002 and a PhD from Anna University, Chennai, in 2013. He has been working as an Associate Professor at Vellore Institute of Technology, Tamil Nadu, India. He has more than 19 years of experience in teaching and research. His major scientific interest is focused on power system optimization and protection, optimal location of FACTS and DG devices, renewable energy systems, and demand-side management. He has been serving as secretary for the IEEE i-PACT conference 2017, 19, and 21. IJ was born in India and received his bachelor's degree in Electrical Engineering from The Indian Engineering College and master's degree in Power Systems Engineering from Annamalai University with first class in 2000 and 2001, respectively. He has completed his Ph.D. degree in the Department of Electrical and Electronics Engineering, Indian Institute of Technology, Roorkee, India, in the year 2007. He is presently working as a Professor in the School of Electrical Engineering, Vellore Institute of Technology (VIT). His field of interest is unit commitment, economic dispatch, power system restructuring and deregulation, artificial intelligence applications to power system, and FACTS. CH has 2.6 years of teaching experience. He received his bachelor's degree in Electrical & Electronics Engineering from Jawaharlal Nehru Technological University, Anantapuramu, India, and a master's degree in Power Electronics & Drives from VIT University, Vellore, India, in 2013 and 2016, respectively. He received his Ph. D from VIT University, Vellore, India, in the year 2022. He has published various SCI, Web of Science, Springer Book Chapters, and SCOPUS indexed journals. His research interests include PV cell modeling, fuel cell modeling, soft computing, artificial intelligence, power point tracking techniques, liquid dielectrics, spectroscopy analysis, and design of high step-up dc-dc converters for electric vehicle application.

Conflict of interest

The authors declare that the research was conducted in the absence of any commercial or financial relationships that could be construed as a potential conflict of interest.

Publisher's note

References

Aalami, H. A., Pashaei-Didani, H., and Nojavan, S. (2019). Deriving nonlinear models for incentive-based demand response programs. *Int. J. Electr. Power & Energy Syst.* 106, 223–231. doi:10.1016/j.ijepes.2018.10.003

Aalami, H., Yousefi, G. R., and Parsa Moghadam, M. (2008). "Demand response model considering EDRP and TOU programs. Transmission and Distribution Exposition Conference," in *2008 IEEE PES powering toward the future*. doi:10.1109/TDC.2008.4517059

Abapour, S., Mohammadi-Ivatloo, B., and Tarafdar Hagh, M. (2020). Robust bidding strategy for demand response aggregators in electricity market based on game theory. *J. Clean. Prod.* 243, 118393. doi:10.1016/j.jclepro.2019.118393

Ajoulabadi, A., Ravadanegh, S. N., and Mohammadi-Ivatloo., Behnam (2020). Flexible scheduling of reconfigurable microgrid-based distribution networks considering demand response program. *Energy* 196, 117024. doi:10.1016/j.energy.2020.117024

Chai, Y., Xiang, Y., Liu, J., Gu, C., Zhang, W., and Xu, W. (2019). Incentive-based demand response model for maximizing benefits of electricity retailers. *J. Mod. Power Syst. Clean. Energy* 7 (6), 1644–1650. doi:10.1007/s40565-019-0504-y

ComEd's Hourly Pricing (2011). *ComEd's hourly pricing*. Retrieved from Available at: https://dataport.pecanstreet.org/academic.

Dhundia, S. (2016). *Real time pricing simulator for a smart grid*.

Hosseini Imani, M., Niknejad, P., and Barzegaran, M. R. (2019). Implementing Time-of-Use Demand Response Program in microgrid considering energy storage unit participation and different capacities of installed wind power. *Electr. Power Syst. Res.* 175, 105916. doi:10.1016/j.epsr.2019.105916

Jiang, J., Kou, Y., Bie, Z., and Li, G. (2019). Optimal real-time pricing of electricity based on demand response. *Energy Procedia* 159, 304–308. doi:10.1016/j.egypro.2019.01.011

Lu, R., and Hong, S. H. (2019). Incentive-based demand response for smart grid with reinforcement learning and deep neural network. *Appl. Energy* 236 (2018), 937–949. doi:10.1016/j.apenergy.2018.12.061

McCracken, B., and George, T. (2014). *Pecan street smart grid demonstration project interim Technology performance report*.

Mohajeryami, S., Schwarz, P., and Baboli, P. T. (2015). *Including the behavioral aspects of customers in demand response model: Real time pricing versus peak time rebate*. North American Power Symposium. doi:10.1109/NAPS.2015.7335116*NAPS*

Monfared, H. J., Ghasemi, A., Loni, A., and Marzband, M. (2019). A hybrid price-based demand response program for the residential micro-grid. *Energy* 185, 274–285. doi:10.1016/j.energy.2019.07.045

Rajendhar, P., and Belwin Edward, J. (2019). "Application of demand response and co-simulation approach for renewable integrated home energy management system: A review," in *IET generation, transmission & distribution* (United Kingdom: Wiley). doi:10.1049/iet-gtd.2018.5791

Rate Structure Information for Time-of-Use Pricing (2011). *Rate structure information for time-of-use pricing*. Retrieved from Available at: https://www.pecanstreet.org/wp-content/uploads/2011/07/Pricing-trial-rate-overview.pdf.

Residential data page of Pecan street data port (2022). *Residential data page of Pecan street data port*. Retrieved from Available at: https://dataport.pecanstreet.org/academic.

Sharifi, R., Fathi, S. H., Anvari-Moghaddam, A., Guerrero, J. M., and Vahidinasab, V. (2018). An economic customer-oriented demand response model in electricity markets. *Proc. IEEE Int. Conf. Industrial Technol.*, 1149. –1153. doi:10.1109/ICIT.2018.8352340

Shi, Q., Chen, C. F., Mammoli, A., and Li, F. (2020). Estimating the profile of incentive-based demand response (IBDR) by integrating technical models and social-behavioral factors. *IEEE Trans. Smart Grid* 11 (1), 171–183. doi:10.1109/TSG.2019.2919601

University of Texas, C. for electromechancis (2011). *Simulink smartgrid simulation 1: The basics*. Retrieved from Available at: https://www.youtube.com/watch?v=UvOJh534cok&t=228s.

Nomenclature

Acronyms

DR demand response
FR flat rate
RTP real-time pricing
DAP day-ahead pricing
PTR peak time rebate
IBDR incentive-based demand response
ESC energy supply charge

Variables

P_{Grid} power drawn from the grid
P_{Used} power consumed by the loads
P_{PV} PV power generated
P_{Total} total power distributed among the legs
$P_{1,2,3}$ power to legs 1, 2, and 3, respectively
V_{pk} voltage phasor (peak)
I_{pk} current phasor (peak)
E demand elasticity
d value of demand
p price of electricity
Δd change in demand
Δp change in price
$I(i)$ incentive($/kWh)
$R(d(i))$ revenue
$IB(i)$ incentive bonus
λ coefficient that represents the actual value of the incentive or reward's payment

Indices

i,j time periods

frontiers | Frontiers in Energy Research

TYPE Original Research
PUBLISHED 06 January 2023
DOI 10.3389/fenrg.2022.1076529

OPEN ACCESS

EDITED BY
Sarat Kumar Sahoo,
Parala Maharaja Engineering College (P.M.E.C), India

REVIEWED BY
Ashwin Sahoo,
C. V. Raman College of Engineering, India
Prabhakar Karthikeyan Shanmugam,
VIT University, India
Sachidananda Prasad,
National Institute of Science and Technology, India
Razia Sultana Wahab,
VIT University, India

*CORRESPONDENCE
Zhanming Li,
lizm@lut.edu.cn

SPECIALTY SECTION
This article was submitted to Smart Grids, a section of the journal Frontiers in Energy Research

RECEIVED 21 October 2022
ACCEPTED 19 December 2022
PUBLISHED 06 January 2023

CITATION
Wang N and Li Z (2023), Short term power load forecasting based on BES-VMD and CNN-Bi-LSTM method with error correction.
Front. Energy Res. 10:1076529.
doi: 10.3389/fenrg.2022.1076529

Short term power load forecasting based on BES-VMD and CNN-Bi-LSTM method with error correction

Nier Wang and Zhanming Li*

College of Electrical and Information Engineering, Lanzhou University of Technology, Lanzhou, China

Aiming at the strong non-linear and non-stationary characteristics of power load, a short-term power load forecasting method based on bald eagle search (BES) optimization variational mode decomposition (VMD), convolutional bi-directional long short-term memory (CNN-Bi-LSTM) network and considering error correction is studied to improve the accuracy of load forecasting. Firstly, a decomposition loss evaluation criterion is established, and the VMD optimal decomposition parameters under the evaluation criterion are determined based on BES to improve the decomposition quality of the signal. Then, the original load sequence is decomposed into different modal components, and the corresponding CNN-Bi-LSTM network prediction models are established for each modal component. In addition, considering the influence of various modal components, holiday and meteorological factors on the error, an error correction model considering short-term factors is established to mine the hidden information contained in the error to reduce the inherent error of the model. Finally, the proposed method is applied to a public dataset provided by a public utility in the United States. The results show that this method can better track the changes of load and effectively improve the accuracy of short-term power load forecasting.

KEYWORDS

short term load forecasting, BES, variational modal decomposition, CNN-Bi-LSTM, error correction

1 Introduction

With the implementation of renewable energy policy, renewable energy has gradually replaced fossil fuels and been rapidly applied to the power system. However, the large-scale renewable energies are connected to the power grid, which could affect customers' electricity consumption behavior and load forecasting (Yang D. et al., 2023). Accurate power demand forecasting is the basis for realizing safe and economic operation of power system and scientific management of power grid, it helps to estimate future loads from recent loads using various techniques in efforts to save energy, reduce costs, perform power management, and implement economic dispatch plans (Talaat et al., 2020). The research shows that if the prediction error is reduced by 1%, a 10 GW power station may save $1.6 million per year (Hobbs et al., 1999). Therefore, establishing an accurate short-term power load forecasting model for a power system is both required and beneficial.

The factors that affect the short-term power load mainly include meteorological, holidays, user habits, etc. These factors are working together to make the power load sequence show obvious volatility and nonlinearity characteristics, which undoubtedly increases the difficulty of accurate prediction (Zhao et al., 2022). Therefore, it is necessary to study more accurate short-

term power load forecasting methods. For the short-term power load forecasting model, the research mainly includes statistical methods and machine learning methods. Among them, the statistical methods mainly include autoregressive integrated moving average model (Lee and Ko, 2011), Kalman filter (Zhao et al., 2016), etc. The principle and modeling of such methods are simple, and the statistical method can fully reflect the temporal relationship between power load data, but its nonlinear characteristics are not fully considered. Machine learning algorithms can effectively deal with nonlinear problems. The traditional machine learning methods mainly include: artificial neural network (ANN) (Garcia-Ascanio and Mate, 2009), support vector machine (SVM) (Jiang et al., 2018), random forest (RF) (Wu et al., 2015), etc. ANN has self-learning ability and can effectively solve the nonlinear problems in load data, but it is difficult to determine the network structure scientifically, and has some defects such as local minimum, large generalization error, the prediction accuracy is usually difficult to meet the requirements. The SVM method solves the local minimum question and has stronger generalization ability, but the disadvantage of SVM is that it is sensitive to parameter adjustment and kernel function selection. The RF algorithm is applied to short-term power load forecasting, which has the advantages of higher prediction accuracy and controllable generalization error, but when the load fluctuation is large, the prediction accuracy is not high. Although the above machine learning methods can better reflect the nonlinear relationship between data, the common problem of these methods lies in the lack of consideration of the temporal correlation of time series data (Rodrigues and Pereira, 2020).

With the development of deep learning, different types of neural networks have been proposed one after another, which provides different solutions to the problem that the timing and nonlinearity of data cannot be considered at the same time in power load forecasting. Such as long short-term memory network (LSTM), convolutional neural network (CNN) and deep belief network (DBN) (Chen et al., 2021). Among them, LSTM network has the characteristics of preserving the timing and nonlinearity of data at the same time, so its application in power load forecasting, renewable energy output power forecasting and other fields is increasing. As an optimization of LSTM network, gated recurrent unit (GRU) not only achieves its approximate accuracy, but also has the advantages of less training parameters and fast speed. In addition, bi-directional long short-term memory (Bi-LSTM) network is used for load forecasting, which has better expression ability for continuous time series, and the reuse of weight parameters makes it have lower requirements for data (Kwon et al., 2020; Zang et al., 2021).

However, although GRU and other models can fully respond to the long-term historical process in the input time series data, the effective information between discontinuous data cannot be extracted, and thus the potential relationship between data cannot be deeply mined. With the diversification of training data types and the increase of power grid demand for load forecasting accuracy, the combined forecasting model came into being to further improve the accuracy of load forecasting (Muhammed et al., 2021). Lu et al. (2019) proposed a short-term load forecasting model combining CNN with LSTM network. CNN is used to extract the potential relationship between continuous data and discontinuous data in the feature map and form the feature vector. Then, the feature vector is used as the input of LSTM for load forecasting. Lee and Cho, (2022) determined the most accurate peak load-forecasting model by comparing the performance of time series (Seasonal autoregressive integrated moving average with exogenous variables, SARIMAX), machine learning (Support vector regression, SVR, etc.) and hybrid models (SARIMAX-ANN, etc.). The results indicate that the hybrid models exhibit significant prediction performance.

With the continuous development of data decomposition algorithm, in order to reduce the impact of volatility and nonlinearity in power load series and further improve the accuracy of short-term load forecasting, the hybrid forecasting method combining data decomposition algorithm with existing forecasting models has been widely used in power load forecasting (Zhang et al., 2022). Empirical mode decomposition (EMD) is an adaptive signal decomposition method based on local characteristics of signals. This method overcomes the difficulty of selecting wavelet basis and determining decomposition scale in wavelet transform (WT), so it is more suitable for nonlinear and non-stationary signal analysis (Zhang et al., 2021). Meng et al. (2021) proposed a short-term load forecasting approach integrating EMD, bi-directional long short-term memory and attention mechanism. EMD decomposes the load series into a finite number of components or modes [called intrinsic mode functions (IMFs)] with different characteristic scales, and decomposes the fluctuations or trends of different scales that actually exist in the signal step by step, then a Bi-LSTM neural network based on attention mechanism is applied on each of the extracted IMFs to predict the tendencies of these IMFs, finally, the prediction results of each component are superposed to obtain the load prediction value. Compared with the original load data series, the decomposed series has stronger regularity and can improve the prediction accuracy. Kassa et al. (2019) proposed a short-term load forecasting model of microgrid by combining empirical mode decomposition, particle swarm optimization (PSO) and adaptive neural fuzzy inference system (ANFIS). The complex load sequence is decomposed into a set of modal functions and a residual by EMD, and then the ANFIS model of each modal function component and residual are optimized by PSO algorithm, each modal function component and residual are predicted separately to improve the prediction accuracy. However, EMD needs to solve the problems of modal mixing, end effect and over envelope. Liang et al. (2018) decomposed the original sequence of power load into multiple modal functions with different characteristics by VMD, and the prediction model is established through DBN optimized by PSO algorithm, to improve the prediction accuracy; Ye et al. (2022) proposed a load forecasting method based on VMD and multi-model fusion to solve the problem of strong volatility and randomness of multi load in user level integrated energy system and the difficulty of accurate forecasting; Yang Y. et al. (2023) used VMD to decompose the original data into several sub-sequences, which enables it to extract the implied features to separately predict each sub-sequence to improve the prediction accuracy of the short-term load forecasting. Compared with WT and EMD, VMD is widely used in the fields of power load forecasting and renewable energy power signal decomposition due to its strong self-adaptability and ability to overcome modal mixing (Zhou et al., 2021). However, the following problems still exist:

(1) In VMD process, there is no evaluation standard to guide parameter setting, and parameters are often given by experience, which leads to unsatisfactory decomposition effect. Yuan and Che, (2022), Dou et al. (2018).

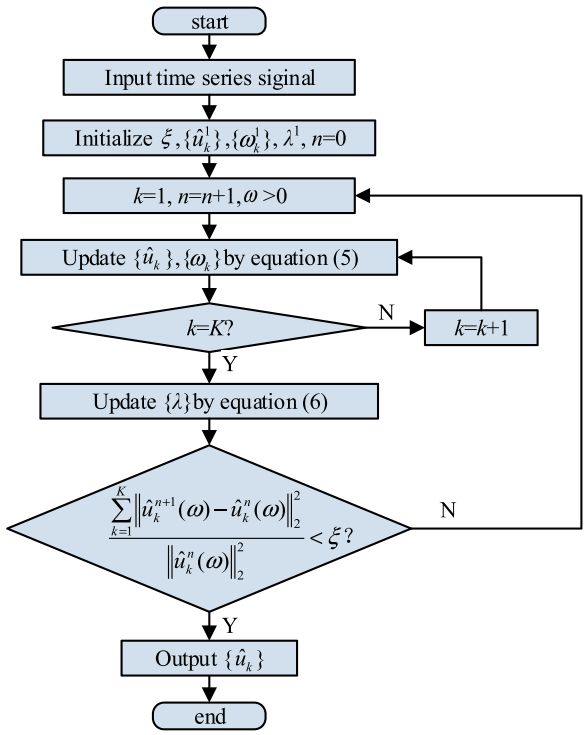

FIGURE 1
Flow chart of VMD.

(2) VMD uses a quadratic penalty factor in the construction of the variational problem, which over punishes the internal jump of the signal, which is easy to generate prediction errors, and the previous research did not make full use of the implicit information in the error. Yan and Tian, (2019).

According to the literatures above, to solve the above problems, meet the challenges of short-term power load forecasting brought by the obvious volatility and nonlinear characteristics of power load due to its vulnerability to various factors, and further improve the accuracy of short-term power load forecasting, a combined short-term power load forecasting method based on BES-VMD-CNN-Bi-LSTM-EC model is proposed in this paper. The forecasting process is divided into two stages: In the first stage, the VMD method optimized by BES algorithm is used to decompose the complex power load data into different subsequence components and then the CNN-Bi-LSTM forecasting model of each load component is established, subsequently, the independent prediction results of each component are reconstructed to obtain the predicted load sequence. In the second stage, an error correction model based on CNN-Bi-LSTM network is established to obtain the predicted error sequence to correct the predicted load sequence before. At last, the final load forecasting results are obtained and further improve the short-term load forecasting effect.

The main contributions of this paper are as follows: 1) The VMD method optimized by bald eagle search (BES) decomposes the non-stationary and nonlinear power load series into components with different frequencies, which effectively reduces the complexity of the load series. 2) The CNN-Bi-LSTM prediction model of each load subsequence is established to improve the feature extraction and dimension reduction ability of the model to the original data. 3) An error correction model considering short-term factors, such as holiday and meteorological factors on the error is established, which reduces the inherent error of the prediction model by mining the effective information hidden in the error. 4) The method proposed in this paper is applied to the actual load verification of the data set published in the 2012 global energy forecasting competition, and the experimental results show its effectiveness in short-term power load forecasting.

The rest of this paper is organized as follows: Section 2 provides the methodology of VMD. Section 3 analyzes the superiority of BES optimization algorithm by simulation experiments. Section 4 introduces the proposed hybrid prediction method in detail. A case study is given to verify the effectiveness of the proposed model in Section 5. Finally, the conclusion is presented in Section 6.

2 Methodology of VMD

VMD is an adaptive signal decomposition method, which can effectively deal with non-stationary and nonlinear signals. By iteratively searching the variational mode, the original time series $f(t)$ is decomposed into different components $u_k(t)$ with limited bandwidth, and its corresponding center frequency is ω_k. Taking the decomposition of power load signal as an example, the steps of constructing the variational problem are as follows:

(1) For each load component $u_k(t)$, Hilbert transform is used to calculate and analyze the signal, and its one-sided spectrum is obtained as follows:

$$\left(\delta(t)+\frac{\mathrm{j}}{\pi t}\right)*u_k(t) \tag{1}$$

(2) For each $u_k(t)$, the spectrum of each component is modulated to the corresponding fundamental frequency band by mixing an exponential term of its corresponding center frequency, as follows:

$$\left[\left(\delta(t)+\frac{\mathrm{j}}{\pi t}\right)*u_k(t)\right]\mathrm{e}^{-\mathrm{j}\omega_k t} \tag{2}$$

(3) The Gaussian smoothing method of demodulated signal is used to estimate the signal bandwidth of each subsequence, and the variational problem with constraints is solved. The objective function is:

$$\begin{cases} \min\limits_{\{u_k\},\{\omega_k\}}\left\{\sum\limits_{k=1}^{K}\left\|\partial_t\left[\left(\delta(t)+\frac{\mathrm{j}}{\pi t}\right)*u_k(t)\right]\mathrm{e}^{-\mathrm{j}\omega_k t}\right\|_2^2\right\} \\ s.t.\sum\limits_{k=1}^{K}u_k = f(t) \end{cases} \tag{3}$$

where, $\{u_k\}=\{u_1,u_2\cdots u_K\}$ is the k modal components obtained after decomposition. $\{\omega_k\}=\{\omega_1,\omega_2\cdots\omega_K\}$ is the center frequency corresponding to each modal component. ∂_t means partial derivative. $\delta(t)$ represents the impulse function. * represents a convolution operation.

By introducing Lagrange multiplication operator λ and the quadratic penalty factor α, the above constrained extreme value

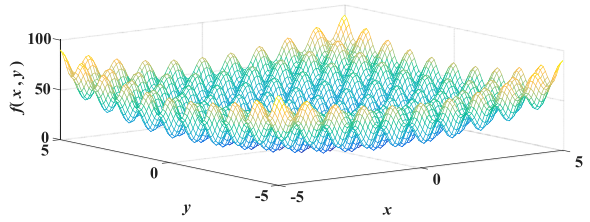

FIGURE 2
Function space.

problem is transformed into an unconstrained problem for solution, as shown in the following formula:

$$L(\{u_k\},\{\omega_k\},\lambda) = \alpha\sum_{k=1}^{K}\left\|\partial_t\left(\left(\delta(t)+\frac{j}{\pi t}\right)*u_k(t)\right)e^{-j\omega_k t}\right\|_2^2 + \left\|f(t)-\sum_{k=1}^{K}u_k(t)\right\|_2^2 + \langle\lambda_t, f(t)-\sum_{k=1}^{K}u_k(t)\rangle \tag{4}$$

The alternating direction multiplier method is used for ω_k and u_k is optimized as follows:

$$\omega_k^{n+1} = \frac{\int_0^\infty \omega\left|\hat{u}_k^{n+1}(\omega)\right|^2 d\omega}{\int_0^\infty \left|\hat{u}_k^{n+1}(\omega)\right|^2 d\omega}$$
$$\hat{u}_k^{n+1}(\omega) = \frac{\frac{\hat{\lambda}^n(\omega)}{2} + \hat{f}(\omega) - \sum_{i=1}^{k}\hat{u}_i^{n+1}(\omega) - \sum_{i=k+1}^{K}u_i^n(\omega)}{1+2\alpha(\omega-\omega_k^n)^2} \tag{5}$$

Where, ω_k^{n+1} is the center of gravity of the power spectrum of the current modal function. $\hat{u}_k^{n+1}$ is the wiener filtering of the current signal. $\hat{}$ is Fourier transform. n is the number of iterations.

Carry out cyclic iterative solution according to (5), update u_k and ω_k, and bring in (6) for update λ:

$$\hat{\lambda}^{n+1}(\omega) = \hat{\lambda}^n(\omega) + \tau\left[\hat{f}(\omega) - \sum_{k=1}^{K}\hat{u}_k^{n+1}(\omega)\right] \tag{6}$$

where τ is the renewal coefficient of λ. For discrimination accuracy $\xi > 0$, iteration stop condition exists:

$$\frac{\sum_{k=1}^{K}\left\|\hat{u}_k^{n+1}(\omega)-\hat{u}_k^n(\omega)\right\|_2^2}{\left\|\hat{u}_k^n(\omega)\right\|_2^2} < \xi \tag{7}$$

If ξ meets the iteration stop condition, the iteration cycle ends and the adaptive decomposition of the input signal is realized. if not, brings u_k and ω_k in (5) again and starts a new round of iteration until the condition is met.

The flow chart of VMD is shown in Figure 1.

3 BES optimization algorithm

3.1 Bald eagle search

BES is a novel metaheuristic algorithm, which has strong global search ability and can effectively solve various complex numerical optimization problems (Ahmed et al., 2022). The selection of VMD parameters can be regarded as an optimization problem. Therefore, this paper decides to use BES algorithm to optimize VMD parameters. BES algorithm simulates the predator-prey mechanism of bald eagle. The core optimization part of each iteration mainly includes three stages: selection space, search space and swooping phase.

(1) Selection space: bald eagles recognize and choose the best space, this selected space should be rich in prey, this can be implemented by the following equation:

$$P_{i,new} = P_{best} + \alpha \times \gamma \times (P_{mean} - P_i) \tag{8}$$

where, P_{best} is the search area selected using the best position identified in the previous search. α is a controlling parameter that adapts the positions' changes. γ is a random number in range of [0,1]. P_{mean} is the mean position. P_i is the current position of ith bald eagle.

(2) Search space: the bald eagle accelerates the search in a spiral shape to determine the best capture position. The position is updated as follows:

$$P_{i,new} = P_i + x(i) \times (P_i - P_{mean}) + y(i) \times (P_i - P_{i+1}) \tag{9}$$

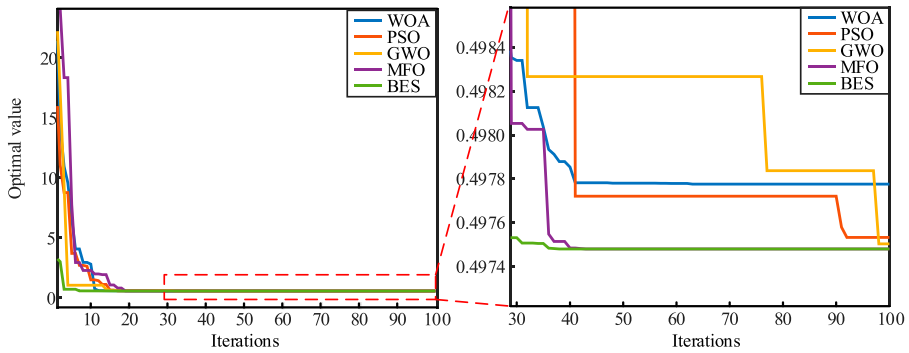

FIGURE 3
Optimization process of multi optimization algorithms.

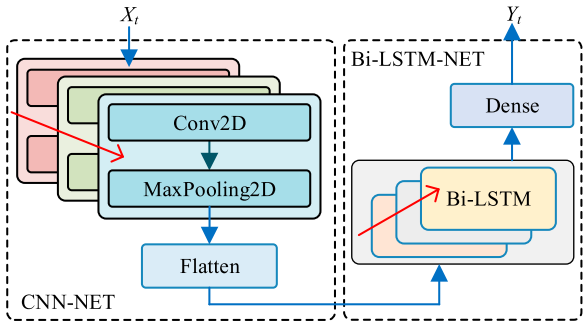

FIGURE 4
CNN-Bi-LSTM hybrid model.

$$\begin{cases} x(i) = \dfrac{xr(i)}{\max(|xr|)}; xr(i) = r(i) \times \sin[\theta(i)] \\ y(i) = \dfrac{yr(i)}{\max(|yr|)}; yr(i) = r(i) \times \cos[\theta(i)] \\ r(i) = \theta(i) + R \times rand \\ \theta(i) = a \times \pi \times rand \end{cases} \tag{10}$$

where, $x(i)$ and $y(i)$ are the position coordinates of ith bald eagle. $r(i)$ is the polar radius of the equation. $\theta(i)$ is the polar angle of the direction. a determines the angle between the search point and the central point, it is assigned in range of [5,10]. R is a parameter that determines the search cycles' number, it is assigned in range of [0.5, 2]. *rand* is a random number.

(3) Swooping phase: the bald eagle quickly pounced on the prey according to the best position obtained in the previous stage and told other bald eagles to start swooping. Its position was updated as follows:

$$P_{i,new} = \mathrm{r\ and} \times P_{best} + x_1(i) \times (P_i - c_1 \times P_{\mathrm{mean}}) + y_1(i) \times (P_i - c_2 \times P_{best}) \tag{11}$$

$$\begin{cases} x_1(i) = \dfrac{xr(i)}{\max(|xr|)}; xr(i) = r(i) \times \sinh[\theta(i)] \\ y_1(i) = \dfrac{yr(i)}{\max(|yr|)}; yr(i) = r(i) \times \cosh[\theta(i)] \\ \theta(i) = a \times \pi \times rand \\ r(i) = \theta(i) \end{cases} \tag{12}$$

where, $x_1(i)$ and $y_1(i)$ denote the position coordinates of the target prey. c_1 and c_2 are the parameters used to control the exercise intensity, and the values are [1,2].

3.2 Simulation experiment and analysis

In order to discuss the significance of the BES algorithm, the optimization comparison experiment of the two-dimensional simulation function in (13) is carried out.

$$f = x^2 + 10 \times \cos(2\pi x) + y^2 + 10 \times \cos(2\pi y) + 20 \tag{13}$$

Whale optimization algorithm (WOA) (Mirjalili and Lewis, 2016), particle swarm optimization (PSO) algorithm (Massaoudi et al., 2021),

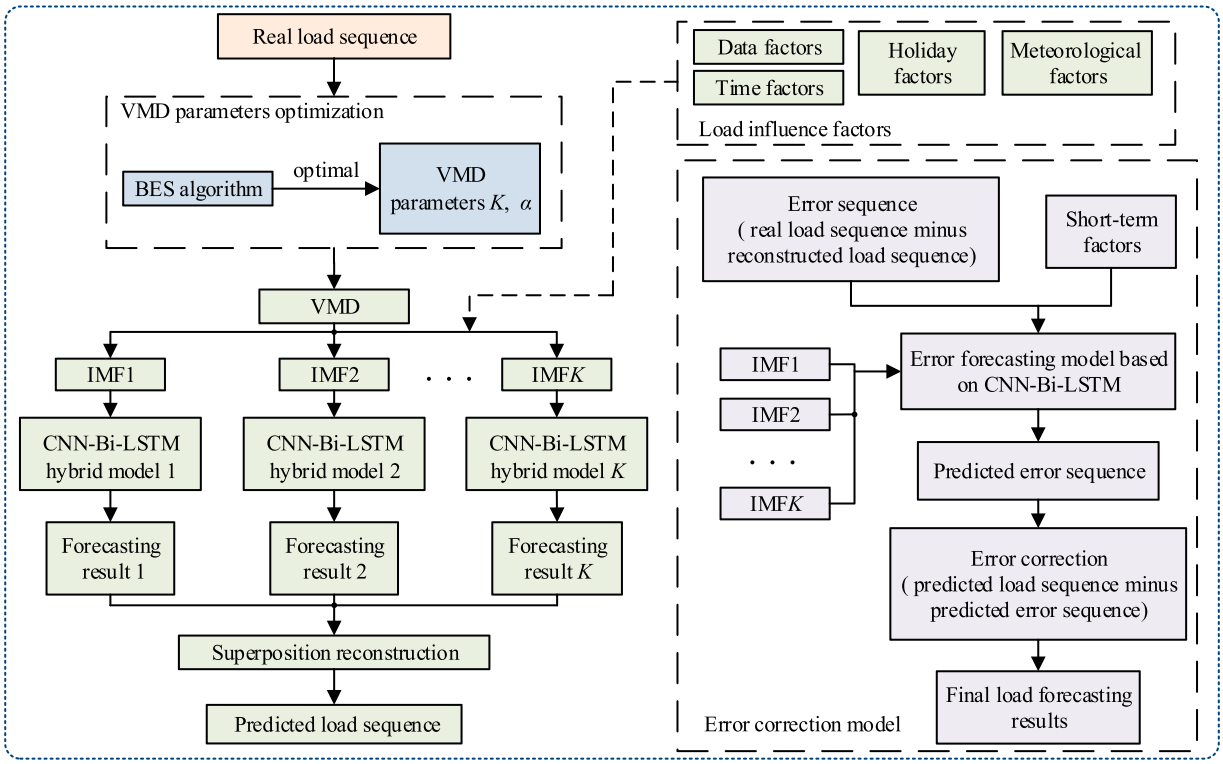

FIGURE 5
Short term load forecasting model *via* BES-VMD-CNN-Bi-LSTM-EC.

TABLE 1 Center frequency of different *K*.

K	3	4	5	6	7	8
u_1	0.7854	0.6283	0.5236	0.4488	0.3927	0.3491
u_2	1.5708	1.2566	1.0472	0.8976	0.7854	0.6981
u_3	2.3562	1.8277	1.5708	1.3464	1.1781	1.0472
u_4		2.5133	2.0808	1.8296	1.5708	1.3077
u_5			2.6180	2.0914	1.8306	1.8298
u_6				2.6156	2.3551	2.0908
u_7					2.6196	2.3566
u_8						2.8729

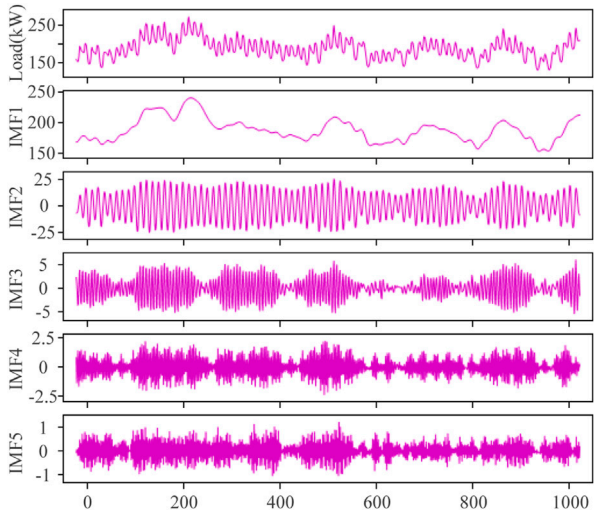

FIGURE 6
Real load sequence and O-VMD results.

grey wolf optimizer (GWO) algorithm (Mirjalili et al., 2014), moth-flame optimization (MFO) algorithm (Mirjalili, 2015) and BES algorithm are used respectively to find the minimum value of this function. In order to maintain the rationality of the experimental results and the consistency of the parameters of various algorithms, the population size is set to 30 and the maximum iterations is set to 100. The function space is shown in Figure 2.

The optimization process of each optimization algorithm is shown in Figure 3.

As can be seen from Figure 3, in terms of optimization speed, WOA finds the minimum value after the 41st iteration, which is 0.49778. PSO finds the minimum value after the 92nd iteration, which is 0.49753. GWO finds the minimum value after the 98th iteration, which is 0.4975. MFO finds the minimum value after the 43rd iteration, which is 0.49748. BES finds the minimum value after the 36th iteration, which is 0.4974797. In terms of optimization accuracy, the accuracy of BES reaches 7 digits after the decimal point, which is closer to the global minimum value. WOA, PSO, GWO, MFO meta heuristic optimization algorithms have certain advantages in optimization, BES optimization is a new meta heuristic optimization algorithm, which has strong global search ability and can effectively solve various complex numerical optimization problems. Based on the above analysis, for VMD parameter selection, it can be regarded as an optimization problem. Compared with WOA, PSO, GWO and MFO, BES optimization algorithm shows certain advantages among them, so this paper uses BES algorithm to optimize VMD parameters.

4 Hybrid models and prediction methods

4.1 CNN-Bi-LSTM hybrid model

CNN model can obtain effective representation directly from the original signal through the alternate use of convolutional layer and pooling layer through local connection and weight sharing, and automatically extract the local features of the data, so as to establish a dense and complete feature vector. So, this paper selects CNN model to extract load data features.

For Bi-LSTM, the input of the model is output after passing through the LSTM network in sequential and reverse directions respectively (Tang et al., 2019; Tian et al., 2021). The output of the model contains the information of the input sequence in forward direction and backward direction at the same time, and the weight reuse further improves the expression ability of the network, while the total amount of data demand remains unchanged, so the risk of under fitting is reduced. Therefore, considering the fluctuation and uncertainty of input data in power load forecasting, CNN is fused on deep Bi-LSTM network to improve the ability of feature extraction and dimension reduction of the model on the original data.

According to the existing experience, there are various factors that affect power load, mainly include: historical load, meteorological factors, date type, etc. Yang J. et al. (2021). Among them, due to the time series characteristics of load, the prediction model can learn the recent change rule of load according to the load daily data that is close to the date to be predicted, which can enrich the prior information of the prediction model. Based on this, this paper selects the historical load data 1 day before the forecast date as one of the characteristics that affect short-term load forecasting; Meteorological factors have a crucial impact on short-term load forecasting. Among them, the common influencing factors are temperature, followed by humidity, wind speed, precipitation, air pressure, etc. Due to the limitations of the experimental data in this paper, only considers temperature as one of the characteristics that affect short-term load forecasting; Date type is another important factor affecting short-term forecast. At present, urban power load is still dominated by industrial power, and the power load on non-working days (Saturday, Sunday, holidays) is significantly less than that on working days (Monday to Friday). Therefore, this paper lists the date type (weather it is Saturday or Sunday, whether it is a legal holiday) as characteristics that affect the load forecasting results.

Based on the above analysis, in this paper, the input $\boldsymbol{X}$ includes the following 8 characteristics: historical load, temperature, data (x year, x month, x day), time (x hour), whether it is Saturday or Sunday, whether it is a legal holiday, expressed as $\boldsymbol{X} = [x^1, x^2, x^3, x^4, x^5, x^6, x^7, x^8]$. And the other prediction models maintain the same input characteristics. The structure of CNN-Bi-LSTM hybrid model proposed in this paper is shown in Figure 4.

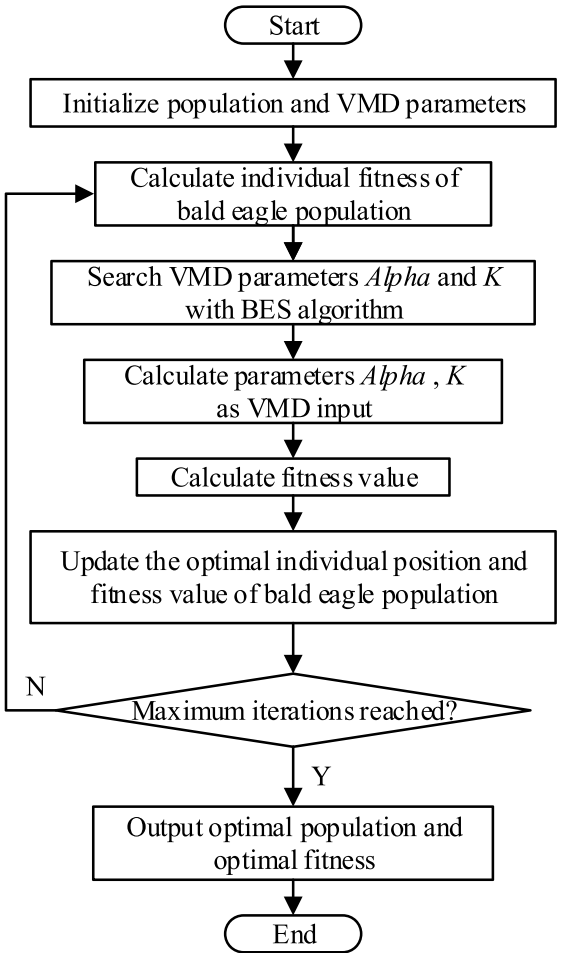

FIGURE 7
VMD parameters optimized by BES algorithm.

As show in Figure 4, CNN is used to extract the effective feature vector, and the feature vector is constructed in the form of time series and used as the input data of Bi-LSTM network. The depth of the prediction model can be increased by adding Bi-LSTM network units to improve the prediction effect of the network. In order to facilitate the subsequent comparison, the sliding window width is 24 records; Step size is 1. The hyperparameters of each CNN-Bi-LSTM model are obtained by grid search method. Dropout technology is used between Bi-LSTM layers to prevent model over fitting. Finally, vectors in the specified format are output through dense.

4.2 BES-VMD-CNN-Bi-LSTM-EC hybrid model

For the data-driven prediction model, it is necessary to determine its input sequence and output sequence. Since the load at the time of the day to be predicted has a strong correlation with the load of the previous day, the 24-h characteristic data of the previous day is selected as the input, and the output is the load value of each hour of the day to be predicted. The short-term power load forecasting model based on BES-VMD-CNN-Bi-LSTM-EC in this paper is shown in Figure 5.

The whole forecasting process is divided into two stages:

(1) In the first stage, several component prediction models based on BES-VMD-CNN-Bi-LSTM hybrid network are constructed. Firstly, a decomposition loss function (*Loss*) is defined as the evaluation criteria, and the optimal number of components K and the penalty factor α are found through the BES algorithm under this evaluation criteria. Then, the real load sequence is decomposed into K modal components by VMD, which are recorded as IMF1, IMF2, . . ., IMFK and the corresponding CNN-Bi-LSTM hybrid network models are established. Finally, the independent prediction results of each sub series are reconstructed to obtain the predicted load sequence.

(2) In the second stage, an error correction model considering short-term factors is proposed. Considering that the influence of nonlinear and short-term fluctuation factors of the sequence itself, various modal components, holiday (whether it is Saturday or Sunday and whether it is a legal holiday) and meteorological factors (ambient temperature) are selected as the input of the error correction model. The error sequence obtained by subtracting the reconstructed load sequence from the real load sequence is used as the output. Subsequently, an error correction model based on CNN-Bi-LSTM network is established to obtain the predicted error sequence to correct the predicted load sequence before. At last, the final load forecasting results are obtained and further improve the short-term load forecasting effect.

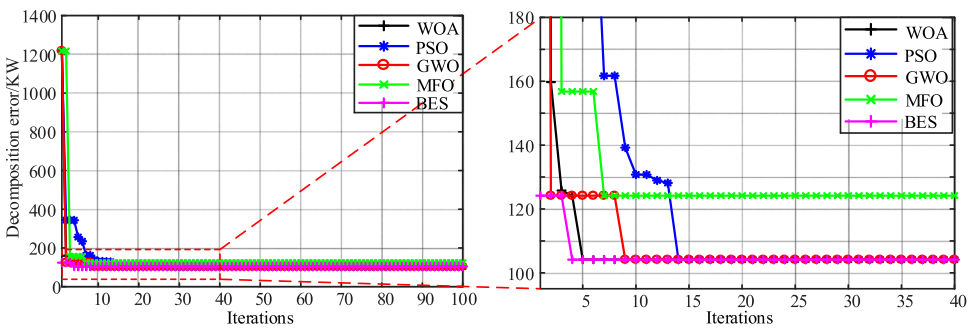

FIGURE 8
Optimization process of multi optimization algorithms.

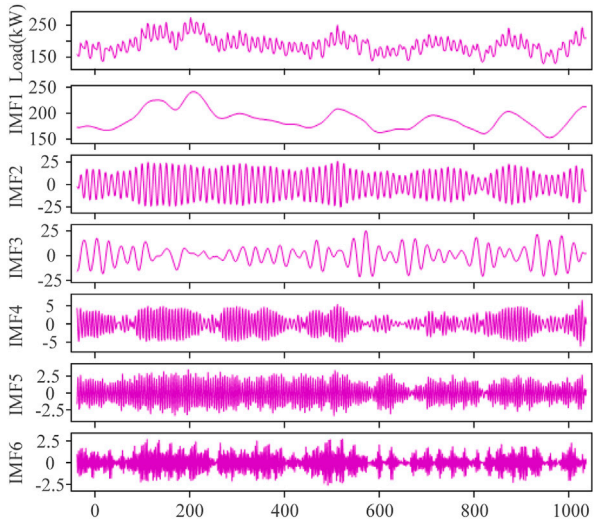

FIGURE 9
Real load sequence and BES-VMD results.

4.3 Evaluation indices

To verify the effectiveness of the proposed model, mean absolute percentage error (MAPE) and root mean square error (RMSE) are used to evaluate the forecasting results, and their specific expressions are as follows:

$$MAPE = \frac{1}{n}\sum_{i=1}^{n}\left|\frac{y_{act}(i) - y_{pred}(i)}{y_{act}(i)}\right| \times 100\%$$
$$RMSE = \sqrt{\frac{\sum_{i=1}^{n}\left(y_{act}(i) - y_{pred}(i)\right)^2}{n}} \quad (14)$$

where, n represents the total number of samples. $y_{act}(i)$ and $y_{pred}(i)$ are the real and predicted load values at time i, respectively.

5 Case study

The experimental computer is configured as: Windows 10 64-bit operating system; Intel(R) Core (TM)i7-8700 CPU; 32GB memory; NVIDIA GeForce RTX 2070 graphics card, which is based on Python 3.6 and tensorflow1.12 operating environment.

5.1 Dataset collection

The experimental data comes from the 2012 global energy forecasting competition published data set, including the hourly load data, the corresponding temperature dataset and holiday information of 20 areas (Hong et al., 2014). The case takes the load data of area 6 from 29 November 2006 to 29 June 2008 as the original data, and divides it into training set, verification set and test set according to the ratio of 8:1:1. The sampling interval is 1 h and 24 points are collected in 1 day. The input includes 8 characteristics: historical load, temperature, year, month, day, hour, whether it is Saturday or Sunday and whether it is a legal holiday. RF, SVM, LSTM, GRU, Bi-LSTM, CNN-LSTM, CNN-GRU, CNN-Bi-LSTM, O-VMD-CNN-LSTM, O-VMD-CNN-GRU, O-VMD-CNN-Bi-LSTM and BES-VMD-CNN-Bi-LSTM are selected as comparison models to verify the feasibility and effectiveness of the proposed model BES-VMD-CNN-Bi-LSTM-EC.

After determining the input characteristics, it is necessary to normalize them to improve the convergence speed of the model. In this paper, the max-min normalization method is used to normalize the characteristic series such as historical load, temperature, year, month, day and hour to the range of [0,1]. The dummy variable is used to represent the weekend and legal holiday characteristics, where logic not represented by 0 and logic yes is represented by 1.

5.2 VMD parameter optimization

5.2.1 Central frequency method

The selection of the number of modal components K directly affects the results of VMD. If K is too large, it will lead to modal

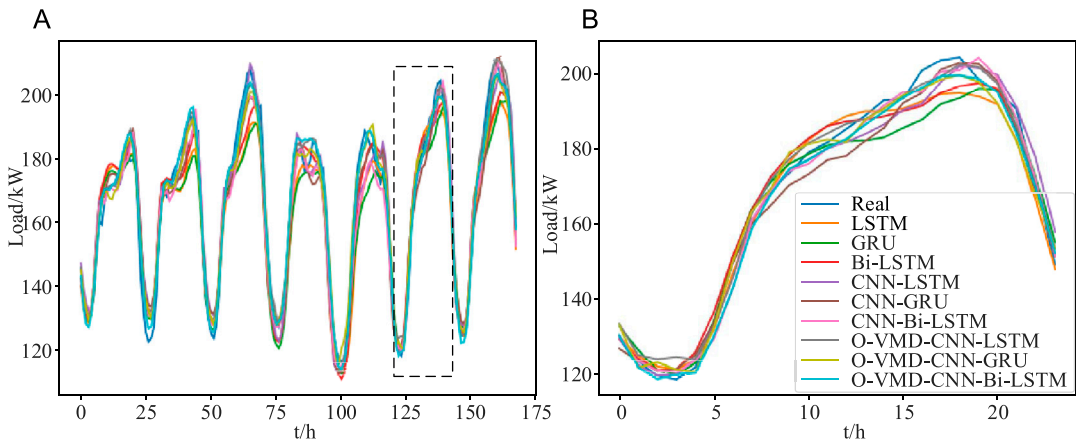

FIGURE 10
(A) Load forecasting results for a continuous week. **(B)** Load forecasting results of 1 day.

TABLE 2 Statistical results of load forecasting of multi models for a week.

Data	Evaluation indices	LSTM	GRU	Bi-LSTM	CNN-LSTM	CNN-GRU	CNN-Bi-LSTM	O-VMD-CNN-LSTM	O-VMD-CNN-GRU	O-VMD-CNN-Bi-LSTM
5.28	MAPE/%	2.239	2.168	2.884	2.372	2.368	2.026	1.779	1.700	1.969
	RMSE/W	4279.803	4268.401	5582.589	5099.821	5084.939	4084.497	4286.851	3643.955	3994.475
5.29	MAPE/%	4.185	4.614	3.984	3.467	3.997	3.370	2.956	3.021	1.861
	RMSE/W	8026.197	8786.023	7128.647	6231.173	7056.000	5852.356	5464.282	5474.566	3603.659
5.30	MAPE/%	4.671	4.241	3.384	2.898	3.505	2.762	2.405	2.536	1.672
	RMSE/W	10412.717	10680.822	7999.168	5289.279	6846.205	5580.044	4522.963	5379.496	3434.211
5.31	MAPE/%	3.716	4.525	2.965	2.138	2.609	2.204	1.522	1.410	1.628
	RMSE/W	6881.564	7956.794	5155.348	3971.573	5705.526	4618.904	3516.774	2874.201	3737.865
6.1	MAPE/%	4.736	4.956	3.816	4.323	3.170	4.058	2.166	2.690	1.733
	RMSE/W	9953.686	10662.705	6840.285	7843.259	5594.357	8415.958	4175.499	4779.977	3057.508
6.2	MAPE/%	2.052	2.211	1.896	1.779	1.999	1.512	1.729	1.571	1.476
	RMSE/W	4466.192	5536.210	4112.376	4076.161	4032.588	3168.142	3151.935	3330.703	3244.042
6.3	MAPE/%	3.546	3.770	2.823	2.157	3.090	1.582	1.189	2.013	1.641
	RMSE/W	8630.803	9190.872	6940.003	4832.514	6498.362	3480.811	2675.668	4500.534	3577.321
Mean	MAPE/%	3.592	3.784	3.107	2.734	2.962	2.502	1.964	2.134	1.711
	RMSE/W	7856.123	8465.215	6374.189	5478.145	5914.324	5296.709	4063.585	4385.787	3533.048

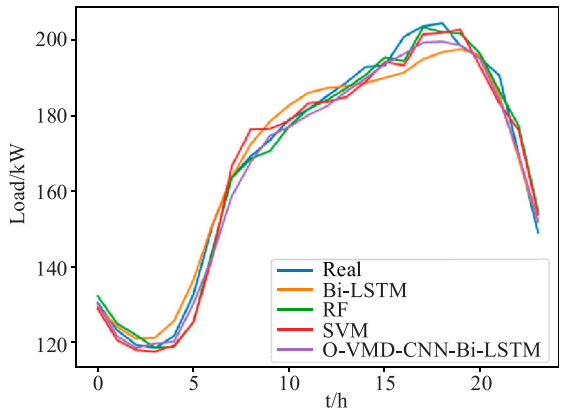

FIGURE 11
Load forecasting results of different models.

repetition or additional noise; if K is too small, the modal under decomposition will occur, resulting in the decline of the accuracy of the subsequent prediction model. Generally, the range of K is set to [3, 8], and the center frequencies corresponding to different components are different (Yang L. et al., 2021). Therefore, set K = 3, 4, . . ., 8 to conduct experiments respectively, and obtain the center frequencies of each component corresponding to different K values. When the K with similar center frequency appears for the first time, it is marked, and determine K-1 as the number of modal components to decompose the original load sequence. In this paper, the method of determining VMD parameter by central frequency method is expressed as O-VMD. 1000 time series load samples with non-linear and non-stationary are randomly selected and decomposed by VMD to obtain different components. Table 1 shows the center frequencies of various component corresponding to different K values.

It can be seen from Table 1 that when K is 6, the center frequencies of modal components u_4 and u_5 are 1.8296 and 2.0914 respectively. The center frequencies of the two components are approximate and it is over decomposed at this time. When K = 8, the center frequencies of u_5 and u_6 are approximate, so the number of components K is determined to be 5. Based on this, the above 1000 time series load samples and their O-VMD decomposition results are shown in Figure 6. It can be seen from Figure 6 that the average amplitude of IMF3, IMF4 and IMF5 is small, with large fluctuations and poor regularity; For mode function IMF2, the regularity is relatively good and the periodicity is relatively obvious; the average amplitude of the modal function IMF1 is large, the change is gentle, and the regularity is easiest to grasp. Later, these five modal functions will be modeled separately for short-term load forecasting of O-VMD combined method.

5.2.2 VMD parameters optimized by BES

In addition to the selection of the value of K, the penalty factor α affects the reconstruction accuracy of VMD signal. Considering the influence of decomposition loss on forecasting accuracy, an evaluation criterion suitable for load forecasting is selected to determine VMD parameters. The evaluation criterion is defined as follows:

$$Loss = \frac{\sum_{t=1}^{T} \left| f(t) - f^{*}(t) \right|}{T} \tag{15}$$

TABLE 3 Statistical results of load forecasting of different models on a certain day.

Time	Real value(W)	Bi-LSTM		RF		SVM		O-VMD-CNN-Bi-LSTM	
		Forecasting value(W)	RMSE/ %	Forecasting value(W)	RMSE/ %	Forecasting value(W)	RMSE/ %	Forecasting value(W)	RMSE/ %
1	130614	129512.86	0.84	132388.69	1.36	129047.94	1.20	130377.37	0.18
2	123397	124323.71	0.75	125145.89	1.42	120801.18	2.10	121825.66	1.27
3	119533	121094.10	1.31	122059.56	2.11	118050.89	1.24	118645.14	0.74
4	118602	121383.05	2.35	118700.41	0.08	117672.35	0.78	119880.66	1.08
5	121868	125849.23	3.27	118977.05	2.37	119324.85	2.09	120348.36	1.25
6	132794	136656.45	2.91	125492.11	5.50	125401.02	5.57	130332.52	1.85
7	151069	151507.06	0.29	144555.89	4.31	142868.50	5.43	142957.33	5.37
8	163931	163753.02	0.11	163603.09	0.20	166685.13	1.68	158739.33	3.17
9	169347	172556.62	1.90	168686.86	0.39	176466.46	4.20	167796.38	0.92
10	173614	178512.38	2.82	170748.00	1.65	176589.88	1.71	174767.69	0.67
11	179066	182815.70	2.09	177240.68	1.02	178650.46	0.23	177099.28	1.10
12	181716	186098.44	2.41	181787.26	0.04	183342.50	0.90	180187.19	0.84
13	185300	187316.34	1.09	184251.57	0.57	183753.65	0.84	182638.75	1.44
14	188863	187857.31	0.53	187338.82	0.81	185012.15	2.04	186455.77	1.28
15	192985	188689.06	2.23	190846.28	1.11	189061.08	2.03	189907.83	1.60
16	193328	190072.86	1.68	195505.85	1.13	194253.84	0.48	193711.31	0.20
17	200931	191464.84	4.71	194401.10	3.25	193330.75	3.78	196395.72	2.26
18	203717	194998.72	4.28	203406.80	0.15	201557.61	1.06	199421.53	2.11
19	204498	196853.17	3.74	202139.56	1.15	201938.72	1.25	199636.78	2.38
20	198605	197631.62	0.49	201826.73	1.62	202803.61	2.11	198720.61	0.06
21	195325	196109.64	0.40	196579.47	0.64	193182.28	1.10	195166.17	0.08
22	190719	185620.56	2.67	186628.00	2.15	183333.71	3.87	184283.45	3.37
23	169934	168566.16	0.81	177329.80	4.35	176176.66	3.67	169751.48	0.11
24	149126	151858.47	1.83	154795.98	3.80	153921.44	3.22	152277.05	2.11
Mean		1.90		1.72		2.19		1.48	

where, $f(t)$ is the original load sequence, $f^*(t)$ is the reconstructed sequence, T is the length of time.

Loss is the average absolute error between the original load sequence and the reconstructed sequence. The smaller *Loss* is, the smaller the signal decomposition loss is and the more accurate the prediction model is. Therefore, the parameter selection problem of VMD is expressed as a constrained optimization problem, as follows:

$$\min_{K,\alpha} \frac{\sum_{t=1}^{T}\left|f(t)-f^*(t)\right|}{T} \tag{16}$$

where, $K\in[3,10]$, $\alpha\in[100,10000]$.

The flow chart of VMD parameters optimized by BES algorithm is shown in Figure 7. WOA, PSO, GWO, MFO and BES algorithms are used to optimize the parameters of the VMD respectively. In order to maintain the consistency of the parameters of various algorithms, the population size is set to 20 and the maximum iterations is set to 100. Figure 8 shows the optimization process of the decomposition loss of different algorithms.

It can be seen from Figure 8 that when the MFO algorithm is used to determine the decomposition parameters, the decomposition loss is high and after the 7th iteration, the minimum decomposition loss is 124.1831. PSO, GWO and WOA algorithms achieve the minimum decomposition loss after the 14th, 9th and 5th iterations respectively. For BES algorithm, the minimum decomposition loss is 104.1395 after the 4th iteration, the optimization speed is the fastest, at this time, the K is 6 and α is 100. Thus, BES-VMD algorithm can adaptively determine the optimal decomposition parameters to improve the decomposition effect of VMD. The original load sequence and their BES-VMD decomposition results are shown in Figure 9. It can be seen from Figure 9 that the average amplitude of IMF4, IMF5 and IMF6 is small, with large fluctuations and poor regularity; For mode function IMF2, IMF3, the regularity is relatively good and the periodicity is relatively obvious; the average amplitude of the modal function IMF1 is large, the change is gentle, and the regularity is easiest to grasp. Later, these six modal functions

TABLE 4 Comparison of statistical results of load forecasting errors for a week.

Data	Evaluation indices	O-VMD-CNN-Bi-LSTM	BES-VMD-CNN-Bi-LSTM	BES-VMD-CNN-Bi-LSTM-EC
5.28	MAPE/%	1.969	1.155	1.266
	RMSE/W	3994.475	2281.845	2929.620
5.29	MAPE/%	1.861	1.397	1.155
	RMSE/W	3603.659	2942.044	2665.914
5.30	MAPE/%	1.672	1.077	0.905
	RMSE/W	3434.211	2727.750	2469.104
5.31	MAPE/%	1.628	1.587	1.401
	RMSE/W	3737.865	4066.452	3152.410
6.1	MAPE/%	1.733	1.653	1.413
	RMSE/W	3057.508	3449.741	2731.502
6.2	MAPE/%	1.476	1.775	1.060
	RMSE/W	3244.042	4294.555	2533.319
6.3	MAPE/%	1.641	1.091	0.801
	RMSE/W	3577.321	2286.436	1722.205
Mean	MAPE/%	1.711	1.391	1.143
	RMSE/W	3533.048	3238.403	2634.082

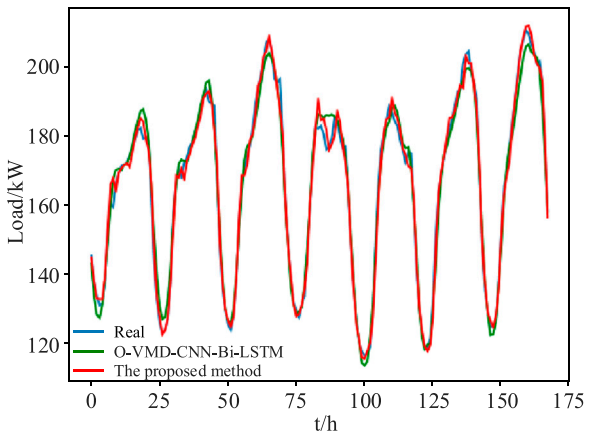

FIGURE 12
Load forecasting results for a week.

will be modeled separately for the short-term load forecasting of BES-VMD combined method.

5.3 Analysis of prediction results

5.3.1 Results analysis of CNN feature extraction and O-VMD

To verify the effectiveness of CNN feature extraction and the effectiveness of VMD decomposition in the load forecasting model, 9 different models are used to conduct short-term load forecasting on the load data of a continuous week (from 28 May to 3 June 2008). Figure 10A shows the load forecasting results for a continuous week; Figure 10B shows the load forecast results of 1 day (June 2). The statistical description of specific prediction results is shown in Table 2.

About the effectiveness of CNN feature extraction prediction model, it can be seen from Figure 10 and Table 2 that, compared with single prediction models like LSTM, GRU and Bi-LSTM, the prediction accuracy of the corresponding CNN-LSTM, CNN-GRU and CNN-Bi-LSTM hybrid models established by CNN feature extraction has been improved to varying degrees. Among them, MAPE decreased by 0.858%, 0.822% and 0.605% respectively. RMSE decreased by 2377.978W, 2550.891W and 1077.48W respectively. Compared with CNN-LSTM and CNN-GRU, the load forecasting accuracy based on CNN-Bi-LSTM model is higher.

About the effectiveness of the VMD (take O-VMD as an example) signal decomposition load forecasting model, According to Figure 10 and Table 2, the outputs of each load forecasting model are compared and analyzed from the perspective of the average value of its evaluation indices. Compared with CNN-LSTM, CNN-GRU and CNN-Bi-LSTM models before VMD, the prediction performance of the corresponding hybrid prediction models O-VMD-CNN-LSTM, O-VMD-CNN-GRU and O-VMD-CNN-Bi-LSTM established after VMD of the original load series has been improved. Among them, MAPE decreased by 0.770%, 0.828% and 0.791% respectively. RMSE decreased by 1414.560W, 1528.537W and 1763.661W respectively. Compared with O-VMD-CNN-LSTM and O-VMD-CNN-GRU models, the MAPE of O-VMD-CNN-Bi-LSTM model decreased by 0.253% and 0.423% respectively. RMSE decreased by 530.537W and 852.739W respectively.

In conclusion, the effectiveness of VMD and CNN feature extraction are verified. Among them, the MAPE and RMSE of O-VMD-CNN-Bi-LSTM model is the smallest. Besides, although

the hybrid prediction model based on Bi-LSTM takes a relatively long time, it obtains the highest prediction accuracy and meets the requirements of engineering applications.

In order to further verify the effectiveness of the proposed O-VMD-CNN-Bi-LSTM model, Bi-LSTM, RF and SVM are used as comparison models to predict the load at 24 h (2 June). The load forecasting results of different models are shown in Figure 11, and the statistical description results are shown in Table 3.

As shown in Figure 11, each model can better predict the change trend of load. Combined with Table 3, compared with Bi-LSTM, RF and SVM prediction methods, the mean RMSE of O-VMD-CNN-Bi-LSTM model at 24 h decreased by 0.42%, 0.24% and 0.71% respectively. Thus, the effectiveness of the prediction method based on O-VMD-CNN-Bi-LSTM is further verified.

5.3.2 Results analysis of BES-VMD and error correction

First, according to the above analysis, the prediction error of O-VMD-CNN-Bi-LSTM model is the smallest, so the comparison experiment is carried out based on this model to analyse the effectiveness of the power load prediction model of BES-VMD-CNN-Bi-LSTM.

Secondly, the prediction error correction experiment is carried out based on BES-VMD-CNN-Bi-LSTM (the prediction model before error correction). Taking various modal components, holidays (whether Saturday or Sunday, and whether it is a legal holiday) and meteorological factors (ambient temperature) as the input of the error correction model, the load prediction model after error correction is established (the proposed method, BES-VMD-CNN-Bi-LSTM-EC).

Table 4 shows the statistical results of load forecasting errors for a week (from 5.28 to 6.3) based on O-VMD-CNN-Bi-LSTM, BES-VMD-CNN-Bi-LSTM and BES-VMD-CNN-Bi-LSTM models.

According to Table 4, compared with O-VMD-CNN-Bi-LSTM method, the weekly mean MAPE and RMSE of BES-VMD-CNN-Bi-LSTM method are reduced by 0.320% and 294.645W respectively, indicating that the overall prediction accuracy and model performance of this method are greatly improved. Thus, the effectiveness of BES optimization algorithm in power load forecasting is further verified.

It can be seen from Table 4 that compared with BES-VMD-CNN-Bi-LSTM method, the weekly mean MAPE and RMSE of BES-VMD-CNN-Bi-LSTM-EC method are reduced by 0.248% and 604.321W respectively, which verifies the effectiveness of the error correction method. Figure 12 shows the prediction results of the proposed method with O-VMD-CNN-Bi-LSTM method.

More intuitively, it can be seen from Figure 12 that the proposed method can better fit the actual load change trend, especially near the peak point, and the prediction accuracy is higher, which further verifies that the BES-VMD-CNN-Bi-LSTM-EC method can effectively reduce the prediction error of short-term power load with excellent prediction performance.

6 Conclusion

Aiming at the characteristics that short-term power load forecasting is easily affected by many factors, in order to improve the accuracy of short-term load forecasting, a short-term load combination forecasting method based on BES-VMD-CNN-Bi-LSTM-EC is proposed in this paper. The conclusions are as follows:

(1) As the current forecasting methods based on traditional statistical analysis and machine learning are difficult to consider both the temporal and nonlinear characteristics of load data, Bi-LSTM model can better fit the temporal and complex nonlinear relationship of load data, it can learn the information of the load sequence in the forward direction and the backward direction at the same time to improve the expression ability of the network, so it is applied to the forecasting model in this paper.

(2) This paper gives full play to the potential feature extraction advantages of CNN model and provides a large amount of effective input data for Bi-LSTM model. It overcomes the defect that a single Bi-LSTM model cannot effectively mine the hidden information between discontinuous data. The simulation results show that compared with the model without CNN feature extraction, which effectively improves the prediction accuracy.

(3) In order to reduce the complexity of load series and further improve the accuracy of short-term load forecasting, this paper uses the advantages of VMD in processing non-stationary and nonlinear signals, and uses BES algorithm to optimize VMD parameters. The load series is decomposed into components with different frequencies, and a CNN-Bi-LSTM forecasting model is established for each component. The simulation results show that compared with the model without signal decomposition, which effectively improves the forecasting accuracy.

(4) An error correction model considering short-term factors is established, which reduces the inherent error of the prediction model by mining the effective information hidden in the error. The simulation results show that compared with the forecasting method without error correction, the VMD-CNN-Bi-LSTM-EC combined forecasting model can further improve the accuracy of short-term load forecasting. The proposed method has better forecasting ability and stability and several application values as follows: 1) It can provide theoretical guidance for power production departments and management departments to formulate production plans and development plans, and determine the power supply quantity and production plans of each power supply area. 2) It can improve the accuracy of power system short-term load forecasting, and further improve the security and economy of power system operation.

The load forecasting feature set established in the proposed method does not considering the diversified load types, and does not include electricity price factors, other meteorological factors, etc. Therefore, in the future work, this paper will further study the impact of load characteristic classification on load forecasting, build a richer feature set including electricity price factors and other meteorological factors such as humidity, wind speed, precipitation, air pressure, etc., explore the internal relationship of input characteristics, and further improve the accuracy of short-term load forecasting. At the same time, the forecasting model needs to be optimized to shorten the prediction time and improve the real-time performance.

Data availability statement

The original contributions presented in the study are included in the article/Supplementary Material, further inquiries can be directed to the corresponding author.

Author contributions

NW and ZL contributed to conception and design of the study. NW organized the database. NW and ZL performed the statistical analysis. NW wrote the first draft of the manuscript. All authors contributed to manuscript revision, read, and approved the submitted version.

Funding

This work was supported in part by the National Natural Science Foundation of China under Grant 51967011 and the Natural Science Foundation of Gansu Province under Grant 21JR7RA207.

Conflict of interest

The authors declare that the research was conducted in the absence of any commercial or financial relationships that could be construed as a potential conflict of interest.

Publisher's note

References

Ahmed, F., Hegazy, R., Dalia, Y., Kandil, T., and Abo-Khalil, A. G. (2022). Real-time bald eagle search approach for tracking the maximum generated power of wind energy conversion system. *Energy* 249 (C), 123661. doi:10.1016/j.energy.2022.123661

Chen, Z., Zhang, D., Jiang, H., Wang, L., Chen, Y., Xiao, Y., et al. (2021). Load forecasting based on LSTM neural network and applicable to loads of "replacement of coal with electricity". *J. Electr. Eng. Technol.* 16 (5), 1–10. doi:10.1007/s42835-021-00768-8

Dou, C., Zheng, Y., Yue, D., Zhang, Z., and Ma, K. (2018). Hybrid model for renewable energy and loads prediction based on data mining and variational mode decomposition. *IET Generation Transm. Distribution* 12 (11), 2642–2649. doi:10.1049/iet-gtd.2017.1476

García-Ascanio, C., and Maté, C. (2009). Electric power demand forecasting using interval time series: A comparison between var and iMLP. *Energy Policy* 38 (2), 715–725. doi:10.1016/j.enpol.2009.10.007

Hobbs, B. F., Jitprapaikulsarn, S., Konda, S., Chankong, V., Loparo, K., and Maratukulam, D. (1999). Analysis of the value for unit commitment of improved load forecasts. *IEEE Trans. Power Syst.* 14 (4), 1342–1348. doi:10.1109/59.801894

Hong, T., Pinson, P., and Fan, S. (2014). Global energy forecasting competition 2012. *Int. J. Forecast.* 30 (2), 357–363. doi:10.1016/j.ijforecast.2013.07.001

Jiang, H., Zhang, Y., Eduard, M., Zhang, J. J., and Gao, D. W. (2018). A short-term and high-resolution distribution system load forecasting approach using support vector regression with hybrid parameters optimization. *IEEE Trans. Smart Grid* 9 (4), 3341–3350. doi:10.1109/tsg.2016.2628061

Kassa, Y., Zhang, J., and Zheng, D. (2019). EMD-PSO-ANFIS based hybrid approach for short-term load forecasting in microgrids. *IET Generation Transm. Distribution* 14 (3), 470–475. doi:10.1049/iet-gtd.2019.0869

Kwon, B. S., Park, R. J., Song, K. B., and Song, K. B. (2020). Short-term load forecasting based on deep neural networks using LSTM layer. *J. Electr. Eng. Technol.* 15 (4), 1501–1509. doi:10.1007/s42835-020-00424-7

Lee, C. M., and Ko, C. N. (2011). Short-term load forecasting using lifting scheme and ARIMA models. *Expert Syst. Appl.* 38 (5), 5902–5911. doi:10.1016/j.eswa.2010.11.033

Lee, J., and Cho, Y. (2022). National-scale electricity peak load forecasting: Traditional, machine learning, or hybrid model? *Energy* 239 (D), 122366–122416. doi:10.1016/j.energy.2021.122366

Liang, Z., Sun, G., and Li, H. (2018). Short-Term load forecasting based on VMD and PSO optimized deep belief network. *Power Syst. Technol.* 42 (2), 598–606. doi:10.13335/j.1000-3673.pst.2017.0937

Lu, J., Zhang, Q., and Yang, Z. (2019). Short-term load forecasting method based on CNN-LSTM hybrid neural network model. *Automation Electr. Power Syst.* 43 (08), 131–137. doi:10.7500/AEPS20181012004

Massaoudi, M., Refaat, S., Chihi, I., Trabelsi, M., Oueslati, F. S., and Abu-Rub, H. (2021). A novel stacked generalization ensemble-based hybrid LGBM-XGB-MLP model for Short-Term Load Forecasting. *Energy* 214, 118874. doi:10.1016/j.energy.2020.118874

Meng, Z., Xie, Y., and Sun, J. (2021). Short-term load forecasting using neural attention model based on EMD. *Electr. Eng.* 104 (3), 1857–1866. doi:10.1007/s00202-021-01420-4

Mirjalili, S., and Lewis, A. (2016). The whale optimization algorithm. *Adv. Eng. Softw.* 95, 51–67. doi:10.1016/j.advengsoft.2016.01.008

Mirjalili, S., Mirjalili, S. M., and Lewis, A. (2014). Grey wolf optimizer. *Adv. Eng. Softw.* 69, 46–61. doi:10.1016/j.advengsoft.2013.12.007

Mirjalili, S. (2015). Moth-flame optimization algorithm: A novel nature-inspired heuristic paradigm. *Knowledge-Based Syst.* 89, 228–249. doi:10.1016/j.knosys.2015.07.006

Muhammad, B., Mohsin, S., Muhammad, A., Ullah, B., Hisham, S. B., and Ali, S. S. A. (2021). Annual cost and loss minimization in a radial distribution network by capacitor allocation using PSO. *Appl. Sci.* 11 (24), 11840. doi:10.3390/app112411840

Rodrigues, F., and Pereira, F. C. (2020). Beyond expectation: Deep joint mean and quantile regression for spatiotemporal problems. *IEEE Trans. Neural Netw. Learn. Syst.* 31 (12), 5377–5389. doi:10.1109/tnnls.2020.2966745

Talaat, M., Farahat, M. A., and Mansour, N. (2020). Load forecasting based on grasshopper optimization and a multilayer feed-forward neural network using regressive approach. *Energy* 196, 1–12. doi:10.1016/j.energy.2020.117087

Tang, X., Dai, Y., Wang, T., and Chen, Y. (2019). Short-term power load forecasting based on multi-layer bidirectional recurrent neural network. *IET Generation, Transm. Distribution* 13 (17), 3847–3854. doi:10.1049/iet-gtd.2018.6687

Tian, P., Zhang, C., Zhou, J., and Nazir, M. S. (2021). An integrated framework of Bi-directional Long-Short Term Memory (BiLSTM) based on sine cosine algorithm for hourly solar radiation forecasting. *Energy* 221 (C), 119887. doi:10.1016/j.energy.2021.119887

Wu, X., He, J., and Zhang, P. (2015). Power system short-term load forecasting based on improved random forest with grey relation projection. *Automation Electr. Power Syst.* 39 (12), 50–55. doi:10.7500/AEPS20140916005

Yan, H., and Tian, C. (2019). A novel two-stage forecasting model based on error factor and ensemble method for multi-step wind power forecasting. *Appl. Energy* 238 (15), 368–383. doi:10.1016/j.apenergy.2019.01.063

Yang, D., Guo, J., and Li, Y. (2023). Short-term load forecasting with an improved dynamic decomposition-reconstruction-ensemble approach. *Energy* 263, 1–16. doi:10.1016/j.energy.2022.125609

Yang, J., Zhang, S., and Liu, J. (2021). Short-term photovoltaic power prediction based on variational mode decomposition and long short-term memory with dual-stage attention mechanism. *Automation Electr. Power Syst.* 45 (3), 174–182. doi:10.7500/AEPS20200226011

Yang, L., Wu, H., and Ding, M. (2021). Short-term load forecasting in renewable energy grid based on Bi-directional long short-term memory network considering feature selection. *Automation Electr. Power Syst.* 45 (03), 166–173. doi:10.7500/AEPS20200202002

Yang, Y., Wang, Z., and Zhao, S. (2023). An integrated federated learning algorithm for short-term load forecasting. *Electr. Power Syst. Res.* 214, 1–10. doi:10.1016/J.EPSR.2022.108830

Ye, J., Cao, J., and Yang, L. (2022). Ultra short-term load forecasting of user level integrated energy system based on variational mode decomposition and multi-model fusion. *Power Syst. Technol.* 46 (07), 2610–2622. doi:10.13335/j.1000-3673.pst.2021.2566

Yuan, F., and Che, J. (2022). An ensemble multi-step M-RMLSSVR model based on VMD and two-group strategy for day-ahead short-term load forecasting. *Knowledge-Based Syst.* 252, 109440–109516. doi:10.1016/j.knosys.2022.109440

Zang, H., Xu, R., Cheng, L., Ding, T., Liu, L., Wei, Z., et al. (2021). Residential load forecasting based on LSTM fusing self-attention mechanism with pooling. *Energy* 229, 120682. doi:10.1016/j.energy.2021.120682

Zhang, L., Mahmoud, A., and Jin, W. (2021). Comparison of time-frequency-analysis techniques applied in building energy data noise cancellation for building load forecasting: A real-building case study. *Energy Build.* 231, 110592–110611. doi:10.1016/j.enbuild.2020.110592

Zhang, S., Li, J., and Jiang, A. (2022). A novel two-stage model based on FPA-VMD and BiLSTM neural network for short-term power load forecasting. *Power Syst. Technol.* 46 (08), 3269–3279. doi:10.13335/j.1000-3673.pst.2021.0969

Zhao, F., Sun, B., and Zhang, C. (2016). Cooling, heating and electrical load forecasting method for CCHP system based on multivariate phase space reconstruction and kalman filter. *Proc. CSEE* 36 (02), 399–406. doi:10.13334/j.0258-8013.pcsee.2016.02.010

Zhao, Y., Wang, H., and Kang, L. (2022). Temporal convolution network-based short-term electrical load forecasting. *Trans. China Electrotech. Soc.* 37 (05), 1242–1251. doi:10.1109/DDCLS49620.2020.9275148

Zhou, M., Hu, T., Bian, K., Lai, W., Hu, F., Hamrani, O., et al. (2021). Short-term electric load forecasting based on variational mode decomposition and grey wolf optimization. *Energies* 14 (16), 4890. doi:10.3390/en14164890

frontiers | Frontiers in Energy Research

TYPE Mini Review
PUBLISHED 09 January 2023
DOI 10.3389/fenrg.2022.1107912

OPEN ACCESS

EDITED BY
Vikram Kulkarni,
SVKM's NMIMS University, India

REVIEWED BY
M. Balamurugan,
Dayananda Sagar College of Engineering, India
Sainath Aher,
Shri Neminath Jain Brahmacharyashram, India
Srikanth Velpula,
SR University, India
C. H. Hussaian Basha,
Nitte Meenakshi Institute of Technology, India

*CORRESPONDENCE
Nishita Parekh,
nishita.parekh@nmims.edu

SPECIALTY SECTION
This article was submitted to Smart Grids, a section of the journal Frontiers in Energy Research

RECEIVED 25 November 2022
ACCEPTED 20 December 2022
PUBLISHED 09 January 2023

CITATION
Parekh N, Kurian J, Patil R and Gautam R (2023), A review on techno managerial approaches to energy optimization in chemical process industries. *Front. Energy Res.* 10:1107912. doi: 10.3389/fenrg.2022.1107912

A review on techno managerial approaches to energy optimization in chemical process industries

Nishita Parekh[1]*, Jinu Kurian[2], Rajesh Patil[3] and Richa Gautam[4]

[1]Chemical Engineering Department, NMIMS (DU), Mumbai, India, [2]Technology Management Department, NMIMS (DU), Mumbai, India, [3]Mechanical Engineering Department, NMIMS (DU), Mumbai, India, [4]National Institute of Industrial Engineering (NITIE), Mumbai, India

The chemical process industries, being energy intensive in nature, still struggle to strategically and sustainably consider energy management issues. Energy sustainability depends on a sustainable energy supply, consumption, and waste disposal. This paper analyses current energy management and optimization in industries and also attempts to identify the significance of incorporating energy management into the strategic perspectives of industry through an exhaustive literature review. To ensure the optimization of energy, the paper illustrates the importance of adopting a techno-managerial approach that integrates the technical aspects of energy conservation with relevant management tactics. This is also a preliminary study for proposing a framework for Indian chemical process SMEs to systematically overcome various challenges and seize the opportunity to ensure optimized energy utilization, thereby highlighting the framework's long- and short-term benefits. The suggestions in the paper would help these industries and local- and national-level policymakers to improve their energy footprint and make the world more energy sustainable.

KEYWORDS

energy, energy management, energy conservation, sustainability, energy sustainability, energy optimization

1 Introduction

Energy sustainability depends on a sustainable energy supply, sustainable energy consumption, and sustainable waste disposal. Energy has been considered a support function in industry, with no to low priority in terms of conservation since the main focus of industry is to enhance productivity (Schulze et al. 2016). Chemical process industries, being energy intensive in nature, still struggle to strategically and sustainably consider energy management issues. This situation is changing rapidly due to a decreasing availability in crude oil, gas, and coal, rising energy prices, increasing awareness about their environmental effects, and a concern to alleviate climate change. Chavan and Jain (2014) proposed that energy management and energy efficiency are separate but interconnected concepts. Energy efficiency is vital part of energy management and is attained when energy intensity (energy required per unit of product) in a specific product, process, or area of production or consumption is lowered without affecting production output or consumption. This paper analyses the current energy management and optimization scenario in industry and also attempts to identify the importance of incorporating energy management into the strategic perspectives of these industries through an exhaustive literature review.

2 Methodology

Kannan & Boie (2003) define "energy management" as "...the judicial and effective use of energy, to maximise profits and to enrich [the] company's competitive positions, through organisational measures and optimising energy efficiency in the [sic.] operations,"—thus combining the skills of engineering and management. Energy management, if carried out properly, decreases energy demand, the operational cost of production, and negative environmental and social impacts. This elevates a company's position in the carbon market, customers' willingness to pay, and shareholders' willingness to invest. To utilize available energy effectively and make industrial systems sustainable, industries must optimize energy through energy management and efficient solutions and tools.

According to Schulze et al. (2016), industries have to realize that energy management can be an effective lever for enhancing their production systems and operations toward improved energy efficiency and hence reduce energy use and related energy costs. This is true for process industries as they are major consumers of energy (electricity, oil, gas, and coal) and emitters of greenhouse gases and carbon.

Several factors must be integrated for successful energy optimization; these are investigated in the academic literature through research into topics such as energy management, energy efficiency, the challenges to and drivers of energy management practices, energy efficient methods, energy conservation techniques, and the development of key performance indicators. This paper builds on this previous research by systematically reviewing the literature, as originally outlined by Tranfield et al. (2003) and applied in the area of energy management by Schulze et al. (2016).

Considering advances in technology, the period from 2000 to 2022 has been chosen since many articles, reports, and case studies have been published on energy management practices, energy efficiency, energy management systems, energy efficient technologies, energy performance indicators, and energy performance measurement. The focus when selecting articles was on the following: the time and type of publication; the availability of full-text articles; the sectors considered; the type of studies undertaken (case study, survey, and literature review); and the content of articles, including energy management practices and/or energy efficient methods or technology (Parekh et. al., 2019; Schulze et al., 2016).

The selected articles include peer-reviewed journal articles, and white papers and reports by national agencies to account for continuous improvement and technology diffusion by industries or national agencies. The contents of articles vary, from an emphasis on energy-efficient technology, its application, its analysis, the importance of energy management, case studies of success, benefits of energy management, reports on energy scenarios across the world, energy management practices, and articles that describe successful energy management systems and energy indicators.

Based on the aforementioned criteria, 95 articles, including 81 peer reviewed articles and 14 reports, were studied to discover the best practices available across the world, and their application to chemical process industries. There are 44 articles that showcase the energy-saving opportunities in manufacturing sectors, followed by 26 articles on the chemical process sector, including chemical manufacturing, the petroleum, pharmaceutical, iron and steel, and paper and pulp industries, cement manufacturing, and water treatment plants.

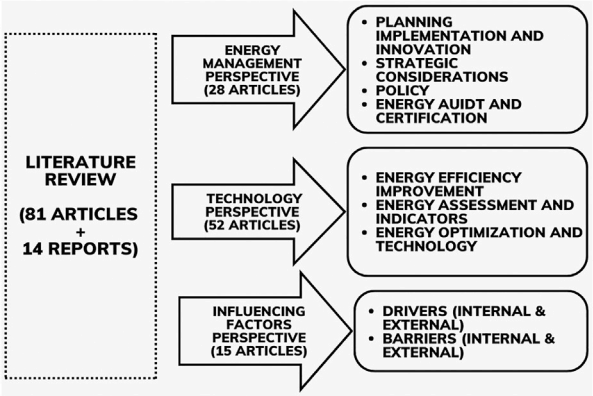

FIGURE 1
Analysis of selected articles.

After identifying the relevant articles, the data were categorised based on their orientation: energy management perspective, energy efficient technology perspective, and positive and negative influencing factors.

3 Categorization of reviewed articles

Many articles are published on energy management practices, but they are fragmented in terms of concepts, industry, country, and policies. Learning from these will help cultivate further research, developments, and innovation unique to relevant sectors, industry types, and countries.

This section analyses and categorises the literature on three major categories: management, technology, and influencing factors. The articles analysed were broadly categorised by their focus of study, highlighting the perspectives of energy management, technology, influencing factors, and energy efficiency (Figure 1).

3.1 Energy management perspective

"Energy management" is planned, monitored, controlled, and executed actions to ensure maximum energy output using minimum energy resources for a predetermined performance by an organization to gain competitive advantage, serve national interests, and adhere to stringent environment standards. Energy management is thus the strategic approach of a company toward its energy usage. The academic literature indicates that energy-intensive organizations that adopt a strategic approach to energy management may reduce energy usage as much as 40%. According to Sivill et al. (2013) and Mulder and Hagens (2008), energy management is below raw materials optimization and production commitment as a priority in energy-intensive industries. Cooremans and Schönenberger (2019) and Schulze et al. (2016) confirm this and argue that considering energy in strategic planning, implementation, and the control, organization, and culture of an organization can exploit a company's energy efficiency potential. Without long-term strategy and the allocation of energy costs, companies will not realise the benefits of energy management. Thollander and Ottosson (2010)

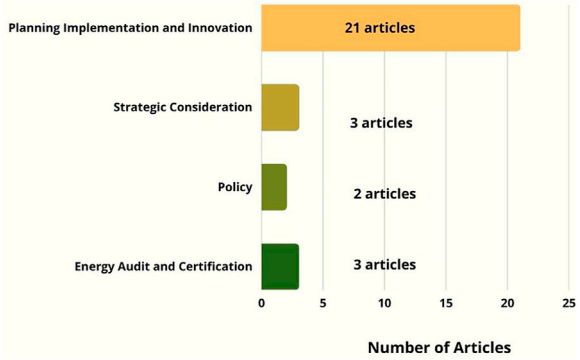

FIGURE 2
Classification of articles with a management perspective.

suggest senior management be involved in developing their company's energy policy, in managing energy-saving projects, and in creating an environment that thus motivates and trains their employees. Schulze et. al. (2016) demonstrated a comprehensive framework for incorporating strategic planning, implementation, control of energy use, reorganizing the organization structure, and modifying an organization's culture to effectively tap its energy efficiency potential. Gopalakrishnan et al. (2014) also suggested a framework of energy management to effectively implement ISO 50001 to reduce the energy costs and losses from minimizing greenhouse gas emissions.

Some 21 articles investigated planning, implementation, and innovation through qualitative and quantitative studies, or a combination of both. Three studies elaborated the process, requirements, and benefits of energy audits and certifications. As illustrated in Figure 2, only three studies investigated the importance of using energy management as a strategic objective; just one article examined the impact of policies on energy management.

Planning and implementation are core to energy management and require a gradual and structured approach that starts from the unit process to the factory facility and multi-facility units, incorporating entire supply chain in the process if possible (Duflou et al. 2012). Alternately, Sivill et al. (2013) focused on incorporating proper change management tools and rewards to make energy management successful. There are many ways to effectively implement energy management in an organization which may differ based on geographic locations, sectors, or the scale of operations. Backlund et al. (2012), using the multiple case study model for Sweden, found energy-intensive firms to be more enthusiastic and successful in adopting energy management.

3.2 Technology perspective

Energy optimization can be achieved through the appropriate channelling of technological interventions and processes by upgrading existing systems or replacing existing systems to achieve energy-efficient systems, depending on the situation. The chemical process industry has a natural scope of energy optimization as it can consume and create energy through various means or can integrate the available energy to achieve higher potential or reduce energy consumption. Lipiäinen et al. (2022) suggest use of bio-alternatives to replace fossil fuels, thus decreasing the carbon intensity of processes.

Exothermic processes release energy into the environment; this can be efficiently trapped for useful energy on-site. Pinch technology and heat exchanger networks (HENs) to integrate process streams are used frequently. Geldermann et al. (2006) took the automobile industry as a case study to demonstrate that blending process integration engineering with operations research can provide economic and environmentally friendly solutions. Waste heat recovery is a big challenge for process industries as it entirely depends on amount, quality, and source of waste heat. Many studies exploit this challenging area of design for recovering low-grade waste heat in the process industry; Law et al. (2016) demonstrated this through a case study, using knowledge-based programs and available plant data. The case study of Oluleye et al. (2016) also investigates different models of on-site waste heat utilization by recording the temperature and duties at the heat source. In a literature review, Chan et al. (2013) illustrated the possibility of recovering low-grade heat using technologies like "Chemical heat pumps, organic Rankine cycles, [and] thermal energy storage. . .". Ammar et al. (2012) evaluated the technical and economic feasibility of extracting low-grade thermal energy using CFD (computational fluid dynamics) for process industries in the United Kingdom, provided that strong government regulations and policies are in place; similar approaches may be applied in other countries.

Even some economical modifications to existing equipment or replacing the energy-intensive with energy-efficient parts can help reduce the energy requirement of the plant. Enhancing awareness and identifying action areas to improve the energy use of processes can be effective if energy analysis is conducted at manufacturing level (Andrei et al.,2022). Saidur et al. (2010) reviewed and further identified energy-saving techniques—such as variable speed drives, energy efficient motors, recovery of waste heat, leakage avoidance, and pressure-drop reduction—for energy-intensive motor-driven process industry equipment. The speed and scale at which technology develops and diffuses across industries, the cost of technology, energy prices, the intensity of chemical industrial activities, and national and international policies will determine the potential effects of mitigation on climate change (Worrell et al., 2009). Xuezhi et al. (2011) emphasised the need for energy saving as a low-cost option with a high potential to benefit the present scenario. Outsourcing energy optimization activities to energy service companies (ESCOs), with the latest know-how required for energy efficiency, and funds to operationalise it, is seen as the latest trend by Benedetti et al. (2015).

According to Lindberg et al. (2015), key performance indicators, used for monitoring operations in industries, need to be benchmarked to similar processes or equipment to classify areas of improvement and necessary actions to be developed and implemented to bridge gaps. Worrell et al. (2003) illustrated the importance of incorporating the productivity benefits associated with energy efficient technologies in terms of cost savings related to conserved energy.

3.3 Influencing factor perspective

Drivers of energy management, as defined by Cagno and Trianni (2013), are ". . .factors facilitating the adoption of both energy-efficient technologies and practices, thus going beyond the

view of investments and including the promotion of an energy-efficient culture and awareness." Stringent environment requirement, government regulations, incentives, and awareness have driven Sweden's iron and steel industries to adopting energy management (Brunke et al.,2014). Trianni et al. (2016) and Singh et al. (2008) listed organizations' policies, long-term strategies, top management commitment, and realizing low-energy benefits as positive influencers for SMEs in the manufacturing industry. Rudberg et al. (2013) described the recognition of non-energy benefits for process industries.

Sorrell et al. (2011) defined a barrier to energy efficiency as a hypothesised mechanism that deters an energy-efficient and cost-effective decision or behaviour. They also suggested that barriers to energy efficiency are multidimensional, varied, and diverse, and are specific to the industry type and the technologies they used. Smith et al. (2022) and Lee KH (2015), emphasised that understanding the barriers and drivers to energy conservation and optimization from frontline workers is also important. As found by Singh et al. (2008) for Indian SMEs, the challenge lies in cost, quality, deliverables, and human resources development. Minciuc et al. (2017) considered limited access to capital and knowledge about energy-efficient technologies alongside poor awareness amongst employees and top management as essential barriers for energy conservation and optimization. These are internal factors within organizations that prevent them shifting toward energy-efficient management. Various myths that are negative influencers were identified by Ammar et al. (2012) and Thollander and Ottosson (2010): perceptions that energy-efficient technologies require higher investment and have a negative impact on production. Factors outside the organization can also hinder their effective energy management, such as support from financial institutions for promoting energy-efficient technologies (Worrell et al.,2009), absence of incentives, limited availability of public information, and lower energy prices in developing countries (Bhattacharya and Cropper, 2010; Alcorta et al.,2014). It is imperative to weaken the barriers to and strengthen the drivers for successfully implementing energy management and mitigate climate change. Parekh et al. (2022) categorize drivers and barriers to energy optimization in the Indian context, using literature and a preliminary survey, into internal and external factors and further analysed them using PESTEL analysis for external factors and SWOT analysis for internal factors. The conclusion from the analysis is the importance to designing energy optimum solutions of evaluating internal and external factors based on the situation and industry type.

4 Discussion and conclusion

Energy optimization is the pressing need to mitigate the impact of energy use on climate change on a macro scale. The extensive use of fossil fuels in industrial operations, rising fuel prices, and its fluctuating availability is driving the global movement to conserve energy, increase energy efficiency, and manage operations with minimal energy resources. The literature focuses on improving energy efficiency, the means to conserving energy, and the importance of managing these within organizations. It also focuses on the barriers to and drivers of energy management practices in industry. We have identified three essential gaps in the available sample of the literature: a lack of integration of management and technology perspectives, lack of policy intervention and implementation, and failure by organizations to consider energy as a strategic objective on par with productivity.

The aforementioned review reveals that the integration of technology and management approaches to energy optimization is still nascent. Such an integrated approach may be termed a "techno managerial approach" which combines the benefits of managerial and technological perspectives, detailed analysis of positive and negative influencing factors, and the local and national energy policies; such an approach would serve as a useful tool for industry.

This review further identifies a gap in the studies related to energy management policy implementation in various industrial sectors across different locations. Energy efficiency policies and initiatives devised by governments do exist, but research shows they are rarely implemented by industry.

Energy cost is normally second to raw material costs in the energy-intensive chemical process industry, thereby making considerable attention on energy conservation and optimization there imperative. To effectively achieve this ambition, energy must be adopted as a strategic objective by business. The strategic importance of optimising energy use percolates from top to bottom in an organization's management, necessitating responsibility and accountability for the wastage of energy resources. Very few articles have considered giving strategic importance, to energy consumption and utilization in chemical process industries. This also helps determine the non-energy benefits of energy-efficient systems and energy management practices, including possibility of generating alternate revenue (Rudberg et al., 2013).

The findings of this paper suggest the relevance and timing of studies which combine energy efficiency and energy management perspectives, thus developing appropriate frameworks for industries is necessary. Ambitious energy efficiency improvement targets need to be set by governments with strategies for implementing them on the ground. The future scope is enormous in the area of energy optimization and realising the revenue benefits of making energy a strategic agenda, which can motivate the industries, academics, and policymakers in a positive direction for future research.

Author contributions

NP: conceptualization and writing—original draft. JK: supervision and editing. RP: supervision and editing. RG: critical reviewing. The authors read and approved the final manuscript.

Conflict of interest

The authors declare that the research was conducted in the absence of any commercial or financial relationships that could be construed as a potential conflict of interest.

The handling editor VK shares second affiliation with authors NP, JK, and RP.

Publisher's note

References

Alcorta, L., Bazilian, M., De Simone, G., and Pedersen, A. (2014). Return on investment from industrial energy efficiency: Evidence from developing countries. *Energy Effic.* 7 (1), 43–53. doi:10.1007/s12053-013-9198-6

Ammar, Y., Joyce, S., Norman, R., Wang, Y., and Roskilly, A. P. (2012). Low grade thermal energy sources and uses from the process industry in the UK. *Appl. Energy* 89 (1), 3–20. doi:10.1016/j.apenergy.2011.06.003

Andrei, M., Thollander, P., and Sannö, A. (2022). Knowledge demands for energy management in manufacturing industry-A systematic literature review. *Renew. Sustain. Energy Rev.* 159, 112168. doi:10.1016/j.rser.2022.112168

Backlund, S., Thollander, P., Palm, J., and Ottosson, M. (2012). Extending the energy efficiency gap. *Energy Policy* 51, 392–396. doi:10.1016/j.enpol.2012.08.042

Benedetti, M., Cesarotti, V., and Introna, V. (2015). Improving Energy Efficiency in manufacturing systems: Literature review and analysis of the impact on the energy network of consolidated practices and upcoming opportunities. *Energy efficiency improvements in smart grid components*, 41–68.

Bhattacharya, S., and Cropper, M. (2010). Options for energy efficiency in India and barriers to their adoption: A scoping study. Available at http://dx.doi.org/10.2139/ssrn.1590510.

Brunke, J. C., Johansson, M., and Thollander, P. (2014). Empirical investigation of barriers and drivers to the adoption of energy conservation measures, energy management practices and energy services in the Swedish iron and steel industry. *J. Clean. Prod.* 84, 509–525. doi:10.1016/j.jclepro.2014.04.078

Cagno, E., and Trianni, A. (2013). Exploring drivers for energy efficiency within small- and medium-sized enterprises: First evidences from Italian manufacturing enterprises. *Appl. Energy* 104, 276–285. doi:10.1016/j.apenergy.2012.10.053

Chan, C. W., Ling-Chin, J., and Roskilly, A. P. (2013). A review of chemical heat pumps, thermodynamic cycles and thermal energy storage technologies for low grade heat utilisation. *Appl. Therm. Eng.* 50 (1), 1257–1273. doi:10.1016/j.applthermaleng.2012.06.041

Chavan, P., and Jain, P. (2014). Sustainable energy for manufacturing industry an Indian scenario. *Int. J. Sci. Res.* 4 (10), 756–761.

Cooremans, C., and Schönenberger, A. (2019). Energy management: A key driver of energy-efficiency investment? *J. Clean. Prod.* 230, 264–275. doi:10.1016/j.jclepro.2019.04.333

Duflou, J. R., Sutherland, J. W., Dornfeld, D., Herrmann, C., Jeswiet, J., Kara, S., et al. (2012). Towards energy and resource efficient manufacturing: A processes and systems approach. *CIRP Annals-Manufacturing Technol.* 61 (2), 587–609. doi:10.1016/j.cirp.2012.05.002

Geldermann, Jutta, Martin, Treitz, and Otto, Rentz (2006). Integrated technique assessment based on the pinch analysis approach for the design of production networks. *Eur. J. Operational Res.* 171 (3), 1020–1032. doi:10.1016/j.ejor.2005.01.015

Gopalakrishnan, B., Ramamoorthy, K., Crowe, E., Chaudhari, S., and Latif, H. (2014). A structured approach for facilitating the implementation of ISO 50001 standard in the manufacturing sector. *Sustain. Energy Technol. Assessments* 7, 154–165. doi:10.1016/j.seta.2014.04.006

Kannan, R., and Boie, W. (2003). Energy management practices in SME––case study of a bakery in Germany. *Energy Convers. Manag.* 44 (6), 945–959. doi:10.1016/s0196-8904(02)00079-1

Law, R., Harvey, A., and Reay, D. (2016). A knowledge-based system for low-grade waste heat recovery in the process industries. *Appl. Therm. Eng.* 94, 590–599. doi:10.1016/j.applthermaleng.2015.10.103

Lee, K. H. (2015). Drivers and barriers to energy efficiency management for sustainable development. *Sustain. Dev.* 23 (1), 16–25. doi:10.1002/sd.1567

Lindberg, C. F., Tan, S., Yan, J., and Starfelt, F. (2015). Key performance indicators improve industrial performance. *Energy procedia* 75, 1785–1790. doi:10.1016/j.egypro.2015.07.474

Lipiäinen, S., Kuparinen, K., Sermyagina, E., and Vakkilainen, E. (2022). Pulp and paper industry in energy transition: Towards energy-efficient and low carbon operation in Finland and Sweden. *Sustain. Prod. Consum.* 29, 421–431. doi:10.1016/j.spc.2021.10.029

Minciuc, E., Diaconescu, I., and Pătrașcu, R. (2017). Energy management for energy efficiency. *FAIMA Bus. Manag. J.* 5 (2), 63.

Mulder, K., and Hagens, N. J. (2008). Energy return on investment: Toward a consistent framework. *AMBIO A J. Hum. Environ.* 37 (2), 74–79. doi:10.1579/0044-7447(2008)37[74:eroita]2.0.co;2

Oluleye, G., Jobson, M., Smith, R., and Perry, S. J. (2016). Evaluating the potential of process sites for waste heat recovery. *Appl. Energy* 161, 627–646. doi:10.1016/j.apenergy.2015.07.011

Parekh, N., Kurian, J., Patil, R., and Gautam, R. (2019). "Drivers and barriers for energy management in process industries: Critical review of literature," in 28th International Conference of the International Association of the Management of Technology on Management of Technology, NITIE, Mumbai, India, 7th – 11th April 2019. ISBN: 978-93-88237-54-3.

Parekh, N., Kurian, J., Patil, R., and Gautam, R. (2022). Influencing factors and challenges to energy management and energy efficiency for chemical process SMEs in India. *Mater. Today Proc.* 57, 1745–1754.

Rudberg, M., Waldemarsson, M., and Lidestam, H. (2013). Strategic perspectives on energy management: A case study in the process industry. *Appl. Energy* 104, 487–496. doi:10.1016/j.apenergy.2012.11.027

Saidur, R., Rahim, N. A., and Hasanuzzaman, M. (2010). A review on compressed-air energy use and energy savings. *Renew. Sustain. energy Rev.* 14 (4), 1135–1153. doi:10.1016/j.rser.2009.11.013

Schulze, M., Nehler, H., Ottosson, M., and Thollander, P. (2016). Energy management in industry–a systematic review of previous findings and an integrative conceptual framework. *J. Clean. Prod.* 112, 3692–3708. doi:10.1016/j.jclepro.2015.06.060

Singh, R. K., Garg, S. K., and Deshmukh, S. G. (2008). Challenges and strategies for competitiveness of SMEs: A case study in the Indian context. *Int. J. Serv. Operations Manag.* 4 (2), 181–200. doi:10.1504/ijsom.2008.016610

Sivill, L., Manninen, J., Hippinen, I., and Ahtila, P. (2013). Success factors of energy management in energy-intensive industries: Development priority of energy performance measurement. *Int. J. energy Res.* 37 (8), 936–951. doi:10.1002/er.2898

Smith, K. M., Wilson, S., and Hassall, M. E. (2022). Barriers and drivers for industrial energy management: The frontline perspective. *J. Clean. Prod.* 335, 130320. doi:10.1016/j.jclepro.2021.130320

Sorrell, S., Mallett, A., and Nye, S. (2011). *Barriers to industrial energy efficiency: A literature review*. Vienna, Austria: United Nations Industrial Development Organization.

Thollander, P., and Ottosson, M. (2010). Energy management practices in Swedish energy-intensive industries. *J. Clean. Prod.* 18 (12), 1125–1133. doi:10.1016/j.jclepro.2010.04.011

Tranfield, D., Denyer, D., and Smart, P. (2003). Towards a methodology for developing evidence-informed management knowledge by means of systematic review. *Br. J. Manag.* 14, 207–222. doi:10.1111/1467-8551.00375

Trianni, A., Cagno, E., and Farné, S. (2016). Barriers, drivers and decision-making process for industrial energy efficiency: A broad study among manufacturing small and medium-sized enterprises. *Appl. Energy* 162, 1537–1551. doi:10.1016/j.apenergy.2015.02.078

Worrell, E., Bernstein, L., Roy, J., Price, L., and Harnisch, J. (2009). Industrial energy efficiency and climate change mitigation. *Energy Effic.* 2 (2), 109–123. doi:10.1007/s12053-008-9032-8

Worrell, E., Laitner, J. A., Ruth, M., and Finman, H. (2003). Productivity benefits of industrial energy efficiency measures. *Energy* 28 (11), 1081–1098. doi:10.1016/s0360-5442(03)00091-4

Xuezhi, L., Zhixia, G., and Yuetong, S. (2011). Analysis of the path to improve the energy saving technologies and management levels in chemical industry. *Energy Procedia* 5, 1269–1273. doi:10.1016/j.egypro.2011.03.221

frontiers | Frontiers in Energy Research

TYPE Review
PUBLISHED 11 January 2023
DOI 10.3389/fenrg.2022.1099890

OPEN ACCESS

EDITED BY
Vikram Kulkarni,
SVKM's NMIMS University, India

REVIEWED BY
Gaddam Sridhar,
Jawaharlal Nehru Technological University, Hyderabad, India
Srikanth Velpula,
SR University, India
Rajendhar Puppala,
Smt. Indira Gandhi College of Engineering, India
Shiva Rama Krishna K.,
J.B. Institute of Engineering & Technology, India

*CORRESPONDENCE
Hossam Kotb,
✉ Hossam.kotb@alexu.edu.eg

SPECIALTY SECTION
This article was submitted to Smart Grids, a section of the journal Frontiers in Energy Research

RECEIVED 16 November 2022
ACCEPTED 08 December 2022
PUBLISHED 11 January 2023

CITATION
Dharavat N, Golla NK, Sudabattula SK, Velamuri S, Kantipudi MVVP, Kotb H and AboRas KM (2023), Impact of plug-in electric vehicles on grid integration with distributed energy resources: A review. *Front. Energy Res.* 10:1099890. doi: 10.3389/fenrg.2022.1099890

Impact of plug-in electric vehicles on grid integration with distributed energy resources: A review

Nagaraju Dharavat[1], Naresh Kumar Golla[1,2], Suresh Kumar Sudabattula[1], Suresh Velamuri[3], M. V. V. Prasad Kantipudi[3], Hossam Kotb[4]* and Kareem M. AboRas[4]

[1]School of Electronics and Electrical Engineering, Lovely Professional University, Phagwara, India, [2]Department of Electrical and Electronics Engineering, B.V Raju Institute of Technology, Telangana, India, [3]Symbiosis Institute of Technology, Symbiosis International Deemed University, Pune, India, [4]Department of Electrical Power and Machines, Faculty of Engineering, Alexandria University, Alexandria, Egypt

The rise of electric vehicles (EVs) has a massive impact on the electricity grid due to the electrification of vehicles in the transportation sector. As a result, various techniques are needed to minimize the effects of charging on the grid. One of these techniques is having intelligent coordination between the various components of the EV charging network. This ensures that the network has enough electricity to support the charging needs of the vehicles. This article provides an overview of the many aspects of the EV industry and its charging infrastructure. It also provides a step-by-step approach for implementing the Vehicle to Grid (V2G) deployment, the utilization of recordings from the data by the EV battery through Artificial Intelligence and the cost-benefit analysis from effective utilization of the V2G method. The paper also explores the various aspects of the EV market and the role of aggregators and consumers. Finally, it assesses the possibility of expansion of the EV charging and grid integration system and outlines its challenges and solutions.

KEYWORDS

electrification, charging infrastructure, V2G, artificial intelligence, cost analysis

Abbreviations: ANN, Artificial neural network; B2G, Battery to Grid; BCS, Battery Charging Station; BSS, Battery Swapping Station; CEM, Consecutive Energy Management; CI, Computational Intelligence; CNN, Convolutional Neural Networks; DGs, Distributed Generators; EGOA, Extended Grasshopper Optimization Algorithm; ESS, Energy Storage System; EV, Electric Vehicle; EVCS, Electric Vehicle Charging Station; FTS, Fuzzy Time Series; G2V, Grid to Vehicle; GOA, Grasshopper Optimization Algorithm; HSLC-PS, Hybrid Soccer League Competition–Pattern Search; LSTM, Long short-term memory; MINLP, Mixed Integer Non-Linear Problem; ML, Machine Learning; PSO, Particle Swarm Optimization; QoS, Quality of Service; SVM, Support Vector Machine; V2G, Vehicle to Grid; VPP, Virtual Power Plant.

Introduction

Due to the rising concerns about the environment and the scarcity of fossil fuels, the electrification of the transportation sector has attracted wide attention. However, the rapid growth of these vehicles has been hampered by the lack of charging facilities. Various policies and guidelines have been established to encourage the development of EVs on a global scale Nallusamy et al. (2016). By 2030, the world's population is expected to reach approximately 130 million. Due to the rapid growth of EVs, the existing power grid infrastructure is expected to face significant challenges in handling the penetration of these vehicles' loads IEA (2022). The grid's components might break down, and the transformer can become overloaded as a result of the successive increase in its dependence. Although renewable energy sources are considered an ideal solution for addressing the issue of fossil fuel shortages, their intermittent nature could make their operation challenging to manage. Dharavat et al. (2022), PEVs (plug-in electrical vehicles) also have challenges such as restricted range, a shortage of charging stations, less power, high cost (due to expensive batteries), expensive insurance, high maintenance, and pollution (due to battery toxicity) as well as the fact that not all energy is generated from renewable sources. PEVs have difficulties in India owing to poor market penetration, high manufacturing costs owing to the drop in the value of the rupee, an inadequate infrastructure, and the need to import lithium batteries from other nations.

High-capacity energy storage devices are required to support the expansion of the EV network. These systems can be integrated into the grid and provide additional storage capacity. The charging infrastructure connects the transport network and distribution system. It's crucial to study charging loads and predict their needs while designing electric vehicle charging stations (EVCS). Installing EVCS will raise distribution system demand, which will affect their performance. Integrating local renewable power into the grid may reduce the adverse effects of charging load and reduce greenhouse gas emissions. The increased demand, however, may not be able to be met at certain times of the day due to the stochiastic nature of renewable energy sources like solar, wind, etc. Cleary and Palmer, (2020). The stability of the power grid will be more affected by the intermittent nature of RES and the lack of coordination among EVs. On the other side, the energy storage capacity of EVs may be used to stabilize the power grid, particularly when collaborating with RES to mitigate power transitions, therefore lowering both energy costs and carbon dioxide emissions. Increasing the percentage of RES integrated into the grid is possible in a variety of ways, but the best one, in terms of both cost and complexity, is to store electricity generated by electric vehicles. By mitigating the negative effects of unplanned EV charging on the grid and enhancing the unpredictability of RES, benefits Reddy and Vijayakumar, (2019). To assist distribution operators in their decision-making processes in the event of system violations, it is crucial to study the consequences of quick charging for EVs. The use of charging stations that are integrated into the smart grid can help to minimize air pollution and provide better energy management.

Smart grid operators must determine an ideal power pricing by examining EV charging behaviour with the enormous quantity of electric energy required by EVs. Regular and irregular EV users may be distinguished from one another from the standpoint of charging behaviour Chung et al. (2018). There is some consistency in how common users charge. The quantity of each charge is constant, and it occurs at a specific time each day. Unusual users do not charge in a predictive manner. V2G technology can also help to reduce the impact of additional load demand on the grid. This mode of operation allows the grid to receive and utilize the collected energy from the vehicles. Due to their environmental benefits, energy storage is becoming an integral part of the electric vehicle industry. Its continuous use enables the grid to monitor and control the distributed generation network. Although the grid operation can be beneficial for consumers, there's a chance that EV batteries could get damaged due to the discharge conditions. To encourage the use of EVs, India is offering subsidies to its buyers. But as the number of EVs on the road increases, so does the need for lithium-ion batteries (LIBs), and therefore measures must be made to guarantee safe battery disposal. This effort contributes to India's larger goal of making the country's future pollution-free EVreporter (2022) and the same given in Table 1. Integrating EVs and the grid can be considered an efficient energy management method. Doing so involves establishing a smart contact connection between the grids and the vehicles. This can help in minimizing the effects of varying load conditions and improve the efficiency of the entire system.

The conventional power infrastructure cannot provide the rising demand for energy needed to enable industrial innovation and the rise in human living standards due to the ongoing

TABLE 1 Penetration of four wheeler EVs in 2022 EVreporter, (2022).

OEMs	August	September	October
Tata Maotors	3845	3655	4277
Mg Motor India	316	286	450
Mahindra and Mahindra	17	112	15
Hyundai Motor India	73	75	82
BYD India	45	65	36
BMW India	25	28	6
Audi Ag	14	10	0
Kia Motors	—	0	33
Mercedes Benz	—	3	23
Others	4	28	13

changes in the climate across the world. By integrating smart communication, artificial intelligence, sensor and automated control technologies with electricity infrastructures, the smart grid is developing as the next-generation electrical grid to solve these issues Sun et al. (2020). In contrast to traditional optimization approaches, using Machine Learning to coordinate EVs is more superficial and takes less time and computational resources Shibl et al., (2020). The machine learning algorithms can forecast the amount of electricity EVCS will consume. Machine learning has been used because of its capacity to use previous information to learn and recognize patterns to make future predictions with minimum input from the user. The use of these technologies for improving future forecasts has yet to be realized and shown, despite the fact that the majority of studies and implementations of ML/CI techniques focus on energy use and associated costs, Shibl et al., (2020). There is a need to emphasize and look forward to the future mobility transition while deploying charging infrastructure. They also believe that developing intelligent charging technologies and measures to reduce range anxiety are crucial components of the EV market strategy, as they would promote the widespread use of EVs.

Non-etheless, EV drivers face range anxiety since charging takes longer than filling a non-EV with petrol at a petrol station. This delays the widespread adoption of EVs and directly results from battery chemistry, charger limitations, and power consumption requirements Wu, (2021). As a result, the BSS model of battery exchange has been presented. Battery swapping has been introduced at commercial and private stations by BSS service providers, prompting academics to study the BSS methodology and propose different operating systems and optimization approaches.

Literature review

There was a period of phenomenal development for the EV industry throughout the last decade. After the previous COP26 summit, India pledged to bring its carbon emissions to zero by 2070. India plans to have a 30% share of the private car industry, a 70% share of the commercial vehicle market, and an 80% share of the two- and three-wheeler market in 2030, originating through sales of EVs. The rising expense of fossil fuels and increased environmental concerns, EVs have attracted the public's attention. EV owners may swiftly charge their vehicles at home with the aid of charging stations. However, these stations can also overload the grid due to their presence (Bossche, 2010). An intelligent charging system should be implemented to avoid this issue. It should use a strategy that considers the varying factors that affect the charging process and provide a reliable and cost-efficient method of operation.

N. Uddin and Islam, (2019) provide a fuzzy logic-based intelligent power management controller that blends wind, solar, and grid power with backup batteries. To assess the suggested method, the smart energy management system uses optimal fuzzy logic and is thus more economical than other conventional methods.

Zahedmanesh et al., (2019), Proposed a model of VPP, which includes parking spots for EVs, connected to the grid through photovoltaic panels. A CEM-based strategy is explored in order to assign a systematic and cost-effective energy management for the VPP and to control the electric constraints for the power systems. For both energy management and the delivery of auxiliary services, the suggested CEM technique makes use of hierarchies. To meet the needs of the commercial entities in the neighborhood, meet the charging needs of the parking lot, and optimize the VPP controller's profit, the CEM's structure employs a daily scheduling strategy. The second-tier aids in satisfying the technical needs of the power system *via* the VPP's provision of reactive power compensation (RPC).

Das et al. (2020) explores a multi-objective optimization problem to establish the simultaneous placement and size of DGs and FCSs, with limitations on the number of EVs in each zone and the maximum number of FCSs achievable based on the road and electrical network in the proposed system. In order to reduce the cost of developing FCS, optimise power loss, and enhance the voltage profile of the electrical distribution system, the challenge is framed as a MINLP.

Gampa et al. (2020), For distribution systems, this work proposes a two-stage GOA based Fuzzy multi-objective approach to the size and location of DGs, Shunt Capacitors (SCs), and EVCS. By addressing the voltage and current limits of the distribution system and limiting the actual power losses to a specific value, the fuzzy-based GOA algorithm determines the optimal size and location of EV charging stations.

Zeb et al. (2020) explore the inclusion of all three categories electric vehicle chargers, which are optimized to achieve the best results by Controlling the electric vehicle load efficiently while reducing installation costs, losses, and distribution transformer loading. Probability has a role in the EV load due to the unpredictable nature of vehicle users. The constrained non-linear stochastic issue is solved using PSO. The model is simulated using MATLAB and OpenDSS.

Dogan, (2021), This paper proposes a weighted sum of Evolutionary-based multi-objective optimization technique for substantially decreasing power loss, improving voltage level, and enhancing the DG, EVCS, and ESS integration capacities. Also presented a hSLC-PS optimization technique to improve the optimization performance.

The overall load demand, the generating profiles of solar and wind energy systems' uncertainties and the DSTATCOM operation capabilities of photovoltaic and wind generating units are taken into account in this research. The potential EV needs are also considered, the time of arrival and departure, the battery's original and current SoC configurations, the charging methods used, and whether the battery was charged in a

regulated or unregulated manner. To handle this complicated planning model, an efficient and accurate bi-level Multiobjective Ant Lion Optimizer (MOALO) solution for the planning model. The MOALO solver has a bi-level structure, with upper-level optimization aimed at maximizing the efficiency of renewable energy sources and lower-level optimization aimed at maximizing the efficiency of personal electric vehicles. The bi-level MOALO solution takes into account sub objectives such as reducing energy losses and maximizing energy from the main grid Ali et al. (2022).

A micro-grid with a fleet of EVs and a confined vehicle-to-grid application is the focus of this research. Chtioui and Boukettaya (2020). The discharging mode is only used when there is a high-demand situation with a long response time. The micro-construction grid's blocks are described and modelled, as well as a simulation of their operation. The research explores the charging and discharging scenarios and the management strategies employed to govern the power in this simulation.

Javed et al. (2020), present the configuration of V2G and the fundamental concerns related to V2G, which are profoundly analyzed in terms of Battery deterioration, Bi-directional chargers, and charging stations using centralized control and management of the battery system. In addition, the economic cost and income from both the EV owner and the power grid are explored, as well as the problems, benefits, and technologies associated with V2G. The influence of V2G on power systems is investigated in this study using typical test networks.

Based on the value-based pricing strategy, this research proposes a unique methodology of placing DGs and V2G parking lots in the most efficient locations at the same time Mousavi-Khademi et al. (2020). The paper's essential contribution is the inclusion of pricing the DGs and V2Gs using a value-based approach for the best position, as well as the suggested optimal search algorithm. The network's technical issues, include improving the voltage profile and lowering the losses, are addressed in this way by identifying and establishing the best capacity of distributed production resources and electric car parking spaces using value-based pricing to attract network investment.

The article's objective is to reduce power loss in the distribution system when DG is present along with more strategic planning of G2V and V2G operating modes of EVs. Velamuri et al. (2022). To identify the optimal size of the DGs to be placed in the system, the suggested method includes a smart charging mechanism, a voltage stability index, and an EGOA. The electric vehicles are simulated by taking into account the most important aspects, such as the EV SoC, journey circumstances, EV battery capacity, and charging/discharging levels.

The work presented here is the size and positioning of DGs in the distribution system, with battery storage installed after the DGs to sustain the grid Chellappan et al. (2022). The genetic algorithm is utilized by radial node distribution systems, IEEE-33, IEEE-69, and IEEE-118, to install the battery energy storage system. At the same time, the heuristic technique PSO is employed for the sizing and positioning of DGs.

Ravi and Aziz (2022), provides a summary of the current V2G technology scenario and some potential ancillary services, such as frequency regulation, voltage regulation, peak shaving, load levelling, spinning reserve, congestion mitigation, renewable energy storage, reduction of intermittentness, and curtailment, that could be offered with an infrastructure that supports vehicle grid integration.

Electric vehicle charging station infrastructure

The global transportation industry is transitioning from cars powered by traditional fossil fuels to vehicles with zero or ultra-low exhaust emissions. We need a well-developed network of charging stations (CSs), data analytics, intelligent decentralized power generation units, and supportive policy initiatives to facilitate this shift. It is crucial to design and locate a charging station to encourage the widespread usage of electric cars and maximize the benefits of cost-efficient, clean electricity from the grid and renewable energy sources. The transportation industry is undergoing these three transformations in terms of autonomous driving, shared mobility, and electrification Ghosh. (2020). As a result, it is vital to consider the interactions and synergies that may arise between these three impending revolutions while designing the infrastructure for EV charging. A new, considerable electrical demand is being added to the power grid as EV usage rises, forcing infrastructure improvements. Only the distribution grid transfers electrical energy, restricting the amount of energy that may travel *via* the transmission lines Zhang et al., 2011). The electrical grid must be extensively rebuilt to accommodate the EV's charging requirements. Figure 1 represents approaches to the conceptualization of the problem regarding the optimal location of EVCS and Figure 2 represents EV Charging Infrastructure.

Optimal allocation and size of charging stations is a fundamental planning challenge for the electric vehicle (EV) industry, with considerations including cost, distribution network operational characteristics, and the needs of EV drivers. For EVs to be extensively employed, a well-thought-out charging infrastructure must be in operation. Figure 1 depicts the many steps involved in designing a charging infrastructure. The forecasting of pricing service demand at various times and places throughout the day is to be measured precisely. Its utilization must be known to determine how often a charger has been used and how many charging cycles it has been supported. Scheduling charging entails scheduling various charging operations with the grid's capacity and the projected charging demand Brenna et al. (2020). Figure 3 represents strategic charging network design: an overview and Figure 4 represents EV charging management structure.

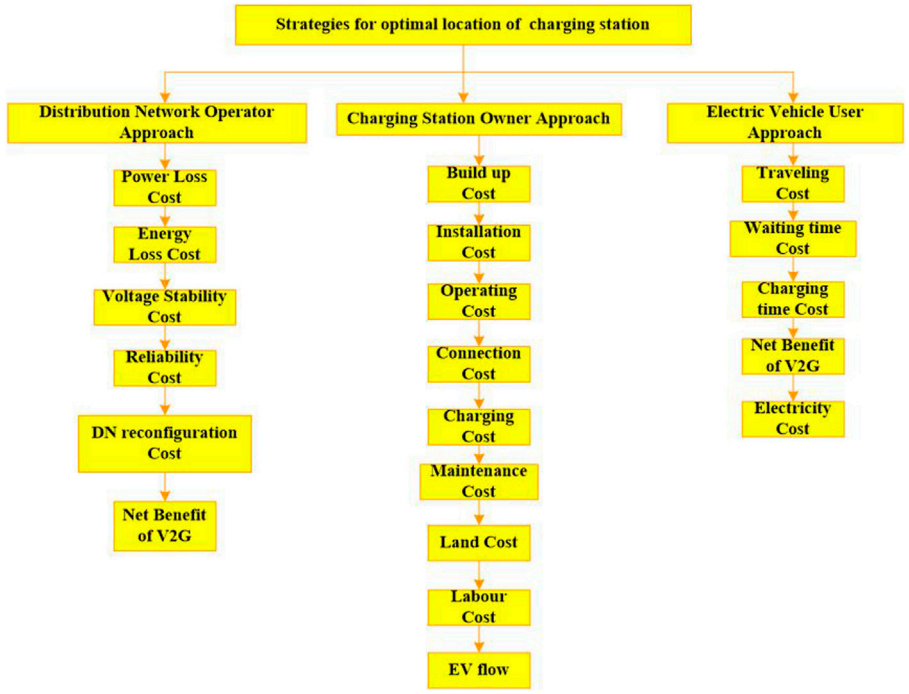

FIGURE 1
Approaches to the conceptualization of the problem regarding the optimal location of EVCS.

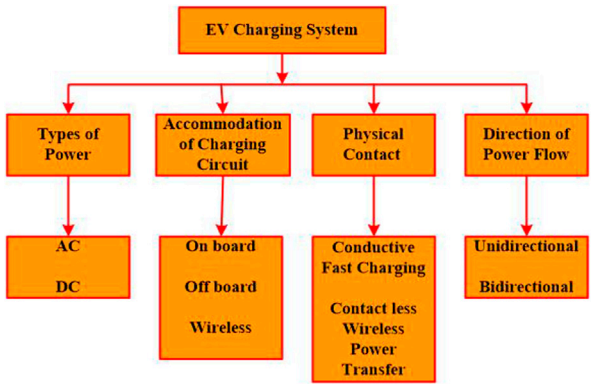

FIGURE 2
EV charging infrastructure.

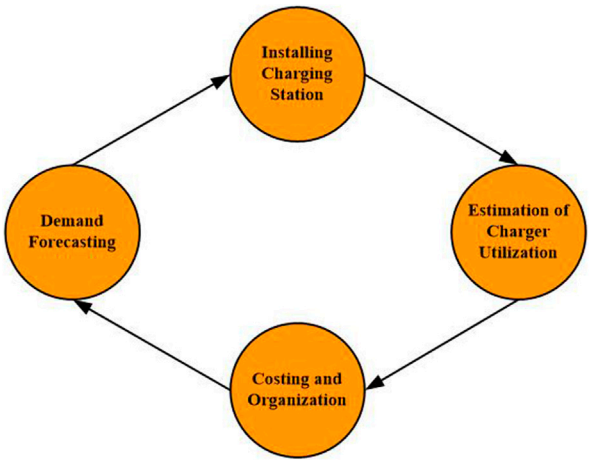

FIGURE 3
Strategic charging network design: An overview.

Management, development, and optimization of charging infrastructure

Location and sizing considerations are vital in optimizing charging infrastructure facilities. Large charging stations are able to handle a greater number of EVs since they have the capacity to house more chargers, but at increased electricity consumption and building expense Iqbal et al. (2021). EV battery capacity and power rates determine future charging infrastructure requirements. The profitability and performance of EVCS are directly correlated to the level of planning and management that goes into the operations of the charging

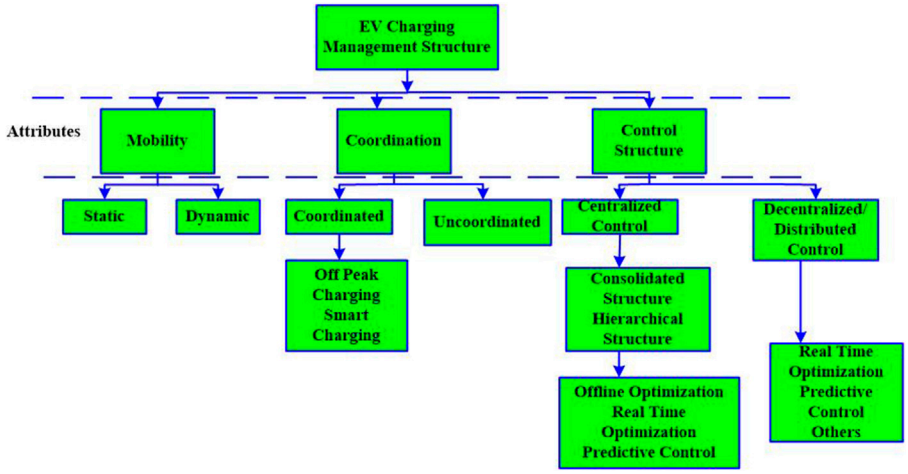

FIGURE 4
EV charging management structure.

stations. The first step in planning an EVCS is to engage in creative thinking and decision-making at different levels. The charging intensity, the expected number of charges, the necessary storage area, the charging infrastructure, and the planned energy storage system are all the factors to be considered. Scheduling charging to support grid functioning, reducing EV charging wait times, and providing a seamless charging experience are all part of a well-managed charging station network. Bhattacharjee et al., (2020). The infrastructure for EVCS, including the distribution system, may be planned, designed, simulated, and optimized using software like MATLAB, HOMER, PVsyst, EVLibSim, etc. Together, EVLib and EVLibSim offer a robust infrastructure for managing EV charging operations at the station level *via* simulation Rigas et al. (2018).

EV charging time reduction with fast, ultra-fast, and battery swapping stations

The pace of EV adoption is crucial to the implementation and profitability of fast and ultra-fast charging stations. Considering that many would-be plug-in electric vehicle (PEV) buyers want public charging times that are on par with traditional refuelling, researchers and policymakers have concentrated on developing rapid charging technologies that can handle larger power loads Sadeghi-Barzani et al. (2014). The public's adoption of EVs may be significantly aided by the widespread availability of fast and ultra-fast charging stations that reduce the charging time to an acceptable level. However, there will be consequences for grid stability, robustness, and efficiency if these technologies are widely used Amiri et al., (2018). Another novel solution to the issue of EVs taking extended periods to charge is the battery swapping station (BSS), which allows drivers to change their discharged battery for a fully charged one. In Iannuzzi and Franzese (2021), a plan is presented for developing ultra-fast EV charging infrastructure. It has a super-fast charging station for EVs powered by a DC microgrid and uses batteries to store energy. In addition to effectively supporting 800 V DC charging, the system allows rapid EV charging in under 10 min. The developed control system uses load-level managing electricity use in order to ease the load on the AC power grid during high demand. According to the system analysis, the ESS's charging power surpasses the grid in the case of a high arrival rate, making it hard to lower the system loss rate successfully. For this reason, to increase profit, the ESS configuration must be adjusted according to the charging load. Optimization often entails formalizing the issue in mathematics and then solving it using an appropriate method. The EVFCS-RP problem is an illustration of an evolutionary computation challenge, since it involves maximizing both profitability and the prospect of satisfying EV consumers. In this research, a multiobjective EVFCS-RP mathematical model is developed to facilitate the attainment of a satisfactory solution Shi and Lee (2015).

Intelligent scheduling of charging the electric vehicles

The widespread adoption of EVs is often viewed as a key component in developing intelligent transportation applications. However, the widespread installation of EVCS presents a number of issues with the electrical grid and other forms of public infrastructure. The straightforward solution of installing

additional charging stations to boost overall charging capacity does not work to mitigate the issue of protracted charging times because of the strain that this would place on existing power grids and the constraints imposed by the availability of physical space Shahriar et al. (2020).

With more recent times, there has been a rising demand in using data-driven methods for simulating electric vehicle charging. As a consequence of this, methods are able to recognize patterns in customer charging behavior in the order to gain insights and the potential to do predictive analytics. As a result, academics have emphasized creating modeling and optimization-based intelligent scheduling methods to reduce the need for public charging. Incorporating network for data exchange, an optimization unit to cut down on wait times at charging stations, and a prediction unit to help the optimization unit will make the most informed decisions possible about charging station placement choice feasible, are the three major impediments to creating an efficient charging infrastructure Sheik Mohammed et al. (2022).

Strategy-based charging station queue management

It is of the utmost importance to manage and effectively plan to charge the electric car at the nearest available charging station to prevent situations in which there is a high demand for charging at one charging station, while there is less demand at other neighbouring stations. This will assist in the strategic management of the queues of vehicles at EVCS. The delays at the charging stations might be more efficiently managed and monitored with an efficient communication network. A negotiating strategy based on agents was developed to schedule charging at an available charging station and allocate EVs to those stations. This system might be used to manage the wait time at the charging station. To facilitate energy trading between individuals and the supply of ancillary services to the grid, Seitaridis et al. (2020) presented an algorithm for bidirectional smart charging of EVs linked to the grid using bidirectional converters. A combination of soft restrictions and optimization variables allows the EV user's preferences to be accounted for in the scheduling model. Mathematical analyses show that taking into account user preferences improved the overall income earned by the EV scheduling scheme. In addition, the established user-centric model increased the number of peer-to-peer energy transactions between the EVs by nearly 90% and the number of ancillary services provided to the grid by about 11% Seitaridis et al. (2020).

Infrastructure management communication system

An optimal EV charging communication protocol is required to provide the following functions when technological innovations like "smart grid" and "V2G" are introduced Dhianeshwar et al., (2017).

- Identifying the vehicle and simplifying the procedure of paying the customer.
- Cost-effective optimization of the charging process is achieved by determining the optimal charging slot and settling on the most economical charging rates.
- Management of charger power rating to grid demand, resulting from loading optimization.
- Vehicle-to-grid (V2G) technology assists the grid during peak demand.
- The ability to charge users and compensate them for their time and energy spent using V2G services.

Several parties, including utilities and vehicle manufacturers, are involved in developing this communication protocol. A joint working group made up of representatives from IEC TC69, ISO TC22 SC3, and TC22 SC21 is addressing the standardization of a communication protocol.

Artificial intelligence-based methods for load forecasting

The operational conditions and equipment capabilities of distribution networks are established based on the predicted loads of EV charging. Therefore, it is crucial to strengthen the distribution system's consistence and efficiency by improving the accuracy of load forecasts. Traditional, non-artificial intelligence approaches, machine learning methods, and artificial intelligence methods are the broad categories that may categorize the many available techniques for load forecasting. The temporal features of the load needs are often the foundation for non-AI approaches. After then, long-term load demand forecasting is usually achieved *via* statistical approaches Yang (2015). Also, the non-linear properties, fluctuating power demands and their time-dependent, unpredictable nature are becoming increasingly apparent as EVs and renewable power production equipment are integrated on a massive scale on the load side. Due to the lack of consistency and precision in conventional forecasting approaches, it is challenging to develop an appropriate mathematical model that can represent the correlations between predicting outcomes and influencing factors.

Artificial intelligence algorithms that are data-driven rather than model-based have shown promising growth in electricity forecasting in recent years. A wide variety of approaches have been used by researchers in power forecasting, including random forests Huang et al., (2016); Lahouar and Ben Hadj Slama (2015), BP neural networks, support vector machines, extended short-term memory networks and convolutional neural networks Choi et al., (2020). FTS and CNN are combined to provide a

short-term load forecasting approach. On the other hand, conventional CNN requires a lot of time to train and fails to adequately capture the temporal information included in the time series. An approach to load forecasting using a genetic algorithm and an extended short-term memory network is presented in Santra et al. (2019). The load curve is the final product after carefully considering the input data as load-demanding elements.

In contrast, the LSTM network augments each hidden-layer neural unit with sophisticated gate components. Therefore, LSTM training efficiency may be poor. The SVM technique suggested in Barman and Nalin Behari, (2020) for load demand forecasting uses grey wolf optimization. SVM approach, on the other hand, when the amount of training data is too large, its classification performance may suffer from a lack of precision due to the continuous nature of the data samples.

Automated charging scheduling using machine learning

To prevent abrupt spikes in peak load demand, it is essential that charging activity at charging stations be managed. V2G technology and scheduled EVCS were the primary emphasis of Dang et al., (2019), which also used reinforcement learning to assess the operational benefit of EVs, also models the scheduling of EV charging and discharging as a constrained Markov Decision Process (CMDP). The constraint is to reduce the cost of charging the EV while still ensuring it can be completely charged, hence a limited charging/discharging scheduling technique is being sought. Model-free safe deep reinforcement learning (SDRL) is offered as a means to resolve the CMDP. With the suggested method, familiarity with randomization is not necessary. It uses a DNN for the constrained optimum charging and discharging schedules directly. The authors of Li et al., (2020) present a method based on reinforcement learning to schedule constrained EV charging times. The authors of Cong Zhang et al. (2021) posed the issue of charging schedule creation as an NP-hard one and then used reinforcement learning to solve it. It was recommended that an intelligent pricing strategy be used at charging stations, and an ANN was presented as a remedy for the issue with charging patterns. Using the Q-learning technique, the authors of Dang et al., (2020) determined that charging electric vehicles at a fast-charging station connected to an intelligent grid was optimum. The attractive feature is the intelligent charging scheduling system, which considers in the state of charge, the distance travelled, the proximity to charging stations, the number of scheduled events, and the average speed. The scenario simulator that creates the labelled datasets needed to train the Machine Learning/Reinforcement Learning algorithms is a unique part of the proposed approach as well, given the scarcity of such datasets Viziteu et al. (2022).

The fields of machine learning and artificial intelligence include the subfield of supervised learning, commonly known as supervised machine learning. It is characterised by training algorithms that properly categorise data or predict outcomes using labelled datasets. Cross-validation is the iterative process of adjusting a model's weights when new data is added until the model is well suited to the data. Predictions based on labelled data may be made more accurately and save time with the help of supervised learning models.

Unsupervised learning makes use of data that has not been labelled. Patterns useful for handling cluster or association difficulties are uncovered within the information. This is especially helpful when domain experts lack knowledge of the similarities present in a dataset. In popular use, methods like the hierarchical, k-means, and Gaussian mixture models cluster data. Machine learning includes the discipline of reinforcement learning. It involves appropriately increasing rewards in a certain circumstance. To determine the optimal course of action to pursue in each circumstance, it is used by different software and robots. The process of reinforcement learning relies heavily on sequential decision-making. To put it another way, the state of one input determines the value of the next input, and the value of the next input determines the value of the preceding output. Figure 5 represents the types of ML Rajbanshi Sabita, (2021).

Coordinated decision making for integrated multiple BSS and BCS

The exponential growth of EV production on the road has shifted the focus of urban planners, utilities, and business owners towards the BSS and BCS initiation. Models of BCS and BSS are included in cutting-edge research on EV charging to provide additional energy sources for EVs. During the BCS mode, EV drivers connect their vehicles to the charging connector and let the batteries recharge over a long time. While in BSS mode, electric vehicle drivers will discharge the spent, then swap it out with one that has been fully charged, which will take less time Wu, (2022). Figure 6 represents battery swaping system.

Charging management of BSS and BCS

Compared to the BCS model, the only direction in which the duration of battery charge is transitioning from the EV to the BSS. In other circumstances, even after switching the batteries, the BSS must spend a significant amount of time for recharging them. The BSS operator may decide on the most effective battery and EV charging schedule based on the battery condition and swapping/charging demand, that supports the station to increase operational profit and reduce power expenses. As a result, the BSS's Quality of Service and

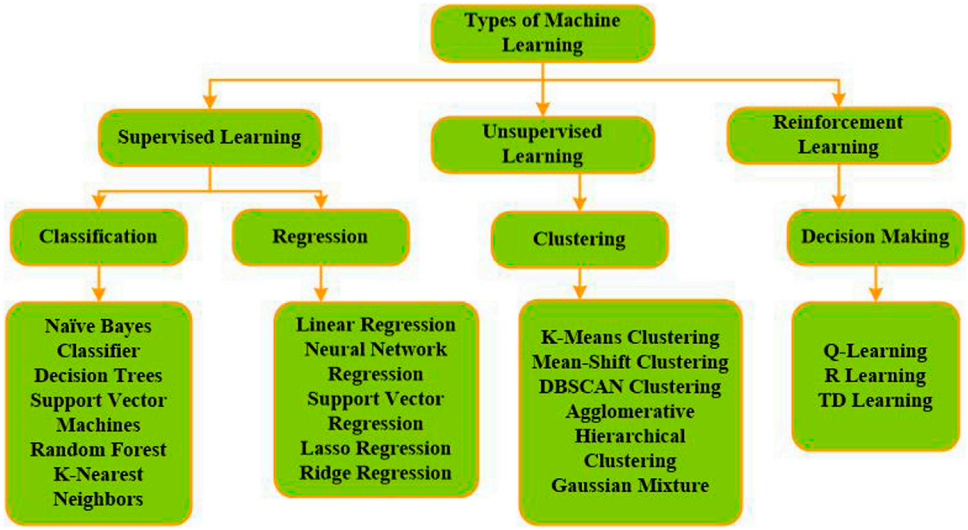

FIGURE 5
Types of machine learning Rajbanshi Sabita (2021).

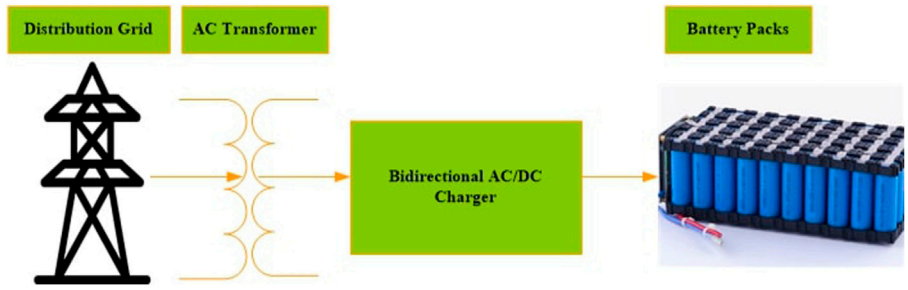

FIGURE 6
Battery swaping system.

service capacity may be enhanced. An ideal charging schedule can also assist the BSS with gratifying more EV swapping and charging demands Wang and Pedram (2019). The following are some of the reasons why charging management is so important while operating in BSS mode:

- If an ideal charging schedule is achieved, then modifying the charging rate at the recharging centre may be used to control the BSS's service availability, which corresponds to the batch of completely recharged batteries.
- The BSS operator is responsible for managing the charging process while considering many factors, such as the needs of EV drivers to swap out their batteries, the limits of the power grid, and the cost to operate (which includes the cost to buy batteries and electricity).
- As the lithium-ion battery's charging power exhibits non-linear features, determining the precise time required to charge one is challenging entirely. To simulate the constant current constant-voltage features Wu et al., (2020), several researchers have developed non-linear mathematical models that can approximate the quantity of power used throughout each period and the time necessary to charge various chargers fully.

EV distribution, road transportation, traffic patterns, and business and residential zones should all be considered when examining the need for charging and switching utilities from an urban planning standpoint Pardo-Bosch et al. (2021). Then, by providing charging facilities, a new charging station may be built, or an existing one can be improved. Additionally, new BSSs

might be designed in a given area to serve commercial EVs, with significant energy demands and the need for quick charging. The charging and switching stations function as high-energy units that impact voltage stability from the standpoint of the power system. Therefore, the power grid's limitations should be considered when choosing BSS or BCS centres. In addition, the BSS/BCS imports supply of electricity from the mains, utilizes it to charge EVs and batteries and then starts selling it to drivers for a profit. As a result, the station manager and the power grid may agree on an electrical strategy. With the aid of V2G and B2G technologies, the BCS/BSS may potentially be able to sell power to the grid., which allow them to benefit from price fluctuations and aid the system in maintaining voltage stability. Providing EV owners with access to battery switching and charging stations is an opportunity for BSS/BCS providers to generate revenue. The operators' primary objective during the planning phase is to choose an area with high swapping/charging demand to optimize their operational profit. On the contrary, intelligent optimization decision models may be used to reduce the cost of their operations, which include things like the BSS's initial stock of batteries, charging infrastructure, and station development. Increasing assessing demand and reducing planning expenses is preferable to optimize the station's operational profit.

If an EV driver wants to switch, the control centre needs to know how far away they are from the BSS and how long it will take them to get there. Due to traffic and travel patterns, it is important to include the unpredictability of appointment information as input to the decision-making model Bonsall, (2004). As a result of needing to travel to their destination BSSs without running out of power, EVs' remaining SoCs are associated with the distance to those BSSs. Because of this, as a constraint in the dispatching and routing problem, the remaining SoC in the EV and the distance to each BSS must be taken into account. In contrast to the single BSS mode, the multiple BSS mode requires the control centre to improve the quality of the choice by synchronizing the needs of EV drivers with the battery status of the dispersed BSSs. To validate their choice, EV drivers will get a response from the control centre. They could negotiate new arrival times or switch to a different BSS if they decided not to accept the assignment. On the BSS side, the control centre should check each BSS's power reserves and make charging adjustments in real time as necessary. Coordination amongst decision makers is, thus, essential in an intelligent BSS system for achieving the best possible outcome.

Models of decentralized decision-making

Decentralized decision-making models that support swapping and charging orders might be used to describe the combined BSS and BCS modes. Due to the integrated nature of these models, they can perform both of these functions. An EV operator may choose battery exchange or recharge when making a service request Sun et al., (2018). Two independent decision models have been established to manage to swap and charge requests from the viewpoint of the control centre. Based on the volatile demands placed on the BSS and BCS, these models determine whether to accept or not to provide access for the request.

Models of centralized decision-making

A centralised decision model might be used to describe the combined BSS and BCS station., in contrast to the decentralized approach, where the BSS and BCS are complimentary while taking into account the order needs from EV drivers and the state of each station. This centralized approach has two operational techniques.

- The control centre makes the assignment without charging or swapping the desired signal from an EV driver. The control centre thus mainly concentrates on the changing battery count at the BSS and BCS, allowing for optimal decision-making given the system's overall state of health.
- If the BSS is overloaded (because of a lack of completely charged batteries), some batteries might be brought to the BSS after being recharged in EVs at the BCS. Once the parking duration of the EVs at the BCS and the switching load at the BSS are known, the interaction may be maximized.

The BSS and BCS models are combined, and the benefits of doing so are addressed. First, the control centre handles the switching and charging requests simultaneously, improving the level of service for EV users. Secondly, by allocating the swapping and charging operations, the choice is optimized, and the overall optimization outcome may be reached. Third, depending on demand and station state, In both the BSS and BCS, the control schedule for the recharging process has been optimised. Fourth, the control centre may ask EV drivers to designate their preferred method, such as swap or charge, since it is believed that they would use a system of distributed decision-making for handling incoming requests Cui et al., (2022). Finally, by synchronising the BCS with the BSS infrastructure, the service capacity may be increased, resulting in enhanced QoS on a Global Scale in BSS and BCS modes due to the adoption of centralized methods.

Possible future scope of this work

The research can be further progressed on the following cases.

- A comparison in the effectiveness of planning issues for charging infrastructure using machine learning approaches, heuristics, and metaheuristics techniques.
- The implementation of various pricing levels for energy based on the intermittent EV load demand, where the price of electricity in EVCS varies and will be calculated based on the overall power use in the region as well as the demand on the power system.
- It is possible to look at leveraging automation and IoT architecture to operate EVCS. As a consequence, EV charging and discharging may be automated based on energy use.
- For EVs to be more sustainable, recycling rates must increase so that valuable metals used in battery production may be reused. The energy density and charging velocity of solid-state batteries are enhanced by the use of ceramic or other solid electrolytes.

Conclusion

This article provides a comprehensive review of studies examining the use of machine learning in various contexts and forecasting of EV charging behaviour. Standard ML algorithms for predicting EV charging behaviour were defined, including supervised and unsupervised methods. Using EV and load volatility, a comparison of different EV modes of operation is accomplished. One might deduce that better EV and DG scheduling contributes to enhanced DS performance. It is also clear that if EV owners can plan their vehicles according to the system consumption pattern, they may generate income using V2G mode.

The article also summarizes various EVs, storage facilities, charging EVs using DGs integrated with EVCS, and a variety of other socio-technical difficulties related to EVs. The adoption rate, as well as the current situation of EVs all around the world, have been emphasized. The increased weight of EVs owing to the inclusion of battery storage mitigates the benefits of EVs' reduced particulate matter production, but only to a limited extent. Electric cars have fundamental problems, such as the absence of high-performance rapid charging infrastructure and the inability to compete in terms of mileage with conventional fuel-based vehicles due to inefficiencies in energy storage and battery management. Government policies that provide attractive incentives and advantages are crucial to boost EV adoption. Willingness to spend and socioeconomic status are two factors influencing consumers' decisions to purchase EVs. The production of EV sales should focus on the variety and design of a model that will appeal to a wide range of buyers. Monadi et al. (2022).

Author contributions

Conceptualization, NG, ND, SS, SV and MVVPK; Methodology, NG, ND, SS, SV and MVVPK; Validation, NG, ND, SS, SV and MVVPK; Formal analysis, NG, ND, SS, SV and MVVPK; Investigation, NG, ND, SS, and SV; Resources, HK and KA; Data curation, NG, ND, SS, SV and MVVPK; Writing—original draft preparation, NG, ND, SS; Writing—review and editing, NG, ND, SS; Visualization, NG, ND, SS, SV, MVVPK, HK, and KA; Supervision, SS, and SV; Project administration, SS, MVVPK, HK and KA; Funding acquisition, HK and KA. All authors have read and agreed to the published version of the manuscript.

Conflict of interest

The authors declare that the research was conducted in the absence of any commercial or financial relationships that could be construed as a potential conflict of interest.

Publisher's note

References

Ali, A., Mahmoud, K., and Lehtonen, M. (2022). Optimal planning of inverter-based renewable energy sources towards autonomous microgrids accommodating electric vehicle charging stations. *IET Generation, Transm. Distribution* 16 (2), 219–232. doi:10.1049/gtd2.12268

Amiri, S., Jadid, S., and Saboori, H. (2018). Multi-objective optimum charging management of electric vehicles through battery swapping stations. *Energy* 165, 549–562. doi:10.1016/j.energy.2018.09.167

Barman, M., and Nalin Behari, D. V. (2020). A similarity based hybrid GWO-SVM method of power system load forecasting for regional special event days in anomalous load situations in Assam, India. *Sustain. Cities Soc.* 61, 102311. doi:10.1016/j.scs.2020.102311

Bhattacharjee, A., Mohanty, R. K., and Ghosh, A. (2020). Design of an optimized thermal management system for Li-ion batteries under different discharging conditions. *Energies* 13 (21), 5695. doi:10.3390/en13215695

Bonsall, P. (2004). "Traveller behavior: Decision-making in an unpredictable world," in *Intelligent transportation systems* (Oxfordshire UK: Taylor & Francis Group), 8, 45–60.1

Bossche, P. (2010). Electric vehicle charging infrastructure. *Electr. Hybrid Veh. Power Sources, Models, Sustain. Infrastructure Mark.*, 517–543. doi:10.1016/B978-0-444-53565-8.00020-8

Brenna, M., Foiadelli, F., Leone, C., and Longo, M. (2020). Electric vehicles charging technology review and optimal size estimation. *J. Electr. Eng. Technol.* 15 (6), 2539–2552. doi:10.1007/s42835-020-00547-x

Chellappan, K., Krishnan, N., Sharma, G., and Senjyu, T. (2022). Real power loss minimization considering multiple DGs and battery in distribution system. *Electr. Power Components Syst.* 49 (6-7), 563–572. doi:10.1080/15325008.2021.2011488

Choi, E., Cho, S., and Kim, K. (2020). Power demand forecasting using long short-term memory (LSTM) deep-learning model for monitoring energy sustainability. *Sustain. Switz.* 12 (3), 1109. doi:10.3390/su12031109

Chtioui, H., and Boukettaya, G. (2020). "Vehicle-to-Grid management strategy for smart grid power regulation," in Proceedings of the 6th IEEE International Energy Conference, Chengdu, China, November 2020, 988–993. doi:10.1109/ENERGYCon48941.2020.92365303

Chung, Y., Khaki, B., Chu, C., and Gadh, R. (2018). "Electric vehicle user behavior prediction using hybrid kernel density estimator," in Proceedings of the 2018 International Conference on Probabilistic Methods Applied to Power Systems, Boise, ID, USA, July 2018. doi:10.1109/PMAPS.2018.8440360

Cleary, K., and Palmer, K. (2020). Renewables 101: Integrating renewable energy resources into the grid. https://www.rff.org/publications/explainers/renewables-101-integrating-renewables/.

Cui, D., Wang, Z., Liu, P., Wang, S., Dorrell, D. G., Li, X., et al. (2022). Operation optimization approaches of electric vehicle battery swapping and charging station: A literature review. *Energy* 263, 126095. doi:10.1016/j.energy.2022.126095

Dang, Q., Wu, D., and Benoit, B. (2019). "A Q-learning based charging scheduling scheme for electric vehicles," in Proceedings of the 2019 IEEE Transportation Electrification Conference and Expo, Seogwipo-si,South Korea, May 2019. doi:10.1109/ITEC.2019.8790603

Dang, Q., Wu, D., and Boulet, B. (2020). "EV charging management with ANN-based electricity price forecasting," in Proceedings of the 2020 IEEE Transportation Electrification Conference & Expo (ITEC), Chicago, IL, USA, June 2020 (IEEE), 626–630.

Das, H. S., Rahman, M. M., Li, S., and Tan, C. W. (2020). Electric vehicles standards, charging infrastructure, and impact on grid integration: A technological review. *Renew. Sustain. Energy Rev.* 120, 109618. doi:10.1016/j.rser.2019.109618

Dharavat, N., Kumar Sudabattula, S., and Suresh, V. (2022). "Review on the integration of distributed generations (solar, wind) and electric vehicles connected to the distribution system to minimize power loss and voltage profile enhancement," in Proceedings of the Innovations and Research in Marine Electrical and Electronics Engineering: Icirmeee, Chennai, India, October 2022, 020001. doi:10.1063/5.01009572455

Dhianeshwar, A., Kaur, P., and Nagarajan, S. (2017). "EV: Communication infrastructure management system," in Proceedings of the 2017 1st International Conference on Sustainable Green Buildings and Communities, SGBC, Chennai, India, December 2017. doi:10.1109/SGBC.2016.7936090

Dogan, A. (2021). Optimum sitting and sizing of WTs, PVs, ESSs and EVCSs using hybrid soccer League competition-pattern search algorithm. *Eng. Sci. Technol. Int. J.* 24 (3), 795–805. doi:10.1016/j.jestch.2020.12.007

Evreporter (2022). *EVreporter magazine*. Bengaluru, India: EVreporter.Com. https://evreporter.com/wp-content/uploads/2022/11/EVreporter-NOV-2022-magazine.pdf.

Gampa, S. R., Jasthi, K., Goli, P., Das, D., and Bansal, R. C. (2020). Grasshopper optimization algorithm based two stage fuzzy multiobjective approach for optimum sizing and placement of distributed generations, Shunt Capacitors and electric vehicle charging stations. *J. Energy Storage* 27, 101117. doi:10.1016/j.est.2019.101117

Ghosh, A. (2020). Possibilities and challenges for the inclusion of the electric vehicle (EV) to reduce the carbon footprint in the transport sector: A review. *Energies* 13 (10), 2602. doi:10.3390/en13102602

Huang, N., Lu, G., and Xu, D. (2016). A permutation importance-based feature selection method for short-term electricity load forecasting using random forest. *Energies* 9 (10), 767. doi:10.3390/en9100767

Iannuzzi, D., and Franzese, P. (2021). Ultrafast charging station for electrical vehicles: Dynamic modelling, design and control strategy. *Math. Comput. Simul.* 184, 225–243. doi:10.1016/j.matcom.2020.04.022

IEA (2022). Global EV outlook 2022 - securing supplies for an electric future. *Glob. EV Outlook* 2022, 221. doi:10.1787/c83f815c-en

Iqbal, M., Kütt, L., Lehtonen, M., Millar, R., Püvi, V., Rassõlkin, A., et al. (2021). Travel activity based stochastic modelling of load and charging state of electric vehicles. *Sustain. Switz.* 13 (3), 1550–1614. doi:10.3390/su13031550

Javed, M., Deb, S., Alam, M., Rafat, Y., and Hameed, S. (2020). "Impact of vehicle to grid on power system," in Proceedings of the 2020 5th IEEE International Conference on Recent Advances and Innovations in Engineering, ICRAIE, Jaipur, India, December 2020. doi:10.1109/ICRAIE51050.2020.9358388

Lahouar, A., and Ben Hadj Slama, J. (2015). Day-ahead load forecast using random forest and expert input selection. *Energy Convers. Manag.* 103, 1040–1051. doi:10.1016/j.enconman.2015.07.041

Li, H., Wan, Z., and He, H. (2020). Constrained EV charging scheduling based on safe deep reinforcement learning. *IEEE Trans. Smart Grid* 11 (3), 2427–2439. doi:10.1109/TSG.2019.2955437

Monadi, M., Farzin, H., Reza Salehizadeh, M., and Rouzbehi, K. (2022). Integrated control and monitoring of a smart charging station with a proposed data exchange protocol. *IET Renew. Power Gener.* 16 (3), 532–546. doi:10.1049/rpg2.12358

Mousavi-Khademi, K., Reza, M., Chamorro, H. R., Vijay, K., Guerrero, J. M., et al. (2020). "Optimal value-based prices placement of der and V2G using planet search algorithm," in Proceedings of the 2020 IEEE Electric Power and Energy Conference, EPEC, Edmonton, Canada, October 2020, 1–6. doi:10.1109/EPEC48502.2020.93200443

Nallusamy, N., Sakthivel, P., Chausalkar, A., and Arumugam, S. (2016). Electric vehicles. *Altern. Fuels Transp.*, 295–320. doi:10.1201/b16260-10

Pardo-Bosch, F., Pujadas, P., Morton, C., and Cervera, C. (2021). Sustainable deployment of an electric vehicle public charging infrastructure network from a city business model perspective. *Sustain. Cities Soc.* 71, 102957. doi:10.1016/j.scs.2021.102957

Ravi, S., and Aziz, M. (2022). Utilization of electric vehicles for vehicle-to-grid services: Progress and perspectives. *Energies* 15 (2), 589. doi:10.3390/en15020589

Reddy, K. R., Meikandasivam, S., and Vijayakumar, D. (2019). A novel strategy for maximization of plug-In electric vehicle's storage utilization for grid support with consideration of customer flexibility. *Electr. Power Syst. Res.* 170, 158–175. doi:10.1016/j.epsr.2018.12.031

Rigas, E. S., Karapostolakis, S., Bassiliades, N., and Ramchurn, S. D. (2018). EVLibSim: A tool for the simulation of electric vehicles' charging stations using the EVLib library. *Simul. Model. Pract. Theory* 87, 99–119. doi:10.1016/j.simpat.2018.06.007

Sabita, R. (2021). Everything you need to know about machine learning. https://www.analyticsvidhya.com/blog/2021/03/everything-you-need-to-know-about-machine-learning/#h2_1.

Sadeghi-Barzani, B., Payam, A., and Kazemi-Karegar, H. (2014). Optimal fast charging station placing and sizing. *Appl. Energy* 125, 289–299. doi:10.1016/j.apenergy.2014.03.077

Santra, A., Samanta, A., and Lin, J. (2019). Integrating long short-term memory and genetic algorithm for short-term load forecasting. *Energies* 12 (11), 2040–2111. doi:10.3390/en12112040

Scott, C., Ahsan, M., and Albarbar, A. (2021). Machine learning based vehicle to grid strategy for improving the energy performance of public buildings. *Sustain. Switz.* 13 (7), 4003. doi:10.3390/su13074003

Seitaridis, A., Rigas, E. S., Bassiliades, N., and Ramchurn, S. D. (2020). An agent-based negotiation scheme for the distribution of electric vehicles across a set of charging stations. *Simul. Model. Pract. Theory* 100, 102040. doi:10.1016/j.simpat.2019.102040

Shahriar, S., Al-Ali, A. R., Osman, A. H., Dhou, S., and Nijim, M. (2020). Machine learning approaches for EV charging behavior: A review. *IEEE Access* 8, 168980–168993. doi:10.1109/ACCESS.2020.3023388

Sheik Mohammed, S., Femin, T., and Sudhakar Babu, T., Sulaiman, S. M., Deb, S., and Kumar, N., (2022). Charge scheduling optimization of plug-in electric vehicle in a PV powered grid-connected charging station based on day-ahead solar energy forecasting in Australia. *Sustain. Switz.* 14 (6), 3498. doi:10.3390/su14063498

Shi, R., and Lee, K. Y. (2015). Multi-objective optimization of electric vehicle fast charging stations with SPEA-II. *IFAC-PapersOnLine* 48 (30), 535–540. doi:10.1016/j.ifacol.2015.12.435

Shibl, M., Ismail, L., and Ahmed, M. (2020). Machine learning-based management of electric vehicles charging: Towards highly-dispersed fast chargers. *Energies* 13 (20), 5429–5524. doi:10.3390/en13205429

Sun, B., Tan, X., Danny, H., and Tsang, K. (2018). Optimal charging operation of battery swapping and charging stations with QoS guarantee. *IEEE Trans. Smart Grid* 9 (5), 4689–4701. doi:10.1109/TSG.2017.2666815

Sun, D., Ou, Q., Yao, X., Gao, S., Wang, Z., Ma, W., et al. (2020). Integrated human-machine intelligence for EV charging prediction in 5G smart grid. *Eurasip J. Wirel. Commun. Netw.* 2020 (1), 139. doi:10.1186/s13638-020-01752-y

Uddin, N., and Islam, M. (2019). "Optimal fuzzy logic based smart energy management system for real time application integrating RES, grid and battery," in Proceedings of the 4th International Conference on Electrical Engineering and Information and Communication Technology, ICEEiCT 2019, Dhaka, Bangladesh, May 2019, 296–301. doi:10.1109/CEEICT.2018.8628057

Velamuri, S., Hari Charan Cherukuri, S., Kumar Sudabattula, S., Natarajan, P., and Hossain, E. (2022). Combined approach for power loss minimization in

distribution networks in the presence of gridable electric vehicles and dispersed generation. *IEEE Syst. J.* 16 (2), 3284–3295. doi:10.1109/JSYST.2021.3123436

Viziteu, A., Furtună, D., Robu, A., Senocico, S., Cioată, P., Marian, R., et al. (2022). Smart scheduling of electric vehicles based on reinforcement learning. *Sensors* 22 (10), 3718–3814. doi:10.3390/s22103718

Wang, L., and Pedram, M. (2019). QoS guaranteed online management of battery swapping station under dynamic energy pricing. *IET Cyber-Physical Syst. Theory Appl.* 4 (3), 259–264. doi:10.1049/iet-cps.2018.5041

Wu, H. (2022). A survey of battery swapping stations for electric vehicles: Operation modes and decision scenarios. *IEEE Trans. Intelligent Transp. Syst.* 23 (8), 10163–10185. doi:10.1109/TITS.2021.3125861

Wu, H., Grantham, K., and Xia, L. (2020). "A realistic and non-linear charging process model for parking lot's decision on electric vehicles recharging schedule," in Proceedings of the 2020 IEEE Transportation Electrification Conference and Expo, ITEC, Chicago, IL, USA, June 2020, 2–7. doi:10.1109/ITEC48692.2020.9161535

Wu, H. (2021). A survey of battery swapping stations for electric vehicles: Operation modes and decision scenarios. *IEEE Trans. Intelligent Transp. Syst.* 23, 10163–10185. doi:10.1109/tits.2021.3125861

Yang, Z. (2015). Electric load movement evaluation and forecasting based on the fourier-series model extend in the least-squares sense. *J. Control, Automation Electr. Syst.* 26 (4), 430–440. doi:10.1007/s40313-015-0186-2

Zahedmanesh, A., Muttaqi, K. M., and Sutanto, D. (2019). "A consecutive energy management approach for a VPP comprising commercial loads and electric vehicle parking lots integrated with solar PV units and energy storage systems," in Proceedings of the 2019 IEEE 1st Global Power, Energy and Communication Conference, GPECOM, Nevsehir, Turkey, June 2019. doi:10.1109/GPECOM.2019.8778609

Zeb, M., Zulqarnain, M., Imran, K., Khattak, A., Janjua, A., Pal, A., et al. (2020). Optimal placement of electric vehicle charging stations in the active distribution network. *IEEE Access* 8, 68124–68134. doi:10.1109/ACCESS.2020.2984127

Zhang, C., Huang, Q., Tian, J., Chen, L., Cao, Y., and Zhang, R. (2011). Smart grid facing the new challenge: The management of electric vehicle charging loads. *Energy Procedia* 12, 98–103. doi:10.1016/j.egypro.2011.10.014

Zhang, C., Liu, Y., Wu, F., Tang, B., and Fan, W. (2021). Effective charging planning based on deep reinforcement learning for electric vehicles. *IEEE Trans. Intelligent Transp. Syst.* 22 (1), 542–554. doi:10.1109/TITS.2020.3002271

frontiers | Frontiers in Energy Research

TYPE Original Research
PUBLISHED 10 February 2023
DOI 10.3389/fenrg.2023.1125408

OPEN ACCESS

EDITED BY
Sarat Kumar Sahoo,
Parala Maharaja Engineering College (P.M.E.C), India

REVIEWED BY
Kandaswamy K. V,
Velammal Educational Trust, India
Vandana Jha,
R.V. College of Engineering (RVCE), India

*CORRESPONDENCE
Mageshvaran Rudramoorthy,
rmageshvaran@vit.ac.in

SPECIALTY SECTION
This article was submitted to Smart Grids, a section of the journal Frontiers in Energy Research

RECEIVED 16 December 2022
ACCEPTED 27 January 2023
PUBLISHED 10 February 2023

CITATION
Ramalingegowda CH and Rudramoorthy M (2023), Transient stability enhancement using optimized PI tuning of static synchronous series compensator in wind power conversion system.
Front. Energy Res. 11:1125408.
doi: 10.3389/fenrg.2023.1125408

Transient stability enhancement using optimized PI tuning of static synchronous series compensator in wind power conversion system

Chethan Hiremarali Ramalingegowda [1] and Mageshvaran Rudramoorthy [2]*

[1]School of Electrical and Electronics Engineering, Vellore Institute of Technology, Vellore, India, [2]School of Electrical and Electronics Engineering, Vellore Institute of Technology, Vellore, India

Power systems are expanding comprehensively with the increase in load demand from both residential and industrial usage. Renewable energy is penetrating the power system to satisfy the power needs of the load demand. With its potential to generate power and compensate for a large portion of the load demand, wind generators make a major renewable power contribution. Power oscillations inherent in wind generator integration with the grid are a power quality issue to be addressed. Oscillation damping using flexible AC transmission system (FACTS) devices is a relevant solution for the power quality issue. There are multiple reasons for power oscillation. Mainly, power systems encounter fault conditions. The faults can be cleared, and the power system tries to retain stability. Sometimes, the system fails due to a longer settling time. A series-connected FACTS device utilized as a series compensator is referred to as a static synchronous series compensator (SSSC). Controlling the flow of electricity over a transmission line using this method is incredibly efficient. The capacity to switch between a capacitive and an inductive reactance characteristic is necessary. The SSSC regulates the flow of power in transmission lines to which it is linked by adjusting both the magnitude of the injected voltage and the phase angle of the injected voltage in series with the transmission line. This allows the SSSC to manage the power flow in the transmission lines. It does it by inserting a voltage that can be controlled into a transmission line in series with the fundamental frequency. This paper develops the optimally tuned SSSC in the wind-integrated grid system to dampen the oscillation. Teacher–learner-based optimization (TLBO) and gray wolf optimization (GWO) algorithms are used to tune the PI controller to improve the damping response. The obtained results show that the damping performance of the proposed controller is better than that of the other traditional controllers.

KEYWORDS

wind integration, static synchronous series compensator, parameter optimized PI tuning, oscillation damping, teacher and learner algorithm (TLBO) and gray wolf optimization (GWO) I

Introduction

The generation of electricity has been almost entirely dependent on fossil fuels, which are a contributing factor to climate change. Many attempts are being made to incorporate renewable energy sources (RES) into the power system to supplant the traditional fuels that are currently used for generation of electricity (Poultangari et al., 2012). One of these renewable energy sources

is wind energy, which, compared to fossil fuels, is both abundant and affordable (Osman et al., 2015). Controlling the pitch angle is one of the control strategies used in wind turbines. It is utilized to achieve the goals of controlling the output power and lowering the loading on the wind turbine components. The PI controller, hydraulic or servo motor, and rate limiter comprise the bulk of its constituent parts. Recent years have seen the implementation of several controllers, including the fuzzy logic controller (FLC), the programmable logic controller (PLC), the maximum point power tracker (MPPT), and the adaptive controller (Burakov and Shishlakov, 2017; Yang et al., 2017). In contrast to the PI controllers, however, these controllers are not only difficult to use but are also expensive. Consequently, PI controllers continue to have a variety of uses in the wind power industry. Finding the gains that are best suited for the PI controller is a challenge. In Civelek et al. (2016), an improved genetic algorithm (IGA) was used to fine-tune the gains of a proportional integral derivative (PID) controller. Compared to the Zeigler and GA tuning methods, the outcome produced by the IGA tuning method is superior.

The gains of the PID controller in the blade pitch angle control were optimized with the help of the PSO algorithm, which increased the amount of power that the variable speed wind turbine was able to produce. Consequently, a larger quantity of power was produced. A considerable performance improvement was observed by switching from the GA tuning strategy to the PSO tuning method. Due to the low efficiency and also the challenges in managing the generator speed of the fixed-speed wind turbines, the variable-speed wind turbines were studied as an alternative to the fixed-speed wind turbines. Regulation of the pitch angle fuzzy is explained in Civelek (2019). Employing PSO to achieve better pitch control is reported in Zahra et al. (2017). The optimization of the PMSG wind turbine grid control is accomplished with the assistance of gray wolf optimizers (Qais et al., 2018) and whale optimization described in Mohamed A and Haridy (2019). Soued et al. (2017) discussed many different metaheuristic optimizers.

Variable-speed wind turbines are more durable, straightforward in construction, and have lower maintenance costs. The PSO tuning approach offers the benefit of rapid convergence, but the GA tuning method is well-accepted due to its high level of accuracy. Nevertheless, the PSO has the potential to converge on a local optimum solution. Additionally, the tuning of the GA can converge too soon, leading to local optimality.

The following is a brief overview of some of the most recent papers written about wind turbines. Choi et al. (2016) made a few suggestions for hybrid power generation. The technical document is beneficial in gaining a grasp of the operation of the wind turbine (Wwd- and Wwd, 2019). A review of hybrid wind–solar energy systems is presented in Sinha and Chandel (2015), which makes use of several optimization strategies. Syahputra et al. (2014) suggested the idea of harnessing wind energy for power generation on the distribution side of the system. A discussion of the Simulink model can be found in Costea et al. (2015). Naik and Gupta (2016) and Ou et al. (2017) provided additional information about the fluctuation of power and the transient study analysis. Bektache and Boukhezzar (2018) discussed optimal power capture, and Naresh and Tripathi (2018) discussed optimal power capture as a hardware solution that uses FPGA. A Java algorithm is utilized in Annamraju and Nandiraju (2019), a fuzzy logic controller is utilized in Duong et al. (2015), an electro-search optimizer is utilized in Dahab et al. (2020), a social search algorithm is utilized in Mohapatra et al. (2019), whale optimization is utilized in Khadanga et al. (2019), gray wolf optimization is utilized in Padhy and Panda (2021), and TLBO is utilized in Pahadasingh (2021) to study stability. However, these algorithms are not widely used in the generation of wind power utilizing doubly fed induction generators (DFIGs) and for power oscillation damping, which is the most important issue.

The integration of wind power generation into the electricity system is done to enhance the power available on the distribution side of the system. The power is disrupted due to wind turbulence. One of the effective series flexible AC transmission systems (FACTS) for increasing the stability of the power system is the static synchronous compensator (SSSC). When managing the injected voltage, the SSSC makes use of the PI controller. Due to the size of the system, PI controller tuning is not a task that can be performed by SSSC controllers. Therefore, the meta-heuristic approach is utilized to modify the PI controller. In this present study, the tuning of the PI controller, which is intended to increase the response, uses the teacher and learner (TLBO) and gray wolf optimization (GWO) algorithms.

Methodology

Figure 1 depicts the planned organizational structure of the proposed system in terms of blocks. In this configuration, the step-up transformer is connected to the DFIG wind generator and the point of common connection (PCC), which is then coupled to the PCC. Then it is wired to the grid using two transmission lines. DFIG causes more oscillations because of the fault in the transmission line system, and eventually, it settles down. The proposed SSSC and associated control will need to dampen these oscillations to be effective.

SSSC modeling

The components of the series injected voltage for the aforementioned two components are expressed by the following equations:

$$V_{dse} = n_c K_{inv} V_{dc_{sssc}} \cos \alpha_{se}, \tag{1}$$

$$V_{qse} = n_c K_{inv} V_{dc_{sssc}} \sin \alpha_{se}, \tag{2}$$

where

n_c—ratio of the coupling transformer

$V_{dc\,sssc}$—Dclink voltage

α_{se}—Series-injected phase angle

K_{inv}—Is a constant to convert the DC to AC using an inverter.

The real (P) and reactive (Q) flows are given as follows:

$$P = \frac{V_s V_r}{X_L} \sin(\delta_s - \delta_r) = \frac{V^2}{X_L} \sin \delta, \tag{3}$$

$$Q = \frac{V_s V_r}{X_L} (1 - \cos(\delta_s - \delta_r)) = \frac{V^2}{X_L} \sin \delta, \tag{4}$$

where V_S and V_r are the magnitudes, and δ_s and δ_r are the phase angles of the voltage sources V_S and V_r, respectively. For simplicity, the voltage magnitudes are chosen such that $V_s = V_r = V$, and the difference between the phase angle is $\delta_s = \delta_r = \delta$.

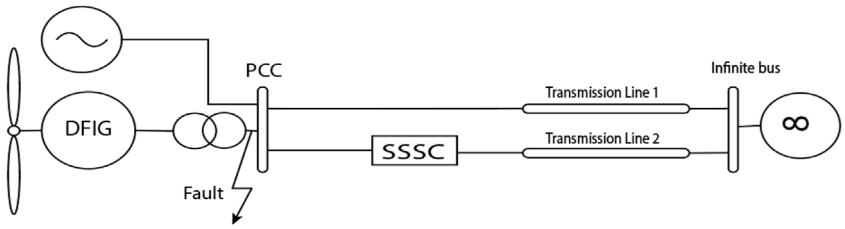

FIGURE 1
Block diagram of the proposed system.

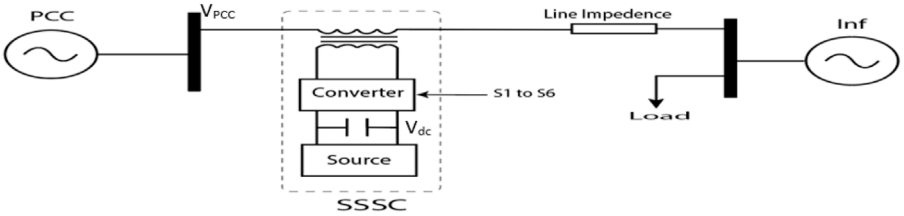

FIGURE 2
Detailed system model of an SSSC without a control.

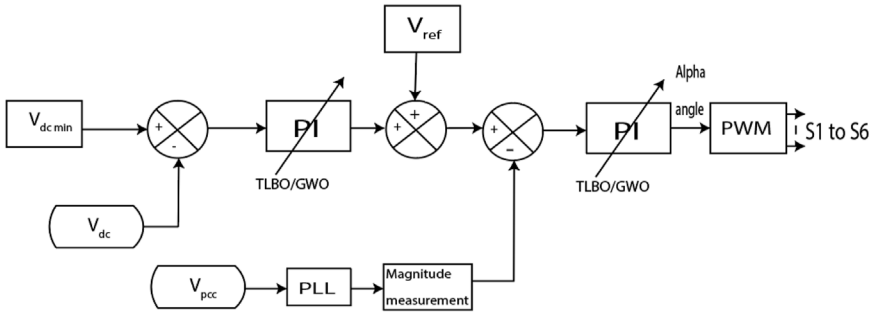

FIGURE 3
Detailed SSSC control system.

$$P_q = \frac{V^2}{X_{eff}} \sin\delta = \frac{V^2}{X_l\left(1 - \frac{X_q}{X_l}\right)} sin\,\delta. \tag{5}$$

$$Q = \frac{V^2}{X_{eff}} (1 - \cos(\delta)) = \left\{\frac{V^2}{X_l\left(1 - \frac{X_q}{X_l}\right)}\right\} \sin\delta. \tag{6}$$

Figure 2 shows the details of the SSSC system. It has capacitors as a storage element, and a converter used is the inverter. The transformer is connected in series. The DC link is connected to the converter, and the three-phase end of the converter is connected to the transformer end. The S1 to S6 switches in the converter are controlled as shown in Figure 3.

Figure 3 shows the control system of the SSSC. The minimum voltage requirement at the DC link ($V_{dc\,min}$) is compared to the DC voltage (V_{dc}) that is measured. This error generated is connected to the PI controller. The PI controller is tuned with TLBO/GWO. This PI controller output is connected to another comparator. Then, the output is compared with the reference voltage (V_{ref}). This output is

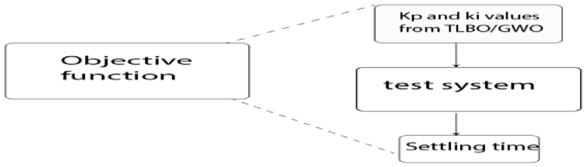

FIGURE 4
Operational diagram for tuning the controller.

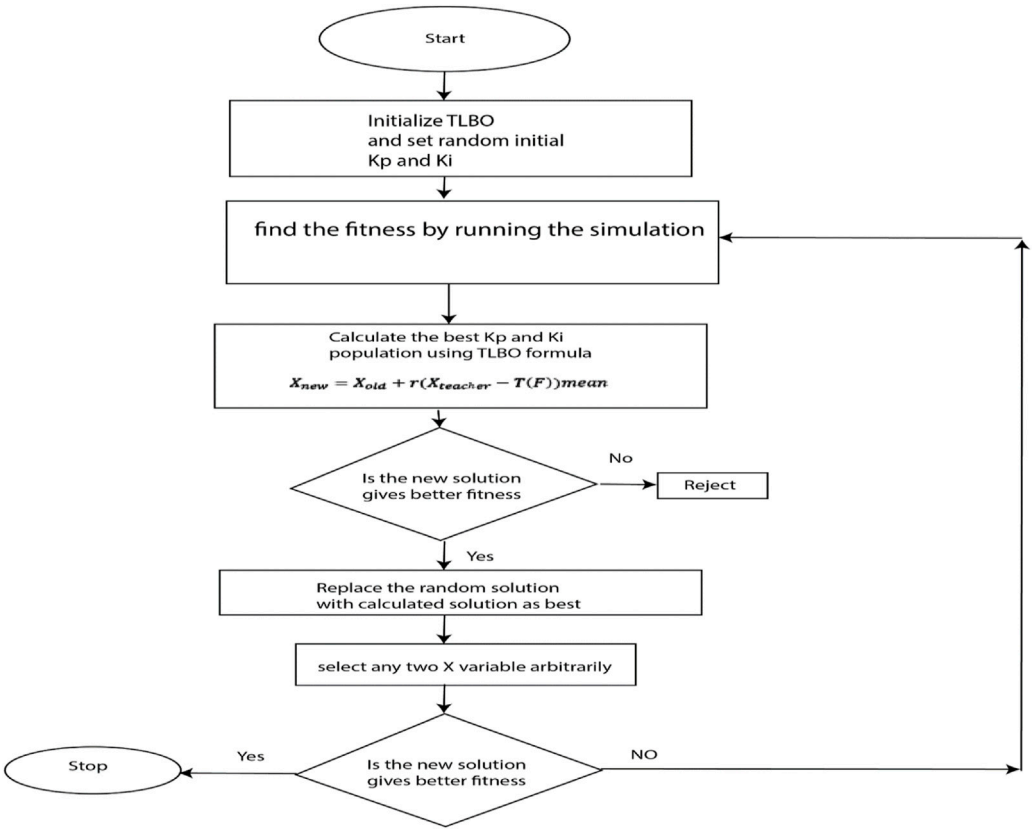

FIGURE 5
Proposed TLBO-based tuning procedure.

again connected to another comparator. The point of common coupling voltage (V_{pcc}) magnitude is compared with this error, and the desired converter alpha angle is determined. This alpha angle is sent to the pulse width modulation (PWM) system. S1 to S6 are the PWM signals, which are connected to the SSSC block as shown in Figure 2.

Objective function

As shown in Figure 3, the PI controller must be tuned using an objective function. This objective function (Figure 4) must be minimized by selecting optimal kp and ki parameters. Eq. 7 is the objective function. Eqs 8, 9 are constraints.

Minimizing voltage settling time

$$\sum_{i=1}^{n} Ts. \tag{7}$$

With respect to constraints

$$K_{p\,min} \le K_p \le K_{p\,max}. \tag{8}$$

$$K_{i\,min} \le K_i \le K_{i\,max}. \tag{9}$$

where Ts—settling time,

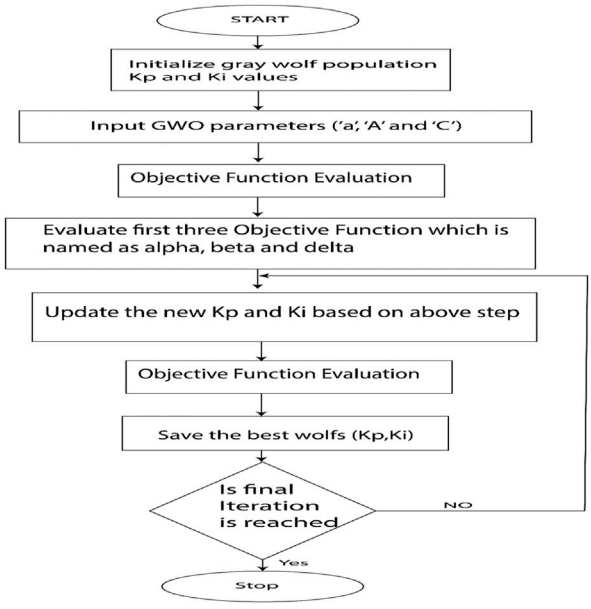

FIGURE 6
Proposed GWO-based tuning procedure flow chart.

$K_{p\,min}$—minimum proportional gain
$K_{p\,max}$—maximum proportional gain
$K_{i\,min}$—minimum integral gain
$K_{i\,max}$—maximum integral gain

The values are obtained by experience while using the PI controller. The problem is formulated using the aforementioned objectives and constraints.

Teacher-learner-based optimization (TLBO)

The optimization techniques used in the present research work are based on the TLBO algorithm, and the steps are presented along with the flow chart (Figure 5).

Step 1: The TLBO algorithm is initialized with the random values of the initial group of Kp and Ki values

Step 2: The Kp and Ki from Step 1 are used in the simulation, and the fitness function is identified.

Step 3: In the group of Kp and Ki values, the values that give lesser fitness are selected.

Step 4: The new Kp and Ki values are calculated using the formula given in the TLBO algorithm, and the fitness is found for new Kp and Ki values.

Step 5: If the new Kp and Ki values give lesser fitness, then replace the best values with the new Kp and Ki values.

Step 6: Else, reject the new Kp and Ki values, go to Step 2, and repeat till the end of the final iteration.

The TLBO algorithm is inspired by the process of teaching and learning in a classroom. The algorithm outlines the two fundamental ways that learning might occur: Through instruction from an instructor, which is called the teaching phase, and through collaboration with other students, which is called learning. The procedure and the flow chart are explained previously.

Gray wolf optimization (GWO)

The second optimization technique used is GWO. The steps involved in the implementation are shown as a flowchart (Figure 6) with a brief description in this section. Here, the wolf is the Kp and Ki values. "Position" means in which the position of the array vector within the group of wolves the Kp and Ki values are placed.

Step 1: Randomly initialize the gray wolf Kp and Ki values for N wolves Yi (i = 1, 2, . . ., n)

Step 2: Find the fit value to reduce the settling time for each individual.

Sort the wolves based on fitness. The three best solutions are named alpha_wolf, beta_wolf, and gamma_wolf.

Alpha_wolf—least fit wolf.
Beta_wolf—second least fit wolf.
Gamma_wolf—third least fit wolf.

Step 3: Do for maximum iteration:

Find the wolf constant "a:"

$$a = 2 * \left(1 - \frac{Iter}{max_{iter}}\right).$$

Do for each wolf till N:

ACalculate the wolf constants Aa1, Aa2, Aa3, Bb1, Bb2, and Bb3, such that

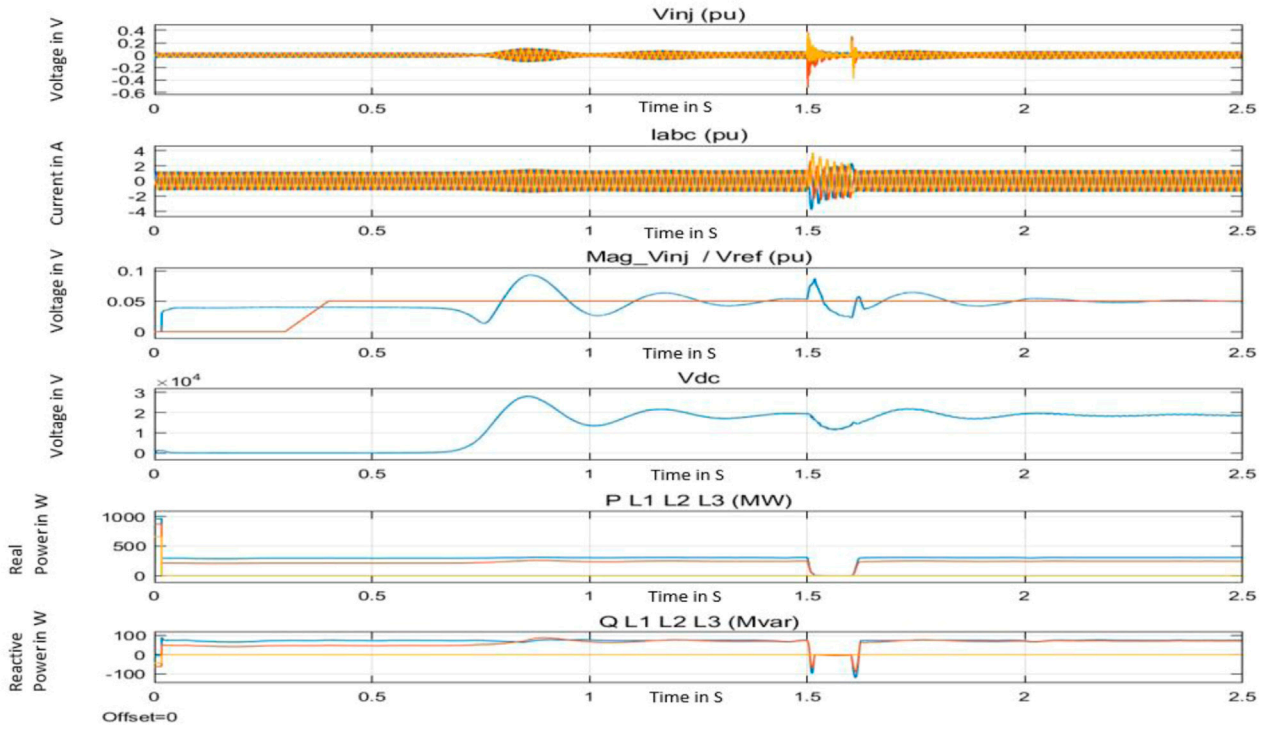

FIGURE 7
PI controller results after connecting the SSSC.

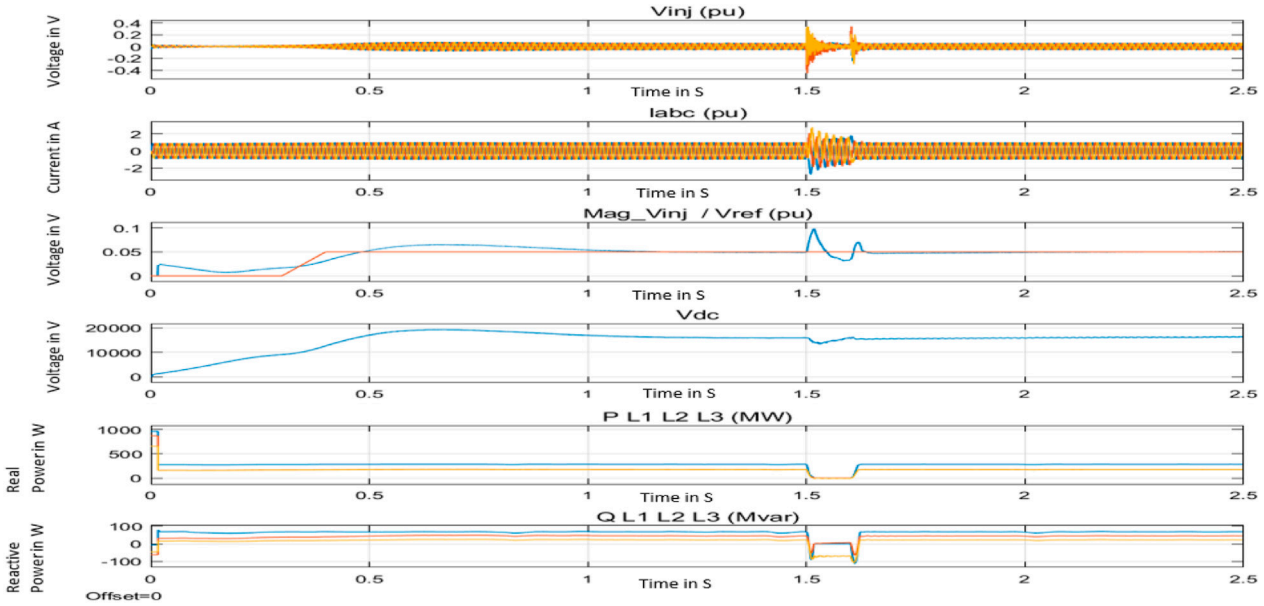

FIGURE 8
TLBO-PI controller results after connecting the SSSC.

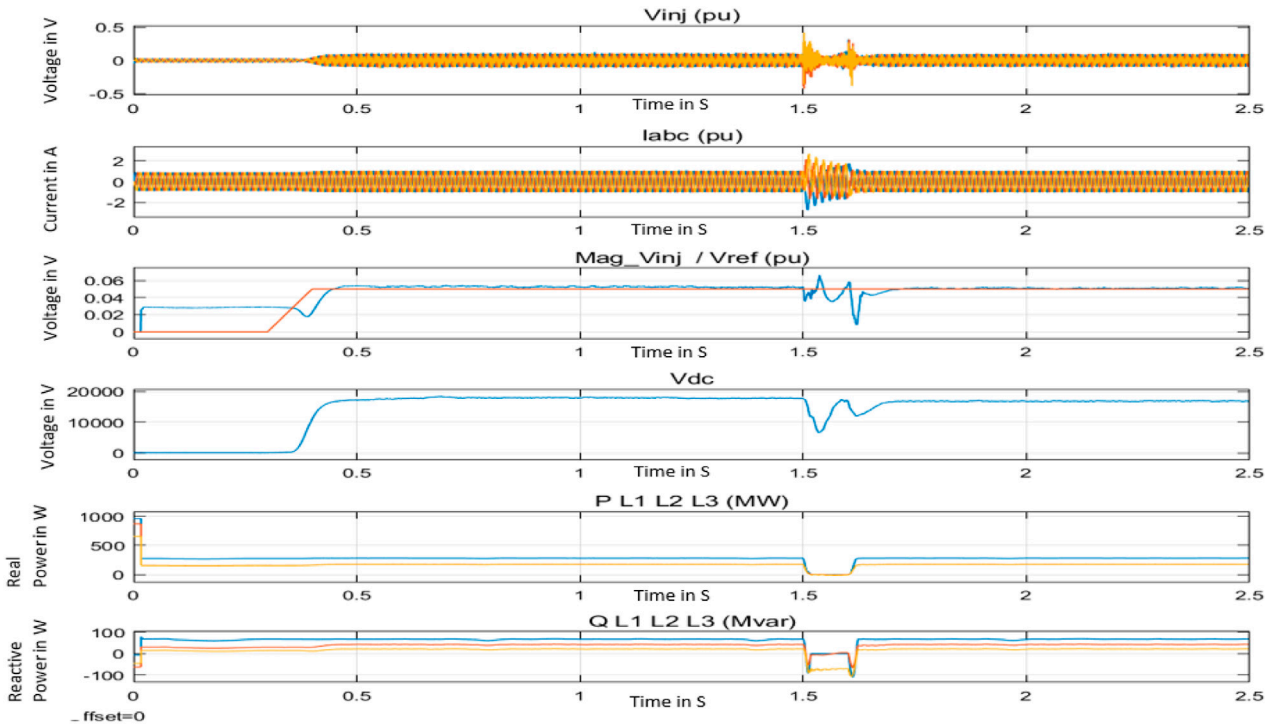

FIGURE 9
GWO-PI controller results after connecting the SSSC.

Aa1 = a*(2*r1 − 1).
Aa2 = a*(2*r2 − 1).
Aa3 = a*(2*r3 − 1).
Bb1 = 2*r1.
Bb2 = 2*r2.
Bb3 = 2*r.

BCalculate Xx1, Xx2, and Xx3, such that

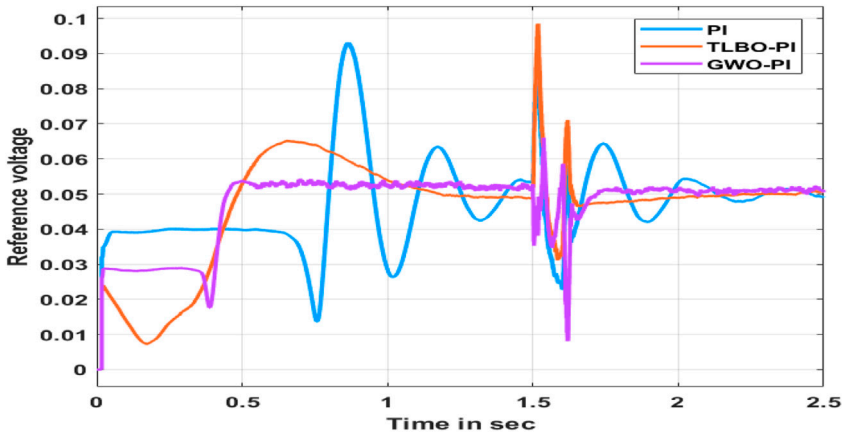

FIGURE 10
Comparison of the measured voltage amplitude of the SSSC injected voltage.

TABLE 1 Kp and Ki values.

Parameter	PI	TLBO-PI	GWO-PI
Kp value	0.77619	0.44402	0.41577
Ki value	2.4481	**2.402**	2.4843

The bold value shows better results.

TABLE 2 Comparative study of waveform properties while using PI, TLBO-PI, and GWO-PI.

Parameter	PI	TLBO-PI	GWO-PI
Rise time (s)	0.77619	0.44402	0.41577
Settling time (s)	2.4481	**2.402**	2.4843
Settling min	0.022728	0.031118	0.008088
Settling max	0.09319	0.098543	0.066098
Overshoot %	89.511	94.518	**30.597**
Peak	0.09319	**0.098543**	0.66098
Peak time (s)	0.86569	1.5184	1.5359

The bold value shows better results.

Xx1 = Aa1*abs (Bb1* position of alpha_wolf—*i*th position of wolf).

Xx2 = Aa2*abs (Bb2*position of beta_wolf—*i*th position of wolf).

Xx3 = Aa3*abs (C3*position of gamma_wolf—*i*th wolf position).

CCompute a new solution and its fitness:

Xnew = (Xx1 + Xx2 + Xx3)/3
Fitnew = fitness (Xnew).

D Update the *i*th wolf greedily:

if the fitnew is less than the *i*th fitness,

*i*th wolf position = Xxnew
*i*th wolf fitness = fitnew
End-for
Find the new values of alpha_wolf, beta_wolf, and gamma_wolf.
Based on the fit value, sort the wolves.
Update with the new value.
Alpha_wolf—least fit wolf.
Beta_wolf—second least fit wolf.
Gamma_wolf—third least fit wolf.
End the for loop.
Step 4: Send the final best wolf.

Results and discussion

The SSSC is connected according to the proposed block diagram shown in Figure 1. The fault is created at the time 1.5 s and released at 1.6 s. The SSSC is connected in the circuit at 0.3 s.

Here, three cases are studied.

Case 1: With the PI controller

Case 2: With TLBO-PI

Case 3: With GWO-PI

Case 1 uses the PI controller in place of the SSSC control. The Case 2 Kp and Ki parameters are tuned using the TLBO algorithm. Then in Case 3, the GWO algorithm is used to tune the PI controller.

The setup and the system are common for all three cases. The results of voltage injection from SSSC (Vinj), the current through the SSSC (Iabc), the reference voltage of SSSC (Vref) and the injected voltage (Mag_inj), the DC voltage measured at the DC link (Vdc), the real power flow and reactive power flow of the power (P L1 L2 L3 and Q L1 L2 L3) are depicted as results for each case. Vinj is the voltage that must be injected when the SSSC is connected at 0.3 s. The current through the SSSC has a phase variation from the voltage of the power system. The magnitude of the Vinj is measured separately and shown as Mag_inj. Then, the SSSC has the DC link as

the capacitor voltage. This voltage should be maintained to get compensation from the SSSC. There are three lines of real and reactive power available in the system labeled P_L1 and Q_L1, P_L2 and Q_L2, and P_L3 and Q_L1.

The SSSC is designed for 10% of injection voltage. The set point of the voltage of SSSC of 0.05 pu is set as the DC link voltage reference. Figure 7 shows the results of PI, Figure 8 shows the results of TLBO-PI, and Figure 9 shows the results of GWO-PI. It can be seen that the Mag_inj takes a very long time to respond, and the oscillations are more in the waveform. This oscillation is also reflected in the other waveforms.

All three methods follow the reference voltage set. However, PI is more oscillatory than TLBO-PI and GWO-PI. The final results show that the settling time is better when using TLBO and GWO than when using PI, while the overshoot is less in GWO than in TLBO. The improvements result in faster stability in the power system, as shown in Figure 10.

Table 1 shows the Kp and Ki values. Here, Table 2 shows the rise time, settling time, minimum and maximum values of settling time, percentage of overshoot, peak value, and the time taken to reach the peak values. The settling time shows that TLBO-PI has a smaller value of 2.402 s, while the PI and GWO-PI take longer to settle. The overshoot value shows 30.597%, which is less than PI and GWO-PI. The peak value of the error is smaller in the PI controller, where the TLBO-PI is slightly higher than the PI and very high in GWO-PI. The research objective is to minimize the settling time, which improves the stability of the system considered. The settling time is less when using the TLBO-PI controller than in other cases. The tendency to reach a peak value is also smaller. However, the percentage of overshoot is less in GWO-PI. Therefore, the TLBO-PI performs better in this study. In addition, the oscillations are smaller, as depicted in Figure 10.

Conclusion

To increase power on the system's distribution side, wind power generation is connected to the power grid. The power is disrupted by this wind's increased disruptions. One of the successful series FACTS for enhancing power system stability is the static synchronous compensator (SSSC). The injected voltage is controlled by the SSSC using a PI controller. Due to the size of the system, SSSC controllers cannot handle this PI controller setting. Therefore, the PI controller is tuned using a meta-heuristic method. This study uses the TLBO and GWO algorithms to tune the PI controller. Improved PI-controller tuning results are shown with the TLBO and GWO. TLBO reduces the settling time by 1.88%, along with a reduction in the peak value of voltage set by the SSSC. The validity of tuning the PI controller and the oscillations is established.

Data availability statement

The raw data supporting the conclusion of this article will be made available by the authors, without undue reservation.

Author contributions

All authors listed have made a substantial, direct, and intellectual contribution to the work and approved it for publication.

Conflict of interest

The authors declare that the research was conducted in the absence of any commercial or financial relationships that could be construed as a potential conflict of interest.

Publisher's note

All claims expressed in this article are solely those of the authors and do not necessarily represent those of their affiliated organizations, or those of the publisher, the editors, and the reviewers. Any product that may be evaluated in this article, or claim that may be made by its manufacturer, is not guaranteed or endorsed by the publisher.

References

Annamraju, A., and Nandiraju, S. (2019). Coordinated control of conventional power sources and PHEVs using Jaya algorithm optimized PID controller for frequency control of a renewable penetrated power system. *Prot. Control Mod. Power Syst.* 4, 28. doi:10.1186/s41601-019-0144-2

Bektache, A., and Boukhezzar, B. (2018). Nonlinear predictive control of a DFIG-based wind turbine for power capture optimization. *Int. J. Electr. Power Energy Syst.* 101, 92–102. doi:10.1016/j.ijepes.2018.03.012

Burakov, M., and Shishlakov, V. (2017). Genetic algorithm optimization for pitch angle control of variable speed wind turbine. *MATEC Web Conf.* 113, 1–6.

Choi, J. W., Heo, S. Y., and Kim, M. K. (2016). Hybrid operation strategy of wind energy storage system for power grid frequency regulation. *IET Gener. Transm. Distrib.* 10 (3), 736–749. doi:10.1049/iet-gtd.2015.0149

Civelek, Z., Çam, E., Lüy, M., and Mamur, H. (2016). Proportional–integral–derivative parameter optimisation of blade pitch controller in wind turbines by a new intelligent genetic algorithm. *Renew. Power Gener.* 10 (8), 1220–1228. doi:10.1049/iet-rpg.2016.0029

Civelek, Z. (2019). Optimization of fuzzy logic (Takagi-Sugeno) blade pitch angle controller in wind turbines by genetic algorithm. *Sci. Technol. Int. J.* 23 (1), 1–9. doi:10.1016/j.jestch.2019.04.010

Costea, M., Vladu, E., and Károly, T. (2015). *Wind turbine modelling in matlab Simulink*. Romania: SSRN, 113–120.

Dahab, Y. A., Abubkar, H., and Tarek Hassan, M. (2020). Adaptive load frequency control of power systems using electro-search optimization supported by balloon effect. *IEEE ACCESS.* 8. 7408–7422. doi:10.1109/ACCESS.2020.2964104

Duong, M. Q., Grimaccia, F., Leva, S., Mussetta, M., Le, K. H., and District, L. (2015). Improving transient stability in a grid-connected squirrel cage induction generator wind turbine system using a fuzzy logic controller. *energies* 8, 6328–6349.

Khadanga, R. K., Kumar, A., and Panda, S. (2019). *A novel modified whale optimization algorithm for load frequency controller design of a two-area power system composing of PV grid and thermal generator", Neural computing and application*. doi:10.1007/s00521-019-04321-7

Mohamed A, H. A. M., and Haridy, A. L. (2019). "The Whale Optimization Algorithm based controller for PMSG wind energy generation system," in 2019 International Conference on Innovative Trends in Computer Engineering (ITCE), no. February, 438–443.

Mohapatra, T. K., Dey, A. K., and Sahu, B. K. (2019). Implementation of SSA based two degrees of freedom fractional order PID controller for AGC with diverse source of generation. *Int. J. Recent Technol. Eng.* 7, 346–356.

Naik, K. A., and Gupta, C. P. (2016). Improved fluctuation behaviour of SCIG based wind energy system using hybrid pitch angle controller. *IEEE Uttar Pradesh Sect. Int. Conf. Electr. Comput. Electron. Eng. UPCON* 1, 508–514., no.

Naresh, M., and Tripathi, R. K. (2018). "Operation and control of doubly fed induction generator based wind energy system using FPGA," in 2017 14th IEEE India Council International Conference (INDICON, 1–6.

Osman, P. A. A., El-wakeel, A. S., and Seoudy, H. M. (2015). Optimal tuning of PI controllers for doubly-fed induction generator-based wind energy conversion system using grey wolf optimizer" J. *Eng. Res. Appl.* 5 (11), 81–87.

Ou, T., Lu, K., and Huang, C. (2017). Improvement of transient stability in a hybrid power multi-system using a designed NIDC. *energies Artic.* 10 (4), 1–16.

Padhy, S., and Panda, S. (2021). Application of a simplified Grey Wolf optimization technique for adaptive fuzzy PID controller design for frequency regulation of a distributed power generation system. *Prot. Control Mod. Power Syst.* 6, 2. doi:10.1186/s41601-021-00180-4

Pahadasingh, S. (2021). "TLBO based CC-PID-TID controller for load frequency control of multi area power system"," in Odisha International Conference on Electrical Power Engineering, Communication and Computing Technology, 1–7. doi:10.1109/ODICON50556.2021.9429022

Poultangari, I., Shahnazi, R., and Sheikhan, M. (2012). RBF neural network based PI pitch controller for a class of 5-MW wind turbines using particle swarm optimization algorithm. *algorithm" ISA Trans.* 51 (5), 641–648. doi:10.1016/j.isatra.2012.06.001

Qais, M. H., Hasanien, H. M., and Alghuwainem, S. (2018). A grey wolf optimizer for optimum parameters of multiple PI controllers of a grid-connected PMSG driven by variable speed wind turbine. *IEEE Access* 6, 44120–44128. doi:10.1109/access.2018.2864303

Sinha, S., and Chandel, S. S. (2015). Review of recent trends in optimization techniques for solar photovoltaic–wind based hybrid energy systems. *Sustain. Energy Rev.* 50, 755–769. doi:10.1016/j.rser.2015.05.040

Soued, S., Ebrahim, M. A., Ramadan, H. S., and Becherif, M. (2017). Optimal blade pitch control for enhancing the dynamic performance of wind power plants via metaheuristic optimisers. *IET Electr. Power Appl.* 11 (8), 1432–1440. doi:10.1049/iet-epa.2017.0214

Syahputra, R., Robandi, I., and Ashari, M. (2014). Performance analysis of wind turbine as a distributed generation unit in distribution system. *J. Comput. Sci. Inf. Technol.* 6 (3), 39–56. doi:10.5121/ijcsit.2014.6303

Wwd-, D., and Wwd, D. T. (2019). *WWD-3 3 MW wind turbine detailed technical-specification," document WWD-1003*. Available at: https://pdf4pro.com/view/wwd-3-3-mw-wind-turbine-ecosource-energy-dc2b5.html.

Yang, B., Zhang, X., Yu, T., Shu, H., and Fang, Z. (2017). Grouped grey wolf optimizer for maximum power point tracking of doubly-fed induction generator based wind turbine. *Convers. Manag.* 133, 427–443. doi:10.1016/j.enconman.2016.10.062

Zahra, B., Salhi, H., and Mellit, A. (2017). "Wind turbine performance enhancement by control of pitch angle using PID controller and particle swarm optimization," in 2017 5th International Conference on Electrical Engineering - Boumerdes (Boumerdes, Algeria: ICEE-B), 1–5.

frontiers | Frontiers in Energy Research

TYPE Brief Research Report
PUBLISHED 16 February 2023
DOI 10.3389/fenrg.2023.1147431

OPEN ACCESS

EDITED BY
Sudhakar Babu Thanikanti,
Chaitanya Bharathi Institute of Technology, India

REVIEWED BY
Damodhar Reddy,
Sasi Institute Technology & Engineering, India
Srikanth Velpula,
S. R University, India
Gaddam Sridhar,
Jawaharlal Nehru Technological University, Hyderabad, India
Rajendhar Puppala,
Smt. Indira Gandhi College of Engineering, India

*CORRESPONDENCE
Vikram Kulkarni,
vikram.kulkarni@nmims.edu

SPECIALTY SECTION
This article was submitted to Smart Grids, a section of the journal Frontiers in Energy Research

RECEIVED 18 January 2023
ACCEPTED 06 February 2023
PUBLISHED 16 February 2023

CITATION
Ravinder M and Kulkarni V (2023), Intrusion detection in smart meters data using machine learning algorithms: A research report.
Front. Energy Res. 11:1147431.
doi: 10.3389/fenrg.2023.1147431

Intrusion detection in smart meters data using machine learning algorithms: A research report

M. Ravinder and Vikram Kulkarni*

Department of Information Technology, SVKM's NMIMS Mukesh Patel School of Technology Management and Engineering, SVKM's NMIMS University, Mumbai, India

The intrusion detection in network traffic for crucial smart metering applications based on radio sensor networks is becoming very important in the Smart Grid area. The network's structure for smart meters under investigation should consider important security factors. The potential of both passive and active cyber-attacks affecting the functioning of advanced metering infrastructure is studied and a novel method is proposed in this article. The proposed method for anomaly identification is efficient and rapid. In the beginning, Cook's distance was employed to recognize and eliminate outlier observations. After observations are made three statistical models Brown's, Holt's, and winter's models were used for exponential smoothing and were estimated using the provided data. Bollinger Bands with the appropriate parameters were employed to estimate potential changes in the forecasts produced by the models that were put into operation. The estimated traffic model's statistical relationships with its actual variations were then investigated to spot any unusual behaviour that would point to a cyber-attack effort. Additionally, a method for updating common models in the event of substantial fluctuations in real network traffic was suggested. The findings confirmed the effectiveness of the proposed method and the precision of the selection of the appropriate statistical model for the under-study time series. The outcomes validated the effectiveness of the proposed approach and the precision in choosing a suitable statistical model for the time series under investigation.

KEYWORDS

smart meter, WSN, AMI, machine learning, intrusion detection, smart grid

1 Introduction

The most essential components of the Smart Grid System are the Smart Metering Communications Networks (SMCN). The reading process can be carried out at an exceptionally high frequency, such as once every 1 s to 15 min for each meter based on the requirement. The Smart Metering Communications Network is made up of three different types of networks: the backbone network, access networks, and last-mile networks (Gao et al., 2022). There are potentially a lot of other creative alternatives, such as meters that are detailed in (Liu et al., 2021). Networks for last-mile smart meters may employ RF, Power Line Communications (PLC), or a combination of the two technologies, which is designed exclusively for the automatic reading of electricity meters (Ravinder and Kulkarni, 2021).

Considering that smart metering systems are a component of the Smart Grid, it is essential to consider the performance of individual infrastructure, they are required to satisfy stringent security requirements. The identification of anomalies in last-mile networks is one such issue (Ji et al., 2015). There are approximately 250 smart metres inside one last-mile network, and it takes a few seconds to read energy consumption data for every 15 min (usually from 1 to 4 s). The aforementioned consumption data, from smart meter will reach a local data-concentrator where the anomaly detection can be done using machine learning algorithms (Wang and Yi, 2011). The data concentrator is mostly constructed using single-board computers, which have a speedy processor, lots of RAM, and ROM memory. Both access and last-mile networks are connected to the data traffic concentrator.

The technique that was described before utilised a way of detecting anomalies that consisted of two stages. The first part of it was primarily concerned with locating and eliminating any abnormalities in the advanced metering infrastructure (AMI) in (Xie et al., 2011) traffic characteristics. This stage was based on Cook's distance, which is an approach that is both straightforward and effective.

A wireless sensor network is used to actualize an AMI network, which is what makes up a last-mile network (WSN) (Liu et al., 2015). Wireless sensors that function in the industrial, scientific, and medical (ISM) frequency bands are included with power meters (Finster and Baumgart, 2015). Lines implemented by technologies such IP networks, General Packet Radio Service (GPRS), or Long-Term Evolution (LTE), receives the traffic from the power meter in (Garcia-Font et al., 2016), which stands in for a link that is realised by a packet communication network (Andrysiak et al., 2017).

In this research, we implement statistical methods for smoothing the data and three machine learning algorithms for detecting abnormal daily power consumption. Based on consumption patterns, which are relatively consistent for a consumer, such as on weekdays or weekends, anomalies in power consumption pattern are detected. To directly identify abnormalities, the proposed methodology may be connected with smart meters. We make the following contributions to this article.

- We create a model to detect anomalies.
- Microservice that receives, processes, stores and exposes meter data.
- Display meter data and anomalies.
- Three machine learning algorithms are implemented for Clustering approach and detecting anomalies based on the means and standard of the readings during the day.
- The proposed system is considered using a cluster environment based on realistic data set. The Monte Carlo model shows the high efficiency for outlier's detection.

The following describes how the article is structured: Section 2 follows the introduction and explains the final mile test-bed network's communication protocol. Section 3 discusses the proposed model. Section 4 presented the Result discussion and Section 5 presented the conclusion of this article followed by references.

2 Literature review

Wireless networking options like ZigBee are cited by Visvakumar et al. in (Aravinthan et al., 2011) as the ideal medium for Smart meter communication. Omid Ardakanian et al. (2014), provide a straightforward, understandable, and useful paradigm for residential consumer profiling that takes temperature and time of day fluctuations into consideration.

In, Robin Berthier et al. (2015) investigated four different strategies for balancing the dual objectives of confidentiality and monitoring by examining their usefulness on a set of real-world packet-level traces obtained at an operational AMI network incongruous with the purpose of intrusion detection systems (IDSes).

Bilal Erman Bilgin et al. (2016) In, developed a plan that makes use of automotive adhoc networks to gather data from smart metres. They are considers average end-end latency and delivery ratio using NS-2 and several routing protocols.

A machine learning-based anomaly detection (MLAD) approach is created by Mingjian Cui et al. (2019) in to efficiently and precisely identify these assaults. Giuseppe Fenza et al. (2019) in, concentrated on the requirement to create anomaly detection methods capable of dealing with idea drift, such as changes in family structure, the conversion of a home into a second dwelling, and other examples. Real power flow on the chosen line in a transmission network is monitored and communicated through a SCADA network to the system operator, according to a suggested method by Annarita Garcia et al. (2015).

The Distributed Denial of Services (DDoS) attack is a possible cyber threat in AMI communication networks, according to Yonghe Guo et al. (2015) in. When using the Markovian decision process framework to examine probable anomalies of malware foot printing, Yonghe Guo et al. (2016) offer an ideal frequency of on-site inquiry and the number of monitoring verification. The greedy quasi-flooding protocol is a novel communication protocol presented by Piotr Kiedrowski et al. (2011).

The smart grid's privacy and cyber security risks are described in general by Jing Liu et al. (2012) in. In (Marnerides et al., 2015), Angelos K, Marne rides, et al. address the problem of finding and attributing anomalies that appear in the sub-meter power consumption data of a smart grid and may be indicative of malicious behavior. A generative model for anomaly detection that takes into consideration the network's hierarchical structure and the information gathered from the SMs was proposed by Ramin Moghaddass et al. in (Moghaddass and Wang, 2018). Amir-Hamed et al. In (Mohsenian-Rad and Leon-Garcia, 2011), list some real-world loads that might be subject to load-altering assaults over the internet. With the help of identity-based signature and encryption schemes, Jia-lun Tsai et al. in (Tsai and Lo, 2016) developed a novel anonymous key distribution system for smart grid scenarios.

3 Proposed model

This proposed model contains Exploratory Data Analysis (EDA) for training the data. Based on the above trained data anomaly detection is estimated using three Machine learning (ML) algorithms discussed in detail in this section below. The dataset

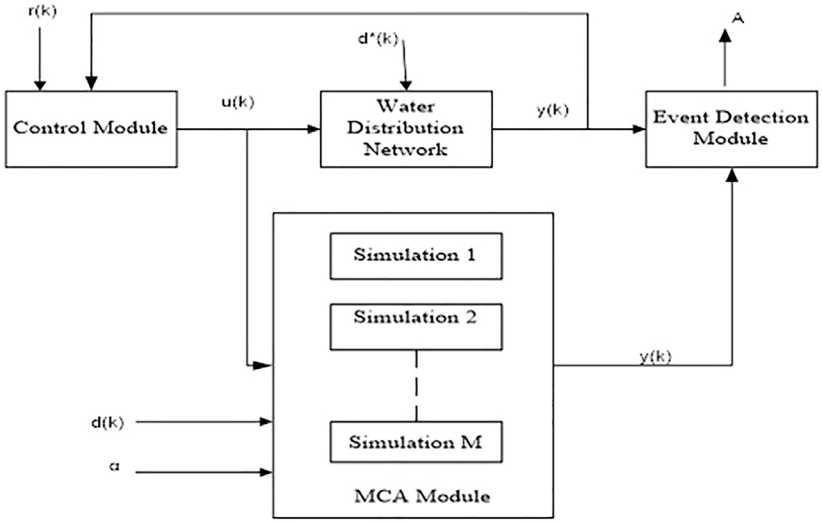

FIGURE 1
Architecture of the proposed system.

consists of time-series forecasting from a single smart meter that is based on the following two models proposed this research.

1. Based on the mean and standard deviation of the day's measurements, a clustering approach for identifying abnormal days has been used.
2. Monte Carlo Algorithm (MCA) for detecting single-meter anomalous readings.

The proposed model is based on, user behavior, mistakes made by humans, poor equipment, energy consumption in buildings and industries that is frequently wasted. In this situation, recognizing anomalous power consumption patterns can be a key step in reducing peak energy use and altering undesired user behavior. Due to the widespread adoption of smart meters, it is now possible to recognize, or flag, anomalous usage by gradually learning what constitutes typical operational consumption. With the use of such information, users may be alerted when their equipment is not functioning as it should, which may modify their behavior. It may even be possible to identify the problematic appliances and make long-term modifications to their behavior. The architecture of proposed system in this paper is shown in Figure 1. The raw data r(k) is given as input to the control model and u(k) is trained data obtained based on EDA. The past data (reference data) d(k) and trained data u(k) are given as input to the MCA the output y(k) is given as input to the Event detection module where the anomaly detection A is identified.

The main purpose of EDA is to analyze the data before making any assumptions. EDA also heps in.

i. Identifying noticeable errors,
ii. Understanding patterns within the data,
iii. Detecting outliers or anomalous events,
iv. Find interesting relations among the variables.

Specific statistical functions and techniques along with EDA tools including clustering and dimension reduction techniques, helps to create graphical displays of high-dimensional data containing many variables.

The algorithm, Density-Based Spatial Clustering of Applications with Noise (DBSCAN) Algorithm (DBSCAN) is utilized to differentiate between clusters with high and low density. DBSCAN performs an excellent job of identifying regions of the data that are highly dense with observations compared to those that are not. DBSCAN also has the capability to group data into clusters of various shapes, which is a significant advantage.

The unsupervised learning method Means shift clustering is non-parametric and does not call for a predetermined shape of the clusters in the feature space, it is frequently utilized in real-world data analysis.

Monte Carlo simulations (MCA) help to clarify how risk and uncertainty impact forecasting and prediction models. An unknown variable must be provided with multiple values in a Monte Carlo simulation to obtain a range of results that must then be averaged to produce an estimate.

3.1 Anomaly detector model

Utilities must identify customers with highly variable consumption and provide them with incentives to smooth out their demand in order to ensure the readiness of the electrical infrastructure for peak demand. An hourly consumption histogram is generated from the algorithms proposed in this research paper, to analyze the data before applying the model to better comprehend its variability.

Next, create a new data frame aggregated from the data generated during weekdays on hourly basis, it is observed that the readings are around 2.75 KWh during weekends with a pick around 5:15 a.m. as shown in Figure 2 in the results section. This might indicate that something is being turned-on automatically at

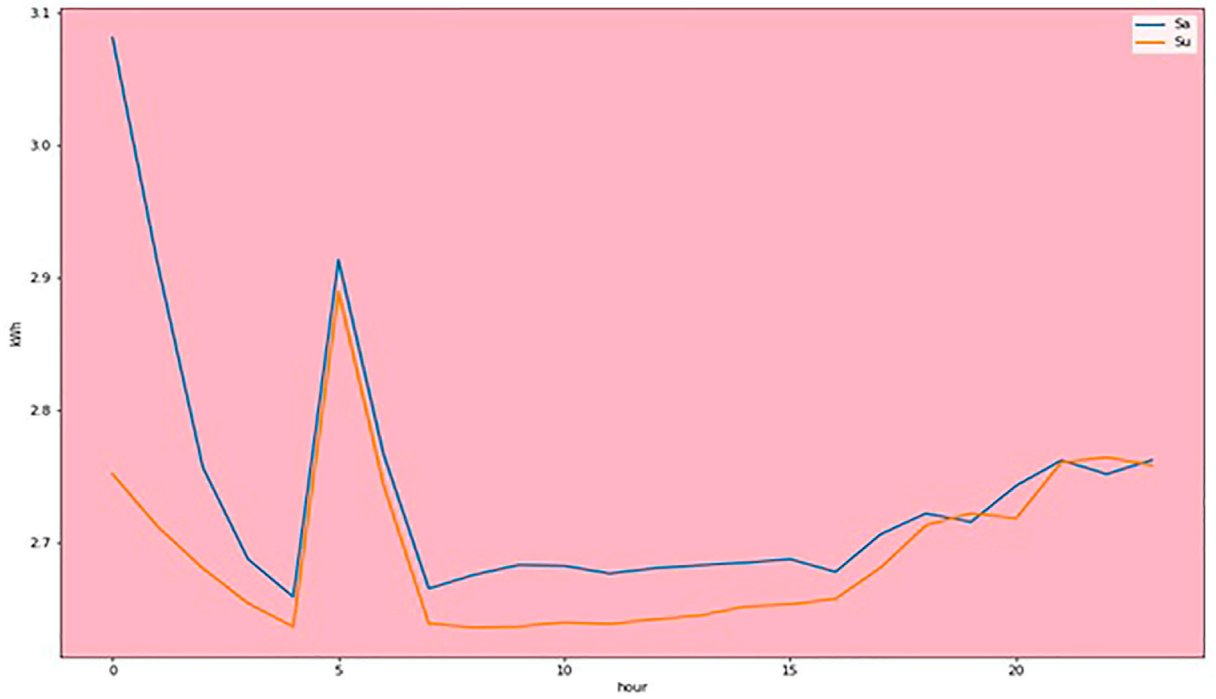

FIGURE 2
Energy consumption in KWh during weekends.

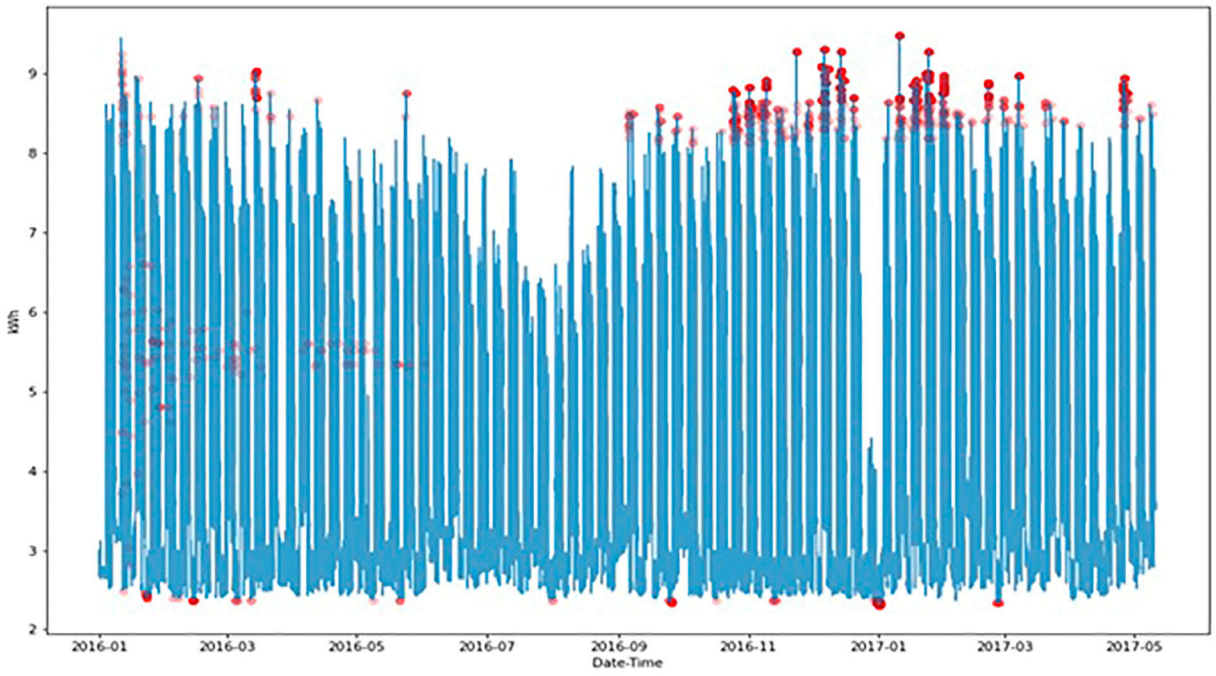

FIGURE 3
Detected outliers.

this time. Lastly, find anomalous days that aggregate the readings for each day in the mean and standard values. The plot below as shown in Figure 3 each day represents with blue standing for Monday to Friday and Green for Saturday to Sunday. As can be seen, there are two big clusters (Blue and Green). However, some blue points fall into the green cluster, and the guess is that these are the non-working Monday to Fridays. To find anomalies, cluster algorithms like DBSCAN, Mean shift and Monte Carlo algorithms are used in this paper.

To find abnormalities, our algorithm includes statistical models and expert knowledge. Furthermore, anomalies should be labelled based on a predefined set of attributes to help us determine whether our model has generated relevant outputs. To locate unique patterns that are difficult to identify by static rules and may not be simple for specialists to quantify, the proposed ML-based models are adapted.

3.2 Density-based spatial clustering of applications with noise (DBSCAN) algorithm

Every data point is encircled by an epsilon (eps) radius circle in DBSCAN before being divided into three categories: Core point, Border point, and Noise. A data point is considered for a core point if a minimum number of points ('min-Points') are present in the circle around it. It is categorized as a Border point if there are less than "minPoints", and as Noise, if there are no other data points within an epsilon radius of any data point.

The values of eps and "minPoints" have a significant impact on DBSCAN. Because of this, it's crucial to know how to choose the values for eps and "minPoints." The DBSCAN algorithm's output can be considerably altered by even a little modification in these numbers. Eq. 1 provides the "min Point" value,

$$\min Point > = Dimensions + 1 \tag{1}$$

Considering "minPoints" as "1"would result in each point becoming its own cluster, which is incorrect. Therefore, it must be at least "3". However, its effectiveness is also determined by domain knowledge. The K-distance graph may be used to determine the value of eps. The graph's elbow, or point of greatest curvature, provides information on the magnitude of eps. More clusters will form and more data points will be viewed as *Noise* if the value of the specified eps is too small. The details will be lost if the size is too large since several little clusters will combine into one large cluster.

```
DBSCAN (dataset, eps, MinPts){
# cluster index
C = 1
for each unvisited point p in dataset {
mark p as visited
# find neighbors
Neighbors N = find the neighboring points of p
if |N|>=MinPts:
N = N U N′
 if p′ is not a member of any cluster:
 add p′ to cluster C
 }
```

Algorithm 1: DBSCAN Algorithm

The DBSCAN pseudo code mentioned above is explained as follows, Finding every neighbor point within an eps and identifying the focal areas or locations that have received visits from neighbors whose number is more than MinPts constitutes step one. For each essential element that hasn't been allocated to a cluster yet in step 2, a new cluster must be created. Recursively finding all of its density-connected points and clustering them with the core point is required in the third stage. A point pair is said to be density connected when "a" and "c" has a sufficient number of points in its neighbors and both "a" and "b" are situated within the eps distance it involves chaining. In consideration of the above, it can be concluded that statement holds true if "b" is a neighbor of "c", "c" is a neighbor of "d", "d" is a neighbor of "e". The fourth step includes repeatedly iterating over the unexplored spots in the dataset. *Noise* is defined as the points that cannot be grouped into a cluster.

3.3 Mean shift algorithm

The "mean point" of the EDA dataset can be obtained by calculating the mean of feature_1 and the mean of feature_2. To note, the "mean point" here is defined by the arithmetic mean of feature_1 and that of feature_2, respectively, because it is calculated based on the equal weights of all points.

$$M_A = \frac{1}{n}\sum_{i=1}^{n} x_i \tag{2}$$

Where M represents the mean, n is the sample size, and x_i is one feature (feature_1 or feature_2) of the data points.

The most widely used weight function in the mean shift algorithm is a flat one,

$$w(d) = \begin{cases} 1, if\ d \le R \\ 0, if\ d > R \end{cases} \tag{3}$$

Where d is the distance between any data point to the currently investigated one, and R is the radius of the circle centered at the investigated point. It's kind of like that we are standing on one local point (center point O) and cannot see the entire picture but are restricted to a local area to calculate the mean. The weighted mean of the investigated area found tends to locate in a region with a high density of points.

```
Initialize k means with random values
 -->For a given number of iterations:
  -->Iterate through items:
   -->Find the mean closest to the item by
      calculating The Euclidean distance of the
      item with each of the means.
   -->Assign item to mean
   -->Update mean by shifting it to the average of
      the items in that cluster
```

Algorithm 2: Mean Shift Algorithm

3.4 Monte Carlo model

Monte Carlo Simulation, is a multiple probability simulation, which is used to estimate the possible outcomes of an uncertain

TABLE 1 Comparison of DBSCAN, mean shift and Monte Carlo algorithms.

S.NO	Performance in %	DBSCAN algorithm (%)	Mean shift algorithm (%)	Monte Carlo algorithm (%)
1	90	87	87	87
2	95	88	88	88
3	100	90	92	96

event. Monte Carlo Algorithm (MCA) based classification is used to estimate every smart meter reading, we calculate the frequency of specific readings in the past and write to the 'freq' column of the data frame. For missing readings, we define the frequency to be −1. A reading is declared anomalous if its frequency is below a set threshold. The threshold value can also be used for estimating the severity of the anomaly.

The Monte Carlo model approach is.

- Easy and Fast
- Tunable
- Adaptive: if the user behavior changes, the algorithm eventually adapts to the new behavior.

This can also be achieved by resetting the clock, i.e., resetting the application dictionary and the count variable after the count reaches a certain threshold, or by setting time-to-live for each reading in the past.

4 Results discussion

The research proposed in this article is implemented on Google Co-lab. The workstation used for the research runs on Intel(R) Core(TM) i3-4005U CPU @ 1.70GHz, 64-bit operating system, the x64-based processor with 8.00 GB RAM. For evaluating algorithms and statistical models proposed in this paper considers open-source data from (kaggle, 2023). Table 1 illustrates the sensitivity of DBSCAN, Mean shift, and Monte Carlo algorithms on anomaly detection. Based on the observation from Table 1 the Monte-Carlo algorithm outperforms the DBSCAN and Mean shift algorithms.

Figure 2 shows the readings of the electrical energy consumption of an office building. The power consumption on weekend (Saturday and Sunday) is observed to be around 2.75 KWh with a pick at 5: 15 a.m. This reading during weekend days is observed to be suspicious.

The location of the detected anomaly is shown in Figure 3. The outliers that were discovered are shown by the red spots on this graph, and the degree of the abnormality is indicated by how transparent the spots are. Brighter red denotes greater severity. This can also be done by setting time-to-live for each reading in the past or by restarting the clock, which involves restarting the application dictionary and the count variable after count reaches a particular threshold.

The observation regarding EDA, DBSCAN, Mean Shift, and Monte Carlo algorithms can be made from the results.

- Observation 1: Implemented three machine learning algorithms to find abnormalities and allow access to a micro-service that collects, modifies, saves, and displays meter data.
- Observation 2: Every data point is encircled by an epsilon-radius circle in DBSCAN before being divided into three categories: Core point, Border point, and Noise. The K-distance graph may be used to determine epsilon's value. The DBSCAN algorithm is a clustering algorithm.
- Observation 3: Mean shift is an unsupervised learning approach that outperforms the DBSCAN algorithm and is mostly used for clustering.
- Observation 4: Monte Carlo classification focuses on individual smart meter measurements. The Monte Carlo model technique is simple, quick, tunable, and adaptable, and it improves results by 15% compared to similar work (Andrysiak et al., 2017).

5 Conclusion

In this paper, a new data-driven approach to identify distribution system abnormalities using time series analysis is proposed. With a high degree of confidence, the developed anomaly detector identified every pre-designed abnormality. The proposed anomaly detector operates unsupervised, which overcomes the issue of data imbalance brought on by a lack of anomalous data. A realistic distribution grid has been successfully used to test the results that correspond to the proposed framework. In the future, this research can analyse and forecast multivariate data from smart grid using a machine learning algorithm.

Data availability statement

The original contributions presented in the study are included in the article/supplementary material, further inquiries can be directed to the corresponding author.

Author contributions

MR is a research scholar and has done the research work. VK is a supervisor and has monitored the work.

Conflict of interest

The authors declare that the research was conducted in the absence of any commercial or financial relationships that could be construed as a potential conflict of interest.

Publisher's note

References

Andrysiak, T., Saganowski, Ł., and Kiedrowski, P. (2017). Anomaly detection in smart metering infrastructure with the use of time series analysis. *J. Sensors* 2017, 1–15. Article ID 8782131, 15 pages. doi:10.1155/2017/8782131

Aravinthan, V., Namboodiri, V., Sunku, S., and Jewell, W. (2011). "Wireless AMI application and security for controlled home area networks," in IEEE Power Energy Soc. Gen. Meet, Detroit, MI, USA, 24-28 July 2011, 1–8. doi:10.1109/PES.2011.6038996

Ardakanian, O., Koochakzadeh, N., Singh, R. P., Golab, L., and Keshav, S. (2014). Computing electricity consumption profiles from household smart meter data. *CEUR Workshop Proc.* 1133, 140–147.

Berthier, R., Urbina, D. I., Cardenas, A. A., Guerrero, M., Herberg, U., Jetcheva, J. G., et al. (2015). "On the practicality of detecting anomalies with encrypted traffic in AMI,"in 2014 IEEE Int. Conf. Smart Grid Commun. SmartGridComm, Venice, Italy, 03-06 November 2014, 890–895. doi:10.1109/SmartGridComm.2014.7007761

Bilgin, B. E., Baktir, S., and Gungor, V. C. (2016). Collecting smart meter data via public transportation buses. *IET Intell. Transp. Syst.* 10 (8), 515–523. doi:10.1049/iet-its.2015.0058

Cui, M., Wang, J., and Yue, M. (2019). Machine learning-based anomaly detection for load forecasting under cyberattacks. *IEEE Trans. Smart Grid* 10 (5), 5724–5734. doi:10.1109/tsg.2018.2890809

Fenza, G., Gallo, M., and Loia, V. (2019). Drift-aware methodology for anomaly detection in smart grid. *IEEE Access* 7, 9645–9657. doi:10.1109/ACCESS.2019.2891315

Finster, S., and Baumgart, I. (2015). Privacy-aware smart metering: A survey. *IEEE Commun. Surv. Tutorials* 17 (2), 1088–1101. doi:10.1109/COMST.2015.2425958

Gao, H.-X., Kuenzel, S., and Zhang, X.-Y. (2022). A hybrid ConvLSTM-based anomaly detection approach for combating energy theft. *IEEE Trans. Instrum. Meas.* 71 (1), 1–10. doi:10.1109/tim.2022.3201569

Garcia, M., Giani, A., and Baldick, R. (2015). Smart grid data integrity attacks: Observable islands. *IEEE Power Energy Soc. Gen. Meet.* 2015 (3), 1244–1253. doi:10.1109/PESGM.2015.7286300

Garcia-Font, V., Garrigues, C., and Rifà-Pous, H. (2016). A comparative study of anomaly detection techniques for smart city wireless sensor networks. *Sensors Switz.* 16, 868–876. doi:10.3390/s16060868

Guo, Y., Ten, C. W., Hu, S., and Weaver, W. W. (2015). Modeling distributed denial of service attack in advanced metering infrastructure. *2015 IEEE Power Energy Soc. Innov. Smart Grid Technol. Conf. ISGT* 2015, 1–5. doi:10.1109/ISGT.2015.7131828

Guo, Y., Ten, C. W., Hu, S., and Weaver, W. W. (2016). Preventive maintenance for advanced metering infrastructure against malware propagation. *IEEE Trans. Smart Grid* 7 (3), 1314–1328. doi:10.1109/TSG.2015.2453342

Ji, S., Chen, T., and Zhong, S. (2015). Wormhole attack detection algorithms in wireless network coding systems. *Wormhole Attack Detect. algorithm Wirel. Netw. Coding Syst.* 14 (3), 660–674. doi:10.1109/tmc.2014.2324572

kaggle (2023). kagle. Available at: https://www.kaggle.com/datasets/portiamurray/anomaly-detection-smart-meter-data-sample (Accessed on 18-Jan 2023).

Kiedrowski, P., Dubalski, B., Marciniak, T., Riaz, T., and Gutierrez, J. (2011). Energy greedy protocol suite for smart grid communication systems based on short range devices. *Adv. Intell. Soft Comput.* 102, 493–502. doi:10.1007/978-3-642-23154-4_54

Liu, J., Xiao, Y., Li, S., Liang, W., and Chen, C. L. P. (2012). Cyber security and privacy issues in smart grids. *IEEE Commun. Surv. Tutorials* 14 (4), 981–997. doi:10.1109/SURV.2011.122111.00145

Liu, Q., Hagenmeyer, V., and Keller, H. B. (2021). A review of rule learning-based intrusion detection systems and their prospects in smart grids. *IEEE Access* 9, 57542–57564. doi:10.1109/ACCESS.2021.3071263

Liu, X., Golab, L., and Ilyas, I. F. (2015). Smas: A smart meter data analytics system. *Proc. - Int. Conf. Data Eng.* 2015, 1476–1479. doi:10.1109/ICDE.2015.7113405

Marnerides, A. K., Smith, P., Schaeffer-Filho, A., and Mauthe, A. (2015). Power consumption profiling using energy time-frequency distributions in smart grids. *IEEE Commun. Lett.* 19 (1), 46–49. doi:10.1109/LCOMM.2014.2371035

Moghaddass, R., and Wang, J. (2018). A hierarchical framework for smart grid anomaly detection using large-scale smart meter data. *IEEE Trans. Smart Grid* 9 (6), 5820–5830. doi:10.1109/TSG.2017.2697440

Mohsenian-Rad, A. H., and Leon-Garcia, A. (2011). Distributed internet-based load altering attacks against smart power grids. *IEEE Trans. Smart Grid* 2 (4), 667–674. doi:10.1109/TSG.2011.2160297

Ravinder, M., and Kulkarni, V. (2021). "Review on energy efficient wireless sensor network protocols," in 21st IEEE Int. Conf. Environ. Electr. Eng. 2021 5th IEEE Ind. Commer. Power Syst. Eur. EEEIC/I CPS Eur. 2021 - Proc., Bari, Italy, 07-10 September 2021, 7. doi:10.1109/EEEIC/ICPSEurope51590.2021.9584696

Tsai, J. L., and Lo, N. W. (2016). Secure anonymous key distribution scheme for smart grid. *IEEE Trans. Smart Grid* 7 (2), 1–914. doi:10.1109/TSG.2015.2440658

Wang, X., and Yi, P. (2011). Security framework for wireless communications in smart distribution grid. *IEEE Trans. Smart Grid* 2 (4), 809–818. doi:10.1109/tsg.2011.2167354

Xie, M., Han, S., Tian, B., and Parvin, S. (2011). Anomaly detection in wireless sensor networks: A survey. *J. Netw. Comput. Appl.* 34 (4), 1302–1325. doi:10.1016/j.jnca.2011.03.004

frontiers | Frontiers in Energy Research

TYPE Original Research
PUBLISHED 22 February 2023
DOI 10.3389/fenrg.2023.1101049

OPEN ACCESS

EDITED BY
Sarat Kumar Sahoo,
Parala Maharaja Engineering College (P.M.E.C), India

REVIEWED BY
Mohammad Amir,
Jamia Millia Islamia, India
S. Padmini,
SRM University, India

*CORRESPONDENCE
Belwin Edward,
belwinedward@vit.ac.in

SPECIALTY SECTION
This article was submitted to Smart Grids, a section of the journal Frontiers in Energy Research

RECEIVED 17 November 2022
ACCEPTED 07 February 2023
PUBLISHED 22 February 2023

CITATION
Gogula V and Edward B (2023), Fault detection in a distribution network using a combination of a discrete wavelet transform and a neural Network's radial basis function algorithm to detect high-impedance faults.
Front. Energy Res. 11:1101049.
doi: 10.3389/fenrg.2023.1101049

Fault detection in a distribution network using a combination of a discrete wavelet transform and a neural Network's radial basis function algorithm to detect high-impedance faults

Vyshnavi Gogula and Belwin Edward*

Department of Electrical Engineering, Vellore Institute of Technology, Vellore, India

High Impedance Fault detection in a solar photovoltaic (PV) and wind generator integrated power system is described in this paper using discrete wavelet transform and a neural network with radial basis function (NNRBF). For this paper, the integration of solar photovoltaic and wind systems was modelled in a MATLAB/Simulink environment to create an IEEE 13-bus system. Microgrids (MG's) are mostly powered by renewable energy. Uncertainty about renewables has shifted attention to ensuring a steady supply and long-term viability. It has been addressed in the paper whether or not a small-scale distant end source connection may be made at the terminal of a radial distribution feeder. Some typical power system problems compromise the reliability of the grid's power supply. To solve this problem, this study suggests a criterion algorithm based on the neural network with radial basis function (NNRBF), and a defect detection method based on the discrete wavelet transform (DWT). The MATLAB/Simulink model of the system is then used to produce fault and travelling wave signals. The db4 wavelet is used to deconstruct the travelling wave signals into detail and approximate signals, which are then combined with the data from the two-terminal travelling wave localization approach for fault detection. After that, the optimal maximum coefficients of the wavelets are extracted and fed into the proposed radial basis function neural network (NNRBF). The results show that both the criterion algorithm and the fault detection algorithm are reliable in their assessments of whether or not faults exist in the power system, and that neither algorithm is particularly sensitive to variations in fault type, fault detection, fault initial angle, or transition resistance. After that, the optimal maximum coefficients of the wavelets are extracted and fed into the proposed radial basis function neural network (NNRBF). Overhead distribution system faults are simulated in Matlab/Simulink, and the technique is rigorously validated across a wide range of system situations. It has been shown through simulations that the proposed method can be relied upon to successfully and dependably protect high impedance fault (Hi-Z).

KEYWORDS

solar photovoltaic, wind, microgrid, high impedance fault, distribution network, neural network with radial basis function, nonlinear load switching

1 Introduction

The widespread recognition of the negative effects of fossil fuel consumption on the environment is a primary cause of this issue. Use of sustainable materials. Hydroelectric power, PV power, wind power, and micro-turbines are all examples of renewable energy sources that can help meet the growing demand for electricity without increasing pollution. Although wind and PV energy show the most promise, their utilization is limited by the fact that they are unpredictable and intermittent, which results in unreliable economic dispatch (Kroposki et al., 2017; Qazi et al., 2019). MG's in remote places that run on renewable energy sources like wind and solar PV are becoming more reliable thanks to the installation of energy storage (Billinton and Karki, 2001; Kroposki et al., 2017). The complementary nature of solar photovoltaics and wind power is an inherent benefit (Al-Masri and Ehsani, 2015). Maximum power point (MPP) extraction is used to get the most efficient amount of energy from the wind and sun. Maximum power point for solar is found using the incremental conductance (De Brito et al., 2012) scheme, whereas for wind it is found using the estimation based perturb and observe (EP&O) (Xiao et al., 2011) scheme. Traditional P&O, MPP schemes perform poorly under conditions of rapid change in the surrounding environment, which can cause tracking to lag or even fail (Ahmed and Salam, 2018). Since the control parameter is an incremental step, it struggles to deliver sufficient dynamic performance. Finding the sweet spot for parameter size can be tricky. The inverter output fluctuates because of the dominating oscillation close to the MPP. EPO offers a more in-depth evaluation of the MPP than what is available through the standard P&O technique. Due to the extremely non-linear nature of the wind, the MPP can only be attained by a combination of the perturb procedure's exhaustive search of the search zone and the estimate procedure's compensation for the perturb procedure's inefficiencies as the wind speed varies. Therefore, PV and wind power together can help with the issue of long-term intermittency. This makes it all the more important to design a solid protection architecture capable of detecting and categorising system failures in order to ensure MG's safe and reliable functioning. Numerous studies were conducted to identify faults, categorize them, and isolate them to lessen the frequency and duration of outages in the transmission and distribution networks. HIF is an annoying system anomaly. A HIF is formed whenever an electrical conductor comes into contact with a high-resistance item, such as a branch, sand, or asphalt. In a grounded system, its fault current is typically between 0 and 75 A, displaying asymmetrical, intermittent, and non-linear arcing behavior (Costa et al., 2015; Wang et al., 2016). Due to the lower current magnitude, the over current relay often fails to detect the HIF in the system, leading to a cascading failure of the system and putting people and their belongings in danger (Sedighi et al., 2005a). Furthermore, the spread of HIF to otherwise functional areas of the grid might cause a domino effect of failure throughout the entire system (Kavi et al., 2018; Santos et al., 2017). To investigate the impact of HIF on distribution networks, a mathematical model is proposed in (Yu et al., 2008) in the form of a non-linear partial differential equation.

According to Figure 1, the most common causes of failures in an urban distribution system are external variables, natural factors, and improper maintenance and operation. The presence of a path to ground is not required for a Hi-Z fault to occur, and the presence of such a path has no bearing on the detection of a Hi-Z fault. Current paper, however, employs a DWT and NNRBF for a distribution network to detect HIF in wind and solar PV power networks. Overhead power lines are the typical method of delivering electricity to homes and businesses. Due to exposure to varying climatic conditions, these are more likely to have power outages. It may be possible to readily detect and localize a subset of these malfunctions. However, there are not many malfunctions that cannot be spotted by standard safety measures (AsghariGovar et al., 2018). Equipment attached to the supply line can be harmed if the distribution system is allowed to run for hours or days with unidentified HIF. Furthermore, the analysis reveals that electric arcs emit a random, unpredictable, and unbalanced current that is then followed by HIF (Chen et al., 2016). Because distribution infrastructure is often located near densely inhabited regions, deaths from electrical arcs are all too often. Despite the fact that the detection of HIFs has been a topic of study since the early 1970s, more work remains to be done to shed light on the process. Using the ratio of harmonics at lower orders, as described in (Emanuel et al., 1990). One problem of this type of method is that it requires setting a number of threshold values, which might negatively impact the detection method's efficiency. Methods based on time-frequency analysis have shown promising results in the identification procedure (Samantaray et al., 2008; Ghaderi et al., 2014). However, the rate of erroneous detection is demonstrated to be a significant barrier to real-world implementations. Faults can be identified by comparing the current or voltage signal before and after the fault occurred, using techniques that operate in the time domain. There are minimal problems associated with an unbalanced network when using the mathematical morphology-based time domain methods presented in (Gautam and Brahma, 2012; Sekar and Mohanty, 2017). Since the DWT can identify both the frequency component and its temporal position, it has found widespread application in signal processing. There has been more than a decade of experience protecting electrical grids with these techniques. Although DWT based techniques are providing a good detection rate with linear loads (Sarlak and Shahrtash, 2011), there is no evidence of non-linear loads inclusion with the

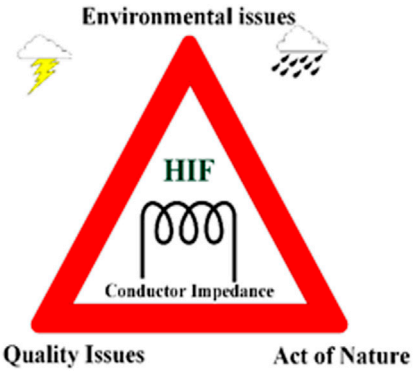

FIGURE 1
Causes of HIF.

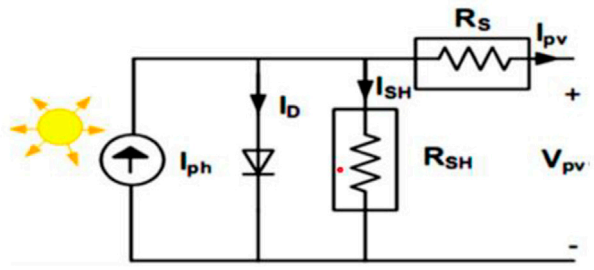

FIGURE 2
PV cell circuit model (Chatrenour et al., 2017).

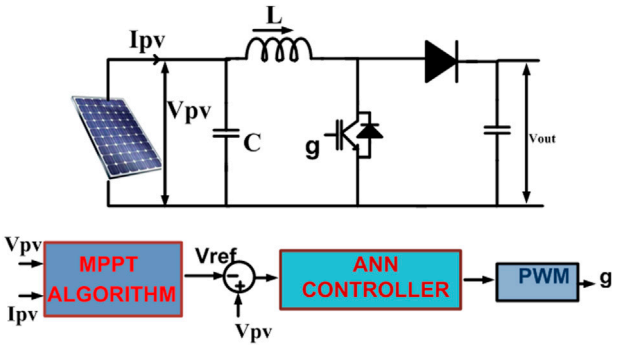

FIGURE 3
PV system configuration using MPPT and DC–DC boost converter (Yahya and Yahya, 2023).

systems while detecting HIFs except in (Chen et al., 2016). All the way through the power distribution networks, the number of non-linear loads (NLLs) has been steadily rising in recent years. While NLLs are a key part of the puzzle when it comes to modelling and building viable HIF detection algorithms, a large proportion of currently available methods ignore them. Similarities between NLL and HIF features will reduce the efficacy of current approaches. The majority of current proposals for defect diagnosis can be broken down into two groups: frequency domain feature identification methods and adaptive detection techniques. Three of the most common methods for finding features in the frequency domain are the Fourier transform, the wavelet transform, and the Hilbert-Huang transform. These days, adaptive detection strategies typically use either expert systems or neural networks. These theoretical studies have produced useful insights, but they are not without their faults. While the single-ended travelling wave fault location approach is commonly used, detecting the wave head is difficult, and placement accuracy is low (Santos et al., 2016). Empirical mode decomposition (EMD) was optimized using integrated EMD (see (Mahari and Seyedi, 2015)). While this approach did not suffer from modal aliasing, it did introduce fake components, which led to poor placement precision. An approach to fault phase selection is proposed in (Sedighi et al., 2005b) that makes use of the high-order multi-resolution singular entropy of active fault components. Though this method works regardless of fault type, fault detection, or transition resistance, finding the right cutoff value can be challenging. When compared to the Fourier transform, the wavelet transform is a marked improvement. Since the Fourier transform is unable to fully express the time-frequency localization property of non-stationary signals, the wavelet transform is used instead. In addition to its strength as a general tool for waveform analysis, the Wavelet Transform excels at analyzing waveforms at the time-frequency level. As a result, it can quickly and accurately identify the signal's focal point, analyze its degree of distortion, and extract precise information from the time and frequency domains (Bakar et al., 2014; He et al., 2014). Fault detection in the fars power distribution system was given a boost in accuracy and efficiency thanks to wavelet transform's application in (Soualhi et al., 2015). When conducting signal analysis using a wavelet transform, extracting both approximation and detailed features is a crucial step. Find the best decomposition level, partition features as finely as feasible, and keep errors isolated from features. Both feature component extraction and fault detection accuracy suffer from the current approaches' reliance on either manually set threshold control or testing with retrieved trend *via* wavelet transform. With the neural network serving as a model for the neuron network in the human brain, the values of the input layer neurons are mapped to the values of the output layer neurons, establishing an implicit function relationship between the input and the output. An asymmetrical fault line searching and locating scheme is developed using the fault direction distinguishing method and its associated communication system. A more up-to-date method for locating faults in a distribution network that includes DG units is the multi-layer perceptron neural network (MLPNN) (Jiang et al., 2003; Gafoor et al., 2014). As a result of the MLPNN's structure and training algorithm, however, its speed is not ideal for applications requiring rapid and precise fault finding (Kordestani et al., 2016; Bayrak, 2018). Non-linear, prior-data-driven processing is employed by the network. Compared to traditional methods of diagnosis, it gives room for more imaginative data manipulation. In contrast, the neural network can learn quickly and tolerates errors better during diagnosis. However, it is not without its flaws. When it comes to power system failure diagnosis, gathering enough data to train a neural network is difficult. It was easy for the neural network to get mired in a cycle of local minima. This study suggests a fault detection system based on wavelet transform and the chaotic neural network as a solution to these problems. The chaotic neural network avoids the drawback of getting stuck at the local optimum. It also has excellent error-handling and associative memory features. With the advent of the internet of things and the cloud-edge-collaboration framework, the authors of (Tonelli-Neto et al., 2017) introduce a DWT and NNRBF for detecting HIF by fusing together information from different distribution networks. To identify HIF in an IEEE 13-bus distribution network, the authors (Rezaei and Haghifam, 2008) opted on a fault-based strategy.

The following outlines the primary inspiration and contribution of this work.

- Electrical Distribution to Rural Areas: Using RESs with energy storage makes it economically feasible to bring electricity to rural areas. Solar PV array, wind turbine, and battery all work together to minimize maintenance costs and maximize clean energy production. When the sun, the wind, the batteries, and

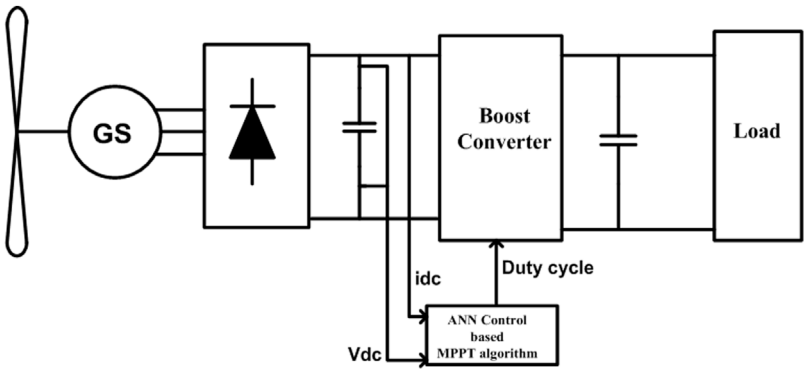

FIGURE 4
WECS configuration (Vas, 1999).

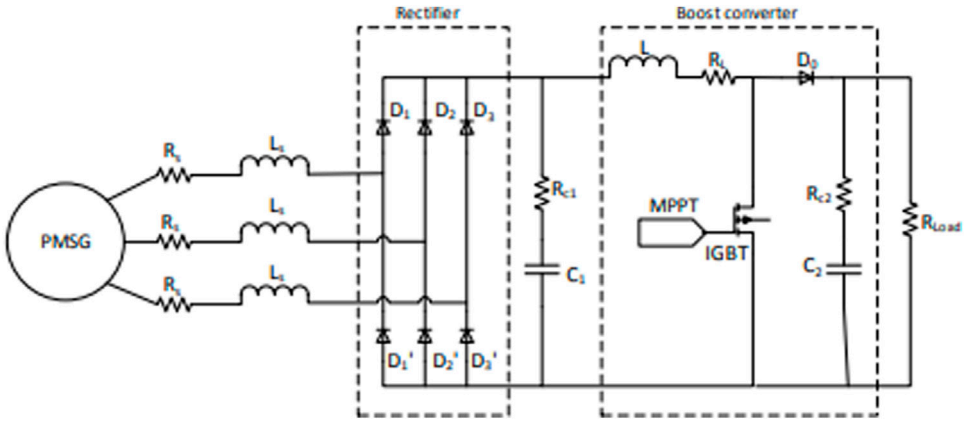

FIGURE 5
Electrical circuit schematic that depicts the PMSG, rectifier, and boost converter (Mishra and Panigrahi, 2019).

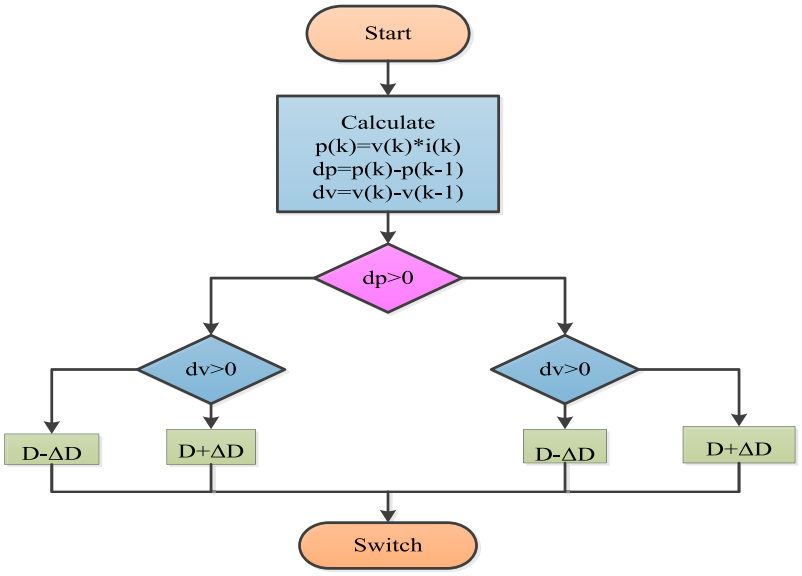

FIGURE 6
MPPT P&O flowchart.

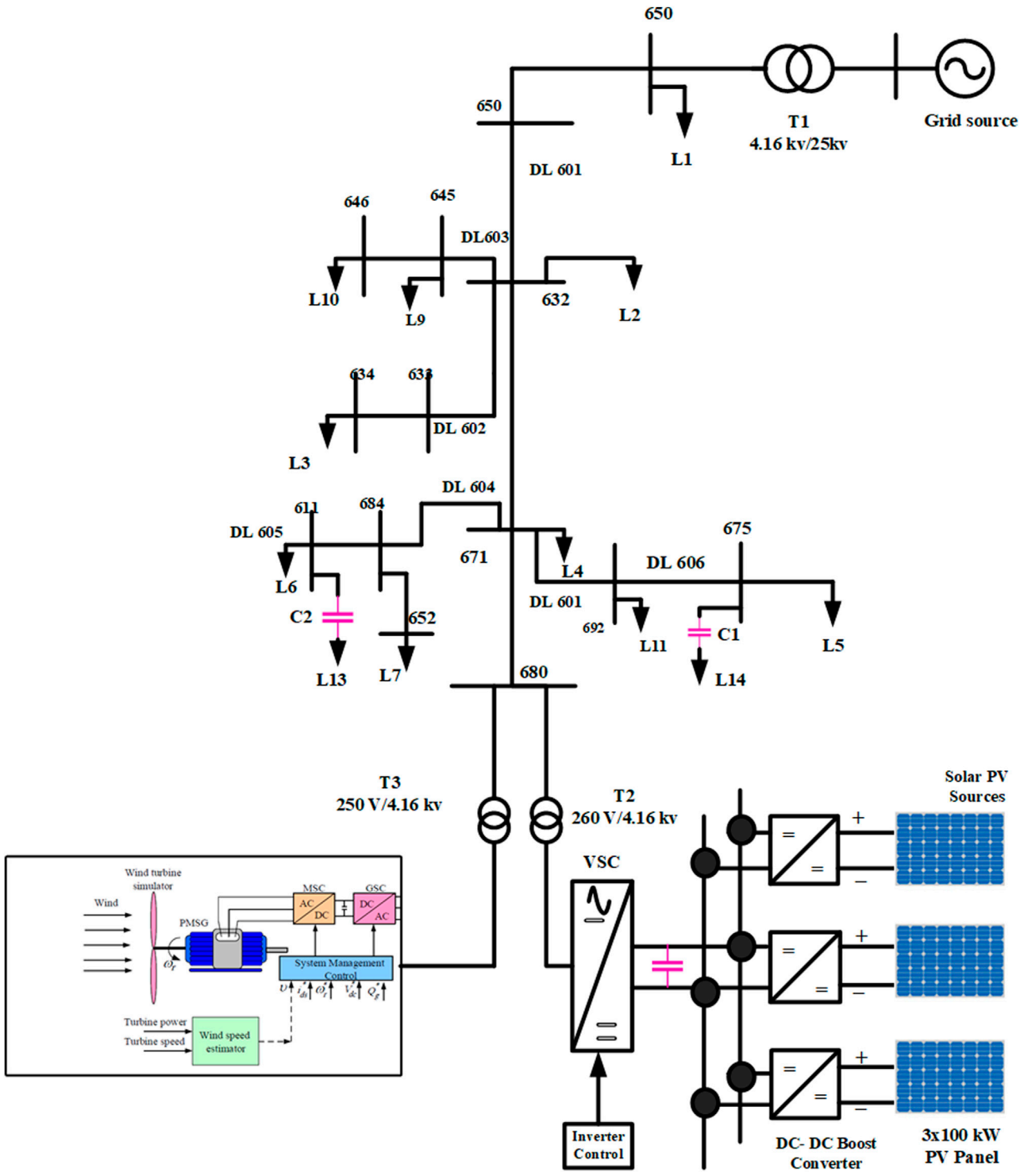

FIGURE 7
IEEE-13 Bus system with the solar PV system & WECS (Mishra and Yadav, 2019).

the load all align, the adopted control will carry out the specified action.

- One MG based on VSI control is created. In addition, a diode rectifier is used to change the AC current produced by PMBLDCG's wind turbines into DC current. Therefore, the overall system cost has decreased thanks to this topology.
- The PMBLDCG saves money by not requiring expensive sensors for MPPT control (like speed/position/wind speed sensors). As the MPP and power converter control become independent, the large operating range and control dependability of a second stage solar design are worth the additional components.

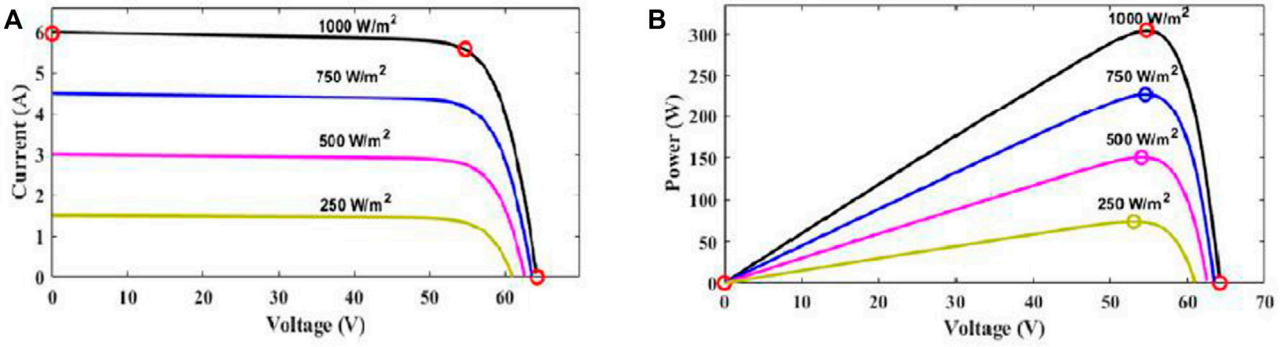

FIGURE 8
(A) Characteristics of the current-voltage curve of a PV array, **(B)** power-voltage characteristics of PV array.

- Renewable energy source used are maintenance free and having high efficiency.
- A neural network called NNRBF is proposed as the basis for an algorithm to select fault phases. An NNRBF neural network is trained on fault features extracted using wavelets, and its output is correlated with inputs to determine the fault type. When it comes to fault and transition resistance, the algorithm is stable.
- There is a proposal for a wavelet-transform-based fault detection algorithm with two terminals. The db4 wavelet is used to detect the travelling wave head to diagnose the issue. This algorithm's fault-detection accuracy is excellent, and it is robust against variations in fault type and transition resistance.

2 Solar PV energy: A brief description

Non-linearity in the I-V curve is a feature of PV cells, and it changes as the cells are exposed to more or less sunlight and are heated or cooled. An ideal solar cell is a circuit that includes a diode and a parallel current source. Yet, we model the losses caused by these cells using the series resistance (Rse) and the parallel resistance (Rsh). This is why the PV cell's orbital model under real-world conditions is shown in Figure 2. RSH has a much higher market value than RS does. Similarly, the Iph source current is zero in total darkness (Zayandehroodi et al., 2010a; Zayandehroodi et al., 2010b).

2.1 The PV module

In a cell, losses are proportional to the resistance in the corresponding circuit. Losses in a cell occur due to multiple processes, including the reflection of incident light at the cell surface, the absorption of photons without electrons and free holes, and the redistribution of electrons and voids. The following equation expresses the solar cell's distinctive behavior as shown in Figure 2 (Chatrenour et al., 2017).

$$I_{pv} = I_{ph} - I_D - I_{SH} \tag{1}$$

Where current PV (Ipv), diode current (ID), and diode voltage (Vd). $I_{SH} = V_{pv} + I_{pv}$, where Ipv is the output current, Vpv is the input voltage, RS and RSH are the solar cell's corresponding series and parallel resistance, and RS/RSH is the leakage current. Shockley diodes have a voltage-current characteristic, and that characteristic can be written as a formula for the diode current, ID.

$$I_D = I_O\left(e^{\frac{v_D}{aV_t}} - 1\right) \tag{2}$$

Here, *Io* is the reverse saturation current; *V*D = *V*pv + *I*pv*RS* is the diode voltage; *a* is the diode ideal constant;

$V_t = \frac{N_s \cdot k_b}{e} T$ T is the operating temperature of the solar cell; Ns is the number of series cells; kb is the Boltzmann constant; e is the electron charge; and T is the diode's thermal voltage. Adding Eq. 2 to the first equation yields the solar panel's defining equation, which is as follows:

$$I_{PV} = I_{ph} - I_o\left(e\frac{V_{PV} + I_{PV}R_S}{aV_t} - 1\right) - \frac{V_{PV} + I_{PV}R_S}{R_{SH}} \tag{3}$$

The value of the photovoltaic current Ipv is related to the variations in light intensity and temperature as shown in Eq. 3.

2.2 DC to DC boost converter configuration

In order to maintain a constant load voltage between the PV array and inverter, a DC-DC boost converter is employed (Necaibia et al., 2017). As the voltage produced by PV systems is typically insufficient to power loads directly, this is an essential component of PV applications. In this study, a novel ANN control based MPPT approach was implemented to maximize power output from a DC-DC boost converter before feeding it into the input of an RS MLI. By calculating the duty cycle for the converter switch and running at a high switching frequency, Maximum Power Point Tracking (MPPT) is a technique for getting the most power out of PV panels. If the converter is in continuous conduction mode, the current through the inductor is

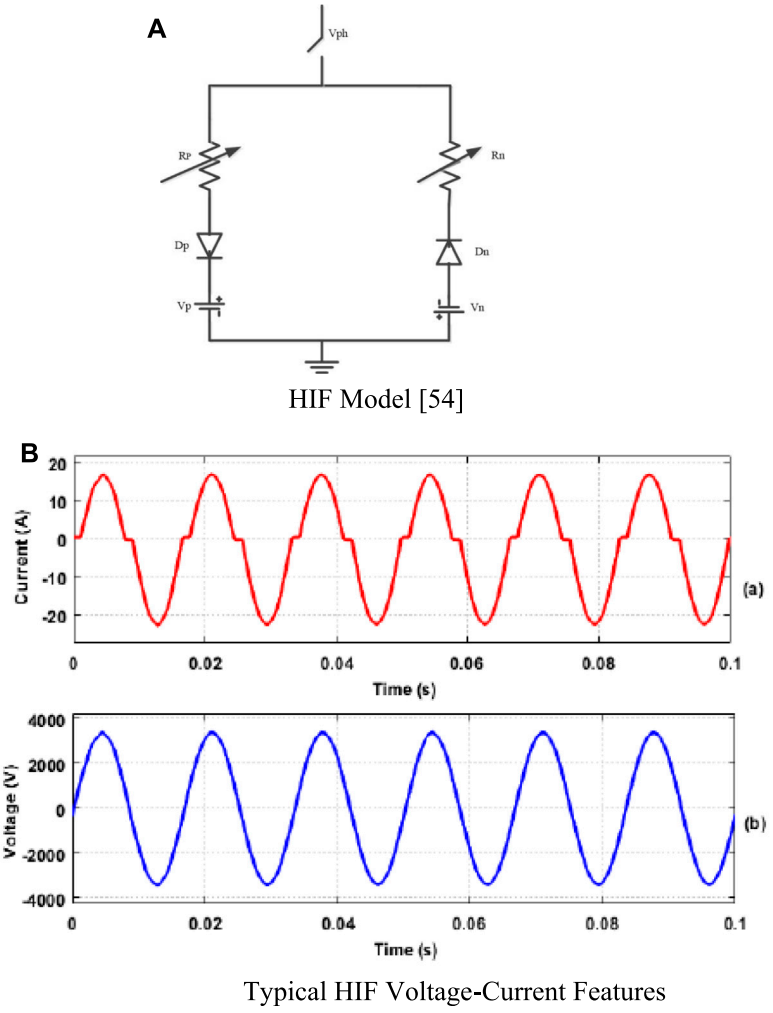

FIGURE 9
(A) HIF model (James et al., 2017) **(B)** Typical HIF voltage-current features.

always present (Abdullah et al., 2012). We provide duty cycle, inductor (L), and capacitor (C) formulas below.

$$\frac{V_{out}}{V_{in}} = \frac{1}{1-D} \tag{4}$$

$$inductor\,(L) = \frac{V_{in} \times D \times T}{\Delta_{iL}} \tag{5}$$

$$Capacitor\ (C) = \frac{V_{out} \times D}{R \times \Delta V_{out} \times f} \tag{6}$$

Vin and V0 are the boost converter's input and output voltages; D is the duty cycle. D > 1 means output voltage > input voltage. Figure 3 depicts a DC-DC boost converter with PV integration and the ANN control based MPPT approach for maximizing PV duty cycle.

When a boost converter is used in conjunction with a PV array, it is discovered that the average current from the PV array increases as the duty cycle rises, resulting in a decrease in the voltage from the PV array as a whole. In order to raise the PV array's break-even point, D modifies its V-I characteristic. When D is decreased, the average current from a PV array drops while the voltage is raised. If the PV array's operating point moves to the right, it means the array's output has been modified. In order to keep the DC voltage output at the VSC terminal constant, the DC-DC converter's value of D is automatically adjusted using the perturb and absorb MPPT approach.

In (Yahya and Yahya, 2023), DC-DC boost converter technology to track the maximum power of a photovoltaic (PV) system using a maximum power point tracking (MPPT) controller based on a modified version of particle swarm optimization (MPSO). A DC-DC boost converter was utilized to increase the input DC voltage of the PV module. The boost converter supplied power for the DC-AC multilevel PWM inverter, which supplied the output AC voltage to a single inductive load. It is common practise to employ cascaded multilayer inverters to condition power in renewable energy applications due to its simplicity and low cost. Modulations in the DC link capacitor voltage result in low order harmonics and inter harmonics at the output of the multilevel inverter. The lowest number of harmonics is achieved using phase disposition pulse width modulation (PDPWM). Energy from the inverter cells.

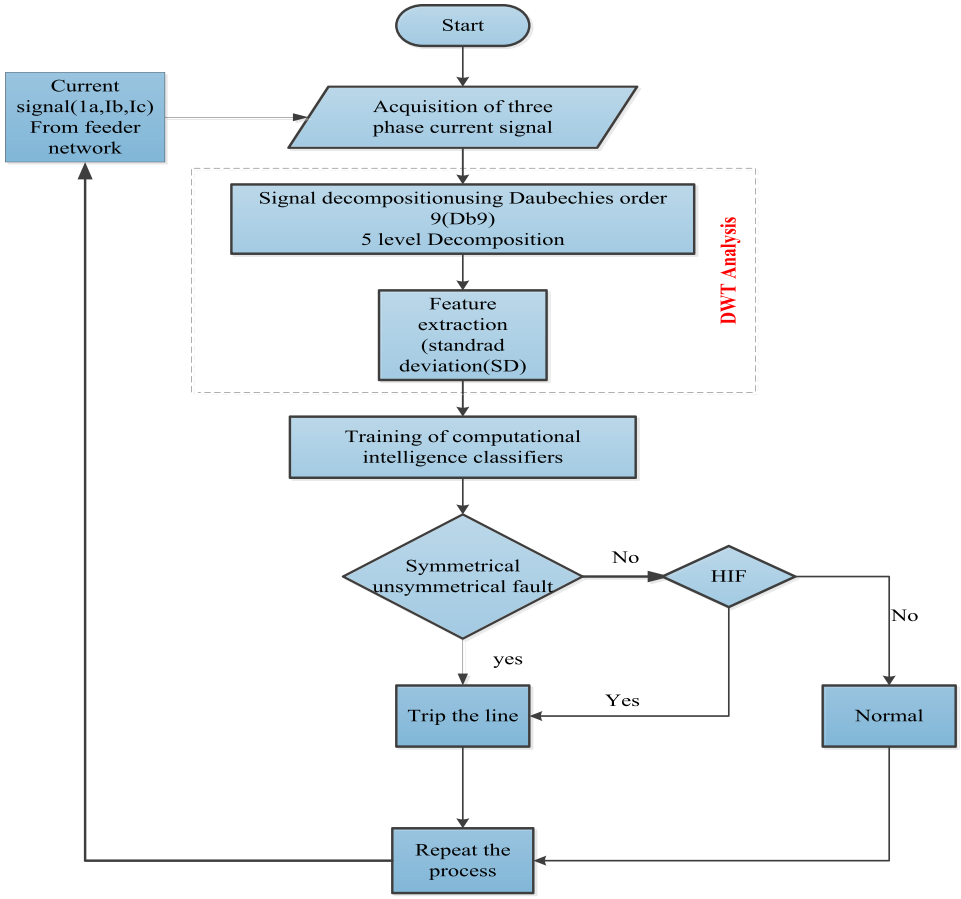

FIGURE 10
Schematic representation of the fault tolerant classification.

2.3 Description of wind source

Solar and wind power dominate the renewable energy market due to their low environmental impact and high irradiation and kinetic energy output, respectively. Figure 4 depicted wind energy conversion system (WECS), purpose of WECS is to exploit the kinetic energy of wind for use in mechanical power generation. Low efficiency, non-linearity and unpredictability in wind speed, and high construction cost are all factors that prevent widespread adoption of wind energy (Manwell et al., 2010). Therefore, a control algorithm is necessary to optimize performance and cut expenses. Using a wind turbine, one can convert wind energy into electricity DWT. DWT are made up of blades and a motorized device. An AC-DC and DC-DC converter are required on the control side. In this study, a horizontal wind turbine with variable speed was used. Since variable speed turbines can generate electricity at varying wind speeds, they have a higher efficiency rating than fixed speed turbines (Nurzaman et al., 2017). In this study, a permanent-magnet synchronous generator is used (PMSG). PMSG's high efficiency at low speeds has made it a popular choice for use in small-scale wind turbines. On the control side, an ANN control based MPPT algorithm locates and maintains the turbine's maximum power point, maximizing its efficiency. Here, we present a DC-DC boost converter that is managed by a ANN control based MPPT algorithm and integrated into a wind power generation setup. In this paper, we'll go over the results of a simulation test of ANN control based MPPT controllers for a residential wind turbine run through the Simulink MATLAB modelling environment.

Wind turbines' peak mechanical power, stated as (Abdullah et al., 2011)

$$P_{max} = \frac{1}{2}\rho C_p A V_w^3 \tag{7}$$

Where ρ is the density of the air (in kg/m3), A is the swept area of the rotor blades (in m2), and Vw is the speed of the wind (in metres per second). Cp is the power coefficient, is written as (Gite and Pawar, 2017).

$$c_p = c_1\left(\frac{C_2}{\lambda_i} - C_3\beta - C_4\right)e_5^{\frac{-C}{\lambda_i}} + C_6\lambda \tag{8}$$

$$\frac{1}{\lambda_i} = \frac{1}{\lambda + 0.08\beta} - \frac{0.035}{\beta^3 + 1} \tag{9}$$

$$\lambda = \omega_m{}^{*}\frac{R}{V_w} \tag{10}$$

C1 to C6 are rotor-specific. In this paper, C1 = 20, C2 = 140, C3 = 0.4, C4 = 28, C5 = 21, and C6 = 0.068.

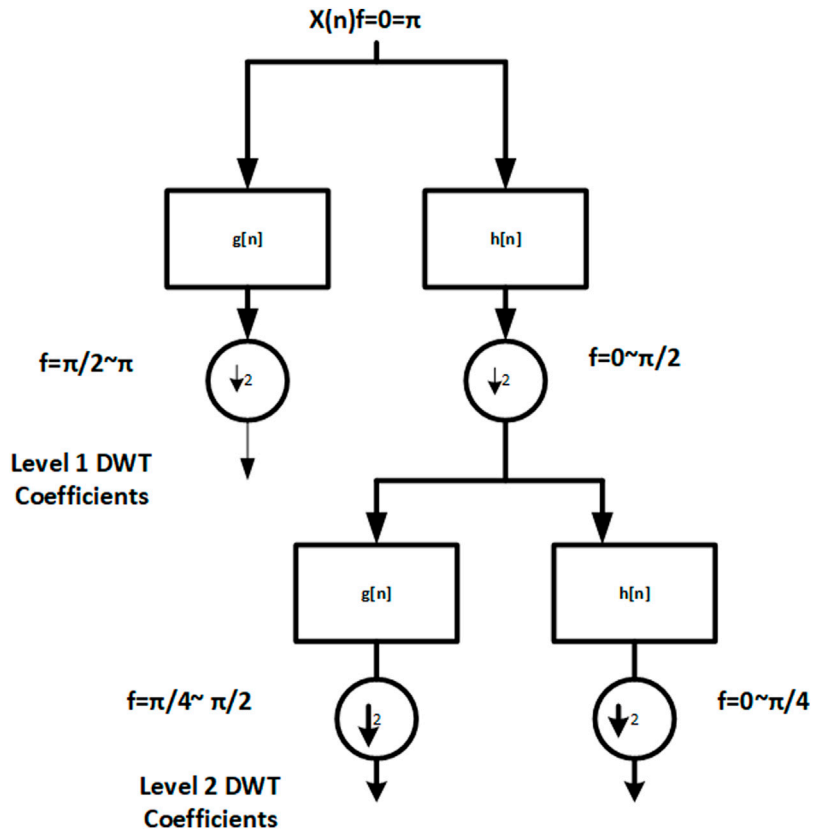

FIGURE 11
DWT decomposition of signal (Daubecheis, 1992).

2.4 Combined boost converter, rectifier, and PMSG in series

Figure 5 is an electrical circuit schematic that depicts the PMSG, rectifier, and boost converter all in one convenient location. This model's goal is to find the relationship between DC grid load current and turbine.

The current in dq reference frame represented as

$$\frac{d}{dt}\begin{bmatrix} i_{sd} \\ i_{sq} \end{bmatrix} = -\begin{bmatrix} \frac{R_s}{L_{sd}} & -\frac{L_{sd}}{L_{sq}}\omega_e \\ \frac{L_{sd}}{L_{sq}}\omega_e & \frac{R_s}{L_{sq}} \end{bmatrix}\begin{bmatrix} i_{sd} \\ i_{sq} \end{bmatrix} + \begin{bmatrix} \frac{1}{L_{sd}} & 0 \\ 0 & \frac{1}{L_{sq}} \end{bmatrix}\begin{bmatrix} v_{sd} \\ v_{sq} \end{bmatrix} \quad (11)$$

Thus, the expression for the mechanical equivalent torque of an electromagnetic force and the mechanical torque of a machine can be written as

$$Te = N\left\{\Psi_f + \left(L_{sd} - L_{sq}\right)i_{sd}\right\}i_{sq} \quad (12)$$

$$Tm = \frac{P}{\omega_m} = \frac{1}{2}\rho\pi R^2 C_P \frac{V_w^3}{\omega_m} \quad (13)$$

Hence the rotor speed can be calculated

$$\frac{d_\omega}{d_t} = \frac{Te - Tm - B\omega_m}{j_t + j_p} \quad (14)$$

2.5 MPPT

A MPPT algorithm known as P&O is utilized to improve performance is shown in Figure 6. The turbine will be operating at its maximum possible efficiency with the help of MPPT. P&O algorithms function by modifying a control parameter and observing the resulting change in output (Kavaskar and Mohanty, 2019). This algorithm is simple, effective, and does not call for any additional hardware or sensors.

$$\Delta P = P(k) - P(k-1) \quad (15)$$

Delta D rises when P is positive and Vs. is negative. If P and the voltage change are positive, delta D will fall. Delta D decreases for a positive voltage change and negative P. If both P and the voltage change are negative, then delta D is too (Alsafasfeh et al., 2012).

3 Systematic illustration of the IEEE-13 bus

The proposed NNRBF classification performance was measured using an IEEE 13-bus network model with high impedance fault, symmetrical and unsymmetrical faults, switching events (heavy load and capacitor bank), and transformer current. The MATLAB/Simulink software environment was used to design the system,

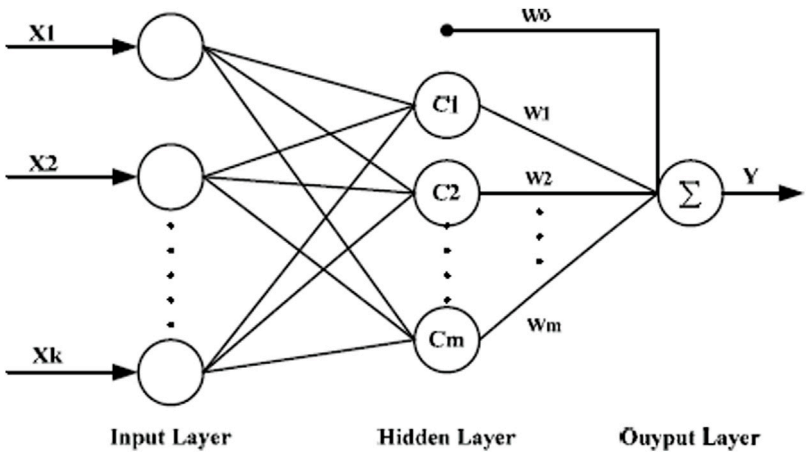

FIGURE 12
A generic architecture of the NNRBF.

which includes a 300 kW solar PV unit (operating under STC) and several load facilities. In this study, an IEEE 13-bus network model was used to evaluate DWT and NNRBF classifiers under high-impedance, symmetrical, and asymmetrical failure conditions. MATLAB/Simulink was used to generate the IEEE 13 bus network model in Figure 7. The test system is connected to the grid with a 200 kVA, 4.16 kV/25 kV transformer (100 MVA, 25 kV, 50 Hz). For the purpose of validating the proposed RNN based classifier's ability to recognize HIF, it was subjected to a battery of tests across a wide range of operating conditions, including normal operation, switching events (capacitor bank and heavy load), transformer inrush current, and abnormal operation (symmetrical and unsymmetrical faults: single line ground, double line, double line to ground, and three-phase fault). The 300 kWp of solar PV comes from three 100 kW PV modules. Each solar cell in the PV array and its specific configuration are described. (Samet et al., 2017). Provides details on modelling transmission line parameters and load. Both normal and unusual circumstances were used to test the classifier's capacity to identify HIF (symmetrical and unsymmetrical faults: single line ground, double line, double line to ground and three-phase fault).

3.1 The characteristics curve of the PV module

Both the input voltage and output current of the PV array play a role in the I-V and P-V curves that define the PV module. Insulation-voltage and potential-voltage plots. This graphic depicts as MPP at a given temperature and radiation level (where 25°C is assumed for the temperature and 100 W/m2 is assumed for the radiation level). This is the sweet spot for maximizing both power output and efficiency from a PV module. In this case, the MPP is the general maximum, which is another name for the MPP.

Solar cell current (a) and power output (voltage) (b) are shown as a function of solar irradiance (W/m2) in Figure 8. The two most important parts of a PV system are the DC-DC boost converter and the DC-AC VSI. As a result of the boost converter, the 280 V DC maximum power point of the PV unit is increased to 480 V (to 500 V). To achieve maximum power tracking, the MPPT controller's incremental conductance approach was used to vary the DC-DC boost converter's duty cycle in response to changes in solar irradiance. We analyzed a three-level IGBT bridge circuit for a PV inverter (VSI) using pulse width modulation (switching frequency of 1980 Hz). The inverter uses synchronous reference frame theory and two-control to regulate the AC voltage at the output. The inverter's 260 V AC output is increased to 4.16 kV so that it can be connected to the IEEE-13 bus power system network.

4 High impedance fault model

Based on the Emanuel model (Gomes et al., 2018), (James et al., 2017) and illustrated in Figure 9, an anti-parallel diode model is used to simulate the waveform features of the HIF current. The ideal HIF V-I characteristics are achieved by adjusting the HIF model parameters V_p, V_n, R_p, and Rn from 550 to 7500 V, 1,100–9000 V, 110 to 4,000, and 120 to 4,000, respectively. HIF's current and voltage waveforms when sampling at 600V, 1100V, and 120R are depicted in Figure 9A and Figure 9B, respectively. Current waveform is found to be non-linear, asymmetrical, and contain harmonics when HIF model is taken into account. In addition, FFT examination revealed that there was a 3.94% and 11.7% content of second- and third-order harmonics, respectively.

4.1 Methodology proposed for the detection of HIF

Using a Figure 10 diagram of the MV distribution power system's solar PV and wind integrated power network, this part discusses the identification of HIF using intelligent classifiers following the below 4steps.

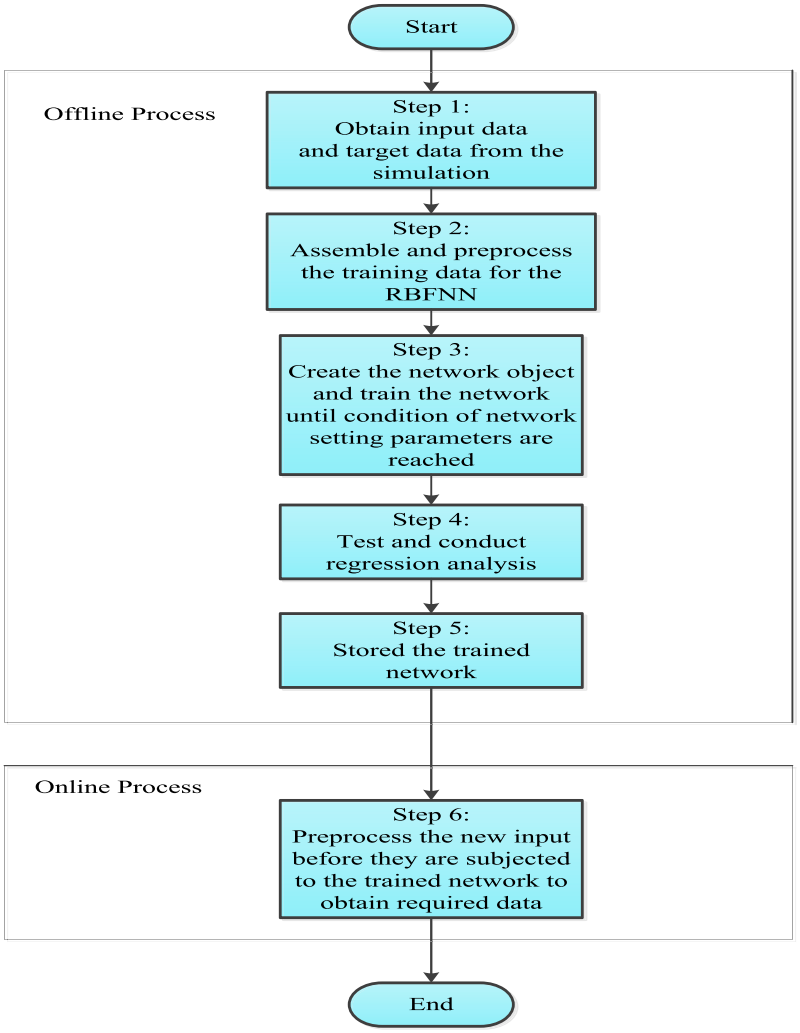

FIGURE 13
Implementation procedures in the training of the NNRBF.

- Create disturbances in MATLAB/Simulink to obtain faulty existing data.
- To train the classifiers, we have taken samples of the current indicative of a fault using the mother wavelet daubechies4 and then use those samples' standard deviation (SD) values as the features.
- Data gathered from the discrete wavelet transform (DDWT) during various power system disturbances was used to train artificial intelligence-based classifiers.
- To ensure the classifiers can distinguish the HIF from other power system disturbances including three-phase faults, line-to-ground faults, line-to-line faults, and double line-to-ground faults, they are put through their paces with a variety of test cases. In order to ensure the system's continued security and dependability, this procedure is repeated during each cycle of operation. Furthermore, as the protective relay is insensitive to fluctuations, the system continued to function normally when the irradiance of the solar and the speed of the wind both fluctuated without triggering any abnormalities.

4.2 The DWT analysis for data collection

The DWT is a powerful method for separating a transient signal into its constituent parts, which it then displays in the domain of time-frequency instead of the conventional time domain (Elkalashy et al., 2008). The basic concept is to analyze the signal by expanding and contracting it. A continuous signal f (t) is defined in both CDWT and DWT, with the definition provided by Eq. 16.

$$CWT(a,b) = \left[\frac{1}{\sqrt{a}}\int_{-\infty}^{\infty} f(t)^{*}h\left(t-\frac{b}{a}\right)d_t\right] \tag{16}$$

The mother wavelet is the initial point from which a wavelet feature is formed. CDWT is an alternate method for avoiding the same resolution issue that plagues STFT. In contrast to the DWT technique, however, this one has low redundancy during signal reconstruction. The DWT is an effective data technique for signal analysis because it permits the signal to be sampled with distinct peaks. For decades, this sophisticated and powerful instrument has

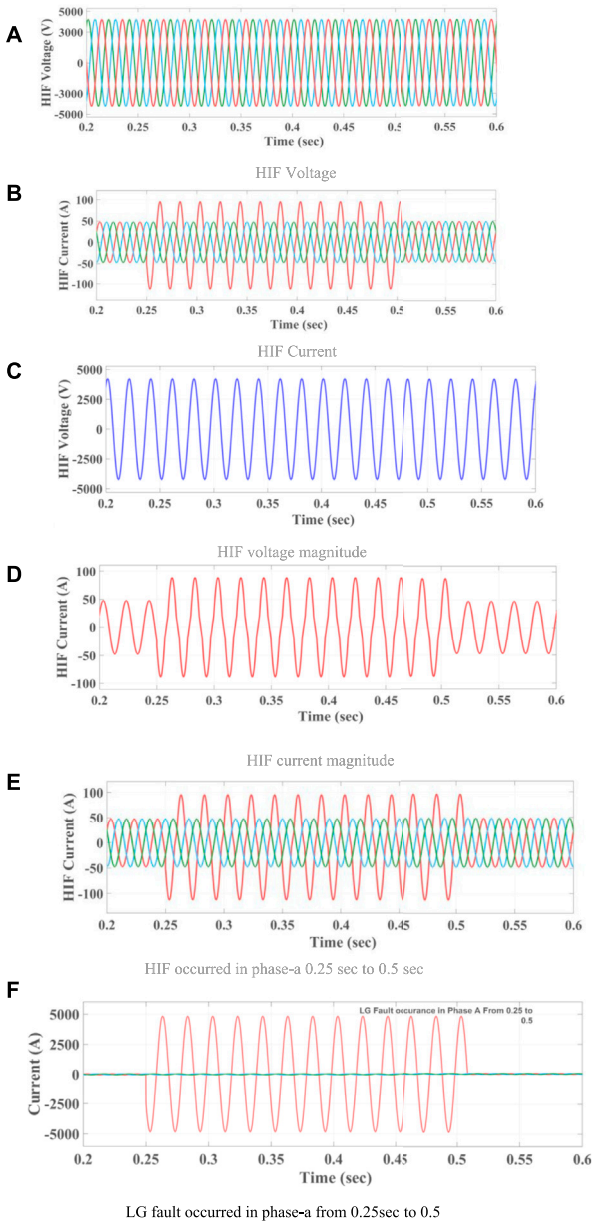

FIGURE 14
The three-phase current waveform observed for the period of 0.25–0.5 s in case of HIF fault and single line to ground (LG). **(A)** HIF Voltage **(B)** HIF Current **(C)** HIF voltage magnitude **(D)** HIF current magnitude **(E)** HIF occurred in phase-a 0.25 sec to 0.5 sec **(F)** LG fault occurred in phase-a from 0.25 sec to 0.5.

been employed to regulate the safety switches. There are other ways to compute time and frequency information, such as with a fast Fourier transform (FFT), a short-time Fourier transform (STFT), or a continuous- (CDWT), but DWT has been utilized because of its quick computing speed and precision (Chen et al., 2016). Since this is the case, we can express DWT as Eq. 17.

$$DWT(m,k) = \left[\frac{1}{\sqrt{a_0^m}} \sum_n f(n)^* h\left(\frac{k - na_0^m}{a_0^m}\right)\right] \quad (17)$$

Algorithm

Below (Chen et al., 2016) we display the various decomposition levels of the signal X(n). Here are the procedures for signal decomposition:

First, through a denoising process, the original X(n) is decomposed into a series of levels.

Choosing a subset of levels from which to reconstruct the signal is the second stage.

Third, re-create the signal using the values you've chosen.

In Step 4, you'll choose the sampling rate, window size, decomposition levels, and mother wavelet.

Where n and m are integers, h is the wavelet function, a_0^m and na_0^m are sizing and interpretation constants, respectively. By using DWT, one can separate a signal into its low-frequency g(n) and high-frequency h(n) approximation and detailed coefficients, respectively as shown in Figure 11. This process of successive approximation is repeated until the signal has been decomposed into a large number of low-resolution sub-signals. In comparison to the Haar wavelet, the Daubechies 4 (db4) is a more effective frequency extractor, it was chosen as the mother wavelet for fault detection in this work. And unlike Coiflet and Meyer wavelets, it reduces signal redundancy and satisfies Parsevall's theorem (Daubecheis, 1992). The condition shown in Eq. 18 represents the optimal decomposition of L-levels

$$N = 2^L \quad (18)$$

Where N is the level, and L is the length.

$$B = \frac{F}{2^{L+1}} \quad (19)$$

From Eqs. 19, B is the level-to-level bandwidth in hertz, and F is the sample rate in hertz. In order to divide the signal into its component parts, a sampling rate of 20 kHz is being considered, with each phase of the current signal receiving 800 samples over a length of 5,000 points. Using Eq. 18, we can determine the different band frequencies that were captured at each level, and they are as follows: Approximation is made using the detailed coefficient d4, which represents frequencies from 5 to 2.5 kHz, 2.5 to 1.25 kHz, 1.25 to 0.625 kHz, and 0.625 to 0.3125 kHz, respectively. In the proposed study, the mother wavelet of db4 is used with detailed coefficients on 5 levels for varied fault current signals captured throughout each cycle.

4.3 The effectiveness of NNRBF for fault detection in a DG-enabled distribution network

NNRBFs are trained with data sets generated from short circuit simulations at all line sections accounting for four different types of failures, and then applied to the problem of fault detection in a simulated DG-based distribution system. By analyzing the three-phase currents coming from the main source at the feeding substation, it is possible to identify a single-phase-to-ground fault, a phase-to-phase fault, a two-phase-to-ground fault, or a three-phase fault. In order to standardize the fault currents in the three-phase output at the main source or feeder substation, the maximum fault currents for each fault type are calculated. This equation is used to standardize currents (Yu et al., 2008):

TABLE 1 Ground resistance 20 Ω detection at 5th bus.

S.No	Types of fault	Max. Coefficient of phase A current	Max coefficient of phase B current	Max coefficient of phase C current	Max coefficient of ground current	NNRBF output for phase A	NNRBF output for phase B	NNRBF output for phase C	NNRBF output for ground current
1	ABC-G	4.6350	29.6395	4.6556	15.6281	1.0000	1.0000	1.0000	1.0000
2	ABC	4.6328	29.6454	4.6534	0.1136	1.0000	1.0000	1.0000	−0.000
3	AB-G	4.1035	30.2836	0.2000	16.5877	1.0000	1.0000	−0.000	1.0000
4	BC-G	0.1914	30.2978	4.1178	16.9470	−0.000	1.0000	1.0000	1.0000
5	AC-G	5.6985	0.3533	5.7190	11.9947	1.0000	−0.000	1.0000	1.0000
6	A-G	5.1419	0.1690	0.1835	5.5964	1.0000	−0.000	−0.000	1.0000
7	B-G	0.3738	30.8997	0.3867	32.5315	−0.000	1.0000	−0.000	1.0000
8	C-G	0.1527	0.1699	5.1566	5.5770	−0.000	−0.000	1.0000	1.0000
9	AB	6.9556	22.3087	0.0324	0.0087	1.0000	1.0000	−0.000	−0.000
10	BC	0.0254	22.1506	6.9803	0.0204	−0.000	1.0000	1.0000	−0.000
11	AC	6.9596	0.8563	6.9853	0.0100	1.0000	−0.000	1.0000	−0.000
12	No fault	0.0254	0.0236	0.0324	1.3901e-32	−0.000	−0.000	−0.000	−0.000

$$I_{normal} = \frac{I}{I_{\max}} \tag{20}$$

The maximum fault current, or Imax, is the product of the fault current and the fault type, and it varies depending on the nature of the defect. The normalized three-phase fault currents are used to classify various fault types. With k input neurons and m hidden neurons, the NNRBF is a three-layer feed-forward neural network. The input layer feeds data into the hidden layer, while the hidden layer is made up of neurons with radial basis activation functions. In Figure 12 we see a typical NNRBF, and in Figure 12 we see an NNRBF used for training.

There are several calculations taken into account during NNRBF training. Input k-dimensional vector X is used to calculate a scalar value by the network, which is then output.

$$Y = f(X) = w_0 + \sum_{i=1}^{m} w_i \phi(D_i) \tag{21}$$

Where (Di) is the RBF and (w0) is the bias, (wi) is the weight parameter, (m) is the number of hidden-layer nodes, and (m) is the bias.

The Gaussian function is used as the RBF in this investigation, and it is given by.

$$\varnothing(D_i) \exp\left(\frac{-D_i^2}{\sigma^2}\right) \tag{22}$$

$$D_i = \sqrt{\sum_{j=1}^{k} \left(X_j - C_{ji}\right)^2} \tag{23}$$

Di is the distance between the input vector X and each data centre, where is the radius of the cluster represented by the centre node. Di, the distance between two points, is typically calculated using the Euclidean norm and is presented as a cypher layer in (Yu et al., 2008). Figure 13 depicts the training procedures for the RBFNN and how they are implemented.

The RBFNNs were implemented in the MATLAB software for the fault detection technique, and training data was generated in the Dig SILENT Power Factory 14.0.523 software by simulating various faults created at the 5th BUS of each line. We can extract the fault distance from each source and the number of defective lines from the RBFNNs' target vector by running simulations. Here, we break down the inputs and outputs of the training data that was used to hone the generated RBFNNs.

4.3.1 A. First RBFNN

Nine neurons are used as input, and these are the short circuit currents in each source's three phases (5th BUS). Three neurons are used as output, and these are the fault detection in the main source and two DG units (DS).

4.3.2 Second RBFNN

In this case, there are three input neurons representing the distances to the three potential sources of the fault, and one output neuron representing the actual number of faulty wires. There are about 138 training and testing data sets available, with 80% used for training the RBFNNs and the remaining 20% used for testing their efficacy. Mean square error (MSE) is used in neural networks as a measure of performance. The maximum epoch for training any of the RBFNNs is set to 100, and the mean square error is kept below 0.0002. The trained RBFNNs are then put through their paces after fault classification.

5 Results and discussions

Data is gathered for analysis and classifier training/testing after faults are applied to a number of buses across the 13-bus system. When doing this research, we used eighty percent of the data for training our classifiers and twenty percent for testing. Initial network simulations were performed in MATLAB/Simulink, yielding results for steady-state,

TABLE 2 Ground resistance 10 Ω location at 5th bus.

S.No	Types of fault	Max. Coefficient of phase A current	Max coefficient of phase B current	Max coefficient of phase C current	Max coefficient of ground current	NNRBF output for phase A	NNRBF output for phase B	NNRBF output for phase C	NNRBF output for ground current
1	ABC-G	7.1967	50.2064	7.2319	8.1605	1.0000	1.0000	1.0000	1.0000
2	ABC	7.7044	29.1686	5.0160	3.8938	1.0000	1.0000	1.0000	−0.0000
3	AB-G	5.8851	51.9080	0.3487	29.3847	1.0000	1.0000	−0.000	1.0000
4	BC-G	0.3433	51.9446	5.9073	30.0053	−0.000	1.0000	1.0000	1.0000
5	AC-G	9.8223	0.6148	9.8575	20.7549	1.0000	−0.000	1.0000	1.0000
6	A-G	8.3985	0.2833	0.2978	9.1754	1.0000	−0.000	−0.000	1.0000
7	B-G	0.6513	53.4671	0.6642	56.3076	−0.000	1.0000	−0.000	1.0000
8	C-G	0.2659	0.2801	8.4224	9.1621	−0.000	−0.000	1.0000	1.0000
9	AB	10.8054	37.7852	0.0324	0.0987	1.0000	1.0000	−0.000	−0.0000
10	BC	0.0254	37.5244	10.8374	0.0504	−0.000	1.0000	1.0000	−0.0000
11	AC	10.8034	0.9405	10.8324	0.0700	1.0000	−0.000	1.0000	−0.0000
12	No fault	0.0254	0.0236	0.0324	$4.6118e^{-32}$	−0.000	−0.000	−0.000	−0.0000

TABLE 3 Comparison on various methods.

References	Classification method	Type of fault considered							% accuracy
		LG	LL	LLG	LLG	LLLG	HIF	Fault resistance R_f Ω)	
Alsafasfeh et al. (2012)	Principal component analysis	√	√	√	√	X	X	5–100	94.54
Mishra and Yadav (2019)	DFT + fuzzy (series compensated line	√	√	√	√	√	X	0.001–100	99.678
Samet et al. (2017)	Improved alienation coefficients method	√	√	√	√	√	X	0–70	92.88
Tonelli-Neto et al. (2017)	WT + fuzzy-ARTMAP	X	X	X	X	X	√	X	97.69
Santos et al. (2017)	Energy spectrum of DWT (Considering DG placement)	X	X	X	X	X	√	X	70
Gomes et al. (2018)	DWT + boosted decision tree	X	X	X	X	X	√	X	98.06
Kavi et al. (2018)	Morphological fault detector algorithm	X	X	X	X	X	√	X	100
AsghariGovar et al. (2018)	Adaptive CWT and extreme learning machine (considering CT saturation)	X	X	X	X	X	√	X	100
Proposed method (DWT + NNRBF)		—	—	—	—	—	—	(0–100)	100

transient and conventional faults (LG, LL, LLG, and LLLG incidence), as well as HIF. Maximum HIF occurs when the load current exceeds the fault current. During this instance, the HIF model observed a non-linear connection between voltage and current, which is seen in Figure 14.

5.1 Distinguish between normal fault and no fault conditions

Table 1 describes that comparison between coefficients of phase a, b, c currents and NNRBF output of phase a, b, c and ground resistance of 20 Ω at bus 5. Conventional fault types like LG, LL, LLG, and both LLLG and HIF occurrence are used here.

Table 2 describes that comparison between coefficients of phase a, b, c currents and NNRBF output of phase a, b, c and ground resistance of 10 Ω at bus 5. Conventional fault types like LG, LL, LLG, and both LLLG and HIF occurrence are used here. In no fault case ground current value is high at 20 Ω when compared to 10 Ω it means when resistance is high ground current value will be very low and *vice versa*.

5.2 HIF voltage and current waveforms

Here, we present the simulation results for the IEEE 13-bus power network that included both PV and Wind. We simulated the PV and Wind method we intend to use to detect and identify HIF in the MV distribution network. To test the viability of the strategy, we run a MATLAB/Simulink simulation of the distribution model shown in Figure 7. In Figure 14A, we can see the time-varying current signal during the typical feeder state, which lasts for 0.25s. The HIF analysis was run alongside simulations of various power system failures to prove the viability of the proposed method. The three-phase current waveform during this time period is shown in Figure 14B in the event of an HIF fault and a single line to ground (LG). As can be seen in Figures 14C, D, the magnitude of the fault current and voltage in the case of an HIF fault in phase C of a three-phase system are small. It is shown in Figures 14E, F that if an LG fails in phase A of a three-phase system, the amplitude of the current signal is quite large, making it challenging to detect HIF in power systems. To address these issues in real time, we extracted the features using a DWT analysis, which decomposes the signal across the temporal and frequency domains. Every cycle, DWT is applied to 800 samples of the phase current signal at four different levels of decomposition. There is a different spectrum of frequencies represented by each tier; Table 1 displays the calculated SD values for each of the detailed coefficient levels and the final decomposed level (d4) (d1, d2, d3, and d4). In this paper, we present a DWT analysis of the A, B, and C stages of the system under normal conditions. Table 2 summarizes the results of the DWT analysis performed on faults with different fault resistance, such as LL, LLG, and three-phase faults, and the SD characteristics derived from these faults that were used to train classifiers to identify HIF in the system. There were 13 buses in the system, and each one had a fault applied to it so that the DWT data could be collected and used to train and test the classifiers. In this research, we used eighty percent of the data for training our classifiers and twenty percent for testing. The current setup consists of three input neurons (representing the various potential root causes of the issue) and a single output neuron (the precise count of faulty lines). Mean square error (MSE) is a common metric used to evaluate the efficacy of neural networks. All RBFNNs are considered well-trained if their MSE is less than 0.0002 and they have undergone no more than 38 training epochs. After faults are categorized, RBFNNs are put through their paces. Initial network simulation and data collection were performed in MATLAB/Simulink, covering both steady-state and transient conditions as well as the occurrence of common faults like LG, LL, LLG, and LLLG, and even HIF. As shown in Figures 14A–F, the normal operation of the power grid results in an asymmetrical current waveform due to the distribution of electrical demand.

Table 3 describes the comparison on various classification methods and % accuracy 'X' represents the fault type/parameter which is not considered for classification, and '/' represents the occurrence of fault.

6 Conclusion

The detection of the HIF procedure is dependent on a number of factors, some of which are unique to the characteristics of a given network. This work considers a more practical PV-integrated IEEE 13-bus system to analyze HIF using the proposed RNN-based network. Initially, a MATLAB/Simulink model of a 13-bus distribution network was built to introduce different types of events (normal operation, inrush current from a transformer, load switching, and capacitor switching, and HIF, LG, LL, LLG, and LLLG, all of which represent malfunctions in the system). Under these conditions, DWT analysis was applied to the three-phase current signal using the db4 mother wavelet. Energy value features for different phases were extracted using the obtained wavelet coefficients (d1, d2, d3, d4, d5, and a5) to train and test classifiers.

Data availability statement

The original contributions presented in the study are included in the article/Supplementary Material, further inquiries can be directed to the corresponding author.

Author contributions

VG and BE have implemented the idea and converted it into a manuscript. This idea was proposed by BE for the article "Hybrid and Neural Network Radial Basis Function Algorithms for High-Impedance Fault Detection in a Distribution Network", and he also supervised the process. VG investigated and collected all data, wrote the draft, and converted it into an original research article.

Conflict of interest

The authors declare that the research was conducted in the absence of any commercial or financial relationships that could be construed as a potential conflict of interest.

Publisher's note

References

Abdullah, M. A., Yatim, A. H. M., and Tan, C. W. (2011). "A study of maximum power point tracking algorithms for wind energy system," in 2011 IEEE Conference on Clean Energy and Technology (CET) (IEEE), 321–326.

Abdullah, M. A., Yatim, A. H. M., Tan, C. W., and Saidur, R. (2012). A review of maximum power point tracking algorithms for wind energy systems. *Renew. Sustain. energy Rev.* 16 (5), 3220–3227. doi:10.1016/j.rser.2012.02.016

Ahmed, J., and Salam, Z. (2018). An enhanced adaptive P&O MPPT for fast and efficient tracking under varying environmental conditions. *IEEE Trans. Sustain. Energy* 9 (3), 1487–1496. doi:10.1109/tste.2018.2791968

Al-Masri, H. M., and Ehsani, M. (2015). Feasibility investigation of a hybrid on-grid wind photovoltaic retrofitting system. *IEEE Trans. Ind. Appl.* 52 (3), 1979–1988. doi:10.1109/TIA.2015.2513385

Alsafasfeh, Q., Abdel-Qader, I., and Harb, A. (2012). Fault classification and localization in power systems using fault signatures and principal components analysis. *Energy Power Eng.* 4 (6), 506–522. doi:10.4236/epe.2012.46064

Asghari Govar, S., Heidari, S., Seyedi, H., Ghasemzadeh, S., and Pourghasem, P. (2018). Adaptive CWT-based overcurrent protection for smart distribution grids considering CT saturation and highimpedance fault. *IET Gener. Transm. Distrib.* 12 (6), 1366–1373. doi:10.1049/iet-gtd.2017.0887

Bakar, A. H. A., Ali, M. S., Tan, C., Mokhlis, H., Arof, H., and Illias, H. A. (2014). High impedance fault location in 11 kV underground distribution systems using wavelet transforms. *Int. J. Electr. Power Energy Syst.* 55, 723–730. doi:10.1016/j.ijepes.2013.10.003

Bayrak, G. (2018). Wavelet transform-based fault detection method for hydrogen energy-based distributed generators. *Int. J. Hydro. Energy* 43 (44), 20293–20308. doi:10.1016/j.ijhydene.2018.06.183

Billinton, R., and Karki, R. (2001). Maintaining supply reliability of small isolated power systems using renewable energy. *IEE Proc. Gen. Trans. Dist.* 148 (6), 530–534. doi:10.1049/ip-gtd:20010562

Chatrenour, N., Razmi, H., and Doagou-Mojarrad, H. (2017). Improved double integral sliding mode MPPT controller based parameter estimation for a stand-alone photovoltaic system. *Energy Convers. Manag.* 139, 97–109. doi:10.1016/j.enconman.2017.02.055

Chen, J., Phung, T., Blackburn, T., Ambikairajah, E., and Zhang, D. (2016). Detection of high impedance faults using current transformers for sensing and identification based on features extracted using wavelet transform. *IET Gener. Transm. Distrib.* 10 (12), 2990–2998. doi:10.1049/iet-gtd.2016.0021

Costa, F. B., Souza, B. A., Brito, N. S. D., Silva, J. A. C. B., and Santos, W. C. (2015). Real-time detection of transients induced by high-impedance faults based on the boundary wavelet transform. *IEEE Trans. Industry Appl.* 51 (6), 5312–5323. doi:10.1109/tia.2015.2434993

Daubecheis, I. (1992). *Ten lectures on wavelets*, Vol. 61. Philadelphia: SIAM.

De Brito, M. A. G., Galotto, L., Sampaio, L. P., e Melo, G. D. A., and Canesin, C. A. (2012). Evaluation of the main MPPT techniques for photovoltaic applications. *IEEE Trans. Indust. Electron.* 60 (3), 1156–1167. doi:10.1109/tie.2012.2198036

Elkalashy, N. I., Lehtonen, M., Darwish, H. A., Taalab, A. I., and Izzularab, M. A. (2008). "Operation evaluation of DDWT-based Earth fault detection in unearthed MV networks," in 2008 12th International Middle-East Power System Conference (IEEE), 208–212.

Emanuel, A. E., Cyganski, D., Orr, J. A., Shiller, S., and Gulachenski, E. M. (1990). High impedance fault arcing on sandy soil in 15 kV distribution feeders: Contributions to the evaluation of the low frequency spectrum. *IEEE Trans. Power Deliv.* 5 (2), 676–686. doi:10.1109/61.53070

Gafoor, S. A., Yadav, S. K., and Prashanth, P. (2014). "Transmission line protection scheme using wavelet based alienation coefficients," in Proceedings of the IEEE International Conference Power and Energy, Kyiv, Ukraine, 32–36.

Gautam, S., and Brahma, S. M. (2012). Detection of high impedance fault in power distribution systems using mathematical morphology. *IEEE Trans. Power Syst.* 28 (2), 1226–1234. doi:10.1109/tpwrs.2012.2215630

Ghaderi, A., Mohammadpour, H. A., Ginn, H. L., and Shin, Y. J. (2014). High-impedance fault detection in the distribution network using the time-frequency-based algorithm. *IEEE Trans. Power Deliv.* 30 (3), 1260–1268. doi:10.1109/tpwrd.2014.2361207

Gite, S. S., and Pawar, S. H. (2017). "Modeling of wind energy system with MPPT control for DC microgrid," in 2017 second international conference on electrical, computer and communication technologies (ICECCT) (IEEE), 1–6.

Gomes, D. P. S., Ozansoy, C., and Ulhaq, A. (2018). High-sensitivity vegetation high-impedance fault detection based on signals highfrequency contents. *IEEE Trans. Power Deliv.* 33 (3), 1398–1407. doi:10.1109/tpwrd.2018.2791986

He, Z.-Y., Liao, K., Li, X.-P., Lin, S., Yang, J.-W., and Mai, R.-K. (2014). Natural frequency-based line fault location in HVDC lines. *IEEE Trans. Power Deliv.* 29 (2), 851–859. doi:10.1109/tpwrd.2013.2269769

James, J. Q., Hou, Y., Lam, A. Y., and Li, V. O. (2017). Intelligent fault detection scheme for microgrids with wavelet-based deep neural networks. *IEEE Trans. Smart Grid* 10 (2), 1694–1703.

Jiang, J. A., Fan, P. L., and Chen, C. S. (2003). A fault detection and faulted phase selection approach for transmission lines with haar wavelet transform. *IEEE PES Transm. Distribution Conf. Expo.* 1 (1), 285–289.

Kavaskar, S., and Mohanty, N. K. (2019). Detection of high impedance fault in distribution networks. *Ain Shams Eng. J.* 10 (1), 5–13. doi:10.1016/j.asej.2018.04.006

Kavi, M., Mishra, Y., and Vilathgamuwa, M. D. (2018). High-impedance fault detection and classification in power system distribution networks using morphological fault detector algorithm. *IET Gener. Transm. Distrib.* 12 (15), 3699–3710. doi:10.1049/iet-gtd.2017.1633

Kordestani, M., Safavi, A. A., and Sadrzadeh, A. (2016). "A new method to diagnose the type and location of disturbances in fars power distribution system," in Proceedings of the 24th Iranian Conference on Electrical Engineering ICEE, Shiraz, Iran (IEEE), 1871–1876.

Kroposki, B., Johnson, B., Zhang, Y., Gevorgian, V., Denholm, P., Hodge, B. M., et al. (2017). Achieving a 100% renewable grid: Operating electric power systems with extremely high levels of variable renewable energy. *IEEE Power energy Mag.* 15 (2), 61–73. doi:10.1109/mpe.2016.2637122

Mahari, A., and Seyedi, H. (2015). High impedance fault protection in transmission lines using a WPT-based algorithm. *Int. J. Electr. Power & Energy Syst.* 67, 537–545. doi:10.1016/j.ijepes.2014.12.022

Manwell, J. F., McGowan, J. G., and Rogers, A. L. (2010). *Wind energy explained: Theory, design and application*. John Wiley & Sons.

Mishra, M., and Panigrahi, R. R. (2019). Taxonomy of high impedance fault detection algorithm. *Measurement* 148, 106955. doi:10.1016/j.measurement.2019.106955

Mishra, P. K., and Yadav, A. (2019). Combined DFT and fuzzy based faulty phase selection and classification in a series compensated transmission line. *Modell. Simul. Eng.* 2019, 1–18. doi:10.1155/2019/3467050

Necaibia, S., Kelaiaia, M. S., Labar, H., and Necaibia, A. (2017). Implementation of an improved incremental conductance MPPT control based boost converter in photovoltaic applications. *Int. J. Emerg. Electr. Power Syst.* 18 (4). doi:10.1515/ijeeps-2017-0051

Nurzaman, I., Harini, B. W., Avianto, N., and Yusivar, F. (2017). "Implementation of maximum power point tracking algorithm on wind turbine generator using perturb and observe method," in 2017 International Conference on Sustainable Energy Engineering and Application (ICSEEA) (IEEE), 45–51.

Qazi, A., Hussain, F., Rahim, N. A., Hardaker, G., Alghazzawi, D., Shaban, K., et al. (2019). Towards sustainable energy: A systematic review of renewable energy sources, technologies, and public opinions. *IEEE access* 7, 63837–63851. doi:10.1109/access.2019.2906402

Rezaei, N., and Haghifam, M. R. (2008). Protection scheme for a distribution system with distributed generation using neural networks. *Int. J. Electr. Power Energy Syst.* 30, 235–241. doi:10.1016/j.ijepes.2007.07.006

Samantaray, S. R., Panigrahi, B. K., and Dash, P. K. (2008). High impedance fault detection in power distribution networks using time–frequency transform and probabilistic neural network. *IET generation, Transm. distribution* 2 (2), 261–270. doi:10.1049/iet-gtd:20070319

Samet, H., Shabanpour-Haghighi, A., and Ghanbari, T. (2017). A fault classification technique for transmission lines using an improved alienation coefficients technique. *Int. Trans. Electr. Energ Syst.* 27, 22355–e2323. doi:10.1002/etep.2235

Santos, W. C., Lopes, F. V., Brito, N. S. D., and Souza, B. A. (2016). High-impedance fault identification on distribution networks. *IEEE Trans. Power Deliv.* 32 (1), 23–32. doi:10.1109/tpwrd.2016.2548942

Santos, W. C., Lopes, F. V., Brito, N. S. D., and Souza, B. A. (2017). High impedance fault identification on distribution networks. *IEEE Trans. Power Deliv.* 32 (1), 23–32. doi:10.1109/tpwrd.2016.2548942

Sarlak, M., and Shahrtash, S. M. (2011). High impedance fault detection using combination of multi-layer perceptron neural networks based on multi-resolution morphological gradient features of current waveform. *IET generation, Transm. distribution* 5 (5), 588–595. doi:10.1049/iet-gtd.2010.0702

Sedighi, A. R., Haghifam, M. R., Malik, O. P., and Ghassemian, M. H. (2005a). High impedance fault detection based on wavelet transform and statistical pattern recognition. *IEEE Trans. Power Deliv.* 20 (4), 2414–2421. doi:10.1109/tpwrd.2005.852367

Sedighi, A. R., Haghifam, M. R., and Malik, O. P. (2005b). Soft computing applications in high impedance fault detection in distribution systems. *Electr. Power Syst. Res.* 76 (1-3), 136–144. doi:10.1016/j.epsr.2005.05.004

Sekar, K., and Mohanty, N. K. (2017). Combined mathematical morphology and data mining based high impedance fault detection. *Energy Procedia* 117, 417–423. doi:10.1016/j.egypro.2017.05.161

Soualhi, A., Medjaher, K., and Zerhouni, N. (2015). Bearing health monitoring based on hilbert-huang transform, support vector machine, and regression. *IEEE Trans. Instrum. Meas.* 64 (1), 52–62. doi:10.1109/tim.2014.2330494

Tonelli-Neto, M. S., Decanini, J. G. M. S., Lotufo, A. D. P., and Minussi, C. R. (2017). Fuzzy based methodologies comparison for high-impedance fault diagnosis in radial distribution feeders. *IET Gener. Transm. Distrib.* 11 (6), 1557–1565. doi:10.1049/iet-gtd.2016.1409

Vas, P. (1999). *Sensorless vector and direct torque control*. Oxford University Press.

Wang, B., Geng, J., and Dong, X. (2016). High-impedance fault detection based on nonlinear voltage–current characteristic profile identification. *IEEE Trans. Smart Grid* 9 (4), 3783–3791. doi:10.1109/tsg.2016.2642988

Xiao, W., Elnosh, A., Khadkikar, V., and Zeineldin, H. (2011). "Overview of maximum power point tracking technologies for photovoltaic power systems," in IECON 2011 - 37th Annual Conference of the IEEE Industrial Electronics Society, Melbourne, VIC, 3900–3905.

Yahya, M. G., and Yahya, M. G. (2023). Modified PDPWM control with MPPT algorithm for equal power sharing in cascaded multilevel inverter for standalone PV system under partial shading. *Int. J. Power Electron. Drive Syst.* 14 (1), 533. doi:10.11591/ijpeds.v14.i1.pp533-545

Yu, L., Lai, K. K., and Wang, S. (2008). Multistage RBF neural network ensemble learning for exchange rates forecasting. *Neurocomputing* 71 (16-18), 3295–3302. doi:10.1016/j.neucom.2008.04.029

Zayandehroodi, H., Mohamed, A., Shareef, H., and Mohammadjafari, M. (2010). "Performance comparison of MLP and RBF neural networks for fault location in distribution networks with DGs," in IEEE International Conference on Power and Energy (PECon 2010), Kuala Lumpur, Malaysia, 341–345.

Zayandehroodi, H., Mohamed, A., Shareef, H., and Mohammadja, M. (2010). Automated Fault location in a power system with distributed generations using radial basis function neural networks. *Int. J. Appl. Sci.* 10, 3032–3041. doi:10.3923/jas.2010.3032.3041

frontiers | Frontiers in Energy Research

TYPE Original Research
PUBLISHED 16 March 2023
DOI 10.3389/fenrg.2023.1088297

OPEN ACCESS

EDITED BY
Franco Fernando Yanine,
Universidad Finis Terrae, Chile

REVIEWED BY
Gudina Terefe Tucho,
Jimma University, Ethiopia
Roman Teodora,
Alexandru Ioan Cuza University, Romania
Alexandru Maxim,
Alexandru Ioan Cuza University, Romania

*CORRESPONDENCE
Muhsan Ehsan,
muhsanehsan98@hotmail.com
Tamer Abu-Alam,
tamer.abu-alam@uit.no

SPECIALTY SECTION
This article was submitted to Smart Grids, a section of the journal Frontiers in Energy Research

RECEIVED 03 November 2022
ACCEPTED 27 February 2023
PUBLISHED 16 March 2023

CITATION
Ud Din S, Wimalasiri R, Ehsan M, Liang X, Ning F, Guo D, Manzoor Z, Abu-Alam T and Abioui M (2023), Assessing public perception and willingness to pay for renewable energy in Pakistan through the theory of planned behavior.
Front. Energy Res. 11:1088297.
doi: 10.3389/fenrg.2023.1088297

Assessing public perception and willingness to pay for renewable energy in Pakistan through the theory of planned behavior

Shahab Ud Din[1,2,3], Ruminda Wimalasiri[2], Muhsan Ehsan[4]*, Xue Liang[1], Fulong Ning[3], Dongdong Guo[5], Zaira Manzoor[6], Tamer Abu-Alam[7]* and Mohamed Abioui[8,9]

[1]Department of Oil-Gas Field Development, College of Petroleum Engineering, China University of Petroleum, Beijing, China, [2]Department of Mechanical Engineering, The Open University of Sri Lanka, Nawala, Nugegoda, Sri Lanka, [3]Faculty of Engineering, China University of Geosciences, Wuhan, China, [4]Department of Earth and Environmental Sciences, Bahria University, Islamabad, Pakistan, [5]School of Earth and Environment, Anhui University of Science and Technology, Huainan, China, [6]Department of Government and Public Policy, Faculty of Contemporary Studies, National Defence University, Islamabad, Pakistan, [7]The Faculty of Biosciences, Fisheries and Economics, UiT The Arctic University of Norway, Tromsø, Norway, [8]Department of Earth Sciences, Faculty of Sciences, Ibnou Zohr University, Agadir, Morocco, [9]MARE-Marine and Environmental Sciences Centre—Sedimentary Geology Group, Department of Earth Sciences, Faculty of Sciences and Technology, University of Coimbra, Coimbra, Portugal

With growing urbanization and increasing world population, energy demand also increases. A significant portion of the world's energy comes from fossil fuels, and these sources of energy are declining rapidly at the current consumption rate. There are also growing environmental concerns on the use of fossil fuels increasing greenhouse gas emissions. In this regard, renewable energy (RE) shows promising solutions which are both sustainable and environmentally friendly. Developed countries and leading organizations are investing heavily in the RE sector. However, the developing world has anxieties over social acceptability and people's willingness to pay for renewable energy. This study is conducted in Pakistan to understand the public perception and willingness to pay. The Theory of Planned Behavior (TPB) was utilized with background factors such as awareness, perceived advantages, perceived challenges, and moral obligations to examine its influence on people's willingness to pay. In addition to this, the study also assessed the indirect effects of background factors (awareness, perceived advantages, and perceived challenges) on willingness to pay through public attitude. Furthermore, the indirect relationship between background factors (awareness and moral obligation) and willingness to pay through subjective norms was also examined. A total of 512 samples were gathered from participants and were analyzed through partial least square–structural equation modeling (PLS-SEM) and SPSS. The study findings are very interesting and back up our hypotheses that the background factors (awareness, perceived advantages, and perceived challenges) are positively associated with public attitude and have an indirect effect on willingness to pay through public attitude. Similarly, variables such as awareness and moral obligation are negatively and positively associated with subjective norms, respectively. However, the variables, awareness and moral obligation, have no indirect relationship with willingness to pay through subjective norms. Additionally, the study reveals that the components (attitude and perceived behavior control) of TPB have a significantly positive effect on willingness to

pay. The study also concludes that the participants having formal education and knowledge about climate change and renewable energy are inclined toward green energy and are willing to pay, and they are hardly influenced by others' opinions. Furthermore, the study also provides insights for policymakers, suggestions, and recommendations for the future.

KEYWORDS

renewable energy, public perception, willingness to pay, theory of planned behavior, PLS-SEM

1 Introduction

Environmental quality and accessibility to natural resources have a direct impact on life. The fundamental requirement for sustaining life is to maintain the ecosystem in equilibrium. The Earth's atmosphere is a very precious resource, but it is fragile too and has to be protected. Contrarily, the unwanted influxes into the environment by human activities can disturb this equilibrium and also have negative effects on lives (Mariani et al., 2010). Human interventions intensify day by day due to large-scale manufacturing, agriculture, and urbanization, which lead to more demands for fossil fuels and a high consumption of transportation and energy (Van Gent and Rietveld, 1993; Lam et al., 2011; Ockenden et al., 2014). As reported by the International Energy Agency (IEA), the world's primary energy consumption has increased 2.5 times from 1971–2014, from 5.5 GTOE to 13.7 GTOE (International Energy Agency I, 2017). A 150% increase in the total primary consumption. Similarly, during the same time, CO_2 emission has also increased twofold (Bell et al., 2011).

Climate change poses very serious threats, such as environmental, social, and economic threats. Global warming is directly linked to increases in carbon emissions associated with human intervention. During the past century, CO_2 emission has increased significantly in comparison to the pre-industrial level (Canadell et al., 2007). One of the major contributors of CO_2 emission is fossil fuels. Burning fossil fuels around the world adds 5×10^9 tons of CO_2 to the atmosphere annually, a significant portion of which remains in the atmosphere (Dyson, 1977). Similarly, the continuous increase in population, urbanization, growing energy consumption, and economic activities are also among the major contributors to global warming. Recent studies have shown that the world average temperature is in excess of 2°C (IPCC, 2014). Although it has been consented in the Paris Agreement that the world's major countries would keep the world's average temperature below 1.5°C by 2050 (Bach, 1979), it is estimated that the average global temperature may exceed 3°C by 2050.

The growing energy demands are increasing the burden on the environment, thus attracting the attention of academia and researchers in the field of energy management and RE. In the developed countries, a significant transition has occurred toward green energy due to their commitment to the Kyoto Protocol and Paris Agreement, as a result of public access to information relevant to the environment and RE (Vasseur and Kemp, 2015; The Paris Agreement, 2018). In order to meet the goals of the Paris Agreement of limiting the average temperature increase to 1.5°C, large-scale RE adoption is required. In recent years, green investment in RE has greatly increased to achieve sustainable growth. However, most developing countries still use fossil fuels for energy generation. Fossil fuels can no longer be used as the primary energy source due to their high price and potential environmental threat. Fossil fuels' unsustainability and potential environmental threat led governments and policymakers to shift to green energy and minimize fossil fuel usage. However, the investment ratio is meager due to their poor infrastructure, poor economies, and related social and cultural issues.

The social acceptability of green energy (renewable energy sources and renewable energy technologies) is to monitor at both the national and international levels. It has also been observed that public attitude varies not only between countries but also between different regions within the same country (Eiser et al., 2010; Walter, 2014; Gallup, 2015). Active ecological awareness has been observed in South Korea, where the majority of South Koreans support policies that promote renewable energy sources (most of them are state owned) (Mroczek and Donata, 2014). The US government is also motivating and encouraging US citizens to use renewable energy resources such as solar energy systems by giving them incentives (Kowalczyk-Juśko and Bogdan, 2015). Similarly, Portugal has a favorable attitude toward investing in renewable energy sources, especially hydropower and solar energy (Dmochowska-Dudek and Bednarek-Szczepańska, 2018). Germany, Italy, the United States, China, Japan, Spain, France, Bulgaria, Australia, and the Czech Republic are countries with the most installed photovoltaic-rated power. Most of these countries' energy policies are on generated kilowatt-hour, low-interest loans, national renewable energy sources, solar development goals, and lower taxations, which attract the masses toward RE (Borges Neto et al., 2010). The local authorities and volunteers have played a very important role and made advancements in technology and large-scale applicability of photovoltaics (Bajpai and Vaishalee, 2012).

Contrarily, the major impediments to the wider adoption of renewable energy sources and renewable energy technologies, except costly infrastructure, are of not sharing relevant information with the public and the behavior of the public against advancements in renewable energy sources and renewable energy technologies (Kaya et al., 2019), where the latter has been more pronounced and observed in developing countries, while the former is in the context of people living in the rural, suburban, and urban regions of China. (Rahman et al., 2014). Another study was conducted in Malaysia (Muhammad-Sukki et al., 2011) about the public views and perceptions on solar energy and photovoltaic installation, which concluded that Malaysians have been very hesitant to invest in photovoltaics since they hardly comprehend the incentives and

significant socioeconomic benefits. Furthermore, there has been social opposition to renewable energy sources and renewable energy technologies in the Middle East and North Africa (Florkowski et al., 2018). A study on the societal acceptance of small hydropower plants (SHPs) in India has found that these projects are difficult to implement in certain regions (Florkowski et al., 2018).

Apart from the social acceptance of, behavior toward, and perception of renewable energy sources and renewable energy technologies, studies have also focused on the economics aspect where the public readiness to pay for expensive renewable energy in their locality and the place of residency, also known as the "willingness to pay" (WTP), was studied (Klepacka et al., 2018). WTP was further investigated by arranged discussions with the public through a questionnaire to record their preferences (Devine-Wright, 2008). A positive relationship has always been noted among WTP, income, and the level of public information (Ekins, 2004; Wüstenhagen et al., 2007). A study on attitude toward renewable energy sources and renewable energy technologies has observed that tourists from Australia are willing to pay more (about 1%–5%) for existing renewable energy sources and renewable energy technologies in accommodation sites (Miranda et al., 2011). In the case of Sweden, it has been reported that renewable energy source acceptance increases with the level of environmental awareness (Wooldridge, 2015). A Chinese study had examined that household income, knowledge about RE, renewable energy technologies (RET), and education were positively associated with WTP, whereas variables like age and neighborhood were negatively associated with WTP (Eurobarometer, 2014).

Pakistan is a developing country, the fifth most populous country with a population of 224.78 million (Pakistan Economic Survey, 2022). Like other developing countries, Pakistan is also facing huge challenges in achieving sustainable green development. The rapid increase in population and urbanization have increased the country's energy demand. In the past 15 years, the total energy consumption has increased by 53.61% (887.4 GWh to 1,363.2 GWh) (Pakistan Economic Survey, 2022). A significant portion of this energy comes from fossil fuels (non-renewable fuels such as oil, gas, and coal). According to the Pakistan Economic Survey 2021–2022 (Pakistan Economic Survey, 2022), a significant portion of the total energy comes from fossil fuels. However, the share of renewable energy sources (other than hydropower) amounts to only 3% (Pakistan Economic Survey, 2022). The country has developed an Alternative and Renewable Energy Policy in 2019, which includes some ambitious goals such as to increase the portion of renewable energy sources (other than hydropower) by 20% by 2025 and 30% by 2030 in the total energy mix (Ministry of Energy, 2019). However, social acceptance is the key factor which will play a key role in achieving this ambitious goal. Social acceptance is the willingness of people to accept renewable energy investment in their communities and countries at large (Liu et al., 2013; Caporale and de Lucia, 2015). According to Rosso-Cerón and Kafarov (2015), social acceptance defines people's positive and negative attitudes toward various green energy resources and technologies. In Pakistan, various studies have been conducted on renewable energy sources and renewable energy technologies (Bhutto et al., 2011; Bhutto et al., 2013; Kamran, 2018; Zafar et al., 2018; Ali et al., 2019; Kashif et al., 2020; Bhutto et al., 2021; Uddin et al., 2021), but no study has been reported on public perception about RE sources, technology, and WTP.

The scope of this article is to investigate the public perception about the environment, climate change, and renewable energy technology, as well as their awareness and willingness to pay for renewable energy. This study also investigates how various variables such as perceived advantages, perceived challenges, and moral obligations effect their willingness to pay for renewable energy. To study all these parameters, the Theory of Planned Behavior (TPB) is utilized. This study provides researchers and policy makers with an understanding of the public perception about renewable energy and factors those affect their attitudes toward renewable energy, as well as their willingness to pay for it and aid in improving their existing models or policies.

2 Literature review

2.1 Theoretical background

Earlier studies have shown that customers' decision-making process is dynamic. Researchers have used models such as self-efficacy, reasoned action theory, and TPB to examine purchasers' purchase intentions. The TPB states that behavioral intentions control behavior. People consider the consequences before doing, which leads to their intended result. Individuals' attitudes are shaped by their strong beliefs and predictions of behavior results (Ajzen, 1991). The TPB offers a framework for looking at the factors those influence behaviors. The TPB contends that individual conduct is the result of behavioral intentions, where intentions are a result of one's attitude toward the action, i.e., one's perception of behavioral control and one's subjective norm. In essence, the TPB states that the greater one's behavioral intentions are, the greater will be one's likelihood of carrying out that behavior. Intentions are further explained by variables like attitude (AT), subjective norms (SNs), and perceived behavior control (PBC) (Ajzen, 2012). The TPB has played an important role in various research areas. Various studies have utilized the TPB for ascertaining consumption and willingness to pay (Al Mamun et al., 2018; Sreen et al., 2018; Kaffashi and Shamsudin, 2019; Bhutto et al., 2021; Masrahi et al., 2021; Nazir and Tian, 2022). Apart from significant support, the TPB also faces criticism. A major criticism is the need to add some additional variables that would improve its predictive and explanatory power. Ajzen (1991); Ajzen (2020) acknowledges that the TPB allows additional variables if it adds significance to the model's predictive and explanatory power. Thus, several researchers have suggested the addition of new variables to the TPB to enhance its predictive and explanatory power. This study expands the TPB by adding variables such as awareness, perceived advantages, perceived challenges, and moral obligations to improve the model's predictive power for assessing public perception and willingness to pay for renewable energy. The study conceptualizes and validates the model in the context of Pakistan.

2.2 Hypotheses

2.2.1 Awareness

Environmental awareness has a direct impact on customers' attitudes and their willingness to pay for goods, and this is related to

buying behavior both directly and indirectly. Eco-label awareness has been found to have a good link with both product knowledge and consumers' propensity to buy environmentally friendly products in studies (Devi et al., 2012). Similarly, increasing people's environmental awareness and encouraging them to buy green or ecologically friendly products might help them make better decisions (Laroche et al., 1996). Customers who are eco-literate are more likely to make rational, rather than irrational, purchases because they understand the problems regarding environmental concerns. The increased ecoliteracy will generally lead to stronger purchasing intentions for green energy, because it suggests a better awareness of environmental symbols, concepts, benefits, and consequences. As a result, attitude's explanatory ability will be improved. However, the explanatory value of attitude is diminished when consumers lack eco-literacy and instead rely on subjective feelings while making purchases. So overall, eco-literacy plays a key role in consumers' attitude and their willingness to pay for renewable energy and technologies.

Hypothesis 1a: Public awareness will have a positive impact on their attitude toward renewable energy.

Hypothesis 1b: Public awareness will also have a positive and indirect effect on their willingness to pay for renewable energy through AT.

2.2.2 Attitude

The term "attitude" refers to a person's mental state of preparedness, which they can develop and plan as a result of their experiences with things, people, and scenarios to which they can connect (Ivancevich et al., 2008). According to the TPB model, a person's behavioral attitude relates to the degree to which they see the activity—positively or negatively (Fishbein and Ajzen, 1975). According to Ajzen (1991), people are more likely to engage in action if they have a good attitude toward it. Positive or negative attitudes toward ecologically friendly items have been documented in the literature with regard to supporting the environment, according to Wang et al. (2016). There is no need for intentions to impact green purchasing and recycling practices according to the findings of Gadenne et al. (2011). Consumers' everyday energy-saving habits may be influenced by their views toward energy conservation, which in turn can help them become more involved in the cause for energy conservation and in using green energy (Egmond et al., 2005; Lopes et al., 2019).

Hypothesis 2: Public attitude positively affects their willingness to pay for renewable energy.

2.2.3 Advantages

Emotional rewards that might result from pure altruistic activity, such as giving to others, are described by economists in the warm-glow hypothesis (Andreoni, 1989; Andreoni, 1990). A "helper's high" is conceptually connected to a warm-glow effect (James Baraz, 2010). Furthermore, a previous study has revealed that consumers may experience a feeling of personal pleasure when they devote themselves not just to charitable acts but also to environmental awareness (Ritov and Kahneman, 1997). Altruism in the context of sustainability has been examined in a number of research studies. It has been shown that those motivated by a strong feeling of dedication and generosity are more likely to utilize environmentally friendly goods and services than those who do not feel the same way (Sánchez-Fernández et al., 2009). Research has revealed that consumers' willingness to pay a higher price for green energy is influenced much more by the expectation of warm-glow advantages than by the perceived decrease in environmental impact (Wüstenhagen and Bilharz, 2006). According to Andreoni (1990), "pure altruism," i.e., an intrinsic purpose without reciprocal expectations, produces a pleasant glow that is idealistic. "Impure altruism," i.e., an extrinsic drive with reciprocal expectations, is the most common source of the warm-glow feeling (Gneezy and Rustichini, 2000). However, a previous study has shown that both altruism and warm-glow effects have considerable influence on customer sentiments toward green energy products (Hartmann and Apaolaza-Ibáñez, 2012; D'Amato et al., 2014; Carrington et al., 2010). In other words, attitudes are influenced by perceptions of warm-glow advantages. Thus,

Hypothesis 3a: The perceived advantages will also have a positive impact on public attitude toward renewable energy.

Hypothesis 3b: The perceived advantage will also have a positive and indirect effect on public willingness to pay for renewable energy through AT.

2.2.4 Perceived challenges and risks

Risk perception is the term used to describe an individual's capacity to evaluate the level of risk that is connected with a certain behavior or activity (Ajzen, 2002). In the context of renewable energy, this means a person's assessment of how they feel about the risks of using renewable energy technologies. This introduces a new concept: risk tolerance. An individual's perception of danger, as well as his or her risk tolerance level, plays a key role in accepting a particular technology. If a person thinks that using renewable energy is less dangerous than using other sources of energy, he or she is more likely to use renewable energy (Aman et al., 2012). Trust is when a person or group is willing to be open to the actions of another person or group in the hope that the other person or group will act in the best interests of the trusting person or group (Zainudin et al., 2014). In the context of renewable energy, confidence in renewable energy refers to an individual's anticipation that employing renewable energy resources will result in acceptable favorable outcomes in terms of benefits (Nguyen, 2018). Trust is a crucial factor in determining the current scenario, which includes the hazards involved and vulnerability of the trusted person. Trust has been viewed as a motivator in adopting new technology and completing transactions involving the provision of services in the hopes of a beneficial exchange relationship between the parties concerned. Thus

Hypothesis 4a: The perceived challenges and risks will negatively affect public attitude toward renewable energy.

Hypothesis 4b: The perceived challenges and risks will also have a negative and indirect effect on public willingness to pay for renewable energy.

2.2.5 Awareness and subjective norms

Subjective norms are determined by a set of cultural beliefs that represent the perceived social pressures that an individual feels to engage in specific types of conduct (Minton et al., 2017). Individuals in modern civilization are inextricably linked to society, and this influences their pro-environmental conduct (Zhang et al., 2019). The majority culture in Pakistan is collectivist, and social results have a part in consumers' purchase decisions (Zhang et al., 2019). Environmentally conscious and literate consumers are more inclined to make purchasing decisions on their own rather than seek recommendations from friends, family, co-workers, and other reference groups. As a result, we believe that growing consumer awareness will lower the explanatory power of subjective norms. Due to their lack of confidence, consumers with less eco-knowledge (eco-literacy) are more likely to rely on social input when making decisions. As a result, we believe that a low level of customer knowledge will boost the strength of subjective standards to explain purchase intent.

Hypothesis 5a: Awareness will have a negative impact on the subjective norm.

Hypothesis 5b: Public awareness will also have a positive and indirect effect on their willingness to pay for renewable energy through SN.

2.2.6 Moral obligations

The term "moral duty" refers to a person's sentiments of accountability, which leads them to perform or avoid certain actions (Beck and Ajzen, 1991). Having moral duties shows that the person has accepted a commitment to perform actions in an environmentally conscientious way (Stern, 2000; Bamberg et al., 2007). Empirical data have substantially supported the positive association between moral duty and environment-friendly intentions in prior investigations (Stern, 2000; Onwezen et al., 2013; Hwang and Lee, 2017). The desire to acquire RE might be sparked by a person's moral duty to preserve natural resources and enhance the environment. In many cases, people who have a strong sense of moral obligation to act in a way that is beneficial to the environment will act in accordance with an internal normative standard that they have established for themselves (Bamberg et al., 2007; Hwang, 2016). Previous research have experimentally examined the link between moral responsibilities and subjective standards (Mamun et al., 2018; Al Mamun et al., 2019; Fatoki, 2020). The relationship between moral duty and the subjective norm was largely neglected by academics in impoverished nations like Pakistan. Consequently, our research implies that moral duty might have a favorable impact on subjective standards for adopting RE. Because of this, this research suggests

Hypothesis 6a: Moral obligations will have a positive effect on subjective norms.

Hypothesis 6b: Moral obligations will also have a positive and indirect effect on public willingness to pay for renewable energy through SN.

2.2.7 Subjective norms

Subjective norms refer to how much people, society, or others approve or disapprove of a specific behavior (Sultan et al., 2020). As defined by the TPB framework, a subjective norm relates to the extent to which people feel that the other person should do (Finlay et al., 1999). It relates to the "social pressure" that people feel and how they interpret the actions of others in their social circles, such as family, friends, or co-workers, which are both parts of the concept. Consumers' ideas of what is and is not acceptable are shaped by these many facets of perception. In the present sustainability movement, behaviors such as adopting new energy sources and using eco-friendly products may be viewed more favorably.

This psychological process has been extensively studied in the context of energy-saving behavior. In the words of Black et al. (1985), customers' ideas about the advantages of energy savings may encourage them to save energy. A similar finding was reported in studies conducted in South Korea and China (Zhao et al., 2014; Ha and Janda, 2017). Subjective norms were demonstrated to have a beneficial influence on Korean customers' purchase intentions for energy-efficient appliances in a recent study performed in South Korea (Park and Kwon, 2017). Energy-efficient appliance purchase intentions were shown to be negatively affected (Wang et al., 2019). Additional research in Asia has bolstered these results (Ajzen, 1991; Zainudin et al., 2014; Tan et al., 2017). However, in a study on Pakistani consumers, subjective standards and energy-saving objectives were not linked (Ali et al., 2019). In addition, Tan et al. (2017) observed that energy-efficient appliance purchase intention did not have a substantially positive association with SNs, which shows that customers may not be readily affected by other people's views. By contrast, Wang et al. (2019) found a stronger influence of social norms on intentions to buy in South Asian collectivistic societies. Thus,

Hypothesis 7: Subjective norms will positively affect public intention to pay for renewable energy.

2.2.8 Perceived behavior control

Perceived behavior control is a measure of how much control a person believes they have over their behavior (Ajzen, 1991). PBC has been studied as a key factor in determining behavioral intentions in the context of green consumption and willingness to pay for renewable energy (Chen and Tung, 2014; Wu and Chen, 2014). Consumers are more likely to engage in the desired activity if they have more control over their actions (Ajzen, 1991). Perceived difficulty or ease of executing a given conduct has also been classified as PBC in the pro-environmental literature (Bamberg, 2003).

Wang et al. (2019) hypothesized that behavioral control has a detrimental effect on customers' willingness to pay for renewable energy, which is counterintuitive. The justification for this is that it is challenging for consumers to obtain relevant energy consumption information or to fully understand energy-efficient rating information when purchasing energy-saving products, which in turn hinders their ability to make educated decisions and feel secure when purchasing renewable energy or green energy products. On the contrary, the results did not back up this theory, but instead indicated that PBC had a significant impact on whether people planned to pay for renewable energy even when controlling for factors like informational details. Thus,

Hypothesis 8: Perceived behavior control positively affects the willingness to pay for renewable energy.

10.3389/fenrg.2023.1088297

TABLE 1 Demographic information of the participants (n = 512).

Components	Categorization	Enumeration	
		Frequency	%
Gender	Male	289	56.45
	Female	223	43.55
	Transgender	—	—
Age	Under 25	187	36.52
	25–35	274	53.52
	36–45	35	6.84
	45+	16	3.13
Province	Baluchistan	123	24.02
	Khyber Pakhtunkhwa	145	28.32
	Punjab	131	25.59
	Sindh	113	22.07
Qualification	Undergraduate	83	16.21
	Master/MS/MPhil	270	52.73
	PhD	109	21.29
	Others	50	9.77

3 Materials and methods

3.1 Participants and sampling procedure

This study utilized a quantitative method to analyze the suggested model. The data were acquired through questionnaires distributed among the inhabitants of four provinces in Pakistan: Baluchistan, Khyber Pakhtunkhwa, Punjab, and Sindh. The questionnaires were distributed among the participants from July to September 2021 at times when there was a smart lockdown imposed in several cities. All the participants were briefed before filling out this questionnaire and signed a written consent. An instruction document was also provided to inform the participants of the aim of the study to avoid any biases. Due to COVID-19, a smart lockdown was imposed in various cities and provinces, so an online sampling technique was applied to reach the maximum number of participants in the study. To ensure a non-biased sample and strictly follow the standard operating procedure (SOPs) during the pandemic, questionnaires were spread with the aid of different social media platforms, such as WhatsApp, WeChat, and QQ through Google Forms (online data collection software), where every respondent had the opportunity of being selected. The target provinces and regions completed a total of 512 usable questionnaires where the participation of each respondent was voluntary.

The demographic information of the participants in the study is given in Table 1. All the respondents belonged to the four different abovementioned provinces in Pakistan. According to the survey's gender breakdown, 56.45% and 43.55% of the respondents were male and female, respectively. In total, 36.52, 53.52, 6.84, and 3.13% of the respondents were from the age groups of under-25, 25–35, 36–45, and 45-plus years, respectively. Based on the qualification of the respondents, 16.21% were undergraduates, 52.73% were Master/MS/MPhils, 21.29% were PhDs, and 9.77% were others (which included post-doctorate or any other level of qualification). Furthermore, among the respondents, 24.02, 28.32, 25.59, and 22.07% belonged to the province of Baluchistan, Khyber Pakhtunkhwa (KPK), Punjab, and Sindh, respectively.

3.2 Measures

The measures of the TPB construct utilized in the present study are those used by prior researchers in various settings, which is consistent with the TPB questionnaire's criteria and structure. Figure 1 shows all the TPB model components and background components that are considered latent variables. The data collection questionnaire comprised two parts. The participant's demographic data were included in the first section, while the second section included questions related to the public perception and WTP for RE, which was measured on the basis of TPB.

The perceived advantages of renewable energy (AD), perceived challenges of renewable energy (CH), and willingness to pay (WTP) were measured by seven, six, and two items, respectively, as proposed by Ntanos et al. (2018) and Buchmayr et al. (2021), whereas the subjective norm (SN), moral obligation (MO), and perceived behavior control (PBC) were measured by two items each proposed by Bhutto et al. (2021). The items reflecting awareness (AW) were adapted from the study by Djurisic et al. (2020); similarly, the items reflecting attitude (AT) were adapted from the studies of Ntanos et al. (2018); Kaya et al. (2019). A Likert scale with a maximum of five points, from "strongly disagree" (1) to "strongly agree" (5), was used to measure the aforementioned items. The questionnaire structure and the proposed model reliability were tested by a pilot test with 50 respondents.

3.3 Common method variance

The data of both the dependent and independent variables in this study were recorded and obtained from the same participants. So, there is a possibility of method bias. The possible method bias was reduced by properly guiding and briefing the participants before attempting the questionnaire (an instruction document containing the aims of the study was also provided with the questionnaire), which helped the participants to better understand the questionnaire before attempting it. To check for any bias in the study, the variance inflation factor (VIF) and tolerance (TOL) tests were used (the most commonly used test for checking biases). Table 2 shows that there is no collinearity problem with the research since all TOL values are larger than 0.1 and all VIF values are less than 10.

3.4 Model assessment

The current study's research model was transformed into structural equation modeling (SEM) for additional investigation (such as outer and inner models). For PLS-SEM, the PLS

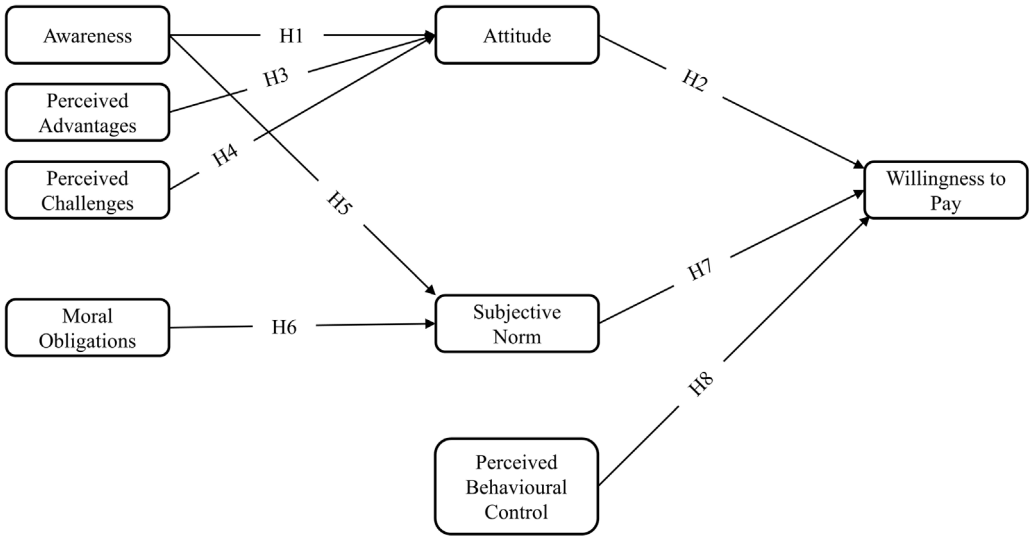

FIGURE 1
Hypothesized model.

TABLE 2 Collinearity assessment.

IVs	Tolerance	VIF
AW	0.218	4.596
AD	0.163	6.14
CH	0.211	4.731
AT	0.108	9.238
MO	0.491	2.035
SN	0.477	2.098
PBC	0.784	1.276

IVs, independent variables; AT, attitude; SN, subjective norm; PBC, perceived behavior control; AW, awareness; AD, perceived advantages; CH, perceived challenges; MO, moral obligation; VIF, variance inflation factor (Latan and Noonan, 2017).

3.0 software was used. The study utilized PLS-SEM, which is normally used to analyze complicated models and comprehend their multidimensional relationships. In the realm of management, PLS-SEM is considered a helpful multivariate analytical approach. Furthermore, the model's adaptability and suitability for analyzing numerous interactions between variables have been acknowledged in prior studies (Sarstedt et al., 2014).

4 Results

4.1 Partial least square–structural equation modeling

To evaluate the model, the study utilized a two-step approach: first, the validity and reliability of the scale employed and customized for the study were evaluated using an outer model or a measurement model; second, the model's efficacy and the proposed relationship between the proposed variables were tested using an inner model or a structural model; the (PLS-SEM) PLS-3 was utilized to assess both the inner and outer models.

4.2 Measurement model

The convergent and discriminant validity analyses were conducted for evaluating the reflective model; the results are given in Tables 3, 4. The convergent validity assessment presumes a high degree of correlation between items measuring the same construct (Hair et al., 2019) and this can be assessed from factor loading (CL), composite reliability (CR), and average variance extracted (AVE). Where the values of CL fall in the range of 0.761–0.951, the value of CL >0.5 is considered satisfactory and to fall in the acceptable range. Similarly, the values of CR that fall between 0.906 and 0.951 are considered acceptable if the values are >0.7, representing good internal consistency. After examining both CL and CR, the AVE values are also calculated. The results show that all the constructs have

TABLE 3 Constructs validity evaluation (*n* = 512).

Constructs and statements	Items	(CL)	(CR)	(AVE)	(Cα)
Awareness					
I am fully aware of climate change.	AW1	0.915	0.917	0.786	0.863
I am fully aware of environmental problems.	AW2	0.892			
I know what is RE.	AW3	0.850			
Perceived advantages					
RE improves life quality.	AD1	0.910	0.956	0.758	0.947
RE can protect the environment.	AD2	0.873			
RE is a source of green development.	AD3	0.869			
RE is a source of economic development.	AD4	0.846			
RE will reduce fossil fuel dependency.	AD5	0.840			
RE will create new job opportunities.	AD6	0.857			
RE will give energy independence.	AD7	0.897			
Perceived challenges					
RE has a high installation cost.	CH1	0.854	0.924	0.670	0.901
RE has low reliability.	CH2	0.769			
RE technologies have complex installation.	CH3	0.809			
RE systems are hazardous.	CH4	0.761			
RE systems have high maintenance costs.	CH5	0.845			
I do not have enough information about RE challenges.	CH6	0.866			
Attitude					
I am concerned about climate change.	AT1	0.900	0.940	0.758	0.920
I like to try new technologies.	AT2	0.839			
Energy-saving/conservation is important.	AT3	0.896			
The govt should set targets for increasing RE.	AT4	0.833			
I will cooperate with the govt for public awareness in my community.	AT5	0.883			
Moral obligations					
I feel it is our moral obligation to save our environment.	MO1	0.938	0.930	0.870	0.851
I feel it is our moral obligation to use clean energy.	MO2	0.928			
Subjective norms					
Most of the people important to me buy and use green energy.	SN1	0.913	0.908	0.832	0.798
Most of the people whose opinion I respect would buy green energy.	SN2	0.911			
Perceived behavior control					
I am confident that I would buy RE instead of conventional energy.	PBC1	0.951	0.950	0.904	0.894
I have the tools, skills, and knowledge to use RE.	PBC2	0.950			
Willingness to pay					
I would like to buy RE.	WP1	0.947	0.946	0.898	0.886

(Continued on following page)

TABLE 3 (*Continued*) Constructs validity evaluation (*n* = 512).

Constructs and statements	Items	(CL)	(CR)	(AVE)	(Cα)
Awareness					
I would like to pay more for RE.	WP2	0.948			

CL, cross-loadings; CR, composite reliability; AVE, average variance extracted; Cα, Cronbach's alpha; AW, awareness; AD, perceived advantages; CH, perceived advantages; AT, attitude; MO, moral obligation; SN, subjective norm; PBC, perceived behavior control; WTP, willingness to pay for renewable energy.

TABLE 4 Discriminant validity evaluation (*n* = 512).

Heterotrait–monotrait ratio (HTMT)							
AD							
AT	0.780						
AW	0.824	0.832					
CH	0.830	0.810	0.820				
MO	0.103	0.064	0.102	0.094			
PBC	0.409	0.417	0.380	0.455	0.209		
SN	0.246	0.158	0.229	0.259	0.846	0.087	
WTP	0.700	0.666	0.662	0.671	0.055	0.415	0.197

The heterotrait–monotrait (HTMT) criterion was used to estimate the results (Al Mamun et al., 2019).

an average value between 0.670 and 0.904, which means that all the constructs' values are above 0.5, which represents that all the items in the construct have a variation of more than 50% (Hair et al., 2017). Additionally, Cronbach's alpha (Cα) was calculated to examine internal reliability. The Cα values fall between 0.798 and 0.947, surpassing the minimum threshold value of 0.70, which validates the data reliability (Table 3).

Furthermore, the discriminant validity of the construct was examined through the heterotrait–monotrait (HTMT) ratio (Henseler et al., 2015), as given in Table 4. According to Henseler et al. (2015), the resulting values are <0.85, representing good discriminant validity of all the constructs of the proposed model.

4.3 Structural model assessment

The structural model assessment was performed after confirming that the structural model had no collinearity issues. The model collinearity assessment was performed by assessing the VIF and TOL values. Table 2 shows the results representing both VIF and TOL in the acceptable range (VIF values <10 and TOL values >0.1), confirming that the model had no collinearity issue and was ready for the structural model assessment.

To evaluate the suggested structural model, a comparison of the path coefficient dimensions and values with other relevant R^2 in t statistics calculation is considered important. The path coefficient and relevant importance of the proposed model are measured by utilizing the bootstrapping technique (to 5,000 resamples). The effect size f^2 measurement is also taken into account for the proposed study (Hair et al., 2017). Furthermore, Stone–Geisser's Q^2 was also considered in the study to measure the model's predictive ability.

Table 5 illustrates the bootstrapping results of the β-coefficient, t-statistics, and f^2 values for all the proposed structural paths. Except for one proposed structural path or relationship, all others were deemed to be significant (with a 99% confidence level). Factors affecting attitude, such as awareness (AW-AT, β = 0.36, t = 3.643, LL = 0.196, UL = 0.52, $p \leq 0.01$), perceived advantages (AD-AT, β = 0.37, t = 2.771, LL = 0.182, UL = 0.617, $p \leq 0.01$), and perceived challenges (CH-AT, β = 0.28, t = 2.794, LL = 0.103, UL = 0.437, $p \leq 0.01$), had a substantial favorable effect on attitude. In the case of subjective norms, both awareness (AW-SN, β = 0.13, t = 1.865, LL = -0.244, UL = −0.016, $p \leq 0.01$) and moral obligations (MO-SN, β = 0.69, t = 12.474, LL = 0.593, UL = 0.773, $p \leq 0.01$) had a substantial favorable effect on subjective norms. Regarding the components of TPB, and based on the data set findings, this study found that the attitude (AT-WTP, β = 0.52, t = 5.778, LL = 0.367, UL = 0.661, $p \leq 0.01$) and perceived behavior control (PBC-WTP, β = 0.18, t = 1.956, LL = 0.035, UL = 0.333, $p \leq 0.01$) had a substantial favorable effect on the willingness to pay, however subjective norm (SN-WTP, β = 0.10, t = 1.544, LL = −0.22, UL = 0.005, $p \leq 0.01$) had no significant effect on WTP for RE. So, overall, the hypotheses H1a, H2, H3a, H4a, H5a, H6, and H8 were accepted, while H7 was rejected. The path coefficient and degree of influence of the proposed model are shown in Figure 2.

To measure the effect size (f^2), the Cohen (1970) criteria were adopted, such as 0.02 for small-, 0.35 for medium-, and ≥0.8 for large-sized effects. All variables, except for one, were greater than the minimal threshold criterion of (0.02), demonstrating that they had an impact on the dependent variable, as shown in Table 5. SN showed no noticeable impact on the WTP for RE.

Additionally, the study also determined the coefficient of determination (R^2) and predictive relevance (Q^2) of variables

TABLE 5 Structural paths evaluation (hypothesis testing).

Structural paths	β-Value	*t*-Value	f^2	LL	UL	Results
AD—AT	0.37	2.771	0.251	0.182	0.617	Accepted
AT-WTP	0.52	5.778	0.373	0.367	0.661	Accepted
AW-AT	0.36	3.643	0.363	0.196	0.52	Accepted
AW-SN	0.13	1.865	0.034	−0.244	−0.016	Accepted
CH-AT	0.28	2.794	0.184	0.103	0.437	Accepted
MO-SN	0.69	12.474	0.946	0.593	0.773	Accepted
PBC-WTP	0.18	1.956	0.044	0.035	0.333	Accepted
SN-WTP	0.10	1.544	0.018	−0.22	0.005	Rejected

**Significance at $p \leq 0.01$. AT, attitude; AD, perceived advantages; AW, awareness; CH, perceived challenges; SN, subjective norm; MO, moral obligation; PBC, perceived behavior control; WTP, willingness to pay for renewable energy; LL, lower limit; UL, upper limit at 99% confidence interval.

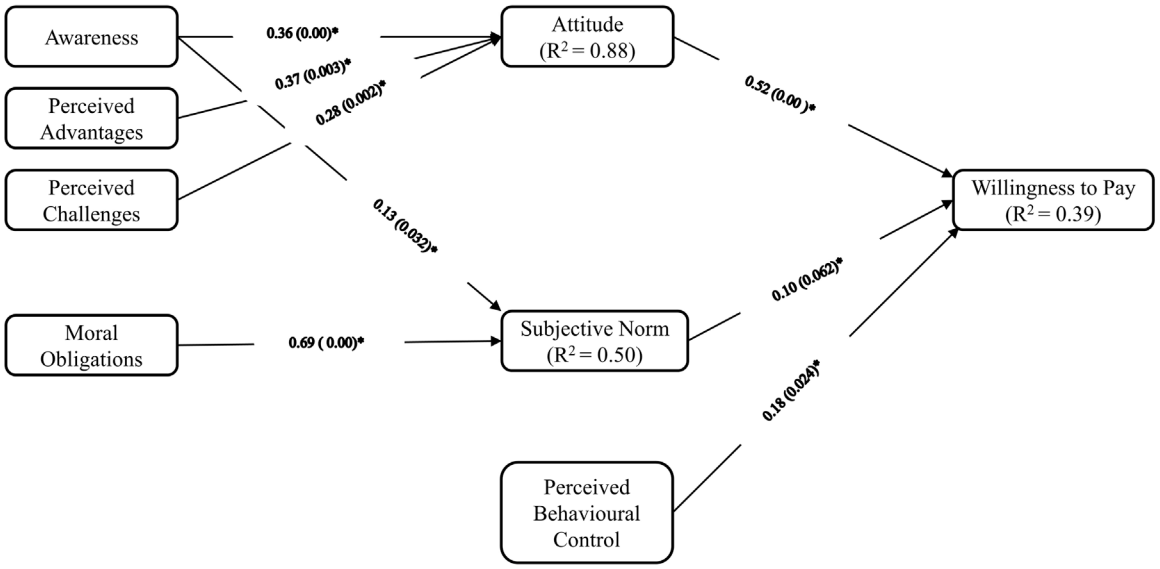

FIGURE 2
Structural equation modeling (SEM) results of complete data (n = 512), PBC, and perceived behavior control. * represents p-values < 0.01, and effect sizes (f^2) are shown in parentheses next to the path coefficient (β).

(independent with respect to dependent). The computed R^2 value for the dependent variable WTP is 0.39, which indicates that the study's overall independent variables, AT, SN, and PBC, collectively account for 39% of the variance in the dependent variable. The R^2 for the dependent variable AT and SN is 0.88 and 0.50, respectively. It is an indication that variables such as AW, AD, and perceived challenges (CH) explain a variance of 88% in the dependent variable AT, similarly variables such as AW and MO explain a variance of 50% in the dependent variable SN.

Furthermore, the study also performed PLS prediction by adopting the Shmueli et al. (2019) procedures. The predictive validity was evaluated using cross-validation with holdout sampling, and the overall findings are shown in Table 6. During the assessment, first the Q^2 values were measured and the corresponding values for AT, SN, and WTP were 0.870, 0.481, and 0.404, respectively, representing the promising predictive performance of the suggested model. In addition to this, the linear regression (LM) model was also used for the prediction assessment (Shmueli et al., 2019). The results of both LM and PLS were compared, which showed that the LM had a lower mean absolute (MAE) and mean square error (RMSE) than did the PLS, indicating a significant predictive ability of the proposed model.

4.4 Mediation effect of TPB components among background factors of behavioral intention

The proposed model presumed that TPB components will mediate the existing factors (such as AW, AD, CH, and MO) and people's WTP for RE. The mediation effect of the proposed

TABLE 6 PLS prediction evaluation.

Summary									
AT		0.870							
SN		0.481							
WTP		0.404							

PLS prediction summary									
	PLS			LM			PLS-LM		
	RMSE	MAE	Q^2 Predict	RMSE	MAE	Q^2 Predict	RMSE	MAE	Q^2 Predict
AT1	0.724	0.585	0.709	0.828	0.665	0.620	−0.104	−0.080	0.089
AT2	0.803	0.670	0.629	0.886	0.713	0.549	−0.083	−0.043	0.080
AT3	0.773	0.651	0.644	0.850	0.680	0.569	−0.077	−0.029	0.075
AT4	0.756	0.591	0.598	0.862	0.653	0.477	−0.106	−0.062	0.121
AT5	0.836	0.682	0.696	0.903	0.711	0.645	−0.067	−0.029	0.051
SN1	1.019	0.827	0.387	1.152	0.908	0.217	−0.133	−0.081	0.170
SN2	0.942	0.741	0.408	1.072	0.836	0.234	−0.130	−0.095	0.174
WTP1	1.023	0.770	0.359	1.135	0.870	0.210	−0.112	−0.100	0.149
WTP2	1.042	0.816	0.368	1.128	0.867	0.259	−0.086	−0.051	0.109

AT, attitude; SN, subjective norm; WTP, willingness to pay for renewable energy; LM, linear regression model; RMSE, root mean square error; MAE, mean absolute error.

TABLE 7 Mediation effect.

Structural paths	β-value	t-value	*p*-values	LL	UL	Results
AW-AT-WTP	0.186	3.204	0.001	0.093	0.284	Supported
CH-AT-WTP	0.146	2.439	0.007	0.048	0.246	Supported
MO-SN-WTP	0.073	1.543	0.061	−0.151	0.003	Not-supported
AD-AT-WTP	0.190	2.472	0.007	0.087	0.341	Supported
AW-SN-WTP	0.013	1.118	0.136	−0.002	0.037	Not-supported

**Significance at $p \leq 0.01$. AT, attitude; SN, subjective norm; PBC, perceived behavior control; WTP, willingness to pay for renewable energy; AW, awareness; MO, moral obligation; LL, lower limit; UL, upper limit at 99% confidence interval.

model was assessed by the bootstrapping technique as mentioned in Section 4.3. The results of the mediation effect such as the specific indirect effect and significance values (*p*-values) with 95% confidence level (bias-corrected) are given in Table 7. The results reveal that the indirect effect of awareness, perceived challenges, and perceived advantages on people's willingness to pay for renewable energy through the mediation effect AT was significant ($\beta = 0.186$, LL = 0.093, UL = 0.284, $p \leq 0.001$; $\beta = 0.146$, LL = 0.048, UL = 0.246, $p \leq 0.007$; and $\beta = 0.190$, LL = 0.087, UL = 0.341, $p \leq 0.007$, respectively). Nevertheless, the indirect effect of awareness and moral obligation on people's willingness to pay for renewable energy through SN turned out to be insignificant ($\beta = 0.013$, LL = −0.002, UL = 0.037, $p \leq 0.136$ and $\beta = 0.073$, LL = -0.151, UL = 0.003, $p \leq 0.061$, respectively). Based on the above results, we conclude that the effect of awareness, perceived advantages, and perceived challenges on WTP is mediated by AT, whereas SN does not mediate the relationship. So overall, Hypothesis 1b, Hypothesis 3b, and Hypothesis 4b are supported, whereas Hypothesis 5b and Hypothesis 6b are not supported.

5 Discussion

Growing energy demand and global warming concerns have changed the priorities of governments and regions, particularly in countries that are facing serious climate change problems. Countries around the globe, especially the developed countries, are continuously taking serious measures to avoid the negative impacts of climate change and continue to invest in green energy. They also discourage the use of energy from non-renewable sources. Developed countries can afford investing in renewable energy sources, and the people there are capable

of buying energy even by paying relatively high amounts. On the contrary, third-world countries (the developing countries) such as Pakistan have serious energy crises (where the governments are trying to meet the energy demand by any means); apart from this, poor infrastructure and economic restrictions do not provide any provision to invest in renewable energy. Also, due to inherited social and cultural issues along with financial limitations, people are reluctant to switch to renewable energy. Several studies have been conducted to check public perception, awareness, attitude, and willingness to pay for RE across the world but not in Pakistan. This study is conducted to investigate these aspects within the context of Pakistan. A highly significant social theoretical framework, TPB, along with factors such as awareness, perceived challenges, perceived advantages, and willingness to pay, was investigated.

The results show that the TPB has a significant explanatory power and is a useful framework for comprehending the intended investigational behavior. To be precise, the relationship between AT, PBC, and WTP are found to be significant and hence supports our proposed Hypothesis 2 and Hypothesis 8. Similar results have been noticed in studies relevant to environmentally friendly purchasing (Roe et al., 2000; Zarnikau, 2003). However, there is no significant relationship between SN and WTP for RE and hence Hypothesis 7is rejected. First, by directly examining the relationship between the TPB components, it is noted that people's attitude toward WTP for RE predicts intention and indirect behavior. Furthermore, this study presumes that people who have positive opinions and attitudes toward renewable energy are more inclined to use renewable energy and are willing to pay for it. As reported by Ajzen (2020), people are more inclined to act if they have a positive attitude toward it. The results also reflect that eco-literate people are hardly influenced by others' opinions or views. The study found pro-environmental behavior that might be due to people's level of understanding and information about environmental issues, climate change, and renewable energy sources. Variables such as perceived advantages, challenges, and awareness about renewable energy resources have a substantial positive effect on their attitude toward renewable energy and hence support our proposed Hypothesis 3a, Hypothesis 4a, and Hypothesis 1a. The abovementioned results are in line with those of previous studies (Nazir and Tian, 2022), and we conclude that all these variables shape people's opinion and attitude. In order to promote renewable energy, the positive aspects should be highlighted further. To effectively inform consumers about environmental challenges and renewable energy technologies, more information is needed. Second, the findings show that awareness (AW) is negatively associated with subjective norms (SNs) and hence support our proposed Hypothesis 5a. Furthermore, this study shows that SNs have no significant impact on public WTP for RE and hence reject Hypothesis 7. It is presumed that those who have proper education and knowledge about climate change and RE will hardly be influenced by others as they have their own say. A similar conclusion is also drawn in a study relevant to check consumers' buying intentions (Zhang et al., 2019). However, moral obligation has been positively associated with the subjective norm and hence supports our proposed Hypothesis H6a. We presume those who are educated and have knowledge about their responsibilities have a sense of moral obligations and act as responsible citizens. Furthermore, the study found that AT is a mediation effect between the variables (AW, AD, and CH) and WTP for RE, hence validating our proposed Hypothesis 1b, Hypothesis 3b, and Hypothesis 4b. The same conclusion had also been drawn in previous studies (Hartmann and Apaolaza-Ibáñez, 2012; Allison et al., 2013; Ntanos et al., 2018). We presume that awareness, perceived challenges, and perceived advantages can affect people's attitudes and behavior toward their willingness to pay. The more they learn about environmental issues and renewable technologies, as well as their benefits, the more likely they are to purchase renewable energy. It indicates that people are willing to pay more for green energy. On the contrary, awareness and moral obligation have no significant indirect effect on willingness to pay for renewable energy through SN and hence Hypothesis 5b and Hypothesis 6b are rejected. This means that those who have knowledge about climate change and renewable energy are hardly influenced by society, and they have their own opinion based on their understanding. Similar results have also been noticed in a study based on consumers' intention to buy energy-efficient appliances (Bhutto et al., 2021).

It is concluded that the relationship between AT, PBC, and WTP was significant. However, the relationship between SN and WTP was found to be insignificant. Similarly, the results indicate that the relationship between all the variables except for one was significant. This is a positive indication that those who have a formal education (also a relatively young population of the country) have a clear understanding of the environmental challenges, climate change, and renewable energy technologies, resulting in favor of renewable energy resources. This means that education and the right information about new technologies and their advantages are the key factors that intensify public intention toward their willingness to pay for renewable energy. Educating the masses with the right information and promoting the advantages of green energy/renewable energy will positively affect public perception toward RE. Additionally, RE plays a vital role in supporting energy security by safeguarding continuous energy provisions without interruption. The possible source of disruption can be natural (flood, heavy rainfall, etc.), technological, human interventions, cyber attitudes, and geopolitics. The International Energy Agency (IEA) defines energy security as continuous supply at affordable prices. The US Department of Energy defines it as access to various energy sources, routes, and supplies. Energy supply is essential for industries (almost all modern industries), such as food, healthcare, telecommunication, water, and sanitation. As mentioned in previous sections, Pakistan primarily depends on imported fossil fuels for energy generation. This high dependency on imported fossil fuels puts energy security at risk and puts pressure on the country's poor economy in the form of large import bills. The country has abundant RE sources such as solar, wind, biomass, geothermal, and hydro energy. The country has plenty of RE sources, which when tapped effectively can satisfy the its energy needs. By shifting to RE, the country can reduce high import bills and get energy independence and clean energy. Furthermore, it can help avoid climate change and consequences like global warming, floods (which destroy all the infrastructure), etc. So, a policy shift is required in this regard.

6 Policy implications

The findings of the study have significant implications for policymakers and relevant organizations. The study's findings

suggest that awareness and information about renewable energy play an essential role in consumers' purchase intentions. The policymakers and energy sector should formulate such policies that increase public awareness and educate the public about environmental issues, climate change, and renewable energy. Similarly, the energy sector and relevant organizations should educate the masses, provide relevant information about renewable energy technologies, and highlight the potential benefits of RE on print, electronic, and social media. This will increase customers' understanding of environmental challenges and renewable energy technologies. Giving more information about renewable energy sources and technologies will reduce the mass skepticism toward it. This will further lead consumers to purchase renewable energy (environmentally friendly and sustainable energy sources).

This study proposed that perceived challenges and advantages affect public attitude toward renewable energy. The perceived challenges and associated risks negatively affect public attitude toward renewable energy, reducing people's intentions to purchase it. Policymakers have to formulate relevant policies to facilitate energy sectors (such as waiving tax on importing relevant technologies and attracting multinational companies to invest) and give incentives to end consumption. This will encourage investors to invest in the energy sector and help reduce renewable energy costs, hence more people will purchase renewable energy. Also, the relevant companies and organizations should focus on reducing the challenges to a minimum (by improving the technology), making the installation simple and reducing installation and maintenance costs. An effective advertisement is required to attract the public to purchase renewable energy.

Similarly, the perceived advantages and warm-glow benefits positively affect public attitude and increase purchase intentions and renewable energy adoption. Policymakers should formulate policies that indicate renewable energy's importance and implement renewable energy advantages. Similarly, marketing organizations should promote the benefits of using renewable energy such as improving the quality of life, creating job opportunities, reducing fossil fuel consumption, promoting energy independence, and most importantly, protecting the environment by reducing the carbon footprints and adverse effects of climate change. This study gives new insights into public perception and willingness to pay for RE in developing countries like Pakistan. It will not only help the local policy maker and energy sectors but also aid the international market in understanding local consumers and the potential of the green energy market in the country. Further results will also help the policymaker and energy sector understand the factors that shape public perception and willingness to pay for RE.

7 Conclusion, limitations, and recommendations

Global energy demand is increasing tremendously and is mainly dependent on fossil fuels, which are exhausted rapidly and pose environmental concerns. These unsustainability and environmental concerns have changed regions' and countries' priorities from fossil fuels to green energy. This transition from non-renewable to renewable energy is more prominent in developed countries. However, developing countries face challenges, and their pace is relatively slow. The study is conducted in Pakistan to understand public perception and willingness to pay for RE. The results of the study are pretty interesting. The study reveals that public attitude and perceived behavior control are positively associated with the public's willingness to purchase renewable energy.

Additionally, the study also finds that a change to background factors such as awareness, perceived challenges, and perceived advantages has a significant positive effect on public attitude and willingness to pay for RE through the mediation effect of attitude. This means that the public will be more inclined and attracted toward renewable energy when they are aware and have the information about the environment, climate change, and renewable energy. Furthermore, the warm-glow benefits will also positively affect the public's purchase intentions. So, it is suggested that the public be educated to minimize their concerns and advertise the warm-glow benefits of renewable energy to attract the public in utilizing RE. Furthermore, the study reveals that subjective norms have no significant effect on willingness to pay for RE, and the background factors (awareness and moral obligations) have no significance on willingness to pay through subjective norms. This indicates that society, friends, and colleagues hardly influence eco-literate people who have their own opinions. So, it is necessary to attract people by equipping them with pertinent information. It will increase public understanding of renewable energy and motivate them to purchase it.

The following are some limitations of this study and recommendations for future research. First, this study only considers the four provinces of Pakistan and does not account for other regions such as Gilgit Baltistan, Azad Kashmir, and Ex-FATA (federally administered tribal areas). So, it is recommended that the study be extended throughout the country to investigate better and more accurate public perception. Second, due to time and resource constraints, the study's sample size was small and may not reflect the entire population. So, it is recommended that in future studies, the sample size should be increased to get a true representation. Third, this study was only based on a questionnaire survey. It is highly recommended that interviews be conducted with the participants. Fourth, the study only represented the educated section of the society (having formal education), which may not represent the complete spectrum of the public. It is recommended to spread out future studies to cover different segments of the society. Fifth, the study does not take subcultural factors into account, so it is highly recommended that future studies should incorporate them into their model to see how it affects public perception and purchase intentions. Finally, this study was conducted in the context of Pakistan only, so in the future, it can be extended to other regions and countries for comparative analysis.

Data availability statement

The raw data supporting the conclusion of this article will be made available by the authors, without undue reservation.

Author contributions

SD: Conceptualization, Formal analysis, Software, Writing—original draft; RW, ME, XL: Supervision, Writing—review, and editing; FN, DG, ZM, and MA: Writing, review, and editing; TA: Funding, Writing—review, and editing. All the authors discussed the results and contributed to the final manuscript.

Funding

Open access funding provided by UiT—The Arctic University of Norway.

Acknowledgments

This study had the support of national funds through Fundação para a Ciência e Tecnologia, I. P (FCT), under the projects UIDB/04292/2020, UIDP/04292/2020, granted to MARE, and LA/P/0069/2020, granted to the Associate Laboratory ARNET.

Conflict of interest

The authors declare that the research was conducted in the absence of any commercial or financial relationships that could be construed as a potential conflict of interest.

Publisher's note

All claims expressed in this article are solely those of the authors and do not necessarily represent those of their affiliated organizations, or those of the publisher, editors, and reviewers. Any product that may be evaluated in this article, or claim that may be made by its manufacturer, is not guaranteed or endorsed by the publisher.

References

Ajzen, I. (2002). *Constructing a TPB questionnaire: Conceptual and methodological considerations*.

Ajzen, I. (1991). The theory of planned behavior. *Theory Plan. Behav.* 50, 179–211. doi:10.1016/0749-5978(91)90020-t

Ajzen, I. (2012). The theory of planned behavior. *Handb. Theor. Soc. Psychol.* 1.

Ajzen, I. (2020). The theory of planned behavior: Frequently asked questions. *Hum Behav Emerg Tech* 2, 314–324. doi:10.1002/hbe2.195

Al Mamun, A., Masud, M. M., Fazal, S. A., and Muniady, R. (2019). Green vehicle adoption behavior among low-income households: Evidence from coastal Malaysia. *Environ. Sci. Pollut. Res.* 26, 27305–27318.

Al Mamun, A., Mohamad, M. R., Yaacob, M. R. B., and Mohiuddin, M. (2018). Intention and behavior towards green consumption among low-income households. *J. Environ. Manage* 227, 73–86. doi:10.1016/j.jenvman.2018.08.061

Ali, S., Ullah, H., Akbar, M., Akhtar, W., and Zahid, H. (2019). Determinants of consumer intentions to purchase energy-saving household products in Pakistan. *Sustainability* 11, 1462. doi:10.3390/su11051462

Allison, T. H., McKenny, A. F., and Short, J. C. (2013). The effect of entrepreneurial rhetoric on microlending investment: An examination of the warm-glow effect. *J. Bus. Ventur* 28, 690–707. doi:10.1016/j.jbusvent.2013.01.003

Aman, A. L., Harun, A., and Hussein, Z. (2012). The influence of environmental knowledge and concern on green purchase intention the role of attitude as a mediating variable. *Br. J. Arts Soc. Sci.* 7, 145–167.

Andreoni, J. (1989). Giving with impure altruism: Applications to charity and ricardian equivalence. *J. Polit. Econ.* 97, 1447–1458. doi:10.1086/261662

Andreoni, J. (1990). Impure altruism and donations to public goods: A theory of warm-glow giving. *Econ. J.* 100, 464–477. doi:10.2307/2234133

Bach, W. (1979). Impact of increasing atmospheric CO 2 concentrations on global climate: Potential consequences and corrective measures. *Environ. Int.* 2, 215–228. doi:10.1016/0160-4120(79)90004-7

Bajpai, P., and Vaishalee, D. (2012). Hybrid renewable energy systems for power generation in stand-alone applications: A review. *Renew. Sustain. Energy Rev.* 16, 2926–2939. doi:10.1016/j.rser.2012.02.009

Bamberg, S. (2003). How does environmental concern influence specific environmentally related behaviors? A new answer to an old question. *J. Environ. Psychol.* 23, 21–32. doi:10.1016/s0272-4944(02)00078-6

Bamberg, S., Hunecke, M., and Blöbaum, A. (2007). Social context, personal norms and the use of public transportation: Two field studies. *J. Environ. Psychol.* 27, 190–203. doi:10.1016/j.jenvp.2007.04.001

Beck, L., and Ajzen, I. (1991). Predicting dishonest actions using the theory of planned behavior. *J. Res. Personal.* 25, 285–301. doi:10.1016/0092-6566(91)90021-h

Bell, A. R., Cook, B. I., Anchukaitis, K. J., Buckley, B. M., and Cook, E. R. (2011). Repurposing climate reconstructions for drought prediction in Southeast Asia. *Clim. Change* 106, 691–698. doi:10.1007/s10584-011-0064-2

Bhutto, A. W., Bazmi, A. A., and Zahedi, G. (2011). Greener energy: Issues and challenges for Pakistan - biomass energy prospective. *Renew. Sustain. Energy Rev.* 15, 3207–3219. doi:10.1016/j.rser.2011.04.015

Bhutto, A. W., Bazmi, A. A., and Zahedi, G. (2013). Greener energy: Issues and challenges for Pakistan - wind power prospective. *Renew. Sustain. Energy Rev.* 20, 519–538. doi:10.1016/j.rser.2012.12.010

Bhutto, M. Y., Liu, X., Soomro, Y. A., Ertz, M., and Baeshen, Y. (2021). Adoption of energy-efficient home appliances: Extending the theory of planned behavior. *Sustain. Switz.* 13, 250. doi:10.3390/su13010250

Black, J., Stern, P., and Elworth, J. (1985). Personal and contextual influences on household energy adaptations. *J. Appl. Psychol.* 70, 3–21. doi:10.1037/0021-9010.70.1.3

Borges Neto, M. R., Carvalho, P. C. M., Carioca, J. O. B., and Canafístula, F. J. F. (2010). Biogas/photovoltaic hybrid power system for decentralized energy supply of rural areas. *Energy Policy* 38, 4497–4506. doi:10.1016/j.enpol.2010.04.004

Buchmayr, A., van Ootegem, L., Dewulf, J., and Verhofstadt, E. (2021). Understanding attitudes towards renewable energy technologies and the effect of local experiences. *Energies (Basel)* 14, 7596. doi:10.3390/en14227596

Canadell, J. G., Kirschbaum, M. U. F., Kurz, W. A., Sanz, M. J., Schlamadinger, B., and Yamagata, Y. (2007). Factoring out natural and indirect human effects on terrestrial carbon sources and sinks. *Environ. Sci. Policy* 10, 370–384. doi:10.1016/j.envsci.2007.01.009

Caporale, D., and de Lucia, C. (2015). Social acceptance of on-shore wind energy in apulia region (southern Italy). *Renew. Sustain. Energy Rev.* 52, 1378–1390. doi:10.1016/j.rser.2015.07.183

Carrington, M. J., Neville, B. A., and Whitwell, G. J. (2010). Why ethical consumers don't walk their talk: Towards a framework for understanding the gap between the ethical purchase intentions and actual buying behaviour of ethically minded consumers. *J. Bus. Ethics* 97, 139–158. doi:10.1007/s10551-010-0501-6

Chen, M-F., and Tung, P-J. (2014). Developing an extended Theory of Planned Behavior model to predict consumers' intention to visit green hotels. *Int. J. Hosp. Manag.* 36, 221–230. doi:10.1016/j.ijhm.2013.09.006

Cohen, J. (1970). Significant measures: *Statistical power Analysis for the behavioral Sciences*. Jacob cohen. Academic press, New York, 1969. Xvi + 416 pp. $13.50. *Science* 169, 167–168. doi:10.1126/science.169.3941.167

D'Amato, A., Susanna, M., and Mariangela, Z. (2014). "Two Shades of (Warm) Glow: multidimensional intrinsic motivation, waste reduction and recycling". *SEEDS Working Papers 2114, SEEDS, Sustainability Environmental Economics and Dynamics Studies.*

Devi, J., Pudaruth, S., and Noyaux, M. (2012). Analysing the impact of green marketing strategies on consumer purchasing patterns in Mauritius. *World J. Entrep. Manag. Sustain Dev.* 8, 36–59. doi:10.1108/20425961211221615

Devine-Wright, P. (2008). "Reconsidering public acceptance of renewable energy technologies: A critical review," in *Delivering a low carbon electricity system: Technologies, economics and policy* (Cambridge: Cambridge University Press).

Djurisic, V., Smolovic, J. C., Misnic, N., and Rogic, S. (2020). Analysis of public attitudes and perceptions towards renewable energy sources in Montenegro. *Energy Rep.* 6, 395–403. doi:10.1016/j.egyr.2020.08.059

Dmochowska-Dudek, K., and Bednarek-Szczepańska, M. (2018). A profile of the Polish rural NIMBYist. *J. Rural. Stud.* 58, 52–66. doi:10.1016/j.jrurstud.2017.12.025

Dyson, F. J. (1977). *Voi 2*. Pergamon Pres, 217–291.

Egmond, C., Jonkers, R., and Kok, G. (2005). A strategy to encourage housing associations to invest in energy conservation. *Energy Policy* 33, 2374–2384. doi:10.1016/j.enpol.2004.05.007

Eiser, J. R., Aluchna, K., and Christopher, R. J. (2010). Local wind or Russian gas? Contextual influences on polish attitudes to wind energy development. *Environ. Plan. C* 28, 590–608.

Ekins, P. (2004). Step changes for decarbonising the energy system: Research needs for renewables, energy efficiency and nuclear power. *Energy Policy* 32, 1891–1904. doi:10.1016/j.enpol.2004.03.009

Eurobarometer (2014). *Climate change, special eurobarometer 409*. Brussels, Belgium: European Commission.

Fatoki, O. (2020). Factors influencing the purchase of energy-efficient appliances by young consumers in South Africa. *Found. Manag.* 12, 151–166. doi:10.2478/fman-2020-0012

Finlay, K. A., Trafimow, D., and Moroi, E. (1999). The importance of subjective norms on intentions to perform Health behaviors. *J. Appl. Soc. Psychol.* 29, 2381–2393. doi:10.1111/j.1559-1816.1999.tb00116.x

Fishbein, M., and Ajzen, I. (1975). *Belief, attitude, intention and behaviour: An introduction to theory and research*, 27. Boston, MA, USA.

Florkowski, W. J., Us, A., and Anna, K. M. (2018). Food waste in rural households support for local biogas production in Lubelskie Voivodship (Poland). *Resour. Conserv. Recycl* 136, 46–52. doi:10.1016/j.resconrec.2018.03.022

Gadenne, D., Sharma, B., Kerr, D., and Smith, T. (2011). The influence of consumers' environmental beliefs and attitudes on energy saving behaviours. *Energy Policy* 39, 7684–7694. doi:10.1016/j.enpol.2011.09.002

Gallup (2015). *Gallup: Energy, survey on topics related to energy*.

Gneezy, U., and Rustichini, A. (2000). Pay enough or don't pay at all. *Q. J. Econ.* 115, 791–810. doi:10.1162/003355300554917

Ha, H-Y., and Janda, S. (2017). "Predicting consumer intentions to purchase energy-efficient products," in *The customer is NOT always right? Marketing orientationsin a dynamic business world* (Cham, Switzerland: Springer International Publishing), 897.

Hair, J. F., Hult, G. T. M., Ringle, C. M., Sarstedt, M., and Thiele, K. O. (2017). Mirror, mirror on the wall: A comparative evaluation of composite-based structural equation modeling methods. *J. Acad. Mark. Sci.* 45, 616–632. doi:10.1007/s11747-017-0517-x

Hair, J. F., Risher, J. J., Sarstedt, M., and Ringle, C. M. (2019). When to use and how to report the results of PLS-SEM. *Eur. Bus. Rev.* 31, 2–24. doi:10.1108/EBR-11-2018-0203

Hartmann, P., and Apaolaza-Ibáñez, V. (2012). Consumer attitude and purchase intention toward green energy brands: The roles of psychological benefits and environmental concern. *J. Bus. Res.* 65, 1254–1263. doi:10.1016/j.jbusres.2011.11.001

Henseler, J., Ringle, C. M., and Sarstedt, M. (2015). A new criterion for assessing discriminant validity in variance-based structural equation modeling. *J. Acad. Mark. Sci.* 43, 115–135. doi:10.1007/s11747-014-0403-8

Hwang, J., and Lee, S. (2017). Cognitive, affective, normative, and moral triggers of sustainable intentions among convention-goers. *J. Environ. Psychol.* 51, 1–13. doi:10.1016/j.jenvp.2017.03.003

Hwang, J. (2016). What motivates delegates' conservation behaviors while attending a convention? *J. Travel Tour. Mark.* 34, 82–98. doi:10.1080/10548408.2015.1130111

International Energy Agency I (2017). *CO2 emissions from fuel combustion 2017 - highlights*.

IPCC (2014). *IPCC. Climate change 2014: Synthesis report. Contribution of working groups I, II and III to the fifth assessment report of the intergovernmental panel on climate change*.

Ivancevich, J. M., Konopaske, R., and Matteson, M. T. (2008). *Organizational behavior and management*. 10th ed. New York, NY, USA: McGraw-Hill Education.

James Baraz, S. A. (2010). *The helper's high*. Berkeley: The Greater Good Science Center at the University of California.

Kaffashi, S., and Shamsudin, M. N. (2019). Transforming to a low carbon society; an extended theory of planned behaviour of Malaysian citizens. *J. Clean. Prod.* 235, 1255–1264. doi:10.1016/j.jclepro.2019.07.047

Kamran, M. (2018). Current status and future success of renewable energy in Pakistan. *Renew. Sustain. Energy Rev.* 82, 609–617. doi:10.1016/j.rser.2017.09.049

Kashif, M., Awan, M. B., Nawaz, S., Amjad, M., Talib, B., Farooq, M., et al. (2020). Untapped renewable energy potential of crop residues in Pakistan: Challenges and future directions. *J. Environ. Manage* 256, 109924. doi:10.1016/j.jenvman.2019.109924

Kaya, O., Florkowski, W., Us, A., and Klepacka, A. (2019). Renewable energy perception by rural residents of a peripheral EU region. *Sustainability* 11, 2075. doi:10.3390/su11072075

Klepacka, A. M., Florkowski;, W. J., and Meng, T. (2018). Clean, accessible, and cost-saving: Reasons for rural household investment in solar panels in Poland. *Resour. Conserv. Recycl* 139, 338–350. doi:10.1016/j.resconrec.2018.09.004

Kowalczyk-Juśko, A., and Bogdan, K. (2015). Assessment of the ecological and energy awareness of the citizens in rural communes. *Barom. Reg.* 13, 161–168. doi:10.56583/br.746

Lam, C. W., Lim, S. R., and Schoenung, J. M. (2011). Environmental and risk screening for prioritizing pollution prevention opportunities in the U.S. printed wiring board manufacturing industry. *J. Hazard Mater* 189, 315–322. doi:10.1016/j.jhazmat.2011.02.044

Laroche, M., Toffoli, R., Kim, C., and Muller, T. E. (1996). The influence of culture on pro-environmental knowledge, attitudes, and behavior: A Canadian perspective. *Adv. Consum. Res.* 23, 196–202.

Latan, H., and Noonan, R. (2017). *Partial least squares path modeling: Basic concepts, methodological issues and applications*. Springer International Publishing. doi:10.1007/978-3-319-64069-3

Liu, W., Wang, C., and Mol, A. P. J. (2013). Rural public acceptance of renewable energy deployment: The case of Shandong in China. *Appl. Energy* 102, 1187–1196. doi:10.1016/j.apenergy.2012.06.057

Lopes, J. R. N., Kalid, R. D. A., Rodríguez, J. L. M., and Ávila Filho, S. (2019). A new model for assessing industrial worker behavior regarding energy saving considering the theory of planned behavior, norm activation model and human reliability. *Resour. Conserv. Recycl* 145, 268–278. doi:10.1016/j.resconrec.2019.02.042

Mamun, A., Mohiuddin, M., Ahmad, G., Ramayah, T., and Fazal, S. (2018). Recycling intention and behavior among low-income households. *Sustainability* 10, 2407. doi:10.3390/su10072407

Mariani, F., Pérez-Barahona, A., and Raffin, N. (2010). Life expectancy and the environment. *J. Econ. Dyn. Control* 34, 798–815. doi:10.1016/j.jedc.2009.11.007

Masrahi, A., Wang, J. H., and Abudiyah, A. K. (2021). Factors influencing consumers' behavioral intentions to use renewable energy in the United States residential sector. *Energy Rep.* 7, 7333–7344. doi:10.1016/j.egyr.2021.10.077

Ministry of Energy (2019). *Alternative & renewable energy policy 2019 (ARE policy 2019)*.

Minton, E., Spielmann, N., Kahle, L., and Kim, C. H. (2017). The subjective norms of sustainable consumption: A cross-cultural exploration. *J. Bus. Res.* 82, 400–408. doi:10.1016/j.jbusres.2016.12.031

Miranda, G., Eberts, R. W., González, E., Foo, V., and Kulawczuk, P. (2011). *Climate change, employment and local development in Poland*. doi:10.1787/5kg0nvfvwjd0-en

Mroczek, B., and Donata, K. (2014). Social attitudes towards wind farms and other renewable energy sources in Poland. *Medycyna Środowiskowa-Environ Med.* 4, 19–28.

Muhammad-Sukki, F., Ramirez-Iniguez, R., Abu-Bakar, S. H., McMeekin, S. G., and Stewart, B. G. (2011). An evaluation of the installation of solar photovoltaic in residential houses in Malaysia: Past, present, and future. *Energy Policy* 39, 7975–7987. doi:10.1016/j.enpol.2011.09.052

Nazir, M., and Tian, J. (2022). The influence of consumers' purchase intention factors on willingness to pay for renewable energy; mediating effect of attitude. *Front. Energy Res.* 10. doi:10.3389/fenrg.2022.837007

Nguyen, T. N. (2018). Determinants which influence purchase behaviour of energy efficient household appliances in emerging markets. *Goals Sustain Dev. Responsib. Gov.*, 97–110.

Ntanos, S., Kyriakopoulos, G., Chalikias, M., Arabatzis, G., and Skordoulis, M. (2018). Public perceptions and willingness to pay for renewable energy: A case study from Greece. *Sustain. Switz.* 10, 687. doi:10.3390/su10030687

Ockenden, M. C., Deasy, C., Quinton, J. N., Surridge, B., and Stoate, C. (2014). Keeping agricultural soil out of rivers: Evidence of sediment and nutrient accumulation within field wetlands in the UK. *J. Environ. Manage* 135, 54–62. doi:10.1016/j.jenvman.2014.01.015

Onwezen, M., Antonides, G., and Bartels, J. (2013). The norm activation model: An exploration of the functions of anticipated pride and guilt in pro-environmental behaviour. *J. Econ. Psychol.* 39, 141–153. doi:10.1016/j.joep.2013.07.005

Pakistan Economic Survey (2022). "Pakistan economic survey 2021-22," in *Energy, climate change, population, labor force and employment*.

Park, E., and Kwon, S. J. (2017). What motivations drive sustainable energy-saving behavior?: An examination in South Korea. *Renew. Sustain Energy Rev.* 79, 494–502. doi:10.1016/j.rser.2017.05.150

Rahman, M., Mahmodul Hasan, M., Paatero, J. V., and Lahdelma, R. (2014). Hybrid application of biogas and solar resources to fulfill household energy needs: A potentially viable option in rural areas of developing countries. *Renew. Energy* 68, 35–45. doi:10.1016/j.renene.2014.01.030

Ritov, I., and Kahneman, D. (1997). "How people value the environment: Attitudes versus economic values," in *Environment, ethics, and behavior: The psychology of environmental valuation and degradation* (Francisco: New Lexington Press), 33–51.

Roe, B., Teisl, M. F., Levy, A., and Russell, M. (2000). *US consumers' willingness to pay for green electricity*.

Rosso-Cerón, A. M., and Kafarov, V. (2015). Barriers to social acceptance of renewable energy systems in Colombia. *Curr. Opin. Chem. Eng.* 10, 103–110. doi:10.1016/j.coche.2015.08.003

Sánchez-Fernández, R., Iniesta-Bonillo, M. Á., and Holbrook, M. B. (2009). The conceptualisation and measurement of consumer value in services. *Int. J. Mark. Res.* 51, 1–17. doi:10.1177/147078530905100108

Sarstedt, M., Ringle, C. M., and Hair, J. F. (2014). PLS-SEM: Looking back and moving forward. *Long. Range Plann* 47, 132–137. doi:10.1016/j.lrp.2014.02.008

Shmueli, G., Sarstedt, M., Hair, J. F., Cheah, J. H., Ting, H., Vaithilingam, S., et al. (2019). Predictive model assessment in PLS-SEM: Guidelines for using PLSpredict. *Eur. J. Mark.* 53, 2322–2347. doi:10.1108/EJM-02-2019-0189

Sreen, N., Purbey, S., and Sadarangani, P. (2018). Impact of culture, behavior and gender on green purchase intention. *J. Retail. Consumer Serv.* 41, 177–189. doi:10.1016/j.jretconser.2017.12.002

Stern, P. (2000). New environmental theories: Toward a coherent theory of environmentally significant behavior. *J. Soc. Issues* 56, 407–424. doi:10.1111/0022-4537.00175

Sultan, P., Tarafder, T., Pearson, D., and Henryks, J. (2020). Intention-behaviour gap and perceived behavioural control-behaviour gap in theory of planned behaviour: Moderating roles of communication, satisfaction and trust in organic food consumption. *Food Qual. Prefer* 81, 103838. doi:10.1016/j.foodqual.2019.103838

Tan, C-S., Ooi, H-Y., and Goh, Y-N. (2017). A moral extension of the theory of planned behavior to predict consumers' purchase intention for energy-efficient household appliances in Malaysia. *Energy Policy* 107, 459–471. doi:10.1016/j.enpol.2017.05.027

The Paris Agreement (2018). *Work programme under the Paris agreement*.

Uddin, R., Shaikh, A. J., Khan, H. R., Shirazi, M. A., Rashid, A., and Qazi, S. A. (2021). Renewable energy perspectives of Pakistan and Turkey: Current analysis and policy recommendations. *Sustain. Switz.* 13, 3349. doi:10.3390/su13063349

Van Gent, H. A., and Rietveld, P. (1993). Road transport and the environment in Europe. *Sci. Total Environ.* 129, 205–218. doi:10.1016/0048-9697(93)90171-2

Vasseur, V., and Kemp, R. (2015). The adoption of PV in The Netherlands: A statistical analysis of adoption factors. *Renew. Sustain. Energy Rev.* 41, 483–494. doi:10.1016/j.rser.2014.08.020

Walter, G. (2014). Determining the local acceptance of wind energy projects in Switzerland: The importance of general attitudes and project characteristics. *Energy Res. Soc. Sci.* 4, 78–88. doi:10.1016/j.erss.2014.09.003

Wang, S., Fan, J., Zhao, D., Yang, S., and Fu, Y. (2016). Predicting consumers' intention to adopt hybrid electric vehicles: Using an extended version of the theory of planned behavior model. *Transportation* 43, 123–143. doi:10.1007/s11116-014-9567-9

Wang, Z., Sun, Q., Wang, B., and Zhang, B. (2019). Purchasing intentions of Chinese consumers on energy-efficient appliances: Is the energy efficiency label effective? *J. Clean. Prod.* 238, 117896. doi:10.1016/j.jclepro.2019.117896

Wooldridge, J. M. (2015). *Introductory econometrics: A modern approach*. 6th ed. Boston: Cengae Learning.

Wu, S-I., and Chen, J-Y. (2014). A model of green consumption behavior constructed by the theory of planned behavior. *Int. J. Mark. Stud.* 6, 119. doi:10.5539/ijms.v6n5p119

Wüstenhagen, R., and Bilharz, M. (2006). Green energy market development in Germany: Effective public policy and emerging customer demand. *Energy Policy* 34, 1681–1696. doi:10.1016/j.enpol.2004.07.013

Wüstenhagen, R., Wolsink, M., and Burer, M. J. (2007). Social acceptance of renewable energy innovation: An introduction to the concept. *Energy Policy* 35, 2683–2691. doi:10.1016/j.enpol.2006.12.001

Zafar, U., Ur Rashid, T., Khosa, A. A., Khalil, M. S., and Rahid, M. (2018). An overview of implemented renewable energy policy of Pakistan. *Renew. Sustain. Energy Rev.* 82, 654–665. doi:10.1016/j.rser.2017.09.034

Zainudin, N., Siwar, C., Choy, E. A., and Chamhuri, N. (2014). Evaluating the role of energy efficiency label on consumers' purchasing behaviour. *Apcbee Procedia* 10, 326–330. doi:10.1016/j.apcbee.2014.10.061

Zarnikau, J. (2003). Consumer demand for "green power" and energy efficiency. *Energy Policy* 31, 1661–1672. doi:10.1016/S0301-4215(02)00232-X

Zhang, L., Fan, Y., Zhang, W., and Zhang, S. (2019). Extending the theory of planned behavior to explain the effects of cognitive factors across different kinds of green products. *Sustain. Switz.* 11, 4222. doi:10.3390/su11154222

Zhao, H., Gao, Q., Wu, Y., Wang, Y., and Zhu, X. (2014). What affects green consumer behavior in China? A case study from qingdao. *J. Clean. Prod.* 63, 143–151. doi:10.1016/j.jclepro.2013.05.021

frontiers | Frontiers in Energy Efficiency

TYPE Original Research
PUBLISHED 21 November 2023
DOI 10.3389/fenef.2023.1258384

OPEN ACCESS

EDITED BY
Juris Burlakovs,
Mineral and Energy Economy Research Institute, Polish Academy of Sciences, Poland

REVIEWED BY
Mariacristina Roscia,
University of Bergamo, Italy
Lina Montuori,
Universitat Politècnica de València, Spain

*CORRESPONDENCE
Fernando Yanine,
fyanine@uft.cl

RECEIVED 13 July 2023
ACCEPTED 06 October 2023
PUBLISHED 21 November 2023

CITATION
Yanine F, Sahoo SK, Sanchez-Squella A, Barrueto A and Krishna Rao C (2023), Energy homeostasis model for electrical and thermal systems integration in residential buildings: a means to sustain distributed generation systems integration.
Front. Energy Effic. 1:1258384.
doi: 10.3389/fenef.2023.1258384

Energy homeostasis model for electrical and thermal systems integration in residential buildings: a means to sustain distributed generation systems integration

Fernando Yanine[1]*, Sarat Kumar Sahoo[2], Antonio Sanchez-Squella[3], Aldo Barrueto[3] and Challa Krishna Rao[4,5]

[1]Universidad Finis Terrae, Santiago, Chile, [2]Parala Maharaja Engineering College, Berhampur, India, [3]Federico Santa María Technical University, Santiago, Chile, [4]Department of Electrical and Electronics Engineering, Aditya Institute of Technology and Management, Tekkali, Andhra Pradesh, India, [5]Department of Electrical Engineering, Parala Maharaja Engineering College, Affiliated to Biju Patnaik University of Technology, Rourkela, Odisha, India

Introduction: Integrating renewables in the distribution sector is a rapidly growing reality in many countries, amongst which Chile's stands out with an increasingly diversifiable electricity matrix. However, incorporating RES into the electricity distribution sector is altogether a steep climb at present, and seen by some as a formidable challenge for utilities. Likewise, the introduction of the Smart Grid agenda in Chile is imposing new challenges to electric utilities, mainly from a regulatory and technical viewpoint. In spite of this, big players like ENEL are moving forward decisively to meet this challenge, together with academia experts.

Methods: We model a sustainable energy system in the form of a smart microgrid operated by ENEL Chile comprising a hypothetical community we term a Sustainable Block™ representing an average residential building in Santiago. We then run simulations under different operating scenarios. The model takes into account the most recent innovation in the legal regulatory framework that governs the energy market in Chile —Law 20,571—which allows for benefits to those that generate and consume part or all of their energy needs while connected to the grid. Thus, the community considers the option of consuming green energy from the microgrid with an energy storage unit to supply electricity to the 60-apartment complex of various sizes. Under this scenario, a set of energy homeostasis strategies that comprise the homeostatic control and energy management systems help balance the electricity supply versus demand.

Results: The model proposed comprises a set of energy homeostasis management strategies that have been designed in the power control and energy management system to balance supply and demand while optimizing the availability and use of green energy. Thus, the energy homeostasis model optimizes the microgrid supply while injecting excess power to the grid. In this context, the community residents exhibit different consumption profiles, therefore they may willingly participate of the sustainable energy strategy as prosumers, displaying a thriftier consumption, and enjoying a lower electric bill while using more renewable energy. The model's energy homeostasis control and

energy management system, especially designed for electric power systems, seeks to maintain a dynamic balance between supply and demand and is being currently discussed with ENEL Chile as part of the intelligent control options for the introduction of distributed generation systems tied to the grid, in order to complement their electric power distribution services.

Discussion: The model being proposed comprises a community of residents that we term a sustainable block™ representing an average residential building in Santiago, Chile, which aims to take advantage of Law 20,571 in Chile that allows independent electric power generators to benefit by selling electricity to the grid and also allows independent consumers (mostly residential) to generate part or all of their energy needs while connected to the grid. The community may consume electricity from the microgrid with energy storage, operated by the local electric company, supplying electricity to the 60-apartment complex of various sizes. In his regard, just like in the human body where the brain, particularly the hypothalamus, is primarily responsible for the regulation of energy homeostasis, by monitoring changes in the body's energy state through various mechanisms, the role of energy storage as well as the role of prosumers are the key enabling factors of energy homeostasis and their interaction are highlighted in the overall analysis.

KEYWORDS

energy homeostasis, electric utility, distributed energy resources, smart grid transformation, electric tariff, sustainable block™

1 Introduction

"Investment in clean energy technologies is significantly outpacing spending on fossil fuels as affordability and security concerns triggered by the global energy crisis strengthen the momentum behind more sustainable options", according to the International Energy Agency (IEA) World Energy Investment 2023 report (International Energy Agency, 2023a). Soaring electricity prices, particularly in Europe, amidst the dire energy shortage situation is afflicting the population in various countries (Lan et al., 2022). Thus, leveraging distributed energy resources (DER) by means of solar, energy storage, flexible loads along with community energy integration and power sharing might well be a potential solution to the current crisis from the electric power distribution side. This is not only important and sensible, but also urgent, especially in today's world where electric tariffs are increasing as never before, and harsh, extreme weather conditions are being felt everywhere. According Fatih Birol, executive director of the International Energy Agency, upon presenting the World Energy Outlook 2022 at the Senate in Rome, stated: "Development of renewables - the key to achieving energy independence" (International Energy Agency, 2023b). His speech focused specifically on the need to increase the use of renewables amidst the current energy crisis that is whiplashing Europe and how it is causing the huge surge in the cost of electrical and thermal energy. On the other hand, Francesco Starace, ENEL's CEO, predicted that the real boom in the worldwide adoption of renewables will happen in the next few years, which seems perfectly feasible and likely given the need to transform the energy matrix, in line with a more sustainable outlook (Paris, 2022). This coincides with the Italian government seeking to provide a legal framework—similar to Law 20,571 in Chile—to incentivize the creation of renewable energy communities (Chamorro et al., 2021; Trevisan et al., 2023).

We are undergoing a profound technological change, where the internet is taking over in every major industry—electricity distribution included—through the incorporation of IOT and the widespread use of 5G networks (De Lotto et al., 2022). Such a change is transforming economies, markets, and industry structures everywhere, wherein products and services are changing rapidly and will change even more in the years to come as the world rides on the digital transformation rollercoaster impacting every aspect of our lives. Consumer behavior, jobs, labor markets and living standards will all change with the rapid pace of the digital transformation, but the impact may be even greater than expected on our society as these new sets of standards set in and people become ever more dependent on electricity and high-speed communication networks (Kimani et al., 2019; Chen et al., 2021). This will no doubt further stretch the need for electric utilities to find new, more sustainable, flexible and resilient energy solutions, that can not only sustain but also foster such societal transformation to a greener, more sustainable energy matrix, with far-reaching implications from there onward (Birol, 2020). Such energy solutions must be incorporated not only to the generation sector but also must extend to the distribution sector. A foreseeable change indeed, that we will expect to witness in the very near future, concomitantly with the advances of IOT and its far-reaching role in this massive networking transformation wave that is set to revolutionize our society as a whole.

1.1 Distributed generation systems (DGS) and the smart grid concept reshaping the electric power distribution industry

Looking at the near future, we can certainly foresee an upsurge in DGS, along with the convergence of AI (artificial intelligence) and systems communication through electric power cables in real time everywhere transforming the electric power industry, in the context of smart grid. These technologies are already changing the electric

power distribution landscape and, along with internet of things (IOT), are expected to redefine the way industries, businesses and countries' economy function. AI needs data in real time and very large processing capacity, which modern computers provide. Thus, AI enabled IoT creates intelligent machines that simulate smart behavior and provide support in decision making with little or no human interference. Looking at microgrids being enabled by AI and IOT applications, we may see that an IoT-based microgrid can provide the community of consumers—whether residential or commercial/industrial—the opportunity to enjoy independent, much more reliable and cost-effective electricity which will empower such communities and allow them to thrive, especially in areas that are rich in renewables. Hence, with the installation of an IoT-based microgrid that also has IOT applications encompassing each and every load and also the grid, owners will be able to improve the efficiency of their energy consumption substantially, which will be a key attractiveness factor for its commercialization. AI also will help to forecast energy supply and demand variations better and faster across a microgrid. With AI, a microgrid can successfully manage a large and complex energy structure, for example, a large power plant (involving several microgrids with large scale energy storage units) that provides power to a large community of residential and commercial loads in an urban area. Intelligent control systems will thus be able to monitor and adjust in real time every system variable, including new variables such as different renewable power generation units or rapidly changing energy prices when there is more power available in storage and/or the grid electric tariff is cheaper. IoT-based technology can also improve the efficiency and reliability of wind energy microgrids in those areas where there is excellent wind speed (Li et al., 2023), like in the south of Chile, especially in all of the Magallanes region. Real-time monitoring and control of the microgrid can help to minimize downtime and optimize the use of available resources, reducing operating costs and maintenance requirements (Li et al., 2023).

1.2 The role of electric utilities like ENEL Chile in the transformation of the electricity distribution sector

The role of electric utilities like ENEL Chile is of paramount importance when we realize that electric power distribution industry is a natural monopoly firmly regulated by government agencies. Hence, if we ever expect to see an overhaul of this industry towards energy sustainability, we must work with local electric companies to advance this agenda. In order to use sustainable energy systems (SES) in the form of distributed generation solutions like the microgrid, we must address the methods of harnessing the available energy resources in the most economically efficient manner. We must also ensure that renewable and alternative energy sources be utilized in conjunction with the grid, as two complex systems coupled together and assisting each other, whereby both systems interact and support each other operationally as is the case with the grid-tied microgrid (Chamorro et al., 2021; Chen et al., 2021; De Lotto et al., 2022; Paris, 2022; Trevisan et al., 2023).

Nowadays, electric power lines can also transmit communication using existing electrical wiring, whether in a building or through the electric utility grid's network cables. Hence, data signals can be sent through the wiring. An example of narrowband application of this technology is automatic meter reading currently being used by many electric utility companies (Qiao et al., 2023). With the possibility of transmitting not only electricity but also data, voice and images through their networks, the electricity distribution industry sector is to become a major player on many fronts in the immediate future if not sooner (Ghelani, 2022). Thus, in order to overcome the challenges of the near future—particularly in regards to climate change perils and the need to further energy sustainability—one of the main concerns of electric utilities must be to ensure a reliable, flexible and resilient distribution of electricity and heat to the diversity of energy consumers in today's society, a strong focus on research and development on new and existing technologies for electricity distribution transformation will be necessary. Hence, as the complexity of the electric power grids increases, along with the growing demand, so will the requirements for greater stability, reliability, security and efficiency, together with environmental and energy sustainability concerns (Lan et al., 2022; Paris, 2022; International Energy Agency, 2023b; International Energy Agency, 2023a).

Public utilities in general, and especially electric utilities have—for the most part— understood the magnitude of this change and its implications, as well as the reasons why such a change is necessary and imminent. Hence, public and private investment and cooperation in the industry, along with incentives to be more sustainable on the electricity consumption side are encouraged so as to further the industry transformation (Jain et al., 2017; Tiep et al., 2021). This is just what electric utilities like ENEL are doing in Chile and elsewhere, while bringing about a true revolution in energy generation and management (Paris, 2022; International Energy Agency, 2023b). Part of the response to the challenges of said transformation is the concept of smart microgrid and the sustainable block™ (Yanine et al., 2018a) and how these two interact with the grid. Microgrids are independent small-scale distributed generation systems, usually situated close the loads and operating connected to the grid. They can be personalized for different energy consumers and climate conditions and can be integrated in urban or rural environments, being capable of autonomously generating and storing energy for the distribution of electricity and heat to consumers (Driesen and Katiraei, 2008; Kroposki et al., 2008; Series, 2009; Rao et al., 2022). Hundreds of microgrid projects have been developed worldwide thus far in different parts of the world, adding up to a total capacity exceeding 1.7 GW (Tiep et al., 2021). The need to attenuate or ameliorate peak demand hurdles and to react swiftly and effectively to unforeseeable events that can affect frequency and voltage levels such as threats emanating from environmental threats are also a major concern of electric companies (Cordova and Yanine, 2012). The need to secure a steady flow and to smooth out abrupt changes in their energy supply in order to respond more effectively and proactively to changing energy needs, variations in the grid's power supply and to environmental disruptions are critical (Yanine et al., 2019; Yanine et al., 2022).

Considering the projected growth rates in electricity consumption, and the cost-effectiveness and the far-reaching implications of distributed generation systems like the microgrid (Adefarati and Bansal, 2019; Wolsink, 2020; Bogdanov et al., 2021), it is time to consider a more active participation of these systems in the distribution sector, with a realistic vision of future energy needs

rather than treating the solution just as an oddity in the energy matrix (Jiayi et al., 2008; ENEL, 2014; Adefarati and Bansal, 2019; Li et al., 2019). This will require incorporating traditional power system elements of analysis such as: stability analysis of microgrids in steady and dynamic states of operation, frequency control, protection coordination issues, and energy quality (Jiayi et al., 2008; ENEL, 2014; Adefarati and Bansal, 2019; Li et al., 2019). The role of the electricity users and their willingness to become more sustainable and mindful in their electricity consumption needs is also of great relevance. These new energy players, called "prosumers" by some authors (Hambridge et al., 2017) due to the nature of their role (producers and consumers), play a key role in the possibility of making DGS in the distribution sector a reality. These new customers require clear signals from the electric tariff viewpoint, so that their electricity consumption behavior is aligned with the electrical energy system's proper functioning and supportive of the sustainable green energy consumption of the community where the DGS is to be installed. We have termed this community of energy prosumers a sustainable block™ so as to act as proactive consumers that aim to benefit the whole while, at the same time, benefiting themselves (Hambridge et al., 2017).

1.3 Distributed generation systems (DGS) as key enabling technologies for advancing energy sustainability

Distributed Generation (DG) is defined as "an electric power source connected directly to the distribution network or on the consumer side of the meter" (Jiayi et al., 2008). Likewise, the IEEE Institute defines DG as the generation of electricity from installations that are sufficiently smaller than the centralized generation units (Bhadoria et al., 2013), something which clearly encompasses an ample range of electric power generation solutions that can interconnect with the grid at any point near the load in a power system. The means and conditions of such interconnection are subject to strict local regulatory operation frame and—unless it is in an isolated area, where there is no distribution grid—the local electric utility operating in the area must be involved. DGS can be of two types: the isolated type, supplying the local consumption on a discrete basis, usually in the case of small communities (Paris, 2022) or else, operating connected to the power grid, supplying electrical energy to the community of users and also to rest of the power system if there is excess generation, after the batteries are fully charged. There are many technical and economic advantages related to the implementation of distributed generation in distribution sector that have been widely researched, such as the reduction of active and reactive energy losses, improvement in reliability, reduction of a blackout probability and peak hours' demand reduction; nevertheless, the regulatory aspects have not been covered in depth (Jiayi et al., 2008; ENEL, 2014). However, there is little research related to the social impact regarding the benefits of new policies and regulations that can foster and advance DG in the electric power distribution sector, along with specific urban challenges or local governance factors are likewise not widely analyzed (Gottwalt et al., 2011; Bhavsar et al., 2015; Jain et al., 2017).

An important area of research for distributed generation has been energy management and differential pricing strategies (Gottwalt et al., 2011; Palensky and Dietrich, 2011; Bhavsar et al., 2015; Cheng et al., 2019), some authors have proposed the establishment of a demand side management (DSM) systems based on an hourly price variation price-structure, as a means to further energy sustainability policies based on energy efficiency and off-peak consumption practices (Wolsink, 2020; Yanine et al., 2022). However, electricity demand peaks are not always of regular occurrence but rather sporadic, and may occur at unforeseen times, usually due to abrupt changes in weather patterns, as well as other environmental or social phenomena, causing a severe strain on the electric power supply services for utilities. One way to minimize such occurrence is by curtailing demand and promoting a more sustainable use of electricity when renewables are present in DGS connected to the grid. Electric utilities may offer alternative tariff structures like, for example, Multi-Time-Of-Use (Multi-TOU) and Multi-Critical-Peak-Pricing (Multi-CPP) (ENEL, 2011; Wolsink, 2012; ENEL, 2017) both of which offer economic incentives to those that willingly accept to use them.

Likewise, in electrical distribution systems, distributed generation (DG) can be beneficial for consumers as well as for electric utilities for a number of reasons, many of which have already been cited in this paper. This is specially so in places where the electric supply from centralized power generation plants is impractical/unfeasible due to technical and/or economic reasons or when—as in Chile's case for the most part—the electricity distribution networks' infrastructure is frail, vulnerable and without the appropriate backup systems should natural disasters or environmental threats strike all of a sudden. The epitome of distributed generation systems (DGS) is no doubt the microgrid, employing renewable and non-renewable energy sources. The main generation resources that comprise a microgrid are wind and solar energy, along with rapid dispatch energy sources like small gas turbines, microturbines, and fuel cells, and sometimes small hydroelectric power plant.

In Chile, in particular, the ENEL Group is actively developing renewable energy generation and advancing its Smart Grid transformation agenda. A good example of this is its Ollagüe project in Chile (ENEL, 2017). The Ollagüe plant is a successful project that combines innovation, taking advantage of the natural sources available in the territory, public-private alliances and the participation of the local community, creating an electrification model that can be replicated in other isolated communities. It is an isolated microgrid capable of providing 24 h of continuous energy to the neighboring Ollagüe village of Chile situated in the far northern region of the country (ENEL, 2017). It is the first hybrid plant in the world that combines solar, wind and cogeneration energy with electrical energy storage in molten salt batteries, providing energy to homes at high altitudes and in extreme climatic conditions, with temperatures between −20°C and +20°C. Ollagüe is a small town located on the border between Chile and Bolivia, at more than 3,500 m above sea level, and at a distance of 160 km from Calama. Less than a hundred families from the Quechua community live there, whose main activity is sheep farming. Since December 2014, part of the reality of these families has changed, since an innovative and sustainable idea was implemented in the place, which allowed the community to have sustainable electricity since then, 24 h a day. Enel Green Power (EGP) built a state-of-the-art renewable energy plant, which uses the

resources of the Sun, wind and storage, configuring an off-grid system, which has allowed the community constant access to electricity.

Another important development in the electric power distribution industry towards the Smart Grid transformation is ENEL's Isernia Project (ENEL, 2011). Isernia is a town and commune in the southern Italian region of Molise, and the capital of the province of Isernia. The Isernia Project, where ENEL is developing its first smart grid in Italy (ENEL, 2011), provides a new approach for distributed generation by connecting and managing a renewable energy generation, distribution network and storage systems using lithium-ion batteries, as well as by encouraging distributors and customers to play a new, more active role as 'prosumers' who can produce and consume energy at the same time (Jiayi et al., 2008). On the other hand, policymakers are increasingly focusing on strategies to decentralize the electricity distribution sector, and also seeking to advance in a more flexible and nimble electric power distribution operation and the advancement of renewables (Lan et al., 2022; International Energy Agency, 2023a).

An incentive for advancing renewable energy generation and consumption is the current law 20/25 in Chile for reconverting the energy matrix to achieve a larger percentage of renewables in the generation sector (Nasirov et al., 2015). In October of 2013, the Chilean government enacted Law 20/25 and announced entry into force of the Concessions Law. Initiative doubled the commitment to clean energy from 10%, established in the previous regulations for the year 2024, to 20% for the year 2025 meaning that 20% of all the energy sold must come from non-conventional renewable energy sources, thus doubling the goal set forth by Law 20,257. Thus, the energy sustainability road map of Chile is set on solar energy as the most abundant and least expensive means of electricity generation, even more so than hydroelectricity generation as of today. This explains itself in part by the stark drop in solar photovoltaic (PV) generation costs, while the technology has attained greater efficiency levels, and also by the many environmental, social and legal hindrances that new hydroelectricity projects have faced over the last 15 years, most of them never seeing the light and therefore, making it very difficult for investors to dare venturing on new such projects which have high infrastructure and civil engineering costs coupled with an uncertain destiny down the road (Nasirov et al., 2015; Silva and Nasirov, 2017).

The path towards energy sustainability is a difficult one, and it must also be walked gradually since, aside from major investments on the part of electric utilities, it requires complex legal and social adjustments, as well as greater societal awareness of its need no matter what. It is a necessity which presupposes the incremental adoption of new and available technologies, many of which are changing drastically with new advances in electronics and communications technologies. A shift in industry practices and policies is indispensable, coupled with the proper economic incentives to take such a big leap if we are serious about advancing towards a more sustainable and secure electric power supply (Moslehi and Kumar, 2010; Basak et al., 2012).

The article comprises five distinct sections, beginning in section one with the introduction to the subject and a preamble addressing the electric power distribution industry's changes and technological transformation of the distribution sector, especially with regard to the Smart Grid agenda that is being led by major electric utilities like ENEL worldwide. The methodology comes in section two and right after, we present the energy homeostasis system model and its unique characteristics and operation for smart microgrid systems tied to the grid. Section three explains the control and energy management of the model and its approach to controlling electric supply based on the demand characteristics of the consumers within a sustainable block—a 60-story residential building in Santiago de Chile. Section four presents the simulation results and discusses their significance and implications in terms of implementing sustainable energy consumption strategies in electricity distribution sector. Conclusions come afterward.

2 Methods

We model a sustainable energy system in the form of a smart microgrid operated by ENEL Chile comprising a hypothetical community we term a Sustainable Block™ representing an average residential building in Santiago. We then run simulations under different operating scenarios. The model takes into account the most recent innovation in the legal regulatory framework that governs the energy market in Chile —Law 20,571—which allows for benefits to those that generate and consume part or all of their energy needs while connected to the grid. Thus, the community considers the option of consuming green energy from the microgrid with an energy storage unit to supply electricity to the 60-apartment complex of various sizes. Under this scenario, a set of energy homeostasis strategies that comprise the homeostatic control and energy management systems help balance the electricity supply *versus* demand. Results are assessed and analyzed thereafter. The overall objective is to maximize green power supply capacity, wherein the different energy users and their energy consumption profiles play a crucial role as "active loads", being able to respond and adapt to the needs of the grid-tied microgrid while enjoying economic benefits.

2.1 The energy homeostasis system's model and its implications for energy sustainability

Here we explore the role of energy homeostasis in regards to electricity tariffs and energy use by consumers. Energy homeostasis is that property of energy systems by which they can reach and maintain a dynamic balance between supply and demand at all times just like a governor would in traditional electric power plants, albeit somewhat differently. Here, the energy system is able to respond to perturbations stemming from technical issues, environmental challenges and fluctuations in demand very rapidly and effectively so as to attain optimal equilibrium between the amount of power available for supplying the loads and the demand for energy coming from the loads (Cordova and Yanine, 2012; Caballero et al., 2013; Yanine and Sauma, 2013; Yanine et al., 2014a; Yanine et al., 2017; Yanine et al., 2018a; Yanine et al., 2018b; Yanine et al., 2019; Yanine et al., 2022). This is essential in order to preserve systems stability and continuity of operations in electric power systems' operation. Here both reactive and predictive homeostasis play a key role in sustaining the energy system's functional integrity. Both reactive and predictive homeostatic control have the same purpose: to maintain the current state of

the energy system within an operationally appropriate range (homeostasis) so as to be able to respond to the energy demand from the loads. Reactive homeostatic control does this by counter-regulatory reactions via a feedback mechanism to deviations of system-critical variables from their operational range. Predictive homeostatic control is distinguished from reactive homeostasis in the sense that the regulatory mechanisms do not operate after the facts (reactive) but before, anticipating (predicting) the occurrence of a given scenario and thus adjusting the energy system accordingly. These system-critical variables are part of the control system's model (Cordova and Yanine, 2012; Caballero et al., 2013; Yanine and Sauma, 2013; Yanine et al., 2014a; Yanine et al., 2017; Yanine et al., 2018b; Yanine et al., 2019; Yanine et al., 2022). The control system's model also measures performance in terms of customer satisfaction when he or she obtains the benefits set forth by the tariff structure and the microgrid takes advantage of Chilean law that regulates self-generation (Yanine et al., 2019; Yanine et al., 2022). The system seeks to offer economic incentives for customers who consume more thriftly and sustainably and also generates economic benefits the electric utility (ENEL, 2014). Predictive homeostasis in energy systems, on the other hand, has to do with the energy system's capability to foresee very near future scenarios, monitor in real time key variables (defined in the control system) of the electric power grid, the loads, along with the weather, and environmental indicators such as heat, wind speed, solar irradiance and also to be able to anticipate events and prepare itself in order to procure the necessary resources, make the necessary adjustments and communicate them to the consumers and to the system's operator (ENEL, 2014; Hambridge et al., 2017).

Our homeostatic control model proposes a hybrid tariff which mixes an hourly rate based on time-of-use (TOU) with a rate based on the deviation of the system's frequency—something which may affect voltage levels—and whose value represents the imbalance between generation and consumption. This hybrid rate, which can be calculated every minute, allows for secondary frequency regulation and becomes an economic incentive for those that exhibit a sustainable and responsible electricity consumption. The homeostatic control model has been tested successfully in our microgrid lab and proof of concept has been discussed with ENEL for the purpose of assessing its potential implementation in the electricity distribution sector in Chile and other parts of the world.

2.2 The difference between a sustainable block™ and the single customer scheme

Customers must have intelligent metering installed by the electric company in order to use this grid-connected microgrid control model that also encompasses communication system between the microgrid operator (the local electric company) and the community residents. The model has been proposed to ENEL, considering the incorporation of a distributed generation (DG) plant like a smart microgrid discussed here, based on solar PV energy with energy storage capability. Customers can evaluate the pros and cons of the contract and choose willingly whether to be part of the energy sharing from the microgrid or not. Those that choose not to be part may continue to use grid supply only just like they regularly do. Those that do agree to be part of the sustainable block™ will be able to access electric power supply at more convenient rates as a whole but abiding by the standards and constraints imposed by the DG plant generating renewable energy.

The above model results in significant economic benefits for the entire community and for the electric utility as well. It is important to note here that difference between the sustainable block™ scheme, as opposed to the usual single load figure, is the fact that a sustainable block™ encompasses not only the electric utility's customers but also the grid-tied microgrid, including the energy storage unit (Cordova and Yanine, 2012; Yanine et al., 2018a; Yanine et al., 2019; Rao et al., 2022; Yanine et al., 2022). The algorithms presented here as part of the control model are based on the energy homeostasis model derived from previous work by the corresponding author, which was done on homeostatic control of sustainable energy systems (SES). The research initiative was born in 2010 upon initiating his doctoral program and continued after that with his postdoctoral fellowship successfully realized with the support and collaboration of ENEL Chile.

2.3 The renewables outlook in the expansion of DGS and how it could change the distribution sector: The case of ENEL in Chile

Unlike the far north and many regions of the south of Chile, where wind is quite abundant and stable thus ensuring a regular wind supply, unlike the central region where solar photovoltaic (PV) is the norm. Currently there are 20 wind power generation projects underway in various regions of northern and southern Chile, and more are expected in the years to come but clearly Chile renewables' investment is much more geared towards solar because of its unique abundance and superior solar irradiance being one of the best in the world (Londono, 2017). Renewable energy projects are large and very complex engineering projects that demand sizeable investments and are required by law to submit several feasibility studies, including an environmental impact assessment, before any work can begin. In the case of wind power plants this is much more so but nevertheless wind generation power plants are not new in Chile, and have been around for some time now and are expected to grow in numbers towards the year 2025 like some of the large projects of wind farms built in northern and southern Chile (Morgan et al., 2014). However, all of these large projects entail significant infrastructure investment and engineering costs plus a good negotiation with the local communities, most of which are reluctant to see their landscapes invaded by such monstrous towers or by large surfaces covered by solar panels. Small hydroelectric plants are also disliked and regarded as invasive (Yanine et al., 2014b; Leal-Arcas et al., 2023). Such endeavors can only be offset by a good size project that fully complies with the local environmental and regulatory legislation, and that can render the expected benefits that such projects yield for investors.

2.4 The residential building case study and the sustainable block™ concept in action

The residential community, as already explained, is termed a sustainable block™. The term comprises the synergistic and positive interaction and emergent behavior supportive of sustainable energy

systems' operation that complex systems interaction of this nature can be expected to exhibit (Caballero et al., 2013; Yanine and Cordova, 2013; Yanine and Sauma, 2013; Yanine et al., 2014a; Yanine et al., 2014b; Yanine et al., 2014c; Yanine et al., 2015; Yanine et al., 2017; Yanine et al., 2018b). The characteristics of the residential community are shown in Table 1 below.

As mentioned before, the scenario under study is comprised of a solar PV system, a group of residential customers, the electric distribution grid and an energy storage unit (battery bank). The microgrid is operated by ENEL Chile and residents can get electricity from the microgrid and from the local grid, albeit with different tariffs, as an incentive to those residents that choose to abide by the sustainable energy system's arrangement of green energy sharing. The microgrid's excess energy generation, after the batteries are fully charged, is to be injected to the grid, as it is not being used by the residential community, thus considering the incentive that the current Net Billing law (law 20,571 in Chile) offers (Energypedia, 2015) and this is reflected in the simulation results.

The model's energy homeostasis control and energy management are shown in Figure 1. It especially designed for electric power systems, seeks to maintain a dynamic balance between supply and demand and is being currently discussed with ENEL Chile as part of the intelligent control options for the introduction of distributed generation systems tied to the grid, in order to complement their electric power distribution services.

2.5 Redefining energy sustainability: How the homeostatic control system works and how the benefits are attained

The control system monitors in real time the available capacity and the power demand from the loads, considering demand side projection, in order to decide whether to use from the microgrid only, including the energy storage unit or to also draw power from the grid, and this goes on throughout the day. In addition, the storage status of the batteries is continually monitored, looking always to minimize operating costs. The energy storage unit managed by the homeostatic control system decides when and how much energy to charge or discharge, drawing energy from the energy storage unit when the electric tariff is more expensive. The system keeps track of each resident's electricity consumption through the smart meter. Those residents who exhibit a sustainable electricity consumption that falls within the consumption ranges that the energy pool can support considering tariffs structure and the microgrid's energy supply for the different hourly blocks, get to enjoy a lower electric bill. On the other hand, those who choose to consume more power in said hourly blocks, falling, outside the sustainable range, foregoing the needs of the rest of the community (thriftless consumption) will be notified through an interface and/or alarm and will be disconnected by smart switches (smart plug), leaving them with the grid-only option.

The billing process is calculated by the electric company with data from the smart meter processed by the billing procedure in the microgrid. The system is responsible for prorating payments between users according to their monthly electric consumption. Those customers who choose to align with the energy sustainability strategy of the community, preferring to consume less energy and to move their power-intensive consumption (e.g., dishwasher, washing machine, vacuum cleaner, electric heater) to hours of less demand receive economic compensation (reward) with a lower electric bill.

TABLE 1 Building description.

Location	Santiago, Chile
Stories	15
Dimensions	30 x 20 x 50 m
Apartments	60

2.6 The energy homeostasis equations behind the power control and energy management systems of the microgrid

Below are the equations that express the energy homeostasis (dynamic balance) model that is the basis of the homeostatic control system operating in the microgrid the energy homeostasis regulation mechanisms are discussed in length in these articles (Caballero et al., 2013; Yanine and Sauma, 2013; Yanine et al., 2014a; Yanine et al., 2017; Yanine et al., 2018a; Yanine et al., 2018b):

$$E_{equilb} = P_{supply}(x)PH(u)RH(v)S(\alpha)$$
$$= E_{consump}(u,v,\alpha) + \frac{d}{dt}E_{consump}(u,v,\alpha)$$

where $P_{supply} = Real\ Power + Reactive\ Power = (P+Q) - Losses$

$$E_{management} = P_{supply}(x) - P_{demand}\ subject\ to\ PH(u)RH(v)S(\alpha)$$

The power supply is a function of the internal state of the energy systems at time t_0 represented by variable x and also conditioned by predictive and reactive homeostasis functions $PH(u)RH(v)$ (Yanine et al., 2017). Variables u and v represent the specific predictive and reactive homeostasis functions respectively. In addition, the conditioning function we term $S(\alpha)$ is a function that represents the overall (operational) sustainability state of the system. Thus, $S(\alpha)$ is in essence a systemic function that conditions the system's output. In order to use a helpful analogy to illustrate and better clarify the role of $S(\alpha)$ let us think of the heart's pumping blood and oxygen in the human body; where cardiac output is the product of stroke volume and heart rate. Both are under the control of the sympathetic nervous system (the controller). Stroke volume is also affected by changes in preload, contractility and afterload, and their interaction. Very similar conditions are present in the sustainable energy system (SES) (Yanine et al., 2017), where we have the interaction of predictive and reactive homeostasis functions with the systemic function $S(\alpha)$. Hence, all three are responsible for the dynamic energy balance that is expected to be maintained at all times within the system and that we term energy equilibrium, E_{equilb} (Yanine et al., 2017). Likewise, the Energy management $E_{management}$ is equal to the power supply minus the power demand subject to predictive and reactive homeostasis functions and the systemic function $S(\alpha)$.

TABLE 2 PV panels' characteristics (Yanine et al., 2020).

Type of module	YL270P-96
Maximum power P_{max}	270 W
Open circuit Voltage V_{OC}	37.9 V
Short circuit current I_{SC}	9.27 A
Maximum power voltage V_{mpp}	30.7 V
Maximum power current I_{mpp}	8.6 A
Module efficiency	16.6%
Dimension	1640 x 990 x 35 mm

$S(\alpha)$ is a systemic function responsible for assessing the overall system's functionalities so as to safeguard the system's sustainability and is dependent upon several functional factors operating adequately in the grid-tied microgrid (Yanine et al., 2017). Sustainable energy systems are composed of subsystems, and each one of them serves its own purpose but also interacts with other systems in ways that help the larger system, that is the grid-tied microgrid connected to the loads, to function as intended. The subsystems that comprise the whole must work well both independently and together for the system to function as intended.

The $E_{management}$ function takes into account the projected power supply minus the projected power demand subject to the predictive and reactive homeostasis functions $PH(u)RH(v)$ but $S(\alpha)$ also plays an important role in terms of assessing the overall system state (Yanine et al., 2017).

The demand response paradigm is an interesting option that makes sense when you are sharing a limited supply of green energy and are seeking economic compensation for keeping a lower, more thrifty and sustainable energy consumption. The benefits to consumers, such as those considered in the example analyzed in this paper, in the form of an economic compensation or reward for their thrifty and efficient electricity consumption particularly during certain times of the day and/or exhibit a willingness to be flexible in the timing of their electricity consumption needs. Hence, one of the emerging trends in this area is the enactment of laws and regulations such as the Net Billing law in Chile (Energypedia, 2015) that incentivizes or encourages the use of distributed generation of electricity by means of renewables (Yanine and Cordova, 2013; Energypedia, 2015).

For this project we used commercial solar panels readily available in the local market, whose characteristics are the following, in standard test conditions (STC) (i.e., irradiance of 1000W/m^2, spectral value of 1.5 a.m. and temperature of 25°C). These are presented below in Table 2. (Yanine et al., 2020). The resulting installed power capacity of the DG plant is 41.58 kW (Yanine et al., 2020).

To obtain the generation profiles of the photovoltaic plant, in the time scale required (15-min time intervals), a simplified model is adopted according to (Van Aubel and Poll, 2019). The power output of the plant will be given by the relation (1).

$$P_g(t) = n \cdot A_p \cdot I_i(t) \cdot \left[1 - 0.0042\left(\frac{I_i}{18} + T_i - 20\right)\right]\eta_0\eta_{inv} \quad (1)$$

P_g: Generated power in time period t by the PV plant in kw
n: Number of photovoltaic (PV) panels, $n = 154$
A_p: Panel area, $A_p = 1.64m^2$
$I_i(t)$: Horizontal plane radiation in time period t for Santiago, Chile.
$T_i(t)$: Temperature in time period t for Santiago, Chile.
η_0: Efficiency of the solar module under STC conditions, $\eta_0 = 0.166$.
η_{inv}: Inverter efficiency, $\eta_{inv} = 0.98$.

Solar irradiation and temperature data are both pieces of information that can be readily obtained from the Department

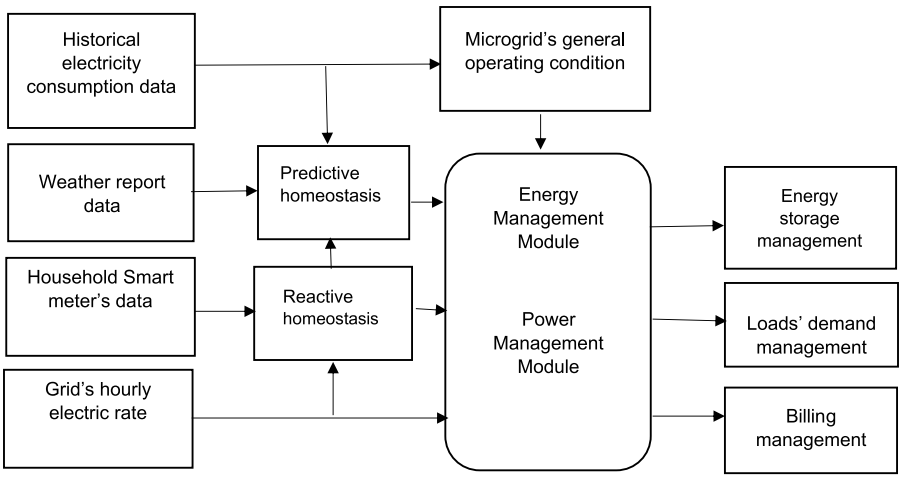

FIGURE 1
Above is the energy homeostasis model for the sustainable block™. Both the energy management system (EMS) and the power management system (PMS) comprise the microgrid's homeostatic control, inspired by energy homeostasis principles (Yanine et al., 2020).

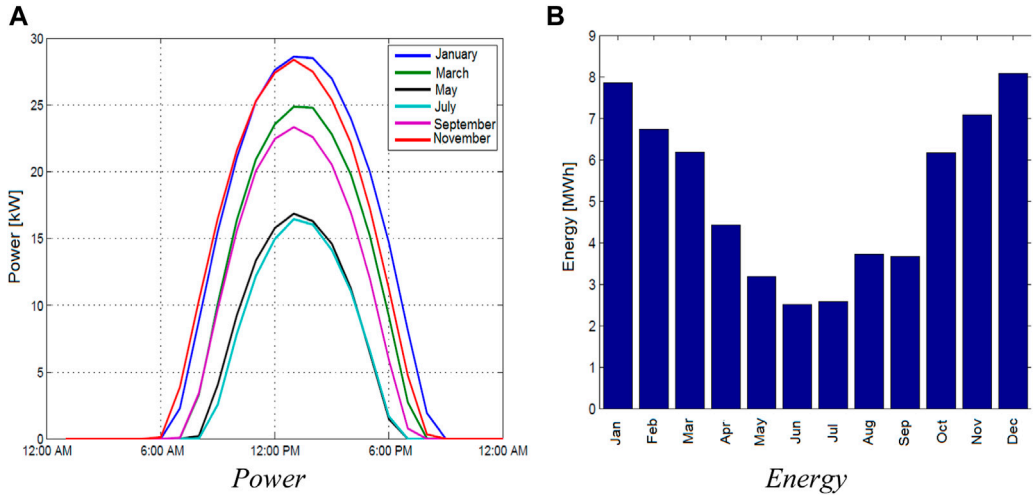

FIGURE 2
Generation of the PV plant. **(A)** depicts the electric power generated per hour on average for the different months of the year, while **(B)** shows the energy generated by the photovoltaic plant per month.

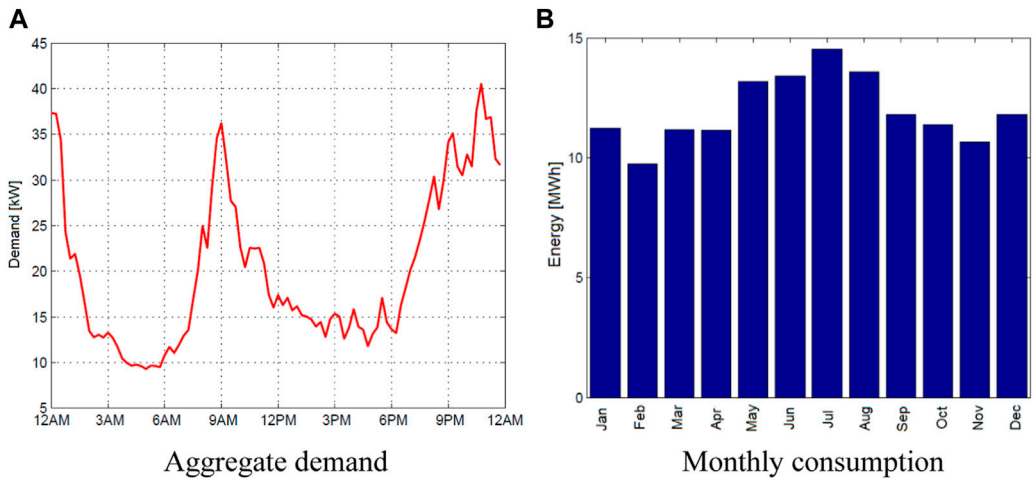

FIGURE 3
Above are curves of aggregate demand and monthly consmption of the community's residents of the 60 apartments in a residential building in Santiago, Chile which, along with the microgrid and the grid comprise a sustainable block™ (Yanine et al., 2020).

of Geophysics of the University of Chile [http://www.dgf.uchile.cl]. To validate the model, the annual energy generated was contrasted with the results obtained and properly adjusted afterwards using a proprietary software especially developed by the research team for this testing. Below are shown the electric power generated per hour on average for the different months of the year in Figure 2A, and the energy generated by the photovoltaic plant per month throughout the whole year in Figure 2B.

Figure 2A depicts the electric power generated per hour on average for the different months of the year, while Figure 2B shows the energy generated by the photovoltaic plant per month.

2.7 The role of smart metering and why should electricity users care to use them

Smart meters are essential for electric companies to keep track of the billing and also of the overall state of the electric supply networks, helping optimize the grid services. A smart meter is an electronic device that records energy consumption of the electric company's customers and exchanges consumption data with energy suppliers, which is used for monitoring and billing. In addition to storing energy consumption data, smart meters also allow real time information on the status of the electricity grid to be collected by the system's operator, including making it possible to identify supply interruptions, inefficient voltages and incorrect connections. The smart meter considered in this study

TABLE 3 Comparison table between lead-acid vs. lithium-ion batteries.

	Lead acid	Lithium-ion
Energy Density (Wh/L)	100	250
Specific Energy (Wh/kg)	40	150
Initial Cost ($/kWh)	120	600
Cycle life	1,200 at 50% DOD	1,900 at 80% DOD
Typical SOC window	50%	80%
Duration	20 years	20 years
Voltage increment	2	3.7 V

TABLE 4 Electricity tariffs according to Chilean electricity law and their characteristics. Source: https://www.cne.cl/tarificacion/electrica/.

	BT4.1 AT4.1	BT4.2 AT4.2	BT4.3 AT4.3
Energy	Measure	Measure	Measure
Power at Peak Hours	contracted	Measure	Measure
Power at off-Peak Hours	contracted	contracted	Measure

(model CERN 1 offered by ENEL Smart Metering Division), measures electrical variables of customers, stores it every 15 min and then sends the data via the power line (known as PLC for power line communications) to where it will be processed. This information reaches a data concentrator, installed close to the distribution transformer, which in turn transfers the information to the electric company via the internet. The smart meter allows the electric company to monitor and process electricity consumption, monitor failures and bill the customers much more accurately than human reading. The energy supplier needs the relevant meter readings, which in many occasions it cannot read directly from the meter (Zheng et al., 2013; Van Aubel and Poll, 2019).

2.7.1 Demand side evolution and its role in the energy homeostasis model

The demand evolution being considered in the model is obtained from a pilot plan supported by ENEL which consists on the installation of 100 residential smart meters in Huechuraba, a suburb of the city of Santiago, Chile which presents large and growing residential and commercial urban communities since 2018.

Figure 3 below illustrates the demand curves and the monthly consumption of the sustainable block™, corresponding to 60 residential customers. In (a) we have the aggregate demand curve throughout the day and in (b) we have the monthly energy consumption throughout the year.

2.8 The role of energy storage systems (ESS) and its relation with energy sustainability in the context of the energy homeostasis model

The role of the energy storage system is of great imperative in order to achieve the energy sustainability objectives of the system. Energy storage is essentially a buffer that acts as an energy homeostasis enabler (Caballero et al., 2013; Yanine and Sauma, 2013; Yanine et al., 2014a; Yanine et al., 2017; Yanine et al., 2018a; Yanine et al., 2018b; Yanine et al., 2020). Energy storage can provide electricity in response to sudden changes or drops in electricity, provide electricity frequency and voltage regulation, and defer or avoid the need for costly investments in transmission and distribution to reduce congestion and also allows the residents to consume cheaper energy during peak hourly demand, especially when the electric tariff is higher during winter months than in spring and summer months. Energy storage also allows for peak shaving to occur, as shown in Figure 4, making possible for the community residents to reduce their power consumption ("load shedding") quickly and for a short period of time to avoid a spike in consumption and higher costs. This is made possible in part by the on-site power generation system, namely the microgrid, but also, and more importantly, by relying on the energy storage system.

Energy storage also provides flexibility to the system and is a key supporting tool for renewable energy integration in the electric power distribution sector (Tejada-Arango et al., 2019; Zsiborács et al., 2019). It can balance centralized and distributed electricity generation, while also contributing to energy security. Energy storage can also provide a complement to grid supply, supporting the integration of higher shares of variable renewable energy in electric transportation services such as buses and subway, buildings or industry (Tejada-Arango et al., 2019; Zsiborács et al., 2019).

Lithium-ion batteries provide 100% of their rated capacity, regardless of the rate of discharge. Lead-acid batteries, on the other hand, are less efficient but cheaper, and typically provide less usable energy with higher rates of discharge. They are usually limited to 50% of the rated capacity to prevent diminished lifespan (Tejada-Arango et al., 2019; Zsiborács et al., 2019). Below in Table 3 there is a comparison between the two types. Notice the difference of cycle life between the two. While the lead-acid battery can reach a maximum of 1,200 cycles at 50% DOD, the lithium-ion battery can reach 1900 cycles at 80% depth of discharge (DOD).

2.9 Electric tariffs' considerations when implementing DGS in the residential sector

An important element to consider in homeostasis-based supervisory control is the rate or tariff regulation being applied by the electric company operating the distribution of electricity, which normally takes into account the fact that the energy demand is differentiated per hour. Therefore, 'peak hours' of electricity demand are considered between 6 p.m. and 11 p.m. from the first of April to the 30th of September, as defined in the Chilean regulation law. The BT2 and AT2 tariffs are purchased power, on the other hand, BT3 and AT3 rates are maximum demand registered. In our model we applied the above rates considering electric consumption during off-peak and on peak hours and according to the following criteria.

a) When the purchased power or the maximum energy demand registered is being used during peak hours, regardless whether said power or energy is or is not used in other hours of the year, the consumption will be qualified as "present on peak" and the corresponding unit price will be applied. It is understood that the purchased power or the maximum energy demand registered is

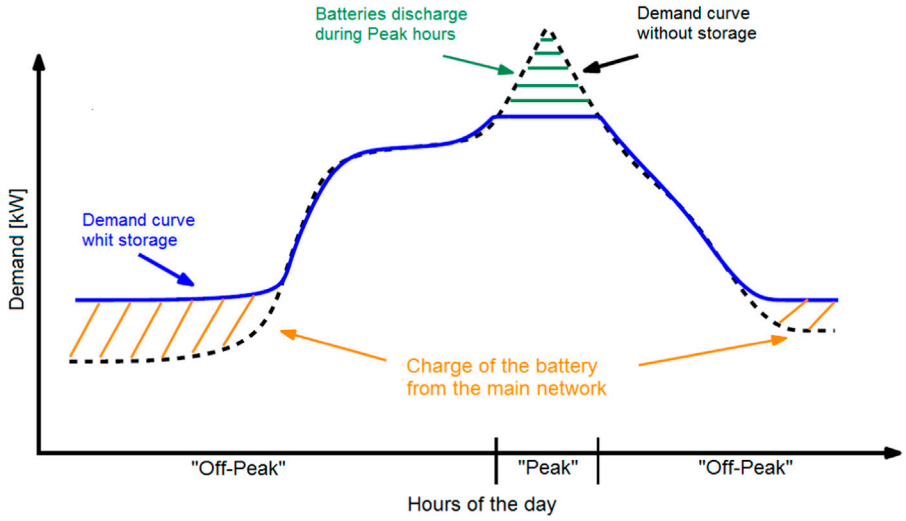

FIGURE 4
The graph depicts the so-called peak shaving, where energy storage helps flatten the demand curve, discharging during peak hourly demand and charging during off-peak hours.

being used during peak hours, when the quotient between the average demand of the customer in peak hours and its purchased power (for BT2 and AT2), or its maximum registered demand (for BT3 and AT3), is greater or equal to 0.5 (ENEL Distribucion, 2023).

b) When the purchased power or the maximum registered energy demand is being used partially during peak hours, regardless of whether power or energy is or is not used during other hours of the year, the consumption will be considered as "partially present in peak", and hence the corresponding price will be applied. It is understood that the purchased power or the maximum registered demand is being used partially during peak hours, when the quotient between the average demand of the customer during those hours and the purchased power (in case of BT2 and AT2), or its maximum registered demand (in case of BT3 and AT3), is less than 0.5. This allows the system to distinguish one particular consumption behavior from another and reflect the pricing and incentives accordingly as discussed in sections 2.5 and 2.6 (ENEL Distribucion, 2023).

However, should it occur that in the period of 60 consecutive minutes during peak hours, the quotient between the average power used by the customer and its purchased power (in case of BT2 and AT2), or its maximum registered demand (in case of BT3 and AT3), exceeds 0.85 and this fact is not an isolated event but occurs frequently, electric consumption will be classified as "present in peak". Hence, monthly charges for maximum demand purchased during peak hours and maximum demand purchased of the BT4.1 tariff, as well as the monthly charge for the maximum purchased demand from tariff BT4.2 will be charged even if the power consumption is zero. They will be obtained by multiplying the kW reading of purchased power by the corresponding unit price (ENEL Distribucion, 2023).

The monthly charges for the maximum power demand registered by the system during peak hours with tariffs BT4.2 and BT4.3 will be charged as follows.

- During the months where peak hourly demand is registered (on-peak hours), it will be applied to the maximum power demand effectively registered during peak hours in each month at the price set by the electric tariff.
- During the months which do not register peak hours, it will be applied the corresponding unit price to the average of the two highest peak demands during peak hours for the peak period months.

Below in Table 4 we have electricity tariffs according to the Chilean electricity law and their characteristics. The monthly charge for maximum power demand supplied from the BT4.3 tariff will be charged to customers, and this charge will be calculated taking the average reading of the two highest maximum power consumption registered during the last 12-month period, including the month when the billing was issued, with the corresponding unit price. Details of different charges and their corresponding prices according to the supply rate electric can be found in (ENEL Distribucion, 2023). For the operation conditions exposed in this work and since it seeks to modify the consumption pattern towards a more efficient use of energy, and thereby receive economic benefits, the chosen tariff to be used in the microgrid is an Hourly dependent. These types of electric tariffs are the ones with the lowest price for energy and provide the necessary flexibility towards an economically efficient operation yielding maximum profit, while the control model ensures stability and service quality as required by the electric company's legal regulatory framework. Thus, the chosen hourly rate will be option 3 (AT-4.3 or BT-4.3) (ENEL Distribucion, 2023).

The above table, taken from the National Energy Commission website (Comision Nacional de Energia) of Chile shows the three possible tariff alternatives for electric company customers. The difference between the BT and AT rates is in the voltage supply. The AT4.3 and BT4.3 tariffs are usually used by

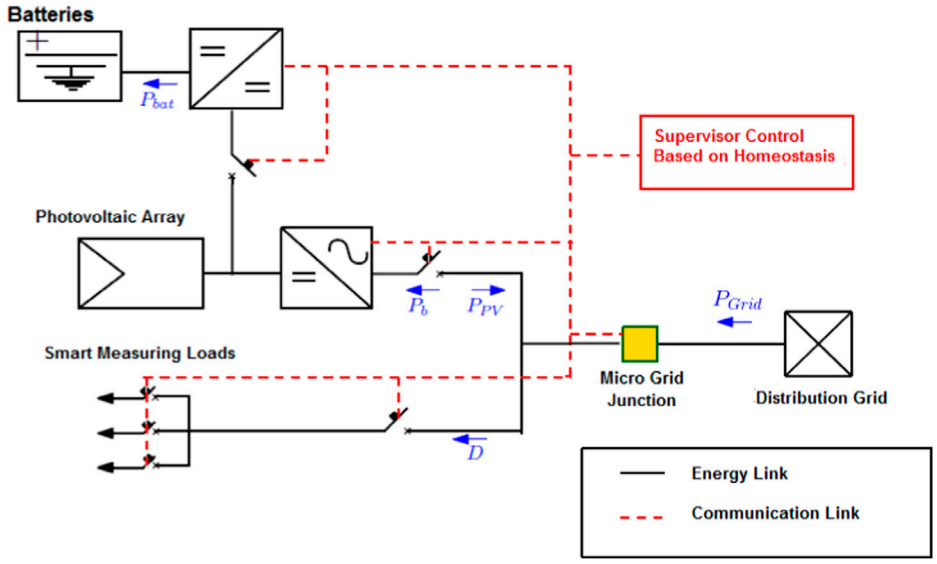

FIGURE 5
The microgrid's logical architecture diagram.

TABLE 5 Components' specification for the microgrid.

Component	Specification
Solar photovoltaic array	41.6 kWp
Inverter DC/AC	42 kW
Batteries	0–50–100–150 kWh

customers who have the possibility of reducing their demanded power during peak hours, hence are more flexible.

3 The system's logical architecture for the grid-tied microgrid

Below on Figure 5 is the logical architecture of the microgrid system developed to operate connected to grid with energy storage, to supply a community of 60 apartments, aiming to reduce the electric supply costs while providing incentives for customers willing to shift habits towards a more efficient, more sustainable energy consumption while enjoying green electricity supply from distributed generation from the electric company.

In the diagram above in Figure 5 depicts the power in the batteries P_{Bat_t} and P_{b_t} which are modeled to represent the efficiency of the batteries upon charging η_c and discharging η_d cycles, and the corresponding charging and discharging processes of the batteries operate as shown in (2).

$$P_{Bat_t} = \begin{cases} \dfrac{P_{b_t}}{\eta_d} & P_{b_t} < 0; \text{Discharge} \\ P_{b_t} & \eta_c P_{b_t} > 0; ; Charge \end{cases} \quad (2)$$

Likewise, each of the component's specifications utilized in the microgrid is summarized below in Table 5.

3.1 The energy homeostasis model behind the control strategy

The energy homeostasis model is what inspired the control strategy applied in this case model. Unlike common control methods, this model encompasses both the grid and the energy consumers as key pillars of the sustainable block™ where each resident can act as a prosumer, not just as a regular, passive consumer of electricity. This behavior can lead to mutual economic benefits for the consumers as well as for the electric utility and is what in previous work has been characterized as sustainable loads (Yanine et al., 2019; Yanine et al., 2020), or active loads, as opposed to passive loads that have no interaction with the network (Yanine et al., 2020). The aim behind this strategy is for the system to be able to self-regulate and adjust to a more sustainable energy consumption habit as a whole community, whenever distributed generation systems, operated by the local electric company and supplying limited renewable generation are present.

The diagram in Figure 6 represents the model's homeostatic control strategy. The control algorithm begins by measuring of the photovoltaic (PV) power generated and the energy demand of each apartment. Then, calculates the total power demanded by the community D_t and also sets the demand limits for the community X_{upper}, so as to keep consumption within the sustainable range considering the renewable generation and supply limitations of the system. The limits will also depend on the hour of the day (low or high demand). The first condition to be evaluated is given by (3) (Yanine et al., 2018a).

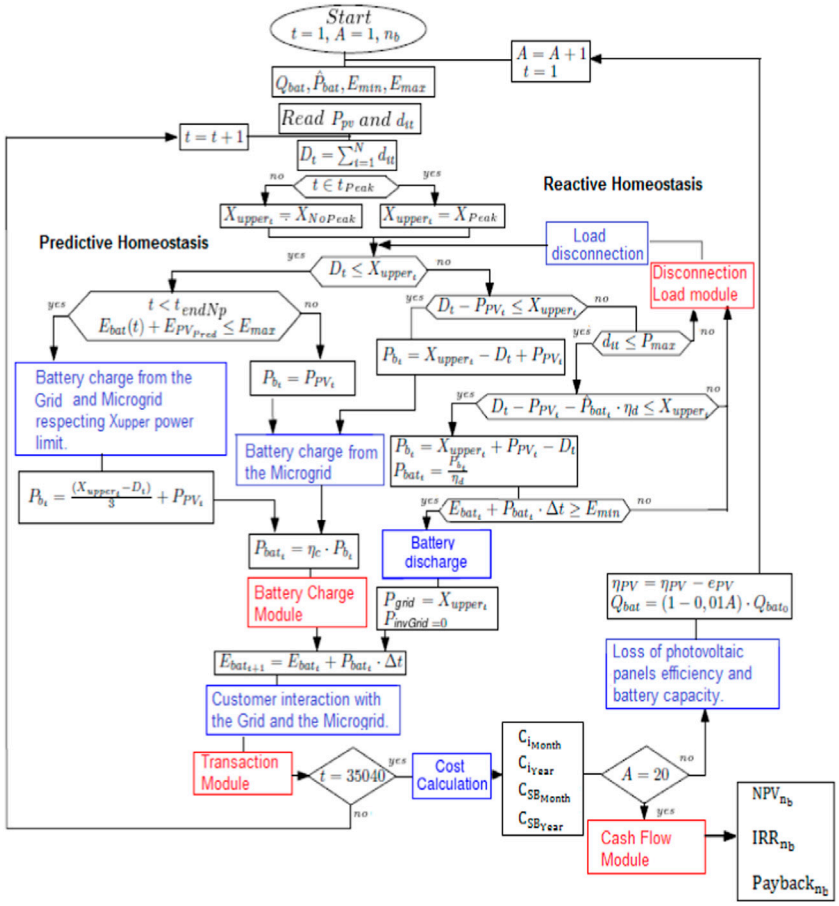

FIGURE 6
Homeostatic control strategy diagram depicting electric power supply to the building's residents considering an hourly tariff (Yanine et al., 2018a).

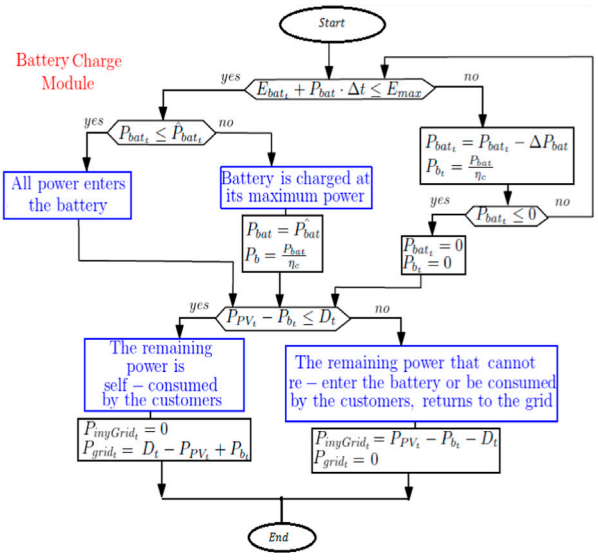

FIGURE 7
The battery charge module algorithm.

$$D_t \leq X\_upper_t \tag{3}$$

As depicted above, if the total electric power demand is less than the demand limit set for the community of residents with the distributed generation supply, all of the photovoltaic (PV) energy generated by the microgrid will be assigned to charge the batteries.

The battery charge algorithm depicted in Figure 7 below takes into account the battery's technical constraints, such as maximum current or the state-of-charge (SOC).

The photovoltaic energy that is not being able to be absorbed by the batteries because they are fully charged, is readily consumed by the residents and the surplus (if there is any) is injected into the grid, taking advantage of the existing Net Billing law (Energypedia, 2015). On the other hand, if condition (3) is not met, the control system proceeds to evaluate condition (4), and if this condition is met, battery is charged by the remaining power (Yanine et al., 2018a).

$$D_t - P_{PV_t} \leq X_{upper_t} \tag{4}$$

Otherwise, if condition set by (4) is not met, the battery will be discharged in order to satisfy the restriction of maintaining the demand of the community in the limit X_{upper_t}. Before discharging the battery, the algorithm makes sure that all customers are

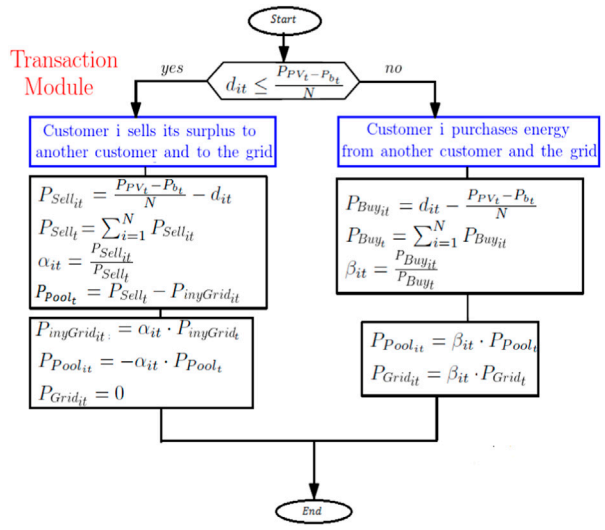

FIGURE 8
Flow diagram depicting renewable energy supply and consumption management under equitable criteria.

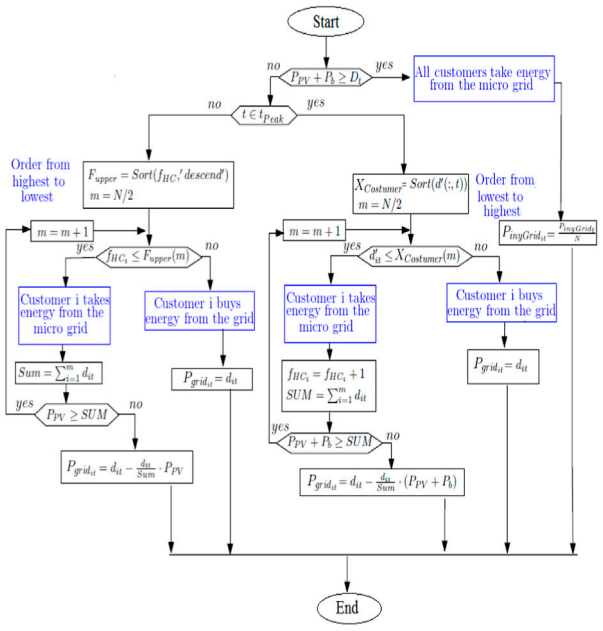

FIGURE 9
Flow diagram depicting renewable energy supply to customers inspired by an energy sustainability strategy based on energy homeostasis.

demanding less than or equal to the maximum allowable demand per customer. In case this condition is not satisfied, alarms will be generated and the controllable loads of the customer who is not complying will be disconnected, leaving him/her with the grid-only option (Yanine et al., 2019; Yanine et al., 2020).

$$D_t - P_{PV_t} - \hat{P}_{bat_t} * \eta_d \leq X_{upper_t} \tag{5}$$

The expression in (5) has total (aggregate) demand of the community minus the power generated by the solar photovoltaic array minus the product of the power stored in the batteries multiplied by the discharging efficiency coefficient η_d check if discharging the battery to the maximum allowed capacity by the controller is sufficient to maintain the X_{upper_t} demand limit. If true, the power to be extracted from the battery is given by,

$$P_{b_t} = X_{upper_t} + P_{PV_t} - D_t \tag{6}$$

During this period, the power demand from the network P_{grid_t} will be equal to X_{upper_t}. Should the power available to the community's aggregate (total) demand D_t not be enough while operating within the boundaries set by the control system in order to maintain power limit of the community, the controller should generate alarms and disconnect specific loads from the residents, starting with non-critical ones. For each load that is disconnected, the expression in (4) is evaluated and the process is repeated over again until the maximum power set by the controller is achieved. Therefore, by changing the parameters of its internal structure (battery discharge and demand), the algorithm is able to control the energy flow and reach an efficient and sustainable operating point where all system limits are satisfied, as part of the reactive homeostasis (RH) component of the energy homeostasis control model (Yanine et al., 2019; Yanine et al., 2020).

In order to bound the power to its established limit point and thus avoid disconnections, the battery must be charged at its maximum capacity before entering peak hours. This procedure is hard to achieve since the energy provided by the PV plant depends directly on weather conditions. An alternative strategy is to introduce an Artificial Neural Networks algorithm that can predict the energy generated by the photovoltaic plant from a given moment until before entering peak hours (Yanine et al., 2019; Yanine et al., 2020). Above in Figure 7, the algorithm diagram shows the logic behind the operation of the battery charge module of the homeostatic control system.

$$E_{bat}(t) + E_{PV_{pred}}\left(t: t_{finNP}\right) \leq E_{batMax} \tag{7}$$

On the other hand, if condition (7) is true, the battery will be fully charged. If otherwise, energy is absorbed from the network to satisfy the limit imposed by the controller (Yanine et al., 2019; Yanine et al., 2020). Renewable energy is produced in limited quantities and its production is affected by intermittence; thus, certain conditions should be imposed to provide cheap energy to consumers while supporting the grid, with a consequent reduction of their electricity bills and carbon footprint (Yanine et al., 2019; Yanine et al., 2020). Figure 8 depicts the transaction module which is in charge for assigning the energy quota for each customer based on the available supply in the system and calculate the energy flow among customers and the grid. In order to accomplish the above mention procedure, criteria A and B could be chosen (Yanine et al., 2019; Yanine et al., 2020).

Criterion A: Customers share the Nth part of generated renewable energy, where each customer owns one Nth part of the renewable energy produced by the microgrid (Yanine et al., 2019; Yanine et al., 2020).

The transaction module begins by discriminating between s with energy in excess or the deficit in energy in the system, by using condition (8) (Yanine et al., 2019; Yanine et al., 2020). Figure 8 below depicts renewable energy supply and consumption management under equitable criteria.

$$d_{it} \leq \frac{P_{PV_t} - P_{b_t}}{N} \tag{8}$$

The customer i that satisfies condition 8) has excess energy, expressed by (9), and can make it available to customers with energy deficit or sell it directly to the network, as convenient (Yanine et al., 2019; Yanine et al., 2020).

$$P_{Sell_{it}} \leq \frac{P_{PV_t} - P_{b_t}}{N} - d_{it} \tag{9}$$

All of the excess energy available in the system, P_{Sell_t}, is given by (10). Part of this excess energy that is available will be used to meet the requirements of those residents that show an energy deficit, and this portion of available energy to meet other residents' needs is represented by P_{Pool_t} on Eq. (12), whereas the rest will be injected into the grid, as denoted by P_{inGrid_t}. The energy made available by each customer, as prosumers by means of an efficient and sustainable energy consumption will be identified defining a factor α_{it} according to Eq. (11) (Yanine et al., 2019; Yanine et al., 2020).

$$\alpha_{it} = \frac{P_{Sell_{it}}}{P_{Sell_t}} \tag{11}$$

Then the energy supplied to customers with energy deficit and injected into the grid by the customers with excess i will be given by (12) and (13), respectively (Yanine et al., 2019; Yanine et al., 2020).

$$P_{Pool_t} = P_{Sell_t} - P_{inGrid_t} \tag{12}$$

$$P_{Pool_{it}} = \alpha_{it} \cdot P_{Pool_t} \tag{13}$$

$$P_{inGrid_{it}} = \alpha_{it} \cdot P_{inGrid_t} \tag{14}$$

If the condition in (8) is not met, this means that there is a resident with energy deficit. Hence, this resident must use energy from the grid P_{grid_t} and/or from the excess energy made available by other residents from the pool of renewable energy P_{Pool_t}. The procedure that describes the energy flow under this condition, is depicted in the flow diagram of Figure 8 to supply renewable energy under an equitable criterion (Yanine et al., 2019; Yanine et al., 2020).

Criterion B: There is substantial renewable energy supply available, based on customer merit.

The flow diagram shown in Figure 9 represents the logic behind the energy sustainability strategy based on energy homeostasis. The strategy calls for community residents to maintain an efficient, sustainable electricity consumption so as to make the renewable energy supply from the microgrid plentiful. This strategy requires residents to be willing to change such power consuming tasks as laundry, dishwashing machines, vacuum cleaner, etc., To those hourly periods when there is more energy available in the system and electric tariff is on off-peak hours.

The condition in (15) checks for available energy in the system considering the power generation from the microgrid and the energy that is available in the energy storage unit (batteries). If condition in (15) is satisfied, all residents may receive the energy supply available in the system from the microgrid and the batteries so as to meet their consumption. The surplus energy generated by the system is injected to the grid and customers will receive an equal economic benefit (prorated) for that contribution (Yanine et al., 2020).

$$P_{PV_t} + P_{b_t} \geq D_t \tag{15}$$

If condition (15) is not met, this means that the energy available in the system is not enough to satisfy the residents' aggregate demand. In this case, those that consume less or whose demand is low compared to others whose demand is higher, may benefit as explained earlier, by allowing their unused energy quota to be available to those in need of more energy and thus be rewarded for it. This is especially relevant for those residents that exhibit a low energy consumption during peak hours (Yanine et al., 2019; Yanine et al., 2020).

The algorithm's control module managing peak hours' demand is in charge of discerning about each resident's consumption profile, thus identifying those that exhibit a thrifty consumption or simply consume less from those that consume more energy and exhibit a higher need for power. It does this by discriminating according to their energy consumption from lowest to highest. The first m customers will have the right to receive energy from the microgrid in proportion to their consumption behavior, as indicated in (16) (Yanine et al., 2019; Yanine et al., 2020).

$$P_{grid_{it}} = d_{it} - \frac{d_{it}}{Sum} \cdot \left(P_{PV_t} + P_{b_t}\right) \tag{16}$$

In expression (16) the grid power supply is equal to the demand of each resident d_{it} minus the same demand divided by the value of Sum which corresponds to the sum of the consumptions of the first m customers. This expression depicts the prioritization that those residents with a thriftier consumption have over those residents that consume more or are more intensive in power demand, especially during peak hourly periods. As seen in (16) the available energy is represented by $P_{PV_t} + P_{b_t}$ The remaining $N - m$ customers must satisfy 100% of their energy consumption from the grid. Customers who are allowed to receive energy from the microgrid at peak hours will increase an index termed "homeostatic index (H_i)" (Yanine et al., 2018a). This index will be used to distribute the renewable energy available during non-peak hours the next day. In addition, customers will be ranked from higher to lower according to the homeostatic index's value H_i, so the first m customers with higher H_i will obtain energy from the microgrid (Yanine et al., 2018a; Yanine et al., 2019; Yanine et al., 2020).

Due to the high cost of electricity during peak hours demand, the control system strategy seeks to encourage residents to consume more during off-peak hours, especially by transferring their power consumption needs to off peak hours. In order achieve this, the cost of the electricity supply is transferred to the residents by means of an internal rate that is applied upon differentiating between those residents whose demand is low from those whose demand is high. Figure 10 bellow illustrate the application of this internal tariff, which will be based on the monomic energy price which consists of a single equivalent price per kWh consumed. The monomic price that considers charging the customer per both, the energy and the power consumption (Yanine et al., 2019; Yanine et al., 2020).

$$C_{m_p}\left(month_p\right) = \frac{\sum_{t \epsilon h_p} P_{grid_t} \cdot \Delta t \cdot C_e + MD_{h_p} \cdot C_p}{\sum_{t \epsilon h_p} P_{grid_t} \cdot \Delta t} \tag{17}$$

$$C_{mop}\left(month_p\right) = \frac{\sum_{t \epsilon h_{op}} P_{grid_t} \cdot \Delta t \cdot C_e + P_{max_t} \cdot C_{op}}{\sum_{t \epsilon h_{op}} P_{grid_t} \cdot \Delta t} \tag{18}$$

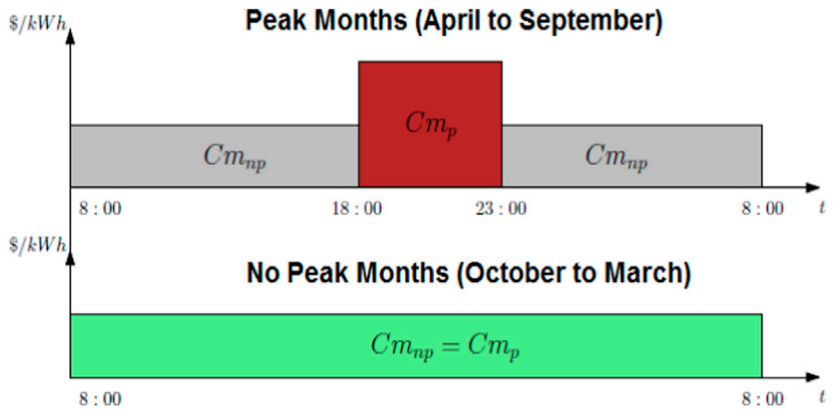

FIGURE 10
Internal rate for the community of 60 residents. The red square block shows the hourly block between 18:00 h (6 p.m.) and 23:00 h (11 p.m.) during which peak hourly demand occurs.

$$C_{m_{op}} = C_{mp}\left(month_{op}\right) = \frac{\sum_{t \in month} P_{grid_t} \cdot \Delta t \cdot C_e + P_{max_t} \cdot C_{op} + P_{max_{pt}} \cdot C_p}{\sum_{t \in month} P_{grid_t} \cdot \Delta t} \quad (19)$$

The monomic price, which is depicted in expressions (17), (18) and (19) is to be used to compute electric consumption billing during peak hours and off-peak hours, respectively. The monomic price for peak hours (C_{mp}) is calculated on the basis of the energy consumed and the maximum demand registered per resident, both during peak hours. On the other hand, the monomic price during off peak hours is computed in similar way, but considering monomic prices that are calculated monthly, together with the billing cycle. During the months that do not contain peak hours (October to March), the monomic cost for peak and non-peak periods are the same and the billing calculation is done according to Equation 19 (Yanine et al., 2019; Yanine et al., 2020).

After 1 year of evaluation ($t = 35040, \Delta t = 15\,min$), the monthly and annual costs are calculated for each resident and for the entire community as a whole, according to the equations shown in (20) through (24) (prices are shown in (Yanine et al., 2019)).

$$C_{SB_{month_{op}}} = \sum_{t \in Month} P_{grid_t} \cdot \Delta t \cdot C_e + \frac{P_{max_m}}{m \in month_p} \cdot C_p + P_{max_t} \cdot C_{op} + C_{fix} \quad (20)$$

$$C_{SB_{month_{op}}} = \sum_{t \in Month} P_{grid_t} \cdot \Delta t \cdot C_e + P_{max_{Pt}} \cdot C_p + P_{max_t} \cdot C_{op} + C_{fix} \quad (21)$$

$$C_{BS_{year}} = \sum_{Month=1}^{12} C_{SB_{Month}} \quad (22)$$

$$C_{i_{Month}} = \left\{ \sum_{t \in Month} P_{Grid_{it}} \cdot C_{m_t} + P_{Pool_{it}} \cdot C_{Pool} - P_{inGrid_{it}} \cdot C_{inGrid} \right\} \cdot \Delta t + C_{fix} \quad (23)$$

$$C_{i_{year}} = \sum_{Month=1}^{12} C_{i_{Month}} \quad (24)$$

We ran the simulation for up to 20 years' time which corresponds to the photovoltaic panels' lifetime, wherein a loss of efficiency per year is expected in the photovoltaic panels as established by the original equipment manufacturer (OEM) that is equal to 0.6% which goes along with a linear reduction of battery capacity, which is also considered, so that the final battery capacity is 80%. The depth of discharge of the battery is adjusted so that no intermediate replacements occur (Yanine et al., 2020).

3.2 Simulation results: The separate customers' case

Customers are free to choose between different electric rates in the corresponding voltage level. Among the rates offered by the local electricity company, described in a previous section, only BT-1 tariffs and THR are competitive for levels and consumption characteristics of individual customers. In this scenario the option of incorporating a microgrid with a photovoltaic array upon the roof of the building with an energy storage system is a good option in terms of distributed generation alternative due to its reliability and cost effectiveness. As illustrated in Figure 11, the smart meter of each resident will register the apartment's electricity consumption but it will not discriminate whether the electricity is supplied by the grid or by the microgrid, unless the proposed energy homeostasis-based control system of the microgrid in the work presented here is implemented through an interface connection operated by the electric company so as to enable the smart meter to differentiate one type of supply from the other (Yanine et al., 2020).

4 Overall simulation results and discussion

Upon confirming the simulation results, we are able to effectively validate the homeostatic control model, and upon looking at the graphs we can ascertain that the energy

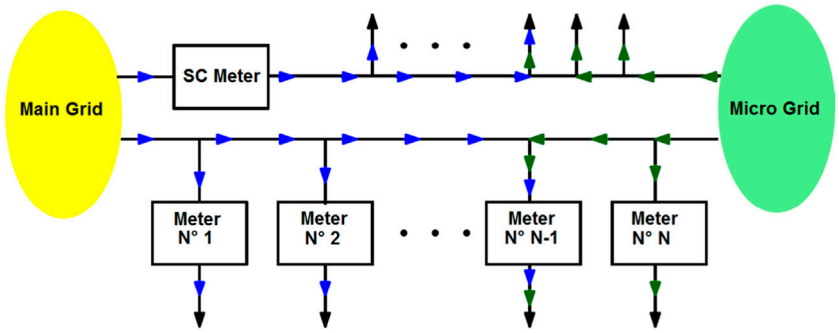

FIGURE 11
Energy flow and smart metering for separate customers.

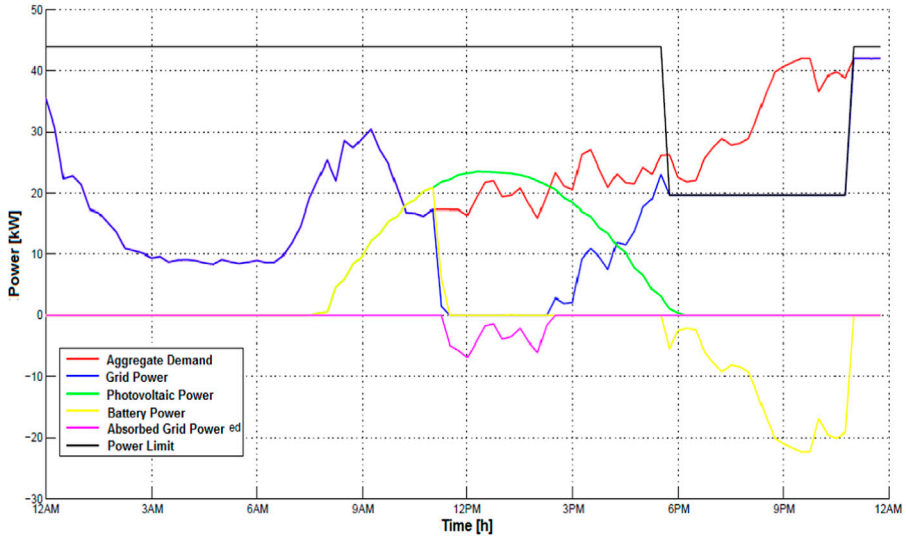

FIGURE 12
the power flow of the microgrid simulated without the energy storage option and depicting the hourly tariff.

homeostasis strategy utilized to manage the available energy supply for the community of residents yields the expected benefits, as opposed to not having the distributed generation alternative but just the grid-only option (Yanine et al., 2020).

Figure 12 below shows the power flow of the microgrid simulated without the energy storage option so as to corroborate the distinct benefits of having this resource available. In this case, what the microgrid cannot supply is supplied by the grid and therefore, the grid is modeled here as an infinite bus. As we can see from the figure's interpretation, the key period, where much of the demand takes place is between 9 a.m. and 4 PM. The period between 10 a.m. and 2 p.m. is where the energy storage should operate at full capacity, supplying its stored energy, but in this case, it is absent, so the yellow line is flat. In the same period, we can also see that the photovoltaic (PV) power generation is at its maximum, and the hump reaches its peak between 12 p.m. and 1 PM. Therefore, during this period of time the grid is absorbing whatever excess power being produced by the grid-tied microgrid. However, later in the day, at around 6 p.m., the power demand intensifies significantly, with the maximum demand period being between 7 p.m. and 10 p.m., and begins to gradually decrease from there onward. During that period the microgrid's production without energy storage is simply not enough to account for the full demand, so the grid comes in to assist and it supplies the rest. Likewise, the aggregate demand (red line) rises between 8 a.m. and 6 p.m. as expected, and this can be seen represented by the yellow straight line that represents the period.

Figure 13, on the other hand, depicts the power flow with the energy storage system operating as part of the microgrid. The homeostatic control system is always prioritizing to charge the batteries (the energy storage system) and, upon reaching the maximum power demand limit in peak hours, the batteries may discharge if required, a process known as load shedding or peak shaving. The controller adjusts the demand limit at peak hours considering the capacity and maximum power delivered by the battery bank. The batteries are also expected be charged (if so needed) by the grid supply when the electric tariff is low (Yanine et al., 2020).

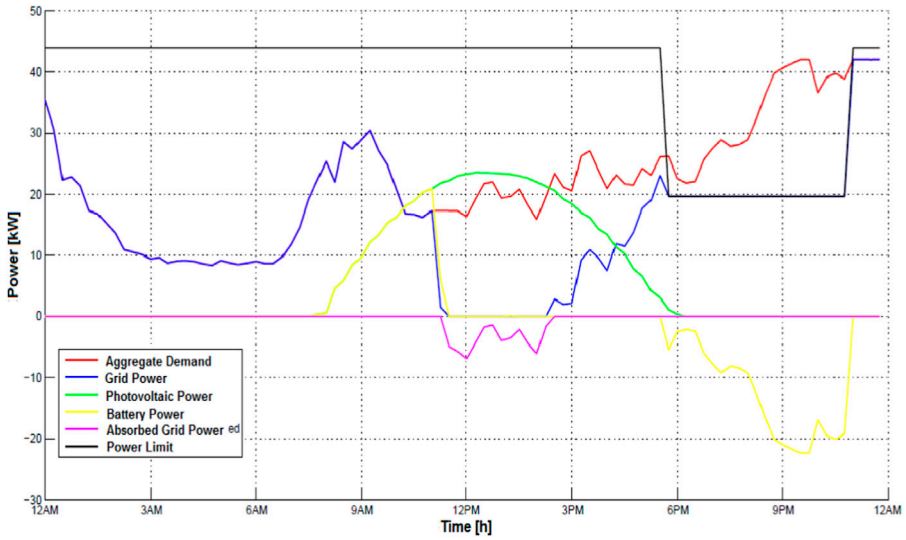

FIGURE 13
the power flow with the energy storage present as part of the microgrid and hourly tariff depiction.

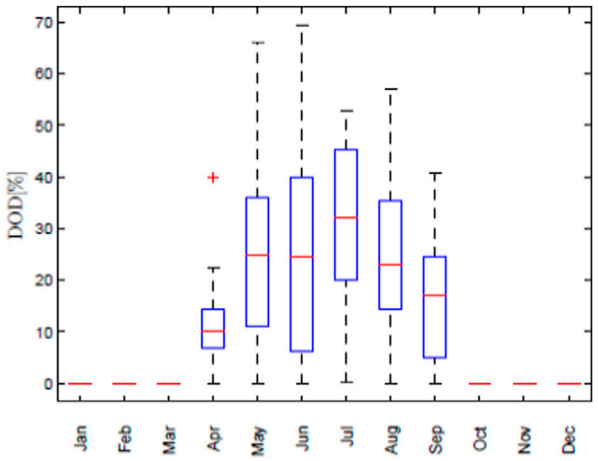

FIGURE 14
First year's monthly depth of discharge (DOD) of the battery bank, showing the months of higher electricity consumption during winter season (April through the end of August).

The practice of load shedding or peak shaving is a strategy very commonly used for avoiding peak demand charges during those hourly periods when electricity tariff is higher accounting for high or peak demand from the electrical grid supply, as is the case illustrated here, and very especially during winter season due to electric heating and hot water pumps operation. This is done by quickly reducing power consumption during intervals of high demand. Energy storage such as on-site energy storage systems depicted here is especially helpful and cost-effective during higher demand periods so as to reduce overall cost associated with residential and commercial electricity consumption.

Again, we see here that the high demand period between 8 a.m. and 10 a.m., we have the batteries operating and supplying power as needed, while the microgrids' full production is on. Grid power reaches a peak in demand right around 9 a.m., and then starts decreasing since the microgrid with energy storage is operating at maximum capacity. The batteries are usually being charged during 2 p.m. and 5 p.m. which is a period of low electricity demand for the community. However, at 6 p.m. demand starts rising and the high demand period is between 7 p.m. and 10 PM. The red line represents the aggregate demand, and we can see that between 12 p.m. and 2 p.m. is a period where we see power being absorbed by the grid, which means that there is excess power being produced so it can be injected to the grid. Like in Figure 12, during the period when the microgrid's production with energy storage is not enough to account for the full electric power demand (between 7 p.m. and 10 p.m.), the grid comes in to assist and supply the rest.

The batteries' state of health depends heavily on the operating conditions, provided that the installation was done properly. Overload, temperature range, intensity and charging cycling are all aspects to be considered. Batteries are used essentially for peak shaving and a solar power plant, as is the case of our grid-tied microgrid. It is highly beneficial to install both, an adequate solar PV capacity and on-site energy storage to ensure that the community can enjoy the highest utility bill savings possible. Thus, during the day, the homeostatic control system charges the on-site batteries with solar energy from the PV panels and batteries may also be charged by the grid supply when electric tariff is low (off-peak hours). Hence, we are still technically saving money, and when we need to power the community, we can use whichever electricity source is cheapest at that precise moment in time–whether it is from the photovoltaic (PV) panels' supply during the day or from the stored solar power (in the batteries) in the evening or during "peak" hours, which in this case is between 7 p.m. and 10 p.m. The only time that the microgrid needs to draw electricity directly from the grid is when PV panels are not operating because of the absence of sunlight and when the batteries are completely empty.

One of the main factors to consider in order to extend the lifetime of the batteries is the Depth of Discharge (DOD) result of the operation cycles. The depth of discharge complements the state of charge (SoC) in the sense that as the depth of discharge increases, the State of Charge decreases. There is a direct relation between the depth of discharge and the cycle life of the batteries (Tejada-Arango et al., 2019; Zsiborács et al., 2019). As shown in Figure 14, batteries are only discharged to do peak shaving, as explained before, when the demand for power is high, during peak months (April through the end of August in Chile); out of this period, the battery bank is in floating state and ready for backup whenever the (grid) main network is not available for whatever reason.

Finally, as a side note, two types of batteries were evaluated for simulation purposes, the traditional Acid-Lead batteries and the Lithium-ion battery. In both cases, technical operating limitations were considered. Keeping the batteries between 40% and 80% ensures that they have a longer lifespan. Particularly in the case of lithium-ion batteries they are stressed the most during the top and bottom 20% of their charging range; and the closer to 100% or to 0% we get, the greater the stress on the batteries. That is why keeping charging up to 80% maximum is much healthier, and never letting it drop (discharge) below 20%. The control system will stop charging at around 80%, more or less, and start recharging at around 20%, so as to keep batteries from aging age rapidly, and last longer, compared to routine full charges (Tejada-Arango et al., 2019; Zsiborács et al., 2019). Hence, we can see in Figure 14 that in the months of June and July, is when the greater use of the batteries is required, as in 75% of the cases the DODs are lower than 40%. This strategy is used to extend the lifetime of the storage devices as much as possible.

5 Conclusion

Urban energy system modeling is an important area of research towards advancing distributed generation and energy sustainability. In this paper we have proposed an energy homeostasis model to ENEL Chile as a proof of concept for a real scale prototype that is to be implemented hopefully in 2024 with ENEL's collaboration. The model envisions a smart microgrid tied to ENEL's distribution grid and operating on a residential building as part of distributed generation agenda being considered moving forward. As shown in this example, for off-peak demand in the spring and summer months, a flat tariff is applied where the price for energy is constant throughout the day. Because of the fact that the payment should be amortized by the maximum power demand and by peak power demand, measured during peak months, with the sale of energy to the grid during the months of low power demand (where not only there is lower consumption but also more photovoltaic (PV) energy is generated).

The energy cost during off-peak months is higher than in the base case (tariff BT-1). Given that the battery bank is used to decrease the demand for power, it is easy to amortize with the sale of energy; hence the incorporation of batteries helps the internal rate to be below the base case during off-peak hours. From the conditions used to define the energy cost at peak and off-peak hours, it can be observed that the tariff is self-regulated and allows to transfer the cost to each individual customer and, at the same time, encourages the efficient consumption of energy. Customers who decide to be more flexible and efficient, exhibiting a thriftier use of electricity, are able to transfer part of their consumption from peak hours to low demand hours, which will cause a decrease in the energy cost in low demand hours, due to the additional available energy. On the other hand, and since there will be less energy to amortize the charge for the maximum peak demand, the monomic cost of peak hour energy will increase. Therefore, without an effective change in peak power demand, the control system simply establishes that customers who exhibit an inefficient and inflexible electricity consumption of the supply that is made available by the microgrid, shall double-subsidize efficient customers. Even more important is the fact that this tariff proposal will allow customers to adapt and have incentives to change their habits and be more efficient, which will trigger thereafter a sustained reduction of the maximum demand in peak hours and with it, an effective saving by the community of energy consumers as a whole.

A singular aspect of the homeostasis model proposed in this work is the fact that customers, being considered as one single load by the electricity company, create the need to establish internal rules regarding the way to consume energy, to identify the diversity of energy consumption habits in the community and how to transfer the costs of operation and power supply to customers individually. A simple way to do so, as demonstrated in the simulation, is to transfer costs through an internal rate based on the monomic price for energy differentiated during peak and non-peak hours, the latter being considerably higher. This monomic price considers the cost per kW of electric power that must be realized and self-regulates by absorbing the dynamics represented by the external tariff and by the customers, so that the costs of supplying the customers of the microgrid are always unequivocally transferred while encouraging the residents to consume more electricity during off-peak hours so as to facilitate the operation of the control system and to reduce the demand limit adjusted for peak hours in the future.

Data availability statement

The original contributions presented in the study are included in the article/Supplementary Material, further inquiries can be directed to the corresponding author.

Author contributions

FY: Conceptualization, Data curation, Formal Analysis, Investigation, Methodology, Software, Validation, Writing–original draft. SS: Conceptualization, Formal Analysis, Investigation, Methodology, Supervision, Validation, Writing–original draft. AS-S: Conceptualization, Investigation, Project administration, Validation, Writing–original draft, Writing–review and editing. AB: Conceptualization, Formal Analysis, Investigation, Methodology, Supervision, Writing–original draft. CK: Conceptualization, Formal Analysis, Investigation, Methodology, Supervision, Validation, Writing–original draft.

Funding

The author(s) declare that no financial support was received for the research, authorship, and/or publication of this article.

Acknowledgments

We wish to thank ENEL Distribucion S.A. (https://www.enel.cl/) in Chile for their great support, unrelenting commitment to advancing this research agenda, and for the valuable technical assistance provided all along.

Conflict of interest

The authors declare that the research was conducted in the absence of any commercial or financial relationships that could be construed as a potential conflict of interest.

The author KS declared that they were an editorial board member of Frontiers at the time of submission. This had no impact on the peer review process and the final decision.

Publisher's note

All claims expressed in this article are solely those of the authors and do not necessarily represent those of their affiliated organizations, or those of the publisher, the editors and the reviewers. Any product that may be evaluated in this article, or claim that may be made by its manufacturer, is not guaranteed or endorsed by the publisher.

References

Adefarati, T., and Bansal, R. C. (2019). Reliability, economic and environmental analysis of a microgrid system in the presence of renewable energy resources. *Appl. energy* 236, 1089–1114. doi:10.1016/j.apenergy.2018.12.050

Basak, P., Chowdhury, S., Halder nee Dey, S., and Chowdhury, S. P. (2012). A literature review on integration of distributed energy resources in the perspective of control, protection and stability of microgrid. *Renew. Sustain. Energy Rev.* 16 (8), 5545–5556. doi:10.1016/j.rser.2012.05.043

Bhadoria, V. S., Pal, N. S., and Shrivastava, V. (2013). "A review on distributed generation definitions and DG impacts on distribution system," in Proceedings of the International Conference on Advanced Computing and Communication Technologies (ICACCT™-2013), Panipa, November 2013, 1–5.

Bhavsar, Y. S., Joshi, P. V., and Akolkar, S. M. (2015). "Simulation of Microgrid with energy management system," in Proceedings of the 2015 International Conference on Energy Systems and Applications, Pune, India, November 2015, 592–596. doi:10.1109/ICESA.2015.7503418

Birol, F. (2020). *The coronavirus crisis reminds us that electricity is more indispensable than ever*. Paris: International Energy Agency.

Bogdanov, D., Ram, M., Aghahosseini, A., Gulagi, A., Oyewo, A. S., Child, M., et al. (2021). Low-cost renewable electricity as the key driver of the global energy transition towards sustainability. *Energy* 227, 120467. doi:10.1016/j.energy.2021.120467

Caballero, F., Sauma, E., and Yanine, F. (2013). Business optimal design of a grid-connected hybrid PV (photovoltaic)-wind energy system without energy storage for an Easter Island's block. *Energy* 61, 248–261. doi:10.1016/j.energy.2013.08.030

Chamorro, H. R., Yanine, F. F., Peric, V., Diaz-Casas, M., Bressan, M., Guerrero, J. M., et al. (2021). "Smart renewable energy communities-existing and future prospects," in Proceedings of the 2021 IEEE 22nd Workshop on Control and Modelling of Power Electronics (COMPEL), Cartagena, Colombia, November 2021 (IEEE), 1–6.

Chen, Y., Liu, Z., Zhang, Y., Wu, Y., Chen, X., and Zhao, L. (2021). Deep reinforcement learning-based dynamic resource management for mobile edge computing in industrial internet of things. *IEEE Trans. Industrial Inf.* 17 (7), 4925–4934. doi:10.1109/tii.2020.3028963

Cheng, Y., Zhang, S., Huan, C., Oladokun, M. O., and Lin, Z. (2019). Optimization on fresh outdoor air ratio of air conditioning system with stratum ventilation for both targeted indoor air quality and maximal energy saving. *Build. Environ.* 147, 11–22. doi:10.1016/j.buildenv.2018.10.009

Cordova, F. M., and Yanine, F. F. (2012). Homeostatic control of sustainable energy grid applied to natural disasters. *Int. J. Comput. Commun. Control* 8 (1), 50–60. doi:10.15837/ijccc.2013.1.168

De Lotto, R., Micciché, C., Venco, E. M., Bonaiti, A., and De Napoli, R. (2022). Energy communities: technical, legislative, organizational, and planning features. *Energies* 15 (5), 1731. doi:10.3390/en15051731

Driesen, J., and Katiraei, F. (2008). Design for distributed energy resources. *IEEE power energy Mag.* 6 (3), 30–40. doi:10.1109/MPE.2008.918703

ENEL Distribucion (2023). Tarifas. https://www.chilectra.cl/tarifas; (Accessed December 4 2022).

ENEL (2011). Enel distribuzione: italy's first smart grid in isernia. https://www.enel.com/media/press/d/2011/11/enel-distribuzione-italys-first-smart-grid-in–isernia; (Accessed February 4 2023).

ENEL (2017). Enel operates world's first "plug and play" micro-grid powered by solar pv and hydrogen-based storage in chile. https://www.enel.com/media/press/d/2017/05/enel-operates-worlds-first-plug-and-play-micro-grid-powered-by-solar-pv-and-hydrogen-based-storage-in-chile (Accessed May 31 2023).

ENEL (2014). Microgrids: the future of energy. https://www.enel.com/media/news/d/2014/05/microgrids-the-future-of-energy; (Accessed June 3 2023).

Energypedia (2015). Net-metering/billing in Chile. https://energypedia.info/wiki/Net-Metering_/_Billing_in_Chile; (Accessed July, 2023).

Ghelani, D. (2022). Cyber security in smart grids, threats, and possible solutions. *Authorea Prepr.*

Gottwalt, S., Ketter, W., Block, C., Collins, J., and Weinhardt, C. (2011). Demand side management—a simulation of household behavior under variable prices. *Energy policy* 39 (12), 8163–8174. doi:10.1016/j.enpol.2011.10.016

Hambridge, S., Lu, N., Huang, A. Q., and Yu, R. (2017). "A frequency based real-time electricity rate for residential prosumers," in Proceedings of the 2017 IEEE Power & Energy Society General MeetingE, Chicago, IL, USA, July 2017 (IEEE), 1–5.

International Energy Agency (2023a). World energy investment 2023 report. https://www.iea.org/reports/world-energy-investment-2023 (Accessed June 30, 2023).

International Energy Agency (2023b). IEA world energy outlook 2022 executive summary. https://www.iea.org/reports/world-energy-outlook-2022 (Accessed June 30 2023).

Jain, S., Kalambe, S., Agnihotri, G., and Mishra, A. (2017). Distributed generation deployment: state-of-the-art of distribution system planning in sustainable era. *Renew. Sustain. Energy Rev.* 77, 363–385. doi:10.1016/j.rser.2017.04.024

Jiayi, H., Chuanwen, J., and Rong, X. (2008). A review on distributed energy resources and MicroGrid. *Renew. Sustain. Energy Rev.* 12 (9), 2472–2483. doi:10.1016/j.rser.2007.06.004

Kimani, K., Oduol, V., and Langat, K. (2019). Cyber security challenges for IoT-based smart grid networks. *Int. J. Crit. infrastructure Prot.* 25, 36–49. doi:10.1016/j.ijcip.2019.01.001

Kroposki, B., Lasseter, R., Ise, T., Morozumi, S., Papathanassiou, S., and Hatziargyriou, N. (2008). Making microgrids work. *IEEE power energy Mag.* 6 (3), 40–53. doi:10.1109/mpe.2008.918718

Lan, J., Khan, S. U., Sadiq, M., Chien, F., and Baloch, Z. A. (2022). Evaluating energy poverty and its effects using multi-dimensional based DEA-like mathematical composite indicator approach: findings from Asia. *Energy Policy* 165, 112933. doi:10.1016/j.enpol.2022.112933

Leal-Arcas, R., Nacht, Y., Madeleine, L., Pelegri, J., Mizrachi, G., and Siebenhirter, J. (2023). Clean energy technologies: assessing advantages and risks. *Renew. Energy Law Policy Rev.* 11 (2-3), 35–47. doi:10.4337/relp.2022.02-03.01

Li, S., Patnaik, S., and Li, J. (2023). IoT-based technologies for wind energy microgrids management and control. *Electronics* 12 (7), 1540. doi:10.3390/electronics12071540

Li, W., Yang, L., Ji, Y., and Xu, P. (2019). Estimating demand response potential under coupled thermal inertia of building and air-conditioning system. *Energy Build.* 182, 19–29. doi:10.1016/j.enbuild.2018.10.022

Londono, E. (2017). *Chile's energy transformation is powered by wind, sun and volcanoes*. New York: New York Times. Available at: https://www.nytimes.com/2017/08/12/world/americas/chile-green-energy-geothermal.html; (Accessed June, 2023).

Morgan, P., Martinez, D., and Maxwell, A. (2014). From good to great: the next step in Chilean energy efficiency. *Nat. Resour. Def. Counc. (NRDC)*. Availble at: https://www.nrdc.org/sites/default/files/chile-energy-efficiency-report.pdf; (Accessed March 2 2023).

Moslehi, K., and Kumar, R. (2010). A reliability perspective of the smart grid. *IEEE Trans. Smart Grid* 1 (1), 57–64. doi:10.1109/tsg.2010.2046346

Nasirov, S., Silva, C., and Agostini, C. (2015). Investors' perspectives on barriers to the deployment of renewable energy sources in Chile. *Energies* 8 (5), 3794–3814. doi:10.3390/en8053794

Palensky, P., and Dietrich, D. (2011). Demand side management: demand response, intelligent energy systems, and smart loads. *IEEE Trans. industrial Inf.* 7 (3), 381–388. doi:10.1109/tii.2011.2158841

Paris, L. (2022). *The integration of sustainability and social innovation practices into the core business: the case of ENEL*.

Qiao, J., Li, M., Liu, J., Lu, Y., Sun, Y., Liu, Y., et al. (2023). Research on decision-making behavior of power suppliers considering multi-market integration and network security. *Front. Energy Res.* 11, 1220751. doi:10.3389/fenrg.2023.1220751

Rao, C. K., Sahoo, S. K., and Yanine, F. F. (2022). "Forecasting electric power generation in a photovoltaic power systems for smart energy management," in Proceedings of the International Conference on Intelligent Controller and Computing for Smart Power (ICICCSP), Hyderabad, India, July 2022, 1–6. doi:10.1109/ICICCSP53532.2022.9862396

Series, I. E. T. R. E. (2009). *Microgrids and active distribution networks*. England: The institution of Engineering and Technology.

Silva, C., and Nasirov, S. (2017). Chile: paving the way for sustainable energy planning. *Energy Sources, Part B Econ. Plan. Policy* 12 (1), 56–62. doi:10.1080/15567249.2014.977464

Tejada-Arango, D. A., Siddiqui, A. S., Wogrin, S., and Centeno, E. (2019). A review of energy storage system legislation in the US and the European Union. *Curr. Sustainable/Renewable Energy Rep.* 6, 22–28. doi:10.1007/s40518-019-00122-7

Tiep, N. C., Wang, M., Mohsin, M., Kamran, H. W., and Yazdi, F. A. (2021). An assessment of power sector reforms and utility performance to strengthen consumer self-confidence towards private investment. *Econ. Analysis Policy* 69, 676–689. doi:10.1016/j.eap.2021.01.005

Trevisan, R., Ghiani, E., and Pilo, F. (2023). Renewable energy communities in positive energy districts: a governance and realisation framework in compliance with the Italian regulation. *Smart Cities* 6 (1), 563–585. doi:10.3390/smartcities6010026

Van Aubel, P., and Poll, E. (2019). Smart metering in The Netherlands: what, how, and why. *Int. J. Electr. Power & Energy Syst.* 109, 719–725. doi:10.1016/j.ijepes.2019.01.001

Wolsink, M. (2020). Distributed energy systems as common goods: socio-political acceptance of renewables in intelligent microgrids. *Renew. Sustain. Energy Rev.* 127, 109841. doi:10.1016/j.rser.2020.109841

Wolsink, M. (2012). The research agenda on social acceptance of distributed generation in smart grids: renewable as common pool resources. *Renew. Sustain. Energy Rev.* 16 (1), 822–835. doi:10.1016/j.rser.2011.09.006

Yanine, F., and Cordova, F. M. (2013). "Homeostatic control in grid-connected micro-generation power systems: a means to adapt to changing scenarios while preserving energy sustainability," in Proceedings of the 2013 International Renewable and Sustainable Energy Conference (IRSEC), Ouarzazate, Morocco, March 2013 (IEEE), 525–530.

Yanine, F., Sanchez-Squella, A., Barrueto, A., Kumar Sahoo, S., and M. Cordova, F. (2018b). Smart energy systems: the need to incorporate homeostatically controlled microgrids to the electric power distribution industry: an electric utilities' perspective. *Int. J. Eng. Technol.* 7 (2), 64–73. doi:10.14419/ijet.v7i2.28.12883

Yanine, F. F., Caballero, F. I., Sauma, E. E., and Córdova, F. M. (2014b). Building sustainable energy systems: homeostatic control of grid-connected microgrids, as a means to reconcile power supply and energy demand response management. *Renew. Sustain. Energy Rev.* 40, 1168–1191. doi:10.1016/j.rser.2014.08.017

Yanine, F. F., Caballero, F. I., Sauma, E. E., and Córdova, F. M. (2014a). Homeostatic control, smart metering and efficient energy supply and consumption criteria: a means to building more sustainable hybrid micro-generation systems. *Renew. Sustain. Energy Rev.* 38, 235–258. doi:10.1016/j.rser.2014.05.078

Yanine, F. F., Córdova, F. M., and Valenzuela, L. (2015). Sustainable hybrid energy systems: an energy and exergy management approach with homeostatic control of microgrids. *Procedia Comput. Sci.* 55, 642–649. doi:10.1016/j.procs.2015.07.060

Yanine, F. F., Sanchez-Squella, A., Barrueto, A., Cordova, F., and Sahoo, S. K. (2017). Engineering sustainable energy systems: how reactive and predictive homeostatic control can prepare electric power systems for environmental challenges. *Procedia Comput. Sci.* 122, 439–446. doi:10.1016/j.procs.2017.11.391

Yanine, F. F., Sauma, E. E., and Cordova, F. M. (2014c). An exergy and homeostatic control approach to sustainable grid-connected microgrids without energy storage. *Appl. Mech. Mater.* 472, 1027–1031. doi:10.4028/www.scientific.net/amm.472.1027

Yanine, F. F., and Sauma, E. E. (2013). Review of grid-tie micro-generation systems without energy storage: towards a new approach to sustainable hybrid energy systems linked to energy efficiency. *Renew. Sustain. Energy Rev.* 26, 60–95. doi:10.1016/j.rser.2013.05.002

Yanine, F., Sánchez-Squella, A., Barrueto, A., Parejo, A., Cordova, F., and Rother, H. (2020). Grid-tied distributed generation systems to sustain the smart grid transformation: tariff analysis and generation sharing. *Energies* 13 (5), 1187. doi:10.3390/en13051187

Yanine, F., Sanchez-Squella, A., Barrueto, A., Sahoo, S. K., Parejo, A., and Cordova, F. M. (2022). Energy homeostasis management strategy for building rooftop nanogrids, considering the thermal model and a HVAC unit installed. *Procedia Comput. Sci.* 199, 10–17. doi:10.1016/j.procs.2022.01.002

Yanine, F., Sanchez-Squella, A., Barrueto, A., Sahoo, S. K., Parejo, A., Shah, D., et al. (2019). Homeostaticity of energy systems: how to engineer grid flexibility and why should electric utilities care. *Periodicals Eng. Nat. Sci. (PEN)* 7 (1), 474–482. doi:10.21533/pen.v7i1.424

Yanine, F., Sanchez-Squella, A., Barrueto, A., Tosso, J., Cordova, F. M., and Rother, H. C. (2018a). Reviewing homeostasis of sustainable energy systems: how reactive and predictive homeostasis can enable electric utilities to operate distributed generation as part of their power supply services. *Renew. Sustain. Energy Rev.* 81, 2879–2892. doi:10.1016/j.rser.2017.06.094

Zakeri, B., Paulavets, K., Barreto-Gomez, L., Echeverri, L. G., Pachauri, S., Boza-Kiss, B., et al. (2022). Pandemic, war, and global energy transitions. *Energies* 15 (17), 6114. doi:10.3390/en15176114

Zheng, J., Gao, D. W., and Lin, L. (2013). "Smart meters in smart grid: an overview," in Proceedings of the 2013 IEEE green technologies conference (GreenTech), Denver, CO, USA, April 2013 (IEEE), 57–64.

Zsiborács, H., Baranyai, N. H., Vincze, A., Zentkó, L., Birkner, Z., Máté, K., et al. (2019). Intermittent renewable energy sources: the role of energy storage in the european power system of 2040. *Electronics* 8 (7), 729. doi:10.3390/electronics8070729

Nomenclature

i	Customera
N	Number of customers of the sustainable block™
t	elapsed time (in minutes)
Y	year
Δt	15 min interval
d_{it}	customer i demands power (kW) during period t
D_t	total power demanded by the sustainable block™ in period t
P_{PV_t}	electric power generated by the microgrid in period t
η_t	number of batteries connected
Q_{Bat_t}	battery capacity in period t [kWh]
P_{Bat_t}	battery power charge/discharge process in period t at the DC side
P_{b_t}	battery power charge/discharge in period t at the AC side
E_{Bat_t}	electrical energy (in kWh) stored in the battery in period t
E_{max}, E_{min}	maximum and minimum electrical energy in the battery
η_c, η_d	efficiency rating of the charging and discharging of the battery
P_{grid_t}	electric power supplied by the distribution grid in period t
$P_{grid_{it}}$	electric power (kW) consumed by customer i in period t
P_{inGrid_t}	electric power injected to the grid in period t
$P_{inGridi_t}$	electric power injected to the grid by customer i in period t
P_{max_t}	average reading of the two highest registered power demands in a 12-month period
$P_{max_{Pt}}$	average of the two highest power demands during peak hour (6 p.m.–11 p.m.) registered in the winter period (April to September in Chile)
P_{pool_t}	electric power being transferred among customers in period t
$P_{pool_{it}}$	electric power supplied by customer i to another customer in period t
C_m	monomic energy price [$/KWh]
$C_{mP}, C_{m_{op}}$	monomic energy price at peak and off-peak hours respectively [$/KWh]
C_p, C_{op}	peak and off-peak power demand cost [$/kW]
C_{im}	cost to supply energy to customer i in month m in [$]
C_{iY}	annual cost to supply energy to customer i [$]
C_{SB_m}	cost of energy supplied to the sustainable block™ in month m [$]
C_e	cost of electric power supply from the grid [$/kWh]
C_{inGrid}	electric power sold back to the grid by the community [$/kW]
C_{pool}	cost of the electrical energy exchange among customers [$/kWh]
MD_{ph}	peak power demand per month during peak hours [kW]
MD_{oph}	peak power demand per month during off-peak hours [kW]
$month_p$	winter season's month (from April to September)
$month_{op}$	summer season's month (from October to March)
h_p	hours of peak electricity consumption, from 6 p.m. to 11 p.m. in winter
h_{op}	off-peak electric consumption hours, from 11:01 p.m. to 5:59 p.m.
C_{BS_A}	cost to supply energy to the sustainable block™ in year Y in [$]

Frontiers in
Energy Research

Advances and innovation in sustainable, reliable and affordable energy

Explores sustainable and environmental developments in energy. It focuses on technological advances supporting Sustainable Development Goal 7: access to affordable, reliable, sustainable and modern energy for all.

Discover the latest Research Topics

See more →

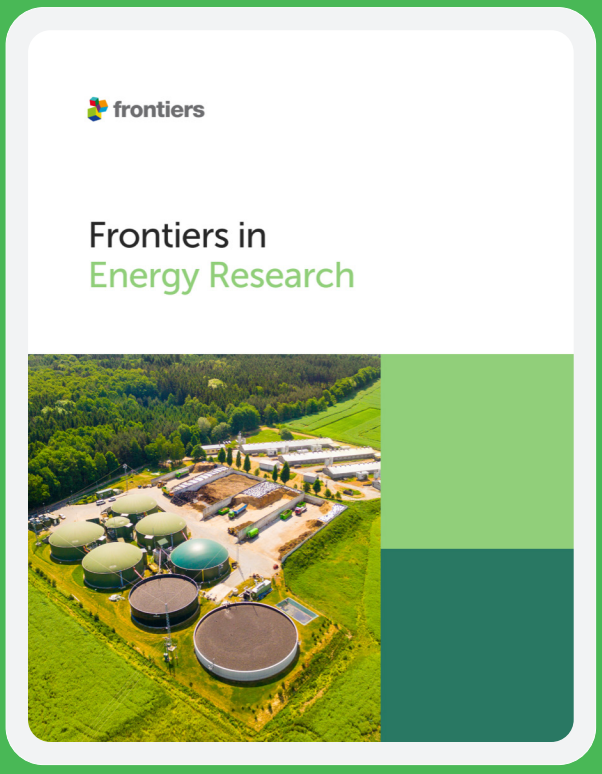

Frontiers

Avenue du Tribunal-Fédéral 34
1005 Lausanne, Switzerland
frontiersin.org

Contact us

+41 (0)21 510 17 00
frontiersin.org/about/contact